REGENERATIVE MEDICINE FOR CARTILAGE AND JOINT REPAIR

EDITED BY: Zhen Li, Laura Creemers and Xiaoling Zhang
PUBLISHED IN: Frontiers in Bioengineering and Biotechnology

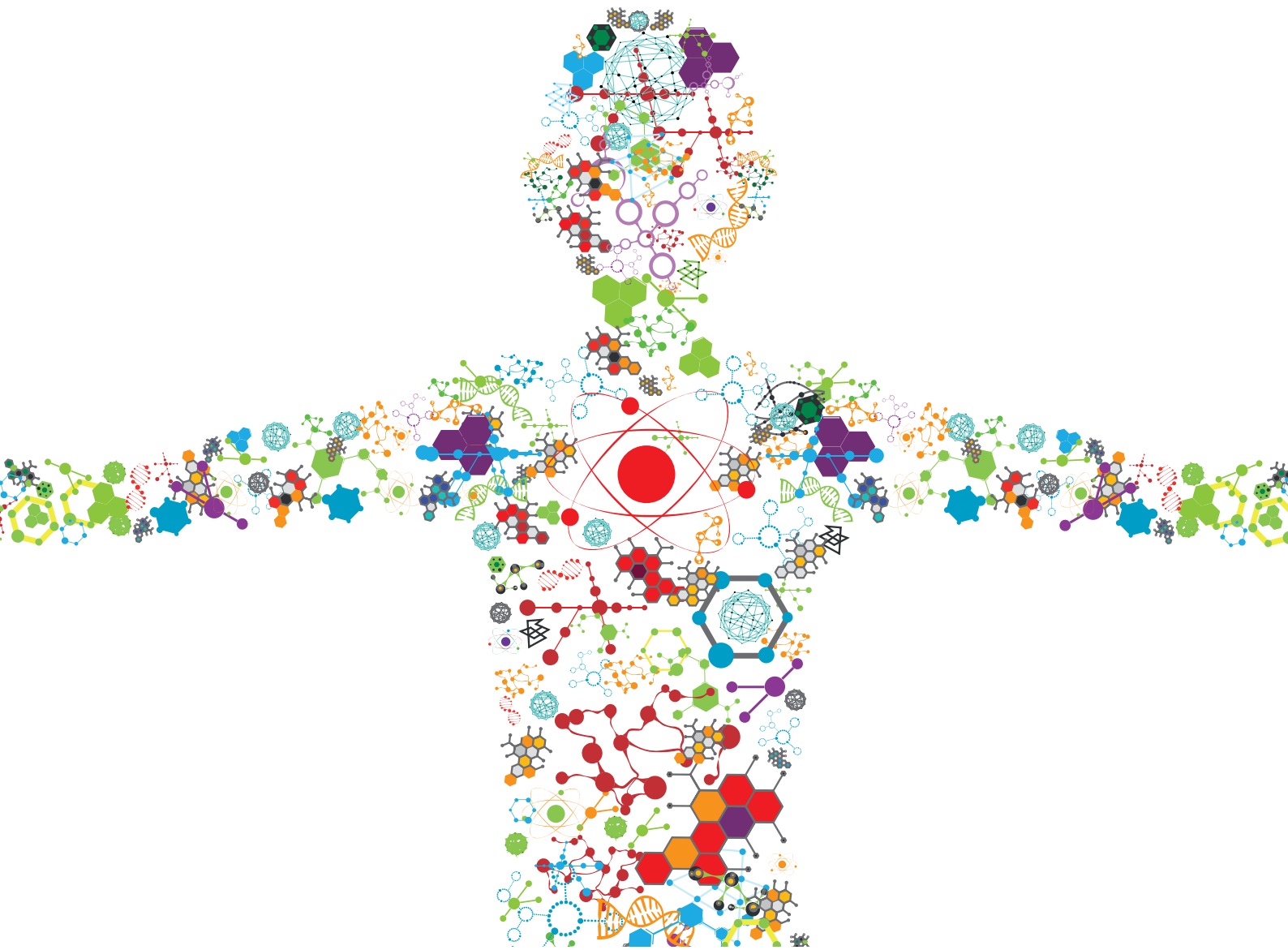

frontiers Research Topics

ISSN 1664-8714
ISBN 978-2-88976-084-8
DOI 10.3389/978-2-88976-084-8

About Frontiers

Frontiers is more than just an open-access publisher of scholarly articles: it is a pioneering approach to the world of academia, radically improving the way scholarly research is managed. The grand vision of Frontiers is a world where all people have an equal opportunity to seek, share and generate knowledge. Frontiers provides immediate and permanent online open access to all its publications, but this alone is not enough to realize our grand goals.

Frontiers Journal Series

The Frontiers Journal Series is a multi-tier and interdisciplinary set of open-access, online journals, promising a paradigm shift from the current review, selection and dissemination processes in academic publishing. All Frontiers journals are driven by researchers for researchers; therefore, they constitute a service to the scholarly community. At the same time, the Frontiers Journal Series operates on a revolutionary invention, the tiered publishing system, initially addressing specific communities of scholars, and gradually climbing up to broader public understanding, thus serving the interests of the lay society, too.

Dedication to Quality

Each Frontiers article is a landmark of the highest quality, thanks to genuinely collaborative interactions between authors and review editors, who include some of the world's best academicians. Research must be certified by peers before entering a stream of knowledge that may eventually reach the public - and shape society; therefore, Frontiers only applies the most rigorous and unbiased reviews.
Frontiers revolutionizes research publishing by freely delivering the most outstanding research, evaluated with no bias from both the academic and social point of view. By applying the most advanced information technologies, Frontiers is catapulting scholarly publishing into a new generation.

What are Frontiers Research Topics?

Frontiers Research Topics are very popular trademarks of the Frontiers Journals Series: they are collections of at least ten articles, all centered on a particular subject. With their unique mix of varied contributions from Original Research to Review Articles, Frontiers Research Topics unify the most influential researchers, the latest key findings and historical advances in a hot research area! Find out more on how to host your own Frontiers Research Topic or contribute to one as an author by contacting the Frontiers Editorial Office: frontiersin.org/about/contact

REGENERATIVE MEDICINE FOR CARTILAGE AND JOINT REPAIR

Topic Editors:
Zhen Li, AO Research Institute, Switzerland
Laura Creemers, University Medical Center Utrecht, Netherlands
Xiaoling Zhang, Shanghai Jiao Tong University, China

Dr. Laura Creemers stands as CSO for Epione Therapeutics, a start-up company on drug delivery in degenerative joint and disc disease. Dr. Xiaoling Zhang holds several patents. All other Topic Editors declare no competing interests with regard to the Research Topic subject.

Citation: Li, Z., Creemers, L., Zhang, X., eds. (2022). Regenerative Medicine for Cartilage and Joint Repair. Lausanne: Frontiers Media SA.
doi: 10.3389/978-2-88976-084-8

Table of Contents

frontiers | Frontiers in Bioengineering and Biotechnology

EDITORIAL
published: 13 April 2022
doi: 10.3389/fbioe.2022.891970

Editorial: Regenerative Medicine for Cartilage and Joint Repair

Zhen Li[1]*, *Laura Creemers*[2] *and Xiaoling Zhang*[3]

[1]AO Research Institute Davos, Davos, Switzerland, [2]Department of Orthopaedics, University Medical Center Utrecht, Utrecht, Netherlands, [3]School of Medicine, Xinhua Hospital, Shanghai Jiaotong University, Shanghai, China

Keywords: cartilage, joint, regenerative medicine, cells, materials

Editorial on the Research Topic

Regenerative Medicine for Cartilage and Joint Repair

INTRODUCTION

Cartilage diseases affect a large population worldwide and are associated with a significant burden to patients and society. Osteoarthritis (OA) is the most common chronic joint disorder and the fastest growing cause of disability. Cartilage focal defects, predisposing to early OA and degeneration impair the function of many joints, including the articular joint, intervertebral disc and temporomandibular joint. Presently, no effective therapy is available, except for palliative care primarily used to delay invasive and often suboptimal surgical interventions. Regenerative medicine therapies directed at the early stage of osteoarthritis, and tissue engineering approaches to reconstruct cartilage defects provide great potential for cartilage and joint repair in the future. This current research topic represents a collected series of articles in this field. Highlights are summarized below.

RESEARCH TOPIC HIGHLIGHTS

Liu et al. provided a timely review describing the factors that affect cartilage homeostasis and function, and the emerging regenerative approaches that are informing the future treatment options. Tissue engineering approaches combining cell and biomaterial strategies to reconstruct the complex and functional cartilage tissue are still under active research. Two review articles in the current topic have described the use of 3D printing technology in cartilage tissue reconstruction in general (Perera et al.) and for irregularly shaped cartilage in particular (Wang et al.). Electrospun gelatin/polycaprolactone (GT/PCL) nanofiber membranes at optimum GT/PCL ratio were used to support *in vivo* cartilage regeneration from autologous chondrocytes in a swine model (Zheng et al.). Also xenogeneic acellular cartilage matrix (ACM) materials encapsulated with autologous chondrocytes showed capacity to promote cell proliferation and cartilage formation in goat, with only a minor immune-inflammatory response (Jia et al.). This provides scientific evidence for future clinical application of ACM in cartilage tissue engineering. Next to biomaterials, appropriate cell sources are important for cartilage repair. Combined physioxia and fibronectin adherence have shown to select and propagate a meniscus progenitor population that can potentially be used to treat meniscal tears or defects (Pattappa et al.). Additional stimuli can further enhance the cartilage repair potential of cells. For example, a magnetic field applied to magnetic nanoparticles-loaded cells decreased cellular senescence and enhanced chondrogenic capability of adipose-derived mesenchymal stem cells (Labusca et al.). Senescence can also be targeted using a senolytic peptide, fork head box O transcription factor 4-D-Retro-Inverso (FOXO4-DRI), which removed the senescent cells among chondrocytes (Huang et al.).

Edited and reviewed by:
Ranieri Cancedda, Independent Researcher, Genova, Italy

***Correspondence:**
Zhen Li
zhen.li@aofoundation.org

Specialty section:
This article was submitted to Tissue Engineering and Regenerative Medicine, a section of the journal Frontiers in Bioengineering and Biotechnology

Received: *08 March 2022*
Accepted: *16 March 2022*
Published: *13 April 2022*

Citation:
Li Z, Creemers L and Zhang X (2022) Editorial: Regenerative Medicine for Cartilage and Joint Repair. Front. Bioeng. Biotechnol. 10:891970. doi: 10.3389/fbioe.2022.891970

Last but not least, appropriate animal models for OA are still lacking and play a pivotal role in the development of regenerative therapies. Bi et al. have established an model combining transection of the anterior and posterior cruciate ligaments, and the meniscus, and a cartilage defect in rhesus macaques, which closely resembled the pathophysiological processes of spontaneous knee OA in humans.

AUTHOR CONTRIBUTIONS

ZL drafted the manuscript. LC and XZ revised the manuscript critically.

Conflict of Interest: The authors declare that the research was conducted in the absence of any commercial or financial relationships that could be construed as a potential conflict of interest.

frontiers in Bioengineering and Biotechnology

BRIEF RESEARCH REPORT
published: 29 April 2021
doi: 10.3389/fbioe.2021.677576

Senolytic Peptide FOXO4-DRI Selectively Removes Senescent Cells From *in vitro* Expanded Human Chondrocytes

Yuzhao Huang[1,2†], Yuchen He[1†], Meagan J. Makarcyzk[1,3] and Hang Lin[1,3,4]*

[1] Department of Orthopaedic Surgery, University of Pittsburgh School of Medicine, Pittsburgh, PA, United States, [2] Department of Orthopaedics, The Third Xiangya Hospital, Central South University, Changsha, China, [3] Department of Bioengineering, University of Pittsburgh Swanson School of Engineering, Pittsburgh, PA, United States, [4] McGowan Institute for Regenerative Medicine, University of Pittsburgh School of Medicine, Pittsburgh, PA, United States

Autologous chondrocyte implantation (ACI) is a procedure used to treat articular cartilage injuries and prevent the onset of post-traumatic osteoarthritis. *In vitro* expansion of chondrocytes, a necessary step in ACI, results in the generation of senescent cells that adversely affect the quality and quantity of newly formed cartilage. Recently, a senolytic peptide, fork head box O transcription factor 4-D-Retro-Inverso (FOXO4-DRI), was reported to selectively kill the senescent fibroblasts. In this study, we hypothesized that FOXO4-DRI treatment could remove the senescent cells in the expanded chondrocytes, thus enhancing their potential in generating high-quality cartilage. To simulate the *in vitro* expansion for ACI, chondrocytes isolated from healthy donors were expanded to population doubling level (PDL) 9, representing chondrocytes ready for implantation. Cells at PDL3 were also used to serve as the minimally expanded control. Results showed that the treatment of FOXO4-DRI removed more than half of the cells in PDL9 but did not significantly affect the cell number of PDL3 chondrocytes. Compared to the untreated control, the senescence level in FOXO4-DRI treated PDL9 chondrocytes was significantly reduced. Based on the result from standard pellet culture, FOXO4-DRI pre-treatment did not enhance the chondrogenic potential of PDL9 chondrocytes. However, the cartilage tissue generated from FOXO4-DRI pretreated PDL9 cells displayed lower expression of senescence-relevant secretory factors than that from the untreated control group. Taken together, FOXO4-DRI is able to remove the senescent cells in PDL9 chondrocytes, but its utility in promoting cartilage formation from the *in vitro* expanded chondrocytes needs further investigation.

Keywords: chondrocyte, senescence, autologous chondrocyte implantation, senolytic, FOXO4-DRI

OPEN ACCESS

Edited by:
Zhen Li,
AO Research Institute, Switzerland

Reviewed by:
Guangli Suo,
Suzhou Institute of Nano-tech and Nano-bionics (CAS), China
Guang Yang,
University of Maryland, College Park, United States

****Correspondence:***
Hang Lin
hal46@pitt.edu

† These authors have contributed equally to this work and share first authorship

Specialty section:
This article was submitted to Tissue Engineering and Regenerative Medicine, a section of the journal Frontiers in Bioengineering and Biotechnology

Received: *07 March 2021*
Accepted: *12 April 2021*
Published: *29 April 2021*

Citation:
Huang Y, He Y, Makarcyzk MJ and Lin H (2021) Senolytic Peptide FOXO4-DRI Selectively Removes Senescent Cells From in vitro Expanded Human Chondrocytes. Front. Bioeng. Biotechnol. 9:677576. doi: 10.3389/fbioe.2021.677576

INTRODUCTION

Autologous chondrocyte implantation (ACI) is a biomedical treatment that repairs cartilage injury in the knee joint, which has been shown to reduce pain and facilitate mobility recovery (Kreuz et al., 2019). It has also been reported that an ACI procedure may prevent the progression of early osteoarthritis in patients with cartilage injuries (Jungmann et al., 2019). However, it is noted that the clinical outcome of ACI is still variable (Andriolo et al., 2017), and the reasons have not been

fully demonstrated. Given that implanted chondrocytes are responsible for the generation of new cartilage in the defect site, it is not surprising that the quality of these cells critically affects the reparative results of ACI treatment (Davies and Kuiper, 2019).

Typically, ACI involves harvesting cartilage, isolating chondrocytes, expanding cells *in vitro*, and re-implanting over an articular cartilage defect. In order to collect a sufficient number of cells for implantation, isolated chondrocytes usually undergo an extensive expansion from 0.1–0.2 million to 40–60 million (Huang et al., 2016). During this period, cultured chondrocytes gradually lose the proliferative capacity and the potential of generating the cartilage-specific matrix, a phenomenon known as dedifferentiation (Sassi et al., 2014). Moreover, the number of senescent cells also increase with culture time, resulting in a loss of division capabilities, resistance to apoptosis, and the acquisition of a robust proinflammatory secretome known as the senescence-associated secretory phenotype (SASP) (Jeon et al., 2018). The representative SASP factors include pro-inflammatory cytokines, chemokines, and proteases, which can cause an imbalance in cartilage hemostasis, resulting in degradation or other dysfunctions (Li and Pei, 2012). In fact, transplanting senescent cells into mice knee joint has been found to induce an osteoarthritis-like change (Xu et al., 2017).

Thus, selectively removing senescent cells in chondrocytes is crucial to assure the quality of cells for ACI. Currently, several senolytics were reported to kill senescent cells (Di Micco et al., 2021). FOXO4-DRI is a peptide antagonist designed to perturbs the interaction of FOXO4 and p53. Disrupting the p53-FOXO4 interaction causes p53 to be excluded from the nucleus and directed to mitochondria for induction of apoptosis in senescent cells, ultimately eliminating senescent fibroblasts through triggering apoptosis (Baar et al., 2017). Whether this novel senolytic can remove senescent chondrocytes, thus finally enhancing the reparative outcome of ACI has not been reported.

In this study, we tested the hypothesis that FOXO4-DRI treatment can selectively remove senescent cells in expanded human chondrocytes, thus enhancing their potential to generate high-quality cartilage. Specifically, to simulate the *in vitro* expansion for ACI, human chondrocytes were expanded to a population doubling level (PDL) 9 to represent chondrocytes ready for implantation. Cells at PDL3 were used as the minimally expanded control. The senescent levels of PDL3 and PDL9 chondrocytes were assessed by senescence-associated beta-galactosidase (SA-β-gal) staining and qRT-PCR analysis of senescence-associated marker genes. Then both PDL3 and PDL9 chondrocytes were treated with FOXO4-DRI for 5 days. Afterward, cell phenotype was examined by testing their senescence level and cartilage formation capacity.

MATERIALS AND METHODS

Isolation and *in vitro* Expansion of Human Chondrocytes

Human chondrocytes were isolated from de-identified knee articular cartilage without signs of osteoarthritis or injury. Tissues were obtained through the National Disease Research Interchange (Philadelphia, PA) with approval from the University of Pittsburgh Committee for Oversight of Research and Clinical Training Involving Decedents (CORID). To isolate chondrocytes, fresh articular cartilage tissues were rinsed with basal medium (BM), consisted of high glucose Dulbecco's modified Eagle's medium (DMEM, Gibco/Thermo Fisher Scientific, Waltham, MA, United States), with 2 × Antibiotics-Antimycotics (anti-anti, Life Technologies, Carlsbad, CA, United States) and then cut into ∼1 mm^3 pieces. The cartilage particles were digested with collagenase type II (0.2% w/v in BM, Worthington Biochemical, Lakewood, NJ, United States) in a 37°C shaker overnight. After passing through the 70 μm cell strainer (BD Falcon, Bedford, MA, United States), the cell suspension was centrifuged at 300 × g for 5 min. Cells resuspended in the growth medium (GM, DMEM containing 10% fetal bovine serum (FBS, Life Technologies) and 1% anti-anti), and the single cells were seeded in a cell culture flask. GM was replaced every 3 days. After chondrocytes reached 80–90% confluency, the cells were dissociated with Trypsin/EDTA (Gibco/Thermo Fisher Scientific) and passaged. The chondrocytes used in this study were isolated from eight donors (15-, 70-, 73-years-old female, and 42-, 69- and 70-years-old male) without the sign of cartilage degradation. For our studies, chondrocytes were expanded *in vitro* in GM and incubated at 37°C with 5% CO_2. Chondrocytes were passaged at 80–90% confluency.

Population Doubling Level Calculation

To calculate the PDL, a formula was used as follows: $\mathbf{n} = 3.32\ (\log \mathbf{UCY} - \log \mathbf{I}) + \mathbf{X}$, where **n** is the final PDL at the end of a given subculture, **UCY** is the cell yield at that point, **I** is the cell number used as inoculum to begin that subculture, and **X** is the PDL of the inoculum used to initiate the subculture being quantitated (Pham et al., 2020). According to the formula, both UCY and I are recorded after each passage. Cell number was assessed by hemocytometer counting.

SA-β-Galactosidase Staining

Cells were seeded in 6-well microplates at 4 × 10^4 cells/well. Cellular senescence was assessed by SA-β-galactosidase staining (SA-β-gal staining) using senescence β-galactosidase Staining Kit (Cell Signaling Technology, Beverly, MA, United States) according to the manufacturer's instructions. Cells stained blue under an optical microscope were counted as positive cells, and DAPI counterstain was used to count the total cell number. The percentage of SA-β-gal staining-positive cells was calculated in at least 3 random fields.

CCK-8 Assay

Chondrocytes were plated at 3 × 10^3 cells/cm^2 in 24-well microplates with growth medium. The ability of proliferation was assessed by a Cell Counting Kit-8 (CCK-8, Dojindo, Rockville, MD, United States) at different time points post-plating. For counting, each condition was plated in triplicate. At each time point, 1/10 volume of culture medium per well CCK-8 solution reagent was added, incubated at 37°C for

3 h, and the absorbance was measured at 450 nm using a microplate reader.

RNA Extraction and qRT-PCR Detection

Chondrocytes were plated at 3×10^3 cells/cm^2 in 6-well microplates (monolayer culture) with GM after treatment. Total RNA was harvested from monolayer and pellet cultures at different time points using Qiazol (Qiagen, Germantown, MD, United States) and purified with RNeasy Plus Universal Mini Kit (Qiagen, Cat. No. 74104) according to the manufacturer's protocol. Then cDNA was synthesized using SuperScript™ IV VILO™ Master Mix (Invitrogen, Waltham, MA, United States) and diluted 10–1 by DNase/RNase-Free Distilled Water (Invitrogen). A 20 μl mix, containing 8 μl of cDNA sample, 10 μl of SYBR Green PCR Master Mix (Thermo Fisher Scientific), and 2 μl of 10 mM forward primer and reverse primer mixture was used to performed Quantitative RT-PCR with a StepOne Plus Real-time PCR system (Applied Biosystems, Foster City, CA, United States). The relative gene expression was calculated using the $2^{-\Delta CT}$ method by Ribosomal protein L13a (*RPL13*α) gene, and the fold change was expressed by $2^{-\Delta\Delta CT}$. For all real-time RT-PCR experiments, each condition was in triplicate. Full name and abbreviation of genes and proteins tested in this study are shown in **Supplementary Table 1**. Sequences of primers for qRT-PCR are listed in **Supplementary Table 2**.

Drug Treatment

In this study, we used FOXO4 D-Retro-Inverso peptide (FOXO4-DRI, NovoPro, Shanghai, China) and ABT-263 (Apexbio Technology, Houston, TX, United States) to selectively remove the senescent chondrocytes. The final concentration of FOXO4-DRI and ABT-263 was 25 and 1.25 μM in 2% FBS basal medium. The duration of treatment was 5 days. After treatment, cells were maintained in GM for 2–3 days before analysis.

Caspase-3/7 Staining

5×10^3 cells/cm^2 chondrocytes were plated in 24-well microplate and cultured with GM. Fluorescent staining for casepase3/7 was done using CellEvent™ Caspase-3/7 Green Detection Reagent Kit (Thermo Fisher Scientific). Diluted reagent was added to cells after treatment and incubated for 30 min at 37°C. Cells were viewed under a fluorescence microscope. Apoptotic cells appeared as bright green, while non-apoptotic cells did not show any signal.

Western Blot

Total proteins were extracted in RIPA buffer (Sigma-Aldrich) that was supplemented with protease inhibitor cocktail (100× Sigma-Aldrich). The protein concentration was measured by BCA kit (Thermo Scientific™ Pierce™ BCA Protein Assay Kit, Waltham, MA, United States). The samples were diluted in RIPA, mixed with Laemmli buffer (Bio-Rad, Hercules, CA), and then denatured at 95°C for 5 min. Proteins were fractionated electrophoretically on NuPAGETM 4–12% Bis-Tris Polyacrylamide Gel (Invitrogen) and then transferred to a polyvinylidene fluoride (PVDF) membrane using the iBlot Dry Blotting System (Invitrogen). The membrane was blocked with 3% non-fat milk (BioRad, Hercules, CA, United States) at room temperature for 1.5 h, washed, and incubated with primary antibodies (**Supplementary Table 3**) at 4°C overnight on a rotating shaker. On the next day, after the membrane was washed with TBST for five times, HRP-conjugated secondary antibody (Thermo Scientific) was applied for 1.5 h at room temperature. Finally, the membrane was incubated in SuperSignal West Dura Extended Duration Substrate (Thermo Fisher Scientific Pierce Protein Biology) and imaged with ChemiDocTMTouch Imaging system (BioRad).

Three-Dimensional Pellet Culture of Chondrocytes

For the 3D pellet culture of chondrocytes, 2.5×10^5 cells were used to form one pellet. Cells were seeded in 96-well MicroWell round-bottom plates (Thermo Fisher Scientific). And then the plate was centrifuged at 300 g for 10 min to condense chondrocytes. The medium used to maintain the pellet was full chondrogenic medium (CM) consisted of DMEM (Gibco), 2× anti-anti (Gibco), 10 μg/ml ITS (Thermo Fisher Scientific), 0.1 μM Dexamethasone (Sigma-Aldrich, St. Louis, MO, United States), 40 μg/ml Proline (Sigma-Aldrich), 50 μg/ml ascorbic acid (Sigma-Aldrich) and 10 ng/ml TGF-β1 (Peprotech, Rocky Hill, NJ, United States). Each pellet was cultured in 200 μl full CM and incubated at 37°C with 5% CO_2. CM was replaced every 48 h. After 14 days of culture, pellets were harvested for histological analysis.

Safranin O Staining

Pellets were fixed overnight at 4°C in 10% buffered formalin (Fisher Chemical, Hampton, NH, United States), dehydrated in gradient ethanol, cleared in xylene, and then embedded in paraffin. The blocks were sectioned at 6 μm thickness using a Leica microtome (Model RM 2255). For Safranin O/Fast Green staining, slides were stained with hematoxylin (Mayer, Sigma) for 5 min, 0.005% Fast Green (Thermo Fisher Scientific, Pittsburgh, PA, United States) for 1 min, rinsed with 1% acetic acid, and stained with 0.1% Safranin O (Millipore, Billerica, MA, United States) for 20 min. Histological staining was imaged using a microscope equipped with a color digital camera (Nikon Eclipse E800).

Statistical Analysis

Each experiment was repeated three or more times with three experimental replicates, and the results were expressed as the mean ± SD. Graphpad Prism 8 (GraphPad Software, San Diego, CA, United States) was applied for statistical analysis. Significant differences among different groups were determined by two-tailed Student's *t*-test for two-group comparisons. One-way or two-way analysis of variance (ANOVA) was used for multiple-group comparisons. Statistical significance was considered at $p < 0.05$.

RESULTS

Extensive *in vitro* Chondrocyte Expansion Results in the Generation of Senescence Cells

We first characterized cells in the early passage (PDL3, 0.1 million cells were expanded to ∼0.8 million cells) and late passage (PDL9, 0.1 million cells were expanded to ∼50 million cells), which, respectively, represented the minimally expanded chondrocytes and chondrocytes ready for ACI. As shown in **Figures 1A,B**, there were more SA-β-gal staining-positive chondrocytes in PDL9 group (>40%) than PDL3 group (<17%). It should be noted that the staining intensity was also higher in the PDL9 group.

Level of senescence was further examined by testing the proliferative ability and expression of SASP genes. Initially, PDL3 and PDL9 cells were seeded at the same density. After 2, 4, and 6 days of culture, the cell number in the PDL9 group was significantly lower than that in the PDL3 group (**Figure 1C**), which indicated that the proliferative ability of senescent chondrocytes was significantly decreased. qRT-PCR analysis revealed the marked upregulation of *CDKN2A (encoding p16)*, *CDKN1A (encoding p21)*, interleukin-8 (*IL-8)*, and matrix metalloproteinase (*MMP)-12* expression (**Figure 1D**). Taken together, PDL9 chondrocytes contained significantly more senescent cells than PDL3 chondrocytes, confirming that extensive *in vitro* expansion led to chondrocyte senescence.

FOXO4-DRI Treatment Removes Cells in PDL9 Chondrocyte Culture

We next test the efficacy of the previously reported senolytics, including ABT263 and FOXO4-DRI, in removing senescent chondrocytes. As shown in **Supplementary Figure 1**, we did not observe a significant difference in the cell number between the control and ABT263 treatment group. In contrast, FOXO4-DRI treatment significantly reduced the cell number in the PDL9 group (**Supplementary Figures 1, 2**). Interestingly, FOXO4-DRI did not affect cell viability in PDL3 group (**Supplementary Figures 1, 2**). Results from **Figure 2A** confirmed that FOXO4-DRI killed the cells through inducing apoptosis.

FOXO4-DRI Treatment Significantly Reduces the Senescence Level in PDL9 Cells

SA-β-gal staining (**Figure 2B**) indicated that FOXO4-DRI treatment led to a significant decrease in the number of senescent cells in the PDL9 group (<5%). qRT-PCR analysis (**Figure 2E**) showed that FOXO4-DRI-treated PDL9 cells displayed enhanced *SOX9* expression, and reduced *MMP12* and *MMP13* expression, which however were at the expense of lower expression levels

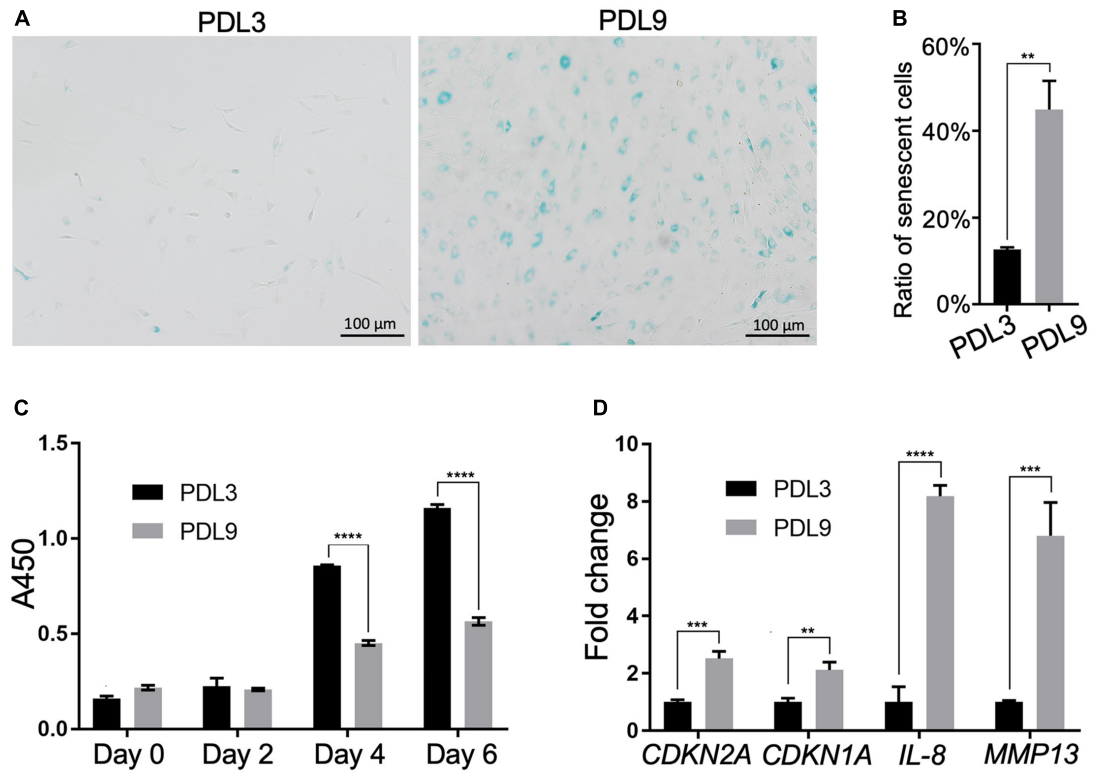

FIGURE 1 | Comparison of senescent level between PDL3 and PDL9 chondrocytes. **(A)** SA-β-gal staining. Bar = 200 μm. (**B**) Ratios of senescent cells. **(C)** CCK-8 assay was used to assess cell proliferation potential. **(D)** Expression levels of senescence-relevant genes. The data was normalized to that in PDL3 group (set as 1). $^{**}p < 0.01$; $^{***}p < 0.001$; $^{****}p < 0.0001$.

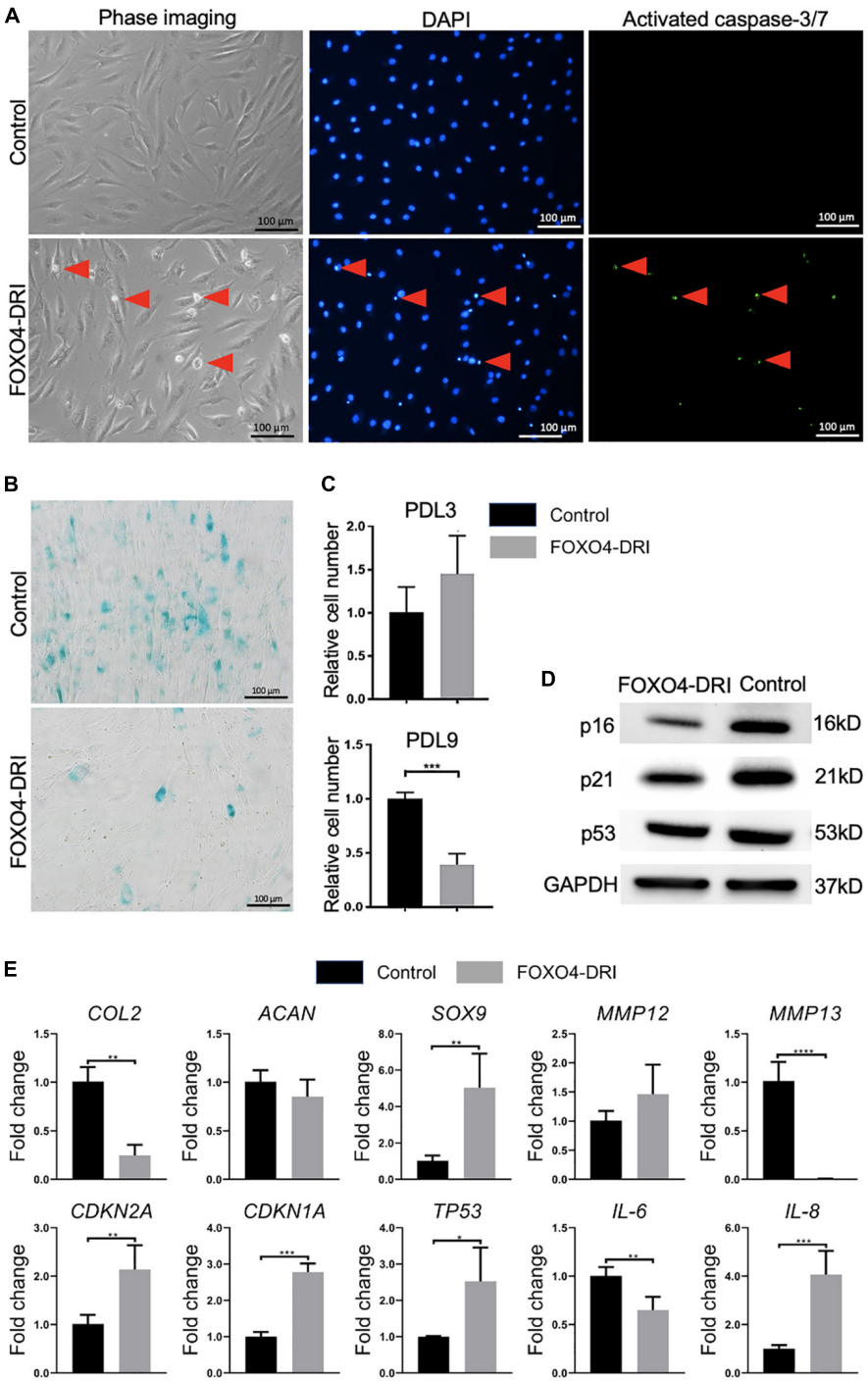

FIGURE 2 | Assessment of senescence level in PDL9 cells after FOXO4-DRI treatment. The samples with (FOXO4-DRI) or without (Control) FOXO4-DRI treatment were analyzed. **(A)** Detection of activated caspase-3/7. Red arrows indicate apoptotic cells. Bar = 100 μm. **(B)** SA-β-gal staining. Bar = 100 μm. **(C)** The relative cell number in PDL3 and PDL9 chondrocytes after FOXO4-DRI treatment was assessed using MTS assay. **(D)** Western blot. **(E)** Expression levels of selective genes. The data was normalized to that in Control group (set as 1). $^{*}p < 0.05$; $^{**}p < 0.01$; $^{***}p < 0.001$; $^{****}p < 0.0001$.

of *COL2*. We also observed a reduction in *IL-6* expression and an increase in *IL-8* expression after FOXO4-DRI treatment. Furthermore, western blot was used to analyze the protein levels of representative senescent markers, including p16, p21, and p53. A significant decrease of these marker proteins was observed in FOXO4-DRI treated group compared with the control group (**Figure 2D**). However, the gene expression levels of these molecules displayed an opposite trend (**Figure 2E**).

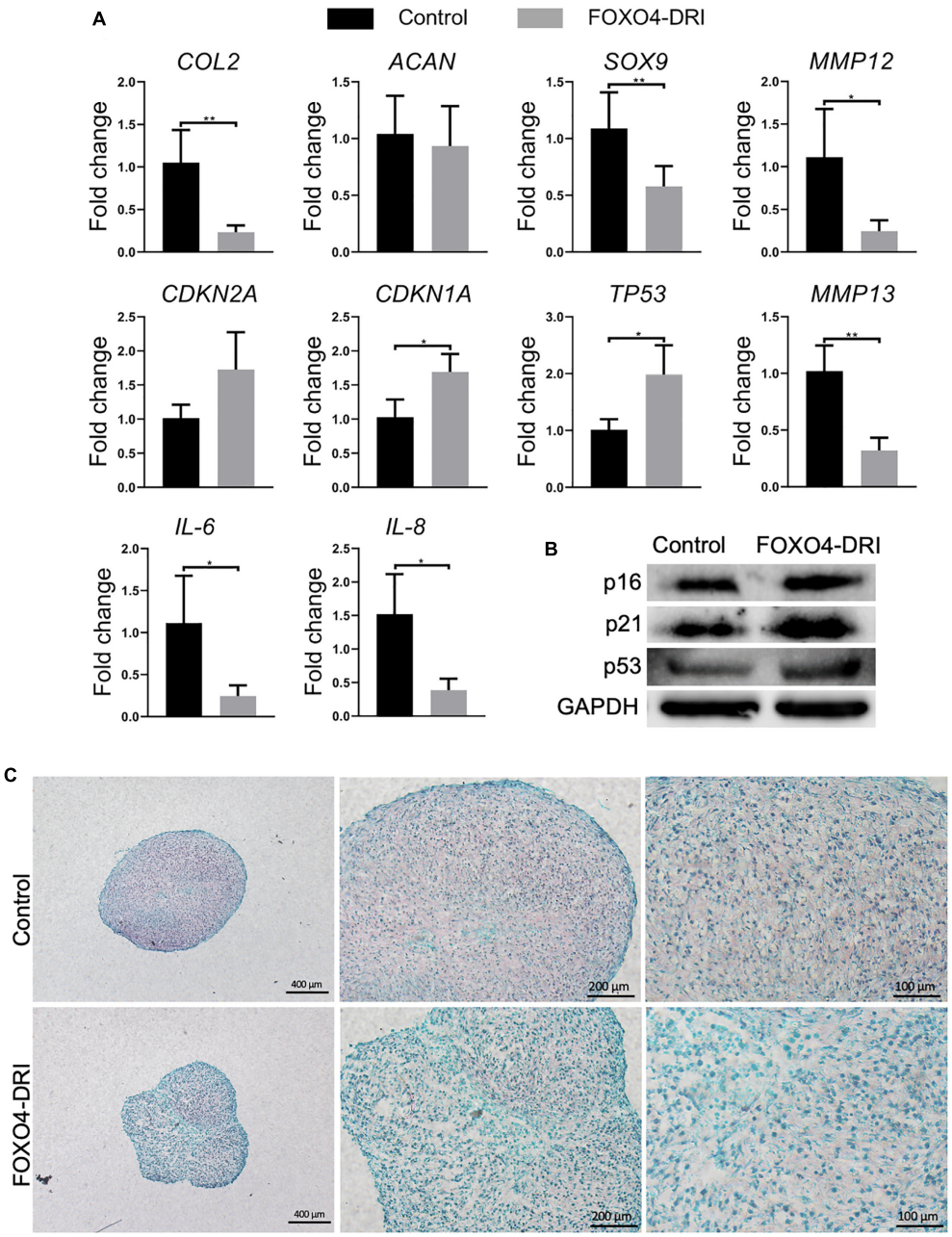

FIGURE 3 | Assessment of senescence level and chondrogenesis in engineered cartilage. PDL9 were pretreated with (FOXO4-DRI) or without (Control) FOXO4-DRI for 5 days and then subjected to 14 days of chondrogenic cultures. **(A)** Expression levels of selective genes. The data was normalized to that in the Control group (set as 1). **(B)** Western blot. **(C)** Safranin O/Fast green staining. Bar = 400, 200, and 100 μm from the left to right. *$p < 0.05$; **$p < 0.01$.

Taken together, FOXO4-DRI is capable of selectively removing senescence cells in PDL9 chondrocytes.

FOXO4-DRI Treatment Does Not Markedly Improve the Regenerative Potential of PDL9 Chondrocytes

The regenerative potential of PDL9 chondrocytes after FOXO4-DRI treatment was assessed by 3D pellet culture. As shown in **Figure 3A**, reduced expression levels of *IL-6 and 8* and *MMP3, 12 and 13* were observed in the FOXO4-DRI treated group, which however were concomitantly accompanied with reduced expression of *SOX9* and *COL2*, as well as increased expression of *CDKN2A*, *CDKN1A*, and *TP53 (encoding p53)*. Western blot analysis further showed that cartilage generated from FOXO4-DRI pre-treated chondrocytes displayed higher protein levels of p16, p21, and p53 (**Figure 3B**). In addition, we did not observe increased deposition of

GAG from FOXO4-DRI pre-treated PDL9 chondrocytes (**Figure 3C**).

DISCUSSION

ACI has been shown to regenerate new tissues, reduce pain, and increase joint function after cartilage injury. However, the clinical outcomes from ACI are not always efficacious or consistent. Given that implanted chondrocytes are major cells that account for creating new tissues, their quality may directly affect the phenotype and function of regenerated cartilage. Surprisingly, no established criteria were available to comprehensively characterize the expanded chondrocytes before they are implanted. In this study, we aimed to analyze senescence during chondrocyte expansion and use senolytics to remove senescent chondrocytes for the enhancement of cartilage formation in ACI.

The loss of the chondrocytic phenotype and proliferative potential during *in vitro* expansion, termed as "dedifferentiation," has been well documented. Chondrocyte dedifferentiation was majorly characterized as the reduced expression of COL2 and ACAN and enhanced expression of type I collagen and versican (Charlier et al., 2019). However, the association between reduced chondrocyte quality during expansion and ACI outcome is less studied. Pietschmann et al. (2009) sampled the newly formed cartilage after ACI and suggested that the number of morphologically abnormal cells was correlated with a poor clinical outcome. Niemeyer et al. (2012) moved one step forward by saving some cells from ACI and studying the correlation between chondrocyte phenotype before implantation, and clinical outcome after 6, 12, and 24 months. Results from this study indicated that the postoperative International Knee Documentation Committee (IKDC) score was significantly influenced by *COL2* expression, but not *ACAN* (Niemeyer et al., 2012). Recently, a cell identity assay was employed to assess the contamination of human chondrocytes by human synovial fibroblasts. The results showed a higher cell identity score, meaning less fibroblast contamination, and was significantly correlated with structural repair quality and graft survival after ACI (Ackermann et al., 2019). These results collectively signified the importance of enhancing chondrocyte quality for the improvement of final clinical outcomes.

In addition to dedifferentiation, another consequence of *in vitro* expansion is replicative senescence, which also significantly influences chondrocyte function. The observation of senescent cells in *in vitro* expanded chondrocytes have been reported as early as 2002. In this study, articular chondrocytes were expanded to a number that was needed for ACI. These chondrocytes displayed a telomere erosion in the range of 900 bp, which was comparable with 30 years of native aging (Parsch et al., 2002). In our study, significantly more SA-β-gal staining-positive cells were observed in PDL9 chondrocytes. Similar results were reported in a recent study (Ashraf et al., 2016). Interestingly, passage 2 and 6 chondrocytes were used, which were roughly equivalent to the PDL3 and PDL9 cells used in our current study. Our results also indicate that senescent chondrocytes present a larger and flatter cell shape, which is consistent with a previous study (Cha et al., 2013).

The detrimental influence of senescence has been previously demonstrated. They negatively influence neighbor cells by secreting SASP (Borodkina et al., 2018). In fact, it has been shown that the translation of senescence chondrocytes in mice knee joint resulted in OA phenotype, characterized by leg pain, impaired mobility, and radiographic and histological changes (Xu et al., 2017). These studies signify the importance of removing the senescence cells in enhancing reparative outcomes from ACI.

In our study, ABT 263 (or UBX0101) was first tested because of its reported capacity in clearing senescent cells. For example, chondrocytes isolated from OA cartilage displayed significant senescence levels, and ABT263 treatment reduced the expression of inflammatory cytokines and promoted cartilage matrix aggregation in OA chondrocytes (Yang et al., 2020). Similar results were found in the radiation-induced senescent chondrocytes (Jeon et al., 2017). It should be noted that expression of p16 actually increased after 3 days of ABT 263 treatment, indicating the potential stress of senolytics on cells. Moreover, although the expression of p21 decreased after treatment, the protein level was higher in cells treated with ABT 263 than the untreated control. Regarding the chondrogenic potential, results from both studies confirmed that the removal of senescent cells significantly increased the cartilage formation with less production of degrative enzymes. However, similar senolytic potential of ABT 263 was not seen in our study. Of note, the senescence chondrocytes tested here were induced by replication stress. In previous studies, senescence chondrocytes were either from OA cartilage, or induced by other methods.

Next, we tested the potential of FOXO4-DRI in removing senescent chondrocytes, which has not been reported before. Mechanistically, the peptide perturbs the FOXO4 interaction with p53, which selectively causes p53 nuclear exclusion and cell-intrinsic apoptosis (Baar et al., 2017). As demonstrated in **Figure 2**, this novel senolytic did remove cells from the PDL9 chondrocytes, which was accompanied by significantly reduced levels of SA-β-gal staining. Surprisingly, there was not a noticeable cell loss in the culture of non-senescent PDL3 chondrocytes, suggesting the selective potential of FOXO4-DRI. Since it is suggested that p53, p16, p21 are directly related to the induction of senescence in chondrocytes (Ashraf et al., 2016), we thus used qRT-PCR and western blot analysis to examine their expression levels. We observe the reduction of both protein and RNA levels of all these three molecules. We also analyzed the expression of *IL-6* and *-8*, which however were not detectable due to the low expression level. Again, in the first study using FOXO4-DRI to induce apoptosis in senescent cells, the senescent cells were generated by irradiation or doxorubicin (Baar et al., 2017). In a recent study, FOXO4-DRI decreased levels of p53, p21, and p16 in the testes of aged mice, when compared to young mice (Zhang et al., 2020). Therefore, our study and published work collectively showed that FOXO4-DRI was able to remove senescent cells created by different methods.

As shown in **Figure 3**, FOXO4-DRI pre-treatment neither resulted in more cartilage formation nor reduced p16 level in the cartilage derived from the PDL9 cells. The possible reason

is the dedifferentiation of chondrocytes during the *in vitro* expansion. Although not all cells in PDL9 were senescent cells, the intrinsic chondrogenic potential has been impaired during the dedifferentiation process. In previous studies that compared the differentiation capacity of chondrocytes from different passages, the results indicated that cells at early passages usually generated more cartilage matrix than those at late passages upon chondroinduction (Schulze-Tanzil et al., 2002; Ma et al., 2013). Therefore, the treatment with senolytics may not be able to reverse the loss of chondrogenic potential in PDL9. However, the new cartilage created by FOXO4-DRI pretreated PDL9 cells indeed displayed reduced expression of several SASP factors, implying the benefit of FOXO4-DRI pre-treatment in enhancing the cartilage quality. Surprisingly, increased p21 level was observed in the FOXO4-DRI pre-treatment groups, suggesting senolytics might be a potential stressor to cells. Similar results were reported in a previous study, which used another type of senolytic, ABT263, to treat chondrocytes isolated from osteoarthritic cartilage (Yang et al., 2020). Therefore, the potential adverse influence of senolytics needs to be further investigated.

There are several limitations in the current study. First, we only examined limited senolytics. Also, we used the doses that were reported in a previous study, which may not be optimal for treating PDL9 chondrocytes. In the future, we will test more senolytics with different doses. Recently, oleuropein, a polyphenol, was shown to have the senolytic potential in OA chondrocytes (Varela-Eirín et al., 2020). Whether it is able to selectively remove senescent chondrocytes created by the *in vitro* expansion requires additional study. Second, the mechanistic analysis was not performed to explain why removing senescent cells did not result in more cartilage formation. Third, the combination of senolytics with other methods for reducing senescence was not examined. Recently, extracellular matrix derived from mesenchymal stem cells were shown to maintain re-differentiation potential of human chondrocytes (Pei and He, 2012; Yang et al., 2018). Also, the low-oxygen environment has been found to suppress senescence (Moussavi-Harami et al., 2004). These methods can be adapted to the current study to increase the potential of senolytics in enhancing ACI. Lastly, the strategy to augment the chondrogenic potential of senolytics-treated chondrocytes needs to be explored. For example, conventional chondrogenic factors (Jonitz et al., 2012), epigenetic manipulation with specific agents (Duan et al., 2017), or co-culture with mesenchymal stem cells (Lai et al., 2013), have been shown to promote or maintain chondrocytic phenotype. These methods can be used either during or after the senolytic treatment.

CONCLUSION

In vitro expanding human chondrocytes to a number that is required by the ACI results in the generation of senescent cells. Although FOXO4-DRI treatment did remove the senescent cells, the cartilage formation capacity of retained chondrocytes was not improved. Of note, cartilage created by FOXO4-DRI pretreated chondrocytes displays a lower senescence level than that from the untreated counterparts. Our results indicate the utility of FOXO4-DRI for removing senescent chondrocytes. In the future, other methods are needed to restore the chondrogenic potential of retained chondrocytes after FOXO4-DRI treatment.

DATA AVAILABILITY STATEMENT

The original contributions presented in the study are included in the article/**Supplementary Material**, further inquiries can be directed to the corresponding author/s.

AUTHOR CONTRIBUTIONS

HL conceived the study. YZH and YH designed and carried out all the experiments. YZH, YH, and HL analyzed the results. YZH, MM, and HL wrote the first draft. All authors reviewed and edited the manuscript.

FUNDING

This work was supported by the Department of Orthopaedic Surgery, University of Pittsburgh School of Medicine (to HL) and the Albert B. Ferguson, Orthopaedic Fund of the Pittsburgh Foundation.

ACKNOWLEDGMENTS

We thank Madalyn Fritch for the help in histology staining.

SUPPLEMENTARY MATERIAL

The Supplementary Material for this article can be found online at: https://www.frontiersin.org/articles/10.3389/fbioe.2021.677576/full#supplementary-material

REFERENCES

Ackermann, J., Merkely, G., Mestriner, A. B., Shah, N., and Gomoll, A. H. (2019). Increased chondrocytic gene expression is associated with improved repair tissue quality and graft survival in patients after autologous chondrocyte implantation. *Am. J. Sports Med.* 47, 2919–2926. doi: 10.1177/0363546519868213

Andriolo, L., Merli, G., Filardo, G., Marcacci, M., and Kon, E. (2017). Failure of autologous chondrocyte implantation. *Sports Med. Arthroscopy Rev.* 25, 10–18. doi: 10.1097/jsa.0000000000000137

Ashraf, S., Cha, B. H., Kim, J. S., Ahn, J., Han, I., Park, H., et al. (2016). Regulation of senescence associated signaling mechanisms in chondrocytes for cartilage tissue regeneration. *Osteoarthritis Cartil.* 24, 196–205. doi: 10.1016/j.joca.2015.07.008

Baar, M. P., Brandt, R. M. C., Putavet, D. A., Klein, J. D. D., Derks, K. W. J., Bourgeois, B. R. M., et al. (2017). Targeted apoptosis of senescent cells restores tissue homeostasis in response to chemotoxicity and aging. *Cell* 169, 132–147. doi: 10.1016/j.cell.2017.02.031

Borodkina, A. V., Deryabin, P. I., Giukova, A. A., and Nikolsky, N. N. (2018). "Social Life" of senescent cells: what Is SASP and why study it? *Acta Nat.* 10, 4–14. doi: 10.32607/20758251-2018-10-1-4-14

Cha, B. H., Lee, J. S., Kim, S. W., Cha, H. J., and Lee, S. H. (2013). The modulation of the oxidative stress response in chondrocytes by Wip1 and its effect on senescence and dedifferentiation during in vitro expansion. *Biomaterials* 34, 2380–2388. doi: 10.1016/j.biomaterials.2012.12.009

Charlier, E., Deroyer, C., Ciregia, F., Malaise, O., Neuville, S., Plener, Z., et al. (2019). Chondrocyte dedifferentiation and osteoarthritis (OA). *Biochem. Pharm.* 165, 49–65. doi: 10.1016/j.bcp.2019.02.036

Davies, R. L., and Kuiper, N. J. (2019). Regenerative medicine: a review of the evolution of autologous chondrocyte implantation (ACI) therapy. *Bioengineering* 6, 22–38. doi: 10.3390/bioengineering6010022

Di Micco, R., Krizhanovsky, V., Baker, D., D'adda, and Di Fagagna, F. (2021). Cellular senescence in ageing: from mechanisms to therapeutic opportunities. *Nat. Rev. Mole. Cell Biol.* 22, 75–95. doi: 10.1038/s41580-020-00314-w

Duan, L., Liang, Y., Ma, B., Wang, D., Liu, W., Huang, J., et al. (2017). DNA methylation profiling in chondrocyte dedifferentiation in vitro. *J. Cell. Physiol.* 232, 1708–1716. doi: 10.1002/jcp.25486

Huang, B. J., Hu, J. C., and Athanasiou, K. A. (2016). Cell-based tissue engineering strategies used in the clinical repair of articular cartilage. *Biomaterials* 98, 1–22. doi: 10.1016/j.biomaterials.2016.04.018

Jeon, O. H., David, N., Campisi, J., and Elisseeff, J. H. (2018). Senescent cells and osteoarthritis: a painful connection. *J. Clin. Invest.* 128, 1229–1237. doi: 10.1172/jci95147

Jeon, O. H., Kim, C., Laberge, R. M., Demaria, M., Rathod, S., Vasserot, A. P., et al. (2017). Local clearance of senescent cells attenuates the development of post-traumatic osteoarthritis and creates a pro-regenerative environment. *Nat. Med.* 23, 775–781. doi: 10.1038/nm.4324

Jonitz, A., Lochner, K., Tischer, T., Hansmann, D., and Bader, R. (2012). TGF-β1 and IGF-1 influence the re-differentiation capacity of human chondrocytes in 3D pellet cultures in relation to different oxygen concentrations. *Int. J. Mole. Med.* 30, 666–672. doi: 10.3892/ijmm.2012.1042

Jungmann, P. M., Gersing, A. S., Baumann, F., Holwein, C., Braun, S., Neumann, J., et al. (2019). Cartilage repair surgery prevents progression of knee degeneration. *Knee Surg. Sports Traumatol. Arthros.* 27, 3001–3013. doi: 10.1007/s00167-018-5321-8

Kreuz, P. C., Kalkreuth, R. H., Niemeyer, P., Uhl, M., and Erggelet, C. (2019). Long-term clinical and MRI results of matrix-assisted autologous chondrocyte implantation for articular cartilage defects of the knee. *Cartilage* 10, 305–313. doi: 10.1177/1947603518756463

Lai, J. H., Kajiyama, G., Smith, R. L., Maloney, W., and Yang, F. (2013). Stem cells catalyze cartilage formation by neonatal articular chondrocytes in 3D biomimetic hydrogels. *Sci. Reports* 3:3553.

Li, J., and Pei, M. (2012). Cell senescence: a challenge in cartilage engineering and regeneration. *Tissue Eng. B Rev.* 18, 270–287. doi: 10.1089/ten.teb.2011.0583

Ma, B., Leijten, J. C., Wu, L., Kip, M., Van Blitterswijk, C. A., Post, J. N., et al. (2013). Gene expression profiling of dedifferentiated human articular chondrocytes in monolayer culture. *Osteoarthr. Cartil.* 21, 599–603. doi: 10.1016/j.joca.2013.01.014

Moussavi-Harami, F., Duwayri, Y., Martin, J. A., Moussavi-Harami, F., and Buckwalter, J. A. (2004). Oxygen effects on senescence in chondrocytes and mesenchymal stem cells: consequences for tissue engineering. *Iowa Orthopaedic J.* 24, 15–20.

Niemeyer, P., Pestka, J. M., Salzmann, G. M., Südkamp, N. P., and Schmal, H. (2012). Influence of cell quality on clinical outcome after autologous chondrocyte implantation. *Am. J. Sports Med.* 40, 556–561. doi: 10.1177/0363546511428879

Parsch, D., Brümmendorf, T. H., Richter, W., and Fellenberg, J. (2002). Replicative aging of human articular chondrocytes during ex vivo expansion. *Arthritis Rheum.* 46, 2911–2916. doi: 10.1002/art.10626

Pei, M., and He, F. (2012). Extracellular matrix deposited by synovium-derived stem cells delays replicative senescent chondrocyte dedifferentiation and enhances redifferentiation. *J. Cell. Physiol.* 227, 2163–2174. doi: 10.1002/jcp.22950

Pham, P. V., Nguyen, S. T., Phan, N. L.-C., Do, N. M., and Vo, P. H. (2020). Adipose-derived stem cells can replace fibroblasts as cell control for anti-tumor screening assay. *OncoTargets Ther.* 13, 6417–6423. doi: 10.2147/ott.s259114

Pietschmann, M. F., Horng, A., Niethammer, T., Pagenstert, I., Sievers, B., Jansson, V., et al. (2009). Cell quality affects clinical outcome after MACI procedure for cartilage injury of the knee. *Knee Surg. Sports Traumatol. Arthroscopy* 17, 1305–1311. doi: 10.1007/s00167-009-0828-7

Sassi, N., Laadhar, L., Allouche, M., Zandieh-Doulabi, B., Hamdoun, M., Klein-Nulend, J., et al. (2014). Wnt signaling is involved in human articular chondrocyte de-differentiation in vitro. *Biotechnic Histochem.* 89, 29–40. doi: 10.3109/10520295.2013.811285

Schulze-Tanzil, G., De Souza, P., Villegas Castrejon, H., John, T., Merker, H. J., Scheid, A., et al. (2002). Redifferentiation of dedifferentiated human chondrocytes in high-density cultures. *Cell Tissue Res.* 308, 371–379. doi: 10.1007/s00441-002-0562-7

Varela-Eirín, M., Carpintero-Fernández, P., Sánchez-Temprano, A., Varela-Vázquez, A., Paíno, C. L., Casado-Díaz, A., et al. (2020). Senolytic activity of small molecular polyphenols from olive restores chondrocyte redifferentiation and promotes a pro-regenerative environment in osteoarthritis. *Aging* 12, 15882–15905. doi: 10.18632/aging.103801

Xu, M., Bradley, E. W., Weivoda, M. M., Hwang, S. M., Pirtskhalava, T., Decklever, T., et al. (2017). Transplanted senescent cells induce an osteoarthritis-like condition in mice. *J. Gerontol. A Biol. Sci. Med. Sci.* 72, 780–785.

Yang, H., Chen, C., Chen, H., Duan, X., Li, J., Zhou, Y., et al. (2020). Navitoclax (ABT263) reduces inflammation and promotes chondrogenic phenotype by clearing senescent osteoarthritic chondrocytes in osteoarthritis. *Aging* 12, 12750–12770. doi: 10.18632/aging.103177

Yang, Y., Lin, H., Shen, H., Wang, B., Lei, G., and Tuan, R. S. (2018). Mesenchymal stem cell-derived extracellular matrix enhances chondrogenic phenotype of and cartilage formation by encapsulated chondrocytes in vitro and in vivo. *Acta Biomater.* 69, 71–82. doi: 10.1016/j.actbio.2017.12.043

Zhang, C., Xie, Y., Chen, H., Lv, L., Yao, J., Zhang, M., et al. (2020). FOXO4-DRI alleviates age-related testosterone secretion insufficiency by targeting senescent Leydig cells in aged mice. *Aging* 12, 1272–1284. doi: 10.18632/aging.102682

Conflict of Interest: The authors declare that the research was conducted in the absence of any commercial or financial relationships that could be construed as a potential conflict of interest.

frontiers in Bioengineering and Biotechnology

ORIGINAL RESEARCH
published: 02 June 2021
doi: 10.3389/fbioe.2021.667161

Immune-Inflammatory Responses of an Acellular Cartilage Matrix Biomimetic Scaffold in a Xenotransplantation Goat Model for Cartilage Tissue Engineering

Litao Jia[1,2†], Peiling Zhang[3,4†], Zheng Ci[1,4], Wei Zhang[1,3], Yu Liu[1,4], Haiyue Jiang[2] and Guangdong Zhou[1,3,4]**

[1] Research Institute of Plastic Surgery, Weifang Medical University, Weifang, China, [2] Research Center of Plastic Surgery Hospital, Chinese Academy of Medical Sciences and Peking Union Medical College, Beijing, China, [3] Department of Plastic and Reconstructive Surgery, Shanghai Key Laboratory of Tissue Engineering, Shanghai Ninth People's Hospital, Shanghai Jiao Tong University School of Medicine, Shanghai, China, [4] National Tissue Engineering Center of China, Shanghai, China

The rapid development of tissue engineering and regenerative medicine has introduced a new strategy for ear reconstruction, successfully regenerating human-ear-shaped cartilage and achieving the first clinical breakthrough using a polyglycolic acid/polylactic acid (PGA/PLA) scaffold. However, its clinical repair varies greatly among individuals, and the quality of regenerated cartilage is unstable, which seriously limits further clinical application. Acellular cartilage matrix (ACM), with a cartilage-specific microenvironment, good biocompatibility, and potential to promote cell proliferation, has been used to regenerate homogeneous ear-shaped cartilage in immunocompromised nude mice. However, there is no evidence on whether ACM will regenerate homogeneous cartilage tissue in large animals or has the potential for clinical transformation. In this study, xenogeneic ACM assisted with gelatin (GT) with or without autologous chondrocytes was implanted subcutaneously into goats to establish a xenotransplantation model and compared with a PGA/PLA scaffold to evaluate the immune-inflammatory response and quality of regenerated cartilage. The results confirmed the superiority of the ACM/GT, which has the potential capacity to promote cell proliferation and cartilage formation. Although there is a slight immune-inflammatory response in large animals, it does not affect the quality of the regenerated cartilage and forms homogeneous and mature cartilage. The current study provides detailed insights into the immune-inflammatory response of the xenogeneic ACM/GT and also provides scientific evidence for future clinical application of ACM/GT in cartilage tissue engineering.

Keywords: immune-inflammatory responses, acellular cartilage matrix, biomimetic scaffold, xenotransplantation model, cartilage tissue engineering

OPEN ACCESS

Edited by:
Zhen Li,
AO Research Institute Davos, Switzerland

Reviewed by:
Karoliina Pelttari, University Hospital of Basel, Switzerland
Yasuhiko Tabata, Kyoto University, Japan

****Correspondence:***
Guangdong Zhou
guangdongzhou@126.com
Haiyue Jiang
jianghaiyue@psh.pumc.edu.cn

† These authors have contributed equally to this work and share first authorship

Specialty section:
This article was submitted to Tissue Engineering and Regenerative Medicine, a section of the journal Frontiers in Bioengineering and Biotechnology

Received: *12 February 2021*
Accepted: *11 May 2021*
Published: *02 June 2021*

Citation:
Jia L, Zhang P, Ci Z, Zhang W, Liu Y, Jiang H and Zhou G (2021) Immune-Inflammatory Responses of an Acellular Cartilage Matrix Biomimetic Scaffold in a Xenotransplantation Goat Model for Cartilage Tissue Engineering. Front. Bioeng. Biotechnol. 9:667161. doi: 10.3389/fbioe.2021.667161

INTRODUCTION

Auricular cartilage defects, including congenital auricle malformation–microtia and acquired auricular cartilage injuries caused by various causes are very common, and the most clinical effective treatment is reconstruction using autologous costal cartilage engraving, which can cause serious complications such as surgical trauma and pneumothorax (Brent, 2002; Zhang et al., 2009; Luquetti et al., 2011, 2012; Bly et al., 2016). Fortunately, the rapid development of tissue engineering and regenerative medicine technologies has introduced a new strategy for ear reconstruction, successfully regenerating human-ear-shaped cartilage and achieving the first clinical breakthrough based on a polyglycolic acid/polylactic acid (PGA/PLA) scaffold (Cao et al., 1997; Haisch, 2010; Zhou et al., 2018; Yin et al., 2020). However, the degradation of implanted polymer scaffolds can cause aseptic inflammation and lead to unstable cartilage regeneration, which seriously limits its further clinical application (Ceonzo et al., 2006; Luo et al., 2013; Liu et al., 2016). Therefore, an appropriate scaffold with good biocompatibility and low immunogenicity is required for cartilage regeneration. Recent studies have found that acellular cartilage matrix (ACM) has a cartilage-specific microenvironment, good biocompatibility, and the potential to promote cell proliferation (Xue et al., 2012; Li Y. et al., 2019; Wiggenhauser et al., 2019; Jian et al., 2021). Combined with 3D printing, cast molding, gelatin (GT) assisted crosslinking, and freeze-drying techniques, a human-ear-shaped scaffold based on ACM has been successfully prepared and used to regenerate homogeneous ear-shaped cartilage in immunocompromised nude mice (Jia et al., 2020). Nevertheless, it is still unproven whether ACM/GT scaffolds will trigger immune-inflammatory responses like PGA/PLA scaffolds and whether ACM/GT scaffolds will regenerate homogeneous cartilage tissue in the subcutaneous environment of large animal models.

To address the issues mentioned above, it is necessary to systematically compare the post-implantation reaction and cartilage regeneration of ACM/GT scaffolds and PGA/PLA scaffolds (which were previously applied clinical) in large animals with sound immune function to predict the possible advantages of ACM/GT scaffolds in reducing immune-inflammatory response and enhancing the quality of regenerated cartilage in future clinical translation. Therefore, the main purpose of this current study is to verify whether ACM/GT scaffold can induce serious immune-inflammatory responses in large animals with sound immune function and whether mature homogeneous cartilage can be successfully regenerated in the subcutaneous environment.

To effectively verify the immune-inflammatory response of xenogeneic ACM in large animals with sound immune function, ACM derived from cow scapular cartilage assisted with gelatin was implanted subcutaneously in goats to establish the xenotransplantation model used in this study. A PGA/PLA scaffold was also implanted subcutaneously to compare immune-inflammatory responses. Two groups of scaffold constructs inoculated with autologous auricular chondrocytes were also implanted subcutaneously in goats to explore the quality of cartilage regeneration and long-term stability *in vivo*. The current study provides detailed insights into the immune-inflammatory responses and cartilage regeneration stability of ACM/GT in the xenotransplantation model and scientific evidence for future clinical application in cartilage tissue engineering.

MATERIALS AND METHODS

Preparation of the Scaffolds

Cartilage pieces obtained from cow scapular cartilage were processed into ACM powder after freeze–grinding and decellularization procedures. The ACM scaffold, using gelatin extracted from bovine Achilles tendon (Gel strength approximately 240 g Bloom, Aladdin) as an auxiliary crosslinker, and PGA/PLA scaffold were fabricated according to our previously reported protocols (Liu et al., 2010; Jia et al., 2020). Briefly, the ACM particles were filtered by 100-mesh (150 ± 10 μm) filtration screens to obtain uniform particles. A certain concentration of gelatin solution (dissolved in deionized water) was first placed at 4°C as a gel for an hour to reduce ACM particles deposition as much as possible before fully mix. Then the suspension was fully frozen at −10°C for 24 h. The specific concentration and proportion of the ACM suspension and GT solution (2% concentrations, ACM: GT = 5:5) optimized in our previous experiment were blended uniformly and freeze-dried to form a porous ACM/GT scaffold. Thirty micrograms of unwoven PGA fibers (National Tissue Engineering Center of China, Shanghai, China) were compressed into cylindrical scaffolds (8 mm in diameter and 2 mm in thickness) and then 1.0% PLA (Sigma, St. Louis, MO, United States) solubilized in dichloromethane was continuously added to form the PGA/PLA scaffold. All scaffolds were sterilized before application using ethylene oxide.

Scanning Electron Microscopy (SEM)

The surface morphology of the two kinds of scaffolds was observed by SEM (Philips XL-30, Amsterdam, Netherlands) at an accelerating voltage of 15 kV. The two kinds of cell–scaffold constructs cultured for 7 days *in vitro* were washed with PBS and fixed overnight in 0.05% glutaraldehyde at 4°C. After dehydration in a graded ethanol series and critical point drying, the surface morphology and extracellular matrix (ECM) production of these constructs were observed by SEM (Chen et al., 2016).

Porosity Analysis of the Scaffolds

The porosity of the ACM/GT scaffold and PGA/PLA scaffold was tested using the ethanol infiltration method as previously described (Serra et al., 2015). Briefly, V1 and V2 were marked as the volume of ethanol in the measuring cylinder before and after the scaffold was immersed in ethanol, respectively. V3 was marked as the remaining ethanol volume after the scaffold was removed from ethanol. The porosity of the scaffold (n = 5 per group) was calculated using the following formula: Porosity = (V1–V3)/(V2–V3) × 100%.

Biocompatibility of the Scaffolds

Cell Seeding Efficiency

Chondrocytes from the auricular tissue of goats were isolated and cultured in a basic medium that Dulbecco's modified Eagle medium (DMEM, Gibco) containing 10% fetal bovine serum (FBS, Gibco) at 37°C with 95% humidity and 5% CO_2 according to the previously established methods (Zhang et al., 2014). Harvested chondrocytes from the second passage were adjusted to a final concentration of 75×10^6 cells/mL, and 200 μL cell suspension was inoculated into each scaffold (n = 5 per group). After 24 h of incubation, the remaining cells were collected, counted, and the cell seeding efficiencies of the two groups were calculated based on the formula: (total cell number-remaining cell number)/total cell number × 100% (Zheng et al., 2014).

Cellular Viability Assessment

After 1, 4, 7, and 14 days of culture in basic medium, the cellular viability of the seeded chondrocytes on the ACM/GT scaffold and PGA/PLA scaffold (n = 5 per group) was evaluated using the Live and Dead Cell Viability Assay (Invitrogen, Carlsbad, CA, United States) following the manufacturer's instructions, and examined by confocal microscope (Nikon, Japan) (Xu et al., 2020a).

Cellular Proliferation Assessment

After 1, 7, and 14 days of culture in basic medium, the cellular proliferation capacity of chondrocytes on the ACM/GT scaffold and PGA/PLA scaffold (n = 5 per group) was assessed by the total DNA quantification assay (PicoGreen dsDNA assay, Invitrogen, Carlsbad, CA, United States) following the manufacturer's protocols (Xia et al., 2018).

In vitro Culture of the Cell–Scaffold Constructs

Chondrocytes were collected and seeded evenly into each scaffold to form cell–scaffold constructs according to a previously described method (Xue et al., 2013). The constructs were incubated for 4 h at 37°C to allow for complete adhesion of the cells to the scaffolds and then cell–constructs were cultured for 2 weeks in the basic medium at 37°C with 95% humidity and 5% CO_2.

Subcutaneous Implantation in Goats

Six 3-month-old goats (4 males and 2 females) were purchased from Shanghai Jiagan Biological Technology Co., Shanghai, China. All protocols with animal use were approved by the Animal Care and Experiment Committee of Shanghai Jiao Tong University School of Medicine (Shanghai, China). Six goats were divided into two groups: in three goats, two kinds of scaffolds without cells (PGA/PLA scaffolds and ACM/GT scaffolds, n = 10 scaffolds per group in each goat) were implanted subcutaneously into both sides of the abdomen of each goat. Five samples per group in each goat were harvested after 1 and 2 weeks of implantation for subsequent analysis, respectively. In the other three goats, two kinds of cell–scaffold constructs (cell-PGA/PLA constructs and cell-ACM/GT constructs, n = 15 constructs per group in each goat) cultured for 2 weeks *in vitro* were implanted subcutaneously into both sides of the abdomen of each donor goat for continue culture *in vivo*. Five samples per group in each goat were harvested after 1, 2, and 8 weeks of implantation for subsequent analysis, respectively. During surgery, each goat was anesthetized and subcutaneous pockets were created in the abdominal area in which the scaffolds and constructs were implanted. After closure of the incisions, the animals were allowed to recover from the anesthesia.

Immune-Inflammatory Response Evaluations

After 1 and 2 weeks of implantation, two kinds of constructs and two kinds of scaffolds (n = 5 samples per group in each goat) were harvested with surrounding tissue for analysis of the immune-inflammatory response. After gross observation, all samples were fixed in 4% paraformaldehyde for 48 h, embedded in paraffin, and sectioned in 5-mm slices according to our previously established methods (Liu et al., 2016). The slices were stained with hematoxylin and eosin (H&E), as well as immunohistochemical techniques as previously reported. CD3 was detected using rabbit anti-CD3 monoclonal antibody (ab16669, 1:200, Abcam, Cambridge, United Kingdom), followed by goat anti-rabbit IgG H&L (HRP) (ab205718, 1:2000, Abcam). CD 68 was detected using mouse anti-CD68 monoclonal antibody (ab955, 1:200, Abcam), followed by goat anti-mouse IgG H&L (HRP) (ab205719, 1:2000, Abcam). The quantification of CD3 and CD68 position area (%) was performed with Image J and IHC Profiler Software (n = 5 per group).

Histological and Immunohistochemical Evaluations of Regenerative Tissues

After 8 weeks of culture *in vivo*, the two kinds of tissue-engineering cartilage tissue (n = 5 samples per group in each goat) were carefully harvested. Part of each sample (the rest of the sample was used for subsequent biochemical and biomechanical analysis) was prepared for histological and immunohistochemical analyses after gross observation and measurement, as described above (Li D. et al., 2019). These slices were stained with H&E, Safranin O, and type II collagen (COL II) to evaluate the histological structure and cartilage ECM deposition of tissue-engineering cartilage tissue. COL II was detected using rabbit anti-collagen II polyclonal antibody (ab34712, 1:100, Abcam), followed by goat anti-rabbit IgG H&L (HRP) (ab205718, 1:2000, Abcam). The quantification of regenerated cartilage area (%) was performed with Image J and IHC Profiler Software (n = 5 per group).

Biochemical and Biomechanical Analysis

Two groups of tissue-engineering cartilage tissue cultured for 8 weeks *in vivo* were collected, weighed with an electronic balance, and the volume of each sample was measured by the water displacement method (n = 5 per group). Biochemical and biomechanical analysis of both regenerated tissues and native auricular cartilage was performed as described previously (Xu et al., 2020b). All samples were collected and

minced to conduct cartilage-related biochemical evaluations (n = 3 per group). Briefly, glycosaminoglycan (GAG), total collagen, and DNA quantifications were quantified by the dimethyl methylene blue assay (DMMB, Sigma-Aldrich, St. Louis, MI, United States), hydroxyproline assay kit (Sigma-Aldrich), and PicoGreen dsDNA assay (Invitrogen, Carlsbad, CA, United States), respectively. The biomechanical analysis was determined using a mechanical testing machine (Instron-5542, Canton, MA, United States). All samples (n = 5 per group) were processed into a cylindrical shape and a constant compressive strain rate of 0.5 mm/min was applied until 80% of the maximal deformation. The Young's modulus of each sample was calculated based on the slope of the stress–strain curve in the range of 0 to 40%.

Statistical Analysis

All quantitative data were collected from at least three replicate tests, and values were expressed as mean ± standard deviation. After confirmation of the normal data distribution, a one-way analysis of the variance was used to determine the statistical significance among groups using GraphPad Prism 8 software, and a value of $p < 0.05$ was considered statistically significant.

RESULTS

Characterization of the Scaffolds

Unwoven PGA fibers coated by PLA were compressed to form a cylindrical scaffold for imaging. Both scaffolds exhibited a porous structure and the SEM examination further confirmed the porous surface (**Figures 1A,B**). The porosity of the ACM/GT scaffold was greater than the PGA/PLA scaffold (**Figure 1E**). Overall, the two scaffolds met the requirements of cartilage tissue regeneration; however, the ACM/GT scaffold was more suitable because of the greater porosity for cell inoculation.

Biocompatibility of the Scaffolds

After analyzing the characterization of the scaffolds, the cell biocompatibility was the focus of the next evaluation for cartilage tissue regeneration. Cell seeding efficiency, SEM, DNA content, and cellular viability analyses were performed to evaluate the biocompatibility of the two scaffolds. After cell seeding, the two scaffolds maintained their original shape and size, and gross observation showed that the cell suspension was quickly absorbed by the whole scaffolds (**Figures 1C$_1$,D$_1$**). After 7 days of culture *in vitro*, SEM observation revealed that the chondrocytes were well attached to the two scaffolds with a small amount of ECM production (**Figures 1C$_2$,D$_2$**). The cell seeding efficiency in the ACM/GT scaffold was more than 90%, which was significantly greater than on the PGA/PLA scaffold (**Figure 1F**). Cellular viability assays showed that chondrocytes grew well on the two scaffolds with significant proliferation over time, and very few dead cells were observed at all observation times (**Figure 2**). DNA quantitative analysis further indicated that the number of chondrocytes gradually increased with time on the two scaffolds. However, the DNA content of chondrocytes on the ACM/GT scaffold was significantly greater than on the PGA/PLA scaffold (**Figure 1G**), which indicates that ACM may have the potential to promote cell proliferation. Collectively, these *in vitro* results indicated that the ACM/GT scaffold was more favorable for cell adhesion and cell proliferation, indicating better biocompatibility of the ACM/GT scaffold when compared with PGA/PLA scaffold.

Immune-Inflammatory Response Evaluations of the Scaffolds

To capture the early stage post-implantation inflammatory reaction, the two kinds of scaffolds were evaluated by H&E staining and immunohistochemical staining of lymphocytes (CD3) and macrophages (CD68) after 1 and 2 weeks of subcutaneous implantation. As shown in **Figure 3**, the contours of the two groups of implants were observed after 1 week of subcutaneous implantation. A large amount of cell infiltration was observed around the PGA/PLA scaffold while much milder infiltration was observed in the ACM/GT scaffold. The immunohistochemical staining results showed homogenous and strong positive staining of CD3 and CD68 around the PGA/PLA scaffold. After 2 weeks of implantation, the cell infiltration, CD3 and CD68 staining, as well as the quantification of CD3 and CD68 position area (%) around the ACM/GT scaffold were significantly reduced, while the degree of cell infiltration around the PGA/PLA scaffold was significantly increased, which may be because of an aseptic inflammatory reaction caused by the acidic degradation products of the PGA/PLA scaffold.

Immune-Inflammatory Response Evaluations of the Cell–Scaffold Constructs

As shown in **Figure 4**, a large number of inflammatory cells adhered to the cell–scaffold constructs after 1 week of subcutaneous implantation. The boundary area of the ACM/GT group was clear and immature cartilage tissue, while the area of the PGA/PLA group was infiltrated and enveloped by inflammatory cells. Positive staining of CD3 and CD68 was also observed around the PGA/PLA constructs. After 2 weeks of subcutaneous implantation, the cell infiltration was significantly reduced at the outer edge of the ACM/GT construct and the cartilaginous islands were surrounded by a thin layer of negative staining of CD3 and CD68. The quantification of the CD3 and CD68 position area (%) confirmed the above histological results. Notably, the degree of cell infiltration around the PGA/PLA construct was remarkably increased and no typical cartilaginous island was observed compared with the ACM/GT scaffold. These results indicate that the PGA/PLA scaffold had a more severe inflammatory response to the host organism than the ACM/GT scaffold, potentially because chondrocytes promote the degradation of the PGA/PLA scaffold, triggering a serious aseptic inflammatory response and seriously affecting the formation of cartilage.

Histological and Immunohistochemical Evaluations of Regenerative Tissues

After 8 weeks of subcutaneous implantation into autologous goats, the two groups of regenerative tissue were harvested

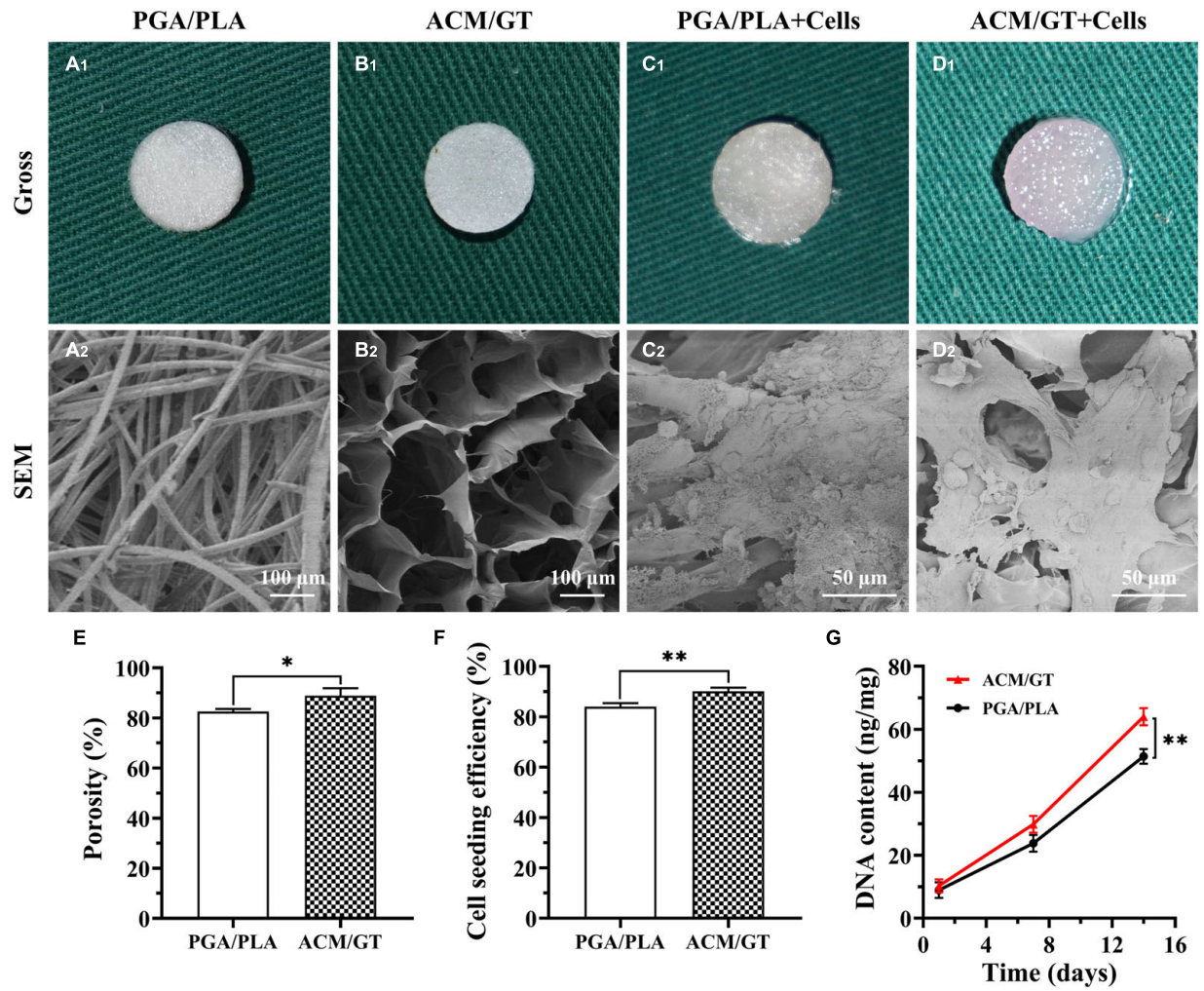

FIGURE 1 | Characterization and biocompatibility of the scaffolds. Gross and SEM images of PGA/PLA scaffold **(A)**, ACM/GT scaffold **(B)**, as well as cell-scaffold constructs **(C,D)**. (**C_1,D_1**) Were the immediate gross images of chondrocytes seeded on scaffolds, while (**C_2,D_2**) were the SEM images of cell-scaffold constructs after 7 days of culture *in vitro*. Characterization analysis of the porosity of two scaffolds **(E)**. Cell seeding efficiency **(F)** and DNA content **(G)** of chondrocytes inoculated into the PGA/PLA scaffold and ACM/GT scaffold. Statistical significance: $^*p < 0.05$, $^{**}p < 0.01$.

to explore the corresponding status of neo-cartilage formation *in vivo*. In the gross observation, the regenerative tissue formed by the PGA/PLA construct had a reddish appearance and soft texture (**Figure 5A**). However, the regenerative tissue formed by the ACM/GT construct also showed a reddish appearance, but with slippery and firmer texture (**Figure 5B**). Histological examinations further confirmed the results from gross observation, where the regenerative tissue formed by the PGA/PLA construct showed a fibrous tissue structure with abundant scaffold fibers, and no obvious cartilaginous tissue was detected (**Figure 5C**). The regenerative tissue formed by the ACM/GT construct showed typical cartilage features with abundant lacuna structures as well as positive staining of Safranin-O and collagen II, although the neo-cartilage tissue was not obviously homogenous (**Figure 5D**). The regenerated cartilage area (%) formed by the ACM/GT constructs were significantly greater than those formed by the PGA/PLA constructs, which supported the above histological results (**Figure 5E**). These results indicated that the ACM might have the potential to enhance the quality of cartilage regeneration in a subcutaneous environment.

Biochemical and Biomechanical Analysis

Naturally, the evaluation of final cartilage formation is the most important criterion to determine whether a scaffold can be suitable for cartilage tissue engineering. The quantitative analysis related to the neo-cartilage formation that is based on the regenerated tissue subcutaneously implanted for 8 weeks further supports the above results. The wet weight and volume of the neo-cartilage tissue formed by the ACM/GT constructs were significantly greater than those formed by the PGA/PLA constructs (**Figures 6A,B**). Similarly, the DNA content, total collagen, and GAG content in the ACM/GT group were close to native cartilage, though significantly greater than

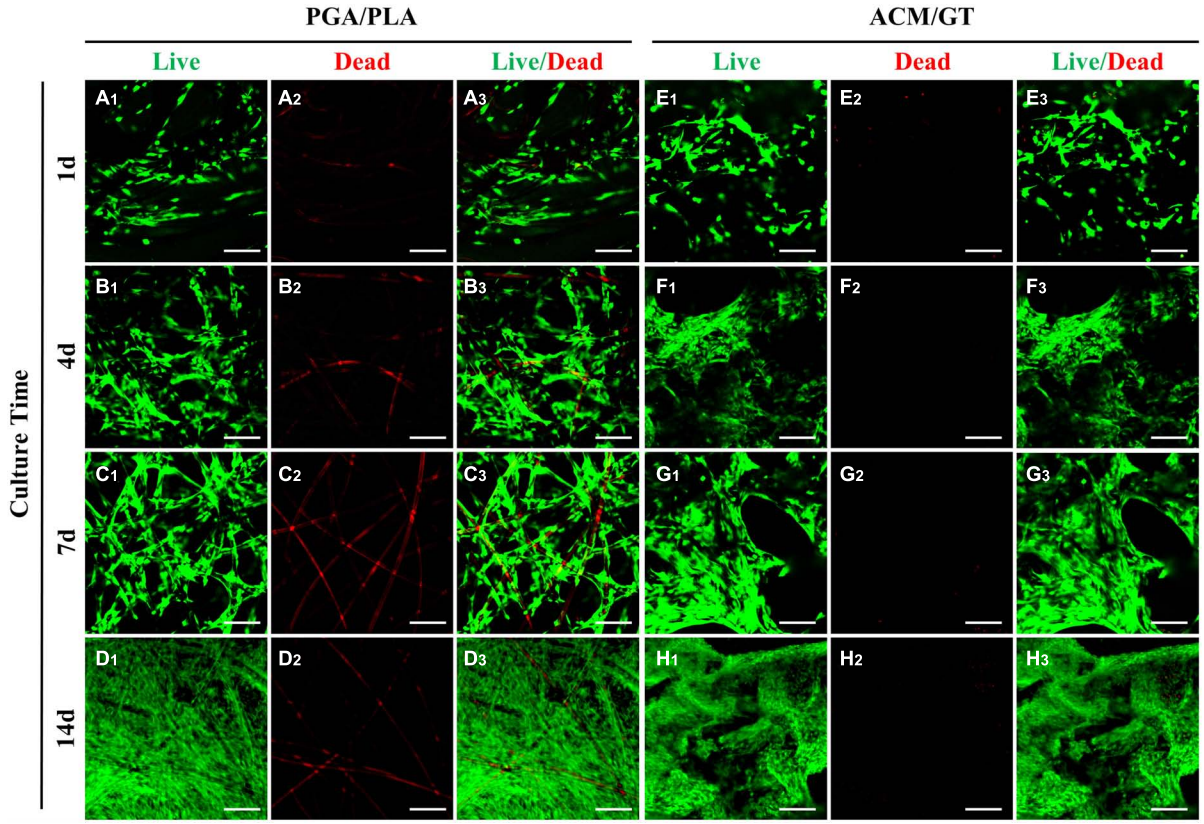

FIGURE 2 | Evaluation of cell viability on the scaffolds. Live/Dead staining showed the number of chondrocytes gradually increased on the PGA/PLA scaffold **(A–D)** and ACM/GT scaffold **(E–H)** as the culture time increased *in vitro*. Almost all chondrocytes survive well (green cells) and few dead cells (red cells) are observed at all observation points. The linear red color (**A_2–D_2**, non-specific staining) is the PGA fibers. Scale bar: 100 μm.

the PGA/PLA group (**Figures 6C–E**). In addition, Young's modulus in the two groups was not statistically different, both reaching more than 75% of the native cartilage (**Figure 6F**). Quantitative analysis results showed that the quality of cartilage regeneration in the ACM/GT group was significantly better than that in the PGA/PLA group, indicating the ACM/GT scaffold was more suitable for cartilage tissue engineering than the PGA/PLA scaffold.

DISCUSSION

The rapid development of tissue engineering and regenerative medicine technology has provided new strategies for auricular reconstruction (Cervantes et al., 2013; Kang et al., 2016; Schroeder and Lloyd, 2017; Wiggenhauser et al., 2017; Jang et al., 2020). Morphological cartilage of human auricular tissue has been successfully regenerated using a PGA/PLA scaffold, and the first clinical breakthrough was achieved (Cao et al., 1997; Zhou et al., 2018). However, its clinical repair varies greatly among individuals, and the quality of regenerated cartilage is unstable, which seriously limits its further clinical application. The poor quality of regenerated cartilage may be related to the acidity of the degradation products of polymer materials, which easily causes an aseptic inflammatory reaction (Asawa et al., 2012; Kanazawa et al., 2013). After PGA/PLA scaffold implantation, acid degradation products accumulate in local tissue, and a large number of inflammatory cells gather and phagocytize the material fibers (Lu et al., 2000; Boland et al., 2004; Pamula and Menaszek, 2008). Concurrently, a series of chemical factors are released, which cause a strong inflammatory response of the host and affect the adhesion of chondrocytes and matrix secretion. The fibrous connective tissue stimulated by inflammation is mixed into the constructed tissue, which weakens the construction quality of the tissue engineered cartilage (Grizzi et al., 1995; Li and McCarthy, 1999). Overall, the engineered cartilage is easily damaged by a severe immune reaction in large animals, causing the implant to not form cartilage tissue well, which limits its transformation to clinical application. However, there are still some problems that need to be addressed for the subcutaneous model of large animals.

Recent studies have found that ACM has a cartilage-specific microenvironment, good biocompatibility, and the potential to promote cell proliferation (Yang et al., 2008, 2010; Utomo et al., 2015; Kim et al., 2020). In the early stage, with the integration of 3D printing, casting molding, and freeze-drying techniques, the human-ear-shaped scaffolds based on ACM have been successfully prepared and further inoculated with

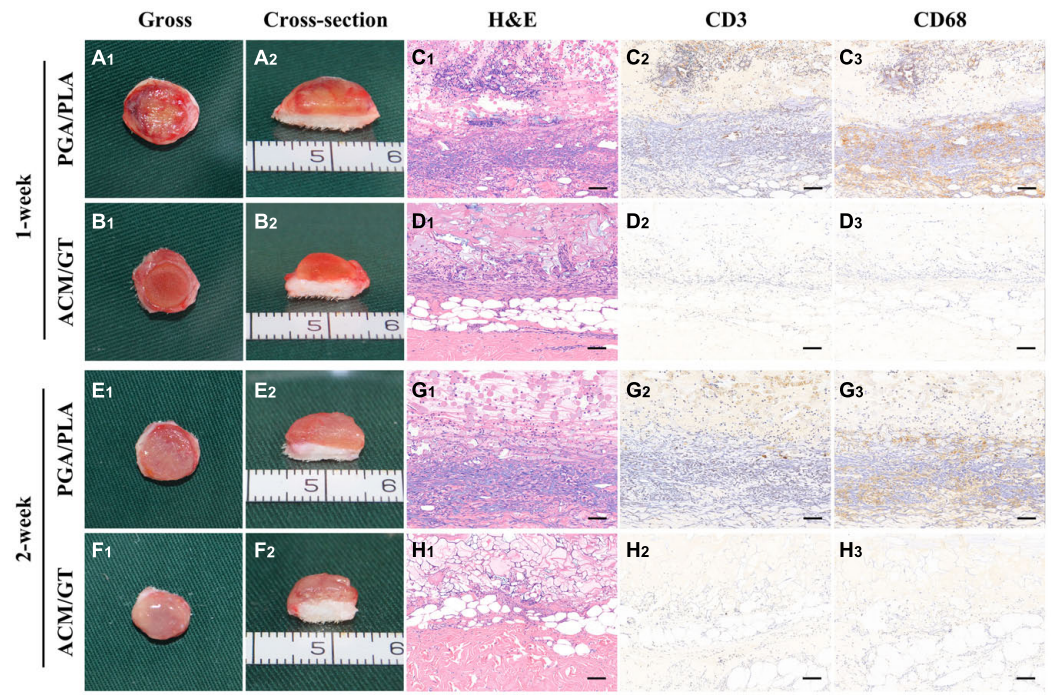

FIGURE 3 | The immune-inflammatory response evaluations of the scaffolds subcutaneously implanted for 1 and 2 weeks. Gross and cross-section observation of the PGA/PLA scaffold and ACM/GT scaffold which subcutaneously implanted for 1 week **(A,B)** and 2 weeks **(E,F)**. Two groups of implanted samples with surrounding tissue were stained with H&E, CD3, and CD68 for immune-inflammatory response analysis **(C,D,G,H)** and the quantification of the CD3 **(I)** and CD68 **(J)** position area (%). Scale bar: 100 μm. Statistical significance: $^{**}p < 0.01$, $^{***}p < 0.001$.

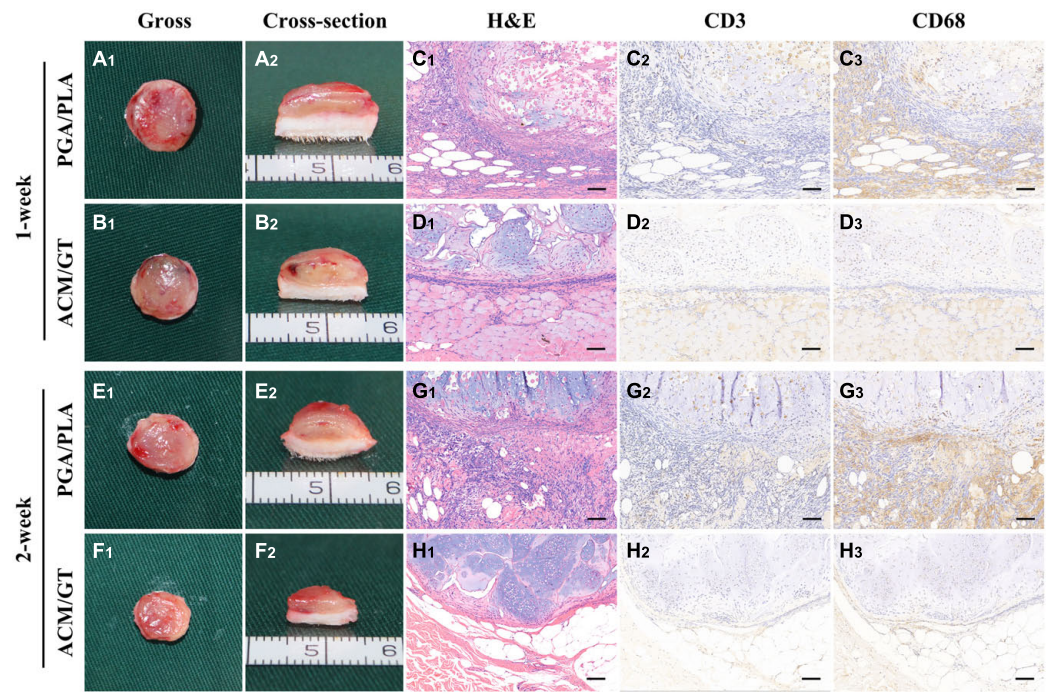

FIGURE 4 | The immune-inflammatory response evaluations of the cell-scaffold constructs subcutaneously implanted for 1 and 2 weeks. Gross and cross-section observation of the cell-PGA/PLA construct and cell-ACM/GT construct which subcutaneously implanted for 1 week **(A,B)** and 2 weeks **(E,F)**. Two groups of implanted samples with surrounding tissue were stained with H&E, CD3, and CD68 for immune-inflammatory response analysis **(C,D,G,H)** and the quantification of the CD3 **(I)** and CD68 **(J)** position area (%). Scale bar: 100 μm. Statistical significance: $^{***}p < 0.001$.

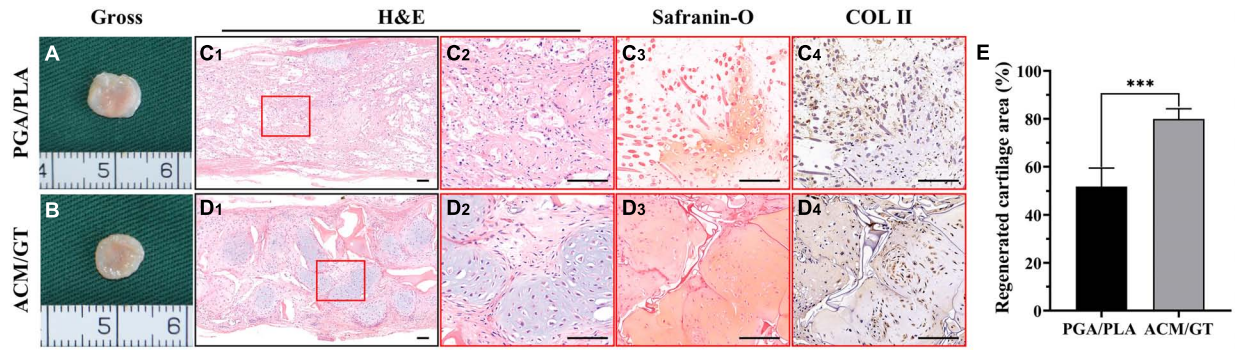

FIGURE 5 | Gross view and histological examination of regenerated cartilage. Gross observation of the cartilage-like tissue regenerated by the cell-PGA/PLA construct **(A)** and cell-ACM/GT construct **(B)** which subcutaneously implanted for 8 weeks. Two groups of regenerated cartilage-like tissue were stained with H&E, Safranin-O, and COL II for the assessment of the quality of cartilage formation **(C,D)** and the quantification of the regenerated cartilage area (%) **(E)**. Scale bar: 100 μm. Statistical significance: ***$p < 0.001$.

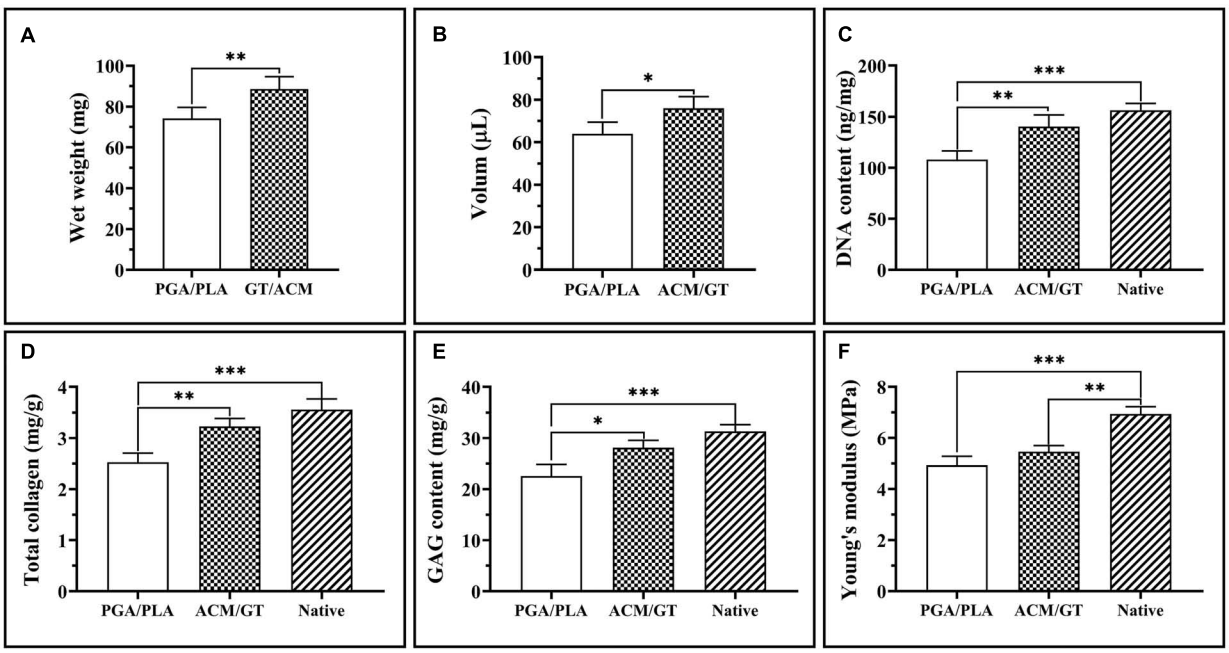

FIGURE 6 | Quantitative analysis of regenerated cartilage. The wet weight and volume of the regenerated cartilage-like tissues by the cell-PGA/PLA construct and cell-ACM/GT construct which subcutaneously implanted for 8 weeks **(A,B)**. The DNA content **(C)**, total collagen **(D)**, GAG content **(E)**, and Young's modulus **(F)** of cartilage-like tissue formatted by two cell-scaffold constructs. Statistical significance: *$p < 0.05$, **$p < 0.01$, ***$p < 0.001$.

chondrocytes to regenerate homogeneous ear-shaped cartilage in immunocompromised nude mice (Jia et al., 2020). However, there is a great difference in the outcome of cartilage regeneration between small animal models and large animal models. That is, the results in small animal models are difficult to be replicated in large animal models, especially in immunocompromised nude mice, which cannot predict the feasibility of clinical application in the future. Therefore, it is necessary to verify the validity and predict the feasibility of clinical translation in pre-clinical large animal models. But so far, there is no specific report on the immune-inflammatory response and cartilage regeneration of ACM in large animal models. So, we specifically conducted current research to systematically compare the post-implantation response and cartilage regeneration of ACM/GT scaffolds and PGA/PLA scaffolds (which were previously applied clinical) in large animal models to predict the potential advantages of ACM/GT scaffolds in reducing immune-inflammatory response and enhancing the quality of regenerated cartilage.

In this study, the cell biocompatibility of ACM derived from cow scapular cartilage was first verified using *in vitro* experiments. The results showed the superiority of the ACM/GT scaffold compared with the PGA/PLA scaffold, especially in cell proliferation, which indicates that ACM may release soluble

growth factors. And our previous studies have identified the presence of some growth factors, such as transforming growth factor-beta (TGF-β), insulin-like growth factor (IGF), and bone morphogenetic protein-2 (BMP-2), which have the potential to promote chondrocyte proliferation (Xue et al., 2012, 2018). This could provide a reasonable explanation for the superior biocompatibility of the ACM/GT scaffold.

To clarify the immune-inflammatory response, xenogeneic ACM/GT with or without autologous chondrocytes was implanted subcutaneously into goats to establish the xenotransplantation model. There was cell infiltration of ACM/GT at an early stage, which was significantly alleviated by 2 weeks, indicating a mild inflammatory response to the host organism. However, the PGA/PLA scaffold showed cell infiltration, which worsened significantly by 2 weeks. This may be induced by the acidic products that are gradually degraded from the PGA/PLA scaffold (Liu et al., 2016). Notably, the immune-inflammatory response of the cell–PGA/PLA scaffolds was more severe, potentially because the chondrocytes promoted degradation of the PGA/PLA scaffold and triggered a severe aseptic inflammatory response.

Furthermore, testing the quality and long-term outcome of tissue-engineered cartilage formatted *in vivo* is the necessary step of preclinical verification. The evaluation of tissue-engineered cartilage showed the ACM/GT construct formed a typical, mature, and homogeneous cartilage tissue, indicating the mild inflammation does not affect cartilage regeneration and the ACM may have the potential to promote the formation of cartilage tissue. Alternatively, no typical cartilage features were observed in the regenerative tissue by the PGA/PLA scaffolds, potentially because of the aseptic inflammatory response hindering the formation of cartilage.

The current research confirmed the potential of ACM to promote cell proliferation and cartilage formation *in vivo* and i*n vitro* experiments. Although there is a slight immune-inflammatory response in large animals that have a sound immune system, it does not affect the quality of the regenerated cartilage. The mild immune-inflammatory response may be related to the remaining galactosyl-alpha-(1,3)-galactose (α-Gal), which is immunogenic in most mammalian species including humans and causes glycan-specific IgG and IgE responses with clinical relevance (Jappe et al., 2018; Bernth Jensen et al., 2020). In the next study, α-Gal in ACM will be removed to obtain a lower immunogenic scaffold. The homogeneous and mature cartilage can be regenerated and maintain long-term stability, which suggests that ACM/GT can replace the PGA/PLA scaffold to improve clinical repair. Additionally, as a natural biodegradable material, ACM has more advantages in microenvironment bionics, biocompatibility, and biosafety, for more prospects of future clinical transformation.

CONCLUSION

In summary, the current study confirmed the superiority of the ACM to PGA/PLA scaffolds with the potential to promote cell proliferation and cartilage formation. Although there is a slight immune-inflammatory response in large animals that have a sound immune system, it does not affect the quality of regenerated cartilage and can form homogeneous and mature cartilage. Although further research is needed to obtain the ACM with lower immunogenicity, the current results provide scientific evidence for its future clinical application in cartilage tissue engineering.

DATA AVAILABILITY STATEMENT

The original contributions presented in the study are included in the manuscript/supplementary material, further inquiries can be directed to the corresponding authors.

ETHICS STATEMENT

The animal study was reviewed and approved by the Animal Care and Experiment Committee of Shanghai Jiao Tong University School of Medicine (Shanghai, China).

AUTHOR CONTRIBUTIONS

LJ: conceptualization, methodology, data curation, formal analysis, and writing original draft. PZ: conceptualization, data curation, and software. ZC and WZ: conceptualization and methodology. YL: conceptualization and supervision. HJ: conceptualization, methodology, and supervision. GZ: conceptualization, methodology, and writing review and editing. All authors contributed to the article and approved the submitted version.

FUNDING

This research was supported by the National Key Research and Development Program of China (2017YFC1103900 and 2018YFC1005800), the National Natural Science Foundation of China (81871502, 81701843, and 81974291), the Chinese Academy of Medical Sciences Innovation Fund for Medical Sciences (2017-I2M-1-007), Shanghai Excellent Technical Leader (18XD1421500), and Shanghai Collaborative Innovation Program on Regenerative Medicine and Stem Cell Research (2019CXJQ01).

REFERENCES

Asawa, Y., Sakamoto, T., Komura, M., Watanabe, M., Nishizawa, S., Takazawa, Y., et al. (2012). Early stage foreign body reaction against biodegradable polymer scaffolds affects tissue regeneration during the autologous transplantation of tissue-engineered cartilage in the canine model. *Cell Transplant* 21, 1431–1442. doi: 10.3727/096368912X640574

Bernth Jensen, J. M., Laursen, N. S., Jensen, R. K., Andersen, G. R., Jensenius, J. C., Sorensen, U. B. S., et al. (2020). Complement activation by human IgG

antibodies to galactose-alpha-1,3-galactose. *Immunology* 161, 66–79. doi: 10.1111/imm.13229

Bly, R. A., Bhrany, A. D., Murakami, C. S., and Sie, K. C. (2016). Microtia Reconstruction. *Facial. Plast. Surg. Clin. North Am.* 24, 577–591. doi: 10.1016/j.fsc.2016.06.011

Boland, E. D., Telemeco, T. A., Simpson, D. G., Wnek, G. E., and Bowlin, G. L. (2004). Utilizing acid pretreatment and electrospinning to improve biocompatibility of poly(glycolic acid) for tissue engineering. *J. Biomed. Mater. Res. B Appl. Biomater.* 71, 144–152. doi: 10.1002/jbm.b.30105

Brent, B. (2002). Microtia repair with rib cartilage grafts: a review of personal experience with 1000 cases. *Clin. Plast. Surg.* 29, 257–271. doi: 10.1016/s0094-1298(01)00013-x

Cao, Y., Vacanti, J. P., Paige, K. T., Upton, J., and Vacanti, C. A. (1997). Transplantation of chondrocytes utilizing a polymer-cell construct to produce tissue-engineered cartilage in the shape of a human ear. *Plast. Reconstr. Surg.* 100, 297–302;discussion303–294. doi: 10.1097/00006534-199708000-00001

Ceonzo, K., Gaynor, A., Shaffer, L., Kojima, K., Vacanti, C. A., and Stahl, G. L. (2006). Polyglycolic acid-induced inflammation: role of hydrolysis and resulting complement activation. *Tissue Eng.* 12, 301–308. doi: 10.1089/ten.2006.12.301

Cervantes, T. M., Bassett, E. K., Tseng, A., Kimura, A., Roscioli, N., Randolph, M. A., et al. (2013). Design of composite scaffolds and three-dimensional shape analysis for tissue-engineered ear. *J. R. Soc. Interface* 10:20130413. doi: 10.1098/rsif.2013.0413

Chen, W., Chen, S., Morsi, Y., El-Hamshary, H., El-Newhy, M., Fan, C., et al. (2016). Superabsorbent 3D scaffold based on electrospun nanofibers for cartilage tissue engineering. *ACS Appl. Mater. Interfaces* 8, 24415–24425. doi: 10.1021/acsami.6b06825

Grizzi, I., Garreau, H., Li, S., and Vert, M. (1995). Hydrolytic degradation of devices based on poly(DL-lactic acid) size-dependence. *Biomaterials* 16, 305–311. doi: 10.1016/0142-9612(95)93258-f

Haisch, A. (2010). Ear reconstruction through tissue engineering. *Adv. Otorhinolaryngol.* 68, 108–119. doi: 10.1159/000314566

Jang, C. H., Koo, Y., and Kim, G. (2020). ASC/chondrocyte-laden alginate hydrogel/PCL hybrid scaffold fabricated using 3D printing for auricle regeneration. *Carbohydr. Polym.* 248:116776. doi: 10.1016/j.carbpol.2020.116776

Jappe, U., Minge, S., Kreft, B., Ludwig, A., Przybilla, B., Walker, A., et al. (2018). Meat allergy associated with galactosyl-alpha-(1,3)-galactose (alpha-Gal)-Closing diagnostic gaps by anti-alpha-Gal IgE immune profiling. *Allergy* 73, 93–105. doi: 10.1111/all.13238

Jia, L., Zhang, Y., Yao, L., Zhang, P., Ci, Z., Zhang, W., et al. (2020). Regeneration of human-ear-shaped cartilage with acellular cartilage matrix-based biomimetic scaffolds. *Appl. Mater. Today* 20:100639. doi: 10.1016/j.apmt.2020.100639

Jian, Z., Zhuang, T., Qinyu, T., Liqing, P., Kun, L., Xujiang, L., et al. (2021). 3D bioprinting of a biomimetic meniscal scaffold for application in tissue engineering. *Bioact. Mater.* 6, 1711–1726. doi: 10.1016/j.bioactmat.2020.11.027

Kanazawa, S., Fujihara, Y., Sakamoto, T., Asawa, Y., Komura, M., Nagata, S., et al. (2013). Tissue responses against tissue-engineered cartilage consisting of chondrocytes encapsulated within non-absorbable hydrogel. *J. Tissue Eng. Regen. Med.* 7, 1–9. doi: 10.1002/term.458

Kang, H. W., Lee, S. J., Ko, I. K., Kengla, C., Yoo, J. J., and Atala, A. (2016). A 3D bioprinting system to produce human-scale tissue constructs with structural integrity. *Nat Biotechnol* 34, 312–319. doi: 10.1038/nbt.3413

Kim, B. S., Das, S., Jang, J., and Cho, D. W. (2020). Decellularized extracellular matrix-based bioinks for engineering tissue- and organ-specific microenvironments. *Chem. Rev.* 120, 10608–10661. doi: 10.1021/acs.chemrev.9b00808

Li, D., Yin, Z., Liu, Y., Feng, S., Liu, Y., Lu, F., et al. (2019). Regeneration of trachea graft with cartilage support, vascularization, and epithelization. *Acta Biomater* 89, 206–216. doi: 10.1016/j.actbio.2019.03.003

Li, S., and McCarthy, S. (1999). Further investigations on the hydrolytic degradation of poly (DL-lactide). *Biomaterials* 20, 35–44. doi: 10.1016/s0142-9612(97)00226-3

Li, Y., Xu, Y., Liu, Y., Wang, Z., Chen, W., Duan, L., et al. (2019). Decellularized cartilage matrix scaffolds with laser-machined micropores for cartilage regeneration and articular cartilage repair. *Mater. Sci. Eng. C. Mater. Biol. Appl.* 105:110139. doi: 10.1016/j.msec.2019.110139

Liu, Y., Li, D., Yin, Z., Luo, X., Liu, W., Zhang, W., et al. (2016). Prolonged in vitro precultivation alleviates post-implantation inflammation and promotes stable subcutaneous cartilage formation in a goat model. *Biomed. Mater.* 12:015006. doi: 10.1088/1748-605X/12/1/015006

Liu, Y., Zhang, L., Zhou, G., Li, Q., Liu, W., Yu, Z., et al. (2010). In vitro engineering of human ear-shaped cartilage assisted with CAD/CAM technology. *Biomaterials* 31, 2176–2183. doi: 10.1016/j.biomaterials.2009.11.080

Lu, L., Peter, S. J., Lyman, M. D., Lai, H. L., Leite, S. M., Tamada, J. A., et al. (2000). In vitro and in vivo degradation of porous poly(DL-lactic-co-glycolic acid) foams. *Biomaterials* 21, 1837–1845. doi: 10.1016/s0142-9612(00)00047-8

Luo, X., Liu, Y., Zhang, Z., Tao, R., Liu, Y., He, A., et al. (2013). Long-term functional reconstruction of segmental tracheal defect by pedicled tissue-engineered trachea in rabbits. *Biomaterials* 34, 3336–3344. doi: 10.1016/j.biomaterials.2013.01.060

Luquetti, D. V., Heike, C. L., Hing, A. V., Cunningham, M. L., and Cox, T. C. (2012). Microtia: epidemiology and genetics. *Am. J. Med. Genet. A* 158A, 124–139. doi: 10.1002/ajmg.a.34352

Luquetti, D. V., Leoncini, E., and Mastroiacovo, P. (2011). Microtia-anotia: a global review of prevalence rates. *Birth Defects Res. A Clin. Mol. Teratol.* 91, 813–822. doi: 10.1002/bdra.20836

Pamula, E., and Menaszek, E. (2008). In vitro and in vivo degradation of poly(L:-lactide-co-glycolide) films and scaffolds. *J. Mater. Sci. Mater. Med.* 19, 2063–2070. doi: 10.1007/s10856-007-3292-2

Schroeder, M. J., and Lloyd, M. S. (2017). Tissue engineering strategies for auricular reconstruction. *J. Craniofac. Surg.* 28, 2007–2011. doi: 10.1097/SCS.0000000000003753

Serra, I. R., Fradique, R., Vallejo, M. C., Correia, T. R., Miguel, S. P., and Correia, I. J. (2015). Production and characterization of chitosan/gelatin/beta-TCP scaffolds for improved bone tissue regeneration. *Mater. Sci. Eng. C Mater. Biol. Appl.* 55, 592–604. doi: 10.1016/j.msec.2015.05.072

Utomo, L., Pleumeekers, M. M., Nimeskern, L., Nurnberger, S., Stok, K. S., Hildner, F., et al. (2015). Preparation and characterization of a decellularized cartilage scaffold for ear cartilage reconstruction. *Biomed. Mater.* 10:015010. doi: 10.1088/1748-6041/10/1/015010

Wiggenhauser, P. S., Schantz, J. T., and Rotter, N. (2017). Cartilage engineering in reconstructive surgery: auricular, nasal and tracheal engineering from a surgical perspective. *Regen. Med.* 12, 303–314. doi: 10.2217/rme-2016-0160

Wiggenhauser, P. S., Schwarz, S., Koerber, L., Hoffmann, T. K., and Rotter, N. (2019). Addition of decellularized extracellular matrix of porcine nasal cartilage improves cartilage regenerative capacities of PCL-based scaffolds in vitro. *J. Mater. Sci. Mater. Med.* 30:121. doi: 10.1007/s10856-019-6323-x

Xia, H., Zhao, D., Zhu, H., Hua, Y., Xiao, K., Xu, Y., et al. (2018). Lyophilized scaffolds fabricated from 3D-printed photocurable natural hydrogel for cartilage regeneration. *ACS Appl. Mater. Interfaces* 10, 31704–31715. doi: 10.1021/acsami.8b10926

Xu, Y., Guo, Y., Li, Y., Huo, Y., She, Y., Li, H., et al. (2020a). Biomimetic trachea regeneration using a modular ring strategy based on poly(sebacoyl diglyceride)/polycaprolactone for segmental trachea defect repair. *Adv. Funct. Mater.* 30:e2004276. doi: 10.1002/adfm.202004276

Xu, Y., Xu, Y., Bi, B., Hou, M., Yao, L., Du, Q., et al. (2020b). A moldable thermosensitive hydroxypropyl chitin hydrogel for 3D cartilage regeneration in vitro and in vivo. *Acta Biomater* 108, 87–96. doi: 10.1016/j.actbio.2020.03.039

Xue, J. X., Gong, Y. Y., Zhou, G. D., Liu, W., Cao, Y., and Zhang, W. J. (2012). Chondrogenic differentiation of bone marrow-derived mesenchymal stem cells induced by acellular cartilage sheets. *Biomaterials* 33, 5832–5840. doi: 10.1016/j.biomaterials.2012.04.054

Xue, J., Feng, B., Zheng, R., Lu, Y., Zhou, G., Liu, W., et al. (2013). Engineering ear-shaped cartilage using electrospun fibrous membranes of gelatin/polycaprolactone. *Biomaterials* 34, 2624–2631. doi: 10.1016/j.biomaterials.2012.12.011

Xue, J., He, A., Zhu, Y., Liu, Y., Li, D., Yin, Z., et al. (2018). Repair of articular cartilage defects with acellular cartilage sheets in a swine model. *Biomed. Mater.* 13:025016. doi: 10.1088/1748-605X/aa99a4

Yang, Q., Peng, J., Guo, Q., Huang, J., Zhang, L., Yao, J., et al. (2008). A cartilage ECM-derived 3-D porous acellular matrix scaffold for in vivo

cartilage tissue engineering with PKH26-labeled chondrogenic bone marrow-derived mesenchymal stem cells. *Biomaterials* 29, 2378–2387. doi: 10.1016/j.biomaterials.2008.01.037

Yang, Z., Shi, Y., Wei, X., He, J., Yang, S., Dickson, G., et al. (2010). Fabrication and repair of cartilage defects with a novel acellular cartilage matrix scaffold. *Tissue Eng. Part C Methods* 16, 865–876. doi: 10.1089/ten.TEC.2009.0444

Yin, Z., Li, D., Liu, Y., Feng, S., Yao, L., Liang, X., et al. (2020). Regeneration of elastic cartilage with accurate human-ear shape based on PCL strengthened biodegradable scaffold and expanded microtia chondrocytes. *Appl. Mater. Today* 20:100724. doi: 10.1016/j.apmt.2020.100724

Zhang, L., He, A., Yin, Z., Yu, Z., Luo, X., Liu, W., et al. (2014). Regeneration of human-ear-shaped cartilage by co-culturing human microtia chondrocytes with BMSCs. *Biomaterials* 35, 4878–4887. doi: 10.1016/j.biomaterials.2014.02.043

Zhang, Q., Zhang, R., Xu, F., Jin, P., and Cao, Y. (2009). Auricular reconstruction for microtia: personal 6-year experience based on 350 microtia ear reconstructions in China. *Plast. Reconstr. Surg.* 123, 849–858. doi: 10.1097/PRS.0b013e318199f057

Zheng, R., Duan, H., Xue, J., Liu, Y., Feng, B., Zhao, S., et al. (2014). The influence of Gelatin/PCL ratio and 3-D construct shape of electrospun membranes on cartilage regeneration. *Biomaterials* 35, 152–164. doi: 10.1016/j.biomaterials.2013.09.082

Zhou, G., Jiang, H., Yin, Z., Liu, Y., Zhang, Q., Zhang, C., et al. (2018). In vitro regeneration of patient-specific ear-shaped cartilage and its first clinical application for auricular reconstruction. *EBioMedicine* 28, 287–302. doi: 10.1016/j.ebiom.2018.01.011

Conflict of Interest: The authors declare that the research was conducted in the absence of any commercial or financial relationships that could be construed as a potential conflict of interest.

frontiers in Bioengineering and Biotechnology

ORIGINAL RESEARCH
published: 06 October 2021
doi: 10.3389/fbioe.2021.734483

Bone-Forming Peptide-4 Induces Osteogenic Differentiation and VEGF Expression on Multipotent Bone Marrow Stromal Cells

Mi Eun Kim[1], Jong Keun Seon[2,3], Ju Yeon Kang[2,3], Taek Rim Yoon[2,3], Jun Sik Lee[1] and Hyung Keun Kim[2,3]**

[1]*Department of Biology, Immunology Research Lab, Integrative Biological Sciences & BK21 FOUR Educational Research Group for Age-Associated Disorder Control Technology, College of Natural Sciences, Chosun University, Gwangju, South Korea,* [2]*Korea Biomedical Materials and Devices Innovation Research Center of Chonnam National University Hospital, Gwangju, South Korea,* [3]*Department of Orthopaedics Surgery, Center for Joint Disease of Chonnam National, University Hwasun Hospital, Jeonnam, South Korea*

OPEN ACCESS

Edited by:
Zhen Li,
AO Research Institute, Switzerland

Reviewed by:
Sophie Verrier,
AO Research Institute, Switzerland
Sorada Kanokpanont,
Chulalongkorn University, Thailand

***Correspondence:**
Jun Sik Lee
junsiklee@chosun.ac.kr
Hyung Keun Kim
chemokines@naver.com

Specialty section:
This article was submitted to Tissue Engineering and Regenerative Medicine, a section of the journal Frontiers in Bioengineering and Biotechnology

Received: *01 July 2021*
Accepted: *21 September 2021*
Published: *06 October 2021*

Citation:
Kim ME, Seon JK, Kang JY, Yoon TR, Lee JS and Kim HK (2021) Bone-Forming Peptide-4 Induces Osteogenic Differentiation and VEGF Expression on Multipotent Bone Marrow Stromal Cells. Front. Bioeng. Biotechnol. 9:734483. doi: 10.3389/fbioe.2021.734483

Bone morphogenetic proteins (BMPs) have been widely used as treatment for bone repair. However, clinical trials on fracture repair have challenged the effectiveness of BMPs and suggested that delivery of multipotent bone marrow stromal cells (BMSCs) might be beneficial. During bone remodeling and bone fracture repair, multipotent BMSCs differentiate into osteoblasts or chondrocytes to stimulate bone formation and regeneration. Stem cell-based therapies provide a promising approach for bone formation. Extensive research has attempted to develop adjuvants as specific stimulators of bone formation for therapeutic use in patients with bone resorption. We previously reported for the first time bone-forming peptides (BFPs) that induce osteogenesis and bone formation. BFPs are also a promising osteogenic factor for prompting bone regeneration and formation. Thus, the aim of the present study was to investigate the underlying mechanism of a new BFP-4 (FFKATEVHFRSIRST) in osteogenic differentiation and bone formation. This study reports that BFP-4 induces stronger osteogenic differentiation of BMSCs than BMP-7. BFP-4 also induces ALP activity, calcium concentration, and osteogenic factors (Runx2 and osteocalcin) in a dose dependent manner in BMSCs. Therefore, these results indicate that BFP-4 can induce osteogenic differentiation and bone formation. Thus, treatment of multipotent BMSCs with BFP-4 enhanced osteoblastic differentiation and displayed greater bone-forming ability than BMP-7 treatment. These results suggest that BFP-4-stimulated cell therapy may be an efficient and cost-effective complement to BMP-7-based clinical therapy for bone regeneration and formation.

Keywords: bone morphogenetic proteins, bone-forming peptides, osteogenic differentiation, bone formation, VEGF

INTRODUCTION

Bone is a constantly renewing tissue by a process that is exquisitely balanced by bone-forming cells, bone-resorbing cells, osteoblasts, and osteoclasts (Douglas et al., 2018; Hamamura et al., 2019; Vesela et al., 2019). Therefore, achieving the proper balance between osteoclastic bone resorption and osteoblastic bone formation is important to prevent osteoporosis (Lerner et al., 2019; Yin et al., 2019). Moreover, bone remodeling is strongly regulated by interactions among cytokines, hormones, and other molecules that affect communication between osteoclasts and osteoblasts. Any disruption in this network may result in abnormal bone mass, including osteoporosis (Florencio-Silva et al., 2015; Han et al., 2018; Owen and Reilly, 2018; Kumar and Roger, 2019).

Various materials for osteogenesis and bone formation have been studied for a long time, and bone morphogenetic proteins (BMPs) is a representative factor with good efficacy in bone formation. Osteogenesis is controlled by multiple factors, including BMPs, and stromal cell-derived factors (SDFs) (Yang F. et al., 2018; Kim et al., 2018). BMPs are the key proteins mediating the differentiation, recruitment, and maturation of mesenchymal stromal cells (MSCs) into osteoblasts via osteogenesis (Sangadala et al., 2019). BMP-7 has been permitted for clinical use in the regeneration of bone in vertebral arthrodesis and fracture healing (Shen et al., 2010). According to previous reports, BMP-7 demonstrated a synergistic effect with microfractures to stimulate cartilage repair *in vivo*. However, some reports induced adipogenesis instead of bone/cartilage differentiation. Therefore, it is still required to find a more stable and economical inducer than BMP-7 as a factor inducing bone formation.

Several signaling pathways play important roles in regulating osteogenesis. BMPs, as a group, are considered one of the strongest osteoinductive factors. The biological activity of BMP-7 is active in the mature region of BMP-7. In contrast, bone-forming peptides (BFPs) is peptide found in the immature precursor of BMP-7. BFPs has a smaller molecular size and is more economical than BMP-7, suggesting the possibility of using it as a new therapeutic agent for bone formation. We previously reported that BFPs, including BFP-1, BFP-2, and BFP-3, are some of the most potent BMPs in inducing osteogenic differentiation (Kim et al., 2012; Kim et al., 2017; Lee et al., 2018). They have been shown to effectively induce osteogenic differentiation of multipotent bone marrow stromal cells (BMSCs) by regulating a panel of important downstream targets and through cross-talk with other important signaling pathways. In the case of BFP-1, we not only found the first reported peptide sequence with osteogenesis effect from the prodomain region of BMP-7, but also confirmed, through animal experiments, that BFP-1 induced bone formation by osteogenic differentiation more strongly than BMP-7. Furthermore, BFP-2 and BFP-3, both found in the prodomain region of BMP-7, have also been shown to have an osteogenic effect. It was reported that BFPs can replace BMP-7 and can be used for economically superior bone resorption-related disease therapies.

Therefore, we investigate to find a new BFP peptide that has more osteogenic effects than BMP-7. We isolated a new peptide sequences with osteogenic activity form the immature region of BMP-7 and investigated its osteogenic effects in multipotent BMSCs.

MATERIALS AND METHODS

Chemical and Reagents

3-(4,5-dimethylthiazol-2-yl)-2,5-diphenyltetrazolium bromide (MTT), phosphate-buffered saline (PBS), dimethylsulfoxide, ethanol, Alizarin red Staining solution, Triton X-100, bovine serum albumin, and paraformaldehyde were purchased from Sigma-Aldrich (St. Louis, MO, United States).

Synthesis and Purification of BFP-4

BFP-4 (FFKATEVHFRSIRST) was synthesized by Fmoc solid-phase peptide synthesis using an ASP48S automated peptide synthesizer (Peptron, Daejeon, South Korea) and purified by reverse-phase high-performance liquid chromatography using a Vydac Everest C18 column (250 mm × 22 mm, 10 μm) (UVISON, Sevenoaks, United Kingdom). Elution was conducted with a water-acetonitrile linear gradient (3–40% (v/v) acetonitrile) containing 0.1% (v/v) trifluoroacetic acid. The molecular mass of the purified peptide was confirmed by liquid chromatography/mass spectroscopy using an Agilent HP1100 series HPLC system (Santa Clara, CA, United States).

Osteogenic Differentiation

Mouse multipotent bone marrow stromal cells were purchased from the American Type Culture Collection (ATCC, Manassas, VA, United States) and maintained in Dulbecco's Modified Eagle Medium (DMEM) containing 10% fetal bovine serum (FBS) (Life Technologies, Grand Island, NY, United States). The multipotent BMSCs were seeded at a density of 1×10^4 cells/well and maintained in culture for 3 days in a humidified atmosphere of 5% CO_2 at 37°C. Experiments were performed after the cells had reached approximately 80% confluency. The culture medium was changed at day 3 to osteogenic differentiation medium (ODM; DMEM supplemented with 50 μg/ml ascorbic acid, 10 nM dexamethasone, and 10 mM β-glycerophosphate; all from Sigma-Aldrich, St. Louis, MO, United States) to induce osteogenic differentiation. After culture for 3 more days, one group of cells was cultured in ODM alone and a second group was cultured in ODM containing BFP-4 (0.01 and 0.1 μg/ml) and BMP-7 (0.01 and 0.1 μg/ml) (Kim et al., 2017; Geng et al., 2019).

Cell Viability Assay

Surviving cells were counted using an MTT assay. Final concentration of 0.5 mg/ml MTT (17.2 mM phosphate-buffered saline (PBS), pH 6.5) was added to each well, and the plates were incubated for an additional 3 h. The solution was removed from the wells, and dimethylsulfoxide/ethanol (1:1 ratio) was added to dissolve the formazan products. The plates were shaken for 20 min, and the absorbance at 570 nm was recorded on a microplate spectrophotometer.

Alizarin Red S Staining

Cell cultures were washed twice with distilled water, fixed for 1 h in ice-cold 70% ethanol, and rinsed twice with deionized water. Cultures were stained for 10 min with 1% Alizarin red S, and excess dye was removed by gently flushing with running water. Calcium deposits, which appeared bright red, were identified by light microscopy and photographed. Osteogenic differentiation was quantified by determining the density and area of Alizarin red S-stained regions with an image analysis program (Multi Gauge V3.0, Fujifilm, Tokyo, Japan).

Calcium Assays

Calcium was assayed with the QuantiChrom Calcium Assay Kit (Gentaur, Voortstraat, Belgium). The calcium concentration was determined based on the formation of a stable blue complex between the phenolsulfonphthalein dye and free calcium, whereby color intensity was directly proportional to the concentration of free calcium in the sample. The cell layers were washed twice with PBS. Calcium in the matrix was dissolved with 0.5 M HCL, assay reagent was added. The color intensity was measured at 612 nm using an Infinite M200 microplate reader (Tecan, Männedorf, Switzerland).

Reverse Transcription-Polymerase Chain Reaction

Total RNA was extracted from harvested BFP-4 treated BMSCs using PicoPure™ RNA Isolation Kit (ThermoFisher, USA) according to the manufacturer's instruction. After isolation of RNA, reverse transcription was carried out using the SMARTer PCR cDNA synthesis Kit (Takara, Japan). One microgram RNA was used for the first-strand cDNA synthesis in a total volume of 20 µl according to the manufacturer's instruction. RT-PCR was performed to assess the effects of BFP-4 on the transcription of the genes encoding alkaline phosphatase (ALP), osteocalcin, RUNX2, and the internal control housekeeping enzyme glyceraldehyde-3-phosphate dehydrogenase (GAPDH). The primers used were as follows: *ALP*, (forward) 5′-ACA CCT TGA CTG TGG TTA CTG CTG A-3′ and (reverse) 5′-CCT TGT AGC CAG GCC CGT TA-3′; *osteocalcin* (forward) 5′-GAG GGC AAT AAG GTA GTG AAC AGA-3′ and (reverse) 5′-AAG CCA TAC TGG TCT GAT AGC TCG-3′; *Runx2*, (forward) 5′-ACA AAC CAC AGA ACC ACA AGT-3′ and (reverse) 5′-GTC TCG GTG GCT GGT AGT GA-3′; and *GAPDH*, (forward) 5′-AAA TGG TGA AGG TCG GTG TG-3′ and (reverse) 5′-TGA AGG GGT CGT TGA TGG-3′ (Bioneer, Daejeon, South Korea). MSCs grown to 70% confluency on plates in the presence and absence of BFP-4 were homogenized in TRIzol reagent (Life Technologies). Total RNA was isolated and used to synthesize cDNA. To determine relative mRNA expression, house-keeping gene (GAPDH) and osteogenic differentiation marker gene with SYBR green I (SYBR advantage qPCR premix, Takara, Japan) were used.

Immunofluorescence Analysis

In brief, a total of 1×10^4 cells/well were seeded in an 6 well cell culture chamber slide containing completed medium for 3 days. The control group was assessed in the absence of osteogenic differentiation medium. At the end of 3 days incubation, the cells were treated by BFP-4 for 24 h. After 24 h incubation, cells were fixed with 4% paraformaldehyde prepared in PBS for 15 min, permeabilized with 0.1% Triton X-100 for 15 min, and blocked with 5% bovine serum albumin in PBS for 30 min. Coverslips were then incubated with a primary antibody against mouse CD44 and CD51 (eBioscience, San Diego, CA, United States) at a dilution of 1:200 followed by incubation with a secondary antibody at a dilution of 1:400, both at room temperature for 1 h. Cells were washed with PBS, and nuclei were counterstained with 4,6-diamidino-2-phenylindole. Coverslips were mounted in 70% glycerol, and micrographs were obtained with an Olympus BX50 fluorescence microscope (Tokyo, Japan).

Flow Cytometry Analysis

A total of 1×10^4 cells/well were seeded in an 6 well containing completed medium for 3 days. At the end of 3 days incubation, the cells were treated by BFP-4 for 24 h. After 24 h incubation, Cells (5×10^5/ml) were incubated in staining buffer (PBS containing 0.5% FBS and 0.1% sodium azide) containing an anti-CD44 and anti-CD51 fluorescein isothiocyanate (FITC) antibody for 30 min on ice. Cells stained with the appropriate isotype-matched were used as negative controls. After staining, cells were fixed with 2% paraformaldehyde and analyzed with an FC500 instrument equipped with Flow ver. 10 (Biosciences, San Diego, CA, United States).

Western Blot Analysis

Multipotent BMSCs (2×10^6 cells/well) were seeded in a 60Φ cell culture dish and starved by incubation in serum-free DMEM for 6 h. Treated cells were washed with cold PBS and lysed with RIPA lysis buffer (Thermo Scientific, PA, United States) at 4°C for 30 min. The lysates were centrifuged at 13,000×*g* for 15 min, and the supernatants were used as protein samples. The protein concentration was measured using a colorimetric bicinchoninic acid kit (Thermo Scientific, PA, United States) according to the manufacturer's instructions. Twenty microgram of each cell protein sample was electrophoresed on 10% or 12% SDS-polyacrylamide gel electrophoresis (PAGE) and transferred to polyvinylidene fluoride (PVDF) membranes (Millipore, MA, United States). The membranes were incubated with blocking solution (5% skim milk prepared in Tris-buffered saline) for 1 h. After blocking, membranes were probed with anti-osteocalcin and anti-GAPDH antibodies (Santa Cruz Biotechnology, CA, United States), and then with a horseradish peroxidase-conjugated anti-rabbit or anti-mouse secondary antibody (Santa Cruz Biotechnology) for 2 h. Bands were visualized using an enhanced chemiluminescence detection system (Bio-Rad, CA, United States) and exposed to radiographic film.

Animal Study

All the animal procedures were carried out in accordance with the guidelines of the Animal Care and Use Committee of Chonnam National University. The animal study was approved by Animal Care and Use Committee of Chonnam National University (Permission number: CNN IACUC-20032). Osteogenically

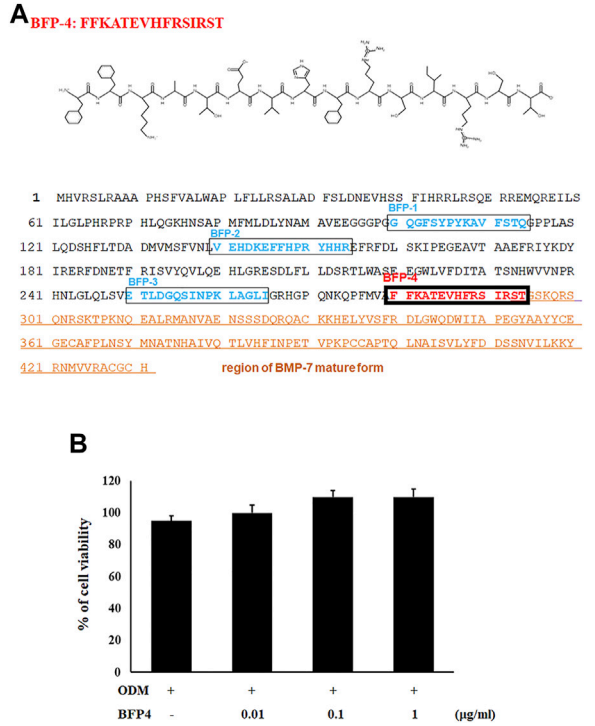

FIGURE 1 | Synthesis of BFP-4 peptide and cell viability. The peptide was synthesized by Fmoc solid-phase peptide synthesis using an automated peptide synthesizer and was purified by reverse-phase high-performance liquid chromatography. The molecular mass of the purified peptide was measured by liquid chromatography/mass spectroscopy **(A)**. BSCs were treated with BFP-4 (0.01 to 1 μg/ml) during the initial phase of osteogenic differentiation. The percentage of viable cells was analyzed by the MTT assay **(B)**. The result is representative of repeated three independent experiments.

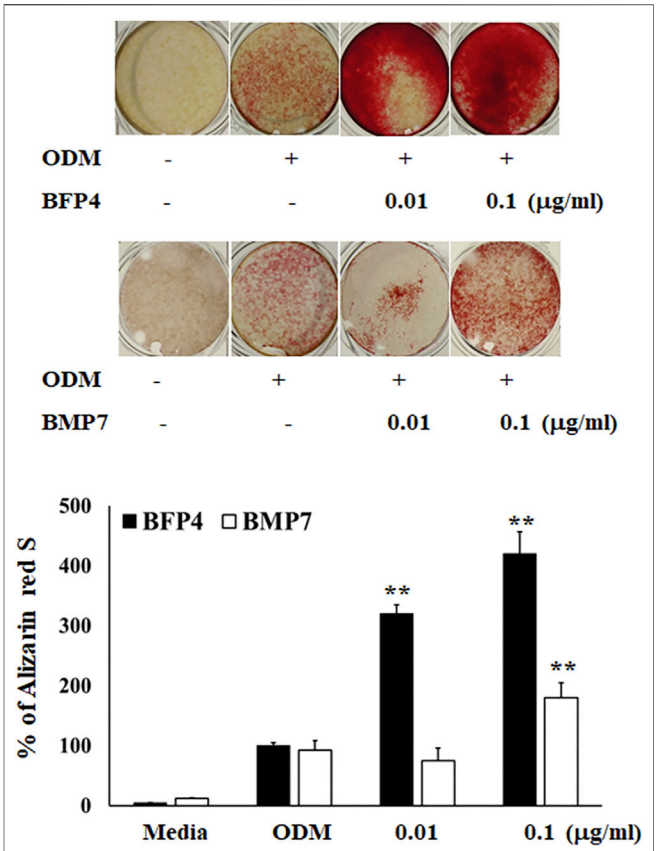

FIGURE 2 | BFP-4 induces osteogenic differentiation BMSCs were treated with a range of concentrations (0.01 and 0.1 μg/ml) of BFP-4 and BMP-7 during the initial phase of osteogenic differentiation and assessed by Alizarin red S staining. Images represent four independent experiments. The result is representative of repeated four independent experiments. Data are mean ± SD of three independent experiments. $^{**}p<0.01$ compared with the ODM control. Magnification, 20×.

differentiated BFP-4–treated and BMP-7–treated BMSCs were suspended in DMEM at a concentration of 1×10^6 cells/200 μl. Cells were implanted subcutaneously into the right flank of 6-week old male C57BL/6 mice and subjected to point projection digital radiography at 26kV for 3 s using a MX-20 digital microradiography system (Faxitron Bioptics, Lincolnshire, IL, United States). X-ray images were processed using Dicom Works software.

Statistical Analysis

Results are presented as means and standard deviation (SD). Data were analyzed by a one-way analysis of variance (ANOVA) followed by Duncan's post-hoc test using SPSS version 11.0 (Chicago, IL, United States). $p < 0.05$ was considered statistically significant.

RESULTS

Synthesis of BFP-4

We previously reported that the BFP series, which is derived from the immature region of BMP-7, is capable of osteogenic differentiation and bone-regeneration activity. Based on this finding, we focused on other potentially osteogenic peptide sequences in the immature region of BMP-7. We identified a new peptide with the sequence FFKATEVHFRSIRST (**Figure 1A**), which we called BFP-4. Therefore, we piloted various experiments to determine the osteogenic efficacy of BFP-4.

BFP-4 Induces Stronger Osteogenic Differentiation of BMSCs Than BMP-7

In the first experiment, we assessed the cytotoxicity of BFP-4 (**Figure 1B**) on multipotent BMSCs by an MTT assay. BFP-4 was not cytotoxic until 1 μg/ml. We next investigated how BFP-4 influences osteogenic differentiation of BMSCs compared with BMP-7. As shown in **Figure 2**, BFP-4 treatment induced greater osteogenic differentiation of BMSCs than BMP-7 treatment as observed by an Alizarin red S staining assay. Interestingly, treatment with 0.01 and 0.1 μg/ml BPF-4 showed a significantly higher osteogenic differentiation effect than the treatment with 0.01 and 0.1 μg/ml BMP-7. This suggests that BFP-4 could be used as an adjuvant in osteoporotic disease therapy instead of BMP-7.

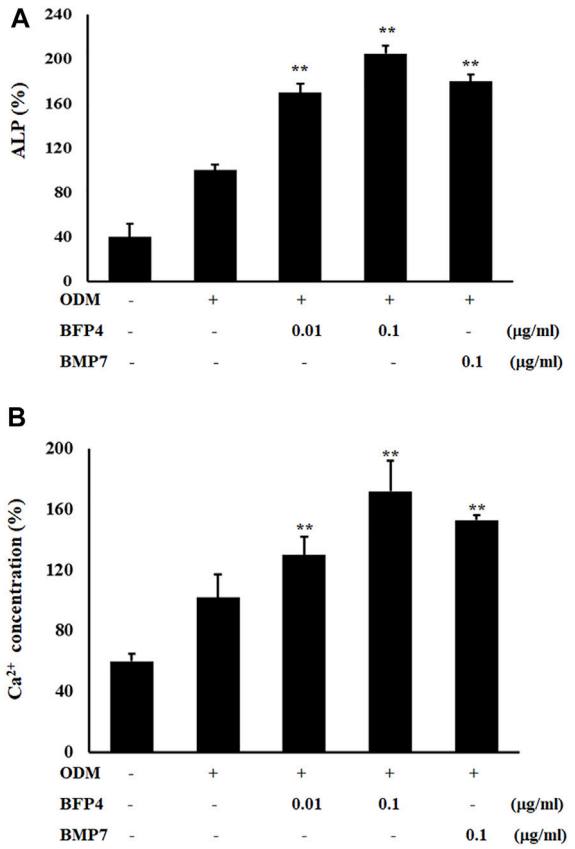

FIGURE 3 | Effect of ALP activity and Ca^{2+} concentration by BFP-4 treatment in BMSCs. Cells were treated with 0.01 or 0.1 μg/ml BFP-4, and 0.1 μg/ml BMP-7 for 24 h. ALP activity **(A)** and Ca^{2+} concentration **(B)** were quantitatively analyzed using a LabAssay™ ALP Assay kit and a calcium detection kit, respectively. Data are mean ± SD of four independent experiments. $^{**}p < 0.01$ compared with the ODM control.

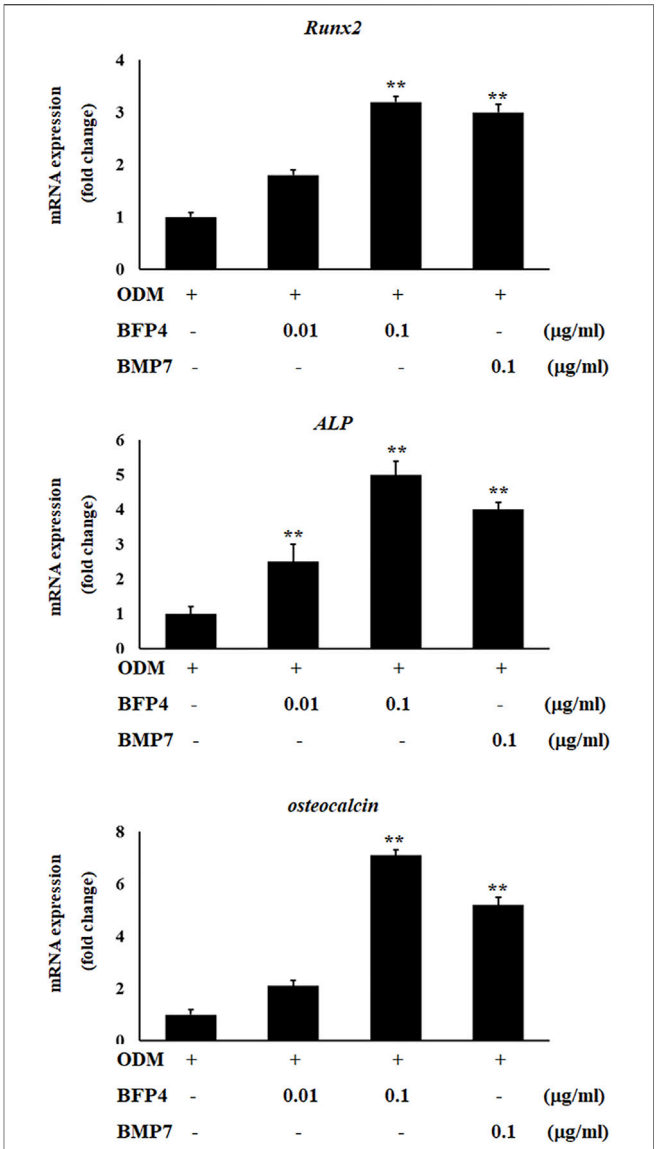

FIGURE 4 | Effect of *ALP, Runx2*, and *osteocalcin* expression by BFP-4 treatment in BMSCs. BMSCs were treated with 0.01–0.1 μg/ml of BFP-4 or 0.1 μg/ml of BMP-7 during osteogenic differentiation. Total RNA was isolated from media only (control) and from cells treated with ODM alone, ODM plus BMP-7, and ODM plus BFP-4. Expression levels were measured by Real-time PCR analysis. The result is representative of repeated three independent experiments. Experimental results were indicated as mean (± SD). $^{**}p < 0.01$ compared with the ODM control.

BFP-4 Induces Biomarkers of Osteogenic Activity

Increased ALP activity and calcium concentration are important biomarkers during osteogenic differentiation. Therefore, we investigated whether BFP-4 induces these osteogenic activity biomarkers in BMSCs. ALP activity and Ca^{2+} concentration were significantly increased by BFP-4 treatment in BMSCs (**Figures 3A,B**). We also determined the effect of BFP-4 on the expression of several genes involved in osteogenesis. Gene expression analysis showed that *ALP, osteocalcin*, and *Runx2* mRNA expression increased during osteogenic differentiation in BFP-4-stimulated cells compared with BMP-7-stimulated cells (**Figure 4**).

BFP-4 Induces CD44 and CD51 Expression in During Osteogenic Differentiation

Transmembrane proteins CD44 and CD51 play important roles in various stages of osteogenesis such as osteoblast proliferation and mineralization. To investigate whether BFP-4 induces expression of CD44 and CD51, we measured CD44 and CD51 expression in BFP-4-stimulated multipotent BMSCs by FACS and immunofluorescence analysis. As shown in **Figures 5A,B**, we found that BFP-4 significantly induced CD44 and CD51 expression in BMSCs. Taken together, these results suggest that the potential osteogenic effects of BFP-4 were manifested through the induction of osteogenic differentiation biomarkers including ALP activity, Ca^{2+} concentration, and the expression of *Runx2, osteocalcin, ALP*, CD44, and CD51.

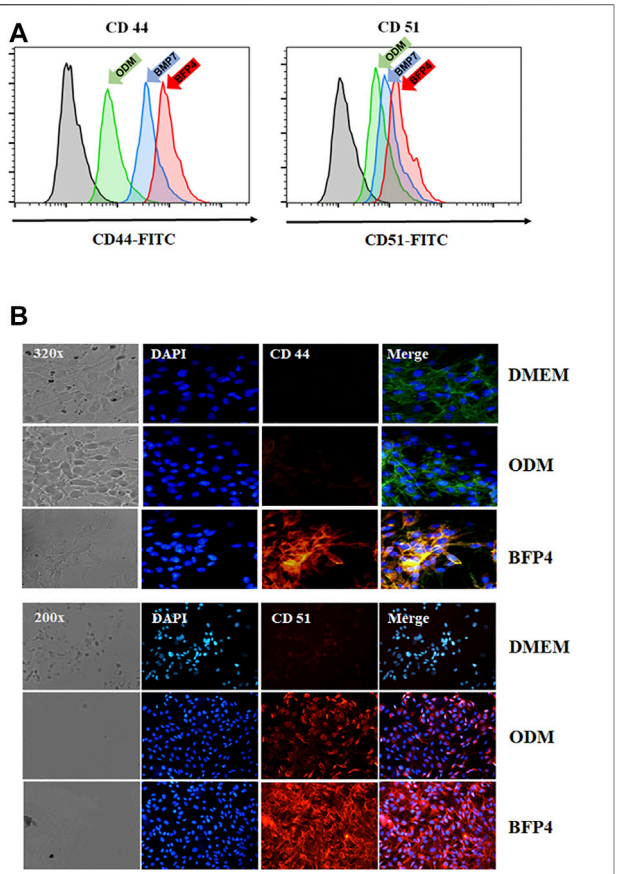

FIGURE 5 | Effect of CD44 and CD51 expression levels by BFP-4 treatment in BMSCs. BMSCs were treated with 0.1 μg/ml BFP-4. After 24 h, CD44 and CD51 expression were measured by flow cytometry (green arrow, ODM only; blue arrow, ODM plus BMP-7; pink arrow, ODM plus BFP4) **(A)**. Immunofluorescence analysis was conducted using anti-CD44 and anti-CD51 antibodies **(B)**. Data represent four independent experiments. Magnification, 400×.

BFP-4 Enhances Bone Formation in BFP-4-Treated BMSCs Transplanted Into Mice

VEGF is not only a factor regulating angiogenesis, but also plays critical roles in bone formation and repair (Hu and Olsen, 2016). BMPs have recently been reported to have angiogenic effects, which are important factors in osteogenesis and bone formation. For this reason, we determined the expression of vascular endothelial growth factor (VEGF) to verify that BFP-4 has an angiogenic effect. As shown in **Figure 6A**, BFP-4 induced VEGF expression in a dose-dependent manner.

Moreover, to determine the potential of BFP-4 for treatment of osteoporotic disease as a therapeutic adjuvant, we next investigated the comparative *in vivo* bone-forming activity of BFP-4 and BMP-7. As shown in **Figures 6A,B** slight bone formation within approximately 4 weeks was observed in the mice transplanted with the BFP-4-stimulated BMSCs, but not the BMP-7-stimulated BMSCs. In a radiography assay conducted 8 weeks after transplantation, BFP-4-stimulated BMSCs in mice had strongly increased bone formation

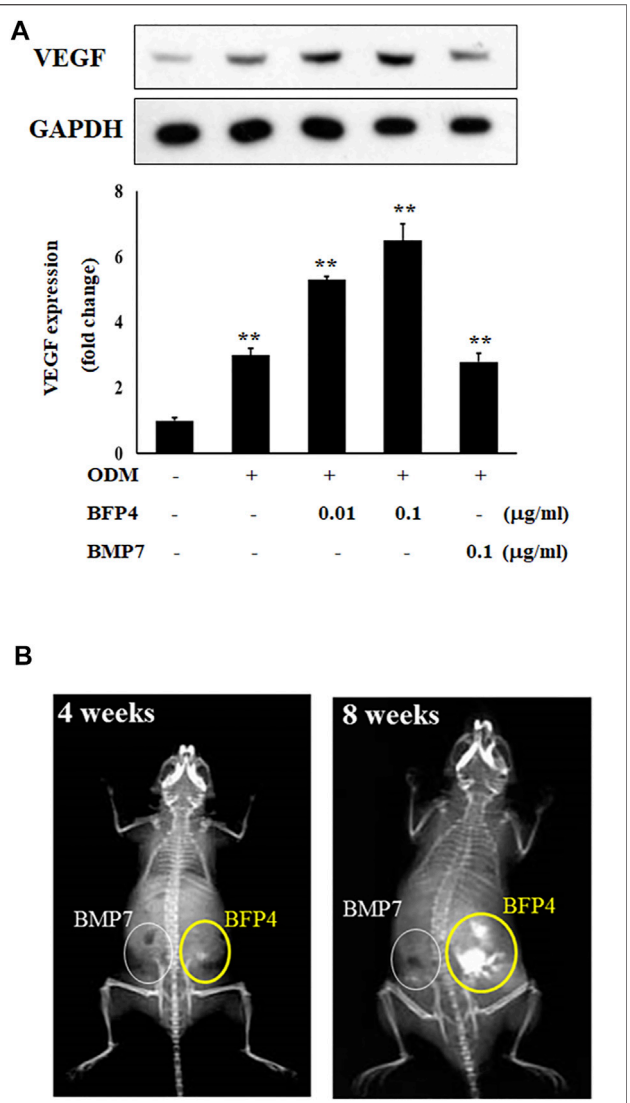

FIGURE 6 | BFP-4 induces VEGF expression and animal bone formation. BFP4-treated cells were lysed, and equal amounts of proteins were separated by SDS-PAGE and transferred to PVDF membranes. Membranes were probed with anti-VEGF and anti-GAPDH antibodies. GAPDH was used as the internal control **(A)**. BMP-7-stimulated and BFP-4-stimulated BMSCs were injected into the left and right flanks of 6-week-old male mice (n = 4 mice for each group). The concentrations of BMP-7 and BFP-4 were 0.1 μg/ml. All mice were examined by radiography at 4 and 8 weeks **(B)**. Data represent four independent experiments. $^{**}p < 0.01$ compared with the ODM control.

compared with BMP-7-stimulated BMSCs. Therefore, these results provide new evidence that BFP-4 may be more useful than BMP-7 as an inducer of osteogenesis for bone-related diseases.

DISCUSSION

BMP was revealed in the 1970s, and demonstrating that these proteins play an important role in osteogenesis and bone

formation (Aluganti Narasimhulu and Singla, 2020). Various types of BMPs have been discovered, and each BMP has been reported to have various functions. For example, BMP-2, −4, and −7 have the ability to induces osteogenesis and bone formation, whereas BMP-9 strongly inhibits angiogenesis. In general, BMP-7 is the most commonly known and used for bone formation and regeneration (Li et al., 2010). However, the development of materials related to bone formation and regeneration that are still excellent in efficacy and economical is still required.

The search for new substances that are more economical and effective than BMP-7 and elucidating the mechanisms by which they operate, are important for the development of new therapeutic adjuvants. Previous findings have indicated that mature BMPs are known to have osteogenic effects, but we discovered that BFP peptides of immature regions of BMPs have osteogenic and bone-formation potency. We previously reported on the osteogenic and bone formation efficacy of BFP-1, BFP-2, and BFP-3. The reason for finding these new peptides is to increase the efficiency of bone regeneration-related treatments as well as economic benefits. In the present study, we not only demonstrated the osteogenic efficacy of the newly-discovered BFP-4, but also provided evidence that it has greater bone-forming activity than BMP-7. Furthermore, BFPs, including BFP-4, induce greater osteogenic differentiation and bone formation at the same concentration as BMP-7. As shown in **Figure 6**, BFP-4-stimulated MSCs have been shown to significantly increase bone formation compared with BMP-7-stimulated BMSCs. Thus it has been demonstrated that BFP-4 is both more effective and more than BMP7.

BMSCs stimulated by BFP-1 and BFP-2 increased levels of ALP, CD44, and CD51 expression as well as Ca^{2+} concentration during osteogenic differentiation (Kim et al., 2012; Kim et al., 2017). Moreover, in the case of BFP-3, the efficacy and molecular mechanism of osteogenic differentiation were elucidated (Lee et al., 2018). It was previously confirmed that BFP-3 not only significantly increased the expression of *osterix* and *Runx2*, which are the major factors of osteogenesis, but also showed osteogenic effect in BMSCs through the regulation of the MAPK signaling pathway. In the present study, we found that BFP-4 induces ALP activity and increases Ca^{2+} concentration in BMSCs (**Figure 2**). We also determined that the expression of osteogenic factors such as *RUNX2, osteocalcin*, and *ALP* expressions were increased by BFP-4 treatment in BMSCs (**Figure 4**). In our previous studies as well as our present results, we found that activation of MAPK and NF-κB are important to osteogenesis by BFPs. From these results, bone formation effects on BFPs were confirmed, and specifics of each were identified. Moreover, it was confirmed that the efficacy of BFP-4 found in this study was also excellent. However, little is known about their target receptor or ligand, and that should be the subject of future research.

Moreover, in recent years, the demand for bone growth factors or accelerators to seed 3D scaffolds has increased, because they are used for tissue regeneration in various therapeutic fields. The regeneration of tissue such as cartilage and bone involves seeding cells into a customized polymer scaffold that provides a 3D environment to promote matrix production. Thus, tissue engineering offers the potential to grow osteoblasts quickly in an injectable form, and these injected cell-polymer constructs can ultimately result in the formation of bone-like structures (Chang et al., 2009). The development of various bone growth inducers such as BFP-4 is important because the differentiation efficacy of BMSCs (stimulated by the inducers) can be demonstrated and applied in 3D scaffold tissue engineering technology to help treat various bone-related diseases. Angiogenesis is also important in bone formation, and the angiogenic effect of BMPs has recently been reported. For example, BMP-2 induces angiogenesis in human endothelial progenitor cells (Chen et al., 2018) and bone regeneration (Yang L. et al., 2018). As described above, various BMP proteins have been reported to have angiogenic effects, and are therefore potentially important therapeutic agents. As shown in **Figure 6**, we found that BFP-4 induces VEGF expression in a dose-dependent manner. Therefore, our results indicated that BFP-4 is an optimal factor for inducing bone formation. In this respect, we believe that the use of peptides is efficient because their synthesis is simple, easy to manipulate, and economical compared to proteins. Although BFPs suggests the possibility of use as a material for bone formation in terms of efficiency and economy, studies on their affinity with receptors or other proteins are needed.

In conclusion, the present study demonstrates that BFP-4 induced greater osteogenic differentiation of BMSCs than BMP-7, both *in vitro* and *in vivo*, and stimulated greater expression of biological markers of osteogenesis than BMP-7. Also, we found that BFP-4 markedly promoted bone formation and also increased the expression of VEGF. Therefore, these results provide new insights into the possible use of BFP-4 as an osteogenic stimulator instead of BMP-7 in clinical trials of bone-related tissue engineering.

DATA AVAILABILITY STATEMENT

The dataset used and/or analyzed during the current study are available from corresponding author on reasonable request.

ETHICS STATEMENT

The animal study was reviewed and approved by the Animal Care and Use Committee of Chonnam National University.

AUTHOR CONTRIBUTIONS

MK, JS, HK, and JL conceived and designed the experiments; MK, JK, and TY performed experiments and analyzed the data. HK and JL wrote the paper.

FUNDING

This research was supported by the National Research Foundation of Korea (NRF) grant (Nos. 2017R1A2B4008676, 2018R1D1A1B07048920, NRF-2016M3A9E9941832, and NRF-2020R1A2C1012984).

REFERENCES

Aluganti Narasimhulu, C., and Singla, D. K. (2020). The Role of Bone Morphogenetic Protein 7 (BMP-7) in Inflammation in Heart Diseases. *Cells* 9 2, 280. doi:10.3390/cells9020280

Chang, S. C.-N., Tai, C.-L., Chung, H.-Y., Lin, T.-M., and Jeng, L.-B. (2009). Bone Marrow Mesenchymal Stem Cells Form Ectopic Woven Bone *In Vivo* through Endochondral Bone Formation. *Artif. Organs* 33, 301–308. doi:10.1111/j.1525-1594.2009.00728.x

Chen, W.-C., Chung, C.-H., Lu, Y.-C., Wu, M.-H., Chou, P.-H., Yen, J.-Y., et al. (2018). BMP-2 Induces Angiogenesis by Provoking Integrin α6 Expression in Human Endothelial Progenitor Cells. *Biochem. Pharmacol.* 150, 256–266. doi:10.1016/j.bcp.2018.02.021

Douglas, T. E. L., Vandrovcová, M., Kročilová, N., Keppler, J. K., Zárubová, J., Skirtach, A. G., et al. (2018). Application of Whey Protein Isolate in Bone Regeneration: Effects on Growth and Osteogenic Differentiation of Bone-Forming Cells. *J. Dairy Sci.* 101, 28–36. doi:10.3168/jds.2017-13119

Florencio-Silva, R., Sasso, G. R., Sasso-Cerri, E., Simões, M. J., and Cerri, P. S. (2015). Biology of Bone Tissue: Structure, Function, and Factors that Influence Bone Cells. *Biomed. Res. Int.* 2015, 421746. doi:10.1155/2015/421746

Geng, W., Shi, H., Zhang, X., Tan, W., Cao, Y., and Mei, R. (2019). Substance P Enhances BMSC Osteogenic Differentiation via Autophagic Activation. *Mol. Med. Rep.* 20, 664–670. doi:10.3892/mmr.2019.10257

Hamamura, K., Hamajima, K., Yo, S., Mishima, Y., Furukawa, K., Uchikawa, M., et al. (2019). Deletion of Gb3 Synthase in Mice Resulted in the Attenuation of Bone Formation via Decrease in Osteoblasts. *Int. J. Mol. Sci.* 20. doi:10.3390/ijms20184619

Han, Y., You, X., Xing, W., Zhang, Z., and Zou, W. (2018). Paracrine and Endocrine Actions of Bone-The Functions of Secretory Proteins from Osteoblasts, Osteocytes, and Osteoclasts. *Bone Res.* 6, 16. doi:10.1038/s41413-018-0019-6

Hu, K., and Olsen, B. R. (2016). Osteoblast-derived VEGF Regulates Osteoblast Differentiation and Bone Formation during Bone Repair. *J. Clin. Invest.* 126, 509–526. doi:10.1172/jci82585

Kim, B., Lee, J.-H., Jin, W. J., Kim, H.-H., Ha, H., and Lee, Z. H. (2018). Trapidil Induces Osteogenesis by Upregulating the Signaling of Bone Morphogenetic Proteins. *Cell Signal.* 49, 68–78. doi:10.1016/j.cellsig.2018.06.001

Kim, H. K., Kim, J. H., Park, D. S., Park, K. S., Kang, S. S., Lee, J. S., et al. (2012). Osteogenesis Induced by a Bone Forming Peptide from the Prodomain Region of BMP-7. *Biomaterials* 33, 7057–7063. doi:10.1016/j.biomaterials.2012.06.036

Kim, H. K., Lee, J. S., Kim, J. H., Seon, J. K., Park, K. S., Jeong, M. H., et al. (2017). Bone-forming Peptide-2 Derived from BMP-7 Enhances Osteoblast Differentiation from Multipotent Bone Marrow Stromal Cells and Bone Formation. *Exp. Mol. Med.* 49, e328. doi:10.1038/emm.2017.40

Kumar, G., and Roger, P. M. (2019). From Crosstalk between Immune and Bone Cells to Bone Erosion in Infection. *Int. J. Mol. Sci.* 20. doi:10.3390/ijms20205154

Lee, J. S., Kim, M. E., Seon, J. K., Kang, J. Y., Yoon, T. R., Park, Y.-D., et al. (2018). Bone-forming Peptide-3 Induces Osteogenic Differentiation of Bone Marrow Stromal Cells via Regulation of the ERK1/2 and Smad1/5/8 Pathways. *Stem Cel Res.* 26, 28–35. doi:10.1016/j.scr.2017.11.016

Lerner, U. H., Kindstedt, E., and Lundberg, P. (2019). The Critical Interplay between Bone Resorbing and Bone Forming Cells. *J. Clin. Periodontol.* 46 (Suppl. 21), 33–51. doi:10.1111/jcpe.13051

Li, J., Li, Y., Ma, S., Gao, Y., Zuo, Y., and Hu, J. (2010). Enhancement of Bone Formation by BMP-7 Transduced MSCs on Biomimetic Nano-Hydroxyapatite/polyamide Composite Scaffolds in Repair of Mandibular Defects. *J. Biomed. Mater. Res.* 95A, 973–981. doi:10.1002/jbm.a.32926

Owen, R., and Reilly, G. C. (2018). *In Vitro* Models of Bone Remodelling and Associated Disorders. *Front. Bioeng. Biotechnol.* 6, 134. doi:10.3389/fbioe.2018.00134

Sangadala, S., Devereaux, E. J., Presciutti, S. M., Boden, S. D., and Willet, N. J. (2019). FK506 Induces Ligand-independent Activation of the Bone Morphogenetic Protein Pathway and Osteogenesis. *Int. J. Mol. Sci.* 20, 1900. doi:10.3390/ijms20081900

Shen, B., Wei, A., Whittaker, S., Williams, L. A., Tao, H., Ma, D. D., et al. (2010). The Role of BMP-7 in Chondrogenic and Osteogenic Differentiation of Human Bone Marrow Multipotent Mesenchymal Stromal Cells *In Vitro*. *J. Cel Biochem* 109, 406–416. doi:10.1002/jcb.22412

Veselá, B., Švandová, E., Bobek, J., Lesot, H., and Matalová, E. (2019). Osteogenic and Angiogenic Profiles of Mandibular Bone-Forming Cells. *Front. Physiol.* 10, 124. doi:10.3389/fphys.2019.00124

Yang, F., Xue, F., Guan, J., Zhang, Z., Yin, J., and Kang, Q. (2018a). Stromal-Cell-Derived Factor (SDF) 1-Alpha Overexpression Promotes Bone Regeneration by Osteogenesis and Angiogenesis in Osteonecrosis of the Femoral Head. *Cell Physiol Biochem* 46, 2561–2575. doi:10.1159/000489684

Yang, L., Wang, S., Zhang, Q., Pan, Y., Lv, Y., Chen, X., et al. (2018b). Clinical Significance of the Immune Microenvironment in Ovarian Cancer Patients. *Mol. Omics* 14, 341–351. doi:10.1039/c8mo00128f

Yin, X., Zhou, C., Li, J., Liu, R., Shi, B., Yuan, Q., et al. (2019). Autophagy in Bone Homeostasis and the Onset of Osteoporosis. *Bone Res.* 7, 28. doi:10.1038/s41413-019-0058-7

Conflict of Interest: The authors declare that the research was conducted in the absence of any commercial or financial relationships that could be construed as a potential conflict of interest.

Publisher's Note: All claims expressed in this article are solely those of the authors and do not necessarily represent those of their affiliated organizations, or those of the publisher, the editors and the reviewers. Any product that may be evaluated in this article, or claim that may be made by its manufacturer, is not guaranteed or endorsed by the publisher.

frontiers in Bioengineering and Biotechnology

ORIGINAL RESEARCH
published: 18 October 2021
doi: 10.3389/fbioe.2021.737132

Magnetic Nanoparticles and Magnetic Field Exposure Enhances Chondrogenesis of Human Adipose Derived Mesenchymal Stem Cells But Not of Wharton Jelly Mesenchymal Stem Cells

Luminita Labusca[1,2], Dumitru-Daniel Herea[1], Anca Emanuela Minuti[1,3], Cristina Stavila[1,3], Camelia Danceanu[1,3], Petru Plamadeala[4], Horia Chiriac[1] and Nicoleta Lupu[1]*

[1]National Institute of Research and Development for Technical Physics, Iasi, Romania, [2]Orthopedics and Traumatology Clinic County Emergency Hospital Saint Spiridon, Iasi, Romania, [3]Faculty of Physics, Alexandru Ioan Cuza University, Iasi, Romania, [4]Pathology Department County Children Emergency Hospital Saint Mary, Iasi, Romania

OPEN ACCESS

Edited by:
Laura Creemers,
University Medical Center Utrecht,
Netherlands

Reviewed by:
Kar Wey Yong,
University of Alberta, Canada
ZuFu Lu,
The University of Sydney, Australia

***Correspondence:**
Dumitru-Daniel Herea
dherea@phys-iasi.ro

Specialty section:
This article was submitted to Tissue Engineering and Regenerative Medicine, a section of the journal Frontiers in Bioengineering and Biotechnology

Received: *06 July 2021*
Accepted: *10 September 2021*
Published: *18 October 2021*

Citation:
Labusca L, Herea D-D, Emanuela Minuti A, Stavila C, Danceanu C, Plamadeala P, Chiriac H and Lupu N (2021) Magnetic Nanoparticles and Magnetic Field Exposure Enhances Chondrogenesis of Human Adipose Derived Mesenchymal Stem Cells But Not of Wharton Jelly Mesenchymal Stem Cells. Front. Bioeng. Biotechnol. 9:737132. doi: 10.3389/fbioe.2021.737132

Purpose: Iron oxide based magnetic nanoparticles (MNP) are versatile tools in biology and medicine. Adipose derived mesenchymal stem cells (ADSC) and Wharton Jelly mesenchymal stem cells (WJMSC) are currently tested in different strategies for regenerative regenerative medicine (RM) purposes. Their superiority compared to other mesenchymal stem cell consists in larger availability, and superior proliferative and differentiation potential. Magnetic field (MF) exposure of MNP-loaded ADSC has been proposed as a method to deliver mechanical stimulation for increasing conversion to musculoskeletal lineages. In this study, we investigated comparatively chondrogenic conversion of ADSC-MNP and WJMSC with or without MF exposure in order to identify the most appropriate cell source and differentiation protocol for future cartilage engineering strategies.

Methods: Human primary ADSC and WJMSC from various donors were loaded with proprietary uncoated MNP. The *in vitro* effect on proliferation and cellular senescence (beta galactosidase assay) in long term culture was assessed. *In vitro* chondrogenic differentiation in pellet culture system, with or without MF exposure, was assessed using pellet histology (Safranin O staining) as well as quantitative evaluation of glycosaminoglycan (GAG) deposition per cell.

Results: ADSC-MNP complexes displayed superior proliferative capability and decreased senescence after long term (28 days) culture *in vitro* compared to non-loaded ADSC and to WJMSC-MNP. Significant increase in chondrogenesis conversion in terms of GAG/cell ratio could be observed in ADSC-MNP. MF exposure increased glycosaminoglycan deposition in MNP-loaded ADSC, but not in WJMSC.

Conclusion: ADSC-MNP display decreased cellular senescence and superior chondrogenic capability *in vitro* compared to non-loaded cells as well as to WJMSC-

MNP. MF exposure further increases ADSC-MNP chondrogenesis in ADSC, but not in WJMSC. Loading ADSC with MNP can derive a successful procedure for obtaining improved chondrogenesis in ADSC. Further *in vivo* studies are needed to confirm the utility of ADSC-MNP complexes for cartilage engineering.

Keywords: adipose derived stem cells, wharton jelly mesenchymal stem cells, magnetic nanoparticles, magnetic field, chondrogenesis, adipose derived mesenchymal stem cell

INTRODUCTION

Musculoskeletal diseases are an increasing burden worldwide and a principal cause of persistent pain and disability. Among them, the incidence of degenerative joint diseases (DJD), mainly of osteochondral defects (OD) and osteoarthritis (OA) is on the rise, affecting hundreds of millions of people worldwide (Kloppenburg and Berenbaum, 2020). Ageing population, sedentary life style but as well increased occurrence of traumatic injuries due to traffic accidents, war casualties or natural disasters have been implicated in DJD. Their impact is even more dramatic due to the fact that such lesions do not heal and have as consequences permanent disabilities and reduced quality of life. In addition, DJD is getting "younger", 16–17% of adults below 40 and up to 60% of adults of 40–65 years of age are reported to having various forms of the disease (Merkely et al., 2018). Current therapies are mainly symptomatic, failing to offer effective joint anatomical and functional rehabilitation. Total joint replacement still represents the ultimate method for treating DJD-induced joint deterioration. Regenerative therapies promise to deliver biological restauration of joint surface and to offer permanent and durable anatomical and functional recovery. Despite more than 30 years of basic and translational research in the field, current available products for joint resurfacing are failing to deliver consistent disease modifying therapeutic solutions. The most appropriate cell source for cartilage bioengineering is still under debate. ADSC are extensively investigated for their use as cell sources in regenerative medicine (RM) (Zizhen et al., 2019; Lima et al., 2015). ADSC are relatively easy to extract by means of enzymatic or mechanical methods from the adipose tissue derived from elective cosmetic procedures. ADSC are available as both autologous and allogeneic sources, can derive larger number of elements per tissue volume (Si et al., 2019) and possess superior proliferative and immunomodulatory capabilities compared with other mesenchymal stem cell sources (Ceccarelli et al., 2020) and could be an attractive modality to generate functional implantable tissue for the treatment of cartilage defects (Rahbar Saadat et al., 2020). However, the efficiency of chondrogenic conversion has proved not to equalize other ADSC sources (such as bone marrow or cord blood) (Wei et al., 2007). Derived from perinatal tissues (namely umbilical cord), Wharton Jelly is as a rich source of allogeneic MSCs with superior proliferative and immunomodulatory capabilities (Esposito et al., 2013). Chondrogenic conversion of Wharton jelly-derived mesenchymal stem cells (WJMSC) was shown to be superior to bone marrow mesenchymal stem cells (BM ADSC). Mechanic stimulation of ADSC was shown to increases differentiation to musculoskeletal lineages (bone, cartilage, skeletal muscle) and efficiently increased ADSC as well as WJMSC chondrogenic potential *in vitro* and *in vivo* (Zha et al., 2021). Previous studies have shown that different types of mechanical loading (such as compression, perfusion, vibration, stretching) are effective in increasing ADSC differentiation (Yong et al., 2020). Delivering the appropriate micro-mechanical stimulation that closely mimic the intensity, duration and orientation of mechanical cues in the developmental niche, at cellular level, has proved to be a challenge for musculoskeletal tissue engineering. Mechanical stem cell preconditioning using biophysical stimulation by applying various types of mechanical stress within dynamic bioreactors (compression, shear stress, and hydrostatic pressure) requires ancillary equipment and often a direct contact with the cells or cell media. This introduces supplementary steps in the process of cell manufacturing when intending clinical application. Moreover, at a cellular level, the distribution of applied forces might be uneven with consequences on quality and reproducibility of chondrogenic conversion (Fahy et al., 2018). Alongside with the perspective of introducing a method that waves the need of supplementary equipment, magneto-mechanical stimulation delivers biomechanical cues at a cellular level, more closely reproducing the natural biomechanics. In plus, the enhancement of the chondrogenic differentiation obtained within a magnetic field has also been demonstrated to having a synergistic effect with biochemical factors delivered by differentiation media resulting in an enhanced chondrogenic differentiation (Amin et al., 2014). The use of MNPs of various structures and coatings has been previously found appealing for regenerative medicine purposes when sought as drug and small molecule delivery vehicles as they have the potential to support regenerative processes *in vitro* and *in vivo* as well as for cell tracking and targeting purposes. Nanoparticle-based manipulation of cell and stem cell fate are recognized as the breakout technology capable to consistently contribute to advancement of biological joint resurfacing toward clinical application (Eftekhari et al., 2020). MNP are particularly appealing for manipulating cell fate due to their excellent biocompatibility, versatility and magnetic proprieties (Wimpenny et al., 2012). Of particular interest when using MNP is the ability to use magnetic actuation as a modality to deliver micromechanical stimulation to differentiating cells (Zhang et al., 2020). Mechanical stimulation consistently increase chondrogenic conversion in ADSC. However, the modality to deliver mechanical preconditioning are difficult to translate for potential clinical applications (O'Conor et al., 2013). Iron oxide MNP internalized by ADSC preserve their proliferative and differentiation capability while inducing cell

magnetization. This is opening fascinating possibilities for remote cell manipulation under magnetic field (MF) aiming for MNP mediated cell actuation. Such particularity can be used as a modality to deliver remote micromechanical stimulation to stem cells differentiating to musculoskeletal lineages—osteoblasts and chondrocytes (Lima et al., 2015).

Due to their magnetic responsiveness, cells loaded with MNP can be traced within living systems using clinically available MRI imagistic equipment or incoming magnetic particle imaging technologies. The magneto-mechanical effect adds to this already versatile stem cell-MNP functionality the ability to potentially control cell fate by improving differentiation to mechanosensitive lineages, especially those required for musculoskeletal regeneration. In our previous studies we have tested the effect of proprietary uncoated MNP in influencing osteogenesis and adipogenesis and found that magneto-mechanical stimulation increase osteogenesis and decrease adipogenesis in primary ADSC. Here we aimed to test comparatively the effect of magneto-mechanical stimulation in human primary ADSC and WJMSC chondrogenesis. The purpose was to test if MNP we are manufacturing can be used as a modality to deliver magneto-mechanical stimulation to stem cells undergoing chondrogenic differentiation *in vitro* and to identify the most appropriate cell source aiming future cartilage engineering strategies.

Remote magnetic actuation of ADSC and WJMSC, with or without MNP, in alternating magnetic field (MF) was investigated as a modality to deliver mechanical stimulation. Its effect on chondrogenic conversion was assessed quantitatively in order to detect the most appropriate cell source for cartilage engineering purposes.

METHODS

MNP Manufacturing and Characterization

MNP. Reagents used for obtaining Fe_3O_4 magnetite MNP were ferrous chloride tetra hydrate ($FeCl_2{\cdot}4H_2O$, 98%), ferric chloride hexahydrate ($FeCl_3{\cdot}6H_2O$, 98%), sodium hydroxide (NaOH, 98%) and hydrochloric acid (HCl, 37%) (Sigma-Aldrich). The reagents were used as purchased, without any further purification.

The MNP synthesis followed an in-house modified hydrothermal approach as previously reported for this study. 2.2 g $FeCl_2{\cdot}4H_2O$ were dissolved in 4 ml deionized water (DW) and mixed with 6 g $FeCl_3{\cdot}6H_2O$. After filtering through a 220 nm filter, the iron salt solution was mixed with 1 ml HCl and added into 200 ml boiling DW. After mixing with solid NaOH (15 g) under magnetic stirring (1,300 rpm), the solution turned immediately black. The solution was further mixed for 30 min (1,000 rpm), whereas the heating was turned off. MNP were magnetically separated and submitted to several washing steps until the pH of the suspension reached 6.5.

Magnetic characterization. The magnetization data were acquired using vibrating sample magnetometer (VSM) (LakeShore 7410) in magnetic fields ranging between −20 and 20 kOe for both bare MNP and WJMSC/ADSC MNP. The morphology and size of MNP was determined through transmission electron microscopy (TEM) (Libra 200 UHR-TEM, Carl Zeiss, Germany). Assessment of the Zeta potential was performed with Malvern Zetasizer NS (Malvern Instruments).

Human Primary Adipose Derived Stem Cells

Human primary ADSC were obtained from healthy donors undergoing elective cosmetic liposuction procedures after institutional ethical approval and informed patient consent. Lipoaspirate was processed within maximum 24 h after surgical procedure (average 3 h) as previously described (Labusca et al., 2018). Briefly, lipoaspirate was washed with PBS, digested with collagenase type I (0.01 mg/ml) for 2 h at 37.5°C, and centrifuged at 300 g for 5 min at room temperature. The supernatant was removed and the medium further centrifuged at 300 g for 5 min. Pelleted cells were re-suspended in complete culture media (CCM) (DMEM, 10% FBS, 2% Antibiotic/antimycotic). Cells were automated counted (TC20™ Automated Cell Counter, Bio-Rad Hungary Ltd.) and plated at 1×10^6 cells/cm^2 in tissue culture flasks (CellBIND surface, Corning). Passage three to four cells were used for experiments. For morphology evaluation, the cells were observed under a fluorescent inverted microscope (EVOS Fl Life Technologies).

Human Primary Wharton Jelly Mesenchymal Stem Cells

Umbilical cord from healthy parturient at term birth was collected after signed informed consent and transported to the laboratory in the first 4 h after delivery. Wharton Jelly was carefully dissected from blood vessels, washed with antibiotic solution, minced with a scalpel in pieces of 1–1.5 mm width, placed in six well plates in complete culture media and kept in the incubator. After 5–7 days, the explanted cells were removed using Trypsin/EDTA and re-plated in appropriate tissue culture flasks. Cells passage two to four were used in the experiments for this study.

ADSC and WJMSC Loading With MNP, Viability and Proliferation

For cytotoxicity assays, ADSC and WJMSC were plated in 96 well plates, at 2×10^4 cells/well and incubated for 48 h. MNP in concentration of 40 µg/ml were added to complete culture media and further incubated for 24 h. MNP suspension was delivered once for all cell types and all experiments without any further addition. Cell viability tests were performed using MTT (5-dimethylthiazol-2-yl-2, 5-diphenyltetrazolium bromide-Vibrant ®TermoFisher Scientific) assay according to supplier's instructions. Absorbance was read at 570 nm. Cell viability (CV) as expressed by MTT optical density (OD) was calculated using the formula CV = 100 × (ODs-ODb)/(ODc-ODb), where ODs = OD of particle treated cells; ODb = OD of blank (media only); ODc = OD of untreated cells. Cell viability and proliferation was investigated at three time points (2, 5 and

10 days) using MTT as well as cell counting after fixation with 80% ethanol and nuclear staining with 4′,6-diamidino-2-phenylindole (DAPI) Termofisher Scientific) 0.1 μg/ml for 5 min, washed twice. Cell count/well 10) was performed using a fluorescent microscope and a grid using the formula X = 2*A/(L*L)*N where A is the surface of the well, L is the size of one square in the grid, N the number of cells per field of view (FOV). Averaged count for at least five FOV were counted/experiment. Cell proliferation expressed as population doubling (PD) was calculated using the formula PDn= [LOG (Nn)-LOG (N0)]/LOG (2) where, N is the number of cells counted at the end of each interval, n represent the time point (day 2, 7 and 14 of cell culture) and N0 number of viable plated cells.

Quantitative Assessment of MNP Content - Ferrozine Assay

ADSC and WJMSC were plated in 24 well plates at 1×10^5 cells/well. MNP were added after 24 h, and the experiments were performed in four replicates. At 1, 7, 14 and 28 days of cell-particle interaction, respectively, the cells were double washed with PBS to remove any extracellular MNP, fixed with 70% ethanol for 15 min and double washed with PBS. 500 μL of 50 nM NaOH were added to three wells per experiment for 2 h on a shaking plate. Aliquots of cell lysates were then transferred to 1.5 ml Eppendorf tubes and mixed with 500 μL of 10 mM HCl, and 500 μL of iron-releasing reagent (a freshly mixed solution of equal volumes of 1.4 M HCl and 4.5% (w/v) KMnO4 (Merck, Germany) in distilled H2O. These mixtures were incubated for 2 h at 60°C within a fume hood. 150 μL of iron-detection reagent (6.5 mM ferrozine (Sigma-Aldrich, St Louis, United States), 6.5 mM neocuproine (Sigma-Aldrich), 2.5 M ammonium acetate and 1 M ascorbic acid (Sigma-Aldrich) dissolved in water) were added to each tube. After 30 min, 500 μL of the solution obtained in each tube was transferred into a well of a 24-well plate, and absorbance was measured at 570 nm with a spectrophotometer. A calibration curve was set up using $FeCl_3$ standards (0–300 μM) in 10 mM HCl to allow calculation of iron content per sample.

Cell Senescence

ADSC, WJMSC, ADSC-MNP and WJMSC were seeded in 24 well plates at 4×10^5cells/well. Beta galactosidase enzyme activity was assessed using β-galactosidase (B-Gal) Detection Kit (Fluorometric) (Abcam) accordingly to manufacturer instructions. Briefly, cells at 14 and 28 days of culture were lysed using lysis buffer, afterwards Fluorescein di-β-D-Galactopyranoside (FDG) stock solution was added to each well and incubated for 1 hour at 37°C, treated with stop buffer solution to increased FDG fluorescence intensity and read using a microplate reader (490–550 nm excitation/emission). Cell number was calculated at each time point as described for ferrozine assay.

Assessment of ADSC and WJMSC Cytoskeleton Fibers in Magnetic Field

2×10^5 cells (passage 3–5) were plated in 35 mm Petri dishes in DMEM with 10% FBS. After 24 h, cells were treated with 40 μg/ml MNP and further cultivated for 24 h. For generation of magnetic field, we used an in house-built system based on four crossed coils programmed to generate a rotating magnetic field (MF) as previously described (Chiriac et al., 2018). ADSC and WJMSC with or without MNP were exposed to MF for 20 min; cells were fixed with 2% paraformaldehide for 15 min, stained with phalloidin (Texas Red™-X PhalloidinTermo Fischer Scientific) and counterstained with DAPI Images were taken using a fluorescent inverted microscope (EVOS Life Technologies).

Chondrogenesis

For *chondrogenesis assays*, 9×10^5 ADSC, WJMSC, ADSC-MNP and WJMSC-MNP were pelleted in incomplete chondrogenic media (ICM) composed of - DMEM (high glucose -HG), Dexamethasone 1mM, Ascorbic acid 2-P: 5 mg/ml L-Proline: 4 mg/ml ITS + supplement Sodium pyruvate). After pelleting, ICM was changed with complete chondrogenic media (ICM plus TGFβ-3 10 ng/ml). Chondrogenic pellets were kept in 15 ml polypropylene tubes in incubator and fed twice/week for 21 days.

Assessment of chondrogenesis. After 21 days, pellets were fixed in 10% formaline solution for 30 min, washed twice with PBS and embedded in paraffin for histological evaluation. Sections were stained with Safranine O 0.1 ml/L. For quantitative chondrogenesis evaluation, pellets were digested using papain and total amount of GAG glycozaminoglycans content was assessed using chondroitin-6-sulphate DMMB (1, 9 Dimethylmethylene blue) method. DMMB absorbance was read using a microplate reader. The results were normalized against pellet total DNA content obtained QuantiTPico Green dsDNA kit (Invitrogen).

ADSC and WJMSC Differentiation in Magnetic Field

Test tubes with chondrogenic pellets were positioned in the center of the coil and subjected to alternating MF for 10 min every 2 h in the first 7 days after chondrogenic induction, Temperature of the samples was measured using an optical fiber thermometer. Non exposed controls were kept in the incubator.

Statistical analysis. Cells from four donors were used in this study. At least 5 technical replicates were used in each experiment per donor. One way analysis of variance (ANOVA) was performed using OriginLab PRO version 9.0 followed by Bonferroni post hoc analysis; between-group and within group differences that were considered significant at $p \leq 0.05$ ($n = 5$).

RESULTS

Magnetic Nanoparticle Characterization

High-resolution TEM (HRTEM) imaging have shown MNP with dimensions ranging between 10 and 15 nm with a fine size distribution. MNP are shown to having different shapes such as cubic, octahedral, or spherical (**Figure 1A**).

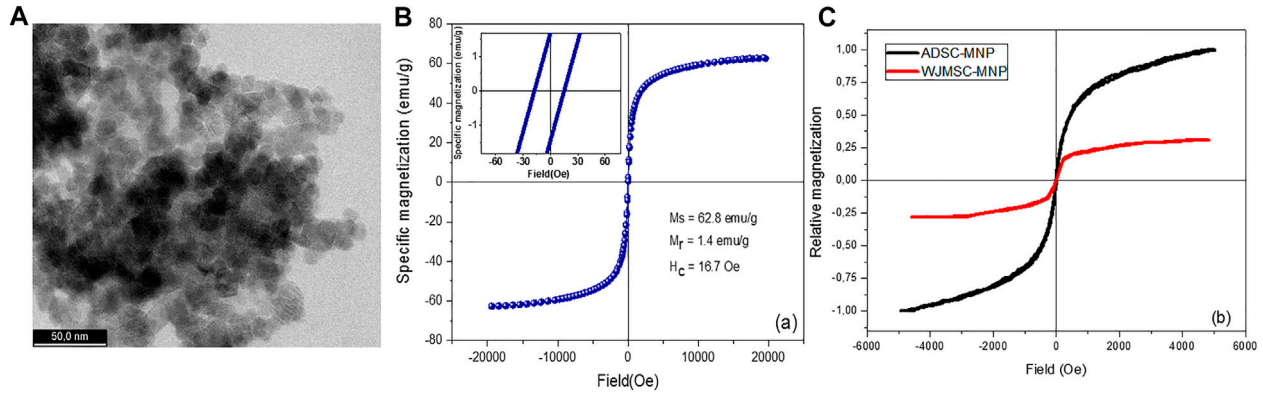

FIGURE 1 | Ultra-high resolution transmission electron microscopy (UHR-TEM) demonstrating the size of Fe_3O_4 nanoparticles **(A)**; magnetization loop of bare magnetite nanoparticles [**(B)**-inset: details from the low-field region]; magnetization loops of WJMSC and ADSC loaded with magnetite nanoparticles **(C)**.

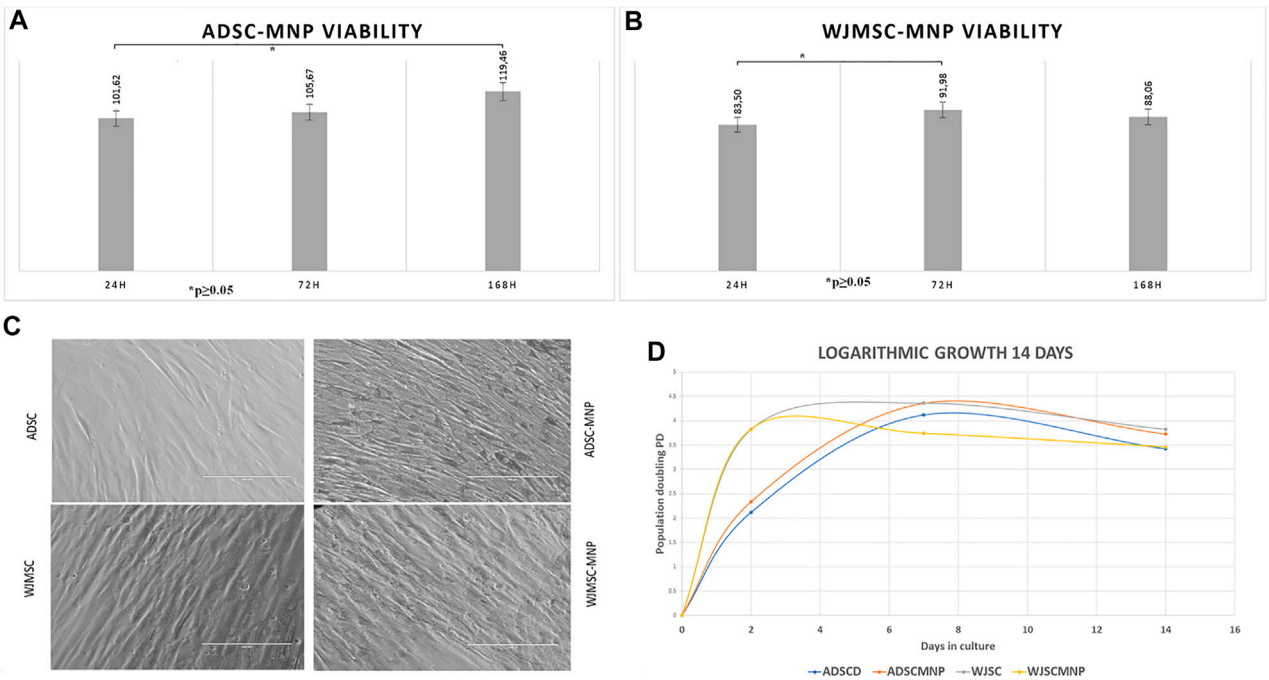

FIGURE 2 | Long term viability in culture MTT assay for cells exposed to 40 μm/ml Fe_3O_4 bare MNP added in the cell culture media; ADSC demonstrate significant increase in MTT activity at 7 days (168 h) compared to 24 h: at all time points viability is more than 100% of non-loaded cells demonstrating good overall viability and lack of MNP cytotoxicity **(A)** WJMSC viability has a minimum at 24 h cell particle interaction increase at 72 h compared to 24 h, slightly decreases at 7 days demonstrating acceptable viability and MNP toxicity **(B)**; morphological evaluation of ADSC-MNP compared to ADSC and WJMSC compared to WJMSC-MNP after 48 h cell particle interaction demonstrating maintenance of cell shape, apparent membrane integrity and even distribution of MNP inside cell body without penetrating nuclei with visible higher amount of incorporated MNP for ADSC-MNP than WJMSC-MNP **(C)**; logarithmic growth curve of MNP loaded and non -loaded ADSC and WJMSC Cell proliferate, with lower, non-significant PD values for WJMSC-MNP and higher, non-significant PD for ADSC-MNP compared to ADSC and WJMSC up to 7 days and plateau afterwards in order to displayed a slight descendent trend at day 14 compared to day 7 most probably due to reaching confluence in the culture dish **(D)**. PD = population doublings.

Zeta potential of the MNP was found to be −32.72 (±1.27), pointing out an excellent stability in aqueous solutions. The strong electrostatic repulsion most probably overcome the remanent magnetization of the MNP. An excellent stability was empirically observed for the MNP aqueous suspensions which remained stable for about 2 months. However, following a short ultrasonication, MNP disperse very well, recovering their initial stability. The hysteresis loop of bare magnetite, obtained for magnetic fields up to 2 T, followed a profile specific to ferromagnetic materials. The relatively low remanent

magnetization, Mr, and coercive field, Hc, allow the MNP to diminish the agglomeration induced by magnetic attraction (**Figure 1B**).

Short and Medium Term ADSC-MNP and WJMSC Viability

ADSC and WJMSC were adherent to tissue culture plastic, displayed volume positivity for CD 105, 76 and 90 and negative for CD 34 and 45 (**Supplementary Charts S1, S2**). All cells underwent three lineage differentiation (chondrogenesis as below, adipogenesis and osteogenesis–**Figures 1**, **2 Supplementary Material**) (Dominici et al., 2006).

Viability of ADSC and WJMSC loaded with MNP, starting 24 h after cell-particle exposure, was tested against non-loaded cells using the MTT assay. This specific assay is based on the quantitative colorimetric assessment of tetrazolium reduction to formazan salt by the mitochondrial dehydrogenase activity in viable and non-quiescent cells, an indirect estimate of mitochondrial metabolic activity and cell viability. Excellent viability was recorded for ADSC-MNP after short and medium term ADSC-MNP interaction (24, 72 h and 7 days–164 h) (**Figure 2A**). A significant time dependent increase in relative dehydrogenase activity between 24 h and 7 days can be attributed to increased ADSC-MNP proliferation compared to non-loaded cells. WJMSC-MNP displayed satisfactory viability after exposure to MNP. The maximum WJSC-MNP viability (91.9% from non-loaded cells) was recorded at 72 h. Unlikely ADSC-MNP, whose relative viability continued to increase in time, WJMSC-MNP viability decreased non-significantly at 7 days and 14 days (**Figure 2**). No visible morphological changes regarding cell shape or membrane integrity could be observed for both cell types after exposure to MNP (**Figure 2C**). ADSC-MNP displayed good to excellent viability over extended time in culture (up to 7 days) and continued to proliferate, displaying more than 100% viability at all time points. WJMSC displayed reduced viability in same culture conditions with a minimum at 24 h (83% viability of non-loaded WJMSC), suggesting MNP presence influence their viability, increasing at 72 h.

ADSC-MNP Proliferation and Senescence

Since MTT results suggested an increase in cell number per well in ADSC-MNP, we further tested the comparative proliferative activity of ADSC-MNP and WJMSC. Logarithmic cell growth was calculated based on number of cells counted after fixation with ethanol 80% and nuclear staining with DAPI. Cells were counted using an inverted fluorescent microscope, the number of cells from at least 5 FOV were averaged and the results were used to determine the number of cells/well (see the methods). ADSC-MNP displayed slightly increased population doubling (PD) compared to non-loaded cells up to 14 days in culture while WJSC-MNP showed decreased proliferation at 7 days compared to non-loaded cells. All cell types continued to proliferate, with lower, non-significant PD values for WJMSC-MNP and higher, non-significant for ADSC-MNP compared to their respective non-loaded counterparts up to 7 days and starting to plateau afterwards most probably reaching confluence in the culture dish. All growth curves displayed a slight descendent trend at day 14 compared to day 7. (**Figure 2D**).

For detection of cell senescence in culture we used quantitative assessment of β-galactosidase (B-Gal) activity calculated per cell. Results revealed lower enzyme expression in ADSC-MNP at 14 days as well as significant lower B-Gal activity in ADSC-MNP after 28 days in culture compared to non-loaded ADSC (**Figure 3A**). WJMSC-MNP however displayed increased B-Gal activity at both time points in culture compared to WJMSC at similar time points (**Figure 3B**).

Iron Content per Cell

The quantity of iron load represented by the up-taken MNP was calculated by subtracting iron content of non-loaded cells from ADSC-MNP and WJSC-MNP respectively. Iron content was determined spectrophotometrically using the ferrozine assay. After 24 h of cell particle interaction, ADSC acquire an average amount of 14.9 pg iron/cell (3.67×10^6 MNP/cell), decreasing to 6.64 (1.63×10^6 MNP/cell) at 7 days in culture. Interestingly, at 14 days the amount of iron/cell was found to be increased to 10.8 pg (1.63×10^6 MNP) in order to reach 14.75 pg/cell (3.62×10^6 MNP) at 28 days, almost similar with content at 24 h. WJMSC-MNP iron load was significantly lower at 24 h (0.4 pg/cell; 9.8×10^4 MNP/cell) and 7 days (0.36 pg/cell; 8.8×10^4 MNP/cell) compared to ADSC-MNP at same time point and reached 3.6 pg/cell after at 14 days and 3.81 at 28 days in culture, respectively (**Figure 3C**).

ADSC-MNP and WJSC-MNP Magnetization

For ADSC and WJMSC loaded with MNP, a marked difference is underlined by the hysteresis loops (**Figure 1C**). The amount of MNP uploaded by WJMSC is very low compared to ADSC, as already confirmed by quantitative evaluation of iron content (see above). ADSC-MNP upload an increased amount of MNP in similar condition (14.95 pg iron/cell) within 24 h of cell particle interaction and culture media preconditioning of MNPcompared to WJMSC (0.4 pg iron/cell). ADSC-MNP become responsive to applied magnetic field while WJMSC display low MF responsiveness and magnetization in similar culture conditions and duration of cell particle interaction.

Qualitative Assessment of ADSC Cytoskeleton Fibers in MF

Both loaded and non-loaded ADSC and WJMSC exposed to 6 mT alternating MF for 20 min displayed distortion of actin fibers. Cell body became edgy and uneven compared to non-exposed cells. Furthermore, in ADSC-MNP exposed to MF, the cytoskeletal fibers became shrunk with multiple edges, while for the WJMSC-MNP this effect was not visible. No obvious distortion of cell nuclei could be observed. (**Figure 4**).

Chondrogenic Conversion

Pelleted ADSC, ADSC-MNP, WJMSC and WJMSC-MNP were treated with chondrogenic differentiation media for 21 days. MF exposure was performed by exposing test tubes to MF for 10 min every 2 h during the first 7 days after chondrogenic induction.

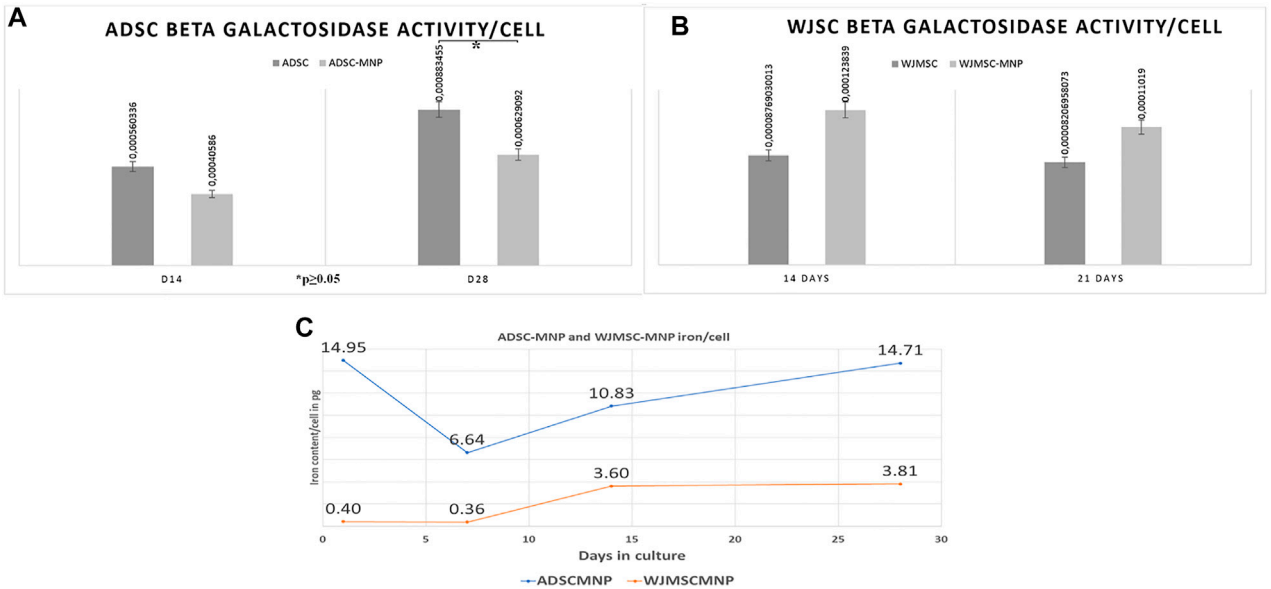

FIGURE 3 | Beta galactosidase activity (B-Gal) in ADSC **(A)** and WJMSC **(B)** demonstrating significant less enzymatic activity in ADSC-MNP at 28 days in culture compared to ADSC at same time point **(C)**; iron content/cell (in picograms) at 1, 7, 14 and 28 days cell-particle interaction; after 24 h cell particle interaction ADSC aquire enough iron content to become remote controllable within MF (14, 0 pg/cell).

Pellets formed from MNP-loaded and MF-exposed cells are more compact, dense and rounded (**Figures 5A,B**) compared to non-loaded (**Figures 5C,D**). Iron presence inferred brownish overall aspect of the pellet, still the characteristic pink color represented by acidic proteoglycan staining could be detected with higher magnification (**Figures 5E,F**). Chondrogenic differentiation was investigated using quantitative colorimetric GAG assay and the results were normalized to cell number/pellet. Cell number/pellet was obtained by dividing DNA content/pellet expressed in pg to 6, the approximated quantity of cellular DNA (Gillooly et al., 2015). In order to exclude a potential interference in colorimetric evaluation of GAG content, for the case of MNP-loaded cells, calculation of GAG content was performed using a standard curve raised for chondroitin sulfate mixed with MNP. The amount of MNP added to each CS dilution was calculated as the iron content per cell resulted from ferrozine assay multiplied by the number of cells/pellet. ADSC-MNP displayed significant increase in GAG content per cells compared to ADSC. Furthermore, ADSC-MNP exposed to MF displayed significant increased GAG/cell ratio compared to non-loaded cells. (**Figure 5I,J**). MF exposed WJMSC and non-exposed WJMSC generated significantly higher amount of GAG/cell compared to WJMSC-MNP and to WJMSC-MNP in MF. Remarkably, the maximum amount of GAG/cell generated by ADSC-MNP-MF (5.55 pg) was almost five times higher compared to maximum amount generated by WJMSC-MF (1.33 pg).

DISCUSSIONS

The ability to produce bioengineered tissues and organs relies on abundant cell sources that have the capability to convert to the desired lineage under appropriate biochemical and mechanical cues. Mesenchymal stem cells have been intensively sought for tissue engineering of cartilage and a large number of research groups are reporting promising *in vitro* and *in vivo* results. The importance of mechanical stimulation for obtaining functional engineered bio equivalents especially in the case of musculoskeletal tissues has been stressed out (Athanasiou et al., 2015). Various methods for mechanical stimulation and dynamic bioreactors have been designed for this specific purpose. However, the ancillary equipment for delivering mechanical load is in many cases bulky, resource consuming and difficult to scale up for translational purposes. We have previously reported good results using magneto-mechanical stimulation for osteogenic and chondrogenic conversion of human primary ADSC using incorporated proprietary MNP and MF exposure. ADSC and WJMSC are considered efficient cell sources for tissue engineering due to their good proliferative and differentiation capabilities, easiness of access and lack of ethical issues with their procurement. WJMSC of allogeneic origin are reportedly non-immunogenic, can generate clinically relevant number of mesenchymal progenitors and are already the object of clinical trials (Liang et al., 2020). In this study we focused on comparing the two cell sources in respect to their capability to undergo chondrogenic lineage differentiation under magnetically delivered mechanical stimulation.

Proprietary bare magnetite MNP are prepared by co-precipitation of iron salts, method that enables production of relatively homogenous nanoparticles (Perlstein et al., 2010). MNP used in this study have average size of 20 nm and display ferromagnetic proprieties and characteristic magnetization curve under MF exposure. Due to their reduced size, sterilization by autoclave induce particle aggregation (data not

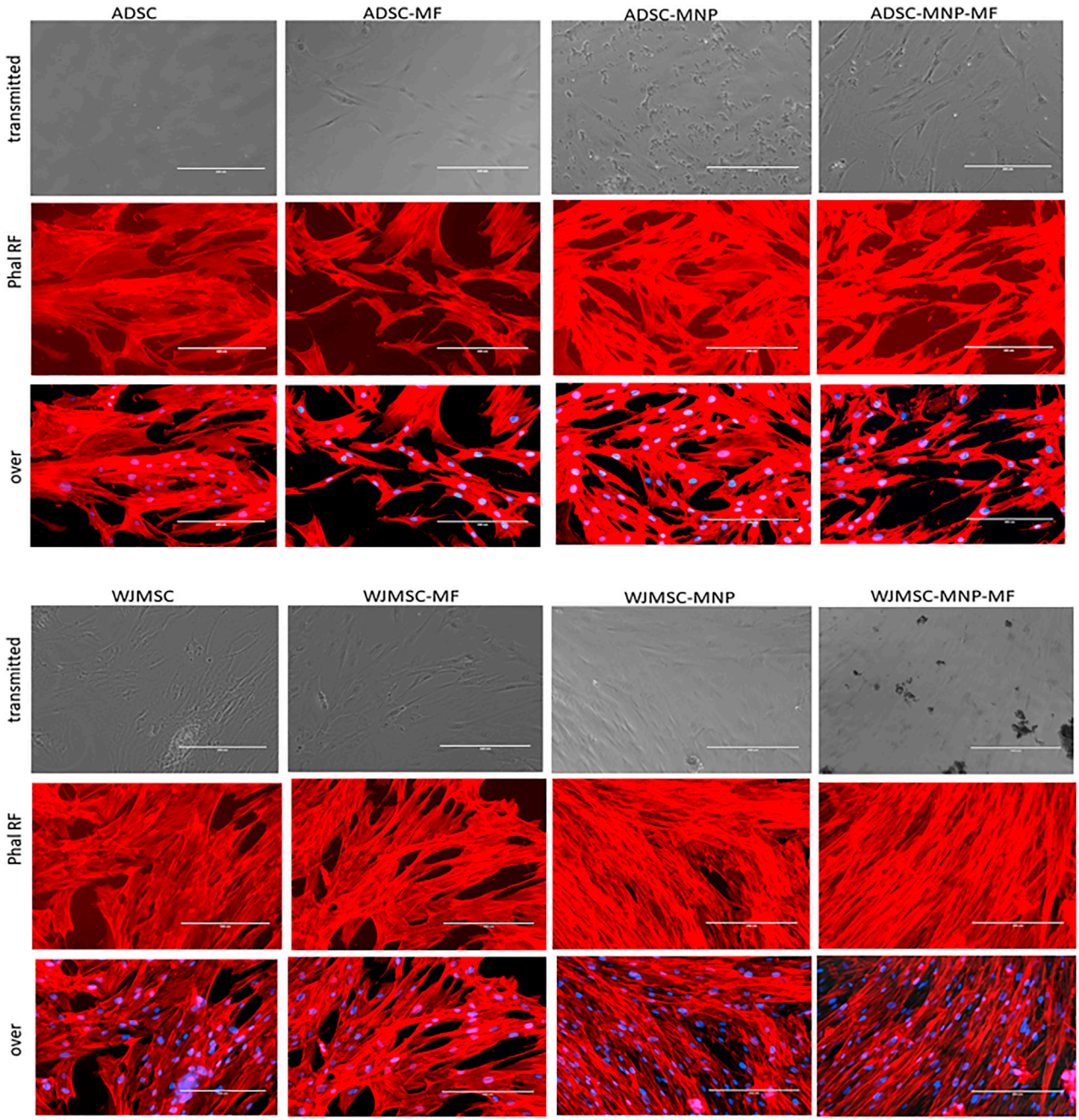

FIGURE 4 | Cytoskeletal fibbers in loaded and non-loaded ADSC and WJMSC demonstrating qualitatively actin fibbers shrinkage in cells exposed to MF, especially for MNP loaded cells. Texas Red™-X Phalloidin staining, nuclei stained with DAPI; EVOS inverted fluorescent microscope 20 × magnification.

shown). Therefore, we used for sterilization UV exposure in the biosafety hood. MNP, in fixed concentration of 40 μg/ml, were first diluted in complete culture media in order to allow formation of a protein corona. Since the protein corona is the major factor that determines MNP biological identity, "presentation" to cell membrane and their internalization (Nierenblerg et al., 2018), one single batch of FBS was used for all experiments in this study for consistency. Simple addition in culture media resulted in different behavior of MNP in relation to the two cell types investigated here. In the first 24 h of cell-particle interaction, MNP were observed to agglomerate around WJMCSs without being internalized. With increasing time in culture, particles were observed in the pericellular area as well as inside cytoplasm. Conversely, MNP could be detected inside ADSC cytoplasm as soon as 24–48 h and further on through all duration of observation (maximum 28 days).

The particularity of WJMSC-MNP interaction could be probably explained by the presence of a dense pericellular

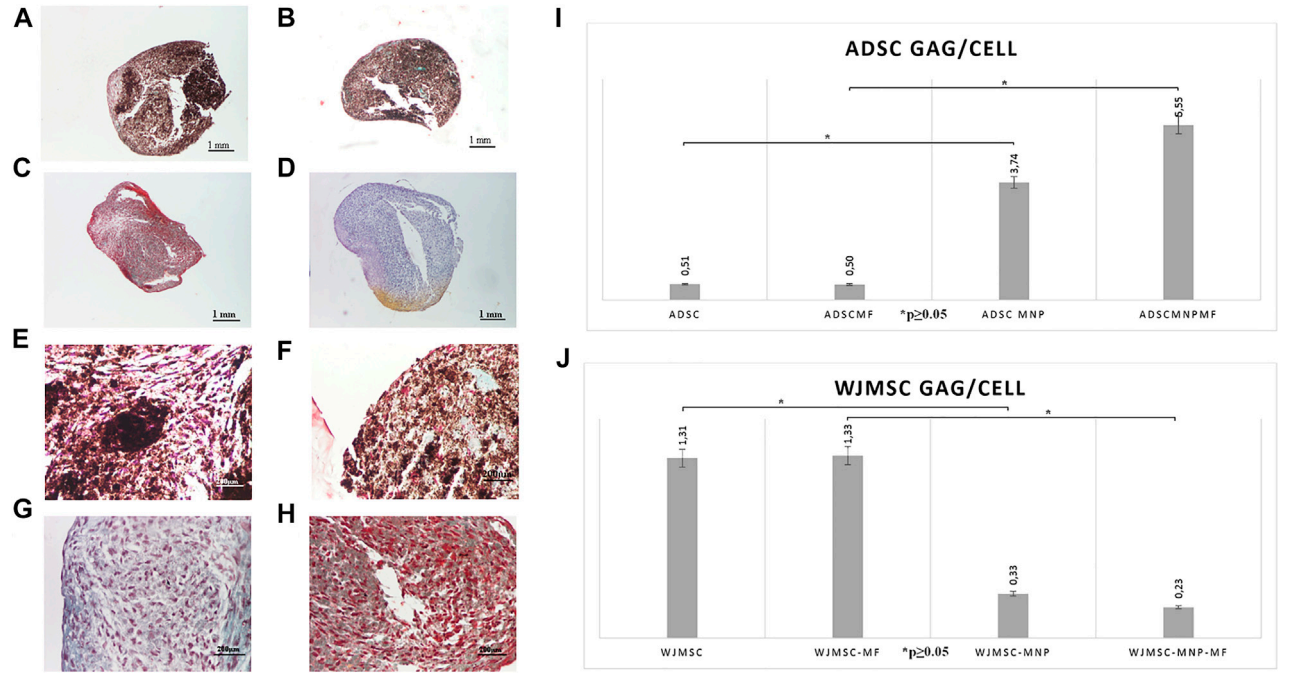

FIGURE 5 | Chondrogensis assay: qualitative: representative histological images of Safranin O stained pellets formed by ADSC-MNP-MF **(A)**; ADSC-MNP **(B)**; ADSC-MF **(C)**; ADSC **(D)** A-D Nikon Eclipse E600 inverted microscope ×4 magnification; ADSC-MNP-MF **(E)**; ADSC-MNP **(F)**; ADSC-MF **(G)**; ADSC **(H) (E–G)** Nikon Eclipse E600 inverted microscope ×20 magnification; quantitative evaluation of glycosaminoglycan (GAG) deposition/cell/pellet in ADSC demonstrating significant increase in GAG deposition in MNP loaded cells as well as in MNP loaded cells submitted to magnetomechanical stimulation within MF compared to non loaded cells **(I)**; WJMSC quantitative evaluation of GAG deposition/cell/pellet demonstrating significant increased GAG deposition in non loaded WJMSC; to note, the maximum amount of GAG deposition is displayed by ADSC-MNP-MF in similar experimental conditions **(J)**.

mesh (Wang et al., 2018) that interfere with initiation of endocytosis. At the initial contact with the cells, MNP are firstly interacting with pericellular matrix and plasma membrane and uploaded by endocytotic mechanisms that vary with their size, coating, and electric charge. MNP are included within intracellular vesicles and finally degraded in the acidic environment of the endo-lysosomal compartment (Kolosnjaj-Tabi, 2013). Bare and as well Fe_3O_4 MNP coated with biocompatible shells are known to be nontoxic, non-genotoxic and not to induce hemolytic processes in contact with blood (Fan et al., 2020). Previous reports have shown good viability in many stem cell types upon internalization of commercially available MNP with different coatings (Wimpenny et al., 2012). Our group has reported good viability in various human stem cells (bone marrow, trabecular bone, adipose derived) with proprietary bare, chitosan and palmitic acid coated Fe_3O_4 MNP. A particularity of MNP that distinguish them from other nanoparticles is the existence of a cellular mechanism for iron storage and metabolism. Ferritin-dependent iron homeostasis is an endogenous mechanism ubiquitous and evolutionary preserved in mammalian cells. Ferritin protein cages accommodate MNP degradation products while concomitantly slowing down the degradation process due to the colloidal behavior in acidic medium (Volatron et al., 2017). A dose dependent reduction in WJMSC viability and proliferation after exposure to commercially available MNP as assessed using MTT was reported (Ohki et al., 2020) suggesting that the maximum iron load the preserves phenotype is cell type dependent. The correlation between maximum iron load that preserves viability and specific cytosolic ferritin activity in various cell type would warrant further investigation. We found that viability of WJMSCs exposed to MNPs after 24 h was only 83,5% compared to non-loaded control as assessed by cell mitochondrial activity. While this is not obligatory a proof that MNPs are cytotoxic to WJMSCs, it is revealing limited mitochondrial activity compared to non-loaded. This could be possible explained by the fact than iron handling enzymatic equipment (especially mitochondrial ferritin) as well as iron overload threshold is cell specific. Mammalian cells response to similar amounts of iron traffic and load is known to not only dependent on cell type but as well on cell status and activity (Ward and Cloonan, 2018). Further investigatings are needed to explore this particularity.

As resulting from population doublings, both cell types, loaded and non-loaded, continue to proliferate up to 14 days when they reach a plateau, most probably due to culture conditions (reaching over confluence). ADSC-MNP display slightly higher PD compared to non-loaded while ADSC-MNP slight decrease proliferation upon MNP exposure. Iron is known to play a crucial role in energy metabolism, being constituent of mitochondrial enzymes of the electron transport chain, involved in ATP production, oxygen consumption, cell cycle progression and

proliferation. Excess of iron, however, generate Fenton reaction producing reactive oxygen species (ROS), especially hydroxyl radicals which can have destructive effects on cellular lipids and DNA (Wessling-Resnick, 2017). The delicate balance between promoting mitochondrial activity and cell proliferation and inducing ROS formation that arrest cell cycle is dependent on complex factors of which free iron ions formation, and availability of intracellular ferritin. Expression of iron transport and metabolism proteins in ADSC, as well as activation of ROS-stimulated pathways are likely to be dependent on tissue of origin, donor age, presence or absence of associated disease (diabetes mellitus, obesity) (Mehta, 2021). Here we found that even if the amount of iron accumulated per cell in the first days in WJMSC is significant lower compared to ADSC-MNP, their growth rate is non-significantly decreased. WJMSC are isolated from WJ, a tissue originating from extraembryonic mesoderm that functions as the very first hematopoietic niche in the developing embryo. WJMSC were shown to support hematopoiesis *in vitro* (Lo Iacono et al., 2018) and to possess a particular transcriptome compared to other ADSC (Jeong et al., 2021), possibly being less equipped for iron internalization. Adenoviral-mediated ferritin overexpression for WJMSC performed as a method to induce their traceability using magnetic resonance imaging (MRI) equipment was found to significantly decrease cell proliferation. (Dai et al., 2017). Further investigation of WJMSC particularities regarding iron transport and metabolism would be necessary.

Bare MNP could be uploaded by ADSC, but not by WJMSC within first 24 h. The average amount of 14.9 pg iron load per cell unit induced efficient cell magnetization in ADSC-MNP suspension as demonstrated by VSM. In WJMSC, the amount of up-loaded iron was significantly lower; however, cells still displayed a magnetic behavior, demonstrating they could respond to an applied MF. This finding was further supported by the configuration of cytoskeletal fibers in loaded and non-loaded cells exposed to MF. After brief exposure (10 min) to a relatively low intensity MF (6 mT), F actin fibers showed the tendency to disorganize and to distort cell contour. Static field exposure (1 mT) of dental pulp stem cells (DPSCs) was shown to rearrange cytoskeleton and to increase their migration proliferation and differentiation by recruiting YAP/TAZ to the nucleus, inhibiting its phosphorylation and upregulating two YAP/TAZ-regulated genes, CTGF and ANKRD1. MF induced YAP/TAZ nuclear localization was inhibited by cytoskeleton inhibitor, cytochalasin D (Zheng et al., 2018). In our study ADSC-MNP and, at a lower extent, WJMSC-MNP displayed increased cytoskeletal fiber rearrangement under MF (**Figure 4**). MNP are known to be trafficked inside cell cytoplasm along cytoskeletal fibbers. It is possible their proximity to actin fibbers during MF exposure to generate micro movements that act as internal mechanical stimulation, influencing YAP/TAZ nuclear translocation and possible other mechano-responsive pathways.

An interesting observation is the particularity of iron load dynamic on the duration of 28 days in ADSC-MNP. After 24 h cell-MNP interaction, cells were found to accumulate the maximum amount of iron/cell (14.9 pg/cell), quantity that was found to decrease to almost one third (6.64 pg/cell) at 7 days, then increased again to reach approximatively the initial amount at 28 days (14.71 pg/cell). The initial decrease in iron content at 7 days can be partly explained by proliferation and consequent distribution of MNP in the dividing cells. Other possible explanations such as particle biodegradation and re-synthesis could be involved. Using magnetism as a modality to demonstrate the MNP presence inside cells, a possible mechanism of biodegradation and "re-biosynthesis" was demonstrated to occur in human ADSC. Cells were found to be "re-magnetized" after degradation of nanoparticles that took place at 7–10 days after particle internalization (Van de Walle et al., 2019). This finding was interpreted as a direct demonstration of a possible neo synthesis of magnetic nanoparticles inside endosomes, a process H-ferritin dependent that could explain, at least in part, the gradual increase in iron content/cell at 14 and 28 days for ADSC-MNP. WJMSC increased iron/cell gradually up to 28 days probably as a result of slow internalization of the MNP due to rich fibronectin pericellular matrix and a possible low expression of transferrin or other iron transporters, fact that needs to be further investigated.

We used assessment of B-Gal activity as a modality to detect culture induced senescence. Not surprisingly, B-Gal expression was found to increase at 28 days in all cell types, loaded and non-loaded, compared to 14 days. However, ADSC-MNP showed less B-Gal activity compared to non-loaded at both time points whereas WJMSC-MNP were found to express increased enzyme activity compared to non-loaded. The presumptive lower activity of cytosolic ferritin and increased ROS formation in WJMSC could be involved. Culture-induced senescence is a well-known phenomenon that impedes *in vitro* cell expansion and negatively influences MSC therapeutic potential (Liu et al., 2020). No significant ROS increase and cell ageing could be observed in human myoblasts loaded with different amounts of superparamagnetic iron oxide nanoparticles (SPIOS) that retained their phenotype *in vitro* and *in vivo* (Wierzbinski et al., 2018). Here we found that non coated MNP internalization decreased B-Gal activity during extended culture in ADSC but not in WJMSC. Further studies focusing on ROS expression as well as on investigating senescence associated phenotype are needed to determine if MNP loading could function as a modality of preventing culture induced senescence in ADSC populations.

Based on quantification of GAG deposition per cell, we found that condrogenic conversion of MF-exposed and non-exposed ADSC-MNP was significantly increased compared to non-loaded. Furthermore, MF exposure increased GAG deposition in ADSC-MNP compared to non-exposed ones, albeit non-significantly. Iron is an essential factor for cartilage formation and its internalization is required for ECM synthesis. Reduced iron is a catalyst of proline and lysine hydroxylation reactions that are essential to the formation of mature collagen molecules (Pacifici and Iozzo, 1988). MNP can provide slow release of reduced iron ions supporting chondrogenic ECM deposition. Stem cells were found to handle iron transport differently depending on differentiation pathways even in the absence of MNP. In MSC chondrogenesis, transferrin is down regulated while

ferroportin is significantly higher expressed compared to osteo and adipogenesis. Moreover, ADSC loaded with MNP, overexpressed L-Ferritin (involved in iron storage as nonmagnetic ferrihydrite in the ferritin cage) during chondrogenesis. Conversely, H-Ferritin, possible involved in *de novo* MNP biosynthesis, was found to be higher expressed during osteogenesis and adipogenesis (Van de Walle et al., 2019). Iron availability and supplementation has been recently confirmed as a modality to increase chondrogenesis *in vitro* and *in vivo* in Guineea pigs. Ascorbic acid and iron supplementation in the form of commercially available ferumoxytol was found to significantly increase chondrogenesis in bone marrow ADSC *in vitro* as well as *in vivo* in Guinea minipig model of cartilage defect (Theruvath et al., 2021). Ferrumoxytol, is used as iron supplement for intravenous administration and occasionally off label as a MRI contrast agent for vascular and nodal metastasis. It consists of carbohydrate-coated ultra-small SPIOs (Vasanawala et al., 2016). Their hydrodynamic size (average 25 nm) and iron oxide composition are similar with particles used in our study. Here we used non-coated MNP, fact that could increase intracellular iron availability and decrease the time of MNP processing by the cells. The fact that WJMSC iron handling mechanisms cannot provide similar amounts of intracellular iron compared to ADSC (as resulting from the quantitative assessment of intracellular iron content) can possible interfere with chondrogenic conversion. Profiling comparatively the cellular iron enzymatic equipment in loaded and non-loaded ADSC and WJMSC during chondrogenic conversion could reveal very useful insights potentially offering molecular targets to enabling future cartilage engineering procedures. ADSC chondrogenesis was previously found inferior to other stem cell sources (Fellows et al., 2016). In this study, significant higher amounts of GAG/cell obtained from non-loaded WJMSC compared to non-loaded ADSC, confirming the fact that non-modified ADSC are not the best source when considering cartilage engineering. However, MNP presence clearly increased GAG deposition in ADSC, especially after MF exposure. Actin cytoskeleton was shown to modulate COL2/aggrecan fragment generation; the factors that control actin dynamic decisively control the chondrocyte phenotype (Lauer et al., 2021). MNP presence, in close relation to actin fibbers (Orynbayeva et al., 2015), can induce the necessary actin dynamics to initiate and promote chondrogenesis. In this study, we showed that MF exposure influences the cytoskeletal fiber organization. GAG deposition in magnetically stimulated ADSC-MNP was almost 5 times higher compared to non-loaded WJMSC, pointing to a possible modality for manipulating ADSC for improved chondrogenic conversion *in vitro* and, possibly, future methods for improving cartilage-repair pulsed magnetic field exposure (PEMF) of BM-ADSC in combination with magnetic hydrogels which were shown to increase repair in rabbit model of cartilage defects (Huang et al., 2019). Further studies are needed to more precisely clarify the molecular mechanism governing the correlation between MNP positioning, MF exposure and increased chondrogenesis in ADSC. Chondrogenic induction of WJMSC was previously shown to result in increased upregulation of cartilage-specific type II collagen synthesis compared to BM-ADSC and decreased osteoinductive Runx2 and collagen X in similar culture conditions (Reppel et al., 2015), suggesting their use could avoid hypertrophic cartilage formation and graft ossification. Previous studies have used human BM ADSC loaded with homogenous sized MNP derived from bacteria (Magnetospirillium sp) for inducing cell aggregation in pellets and for delivering magnetic mediated shear stress during initial stages of chondrogenic conversion. Increased levels of GAGs and collagen production as well as the absence of hypertrophic conversion was observed in the MNP loaded cells (Son et al., 2015).

In our experience, MNP mediated aggregation in spheroid culture under MF was not efficient in increasing the amount of GAG production compared to simple pellet procedure, probably due to increase compaction of three dimensional structure and decreased nutrient availability (Labusca et al., 2021).

A limitation of this study is that we have not investigated hypertrophic markers. However, previous evidence supports the fact that significant GAG increase in ADSC-MNP at protein level is an indicator of normal articular cartilage, being correlated with collagen type expression II and absence of hypertrophy (Kamisan et al., 2013). Further studies will be needed as well to address donor variability especially for the case of ADSC. WJMSC donor population is more likely to being homogenous as it involves processing umbilical cord sample from women of fertile age and with healthy pregnancies. ADSC donors, however, could be more heterogeneous, especially if the use of autologous cells is envisaged for a future therapeutic purpose. A comparative study including a larger number of donors stratified based on age, gender and BMI as well as profiling ADSC characteristics relative to their chondrogenic conversion capability will to enable further donor selection for cartilage regeneration purposes.

CONCLUSION

ADSC upload proprietary MNP by simple addition in culture media after 24 h in quantities that endows the cells with magnetic properties. ADSC-MNP, submitted to low-frequency MF during initial stages of chondrogenic induction, generated the highest amount of chondrogenic conversion at protein level as assessed by GAG/cell deposition after 21 days pellet culture. WJSC displayed low MNP internalization and significant lower amount of GAG deposition in similar conditions. B-Gal activity, after extended culture *in vitro*, was significantly decreased in ADSC-MNP compared to non-loaded, but not in WJMSC, suggesting a possible senescent protective mechanism that needs further investigation. Magneto-mechanical stimulation of MNP-loaded cells could be an efficient modality to increase the efficiency of ADSC, but not of WJMSC for cartilage engineering. Further studies are necessary to confirm the feasibility of this method in animal models of cartilage

defects and to detect the molecular basis of MNP mediated magneto-mechanical stimulation.

DATA AVAILABILITY STATEMENT

The raw data supporting the conclusion of this article will be made available by the authors, without undue reservation.

AUTHOR CONTRIBUTIONS

LL designed the experiment and collected data, drafted the manuscript D-DH manufactured MNPs and performed their characterisation collected and interpreted MNP characterisation results, AEM, CS, and CD performed the experiments and collected data, PP performed histological examination, HC and NL supervised data collection and manuscript editing.

FUNDING

Financial support by the MCID NUCLEU Program (PN 19 28 01 01) and UEFISCDI Contract no. PCE20/2021 (PN-III-P4-ID-PCE-2020-2381) is gratefully acknowledged.

SUPPLEMENTARY MATERIAL

The Supplementary Material for this article can be found online at: https://www.frontiersin.org/articles/10.3389/fbioe.2021.737132/full#supplementary-material

REFERENCES

Amin, H. D., Brady, M. A., St-Pierre, J. P., Stevens, M. M., Overby, D. R., and Ethier, C. R. (2014). Stimulation of Chondrogenic Differentiation of Adult Human Bone Marrow-Derived Stromal Cells by a Moderate-Strength Static Magnetic Field. *Tissue Eng. Part. A.* 20 (11-12), 1612–1620. doi:10.1089/ten.tea.2013.0307

Athanasiou, K. A., Responte, D. J., Brown, W. E., and Hu, J. C. (2015). Harnessing Biomechanics to Develop Cartilage Regeneration Strategies. *J. Biomech. Eng.* 137 (2), 020901. doi:10.1115/1.4028825

Ceccarelli, S., Pontecorvi, P., Anastasiadou, E., Napoli, C., and Marchese, C. (2020). Immunomodulatory Effect of Adipose-Derived Stem Cells: The Cutting Edge of Clinical Application. *Front Cel Dev Biol* 8, 236. doi:10.3389/fcell.2020.00236

Dai, H. Y., He, R., Zhang, Y., Wu, R. H., and Xiao, Y. Y. (2017). Adenoviral Vector Mediated Ferritin Over-expression in Mesenchymal Stem Cells Detected by 7T MRI *In Vitro*. *PLoS One* 12 (9), e0185260. doi:10.1371/journal.pone.0185260

Dominici, M., Le Blanc, K., Mueller, I., Slaper-Cortenbach, I., Marini, F., Krause, D., et al. (2006). Minimal Criteria for Defining Multipotent Mesenchymal Stromal Cells. The International Society for Cellular Therapy Position Statement. *Cytotherapy* 8 (4), 315–317. doi:10.1080/14653240600855905

Esposito, M., Lucariello, A., Costanzo, C., Fiumarella, A., Giannini, A., Riccardi, G., et al. (2013). Differentiation of Human Umbilical Cord-Derived Mesenchymal Stem Cells, WJ- ADSC, into Chondrogenic Cells in the Presence of Pulsed Electromagnetic fields. *Vivo* 27 (4), 495–500.

Fahy, N., Alini, M., and Stoddart, M. J. (2018). Mechanical Stimulation of Mesenchymal Stem Cells: Implications for Cartilage Tissue Engineering. *J. Orthop. Res.* 36 (1), 52–63. doi:10.1002/jor.23670

Fan, D., Wang, Q., Zhu, T., Wang, H., Liu, B., Wang, Y., et al. (2020). Recent Advances of Magnetic Nanomaterials in Bone Tissue Repair. *Front. Chem.* 8, 745. doi:10.3389/fchem.2020.00745

Fellows, C. R., Matta, C., Zakany, R., Khan, I. M., and Mobasheri, A. (2016). Adipose, Bone Marrow and Synovial Joint-Derived Mesenchymal Stem Cells for Cartilage Repair. *Front. Genet.* 7, 213. doi:10.3389/fgene.2016.00213

Gillooly, J. F., Hein, A., and Damiani, R. (2015). Nuclear DNA Content Varies with Cell Size across Human Cell Types. *Cold Spring Harb Perspect. Biol.* 7 (7), a019091. doi:10.1101/cshperspect.a019091

Huang, J., Jia, Z., Liang, I., Huang, Z., Rong, Z., Xiong, J., et al. (2019). Pulse Electromagnetic fields Enhance the Repair of Rabbit Articular Cartilage Defects with Magnetic Nano-Hydrogel. *ACS Biomater. Sci. Eng.* 5 (5), 2200–2207.

Jeong, J. E., Seol, B., Kim, H. S., Kim, J. Y., and Cho, Y. S. (2021). Exploration of Alternative Splicing Events in Mesenchymal Stem Cells from Human Induced Pluripotent Stem Cells. *Genes (Basel)* 12 (5), 737. doi:10.3390/genes12050737

Kamisan, N., Naveen, S. V., Ahmad, R. E., and Kamarul, T. (2013). Chondrocyte Density, Proteoglycan Content and Gene Expressions from Native Cartilage Are Species Specific and Not Dependent on Cartilage Thickness: a Comparative Analysis between Rat, Rabbit and Goat. *BMC Vet. Res.* 9, 62. doi:10.1186/1746-6148-9-62

Kloppenburg, M., and Berenbaum, F. (2020). Osteoarthritis Year in Review 2019: Epidemiology and Therapy. *Osteoarthritis and Cartilage* 28 (3), 242–248. doi:10.1016/j.joca.2020.01.002

Labusca, L., Herea, D. D., Minuti, A. E., Stavila, C., Danceanu, C., Grigoras, M., et al. (2021). Magnetic Nanoparticle Loaded Human Adipose Derived Mesenchymal Cells Spheroids in Levitated Culture. *J. Biomed. Mater. Res. B Appl. Biomater.* 109 (5), 630–642. doi:10.1002/jbm.b.34727

Labusca, L. S., Herea, D. D., Radu, E., Danceanu, C., Chiriac, H., and Lupu, N. (2018). Human Adipose Derived Stem Cells and Osteoblasts Interaction with Fe-Cr-Nb-B Magnetic Nanoparticles. *J. Nanosci Nanotechnol* 18 (7), 5143–5153. doi:10.1166/jnn.2018.15330

Lauer, J. C., Selig, M., Hart, M. L., Kurz, B., and Rolauffs, B. (2021). Articular Chondrocyte Phenotype Regulation through the Cytoskeleton and the Signaling Processes that Originate from or Converge on the Cytoskeleton: Towards a Novel Understanding of the Intersection between Actin Dynamics and Chondrogenic Function. *Int. J. Mol. Sci.* 22 (6), 3279. doi:10.3390/ijms22063279

Liang, H., Suo, H., Wang, Z., and Feng, W. (2020). Progress in the Treatment of Osteoarthritis with Umbilical Cord Stem Cells. *Hum. Cel* 33 (3), 470–475. doi:10.1007/s13577-020-00377-z

Lima, J., Gonçalves, A. I., Rodrigues, M. T., Reis, R. L., and Gomes, M. E. (2015). The Effect of Magnetic Stimulation on the Osteogenic and Chondrogenic Differentiation of Human Stem Cells Derived from the Adipose Tissue (hASCs). *J. Magnetism Magn. Mater.* 393, 526–536. doi:10.1016/j.jmmm.2015.05.087

Liu, J., Ding, Y., Liu, Z., and Liang, X. (2020). Senescence in Mesenchymal Stem Cells: Functional Alterations, Molecular Mechanisms, and Rejuvenation Strategies. *Front. Cel Dev Biol* 8, 258. doi:10.3389/fcell.2020.00258

Lo Iacono, M., Russo, E., Anzalone, R., Baiamonte, E., Alberti, G., Gerbino, A., et al. (2018). Wharton's Jelly Mesenchymal Stromal Cells Support the Expansion of Cord Blood-Derived CD34+ Cells Mimicking a Hematopoietic Niche in a Direct Cell-Cell Contact Culture System. *Cel Transpl.* 27 (1), 117–129. doi:10.1177/0963689717737089

Mehta, K. J. (2021). Role of Iron and Iron-Related Proteins in Mesenchymal Stem Cells: Cellular and Clinical Aspects. *J. Cel Physiol*, 1–24. doi:10.1002/jcp.30383

Merkley, G., Aakerman, J., and Letterman, D. (2018). Articular Cartilage Defects: Incidence, Diagnosis, and Natural History, Op. *Techn Sports Med.* 23, 156–161. doi:10.1053/j.otsm.2018.06.008

Nierenberg, D., Khaled, A. R., and Flores, O. (2018). Formation of a Protein corona Influences the Biological Identity of Nanomaterials. *Rep. Pract. Oncol. Radiother.* 23 (4), 300–308. doi:10.1016/j.rpor.2018.05.005

O'Conor, C. J., Case, N., and Guilak, F. (2013). Mechanical Regulation of Chondrogenesis. *Stem Cel Res Ther* 4 (4), 61. doi:10.1186/scrt211

Orynbayeva, Z., Sensenig, R., and Polyak, B. (2015). Metabolic and Structural Integrity of Magnetic Nanoparticle-Loaded Primary Endothelial Cells for Targeted Cell Therapy. *Nanomedicine (Lond)* 10 (10), 1555–1568. doi:10.2217/nnm.15.14

Pacifici, M., and Iozzo, R. V. (1988). Remodeling of the Rough Endoplasmic Reticulum during Stimulation of Procollagen Secretion by Ascorbic Acid in Cultured Chondrocytes. A Biochemical and Morphological Study. *J. Biol. Chem.* 263 (5), 2483–2492.

Perlstein, B., Lublin-Tennenbaum, T., Marom, I., and Margel, S. (2010). Synthesis and Characterization of Functionalized Magnetic Maghemite Nanoparticles with Fluorescent Probe Capabilities for Biological Applications. *J. Biomed. Mater. Res.* 92B, 353–360. doi:10.1002/jbm.b.31521

Rahbar Saadat, Y., Zununi Vahed, S., Samiei, M., Ardalan, M., Rameshrad, M., Ahmadian, E., et al. (2020). The Use of Nanomaterials in Tissue Engineering for Cartilage Regeneration; Current Approaches and Future Perspectives. *Int. J. Mol. Sci.* 21 (2), 536. doi:10.3390/ijms21020536

Reppel, L., Schiavi, J., Charif, N., Leger, L., Yu, H., Pinzano, A., et al. (2015). Chondrogenic Induction of Mesenchymal Stromal/stem Cells from Wharton's Jelly Embedded in Alginate Hydrogel and without Added Growth Factor: an Alternative Stem Cell Source for Cartilage Tissue Engineering. *Stem Cel Res Ther* 30 (6), 260. doi:10.1186/s13287-015-0263-2

Si, Z., Wang, X., Sun, C., Kang, Y., Xu, J., Wang, X., et al. (2019). Adipose-derived Stem Cells: Sources, Potency, and Implications for Regenerative Therapies. *Biomed. Pharmacother. = Biomedecine pharmacotherapie* 114, 108765. doi:10.1016/j.biopha.2019.108765

Son, B., Kim, H. D., Kim, M., Kim, J. A., Lee, J., Shin, H., et al. (2015). Physical Stimuli-Induced Chondrogenic Differentiation of Mesenchymal Stem Cells Using Magnetic Nanoparticles. *Adv. Healthc. Mater.* 4 (9), 1339–1347. doi:10.1002/adhm.201400835

Theruvath, A. J., Mahmoud, E. E., Wu, W., Nejadnik, H., Kiru, L., Liang, T., et al. (2021). Ascorbic Acid and Iron Supplement Treatment Improves Stem Cell-Mediated Cartilage Regeneration in a Minipig Model. *Am. J. Sports Med.* 49 (7), 1861–1870. doi:10.1177/03635465211005754

Van de Walle, A., Plan Sangnier, A., Abou-Hassan, A., Curcio, A., Hémadi, M., Menguy, N., et al. (2019). Biosynthesis of Magnetic Nanoparticles from Nano-Degradation Products Revealed in Human Stem Cells. *Proc. Natl. Acad. Sci. U S A.* 116 (10), 4044–4053. doi:10.1073/pnas.1816792116

Vasanawala, S. S., Nguyen, K. L., Hope, M. D., Bridges, M. D., Hope, T. A., Reeder, S. B., et al. (2016). Safety and Technique of Ferumoxytol Administration for MRI. *Magn. Reson. Med.* 75 (5), 2107–2111. doi:10.1002/mrm.26151

Volatron, J., Carn, F., Kolosnjaj-Tabi, J., Javed, Y., Vuong, Q. L., Gossuin, Y., et al. (2017). Ferritin Protein Regulates the Degradation of Iron Oxide Nanoparticles. *Small* 13 (2). doi:10.1002/smll.201602030

Ward, D. M., and Cloonan, S. M. (2019). Mitochondrial Iron in Human Health and Disease. *Annu. Rev. Physiol.* 81, 453–482. doi:10.1146/annurev-physiol-020518-114742

Wei, Y., Sun, X., Wang, W., and Hu, Y. (2007). Adipose-derived Stem Cells and Chondrogenesis. *Cytotherapy* 9 (8), 712–716. doi:10.1080/14653240701620596

Wessling-Resnick, M. (2017). Excess Iron: Considerations Related to Development and Early Growth. *Am. J. Clin. Nutr.* 106 (Suppl. 6), 1600S–1605S. doi:10.3945/ajcn.117.155879

Wierzbinski, K, R., Szymanski, T., Rozwadowska, N., Rybka, J. D., Zimna, A., Zalewski, T., et al. (2018). Potential Use of Superparamagnetic Iron Oxide Nanoparticles for *In Vitro* and *In Vivo* Bioimaging of Human Myoblasts. *Sci. Rep.* 8 (1), 3682. doi:10.1038/s41598-018-22018-0

Wimpenny, I., Markides, H., and El Haj, A. J. (2012). Orthopaedic Applications of Nanoparticle-Based Stem Cell Therapies. *Stem Cel Res Ther* 3, 13. doi:10.1186/scrt104

Yong, K. W., Choi, J. R., Choi, J. Y., and Cowie, A. C. (2020). Recent Advances in Mechanically Loaded Human Mesenchymal Stem Cells for Bone Tissue Engineering. *Int. J. Mol. Sci.*, 21, 5816. doi:10.3390/ijms21165816

Zha, K., Sun, Z., Yang, Y., Chen, M., Gao, C., Fu, L., et al. (2021). Recent Developed Strategies for Enhancing Chondrogenic Differentiation of MSC: Impact on MSC-Based Therapy for Cartilage Regeneration. *Stem Cell Int* 2021, 8830834. doi:10.1155/2021/8830834

Zhang, C., Cai, Y. Z., Lin, X. J., and Wang, Y. (2020). Magnetically Actuated Manipulation and its Applications for Cartilage Defects: Characteristics and Advanced Therapeutic Strategies. *Front. Cel Dev Biol.* 8, 526. doi:10.3389/fcell.2020.00526

Zheng, L., Zhang, L., Chen, L., Jiang, J., Zhou, X., Wang, M., et al. (2018). Static Magnetic Field Regulates Proliferation, Migration, Differentiation, and YAP/TAZ Activation of Human Dental Pulp Stem Cells. *J. Tissue Eng. Regen. Med.* 12 (10), 2029–2040. doi:10.1002/term.2737

Conflict of Interest: The authors declare that the research was conducted in the absence of any commercial or financial relationships that could be construed as a potential conflict of interest.

Publisher's Note: All claims expressed in this article are solely those of the authors and do not necessarily represent those of their affiliated organizations, or those of the publisher, the editors and the reviewers. Any product that may be evaluated in this article, or claim that may be made by its manufacturer, is not guaranteed or endorsed by the publisher.

frontiers in Bioengineering and Biotechnology

REVIEW
published: 22 October 2021
doi: 10.3389/fbioe.2021.754113

3D Bioprinted Implants for Cartilage Repair in Intervertebral Discs and Knee Menisci

Kalindu Perera[1†], Ryan Ivone[1†], Evelina Natekin[2], Cheryl. A. Wilga[3,4], Jie Shen[1,5]* and Jyothi U. Menon[1,5]**

[1]Department of Biomedical and Pharmaceutical Sciences, College of Pharmacy, University of Rhode Island, Kingston, RI, United States, [2]Department of Biological Sciences, University of Alaska Anchorage, Anchorage, AK, United States, [3]Department of Biological Sciences, University of Rhode Island, Kingston, RI, United States, [4]Department of Electrical, Computer and Biomedical Engineering, University of Rhode Island, Kingston, RI, United States, [5]Department of Chemical Engineering, University of Rhode Island, Kingston, RI, United States

OPEN ACCESS

Edited by:
Zhen Li,
AO Research Institute, Switzerland

Reviewed by:
Yasuhiko Tabata,
Kyoto University, Japan
Feng-Huei Lin,
National Taiwan University, Taiwan

***Correspondence:**
Cheryl. A. Wilga
cwilga@uri.edu
Jie Shen
jie_shen@uri.edu
Jyothi U. Menon
jmenon@uri.edu

[†]These authors have contributed equally to this work

Specialty section:
This article was submitted to Tissue Engineering and Regenerative Medicine, a section of the journal Frontiers in Bioengineering and Biotechnology

Received: 05 August 2021
Accepted: 30 September 2021
Published: 22 October 2021

Citation:
Perera K, Ivone R, Natekin E, Wilga CA, Shen J and Menon JU (2021) 3D Bioprinted Implants for Cartilage Repair in Intervertebral Discs and Knee Menisci. Front. Bioeng. Biotechnol. 9:754113. doi: 10.3389/fbioe.2021.754113

Cartilage defects pose a significant clinical challenge as they can lead to joint pain, swelling and stiffness, which reduces mobility and function thereby significantly affecting the quality of life of patients. More than 250,000 cartilage repair surgeries are performed in the United States every year. The current gold standard is the treatment of focal cartilage defects and bone damage with nonflexible metal or plastic prosthetics. However, these prosthetics are often made from hard and stiff materials that limits mobility and flexibility, and results in leaching of metal particles into the body, degeneration of adjacent soft bone tissues and possible failure of the implant with time. As a result, the patients may require revision surgeries to replace the worn implants or adjacent vertebrae. More recently, autograft – and allograft-based repair strategies have been studied, however these too are limited by donor site morbidity and the limited availability of tissues for surgery. There has been increasing interest in the past two decades in the area of cartilage tissue engineering where methods like 3D bioprinting may be implemented to generate functional constructs using a combination of cells, growth factors (GF) and biocompatible materials. 3D bioprinting allows for the modulation of mechanical properties of the developed constructs to maintain the required flexibility following implantation while also providing the stiffness needed to support body weight. In this review, we will provide a comprehensive overview of current advances in 3D bioprinting for cartilage tissue engineering for knee menisci and intervertebral disc repair. We will also discuss promising medical-grade materials and techniques that can be used for printing, and the future outlook of this emerging field.

Keywords: cartilage, bone repair, tissue engineering, 3D printing, bioprinting

INTRODUCTION

Treatment of cartilage injuries presents a significant challenge in modern orthopedics. Damage to the articular cartilage due to trauma, degenerative diseases or normal wear and tear affects everyone from children to the elderly. Poorly-healed cartilage defects cause serious and degenerative morbidities like osteoarthritis, which is the predominant cause of joint pain worldwide, affecting nearly 303 million people globally (Wei et al., 2021). The limited self-repair capabilities of the cartilage due to absence of

vascularization, in which nutrients only reach chondrocytes *via* diffusion from the surrounding environment, and low chondrocyte density (comprising 1–5% of total cartilage) attributed to the high matrix to cell volume ratio, and the lack of operative and medical therapies that can significantly facilitate the healing process has led to an urgent need for new and durable treatments and grafting strategies to regenerate and repair these defects (Zhang et al., 2009; Akkiraju and Nohe, 2015; Dai and Gao, 2016).

Metal and plastic prosthetics that can recapitulate the surface of joints are currently the gold standard in cartilage and bone replacement. However, these are often rigid, limiting patient flexibility and mobility. Friction can lead to rapid wear of these implants, leading to damage and inflammation in adjacent tissues. Furthermore, the leaching of metal particles from the implants into the body can lead to adverse effects including tissue damage and poisoning (Prezyna, 2000; Sansone, 2013). Although current strategies to repair cartilage defects exist, including microfracture surgery, autologous chondrocyte implantation and osteochondral transplantation, these procedures have drawbacks such as high failure rates (25–50% within 10 years) and reduced effectiveness among elderly patients (Lansdown et al., 2018). Furthermore, autologous chondrocyte transplantation is marred by shortage of chondrocyte sources, while microfracture surgery is limited by the development of fibrocartilage instead of natural hyaline cartilage in the region, which can worsen joint function (Zhang et al., 2019; Yang et al., 2020a; Wei et al., 2021). Other methods such as debridement and spongialization have been hindered by their clinical invasiveness and the high inherent risk of developing osteoarthritis (Zhang et al., 2019).

As an alternative to existing strategies, cartilage tissue engineering is being increasingly explored as a method of fabricating functional constructs that can facilitate the regeneration of joint cartilage. Among the many strategies under consideration, 3D bioprinting has emerged as a promising method that allows precise control over the properties of the construct including shape, architecture, mechanical strength and placement of cells and bioactive cues, to mimic native cartilage. In this review, we will explore in detail current technologies being developed for the repair of joint cartilage as well as 3D printing strategies and materials being used to improve the properties and functionality of 3D bioprinted constructs for the development of functional and durable implants. In particular, we will focus on high-risk, high-load bearing and motion-critical cartilage: namely, intervertebral discs and knee menisci, for which current treatment options (e.g., implants) do not offer satisfactory biological functionality.

BIOMECHANICS OF JOINT CARTILAGE

In the human body, the three main types of cartilage produced include hyaline cartilage, elastic cartilage, and fibrocartilage. Hyaline cartilage, the most common cartilage found in the body, functions to provide lubrication and load-bearing support for the articulating surfaces of bones in synovial joints, essential for joint movement, in addition to playing a key role in skeletal growth and development (Krishnan, 2018). Hyaline cartilage is comprised primarily of different types of collagen, as well as proteoglycans such as aggrecan, which provides compressive strength and load-bearing support for tissues due to intermolecular repulsive interactions (Ng et al., 2003). Similar to hyaline cartilage, elastic cartilage is comprised mainly of collagen (type II) and proteoglycans. However elastic cartilage, which can be found in the ear and larynx also contains elastin fibers, allowing for increased flexibility while maintaining structural support (Chizhik et al., 2010). Knee menisci and intervertebral discs (IVDs) are comprised predominately of fibrocartilage, which exhibits high tensile strength due to the presence of thick, bundled, and highly ordered collagen (type I) fibers (Murphy et al., 2015).

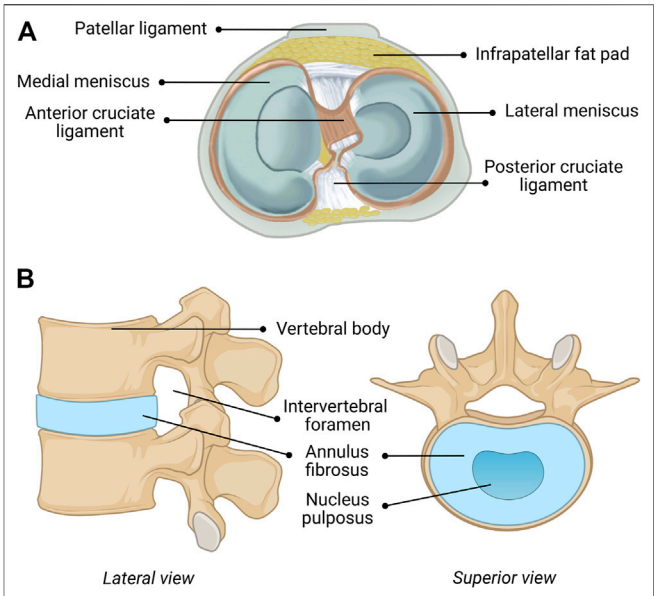

FIGURE 1 | Anatomical composition of the **(A)** human knee (including menisci) and **(B)** human intervertebral disc (IVD). **Figure 1A** reprinted with minor alterations from (Guo et al., 2015) under Creative Commons Public Domain Dedication waiver (creativecommons.org/publicdomain/zero/1.0).

Knee Menisci

The menisci are critical for maintaining the health and performance of the knee joint, providing nutrition, lubrication, shock absorption, load distribution, and stability of the joint (Fox et al., 2012; Kester et al., 2021). The semicircular medial- and circular lateral menisci are fibrocartilaginous wedges that are attached to the femur *via* multiple ligaments, as shown in **Figure 1B**. The menisci are concave at the femoral surface for articulation with the condyles and flat on the tibial surface to connect with the plateau. The outer border is thick and vascular allowing for firm attachment to the joint capsule, while the inner border is thin and avascular, allowing for correct orientation within the joint. The fibrochondrocytes (meniscal cells) maintain the dense extracellular matrix (ECM) and synthesize the collagen,

proteoglycans, and other proteins embedded within (Makris et al., 2011). Tissue fluid comprises 65–70% of the total weight of menisci as most of the water is sequestered within proteoglycans (Herwig et al., 1984). The orientation of the collagen bundles in the center third region are primarily radially oriented suggesting that they function in compression, while those in the outer two-thirds are circumferentially oriented suggesting a tensile function (McDermott et al., 2008). In contrast, the collagen bundles are randomly oriented in the surface layer suggesting they function to decrease friction (McDermott et al., 2008).

Material properties of the shaped human meniscus is challenging due to the complexity of the structure. Three regions (anterior, middle, posterior) of fresh-frozen human meniscus were tested in compression at four strain rates (3, 6, 9, and 12%) at a physiologically relevant walking strain rate of $32\%^{-s}$ (Chia and Hull, 2008). Young's Modulus increased with greater strain and was higher in the anterior region (1,048 kPa at 12%) than the posterior region (329 kPa at 12% strain), which is 8x larger than at physiological equilibrium (Chia and Hull, 2008). Stiffness in the circumferential direction is greater than that in the axial and radial direction, which are similar, while thickness varies inversely with modulus (Lechner et al., 2000; Chia and Hull, 2008; Norberg et al., 2021). Meniscal biomechanics show that the lateral meniscus demonstrates greater mobility than the medial meniscus as the lateral meniscus has 9–11 mm of anteroposterior displacement and 11.2 mm of mediolateral displacement, while the medial meniscus exhibits only 2–3 mm of anteroposterior displacement and 5.1 mm of mediolateral displacement (Thompson et al., 1991).

Intervertebral Discs

The repair and regeneration of the cartilage of the human spine, which functions as the body's central support system and key to movement, has been the subject of intensive research and the results have been extensively described and summarized (Panjabi and White, 1980; Oxland, 2016). The human IVD functions to give a bipedal upright human spine motion, stability, and durability. The human IVD, shown in **Figure 1A**, consists of three components, including a multilayered outer ring of elastic collagen tissue fibers [annulus fibrosus (AF)], which is oriented at alternating angles (50–60 + degrees) that provides stability in torsion, compression and tension (Panjabi and White, 1980; Oxland, 2016). The concentric rings do not fully form complete circles in the posterior and posterolateral regions, which make these areas susceptible to herniation, fissures and failure (Panjabi and White, 1980; Oxland, 2016). The gelatinous elastic center (nucleus pulposus (NuP)) transmits stress and weight between vertebrae (Panjabi and White, 1980; Oxland, 2016). The NuP has semi-solid-like properties and therefore expands outward when compressed, which also expands the elastic fibers of the AF. This structure is connected to adjacent vertebrae by the Sharpey's fibers of the relatively flat cartilaginous end plates (CEP) of the vertebral bodies (Panjabi and White, 1980; Oxland, 2016). These three components, the AF, the NuP and the CEP are intimately integrated to function as a unit with the vertebrae above and below forming a spinal unit or motion unit that allows combinations of flexion, extension, lateral bending, and rotation of the spine at varying degrees depending on the location in the spine.

Mechanical properties of the human IVD are the topic of interest in many studies, and for good reason, given the debilitating results of their malfunction/degeneration (Markolf, 1974; Yoganandan et al., 1989; Iida et al., 2002; Stemper, 2010). While it had been believed that the NuP is mainly responsible for the elastic properties of the IVD, all components contribute significantly (Markolf, 1974). The compressive stiffness (E modulus: 19.5 ± 4.1 MPa in 28 ± 8 year old persons and 10.6 ± 3.4 MPa in 70 ± 7 year old persons) of the healthy IVD is 6–7 times higher than the tensile stiffness (E modulus: 2.9 ± 0.8 MPa in 28 ± 8 year old persons and 1.7 ± 1 MPa in 70 ± 7 year old persons 3.3 ± 2.1 MPa) (Iida et al., 2002; Stemper, 2010). Stiffness of the spine can vary depending on the spinal region (Shea et al., 1991). The loading of the IVD measured during normal activities was 0.1–0.5 MPa and increased up to 2.3 MPa during lifting 20 kg weight (Wilke et al., 1999). Studies on sheep IVDs showed increased stiffness of IVD after cycled loading, which fully recovered after a period of unloading (Johannessen et al., 2004).

CURRENT TECHNOLOGIES FOR JOINT CARTILAGE REPAIR

Damage to- or degeneration of joint cartilage can lead to the development of debilitating arthritis, thereby impairing joint function (Abrams et al., 2013). In response to this, the number of research papers published on cartilage repair have nearly doubled in recent years, with the main focus being on replacement or regeneration of the knee meniscus and replacement of intervertebral discs (Abrams et al., 2013).

Knee Cartilage

The critical role of the meniscus in knee biomechanics and joint health is well known (Kester et al., 2021). Preservation of knee meniscus by repair, allograft transplantation and partial meniscectomy in the US is the current standard of care (Abrams et al., 2013; Kester et al., 2021). Over a 7 year period, the number of meniscectomies increased by 14% while the number of meniscus repairs increased by 100% (Abrams et al., 2013). Failure rates for meniscal repair were relatively low: 12% up to 1 year, 15% up to 2–3 years, and 16.5–19% up to 4–6 years post-repair (Ow, 2021). Meniscal repairs typically result in more revision surgeries, but remain a more effective long-term treatment than meniscectomies. Accordingly, while total meniscectomy can provide short-term relief and improve function, there remains a high risk of developing osteoarthritis over the long term (Abrams et al., 2013; Kester et al., 2021; Veronesi et al., 2021). The chondroprotective effects as well as the stabilizing and load-distributing function of the meniscus are thought to have led to the increase in the choice of repair over removal (Abrams et al., 2013). Advances in arthroscopic techniques, instrumentation, and postoperative care have also likely contributed to the rise in repairs (Abrams et al., 2013).

Allograft transplants and implants show promise for restoring meniscal function. Transplant of meniscal allograft tissue to replace removed meniscus has shown encouraging results, however the availability of such tissue is limited, and can be subject to strict regulation in some countries (Veronesi et al., 2021). Meniscal scaffolds can stimulate repair and even regeneration of meniscal tissue, and is therefore an area of increasing research interest (Veronesi et al., 2021). Two acellular scaffolds are currently in clinical use, including Actifit (polyurethane-based) and collagen meniscus implant (CMI) (collagen-based). Both have demonstrated promising results in terms of moderate-to significant pain relief (measured on multiple scales) and improved movement/joint functionality over the mid-to long term (study durations lasting <10 years post-implantation) although regeneration is limited (Veronesi et al., 2021). These scaffolds remained biocompatible, while promoting limited meniscal healing, and therefore chondroprotection, which in turn decreased patient pain (Veronesi et al., 2021). Despite these early achievements, there has been a distinct lack of new meniscal implants (of any kind) approved for clinical use over the last decade.

Intervertebral Discs

Total disc replacement (TDR) and fusion of the spinal column have been used to treat degenerative disc disease for several years (Punt et al., 2008). Despite rising rates of fusion, procedures still come with concerns regarding failure to achieve a solid fusion mass (pseudarthrosis) and adjacent segment degeneration (Salzmann et al., 2017). TDR implantation rates have remained steady in the U.S. over the last decade, possibly due to issues with correct sizing and placement of the implant, the difficult nature of the surgery, lack of device selection, or fear of postoperative complications (Punt et al., 2008; Salzmann et al., 2017). The only TDR implants currently approved by the Food and Drug Administration (FDA) are metal based (U.S. Food and Drug Administration, 2020). THE PRODISC L TOTAL DISC REPLACEMENT -P050010/S020; U.S Food and Drug Administration (2015) activL® Artificial DiscPatient Information -P120024. A006; Geisler, 2006).

Damaged IVDs of the spine can be fixed by replacing the disc with non-flexible material and then fusing the adjacent vertebrae using titanium plates, which results in reduced joint mobility (Rajaee et al., 2012). The number of patients having spinal fusion surgery increased from 203,053 to 442,776 annually from 1998 to 2014 (Sheikh et al., 2020). Despite providing temporary relief, adjacent spinal discs are often damaged due to increased stresses imposed on them as a result of lack of flexibility of fused vertebrae (Rajaee et al., 2012).

Artificial disc replacement has recently emerged as an alternative to fusion due to safer surgical procedures and better preservation of joint mobility (Park, 2015; Salzmann et al., 2017). However, total disc replacement (TDR) rates for intervertebral discs are low due to strict regulations for implant surgeries, demanding surgical techniques, low implant selection, and complications, requiring further surgery (Salzmann et al., 2017). Current TDR devices are composed of metal alloy plates sandwiching a plastic core, or a titanium mesh cage for bone infiltration that replaces the intervertebral disc, both of which can leach metal particles into the body and cause degeneration of relatively softer adjacent vertebrae and facets (FDA clears "first ever" 3D printed spine implant to treat of multiple injuries, 2018; Salzmann et al., 2017). One solution to preventing the development of adjacent segment disease is to preserve native biomechanics by replacing fusion techniques with motion sparing artificial discs. A new artificial cervical (SECURE-C TDR) metal disc has recently been developed to maintain physiologic motion, thereby reducing the risk of adjacent segment degeneration (McConnll, 2016).

There are currently three implants approved by the FDA for total disc replacement in the spine, including the Charité III Artificial Disc (DePuy Spine Inc., Raynham, MA), ProDisc-L (Synthes Spine, Paoli, PA) and the activL Artificial Disc (Aesculap Implant Systems, LLC), which are shown in **Figures 2A,B**, respectively (Salzmann et al., 2017). The Charité Artificial Disc consists of an ultra-high molecular weight polyethylene core that slides between the metallic alloy (containing cobalt, chromium, and molybdenum) endplates, with anchoring teeth on both top and bottom for attachment (Putzier et al., 2006). ProDisc-L consists of two metallic (containing cobalt and chromium) endplates and a plastic (ultra-high molecular weight polyethylene) ball-and-socket style center, with corrugated metal teeth on the top and bottom plates for attachment (U.S. Food and Drug Administration, 2020). THE PRODISC L TOTAL DISC REPLACEMENT-P050010/S020). The activL Artificial Disc is made of two cobalt-chromium alloy endplates and one polyethylene inlay. The plastic center is attached to the bottom endplate, and the top plate is designed to move over the center, allowing motion in all directions (U.S Food and Drug Administration, 2015) activL® Artificial DiscPatient Information-P120024. A006; Miller et al., 2016). There are three anchoring spikes on each of the top and bottom end plates. Additional materials used in intervertebral disc implants may include other cobalt-chromium alloys, stainless steel, titanium alloys, polyurethanes, and titanium alloy-ceramic composites (Pham et al., 2015).

Despite the successful use of metallic implants, there are still biomechanical-and toxicity concerns regarding wear debris (Salzmann et al., 2017). Wear reduces the lifetime of a prosthetic and leaves potentially harmful debris, potentially requiring the need for additional surgeries (Shankar and Kesavan, 2016). Several researchers have reported elevated levels of metal ions in the blood and urine of patients with metal-on-metal devices (Jacobs et al., 1996; Massè et al., 2003; Savarino et al., 2003). Postmortem studies have also found significant metal ion bioaccumulation in the liver, kidney, spleen, heart, and lymphatics of those patients outfitted with metallic implants (Urban et al., 2000). This metallosis is suspected to be an underreported or underdiagnosed issue, and has been shown to result in chronic inflammation, causing a host of unpleasant symptoms (nausea, cognitive impairment, hematological aberrations etc.) and more serious complications such as osteolysis or pseudotumors (Vaz et al., 2019). Further, more systemic and long-term impacts of circulating or accumulated metal ions is not completely understood, making

FIGURE 2 | Three intervertebral disc implants currently approved for use by the FDA including: **(A)** Charité III disc replacement (Depuy Spine) and **(B)** Prodisc-L (Centinel Spine) and **(C)** ActivL® artificial disc (Aesculap Implant Systems). **Figures 2A,B** reprinted with no alterations from (Kaner and Ozer, 2013) under Creative Commons Public Domain Dedication waiver (creativecommons.org/publicdomain/zero/1.0). **Figure 2C** (Aesculap's activL® Artificial Disc product image) used with permission from Aesculap Implant Systems, LLC, Center Valley, PA.

their avoidance desirable. The AcroFlex lumbar disc replacement is one example of a metallic implant that was discontinued after poor clinical outcomes (mechanical failures, osteolysis, etc.) (Germain and Tumialan, 2012; Meir et al., 2013). There is a need to fill this gap in available synthetic and non-metallic implants that exhibit some degree of flexibility and can conserve motion while providing sufficient load-bearing support.

Overcoming Wear: The Evolution of Traditional Cartilage Repair

Some attempts have been made to improve upon the wear-resistance of materials used for the repair of cartilage injury. These encompass various nanocomposites, metal-on-polymer arrangements, ceramics and their composites, as well as woven materials, all with the goal of increasing wear resistance and decreasing wear debris and their physiological effects. One such example is oxidized zirconium (oxinium, possessing ceramic-like properties) with cross-linked polyethylene. Originally utilized for hip replacements, this technology has recently found its way to knee replacements, wherein the ends of the femur and tibia are capped with oxinium, with a polyethylene-based disc acting as the meniscus (Bhandari et al., 2012). The expected end-result is less metal-on-metal friction and wear. While touted as a replacement to older cobalt-containing setups, long-term studies have shown almost comparable (low) rates of wear, and no reduction in revision rates (Kim et al., 2012; Zou et al., 2020). Polymer through-wear followed by wear debris release has also been documented in some patients (Frye et al., 2021). Moreover, this technology involves surgery of even greater invasiveness owing to the complicated capping process. Oxinium debris has, however, shown lower inflammation elicitation than older cobalt counterparts (Rose et al., 2012). Other ceramics have also been used in this area, although mostly for hip arthroplasty. Ceramics have a low coefficient of friction and excellent wear resistance but are generally poor in terms of fracture-resistance owing to their brittleness, and sub-optimal load-bearing and flexibility capabilities (Yup Lee and Kim, 2010). Frequent squeaking of the joints during movement is a common patient complaint when using ceramic-on-ceramic joint replacements (Jarrett et al., 2009). A quite recent development has been the exploration of woven materials: being made of polymeric or hybrid polymer-natural fiber composites, these would have less harmful wear debris. Rodts et al. presented some interesting early work in this area, using laser welding to impart high wear-resistance to their constructs, but–focusing entirely on wear resistance–did not provide any notable data with regard to mechanical properties or *in vivo* performance (Rodts et al., 2019). With no load-bearing substructure, it is difficult to envision these being applied successfully in cartilage or other constructs by themselves.

3D PRINTING FOR CARTILAGE ENGINEERING

As a result of the limitations of current treatment options, there has been increased attention focused on cartilage and tissue engineering to overcome these limitations and facilitate joint regeneration. 3D printing is a popular type of additive manufacturing (AM) technology in which constructs are built in a layer-by-layer fashion, allowing for the design and production of patient-centric implants. 3D printing technology can be used to produce patient-personalized constructs (e.g., IVD's) in a time- and cost-effective manner, allowing for greater flexibility in terms of material selection, typically resulting in the production of more biocompatible constructs compared to metallic implants produced *via* traditional manufacturing methods (Lim et al., 2019). Various computer aided design (CAD) programs can be used to construct digital models, typically based on patient centric data obtained *via* computer tomography (CT) and magnetic resonance imaging (MRI) scans. These models can then be imported into software capable of editing and segmenting files, retaining only particular regions of interest. Lastly, files can be uploaded into a slicing software, where printing parameters such as number of layers and layer height are determined. This process can greatly improve the accuracy and translational potential of printed constructs.

Bioprinting is a subtype of 3D printing, in which the materials used in the 3D printing process contain cells and other biomaterials to produce a final construct. It is an emerging manufacturing technique used to develop tissue engineered constructs with very precise size and shape attributes, while maintaining excellent cell adhesion and proliferation abilities.

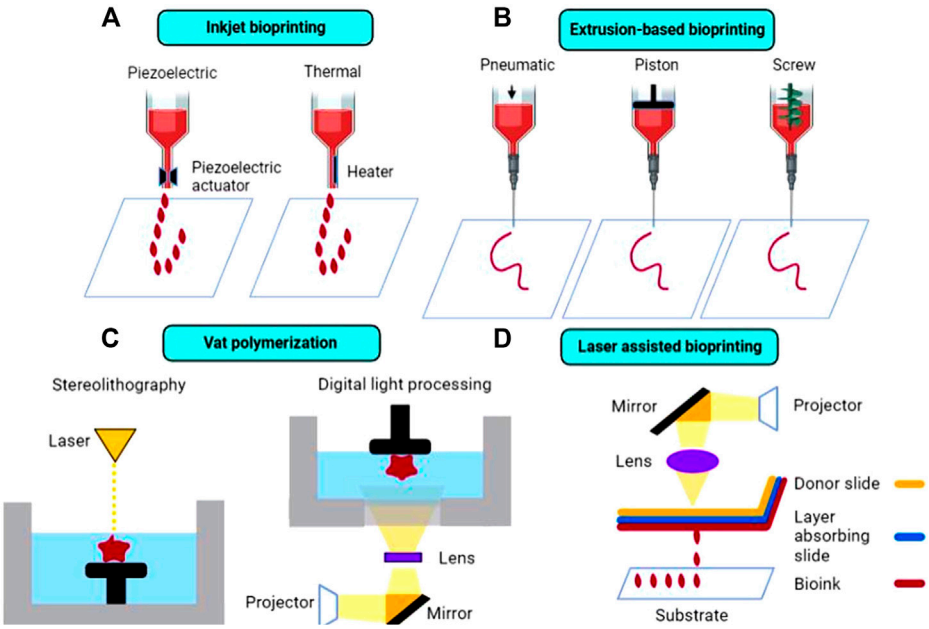

FIGURE 3 | Schematic diagram of the most common 3D bioprinting techniques in cartilage tissue engineering, including **(A)** inkjet bioprinting, **(B)** extrusion-based bioprinting, **(C)** vat polymerization, and **(D)** laser-assisted bioprinting.

Conventionally used metallic implants for meniscus and IVD repair fail to recapitulate the complex biological environment and mechanical structure of native tissue, while also presenting potential toxicity concerns via metal particle leaching in the body (Tavakoli et al., 2020). Overall biocompatibility of printed implants is intimately linked to the materials used in the printing process, which has been the focus of many review papers in recent years (Tappa and Jammalamadaka, 2018). In addition, traditional cartilage tissue engineering approaches result in scaffolds with a homogeneous distribution of chondrocytes or cartilage progenitor cells, and fail to recapitulate the complexity of native cartilage tissue (Daly and Kelly, 2019). Through meticulous material and printing parameter optimization, bioprinting allows for the fabrication of printed constructs demonstrating precise spatial and temporal control on the placement of cells and other bioactive substances (such as growth factors) while exhibiting similar chemical and mechanical properties as native tissue to better guide tissue formation, ideal for cartilage and tissue regeneration applications (Buj-Corral et al., 2018).

To produce 3D printed implants for cartilage repair, available 3D bioprinting techniques include inkjet bioprinting, extrusion-based bioprinting, vat polymerization (VP), and laser assisted bioprinting (LAB). Currently, inkjet and extrusion-based printers remain the most common types of printers used for cartilage tissue engineering applications.

Inkjet Bioprinting

Inkjet printing is a type of powder bed printing technology in which binder droplets, containing cells and other biomaterials (such as growth factors) are dispensed through overhead printheads and deposited onto a substrate, as shown in **Figure 3A** (Shirazi et al., 2015). Inkjet printing is advantageous compared to other traditional bioprinting techniques due to the capability to produce constructs in a cost-effective and high throughput manner (Li et al., 2020). For example, Daly et al. used an inkjet printing approach to produce stratified cartilage tissue by developing a bioink consisting of mesenchymal stem cells (MSC), chondrocytes and either pluronic or gelatin methacrylate (GelMA) and injecting this bioink into polymeric microchambers to guide cell growth and more representatively mimic native cartilage tissue (Daly and Kelly, 2019). However, the droplet ejection process, which can be achieved either *via* thermal or piezoelectric actuation, can be detrimental to maintaining adequate cell viability in printed constructs due to incurred shear and thermal stresses leading to cell death (Li et al., 2016). In addition, depending on bioink viscosity, nozzle clogging can occur, preventing a smooth print from being achieved. Cui et al. (2014) modified an HP Deskjet 500 thermal inkjet printer, allowing it to print a photopolymerizable bioink containing human chondrocytes suspended in poly (ethylene glycol) diacrylate (PEGDA), suitable for cartilage tissue engineering applications.

Extrusion-Based Bioprinting

Traditionally, extrusion-based 3D printing, including fused deposition modeling (FDM) is accomplished by feeding a solid, thermoplastic filament through a high temperature nozzle, in which the material is then continuously extruded and deposited onto a lower temperature build plate, facilitating material solidification (Long et al., 2016). Despite

allowing for rapid and efficient prototyping, FDM is not suitable for thermolabile components, including cell and proteins which can degrade under high temperatures. In addition, this method is only suitable for printing using solid filaments and is not capable of printing liquid cell suspensions. Thus, commercial bioprinters have been developed in recent years to overcome these obstacles. Extrusion-based commercial bioprinters rely on either pneumatic, piston, or screw-driven configurations to achieve continuous bioink extrusion, as shown in **Figure 3B**. In pneumatic-based extrusion, air pressure provides the main driving force for bioink dispensing, whereas in piston and screw-driven extrusion, vertical rotational forces are exerted on the bioink resulting in extrusion (Derakhshanfar et al., 2018). It is important to note that certain configurations, such as screw-driven extrusion, may negatively impact cell viability due to large pressure drops that occur along the nozzle (Ozbolat and Hospodiuk, 2016). Commercial bioprinters are typically considerably more expensive than traditional 3D printers, which may present a significant barrier to entry for some researchers interested in bioprinting, although more cost-effective options have become available. Thus, some researchers have modified existing extrusion-based printers, enabling them to print liquid bioinks. For example, Gantumur et al. (2020) developed an alginate-based bioink containing fibroblast cells that can be printed at room temperature using a modified Prusi i3 3D printer *via* an enzyme-mediated hydrogelation method. Cell viability was similar in printed and non-printed hydrogels (54.1% in printed vs 50.4% in non-printed after 1 day of culture), showing that this printing process did not adversely impact the fate of the cells and demonstrating the feasibility of this technique for bioprinting applications.

Vat Polymerization Bioprinting

Unlike extrusion-based printing, VP techniques rely on the layer-by-layer solidification of liquid photopolymerizable resin, containing photopolymerizable monomer(s) and photoinitiator(s), as shown in **Figure 3C**. A build plate moves along the z-axis inside a resin-containing vat. Upon exposure to a specific wavelength of light (dependent on resin components), the resin polymerizes and solidifies (Martinez et al., 2017). Layer adherence/formation is facilitated by unreacted monomers in the previous layer polymerizing upon light exposure. Stereolithography (SLA) and digital light processing (DLP) are the two main types of VP techniques, with the former using a laser beam and the latter using UV light from a projector to cure the resin. VP printing can overcome limitations inherent to other printing techniques, such as avoiding physical stresses imposed on bioinks (e.g., extrusion-based printing), which can ultimately lead to improved cell viability while maintaining high print resolution of final constructs (Kadry et al., 2019). Grogan et al. (2020) developed scaffold-free cartilage tissue constructs *via* a Regenova bioprinter in which microspheroids, held in place by a microneedle array, eventually fuse together to form neotissues. Li et al. (2017) combined 3D scanning technology with VP-based 3D printing (modified Bio-Architect, Regenovo) to more accurately replicate bone and cartilage defects, using either an alginate- or a hyaluronic acid (HA) based photopolymerizable hydrogel platform. Despite the advantages, concerns regarding photopolymer biocompatibility remains an issue, as unreacted resin components can present cytotoxicity issues at certain concentrations (Sabnis, 2010; Choi and Cha, 2019; Nguyen et al., 2019).

Laser Assisted Bioprinting

LAB is a technique in which a pulsed laser source (UV or near-UV wavelengths) is focused through a donor slide onto an absorbing layer, causing immediate vaporization and resulting in an area of high vapor pressure, facilitating droplet formation of the bioink layer underneath, which then deposits onto a substrate below (**Figure 3D**; Li et al., 2016). Printing *via* LAB circumvents issues typically encountered in traditional bioprinting processes, such as thermal and shear stresses that often lead to lowered cell viability in printed constructs. In addition, high resolution constructs and enhanced cellular organization can be achieved *via* LAB through optimization of ink droplet characteristics, such as ink viscosity and laser energy (Guillotin et al., 2013). However, LAB is a relatively time-consuming and expensive bioprinting method compared to conventional bioprinting techniques. Keriquel et al. (2017) developed a clinically feasible *in situ* forming collagen-nano hydroxyapatite (HAp) composite bioink containing mesenchymal stromal cells suitable for bone defect repair applications using a LAB technique. The LAB setup consisted of a near-infrared pulsed laser beam coupled to a scanning mirror, which focused the laser beam onto the absorbing layer (containing a thin layer of bioink), leading to droplet generation and deposition.

BIOINKS

Materials used to successfully produce bioprinted knee menisci and IVD's need to exhibit certain characteristics, such as biocompatibility to minimize immune response in the body; similar mechanical properties as native cartilage tissue to provide support to high load bearing regions such as in meniscus repair; and capability of promoting cell adhesion and proliferation, leading to cartilage tissue regeneration (Ahmed et al., 2019). Bioink components such as transforming growth factor beta-3 (TGF-β3) and bone morphogenetic protein-6 (BMP-6), can bind to cellular receptors, leading to cell differentiation and proliferation (Roseti et al., 2018). Daly et al. (2016) investigated properties of extrusion-based printing and the *in vitro* cartilage development achievable *via* the use of common bioinks, containing MSC and TGF-β3, including agarose, alginate, GelMA and polyethylene glycol methacrylate (PEGMA, BioINK™). Results demonstrated that agarose and alginate (which lack cell binding motifs) better supported the development of hyaline-like cartilage, while GelMA and PEGMA-based bioinks (which exhibit natural cell binding motifs and can promote cell spreading) were more suitable for fibrocartilaginous tissue development, illustrating that bioink composition plays a key role in determining cell phenotype. In addition, incorporation of polycaprolactone (PCL) fibers allowed for tailored mechanical properties to make printed constructs

TABLE 1 | Examples of cartilage tissue constructs printed using different bioprinting techniques.

Type of bioprinting	Cell type	Bioink materials	Cell viability	Ref
Inkjet	Chondro-cytes	PEGDA	90%	Cui et al. (2014)
	MSC	PEGDMA GelMA	>80%	Gao et al. (2015a)
Extrusion-based	CPC	Alginate	Up to 89%	Yu et al. (2013)
	Chondro-cytes	HA alginate PLA scaffold	>85%	Antich et al. (2020)
	Chondro-cytes	Alginate TGFβ PCL scaffold	85–97%	Kundu, (2013)
Vat polymerization	Chondro-cytes	GelMA Decellularized cartilage ECM	—	Chen et al. (2019)
	Chondro-cytes	GelMA HAMA	Up to 95%	Lam et al. (2019)
Laser-assisted	Mesench-ymal stromal cells	Collagen Nano-hydroxyapatite	—	Keriquel et al. (2017)
	MSC	Alginate	—	Gruene et al. (2010)

CPC, cartilage progenitor cells; ECM, extracellular matrix; GelMA, gelatin methacrylate; HA, hyaluronic acid; HAMA, methacrylated hyaluronic acid; MSC, mesenchymal stem cell; PEGDA, poly(ethylene glycol) diacrylate; PEGDMA, poly(ethylene glycol) dimethacrylate; PLA, polylactic acid; PCL, polycaprolactone; TGF-β, transforming growth factor-β.

more suitable for load-bearing applications (e.g., articular cartilage designed for joint movement) and improve their translational potential. Examples of cartilage tissue constructs fabricated *via* different bioprinting techniques with various types of bioinks are shown in **Table 1**.

Natural Polymers

Natural polymers with excellent biocompatibility and biological activity are an ideal class (relative to synthetic polymers) of materials suitable for use in bioinks, as they are capable of supporting cell attachment and differentiation (Liu et al., 2018). Despite the inherent advantages, natural polymers typically exhibit weaker mechanical properties than synthetic polymers, which can lead to poor printability and hinder *in vivo* performance. Constructs produced using solely natural polymers are typically more prone to failure within the body, as their mechanical properties are often not sufficient to withstand forces exerted *in vivo*. Thus, addition of materials that exhibit enhanced mechanical properties to form composites, and optimization of material crosslinking are strategies that are often used to develop more suitable natural polymer-based bioinks (Peng et al., 2020).

Alginate is a polysaccharide originally derived from brown algae and is often used to produce constructs capable of mimicking ECM structure by crosslinking with calcium ions (Ca^{2+}). Alginate is a promising bioink material due to its biocompatibility and rapid gelation process, leading to suitable printability. Yu et al. (2013) produced tubular channels, designed to mimic native vasculature, *via* an extrusion-based printer using a sodium alginate based bioink containing cartilage progenitor cells, capable of achieving cell viability up to 89%. To improve printability and cell proliferation ability of alginate-based bioinks, composite materials have been developed. For example, Antich et al. (2020) developed a HA-alginate composite bioink able to produce chondrocyte-laden constructs that exhibited improved mechanical properties (e.g., increased viscosity) leading to enhanced printability, while maintaining impressive cell viability (>85%) immediately after printing, with similar cell viability up to 4 weeks later.

HA is a linear polysaccharide and natural glycosaminoglycan (GAG) that plays numerous roles in the human body, such as maintaining ECM structure and acting as a signaling molecule capable of interacting with many cell surface receptors (Dicker, 2014). HA is a biocompatible and biodegradable material and can be easily chemically modified to alter its biological functions, thereby making it an ideal material for cartilage tissue engineering applications. However, like other natural polymers, HA exhibits relatively weak mechanical properties, leading to decreased printability. Ouyang et al. (2016) developed a 3D printable modified HA-based hydrogel ink, relying on guest-host supramolecular assembly *via* adamantane and β-cyclodextrin coupled to HA, resulting in increased viscosity and storage modulus values for modified HA hydrogels. In addition, fibroblast cells were seeded onto printed hydrogels and displayed adequate cell adhesion, illustrating the potential for this material to be used for cartilage tissue engineering applications. Park et al. (2014) developed a bioprinted (in-house extrusion based printer) multicompartment hydrogel platform designed to promote osteochondral tissue regeneration, comprised of a chondrocyte-encapsulated HA compartment and osteoblast-encapsulated collagen (type I) compartment, capable of maintaining good cell viability of both cell types.

Collagen is the most abundant protein in the human body, and has been used to produce bioinks that effectively mimic the ECM structure while promoting cell adhesion, proliferation, and migration (Somaiah et al., 2015). As with other natural polymers, collagen suffers from relatively weak mechanical properties. Rhee et al. (2016) developed a bioink consisting of high concentration (>10 mg/ml) pure collagen containing meniscal fibrochondrocytes, and demonstrated that fabricated constructs could not accurately recapitulate the mechanical properties of native meniscal tissue. Shim et al. (2016) developed a multilayered construct using a bioink comprised

of modified HA (Cucurbit [6]uril and 1,6-diaminohexane (DAH)-conjugated HA) and pepsin-treated collagen (atelocollagen) containing human turbinate-derived mesenchymal stromal cells as well as additional biomaterials (e.g., BMP-2 and TGF-β) capable of inducing cartilage regeneration in an *in vivo* rabbit model.

Gelatin is a linear peptide produced from the denaturation of collagen. Gelation can occur *via* chemical/enzymatic reactions or physical crosslinking, which requires heating and subsequent cooling to produce a semi-solid gel (Bello et al., 2020). Gelatin is an attractive bioink material due to its biocompatibility, biodegradability, and ease of modification (e.g., GelMA), allowing for facile crosslinking and enhanced cellular interactions (Gungor-Ozkerim et al., 2018). However, crosslinking of pure gelatin can be slow and may result in printed constructs that are mechanically inferior to native tissue. To overcome these issues, Singh et al. (2019) developed a gelatin encapsulated composite bioink containing a silk blend (*Bombyx mori* and *Philosamia ricini*) designed to enhance bioink mechanical properties, leading to enhanced printing fidelity while promoting the growth and proliferation of chondrocytes for cartilage tissues regeneration applications. Bioinks have also been developed containing modified gelatin, such as GelMA, in which the degree of methacryloylation and GelMA concentration have been shown to play a key role in modulating overall mechanical properties, including viscosity and stiffness (Leucht et al., 2020).

Other natural polymers, such as silk fibroin and elastin have recently been used in bioinks to produce more physiologically relevant IVD components (i.e., annulus fibrosus) (Costa et al., 2019). Such constructs demonstrate tunable degradation profile and mechanical properties, while remaining biocompatible. On a similar note, Tamo et al. developed a 3D printable chitosan-based hydrogel reinforced with cellulose nanofibers to better address the needs of developing mechanically demanding tissue repair strategies, for use in IVD and menisci repair applications, amongst others (Kamdem Tamo et al., 2021).

Synthetic Polymers

Compared to natural polymers, synthetic polymers such as polycaprolactone (PCL), polyethylene glycol (PEG), and PEG derivatives, such as Pluronic, exhibit more suitable mechanical properties, and are thus better able to withstand the forces exerted during the bioprinting process (Liu and Wang, 2020). In addition, they can support the development of porous structures and microchannels, which serve to recapitulate the vasculature of native tissue. Typically, however, synthetic polymers lack the biological activity necessary for promoting cell growth and proliferation and are thus used primarily for their role in providing structural support for bioinks (Wu et al., 2011).

PCL is a slow-degrading biocompatible polyester that has been used previously in bone tissue scaffold fabrication, and other medical products such as suture and bone screws (Chen et al., 2015; Cho et al., 2019; Dwivedi et al., 2020). PCL is commonly used in bioprinting applications to enhance the mechanical properties of printed constructs. Previous studies have supported this notion, as constructs have been fabricated using PCL as a scaffold material demonstrating an increase in elastic moduli that more closely mimic native articular cartilage (Daly et al., 2016). Kundu (2013) developed a chondrocyte-containing alginate-based bioink able to be printed onto a PCL scaffold using an extrusion-based multi-head deposition system for cartilage tissue engineering. In this study, PCL was used as a support structure for the cell-laden alginate hydrogel, while facilitating cartilage tissue regeneration up to 14 days post-implantation, as demonstrated using a nude mice model.

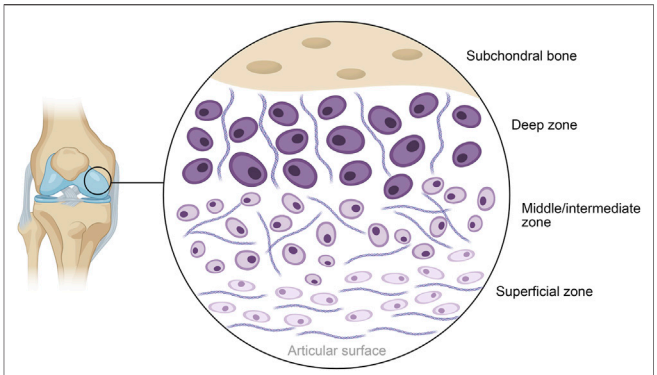

FIGURE 4 | Schematic diagram of the general structure of human articular cartilage, shown in the context of the knee. The deep zone contains hypertrophic chondrocytes interspersed with radially arranged collagen fibers, progressing to polymorphic chondrocytes and randomly arranged collagen in the middle layer. The superficial layer closest to the articular surface contains flattened chondrocytes packed in between horizontally arranged fibers of collagen.

PEG is a highly tunable, relatively inert synthetic polymer synthesized *via* the polymerization of ethylene oxide, that exhibits favorable mechanical properties suitable for cartilage tissue applications. Poloxamer, also known as pluronic, is a PEG-based block copolymer and is also commonly used in bioink development. PEG-based derivatives are attractive bioink materials due to their tunable gelation and favorable mechanical properties, both of which can be modulated by altering pluronic concentration (Geng et al., 2011). For instance, Ribeiro et al. (2018) investigated the printability of PEG/poloxamer-based bioink blends and demonstrated that bioink mechanical properties could be tuned by changing the PEG/poloxamer ratio, noticing that as this ratio increased, mechanical properties (i.e., yield stress, viscosity and storage modulus) decreased correspondingly. PEG and PEG derivatives have been combined with other biologically-active materials to facilitate cell adhesion and proliferation on printed constructs (Hutson et al., 2011; Rutz, 2015). For example, Armstrong et al. (2016) developed a pluronic-alginate composite bioink capable of producing constructs exhibiting a highly porous structure ideal for cell growth and nutrient transport, that supported the proliferation and differentiation of hMSCs over a 5-week period. In addition, photopolymerizable PEG-based materials, such as PEGMA, PEGDA and polyethylene-tetracrylate (PEGTA)–which can crosslink *via* light irradiation–have been developed and are commonly used in bioink formulations for their tunable mechanical properties

and facile crosslinking abilities (Skardal et al., 2010). Gao et al. (2015b) developed a hMSC-encapsulated photopolymerizable PEGDMA-peptide bioink demonstrating good printability capable of producing scaffolds promoting bone-and cartilage regeneration.

CELL-BASED 3D BIOPRINTING

The earliest record of 3D bioprinting with cells being utilized for the regeneration or repair of cartilage is provided by the work of Cui et al. (2012). Fine spatial control and print resolution is highly useful when one considers the distinct structural zones that exist within articular cartilage, particularly the stratification by cell type. Chondrocyte organization, shape and expression patterns have been observed to vary markedly across three distinct layers: the superficial-, middle- and deep zones, as shown in **Figure 4** (Akkiraju and Nohe, 2015). Alternatives to 3D bioprinting such as micromolding or other conventional techniques struggle to recreate these delicate features without significant and painstaking work, often with no guarantee of success. Bioprinting can allow cells with pre-induced expression profiles to be printed in distinct organizational patterns, densities, and depths, while other techniques with low control makes achieving local homogeneity in cell distribution a tough task. Tight spatial control also allows for the use of multiple polymer or matrix materials in complex patterns to achieve desired local-or global mechanical characteristics. This cell-friendly fabrication process allows cells to be seeded earlier on in the fabrication process, further improving fabrication times that have already been made shorter by bioprinting's automated nature. In all, these serve collectively to produce high quality, highly biomimetic cartilage structures.

Cell-Based Bioprinting of Knee Cartilage

Articular cartilage of the knee is one of the most commonly damaged type of cartilage in the human body, as a result of a variety of factors such as age, physical activity or diseases such as osteoarthritis, compounded by the joint's sheer complexity and load-bearing role (Gracitelli et al., 2015). As a result, most bioprinted cartilage applications have focused on regenerating the cartilage of the knee. Given that articular cartilage damage frequently co-occurs with lesions on the subchondral bone, a recent paper by Yang et al. (2020b) sought to produce an integrated, 3D bioprinted construct capable of regenerating both the damaged cartilage and the bone below it. To this end, they printed a layered composite consisting of sodium alginate and gelatin in the "cartilage" layer, and sodium alginate, gelatin and hydroxyapatite in the "bone" layer (the latter being an essential component of the bone regeneration process) with pore sizes of approximately 500 µm (Kattimani et al., 2016). These inks were seeded with pre-differentiated osteogenic and chondrogenic bone marrow mesenchymal stem cells (BMSCs) prior to implantation on rabbit knee lesions for *in vivo* studies. The mechanical properties of this construct were inferior to that of natural cartilage, with a compressive strength of 11 MPa after 6 months post-implantation (30 MPa in natural cartilage) and a maximum tolerable load of 183 N (480 N in natural cartilage), which may be attributed to the mechanical properties of the chosen bioink in this study. Despite this, cell viability *in vitro* was sufficiently high (>70% by day 7) and mechanical properties were significantly better than cell-less controls. Notably, the complete implants could produce hyaline-like cartilage with a still-disorganized structure and delicate links to the surrounding cartilage by 3 months post-implantation, and by 6 months, was histologically indistinguishable from the surrounding cartilage, although a small 'transition area' was visible. This stood in contrast to blank or even cell-less controls where repair either did not happen or was much slower and did not show the key integration with the surrounding cartilage or the subchondral bone. Another research group attempted a similar approach, printing a HAp-doped gelatin hydrogel (10–50 µm pore size) with human umbilical cord blood-derived mesenchymal stem cells (Huang, 2021). The construct was demonstrated to possess a compressive modulus of approximately 77 kPa, with HAp's role in lending compressive strength apparent in the lower compressive modulus of gelatin-only constructs (70.5 kPa). This work demonstrated that HAp was able to induce a certain degree of chondrogenic differentiation as well, noting upregulation in the expression of chondrogenic markers aggrecan (ACAN) and Collagen Type II Alpha 1 Chain (COL2A1) from

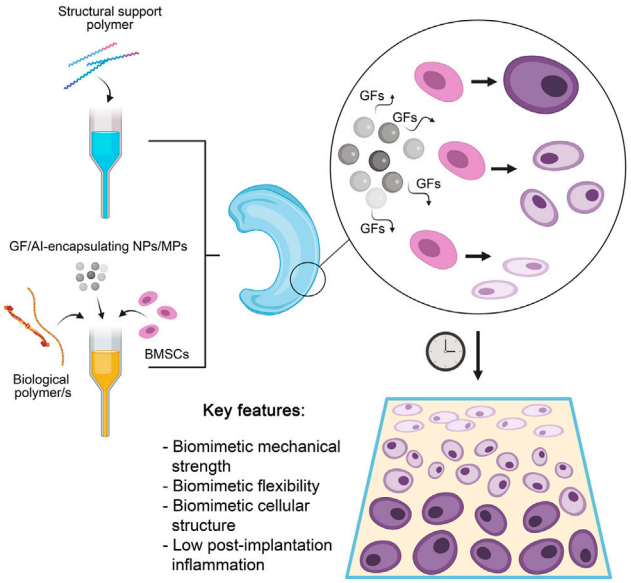

FIGURE 5 | A summary of the most optimal current approach to 3D bioprinting of cartilage structures. A structural support polymer (usually synthetic) is chosen based on desired load-bearing capabilities and co-printed with a range of biological polymers that provide elasticity and a growth medium for seeded cells. Also included are stem cells capable of differentiation into chondrocytes, and nano- (NPs) or microparticles (MPs) encapsulating various growth factors (GFs) to induce differential differentiation of stem cells and anti-inflammatory agents (AIs) to reduce post-implantation inflammation. The release of GFs results in a gradual differentiation of seeded stem cells into mature chondrocytes in a stratified manner. The resultant construct has several key features that allows successful clinical translation.

day 7 on, while levels of SRY-Box Transcription Factor 9 (SOX9) were elevated considerably from day 14 on. The authors did not, however, examine effects of the HAp on the construct's interaction with the subchondral bone, focusing instead on the HAp's ability to induce differentiation, provide strength/stiffness and their ability to act as excellent surfaces for chondrocyte growth and proliferation. In all, this integrative approach is one that merits inclusion in more works in the field of bioprinted cartilage.

The meniscus of the knee has also garnered the attention of 3D bioprinting, mostly due to the inability of current techniques of meniscus repair to address damage deeper in its structure (Guo et al., 2021). Luo et al. (2020) described the design and optimization of a bioink of gelatin, alginate and cellulose nanofibers loaded with rabbit fibrochondrocytes (rFCs). Several different formulations were tested, with pore size increasing proportional to both gelatin and cellulose content: low-gelatin alginate modified with cellulose nanofibers had pore sizes of approximately 180 μm relative to the 300 μm observed in high-gelatin alginate modified with cellulose. Their final construct was printed based on translated MRI imaging data and was thus patient-specific; it could maintain very high cell viabilities (>90% over 14 days) and displayed markedly high levels of collagen types II and X (Col II/X) *in vitro*. These are both indicators of healthy cartilage, the latter being indicative of the hypertrophic chondrocyte phenotype found deep in cartilage structure.

The incorporation of growth factors (GFs) and other molecules to initiate *in situ* differentiation of cells in bioprinted cartilage constructs (as illustrated in **Figure 5**) has been a growing area of interest. Several groups have published on this topic in recent years, examining in various ways how GF can influence cell-laden 3D bioprinted constructs (Henrionnet et al., 2020; Chawla et al., 2021). This has provided an impetus for the printing of constructs pre-loaded with GFs, in a major shift towards biological biomimicry over simple mechanical or morphological biomimicry. Sun et al. (2019) have been frequent contributors to the area, with one of their earlier works translating the findings of a genomics investigation into a viable cartilage regeneration/replacement strategy using 3D bioprinting. Having identified growth differentiation factor 5 (GDF5) as a chondroprotective agent capable of inducing chondrogenic differentiation in rabbit BMSCs, they encapsulated this agent within poly lactic-co-glycolic acid (PLGA) microparticles (MPs) which were then printed into the interfibrillar spaces of a PCL-based support structure, alongside a composite hydrogel made of gelatin, fibrinogen, hyaluronic acid and glycerol laden with rabbit BMSCs. More than 80% of encapsulated GDF5 was observed to be released from the microspheres within 60 days (*in vitro*), and cell proliferation increased exponentially *in vitro* in the 21-day period tested. Most notably, ultimate tensile strength (UTS) was very close to native knee cartilage, as implants exhibited a UTS value of 24 MPa vs. the physiological UTS of 28 MPa. *In vivo*, GDF5 laden constructs were better able to produce hyaline-like neocartilage than constructs without GDF5 MPs, alongside higher GAG and Col II (also indicators of healthy native cartilage, and of chondrocyte phenotype) and displayed better cell spreading and proliferation. Continuing their work, the authors employed 3D bioprinting in the construction of a goat meniscus using a similar approach as above (Sun et al., 2021b). A hydrogel of the same type loaded with goat BMSCs and PLGA MPs containing connective tissue growth factor (CTGF) and (TGFβ3) were printed within a PCL scaffold. Of interest were the conversion of imaging data of a goat meniscus into a 3D model for the print and the differential distribution of the MPs within the meniscus (CTGF-containing MPs in the outer 1/3, TGFβ3 MPs in the inner 2/3) to stimulate differential BMSC differentiation, an improvement upon the indiscriminate differentiation in their previous work. Levels of SOX9 were observed to be elevated by 2x (CTGF MPs) to 3.5x (TGF β3 MPs) *in vitro*, relative to controls. Similar patterns of GAG and Col II vs Col I in the inner- and outer layers were also observed as in their previous work. *In vivo*, qualitative data showed that goats implanted with the complete construct had better 24-week mobility than those with control implants. Histological analysis of the implanted menisci in that period showed the expected native structure of an inner layer with an abundance of Col I-expressing fibroblast-like cells and the outer layer with Col II-expressing chondrocyte-like cells. Post-24 week implants displayed mechanical properties nearly identical to native cartilage, with statistically insignificant differences. Ultimate tensile strength, for instance, stood at approximately 29 MPa in native cartilage *vs.* 28 MPa in the implants; overall tensile modulus was higher in the implants by approximately 10 MPa. Radial and circumferential (both outer and inner layers) tensile modulus readings showed that implants lagged behind native cartilage by margins of less than 5%. By contrast, Deng et al. employed human parathyroid hormone (PH) to prevent chondrocyte hypertrophy in order to achieve and maintain hyaline-like properties (Deng, 2021). They achieved this using a biphasic, layered 3D bioprinted construct made of two distinct bioinks. The first was a mix of GelMA and PH-conjugated SF loaded with rabbit articular cartilage cells, while the second was a mix of GelMA and methacrylated silk fibroin (MSF) loaded with BMSCs, whose pore sizes ranged from 150 to 300 μm. The SF-containing construct was shown to possess a compressive elastic modulus of approximately 102.5 kPa *vs.* 211.1 kPa in the MSF-containing constructs; compressive elastic strength was also higher when MSF was present (260 kPa, a 4x increase over the SF-containing constructs). Significantly lower levels of collagen X and matrix metalloproteinase 13 (MMP13) were expressed by cells grown in the complete construct relative to PH-negative controls. PH was also successful in engendering higher levels of Col II and ACAN in the cells, further confirming its role in maintaining hyaline-like phenotype. *In vivo,* the complete construct had filled lesions on rabbit knee cartilage by week 12 post-implantation. Yang et al. (2021) combined both GFs and MSC-recruiting aptamers in an interesting novel approach. Carbodiimide-mediated conjugation of HM69 aptamer was carried out on decellularized ECM, which was in turn dissolved in TGFβ3-containing GelMA. This bioink was then co-printed with PCL to produce a layered, dual-functional lattice structure with a heterogeneous macro- (800–1,000 μm) and microporous (80–200 μm) structure. The compressive modulus

of this material was observed to be approximately 25 kPa, comparing favorably to expected *in vivo* physiological strain. While cells were later externally cultured on these constructs, what is of note was the ability of the HM69 to recruit adipose-derived stem cells deeper into the construct both *in vitro* and *in vivo*. These GF-loaded, bioprinted constructs are of great use to this field as cell differentiation properties of printed constructs remains paramount to the success of biomimetic cartilage replacement/regeneration strategies. In particular, the inclusion of GFs in extended release micro-/nanoformulations into 3D bioprinted cartilage constructs circumvents a key stumbling block these constructs face during clinical translation-namely, the lack of long-term GF-based support once implanted (Francis et al., 2018).

Recognizing the need for anisotropy for clinical translation, Sun et al. (2020a) have also investigated the significance of construct pore sizes on vascularization and oxidative stress (which in turn influence cellular differentiation). Their design was a four-layer 3D bioprinted construct with gradients of both pore size and GFs. Using their BMSC-loaded, four-component hydrogel within a PCL support referred to previously, the construct was made such that the first layer was endowed with a pore size of 150 μm, which steadily increased to 750 μm in the final, innermost layer. This gradient was designed to accommodate and encourage differentiation of rabbit BMSCs into the smaller flattened chondrocytes observed in the superficial zone of natural cartilage, then into the progressively larger polymorphic- and columnar chondrocytes of the middle zone, and finally, the hypertrophic chondrocytes of the deep zone. This approach was supplemented with PLGA microparticles encapsulating bone morphogenetic protein 4 (BMP4) in the innermost layer of the construct and transforming growth factor-β3 (TGFβ3) in the outermost/superficial one.

In vitro, a clear gradient in the expression of COL2A1 and proteoglycan 4 (PRG4) (markers of the superficial zone of natural cartilage) was observed, decreasing steadily from superficial to deep layers (12x *vs* 1x for PRG4 and 9x *vs* 1x for COL2A1). Cells in this region were observed to be fibroblast-like. Conversely, the levels of Collagen Type X Alpha 1 Chain (COL10A1; cartilage deep zone marker) were 9 times higher in the deep layer (relative to superficial), resulting in clear chondrocyte hypertrophy. The authors also managed to match physiological mechanical properties (a Young's modulus of approx. 300 MPa 12 weeks post-implantation), maintain >70% cell viability *in vitro* and confirm good functional capabilities/performance *in vivo* (with consistently higher histological scores and virtually indistinguishable integration with surrounding cartilage by week 24, relative to single-GF controls. Better microvessel ingrowth was also observed in the dual-GF constructs). These so-called 'dual stimuli' constructs also fared better than controls that either only had the pore size gradient alone or the growth factor gradient alone. Yet another work by the same group directed these anisotropic 3D bioprinting efforts at improving their meniscus construct mentioned previously (Sun et al., 2020b). Seeking again for better biomimicry, they repeated their goat meniscus work within a rabbit model, this time with the addition of microparticles carrying magnesium ions for enhanced vascularization of the superficial zone and skeletal muscle stem cells in place of BMSCs. Again, gradient cell differentiation was recapitulated, and the neovascularization of the superficial layer was observed to closely match the vascular pattern observed in natural menisci (confirmed with endothelial tube-forming assays, which showed the construct was highly capable of inducing the same). *In vivo*, the constructs matched natural cartilage in morphology, histological aspects, and mechanical properties by week 24 (the latter being almost identical to those seen in their earlier work). Anisotropy is a key feature of natural systems and replicating this is especially challenging *in vitro*. Nevertheless, these works discussed above have shown how 3D bioprinting can overcome this issue, and how established growth factor-loaded systems can be adapted for such. Moreover, vascularization of tissue constructs (vital particularly for menisci, which are naturally vascularized along one facet) has long been a significant obstacle for clinical translation of these technologies (Laschke and Menger, 2012; Francis et al., 2018). The work last discussed in this section has elegantly transcended this problem, combining anisotropy, spatial control of cell/ink placement and controlled release of GFs to set a benchmark for the field.

Cell-Based Bioprinting of Intervertebral Discs

Damage to the cartilage of the intervertebral discs (IVDs) can be particularly debilitating, given the key role the spine plays in support and movement. Recapitulating–both biologically and mechanically–the AF and NuP are important steps in producing replacements or regeneration strategies for IVDs. Composed of GAG and Col II, the NuP is a softer, elastic tissue at the core of the IVD, helping distribute pressure through it. The surrounding, harder AF is composed of collagen type I (Col I), and acts as the tougher, load-bearing and shape-maintaining portion of the IVD (Sun et al., 2021a). Bioprinting efforts in this area (particularly in mimicking the AF) have been stymied by the lack of dedicated bioinks for IVDs, as others have already pointed out (Tavakoli et al., 2020). A notable example of a novel bioink for IVDs was presented by Hu et al., who combined thermoplastics and hydrogels in a tunable, 3D printed cartilage system using gellan gum-poly (ethylene glycol) diacrylate (GG-PEGDA) and PLA (Wu et al., 2018). A dual-nozzle printing mechanism formed an outer ring of PLA to replicate the stiffer AF and GG-PEGDA hydrogels seeded with murine bone marrow mesenchymal stem cells (BMSCs) occupying the cavities of the PLA honeycomb substructure standing in for the softer NuP. A Young's modulus of 184 kPa and a compressive strength of 55 kPa was observed in the final construct. The near-total degradation of the PLA within 6 months, excellent cell viability (>90%, 7 days) within the GG-PEGDA hydrogels and progressively high levels of F-actin observed through immunostaining after 7 days (indicating good cell spreading through the construct) were all signs that their bioprinted structure would be a highly biomimetic IVD replacement *in vivo*. Stevens et al. provides an overview of the development of GG-based bioinks, while a recent review by Pieri

et al. provide a more comprehensive review of possible novel bioinks for IVD (Stevens et al., 2016; Pieri et al., 2020). Notwithstanding advances in this field, truly biomimetic IVD replacement/regeneration strategies are only beginning to be researched. Two recent pieces of work stand out for being on this cutting edge. Wu et al. (2021) recently outlined a PLA-based scaffold printed parallelly alongside GG-PEGDA/rat BMSCs, with the NuP and AF differentiated by the patterning of the printed strands, aiming to mimic the porosity and mechanical strength of the two. Of interest was the achievement of an excellent, physiological Young's modulus (remaining >8 MPa over 14 days). When combined with the >80% *in vitro* cell viability 2 weeks post-seeding, the maintenance of >75% disc height *in vivo* over 6 months and comparable levels of proteoglycan expression by the bioprinted implant as in the case of reimplanted natural IVDs over the same period, this is a clear sign that properly designed and -executed thermoplastic-hydrogel composites still hold real promise in this area. The authors did not, however, examine cellular differentiation along their NuP-AF axis, crucial for true biomimicry. Sun et al. (2021a) combined biomaterials, polymers, GFs, cells, and NPs in a complex milieu to form a highly biomimetic IVD replacement capable of inducing site-specific cell differentiation over time. Their NuP consisted of their characteristic gelatin-sodium alginate-hyaluronic acid hydrogel containing rat BMSCs and polydopamine (PDA) NPs decorated with TGF-β3, while the AF consisted of the same hydrogel with BMSCs, and PDA NPs decorated with CTGF. Both were printed in a highly specific pattern within a 3D printed PCL scaffold and capped with cartilage endplates made of the same. Both GFs were found to be released steadily over more than 30 days, while good cell viability over this period *in vitro* predicted good differentiation of BMSCs into AF- and NuP-specific tissue *in vivo*. Most notably, these differentiations were observed to be clearly contained within the envisioned NuP/AF divide, with cells in the NuP portion expressing significantly higher GAG/Col II than those in the AF, and cells in the AF expressing higher Col I levels relative to those in the NuP. While the mechanical properties were not ideal (approaching, but not closely matching physiological compressive modulus), this is cause for excitement in this nascent field, showing how *in situ* differentiation along with the spatial control offered by 3D bioprinting can achieve remarkably biomimetic results.

One notable drawback of the cartilage constructs described so far is a phenomenon the authors themselves have highlighted- 3D bioprinted constructs, no matter how biomimetic, tend to elicit an immune response post-implantation that may last for weeks. Several recent works have outlined bioprinting strategies to solve this problem, albeit based more on traditional 3D printing supplemented with later cell seeding rather than direct bioprinting (Sun et al., 2019; 2020a). Zhu et al. (2020) described a PEGDA and decellularized ECM composite cartilage construct loaded with a natural anti-inflammatory agent (honokiol; 3′,5-Di (prop-2-en-1-yl)[1,1′-biphenyl]-2,4′-diol). This was observed to suppress the release of pro-inflammatory cytokines including TNF-α, IL-1β and IL-6 *in vitro* (by approximately 2.5x, 3x, and 2x, respectively, all matching non-inflamed controls except in the case of IL-6). While levels of inflammation were not measured *in vivo* post-implantation, the use of mild natural compounds may certainly be helpful in forming bioprinted constructs that can manage inflammation without stressing the seeded cells. Lee et al. (2019) outlined a possible role for curcumin in bioprinted cartilage constructs (*viz.* a gelatin-curcumin bioink) but did not elaborate on any anti-inflammatory properties observed in their work. Indeed, natural anti-inflammatory, analgesic compounds such as curcumin, gingerol, resveratrol and others hold much promise in this area- Buhrmann et al. (2020) provide a good recent review of these compounds and their myriad benefits in the context of cartilage tissue engineering in particular. Gong et al. (2020) too presented a method wherein anti-inflammatory IL-4 was printed into a GelMA hydrogel/PCL-hydroxyapatite support to achieve lower immune responses in their cartilage regeneration model. *In vivo,* they observed success in the form of higher histological scores and qualitatively better chondrocyte development post-implantation in the IL-4 loaded constructs compared to controls. This incorporation of anti-inflammatories–while not essential–is a relatively under-researched area in the field, and advances in this area will enhance clinical translation immensely. **Figure 5** provides a summary and most optimal approach to cartilage bioprinting discussed herein.

FUTURE OUTLOOK

3D bioprinting is a fast-moving field, and applications of this technology stand to benefit from this rapid pace of advancement. A recent development of interest is Samandari et al. report of multicompartmental bioprinting and its ability to successfully orient cells during printing (Samandari, 2021). The bioprinting of cartilage stands to gain from technologies such as this, as the spatial orientation of chondrocytes in constructs plays a significant role in *in vitro* and -*vivo* success. However, the need for such developments to be complemented by advances in polymer science and more significant contributions from nano- and microscale engineering must be recognized.

There is still much work to be done in the identification of polymer blends that accurately mimic the mechanical properties and biomechanics of natural cartilage, as well as blends that provide high load-bearing and wear-resistant capabilities. As menisci are responsible for stabilizing joints and acting as shock absorbers, mechanical properties remain one of the most important characteristics to consider when designing appropriate implants for meniscal repairs (Inyang and Vaughan, 2020). This is also of particular concern for IVDs, which differ in anatomy and function by location in the spinal column. For instance, in flexion and extension of the lumbar spine, anterior translation of one vertebra or the other should be 8% or less, while posterior translation should be 9% or less. Translation exceeding this is

known as alteration of motion segment integrity (AOMSI). Additionally, angular motion of one lumbar vertebra to adjacent vertebra should allow no greater than 15 degrees difference within the first three lumbar units, L1/L2, L2/L3, or L3/L4 or no more than 20 degrees at L4/L5 and 25 degrees at L5/S1 (Keeney, 1984). This is a level of complexity that the field cannot yet achieve but must aim for eventually and must mostly be addressed using polymer science. Further, it has been demonstrated that mechanical properties, as well as mesh size (both of which can be impacted by polymer molecular weight) play a key role in modulating the viability and proliferation of chondrocyte-laden constructs (Lin et al., 2011). In addition, several studies have shown that modifications in polymer surface nanotopography (i.e., surface roughness) can lead to increased chondrocyte density and protein production due to enhanced protein binding on micro- and nano-rough surfaces (Storey and Webster, 2014). Advances in anti-inflammatory polymers or polymeric coatings may be of great use to this field as well-this is an active area of research for surgical implants in general, reviewed recently by both Sánchez-Bodón et al. and Lebaudy et al (Bridges and García, 2008; Al-Khoury et al., 2019; Lebaudy et al., 2021; Sánchez-Bodón et al., 2021). Recent work in this field has also evolved to incorporate decellularized extracellular matrix (dECM) from cartilage and IVD into 3D-printable bioinks to aid in guiding cell proliferation, attachment, and differentiation (Vernengo et al., 2020). For example, Kesti et al. (2015) developed a novel composite bioink comprised of gellan and alginate containing micronized BioCartilage, a commercially available extracellular matrix material native to articular cartilage, which supported chondrocyte proliferation and a favorable deposition of cartilage matrix proteins. While this particular bioink was developed for a broad range of tissue engineering applications, advancements like these may serve as a stepping-stone for the development of more finely-tuned bioinks to better address deficiencies in knee menisci and IVD repair strategies. The factors outlined above must all be considered when developing novel bioink formulations for this area of research.

Slow-release nano- or microformulations encapsulating growth factors and other signaling molecules to encourage proper cell differentiation, or those encapsulating agents such as anti-inflammatories or even anti-microbials to enhance post-implantation success are also of great interest to the field. Novel dual-action molecules tailored for cartilage repair like REG-O3 may be of interest to future researchers in this regard (Montjean et al., 2020). A possible way to integrate all this with traditional bioprinting may be to involve nano- or microscale fibers, such as carbon nanotubes (CNTs), that can lend structural support to constructs as well as releasing such agents from their core or their surface. Szymański (2020) provide an excellent review of recent tissue engineering work that has involved CNTs. Capable of self-assembly into nanostructures and acting as cell adhesion points or growth factor binding sites, peptide amphiphiles are also possible additives to cartilage bioinks that are already being explored in other tissue engineering approaches (Lewis et al., 2020; Di Marzio et al., 2020). The next wave of bioink development should also most certainly focus on biomaterials that exhibit 4D bioprinting properties, consisting of materials that can be 3D printed, yet also respond to environmental stimuli (e.g., temperature, pH, etc.) over a desired duration of time (Saska et al., 2021). For example, Betsch et al. (2018) developed a magnetically responsive iron nanoparticle-based bioink capable of producing constructs exhibiting alternating layers of aligned and random collagen fibers able to more accurately recapitulate the complex architecture of native articular cartilage, leading to enhanced collagen II production. Multilayered nano-/microparticles or -fibers can lend additional complexity to cartilage bioprinting by effecting fine control of chondrocyte differentiation and growth through temporally-controlled release of growth factors and other signaling molecules (Go et al., 2011; Asiri et al., 2021). Despite the availability of a considerable body of non-human *in vivo* data, 3D bioprinted cartilage constructs have–so far–not moved on to clinical trials. While fundamental research paves the way to more advanced applications, a field as nascent as this will eventually require clinical data for the refinement and evolution of the field, identifying shortcomings that exist in the *in vitro* development process that impact downstream clinical translation. In this light, it is heartening to note that such trials are now almost underway, with 3DBio Therapeutics' AuriNovo technology (3D bioprinted auricular cartilage for microtia) on the verge of recruiting trial subjects (NCT04399239). The technology is based on a proprietary bioink containing patient-derived (autologous) chondrocytes (AuriNovo for Auricular Reconstruction, 2020). This technology has been spurred in part by the introduction of personalized medicine to this field-a development rooted in the problem of possible implant rejection in a clinical setting as discussed earlier, and the autologous approaches needed to overcome it (Edri et al., 2019).

The need for printed constructs to encourage proper differentiation of seeded stem cells in the correct spatial orientation and patterning is another area that merits further investigation. The majority of works discussed in this review have opted for a static pore size, for instance. While there is evidence in literature that pore sizes of 100–300 μm are optimal for cell differentiation and orientation within constructs, anisotropy in both this and in the release of growth factors, anti-inflammatory agents, anti-microbials etc. from nano/microparticles or -fibers may provide exciting new avenues of producing constructs that are more physiologically relevant, particularly when combined. This is highlighted by Sun and others' work (Zhang et al., 2014; Han et al., 2015; Naseri et al., 2016; Song et al., 2017; Sun et al., 2020a).

As tissue constructs go, cartilage has a relatively simple and straightforward structure to attempt to mimic than many other tissues in the human body. A successful convergence of new and improved polymers, precise bioprinting techniques focusing on anisotropy and dedicated "regions" of cartilage structure, optimized additives, and translation-friendly cell isolation, all complemented with regular feedback in the form of clinical data will define the direction this promising technology will take in the coming years.

AUTHOR CONTRIBUTIONS

KP, RI, and EN wrote and prepared original draft; KP and RI edited and prepared final draft. CW, JS, and JUM reviewed and edited drafts and conceptualized this work.

FUNDING

We acknowledge funding support from the Rhode Island Institutional Development Award (IDeA) Network of Biomedical Research Excellence from the National Institute of General Medical Sciences of the National Institutes of Health under grant number P20GM103430 (JUM), the Rhode Island Foundation Medical Research grant number 2797_20190601 (JS) and the University of Rhode Island Proposal Development Grant (JS, JUM).

ACKNOWLEDGMENTS

Figures 1B, 2, 3 and 4 were created with Biorender.com, with some post-modification by the authors.

REFERENCES

Abrams, G. D., Frank, R. M., Gupta, A. K., Harris, J. D., McCormick, F. M., and Cole, B. J. (2013). Trends in Meniscus Repair and Meniscectomy in the United States, 2005-2011. *Am. J. Sports Med.* 41, 2333–2339. doi:10.1177/0363546513495641

Ahmed, K. K., Tamer, M. A., Ghareeb, M. M., and Salem, A. K. (2019). Recent Advances in Polymeric Implants. *AAPS PharmSciTech.* 20, 300. doi:10.1208/s12249-019-1510-0

Akkiraju, H., and Nohe, A. (2015). Role of Chondrocytes in Cartilage Formation, Progression of Osteoarthritis and Cartilage Regeneration. *J. Dev. Biol.* 3, 177–192. doi:10.3390/jdb3040177

Al-Khoury, H., Espinosa-Cano, E., Aguilar, M. R., Román, J. S., Syrowatka, F., Schmidt, G., et al. (2019). Anti-inflammatory Surface Coatings Based on Polyelectrolyte Multilayers of Heparin and Polycationic Nanoparticles of Naproxen-Bearing Polymeric Drugs. *Biomacromolecules.* 20, 4015–4025. doi:10.1021/acs.biomac.9b01098

Antich, C., de Vicente, J., Jiménez, G., Chocarro, C., Carrillo, E., Montañez, E., et al. (2020). Bio-Inspired Hydrogel Composed of Hyaluronic Acid and Alginate as a Potential Bioink for 3D Bioprinting of Articular Cartilage Engineering Constructs. *Acta Biomater.* 106, 114–123. doi:10.1016/j.actbio.2020.01.046

Armstrong, J. P. K., Burke, M., Carter, B. M., Davis, S. A., and Perriman, A. W. (2016). 3D Bioprinting Using a Templated Porous Bioink. *Adv. Healthc. Mater.* 5, 1724–1730. doi:10.1002/adhm.201600022

Asiri, A., Saidin, S., Sani, M. H., Al-Ashwal, R. H., and Ashwal, A. (2021). Epidermal and Fibroblast Growth Factors Incorporated Polyvinyl Alcohol Electrospun Nanofibers as Biological Dressing Scaffold. *Sci. Rep.* 11, 5634. doi:10.1038/s41598-021-85149-x

AuriNovo for Auricular Reconstruction (2020). Available at: https://clinicaltrials.gov/ct2/show/NCT04399239.

Bello, A. B., Kim, D., Kim, D., Park, H., and Lee, S.-H. (2020). Engineering and Functionalization of Gelatin Biomaterials: From Cell Culture to Medical Applications. *Tissue Eng. B: Rev.* 26, 164–180. doi:10.1089/ten.TEB.2019.0256

Betsch, M., Cristian, C., Lin, Y.-Y., Blaeser, A., Schöneberg, J., Vogt, M., et al. (2018). Incorporating 4D Into Bioprinting: Real-Time Magnetically Directed Collagen Fiber Alignment for Generating Complex Multilayered Tissues. *Adv. Healthc. Mater.* 7, 1800894–1800899. doi:10.1002/adhm.201800894

Bhandari, M., Pascale, W., Sprague, S., and Pascale, V. (2012). The Genesis II in Primary Total Knee Replacement: A Systematic Literature Review of Clinical Outcomes. *The Knee.* 19, 8–13. doi:10.1016/j.knee.2011.02.003

Bridges, A. W., and García, A. J. (2008). Anti-Inflammatory Polymeric Coatings for Implantable Biomaterials and Devices. *J. Diabetes Sci. Technol.* 2, 984–994. doi:10.1177/193229680800200628

Buhrmann, C., Honarvar, A., Setayeshmehr, M., Karbasi, S., Shakibaei, M., Valiani, A., et al. (2020). Herbal Remedies as Potential in Cartilage Tissue Engineering: An Overview of New Therapeutic Approaches and Strategies. *Molecules.* 25, 3075–3125. doi:10.3390/molecules25133075

Buj-Corral, I., Bagheri, A., and Petit-Rojo, O. (2018). 3D Printing of Porous Scaffolds With Controlled Porosity and Pore Size Values. *Materials.* 11, 1532–1618. doi:10.3390/ma11091532

Chawla, S., Turner, N., Terlizzo, M., and Heelan, K. (2021). Annular Atrophic Lichen Planus Induced by Anti-HER2 Antibodies. *Australas. J. Dermatol.* 62, 210–212. doi:10.1111/ajd.13501

Chen, P., Zheng, L., Wang, Y., Tao, M., Xie, Z., Xia, C., et al. (2019). Desktop-Stereolithography 3D Printing of a Radially Oriented Extracellular Matrix/Mesenchymal Stem Cell Exosome Bioink for Osteochondral Defect Regeneration. *Theranostics.* 9, 2439–2459. doi:10.7150/thno.31017

Chen, T., Cai, T., Jin, Q., and Ji, J. (2015). Design and Fabrication of Functional Polycaprolactone. *E-Polymers.* 15, 3–13. doi:10.1515/epoly-2014-0158

Chia, H. N., and Hull, M. L. (2008). Compressive Moduli of the Human Medial Meniscus in the Axial and Radial Directions at Equilibrium and at a Physiological Strain Rate. *J. Orthop. Res.* 26, 951–956. doi:10.1002/jor.20573

Chizhik, S. A., Wierzcholski, K., Trushko, A. V., Zhytkova, M. A., and Miszczak, A. (2010). Properties of Cartilage on Micro- and Nanolevel. *Adv. Tribology.* 2010, 1. doi:10.1155/2010/243150

Cho, Y. S., Choi, S., Lee, S.-H., Kim, K. K., and Cho, Y.-S. (2019). Assessments of Polycaprolactone/Hydroxyapatite Composite Scaffold with Enhanced Biomimetic Mineralization by Exposure to Hydroxyapatite via a 3D-Printing System and Alkaline Erosion. *Eur. Polym. J.* 113, 340–348. doi:10.1016/j.eurpolymj.2019.02.006

Choi, G., and Cha, H. J. (2019). Recent Advances in the Development of Nature-Derived Photocrosslinkable Biomaterials for 3D Printing in Tissue Engineering. *Biomater. Res.* 23, 18–27. doi:10.1186/s40824-019-0168-8

Costa, J. B., Silva-Correia, J., Ribeiro, V. P., da Silva Morais, A., Oliveira, J. M., and Reis, R. L. (2019). Engineering Patient-Specific Bioprinted Constructs for Treatment of Degenerated Intervertebral Disc. *Mater. Today Commun.* 19, 506–512. doi:10.1016/j.mtcomm.2018.01.011

Cui, X., Breitenkamp, K., Finn, M. G., Lotz, M., and D'Lima, D. D. (2012). Direct Human Cartilage Repair Using Three-Dimensional Bioprinting Technology. *Tissue Eng. A.* 18, 1304–1312. doi:10.1089/ten.tea.2011.0543

Cui, X., Gao, G., Yonezawa, T., and Dai, G. (2014). Human Cartilage Tissue Fabrication Using Three-Dimensional Inkjet Printing Technology. *JoVE.* 88, 1–5. doi:10.3791/51294

Dai, Y., and Gao, C. (2016). Cartilage Regeneration. *Poly. Bio. Tiss. Regen.* 21, 255–287. doi:10.1007/978-981-10-2293-7_9

Daly, A. C., Critchley, S. E., Rencsok, E. M., and Kelly, D. J. (2016). A Comparison of Different Bioinks for 3D Bioprinting of Fibrocartilage and Hyaline Cartilage. *Biofabrication.* 8, 045002–045010. doi:10.1088/1758-5090/8/4/045002

Daly, A. C., and Kelly, D. J. (2019). Biofabrication of Spatially Organised Tissues by Directing the Growth of Cellular Spheroids Within 3D Printed Polymeric Microchambers. *Biomaterials.* 197, 194–206. doi:10.1016/j.biomaterials.2018.12.028

Deng, C., Yang, J., He, H., Ma, Z., Wang, W., Zhang, Y., et al. (2021). 3D Bio-Printed Biphasic Scaffolds With Dual Modification of Silk Fibroin for the Integrated Repair of Osteochondral Defects. *Biomater. Sci.* 9, 4891–4903. doi:10.1039/d1bm00535a

Derakhshanfar, S., Mbeleck, R., Xu, K., Zhang, X., Zhong, W., and Xing, M. (2018). 3D Bioprinting for Biomedical Devices and Tissue Engineering: A Review of Recent Trends and Advances. *Bioactive Mater.* 3, 144–156. doi:10.1016/j.bioactmat.2017.11.008

Di Marzio, N., Eglin, D., Serra, T., and Moroni, L. (2020). Bio-Fabrication: Convergence of 3D Bioprinting and Nano-Biomaterials in Tissue Engineering and Regenerative Medicine. *Front. Bioeng. Biotechnol.* 8, 1–11. doi:10.3389/fbioe.2020.00326

Dicker, K. T., Gurski, L. A., Pradhan-Bhatt, S., Witt, R. L., Farach-Carson, M. C., and Jia, X. (2014). Hyaluronan: A Simple Polysaccharide With Diverse Biological Functions. *Acta Biomater.* 10, 1558–1570. doi:10.1016/j.earlhumdev.2006.05.022

Dwivedi, R., Kumar, S., Pandey, R., Mahajan, A., Nandana, D., Katti, D. S., et al. (2020). Polycaprolactone as Biomaterial for Bone Scaffolds: Review of Literature. *J. Oral Biol. Craniofac. Res.* 10, 381–388. doi:10.1016/j.jobcr.2019.10.003

Edri, R., Gal, I., Noor, N., Harel, T., Fleischer, S., Adadi, N., et al. (2019). Personalized Hydrogels for Engineering Diverse Fully Autologous Tissue Implants. *Adv. Mater.* 31, 1803895–1803899. doi:10.1002/adma.201803895

Edri, R.. (2018). FDA Clears "First Ever" 3D Printed Spine Implant to Treat of Multiple Injuries

Fox, A. J. S., Bedi, A., and Rodeo, S. A. (2012). The Basic Science of Human Knee Menisci. *Sports Health.* 4, 340–351. doi:10.1177/1941738111429419

Francis, S. L., Di Bella, C., Wallace, G. G., and Choong, P. F. M. (2018). Cartilage Tissue Engineering Using Stem Cells and Bioprinting Technology-Barriers to Clinical Translation. *Front. Surg.* 5, 1–12. doi:10.3389/fsurg.2018.00070

Frye, B. M., Laughery, K. R., and Klein, A. E. (2021). The Oxinium Arthrogram: A Sign of Oxidized Zirconium Implant Failure. *Arthroplasty Today.* 8, 103–109. doi:10.1016/j.artd.2021.02.001

Gantumur, E., Nakahata, M., Kojima, M., and Sakai, S. (2020). Extrusion-Based Bioprinting Through Glucose-Mediated Enzymatic Hydrogelation. *Int. J. Bioprint.* 6, 43–52. doi:10.18063/ijb.v6i1.250

Gao, G., Schilling, A. F., Hubbell, K., Yonezawa, T., Truong, D., Hong, Y., et al. (2015a). Improved Properties of Bone and Cartilage Tissue From 3D Inkjet-Bioprinted Human Mesenchymal Stem Cells by Simultaneous Deposition and Photocrosslinking in PEG-GelMA. *Biotechnol. Lett.* 37, 2349–2355. doi:10.1007/s10529-015-1921-2

Gao, G., Yonezawa, T., Hubbell, K., Dai, G., and Cui, X. (2015b). Inkjet-Bioprinted Acrylated Peptides and PEG Hydrogel With Human Mesenchymal Stem Cells Promote Robust Bone and Cartilage Formation With Minimal Printhead Clogging. *Biotechnol. J.* 10, 1568–1577. doi:10.1002/biot.201400635

Geisler, F. H. (2006). The CHARITE Artificial Disc: Design History, FDA IDE Study Results, and Surgical Technique. *Clinical Neurosurgery*. Editors G. McKhann II and G. A. Grant. (Philadelphia, PA: Lippincott Williams and Wilkins) 53, 223–228.

Geng, H., Song, H., Qi, J., and Cui, D. (2011). Sustained Release of VEGF from PLGA Nanoparticles Embedded Thermo-Sensitive Hydrogel in Full-Thickness Porcine Bladder Acellular Matrix. *Nanoscale Res. Lett.* 6, 312. doi:10.1186/1556-276X-6-312

Germain, R., and Tumialan, L. M. (2012). Cervical and Lumbar Spinal Arthroplasty: Clinical Review. *Am. J. Neuroradiol.* 33, 1631–1641. doi:10.3174/ajnr.A2758

Go, D. P., Gras, S. L., Mitra, D., Nguyen, T. H., Stevens, G. W., Cooper-white, J. J., et al. (2011). Multilayered Microspheres for the Controlled Release of Growth Factors in Tissue Engineering. *Biomacromolecules.* 12, 1494–1503. doi:10.1021/bm1014574

Gong, L., Li, J., Zhang, J., Pan, Z., Liu, Y., Zhou, F., et al. (2020). An Interleukin-4-Loaded Bi-layer 3D Printed Scaffold Promotes Osteochondral Regeneration. *Acta Biomater.* 117, 246–260. doi:10.1016/j.actbio.2020.09.039

Gracitelli, G. C., Meric, G., Pulido, P. A., McCauley, J. C., and Bugbee, W. D. (2015). Osteochondral Allograft Transplantation for Knee Lesions after Failure of Cartilage Repair Surgery. *Cartilage.* 6, 98–105. doi:10.1177/1947603514566298

Grogan, S. P., Dorthé, E. W., Glembotski, N. E., Gaul, F., and D'Lima, D. D. (2020). Cartilage Tissue Engineering Combining Microspheroid Building Blocks and Microneedle Arrays. *Connect. Tissue Res.* 61, 229–243. doi:10.1080/03008207.2019.1617280

Gruene, M., Deiwick, A., Koch, L., Schlie, S., Unger, C., Hofmann, N., et al. (2011). Laser Printing of Stem Cells for Biofabrication of Scaffold-Free Autologous Grafts. *Tissue Eng. C: Methods.* 17, 79–87. doi:10.1089/ten.tec.2010.0359

Guillotin, B., Ali, M., Ducom, A., Catros, S., Keriquel, V., Souquet, A., et al. (2013). Laser-Assisted Bioprinting for Tissue Engineering. *Biofabrication: Micro- and Nano-fabrication, Printing, Patterning and Assemblies*. Editors G. Forgacs and W. Sun. (Waltham, MA: William Andrew), 95–118. doi:10.1016/B978-1-4557-2852-7.00006-8

Gungor-Ozkerim, P. S., Inci, I., Zhang, Y. S., Khademhosseini, A., and Dokmeci, M. R. (2018). Bioinks for 3D Bioprinting: An Overview. *Biomater. Sci.* 6, 915–946. doi:10.1039/c7bm00765e

Guo, W., Chen, M., Wang, Z., Tian, Y., Zheng, J., Gao, S., et al. (2021). 3D-Printed Cell-Free PCL-MECM Scaffold With Biomimetic Micro-Structure and Micro-Environment to Enhance *In Situ* Meniscus Regeneration. *Bioactive Mater.* 6, 3620–3633. doi:10.1016/j.bioactmat.2021.02.019

Guo, W., Liu, S., Zhu, Y., Yu, C., Lu, S., Yuan, M., et al. (2015). Advances and Prospects in Tissue-Engineered Meniscal Scaffolds for Meniscus Regeneration. *Stem Cell Int.* 2015, 1–13. doi:10.1155/2015/517520

Han, K.-S., Song, J. E., Tripathy, N., Kim, H., Moon, B. M., Park, C. H., et al. (2015). Effect of Pore Sizes of Silk Scaffolds for Cartilage Tissue Engineering. *Macromol. Res.* 23, 1091–1097. doi:10.1007/s13233-015-3156-4

Henrionnet, C., Pourchet, L., Neybecker, P., Messaoudi, O., Gillet, P., Loeuille, D., et al. (2020). Combining Innovative Bioink and Low Cell Density for the Production of 3D-Bioprinted Cartilage Substitutes: A Pilot Study. *Stem Cell Int.* 2020, 1–16. doi:10.1155/2020/2487072

Herwig, J., Egner, E., and Buddecke, E. (1984). Chemical Changes of Human Knee Joint Menisci in Various Stages of Degeneration. *Ann. Rheum. Dis.* 43, 635–640. Available at: https://orthoinfo.aaos.org/en/treatment/artificial-disk-replacement-in-the-lumbar-spine/. doi:10.1136/ard.43.4.635

Huang, J., Huang, Z., Liang, Y., Yuan, W., Bian, L., Duan, L., et al. (2021). 3D Printed Gelatin/Hydroxyapatite Scaffolds for Stem Cell Chondrogenic Differentiation and Articular Cartilage Repair. *Biomater. Sci.* 9, 2620–2630. doi:10.1039/d0bm02103b

Hutson, C. B., Nichol, J. W., Aubin, H., Bae, H., Yamanlar, S., Al-Haque, S., et al. (2011). Synthesis and Characterization of Tunable Poly(ethylene Glycol): Gelatin Methacrylate Composite Hydrogels. *Tissue Eng. Part A.* 17, 1713–1723. doi:10.1089/ten.tea.2010.0666

Iida, T., Abumi, K., Kotani, Y., and Kaneda, K. (2002). Effects of Aging and Spinal Degeneration on Mechanical Properties of Lumbar Supraspinous and Interspinous Ligaments. *Spine J.* 2, 95–100. doi:10.1016/S1529-9430(02)00142-0

Inyang, A. O., and Vaughan, C. L. (2020). Functional Characteristics and Mechanical Performance of PCU Composites for Knee Meniscus Replacement. *Materials.* 13, 1886. doi:10.3390/MA13081886

Jacobs, J. J., Skipor, A. K., Doorn, P. F., Campbell, P., Schmalzried, T. P., Black, J., et al. (1996). Cobalt and Chromium Concentrations in Patients With Metal on Metal Total Hip Replacements. *Clin. Orthop. Relat. Res.* 1, S256–S263. doi:10.1097/00003086-199608001-00022

Jarrett, C., Ranawat, A., Bruzzone, M., Blum, Y., Rodriguez, J., and Ranawat, C. (2009). The Squeaking Hip: A Phenomenon of Ceramic-on-Ceramic Total Hip Arthroplasty. *J Bone Joint Surg Am*, 91, 1344–1350. doi:10.2106/JBJS.F.00970

Johannessen, W., Vresilovic, E. J., Wright, A. C., and Elliott, D. M. (2004). Intervertebral Disc Mechanics Are Restored Following Cyclic Loading and Unloaded Recovery. *Ann. Biomed. Eng.* 32, 70–76. doi:10.1023/b:abme.0000007792.19071.8c

Kadry, H., Wadnap, S., Xu, C., and Ahsan, F. (2019). Digital Light Processing (DLP) 3D-Printing Technology and Photoreactive Polymers in Fabrication of Modified-Release Tablets. *Eur. J. Pharm. Sci.* 135, 60–67. doi:10.1016/j.ejps.2019.05.008

Kamdem Tamo, A., Doench, I., Walter, L., Montembault, A., Sudre, G., David, L., et al. (2021). Development of Bioinspired Functional Chitosan/Cellulose Nanofiber 3d Hydrogel Constructs by 3d Printing for Application in the Engineering of Mechanically Demanding Tissues. *Polymers.* 13, 1663. doi:10.3390/polym13101663

Kaner, T., and Ozer, A. F. (2013). Dynamic Stabilization for Challenging Lumbar Degenerative Diseases of the Spine: A Review of the Literature. *Adv. Orthopedics.* 2013, 1–13. doi:10.1155/2013/753470

Kattimani, V. S., Kondaka, S., and Lingamaneni, K. P. (2016). Hydroxyapatite--Past, Present, and Future in Bone Regeneration. *Bone Tissue Regen. Insights.* 7, BTRI.S36138–19. doi:10.4137/btri.s36138

Keeney, A. H. (1984). Guides to the Evaluation of Permanent Impairment, 2nd Ed. *Am. J. Ophthalmol.* 98, 659. doi:10.1016/0002-9394(84)90290-3

Keriquel, V., Oliveira, H., Rémy, M., Ziane, S., Delmond, S., Rousseau, B., et al. (2017). *In Situ* printing of Mesenchymal Stromal Cells, by Laser-Assisted Bioprinting, for *In Vivo* Bone Regeneration Applications. *Sci. Rep.* 7, 1–10. doi:10.1038/s41598-017-01914-x

Kester, C. R., Caldwell, P. E., and Pearson, S. E. (2021). Lateral Meniscal Allograft Transplant: Dovetail Bone Bridge Preparation. *Arthrosc. Tech.* 10, e969–e973. doi:10.1016/j.eats.2020.11.008

Kesti, M., Eberhardt, C., Pagliccia, G., Kenkel, D., Grande, D., Boss, A., et al. (2015). Bioprinting Complex Cartilaginous Structures With Clinically Compliant Biomaterials. *Adv. Funct. Mater.* 25, 7406–7417. doi:10.1002/adfm.201503423

Kim, Y.-H., Park, J.-W., and Kim, J.-S. (2012). Comparison of the Genesis II Total Knee Replacement With Oxidised Zirconium and Cobalt-Chromium Femoral Components in the Same Patients. *The J. Bone Jt. Surg. Br.* 94, 1221–1227. doi:10.1302/0301-620X.94B9.28854

Krishnan, Y. (2018). Cartilage Diseases. *Matrix Biol.* 71–72, 1–31. doi:10.1016/j.matbio.2018.05.005.Cartilage

Kundu, J., Shim, J.-H., Jang, J., Kim, S.-W., and Cho, D.-W. (2013). An Additive Manufacturing-Based PCL-Alginate-Chondrocyte Bioprinted Scaffold for Cartilage Tissue Engineering. *J. Tissue Eng. Regen. Med.* 9, 1286–1297. doi:10.1002/term.1682

Lam, T., Dehne, T., Krüger, J. P., Hondke, S., Endres, M., Thomas, A., et al. (2019). Photopolymerizable Gelatin and Hyaluronic Acid for Stereolithographic 3D Bioprinting of Tissue-Engineered Cartilage. *J. Biomed. Mater. Res.* 107, 2649–2657. doi:10.1002/jbm.b.34354

Laschke, M. W., and Menger, M. D. (2012). Vascularization in Tissue Engineering: Angiogenesis Versus Inosculation. *Eur. Surg. Res.* 48, 85–92. doi:10.1159/000336876

Lebaudy, E., Fournel, S., Lavalle, P., Vrana, N. E., and Gribova, V. (2021). Recent Advances in Antiinflammatory Material Design. *Adv. Healthc. Mater.* 10, 2001373–2001420. doi:10.1002/adhm.202001373

Lechner, K., Hull, M. L., and Howell, S. M. (2000). Is the Circumferential Tensile Modulus Within a Human Medial Meniscus Affected by the Test Sample Location and Cross-Sectional Area? *J. Orthop. Res.* 18, 945–951. doi:10.1002/jor.1100180614

Lee, M. J., Kim, S. E., Park, J., Ahn, G. Y., Yun, T. H., Choi, I., et al. (2019). Curcumin-Loaded Biodegradable Polyurethane Scaffolds Modified With Gelatin Using 3D Printing Technology for Cartilage Tissue Engineering. *Polym. Adv. Technol.* 30, 3083–3090. doi:10.1002/pat.4740

Leucht, A., Volz, A.-C., Rogal, J., Borchers, K., and Kluger, P. J. (2020). Advanced Gelatin-Based Vascularization Bioinks for Extrusion-Based Bioprinting of Vascularized Bone Equivalents. *Sci. Rep.* 10, 1–15. doi:10.1038/s41598-020-62166-w

Lewis, J. A., Freeman, R., Carrow, J. K., Clemons, T. D., Palmer, L. C., and Stupp, S. I. (2020). Transforming Growth Factor β-1 Binding by Peptide Amphiphile Hydrogels. *ACS Biomater. Sci. Eng.* 6, 4551–4560. doi:10.1021/acsbiomaterials.0c00679

Li, J., Chen, M., Fan, X., and Zhou, H. (2016). Recent Advances in Bioprinting Techniques: Approaches, Applications and Future Prospects. *J. Transl. Med.* 14, 1–15. doi:10.1186/s12967-016-1028-0

Li, L., Yu, F., Shi, J., Shen, S., Teng, H., Yang, J., et al. (2017). *In Situ* repair of Bone and Cartilage Defects Using 3D Scanning and 3D Printing. *Sci. Rep.* 7, 1–12. doi:10.1038/s41598-017-10060-3

Li, X., Liu, B., Pei, B., Chen, J., Zhou, D., Peng, J., et al. (2020). Inkjet Bioprinting of Biomaterials. *Chem. Rev.* 120, 10793–10833. doi:10.1021/acs.chemrev.0c00008

Lim, W., Kim, B., and Moon, Y. L. (2019). Three-Dimensional Bioprinting for Bone and Cartilage Transplantation. *Ann. Jt.* 4, 7. doi:10.21037/aoj.2018.12.06

Lin, S., Sangaj, N., Razafiarison, T., Zhang, C., and Varghese, S. (2011). Influence of Physical Properties of Biomaterials on Cellular Behavior. *Pharm. Res.* 28, 1422–1430. doi:10.1007/s11095-011-0378-9

Liu, F., Chen, Q., Liu, C., Ao, Q., Tian, X., Fan, J., et al. (2018). Natural Polymers for Organ 3D Bioprinting. *Polymers.* 10, 1278–1326. doi:10.3390/polym10111278

Liu, F., and Wang, X. (2020). Synthetic Polymers for Organ 3D Printing. *Polymers.* 12, 1765. doi:10.3390/polym12081765

Long, J., Gholizadeh, H., Lu, J., Bunt, C., and Seyfoddin, A. (2016). Application of Fused Deposition Modelling (FDM) Method of 3D Printing in Drug Delivery. *Curr. Pharm. Des.* 23, 433–439. doi:10.2174/1381612822666161026161

Luo, W., Song, Z., Wang, Z., Wang, Z., Li, Z., Wang, C., et al. (2020). Printability Optimization of Gelatin-Alginate Bioinks by Cellulose Nanofiber Modification for Potential Meniscus Bioprinting. *J. Nanomater.* 2020, 1–13. doi:10.1155/2020/3863428

Makris, E. A., Hadidi, P., and Athanasiou, K. A. (2011). The Knee Meniscus: Structure-Function, Pathophysiology, Current Repair Techniques, and Prospects for Regeneration. *Biomaterials.* 32, 7411–7431. doi:10.1016/j.biomaterials.2011.06.037

Markolf, K. L., and Morris, J. M. (1974). The Structural Components of the Intervertebral Disc. *J. Bone Jt. Surg.* 56, 675–687. doi:10.2106/00004623-197456040-00003

Martinez, P. R., Goyanes, A., Basit, A. W., and Gaisford, S. (2017). Fabrication of Drug-Loaded Hydrogels With Stereolithographic 3D Printing. *Int. J. Pharmaceutics.* 532, 313–317. doi:10.1016/j.ijpharm.2017.09.003

Massè, A., Bosetti, M., Buratti, C., Visentin, O., Bergadano, D., and Cannas, M. (2003). Ion Release and Chromosomal Damage From Total Hip Prostheses With Metal-On-Metal Articulation. *J. Biomed. Mater. Res.* 67B, 750–757. doi:10.1002/jbm.b.10070

McConnll, J. (2016). Motion Preservation at the Operative Level and the Incidence of Symptomatic Adjacent Segment Disease After Treatment With SECURE®-C or ACDF. *Spine J.* 16, 189. doi:10.1016/j.spinee.2016.07.179

McDermott, I. D., Masouros, S. D., and Amis, A. A. (2008). Biomechanics of the Menisci of the Knee. *Curr. Orthopaedics.* 22, 193–201. doi:10.1016/j.cuor.2008.04.005

Meir, A. R., Freeman, B. J. C., Fraser, R. D., and Fowler, S. M. (2013). Ten-Year Survival and Clinical Outcome of the AcroFlex Lumbar Disc Replacement for the Treatment of Symptomatic Disc Degeneration. *Spine J.* 13, 13–21. doi:10.1016/j.spinee.2012.12.008

Miller, L. E., Yue, J., and Garcia, R. (2016). The activL® Artificial Disc: A Next-Generation Motion-Preserving Implant for Chronic Lumbar Discogenic Pain. *Med. Devices: Evidence Res.* 9, 75–84. doi:10.2147/MDER.S102949

Montjean, R., Escaich, S., Paolini, R., Carelli, C., Pirson, S., Neutelings, T., et al. (2020). REG-O3 Chimeric Peptide Combining Growth Hormone and Somatostatin Sequences Improves Joint Function and Prevents Cartilage Degradation in Rat Model of Traumatic Knee Osteoarthritis. *PLoS One.* 15, e0231240–17. doi:10.1371/journal.pone.0231240

Murphy, M. K., Masters, T. E., Hu, J. C., and Athanasiou, K. A. (2015). Engineering a Fibrocartilage Spectrum Through Modulation of Aggregate Redifferentiation. *Cell Transpl.* 24, 235–245. doi:10.3727/096368913X676204

Naseri, N., Poirier, J.-M., Girandon, L., Fröhlich, M., Oksman, K., and Mathew, A. P. (2016). 3-Dimensional Porous Nanocomposite Scaffolds Based on Cellulose Nanofibers for Cartilage Tissue Engineering: Tailoring of Porosity and Mechanical Performance. *RSC Adv.* 6, 5999–6007. doi:10.1039/c5ra27246g

Ng, L., Grodzinsky, A. J., Patwari, P., Sandy, J., Plaas, A., and Ortiz, C. (2003). Individual Cartilage Aggrecan Macromolecules and Their Constituent Glycosaminoglycans Visualized via Atomic Force Microscopy. *J. Struct. Biol.* 143, 242–257. doi:10.1016/j.jsb.2003.08.006

Nguyen, A. K., Goering, P. L., Reipa, V., and Narayan, R. J. (2019). Toxicity and Photosensitizing Assessment of Gelatin Methacryloyl-Based Hydrogels Photoinitiated with Lithium Phenyl-2,4,6-Trimethylbenzoylphosphinate in Human Primary Renal Proximal Tubule Epithelial Cells. *Biointerphases.* 14, 021007–021008. doi:10.1116/1.5095886

Norberg, C., Filippone, G., Andreopoulos, F., Best, T. M., Baraga, M., Jackson, A. R., et al. (2021). Viscoelastic and Equilibrium Shear Properties of Human Meniscus: Relationships With Tissue Structure and Composition. *J. Biomech.* 120, 110343. doi:10.1016/j.jbiomech.2021.110343

Ouyang, L., Highley, C. B., Rodell, C. B., Sun, W., and Burdick, J. A. (2016). 3D Printing of Shear-Thinning Hyaluronic Acid Hydrogels With Secondary Cross-Linking. *ACS Biomater. Sci. Eng.* 2, 1743–1751. doi:10.1021/acsbiomaterials.6b00158

Ow, Z. (2021). All-Cause Failure Rates Increase With Time Following Meniscal Repair Despite Favorable Outcomes: A Systematic Review and Meta-Analysis. *J. Arthrosc. Relat. Surg.* 5, 00519. doi:10.1016/j.arthro.2021.05.033

Oxland, T. R. (2016). Fundamental Biomechanics of the Spine-What We Have Learned in the Past 25 Years and Future Directions. *J. Biomech.* 49, 817–832. doi:10.1016/j.jbiomech.2015.10.035

Ozbolat, I. T., and Hospodiuk, M. (2016). Current Advances and Future Perspectives in Extrusion-Based Bioprinting. *Biomaterials.* 76, 321–343. doi:10.1016/j.biomaterials.2015.10.076

Panjabi, M. M., and White, A. A. (1980). Basic Biomechanics of the Spine. *Neurosurgery.* 7, 76–93. doi:10.1097/00006123-198007000-00013

Park, C. K. (2015). Total Disc Replacement in Lumbar Degenerative Disc Diseases. *J. Korean Neurosurg. Soc.* 58, 401–411. doi:10.3340/jkns.2015.58.5.401

Park, J. Y., Choi, J.-C., Shim, J.-H., Lee, J.-S., Park, H., Kim, S. W., et al. (2014). A Comparative Study on Collagen Type I and Hyaluronic Acid Dependent Cell Behavior for Osteochondral Tissue Bioprinting. *Biofabrication.* 6, 035004–035011. doi:10.1088/1758-5082/6/3/035004

Peng, Y.-Y., Dussan, D. D., and Narain, R. (2020). Thermal, Mechanical, and Electrical Properties. *Polym. Sci. Nanotechnology Fundamentals Appl.*. Editors R. Narain. Cambridge, MA: Elsevier, 179–201. doi:10.1016/b978-0-12-816806-6.00009-1

Pham, M. H., Mehta, V. A., Tuchman, A., and Hsieh, P. C. (2015). Material Science in Cervical Total Disc Replacement. *Biomed. Res. Int.* 2015, 1–9. doi:10.1155/2015/719123

Pieri, A., Byerley, A. M., Musumeci, C. R., Salemizadehparizi, F., Vanderhorst, M. A., and Wuertz-Kozak, K. (2020). Electrospinning and 3D Bioprinting for Intervertebral Disc Tissue Engineering. *Jor Spine.* 3, 1–11. doi:10.1002/jsp2.1117

Prezyna, A. P. (2000). Adverse Biologic Reactions to Polymers, Metals and Other Prosthetic Materials. *Mol. Crystals Liquid Crystals Sci. Technology. Section A. Mol. Crystals Liquid Crystals.* 354, 239–242. doi:10.1080/10587250008023617

Punt, I. M., Visser, V. M., Van Rhijn, L. W., Kurtz, S. M., Antonis, J., Schurink, G. W. H., et al. (2008). Complications and Reoperations of the SB Charité Lumbar Disc Prosthesis: Experience in 75 Patients. *Eur. Spine J.* 17, 36–43. doi:10.1007/s00586-007-0506-8

Putzier, M., Funk, J. F., Schneider, S. V., Gross, C., Tohtz, S. W., Khodadadyan-Klostermann, C., et al. (2006). Charité Total Disc Replacement-Clinical and Radiographical Results After an Average Follow-Up of 17 Years. *Eur. Spine J.* 15, 183–195. doi:10.1007/s00586-005-1022-3

Rajaee, S. S., Bae, H. W., Kanim, L. E. A., and Delamarter, R. B. (2012). Spinal Fusion in the United States: Analysis of Trends From 1998 to 2008. *Spine.* 37, 67–76. doi:10.1097/BRS.0b013e31820cccfb

Rhee, S., Puetzer, J. L., Mason, B. N., Reinhart-king, C. A., and Bonassar, L. J. (2016). 3D Bioprinting of Spatially Heterogeneous Collagen Constructs for Cartilage Tissue Engineering. *ACS Biomater. Sci. Eng.* 2, 1800–1805. doi:10.1021/acsbiomaterials.6b00288

Ribeiro, A., Blokzijl, M. M., Levato, R., Visser, C. W., Castilho, M., Hennink, W. E., et al. (2018). Assessing Bioink Shape Fidelity to Aid Material Development in 3D Bioprinting. *Biofabrication.* 10, 014102–014116. doi:10.1088/1758-5090/aa90e2

Rodts, T., Schmid, S. R., Selles, M. A., Pasang, T., and Sanchez-Caballero, S. (2019). Selective Laser Fiber Welding on Woven Polymer Fabrics for Biomedical Applications. *Mater. Sci. Eng. C.* 94, 628–634. doi:10.1016/j.msec.2018.10.018

Rose, S. F., Weaver, C. L., Fenwick, S. A., Horner, A., and Pawar, V. D. (2012). The Effect of Diffusion Hardened Oxidized Zirconium Wear Debris on Cell Viability and Inflammation-An *In Vitro* Study. *J. Biomed. Mater. Res.* 100B, 1359–1368. doi:10.1002/jbm.b.32704

Roseti, L., Cavallo, C., Desando, G., Parisi, V., Petretta, M., Bartolotti, I., et al. (2018). Three-Dimensional Bioprinting of Cartilage by the Use of Stem Cells: A Strategy to Improve Regeneration. *Materials.* 11, 1749–1820. doi:10.3390/ma11091749

Rutz, A. L., Hyland, K. E., Jakus, A. E., Burghardt, W. R., and Shah, R. N. (2015). A Multimaterial Bioink Method for 3D Printing Tunable, Cell-Compatible Hydrogels. *Adv. Mater.* 27, 1607–1614. doi:10.1002/adma.201405076.A

Sabnis, A., Rahimi, M., Chapman, C., and Nguyen, K. T. (2010). Cytocompatibility Studies of an *In Situ* Photopolymerized Thermoresponsive Hydrogel Nanoparticle System Using Human Aortic Smooth Muscle Cells. *J. Biomed. Mater. Res. A.* 91, 52–59. doi:10.1002/jbm.a.32194.Cytocompatibility

Salzmann, S. N., Plais, N., Shue, J., and Girardi, F. P. (2017). Lumbar Disc Replacement Surgery-Successes and Obstacles to Widespread Adoption. *Curr. Rev. Musculoskelet. Med.* 10, 153–159. doi:10.1007/s12178-017-9397-4

Samandari, M., Alipanah, F., Majidzadeh-A, K., Alvarez, M. M., Trujillo-de Santiago, G., and Tamayol, A. (2021). Controlling Cellular Organization in Bioprinting through Designed 3D Microcompartmentalization. *Appl. Phys. Rev.* 8, 021404. doi:10.1063/5.0040732

Sánchez-Bodón, J., Ruiz-Rubio, L., Hernáez-Laviña, E., Vilas-Vilela, J. L., and Moreno-Benítez, M. I. (2021). Poly(L-lactide)-Based Anti-inflammatory Responsive Surfaces for Surgical Implants. *Polymers.* 13, 34–15. doi:10.3390/polym13010034

Sansone, V. (2013). The Effects on Bone Cells of Metal Ions Released from Orthopaedic Implants. A Review. *Ccmbm.* 10, 34–40. doi:10.11138/ccmbm/2013.10.1.034

Saska, S., Pilatti, L., Blay, A., and Shibli, J. A. (2021). Bioresorbable Polymers : Advanced Materials and 4D Printing for Tissue Engineering. *MDPI Polym.* 13, 1–22. doi:10.3390/polym13040563

Savarino, L., Granchi, D., Ciapetti, G., Cenni, E., Greco, M., Rotini, R., et al. (2003). Ion Release in Stable Hip Arthroplasties Using Metal-On-Metal Articulating Surfaces: A Comparison between Short- and Medium-Term Results. *J. Biomed. Mater. Res.* 66A, 450–456. doi:10.1002/jbm.a.10595

Shankar, S., and Kesavan, D. (2016). Wear Prediction of the Lumbar Total Disc Replacement Using Finite Element Method. *J. Mech. Med. Biol.* 16, 1650004–1650012. doi:10.1142/S0219519416500044

Shea, M., Edwards, W. T., White, A. A., and Hayes, W. C. (1991). Variations of Stiffness and Strength Along the Human Cervical Spine. *J. Biomech.* 24, 95–107. doi:10.1016/0021-9290(91)90354-P

Sheikh, S. R., Thompson, N. R., Benzel, E., Steinmetz, M., Mroz, T., Tomic, D., et al. (2020). Can We Justify it? Trends in the Utilization of Spinal Fusions and Associated Reimbursement. *Clin. Neurosurg.* 86, E193–E202. doi:10.1093/neuros/nyz400

Shim, J.-H., Jang, K.-M., Hahn, S. K., Park, J. Y., Jung, H., Oh, K., et al. (2016). Three-Dimensional Bioprinting of Multilayered Constructs Containing Human Mesenchymal Stromal Cells for Osteochondral Tissue Regeneration in the Rabbit Knee Joint. *Biofabrication.* 8, 014102. doi:10.1088/1758-5090/8/1/014102

Shirazi, S. F. S., Gharehkhani, S., Mehrali, M., Yarmand, H., Metselaar, H. S. C., Adib Kadri, N., et al. (2015). A Review on Powder-Based Additive Manufacturing for Tissue Engineering: Selective Laser Sintering and Inkjet 3D Printing. *Sci. Technology Adv. Mater.* 16, 033502–033520. doi:10.1088/1468-6996/16/3/033502

Singh, Y. P., Bandyopadhyay, A., and Mandal, B. B. (2019). 3D Bioprinting Using Cross-Linker-Free Silk-Gelatin Bioink for Cartilage Tissue Engineering. *ACS Appl. Mater. Inter.* 11, 33684–33696. doi:10.1021/acsami.9b11644

Skardal, A., Zhang, J., and Prestwich, G. D. (2010). Bioprinting Vessel-Like Constructs Using Hyaluronan Hydrogels Crosslinked With Tetrahedral Polyethylene Glycol Tetracrylates. *Biomaterials.* 31, 6173–6181. doi:10.1016/j.biomaterials.2010.04.045

Somaiah, C., Kumar, A., Mawrie, D., Sharma, A., Patil, S. D., Bhattacharyya, J., et al. (2015). Collagen Promotes Higher Adhesion, Survival and Proliferation of Mesenchymal Stem Cells. *PLoS One.* 10, e0145068–15. doi:10.1371/journal.pone.0145068

Song, X., Zhu, C., Fan, D., Mi, Y., Li, X., Fu, R., et al. (2017). A Novel Human-Like Collagen Hydrogel Scaffold With Porous Structure and Sponge-Like Properties. *Polymers.* 9, 638–716. doi:10.3390/polym9120638

Stemper, B. D., Board, D., Yoganandan, N., and Wolfla, C. E. (2010). Biomechanical Properties of Human Thoracic Spine Disc Segments. *J. Craniovertebr Junction Spine.* 1, 18–22. doi:10.4103/0974-8237.65477

Stevens, L. R., Gilmore, K. J., Wallace, G. G., and in het Panhuis, M. (2016). Tissue Engineering With Gellan Gum. *Biomater. Sci.* 4, 1276–1290. doi:10.1039/c6bm00322b

Storey, D. M., and Webster, T. J. (2014). Novel Nano-Rough Polymers for Cartilage Tissue Engineering. *Int. J. Nano.* 9, 1845–1853.

Sun, B., Lian, M., Han, Y., Mo, X., Jiang, W., Qiao, Z., et al. (2021a). A 3D-Bioprinted Dual Growth Factor-Releasing Intervertebral Disc Scaffold Induces Nucleus Pulposus and Annulus Fibrosus Reconstruction. *Bioactive Mater.* 6, 179–190. doi:10.1016/j.bioactmat.2020.06.022

Sun, Y., Zhang, Y., Wu, Q., Gao, F., Wei, Y., Ma, Y., et al. (2021b). 3D-Bioprinting Ready-To-Implant Anisotropic Menisci Recapitulate Healthy Meniscus Phenotype and Prevent Secondary Joint Degeneration. *Theranostics.* 11, 5160–5173. doi:10.7150/thno.54864

Sun, Y., You, Y., Jiang, W., Wang, B., Wu, Q., and Dai, K. (2020a). 3D Bioprinting Dual-Factor Releasing and Gradient-Structured Constructs Ready to Implant for Anisotropic Cartilage Regeneration. *Sci. Adv.* 6, eaay1422–10. doi:10.1126/sciadv.aay1422

Sun, Y., You, Y., Jiang, W., Wu, Q., Wang, B., and Dai, K. (2020b). Generating Ready-To-Implant Anisotropic Menisci by 3D-Bioprinting Protein-Releasing Cell-Laden Hydrogel-Polymer Composite Scaffold. *Appl. Mater. Today.* 18, 100469. doi:10.1016/j.apmt.2019.100469

Sun, Y., You, Y., Jiang, W., Zhai, Z., and Dai, K. (2019). 3D-bioprinting a Genetically Inspired Cartilage Scaffold With GDF5-Conjugated BMSC-

Laden Hydrogel and Polymer for Cartilage Repair. *Theranostics.* 9, 6949–6961. doi:10.7150/thno.38061

Szymański, T. (2020). Utilization of Carbon Nanotubes in Manufacturing of 3D Cartilage and Bone Scaffolds. *Materials (Basel).* 13, 1–25.

Tappa, K., and Jammalamadaka, U. (2018). Novel Biomaterials Used in Medical 3D Printing Techniques. *J. Funct. Biomater.* 9, 17. doi:10.3390/jfb9010017

Tavakoli, J., Diwan, A. D., and Tipper, J. L. (2020). Advanced Strategies for the Regeneration of Lumbar Disc Annulus Fibrosus. *Int. J. Mol. Sci.* 21, 4889–4920. doi:10.3390/ijms21144889

Thompson, W. O., Thaete, F. L., Fu, F. H., and Dye, S. F. (1991). Tibial Meniscal Dynamics Using Three-Dimensional Reconstruction of Magnetic Resonance Images. *Am. J. Sports Med.* 19, 210–216. doi:10.1177/036354659101900302

Urban, R. M., Jacobs, J. J., Tomlinson, M. J., Gavrilovic, J., Black, J., and Peoc'H, M. (2000). Dissemination of Wear Particles to the Liver, Spleen, and Abdominal Lymph Nodes of Patients With Hip or Knee Replacement*. *The J. Bone Jt. Surgery-American.* 82, 457–477. doi:10.2106/00004623-200004000-00002

U.S Food and Drug Administration (2015). *Center for Devices and Radiological Health*. MD: Silver Spring. Available at: https://www.accessdata.fda.gov/cdrh_docs/pdf18/K181644.pdf.

U.S. Food and Drug Administration (2020). *Center for Devices and Radiological Health*. MD: Silver Spring. Available at: https://www.accessdata.fda.gov/cdrh_docs/pdf5/P050010S020A.pdf.

Vaz, R. A., Xavier, P., Brito, S., Dantas, J., Duque, S., Consciência, J. G., et al. (2019). Metallosis: A New Form of Autoimmune/Autoinflammatory Syndrome Induced by Adjuvants Syndrome (ASIA)? *Eur. J. Case Rep. Intern. Med. Met.* 6, 1–3. doi:10.12890/201910.12890/2019_001034

Vernengo, A. J., Grad, S., Eglin, D., Alini, M., and Li, Z. (2020). Bioprinting Tissue Analogues With Decellularized Extracellular Matrix Bioink for Regeneration and Tissue Models of Cartilage and Intervertebral Discs. *Adv. Funct. Mater.* 30, 1909044. doi:10.1002/adfm.201909044

Veronesi, F., Di Matteo, B., Vitale, N. D., Filardo, G., Visani, A., Kon, E., et al. (2021). Biosynthetic Scaffolds for Partial Meniscal Loss: A Systematic Review From Animal Models to Clinical Practice. *Bioactive Mater.* 6, 3782–3800. doi:10.1016/j.bioactmat.2021.03.033

Wei, W., Ma, Y., Yao, X., Zhou, W., Wang, X., Li, C., et al. (2021). Advanced Hydrogels for the Repair of Cartilage Defects and Regeneration. *Bioactive Mater.* 6, 998–1011. doi:10.1016/j.bioactmat.2020.09.030

Wilke, H. J., Neef, P., Caimi, M., Hoogland, T., and Claes, L. E. (1999). New *In Vivo* Measurements of Pressures in the Intervertebral Disc in Daily Life. *Spine.* 24, 755–762. doi:10.1097/00007632-199904150-00005

Wu, D., Tan, J., Yao, L., Tian, J., Luo, B., Li, L., et al. (2021). Customized Composite Intervertebral Disc Scaffolds by Integrated 3D Bioprinting for Therapeutic Implantation. *Composites A: Appl. Sci. Manufacturing.* 147, 106468–106511. doi:10.1016/j.compositesa.2021.106468

Wu, D., Yu, Y., Tan, J., Huang, L., Luo, B., Lu, L., et al. (2018). 3D Bioprinting of Gellan Gum and Poly (Ethylene Glycol) Diacrylate Based Hydrogels to Produce Human-Scale Constructs with High-Fidelity. *Mater. Des.* 160, 486–495. doi:10.1016/j.matdes.2018.09.040

Wu, W., Deconinck, A., and Lewis, J. A. (2011). Omnidirectional Printing of 3D Microvascular Networks. *Adv. Mater.* 23, H178–H183. doi:10.1002/adma.201004625

Yanke, A., and Cole, B. (2019) Editor. *Joint Preservation of the Knee: A Clinical Casebook*. Cham, Switzerland: Springer, 1–8.

Yang, F., Zhao, J., Koshut, W. J., Watt, J., Riboh, J. C., Gall, K., et al. (2020a). A Synthetic Hydrogel Composite With the Mechanical Behavior and Durability of Cartilage. *Adv. Funct. Mater.* 30, 2003451–2003458. doi:10.1002/adfm.202003451

Yang, Y., Yang, G., Song, Y., Xu, Y., Zhao, S., and Zhang, W. (2020b). 3D Bioprinted Integrated Osteochondral Scaffold-Mediated Repair of Articular Cartilage Defects in the Rabbit Knee. *J. Med. Biol. Eng.* 40, 71–81. doi:10.1007/s40846-019-00481-y

Yang, Z., Zhao, T., Gao, C., Cao, F., Li, H., Liao, Z., et al. (2021). 3D-Bioprinted Difunctional Scaffold for *In Situ* Cartilage Regeneration Based on Aptamer-Directed Cell Recruitment and Growth Factor-Enhanced Cell Chondrogenesis. *ACS Appl. Mater. Inter.* 13, 23369–23383. doi:10.1021/acsami.1c01844

Yoganandan, N., Sances, A., and Pintar, F. (1989). Biomechanical Evaluation of the Axial Compressive Responses of the Human Cadaveric and Manikin Necks. *J. Biomech. Eng.* 111, 250–255. doi:10.1115/1.3168374

Yu, Y., Zhang, Y., Martin, J. A., and Ozbolat, I. T. (2013). Evaluation of Cell Viability and Functionality in Vessel-Like Bioprintable Cell-Laden Tubular Channels. *J. Biomech. Eng.* 135, 1–9. doi:10.1115/1.4024575

Yup Lee, J., and Kim, S.-Y. (2010). Alumina-on-Polyethylene Bearing Surfaces in Total Hip Arthroplasty. *Toorthj.* 4, 56–60. doi:10.2174/1874325001004010056

Zhang, L., Hu, J., and Athanasiou, K. A. (2009). The Role of Tissue Engineering in Articular Cartilage Repair and Regeneration. *Crit. Rev. Biomed. Eng.* 37, 1–57. doi:10.1615/CritRevBiomedEng.v37.i1-2.10

Zhang, Q., Lu, H., Kawazoe, N., and Chen, G. (2014). Pore Size Effect of Collagen Scaffolds on Cartilage Regeneration. *Acta Biomater.* 10, 2005–2013. doi:10.1016/j.actbio.2013.12.042

Zhang, Y., Yu, J., Ren, K., Zuo, J., Ding, J., and Chen, X. (2019). Thermosensitive Hydrogels as Scaffolds for Cartilage Tissue Engineering. *Biomacromolecules.* 20, 1478–1492. doi:10.1021/acs.biomac.9b00043

Zhu, S., Chen, P., Chen, Y., Li, M., Chen, C., and Lu, H. (2020). 3D-Printed Extracellular Matrix/Polyethylene Glycol Diacrylate Hydrogel Incorporating the Anti-Inflammatory Phytomolecule Honokiol for Regeneration of Osteochondral Defects. *Am. J. Sports Med.* 48, 2808–2818. doi:10.1177/0363546520941842

Zou, A. H., Feng, J. E., Novikov, D., O'Connor, C. M., Anoushiravani, A. A., Schwarzkopf, R., et al. (2020). Are Oxinium Femoral Heads Superior to Alternative Bearing Surface Materials? A Systematic Review. *J. Hip Surg.* 4, 142–148. doi:10.1055/s-0040-1718506

Conflict of Interest: The authors declare that the research was conducted in the absence of any commercial or financial relationships that could be construed as a potential conflict of interest.

frontiers in Bioengineering and Biotechnology

ORIGINAL RESEARCH
published: 04 November 2021
doi: 10.3389/fbioe.2021.727643

A New Method to Develop the Primate Model of Knee Osteoarthritis With Focal Cartilage Defect

Xin Bi[1,2†], Tao Li[1†], Min Li[3†], Shutian Xiang[4], Junhong Li[1], Bin Ling[5], Zhaoxiang Wu[6] and Zhong Chen[1*]*

[1]Department of Orthopaedic and Trauma Surgery, The Second People's Hospital of Yunnan Province, Kunming, China, [2]Department of Plastic and Reconstructive Surgery, Nanfang Hospital, Southern Medical University, Guangzhou, China, [3]Cadre's Physical Examination Center, The Second People's Hospital of Yunnan Province, Kunming, China, [4]Department of Medical Imaging, The Second People's Hospital of Yunnan Province, Kunming, China, [5]Department of Intensive Care Unit, The Second People's Hospital of Yunnan Province, Kunming, China, [6]Department of Emergency Surgery, The Second People's Hospital of Yunnan Province, Kunming, China

Objective: Osteoarthritis (OA) is a common degenerative joint disease, and animal models have proven pivotal in investigating this disease. This study aimed to develop a primate model of OA that may be more relevant to research studies on OA in humans.

Method: Twelve female rhesus macaques were randomly divided into three groups. Four animals were untreated (Control group); four were subjected to the modified Hulth method, involving cutting of the anterior and posterior cruciate ligaments, and transecting the meniscus (Hulth group); and four were subjected to the modified Hulth method combined with cartilage defect (MHCD group). Each primate was subjected to motor ability tests, and underwent arthroscopic, radiographic, morphological, and pathological observation of the knee joints at various times for up to 180 days.

Results: Motor ability on Day 180 was significantly lower in the MHCD group than in the Control ($p < 0.01$) and Hulth ($p < 0.05$) groups. Radiographic and morphological examination showed that the severity of knee joint deformity and articular cartilage injury were greater in the MHCD group than in the other groups. Pathological examination showed that cartilage thickness was significantly lower in the MHCD group than in the other groups at the same time points. The Mankin score on Day 180 was markedly higher in the MHCD group than in the Hulth ($p < 0.05$) and Control ($p < 0.001$) groups.

Conclusion: The MHCD model of OA closely resembles the pathophysiological processes of spontaneous knee OA in humans. The time required to develop knee OA is shorter using the MHCD model than using the Hulth method.

Keywords: knee, osteoarthritis, animal models, rhesus macaques, modified hulth method, cartilage injury

OPEN ACCESS

Edited by:
Laura Creemers, University Medical Center Utrecht, Netherlands

Reviewed by:
Yong-Can Huang, Peking University Shenzhen Hospital, China
Andrea Barbero, University Hospital of Basel, Switzerland

***Correspondence:**
Zhaoxiang Wu
wzx314159@163.com
Zhong Chen
chenzhongdr@163.com

†These authors have contributed equally to this work and share first authorship

Specialty section:
This article was submitted to Tissue Engineering and Regenerative Medicine, a section of the journal Frontiers in Bioengineering and Biotechnology

Received: *19 June 2021*
Accepted: *20 October 2021*
Published: *04 November 2021*

Citation:
Bi X, Li T, Li M, Xiang S, Li J, Ling B, Wu Z and Chen Z (2021) A New Method to Develop the Primate Model of Knee Osteoarthritis With Focal Cartilage Defect. Front. Bioeng. Biotechnol. 9:727643. doi: 10.3389/fbioe.2021.727643

INTRODUCTION

Osteoarthritis (OA) is a common degenerative joint disease that adversely affects the quality of life of millions of people around the world (Johnson and Hunter, 2014; Glyn-Jones et al., 2015). Symptoms of OA include persistent joint pain, swelling, stiffness, and limited range of motion, accompanied by progressive cartilage degradation, subchondral bone sclerosis, osteophyte formation, and synovium inflammation (Goldring and Goldring, 2010; Sokolove and Lepus, 2013). OA commonly affects the hands, feet, spine, and large weight-bearing joints, particularly the knee (Michael et al., 2010). Knee OA (KOA) is a major cause of physical disability and morbidity, imposing enormous medical and socioeconomic burdens on individuals and society (Alkan et al., 2014; Cross et al., 2014; Hawker et al., 2014). Factors associated with the development of KOA include age, strain, trauma, obesity, and genetic factors; the incidence of KOA does not differ significantly according to race or geographical location (Blagojevic et al., 2010; Guilak, 2011). To date, however, the exact causes and pathogenesis of KOA remain largely unknown, and no treatments have been found to effectively inhibit KOA progression and/or repair injured cartilage.

Animal models are an essential tool to explore the pathogenesis or KOA and to develop effective therapies (Lampropoulou-Adamidou et al., 2014). Various experimentally induced and spontaneous KOA models have been developed in several animal species, including mice, rats, rabbits, guinea pigs, dogs, sheep, goats, and horses (Kuyinu et al., 2016; Cope et al., 2019). However, the patterns of disease, particularly chronic degenerative diseases, in these animals differ markedly from those in humans (Teeple et al., 2013; Mccoy, 2015; Thysen et al., 2015). Because nonhuman primates are phylogenetically close to humans, they make powerful experimental models for studying human diseases. Monkeys, such as rhesus and cynomolgus macaques, are particularly appropriate for studying the molecular processes innate to OA development and progression, as they naturally develop OA at rates similar to those observed in humans (Bailey et al., 2014). To date, however, few KOA models have been developed in monkeys and other primates.

Surgical models of KOA developed in animals involve transaction of the anterior cruciate ligament (ACL), meniscectomy, meniscus injury, and focal cartilage defect (Gregory et al., 2012). These methods are rapid and reproducible, and are similar to the disease-initiating events and pathology of human KOA (Fang and Beier, 2014). One of the most common surgical methods used to induce OA is the Hulth method, which involves cutting the ACL and posterior cruciate ligament (PCL), and transecting the meniscus (Zhou et al., 2018). Compared with other models, KOA induced by the Hulth method is more similar to the spontaneous induction of OA observed in humans. However, the Hulth method may take a long time to produce the same degree of joint damage as a naturally degenerative model. To develop an OA model in which spontaneous development of OA is similar to that in humans, but more rapid and effective than the Hulth model, we explored a potential animal model of KOA based on rhesus macaques. This model involved using a modified Hulth method combined with focal cartilage defect (MHCD). The feasibility and validity of the MHCD method were assessed in comparison with the Hulth model.

MATERIALS AND METHODS

Ethics Statement

All animal procedures were approved by the Institutional Animal Care and Use Committee of The Second People's Hospital of Yunnan Province and the Kunming Institute of Zoology. CAS (SCXK(滇)K2017-0008). All animals were treated according to the guidelines of the Association for Assessment and Accreditation of Laboratory Animal Care International (AAALAC) for the ethical treatment of primates.

Animals

Twelve female specific pathogen-free rhesus macaques (*Macaca mulatta*), aged 12.5–13.9 years and weighing 6.7–8.3 kg, were provided by the Kunming Institute of Zoology of the Chinese Academy of Sciences. The monkeys were housed individually in cages measuring 2.2 m (H) × 2.0 m (W) × 1.5 m (D) and kept in an environment with a 12 h light/dark cycle, a temperature of 22–24°C, and relative humidity of 45–55%. They were fed a standard nonhuman primate diet, and both food and water were available *ad libitum*. Additionally, the monkeys were allowed to move freely for 6–8 h each day in a spacious activity room (12.5 × 10 × 6 m) equipped with a small rockery, swings, and ball games. Occasionally, videos and music were played to relax the monkeys. The animal care staff, as well as the study staff, provided the monkeys with positive interactions.

Grouping and Modeling

The 12 rhesus macaques were randomly divided into three groups of four. Monkeys in the Control group did not undergo surgery; monkeys in the Hulth group underwent unilateral knee surgery during which the ACL and PCL were cut and the meniscus was transected; and monkeys in the MHCD group underwent unilateral knee surgery using the MHCD method.

The monkeys were anesthetized by intramuscular injection of ketamine (0.2 mg/kg; Virbac, France) and fixed in a supine position on the surgical table. The site of incision on the proximal left leg was marked, and a tourniquet was applied. Anterior medial and anterior lateral approaches to the knee joint were made (incisions 4 cm in length) to enable exploration of the knee joints. Operative exploration indicated that the ACL, meniscus, articular cartilage, and other structures were all good. Subsequently, monkeys randomized to the Hulth group underwent transection of the ACL and PCL, and resection of the medial meniscus. By contrast, monkeys in the MHCD group underwent transection of the ACL, the medial collateral ligament (MCL), and the medial meniscus, along with resection of full-thickness cartilage (0.5 × 0.5 × 0.1 cm) in the weight-bearing area of the medial femoral condyle; the procedure was carried using a No. 15 blade scalpel (Jinzhong, Shanghai, China) (**Figure 1**). The articular cavity and incision were flushed with saline and closed

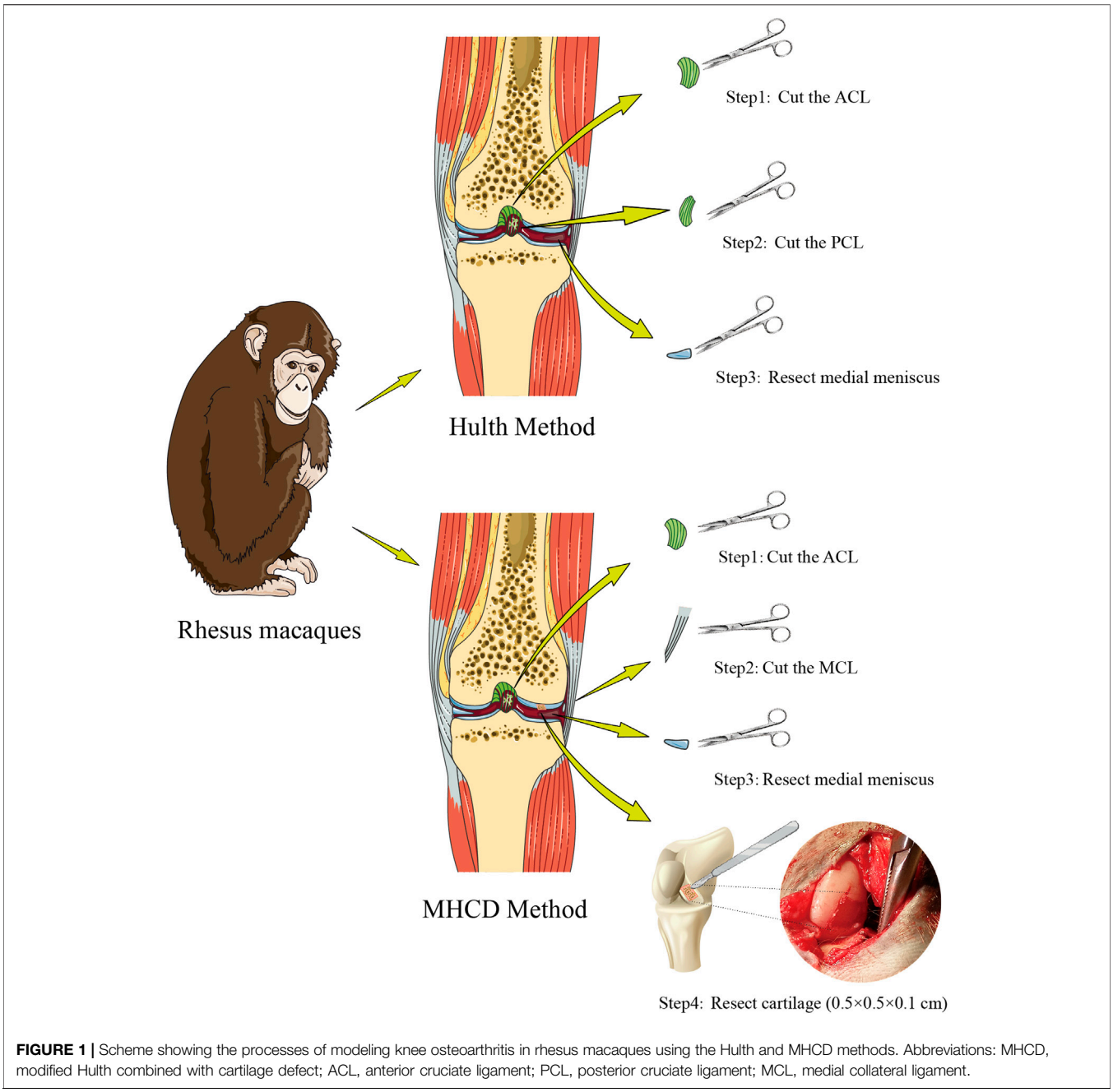

FIGURE 1 | Scheme showing the processes of modeling knee osteoarthritis in rhesus macaques using the Hulth and MHCD methods. Abbreviations: MHCD, modified Hulth combined with cartilage defect; ACL, anterior cruciate ligament; PCL, posterior cruciate ligament; MCL, medial collateral ligament.

TABLE 1 | Baseline characteristics of the three groups of rhesus macaques ($\bar{x}$±s)

Groups	Age (year)	Weight (kg)	Knee circumference (cm)	Crown sacral length (cm)
Control group	12.93 ± 1.24	6.43 ± 0.28	15.29 ± 0.47	46.12 ± 1.36
Hulth group	13.09 ± 1.20	6.45 ± 0.30	15.20 ± 0.50	46.30 ± 1.51
MHCD group	13.16 ± 1.58	6.37 ± 0.34	15.50 ± 0.85	46.48 ± 1.71
F	1.333	2.809	2.363	0.506
P	0.311	0.113	0.150	0.619

with 3-0 absorbable sutures (3L Medical Products Co, Nanchang, China), followed by external fixation with a plaster cast. A soft-padded bandage was placed over the limb and maintained for 2 weeks. Starting within 3 days post-operation, cefodizime sodium (25 mg/kg; Suzhou Chung Hwa Chemical & Pharmaceutical Industrial Co, Suzhou, China) was injected intramuscularly once every 12 h to prevent infection, and parecoxib (0.8 mg/kg; Pfizer, United States) was injected intramuscularly once daily to relieve pain. Animals were monitored daily.

Motor Ability Test

To evaluate the effect of pain caused by KOA on the motor ability of monkeys, all monkeys were monitored by video surveillance (Hikvision, China) from Day 3 to Day 180. The time for which each monkey walked and/or ran during each 24 h period was recorded.

Radiographic Examination

On Days 60, 120, and 180, all animals were anesthetized with 10% chloral hydrate and subjected to radiographic evaluation. X-ray images of the knee joint were taken using an Axiom Multix M radiographic unit (Siemens, Germany). Magnetic resonance imaging (MRI) (Philips, the Netherlands) was also performed to assess changes in articular cartilage. X-ray images and MR images were evaluated by two radiologists and by one specialized orthopedic surgeon independently. One observer (orthopedic surgeon) evaluated all MR images twice with a 3-months interval between the two reading sessions.

Arthroscopic Examination

Following anesthetization with 10% chloral hydrate on Day 120, the monkeys underwent arthroscopic examination (Stryker, United States) of the targeted knee joint to obtain pictures of articular surface injury.

Morphological Examination

All animals were euthanized by administration of intensive anesthesia 180 days after the operation. The monkeys were placed in the supine position and the sites of the surgical areas were shaved. Incisions over the knee joint were made, the knee joint cavity was exposed to collect the fluid, and the articular cartilage surface was examined. Articular cartilage of the medial femoral condyle was cut from the excised knee joints and stored at −20°C before analysis.

Histological Examination

Cartilage specimens were fixed with 4% paraformaldehyde (Solarbio Beijing, China) for 48 h at 4°C, decalcified in 20% EDTA solution (Merck, Germany), dehydrated through graded ethanol solutions, embedded in paraffin, and sliced into 5-μm sections. Sections were stained with hematoxylin and eosin (H&E; Solarbio), Safranin O (Solarbio), and toluidine blue (Solarbio), and then sealed with neutral gum. Finally, the specimens were assessed under a light microscopy (Nikon, Japan). Five slices of each articular cartilage specimen were selected, and KOA was evaluated by measuring the Mankin score(Van Der Sluijs et al., 1992).

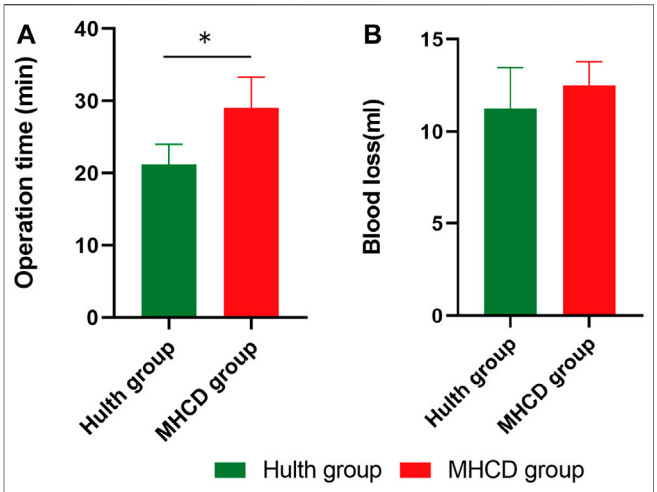

FIGURE 2 | Evaluation of operation time **(A)** and blood loss **(B)** in rhesus macaques subjected to the Hulth and MHCD methods. *$p < 0.05$. Data are presented as the mean ± SD.

Enzyme-Linked Immunosorbent Assay

Synovial fluid was aspirated from the knee joints of all monkeys on Day 120. The concentrations of interleukin-1β (IL-1β), transforming growth factor-β1 (TGF-β1), and matrix metalloproteinase-13 (MMP-13) in these specimens were measured using commercially available kits (Human Quantikine ELISA kits; R&D Systems).

Statistical Analysis

All data are presented as mean ± standard deviation (SD) and were analyzed using the SPSS 13.0 statistical package. Data distributed normally were analyzed using a *t* test, whereas non-normally distributed data were analyzed using the Mann-Whitney U test. *p*-values <0.05 were considered statistically significant.

RESULTS

Baseline Characteristics and Intraoperative Condition of Rhesus Macaques

There was no significant difference between the Control, Hulth, and MHCD groups with respect to age, body weight, knee circumference, and crown sacral length ($p > 0.05$) (**Table 1**). Operation time was longer for the MHCD group than for the Hulth group ($p < 0.05$) (**Figure 2A**), but there was no significant difference in blood loss ($p > 0.05$) (**Figure 2B**). None of the monkeys experienced infection or died.

Analysis of Motor Ability

Compared with the Control group, motor ability at 3 and 7 days post-surgery was significantly lower in the Hulth ($p < 0.01$ on both days) and MHCD ($p < 0.001$ on Day 3, $p < 0.01$ on Day 7) groups due to postoperative pain. Removal of the plaster cast led to rapid relief of pain in the Hulth group, with motor ability being significantly greater than that of the MHCD group on Day 14 ($p < 0.05$). By contrast, the motor ability of the MHCD group was

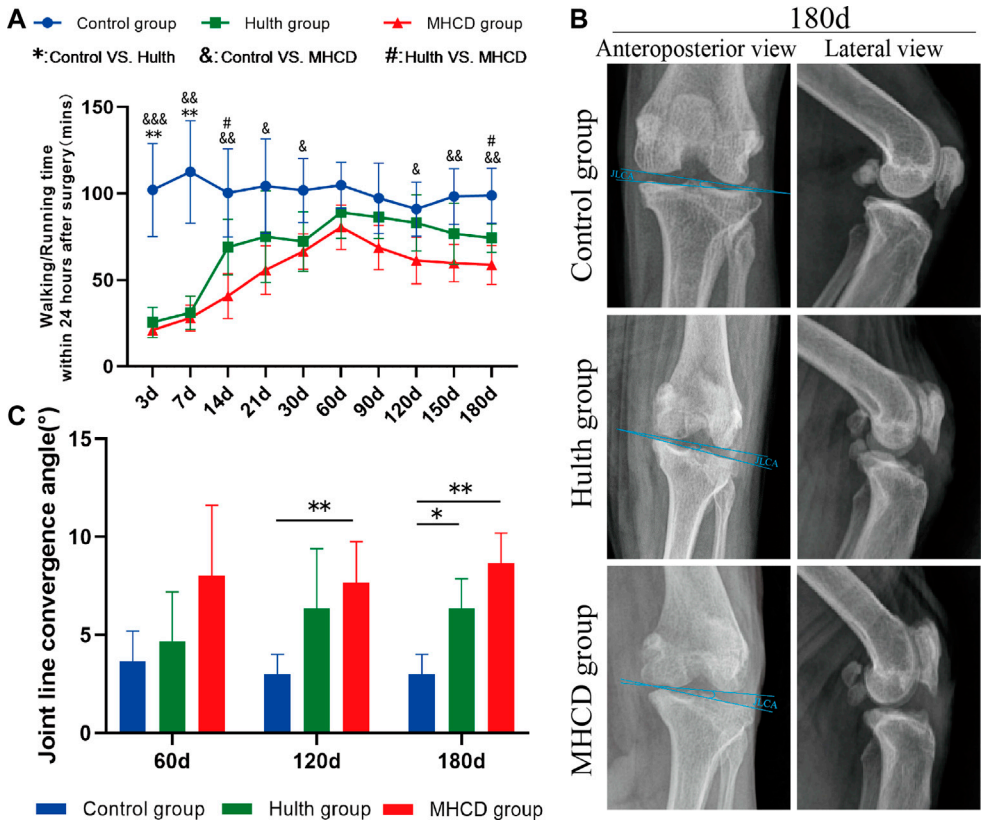

FIGURE 3 | Evaluation of motor activity and postoperative X-rays in the three groups of rhesus macaques. **(A)** Motor activity within 24 h after surgery. **(B)** Representative X-rays of the knee joints on Day 180. **(C)**. Changes in joint convergence angles of the left knee. *$p < 0.05$, **$p < 0.01$, ***$p < 0.001$. Data are presented as the mean ± SD.

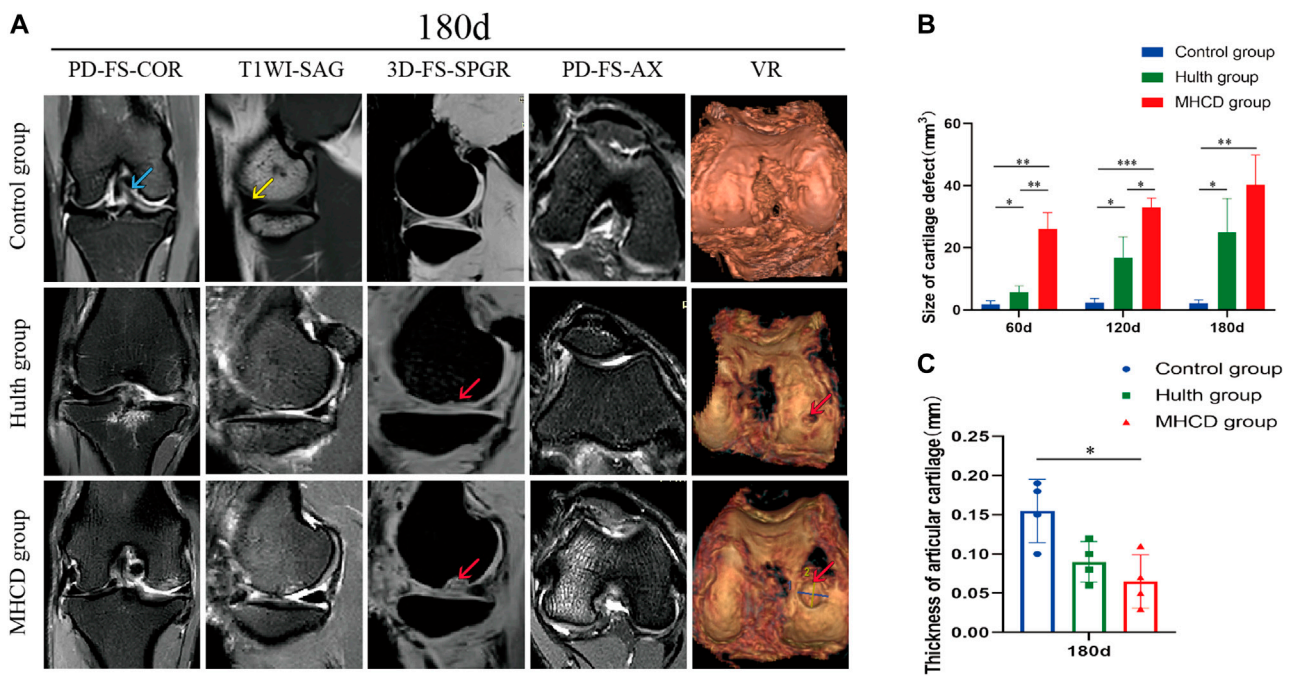

FIGURE 4 | MRI findings of the knee joints of the three groups of rhesus macaques. **(A)** Representative MRI findings of the knee joints on Day 180. **(B)** Sizes of articular cartilage defects on Days 60, 120, and 180. **(C)** Thicknesses of articular cartilage in the weight-bearing part of the knee joint on Day 180. (blue arrows, ACL; yellow arrows, medial meniscus; red arrows, cartilage defects). *$p < 0.05$, **$p < 0.01$, ***$p < 0.001$. Data are presented as the mean ± SD.

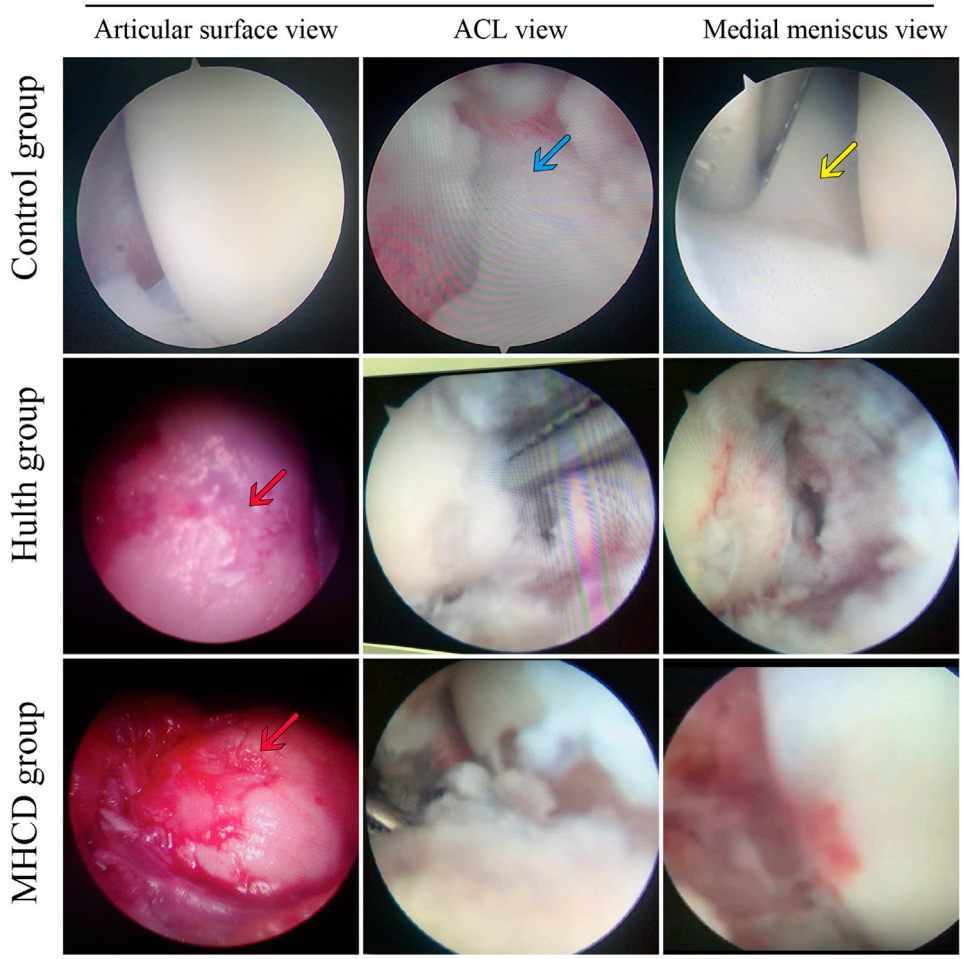

FIGURE 5 | Representative arthroscopic findings of the knee joints of rhesus macaques from the Control, Hulth, and MHCD groups on Day 120 (blue arrows, ACL; yellow arrows, medial meniscus; red arrows, cartilage defects).

significantly lower than that of the Control group on Days 14 ($p < 0.01$), 21 ($p < 0.05$), and 30 ($p < 0.05$). Subsequent progression of KOA after surgery in the MHCD group resulted in gradual weakening of motor ability, which was significantly lower in the MHCD than in the Control group on Days 120 ($p < 0.05$), 150 ($p < 0.01$), and 180 ($p < 0.01$). Interestingly, motor ability on Day 180 was significantly higher in the Hulth than in the MHCD group ($p < 0.05$), but did not differ significantly between the Hulth and Control groups (**Figure 3A**).

Radiographic Analysis of the Knee Joint

After surgery, monkeys showed a reduced knee joint space and other gradual changes associated with KOA (**Figure 3B** and **Figure 4A**). X-rays of animals in the MHCD group showed collapse and sclerosis of the articular surface, deformity of the knee joint, and narrowing of the joint space, whereas X-rays of animals in the Hulth group showed sclerosis of the articular surface without collapse. By contrast, X-rays of the Control group showed knee joints with smooth appearance and regular surfaces (**Figure 3B**). On Days 120 and 180, the joint line convergence angle (JLCA) in the MHCD group was significantly greater than that in the Control group ($p < 0.01$), whereas, on Day 180, the JLCA was more extensive in the Hulth group than in the Control group ($p < 0.05$) (**Figure 3C**).

MRI of animals in the Hulth and MHCD groups showed slight increases in suprapatellar capsule and articular cavity effusion, medial subluxation of the patella, and injury to the articular cartilage of the medial femoral condyle (**Figure 4A**). Monkeys in the Hulth group showed subchondral cystic lesions in the medial femoral condyle, whereas animals in the MHCD group showed cartilage and subchondral bone damage in the medial tibial condyle, as well as joint space narrowing. The size of the cartilage defect was significantly larger in the MHCD than in the Control group on Days 60 ($p < 0.01$), 120 ($p < 0.001$), and 180 ($p < 0.01$), and was also significantly larger in the Hulth than in the Control group on Days 60, 120, and 180 ($p < 0.05$ each). In

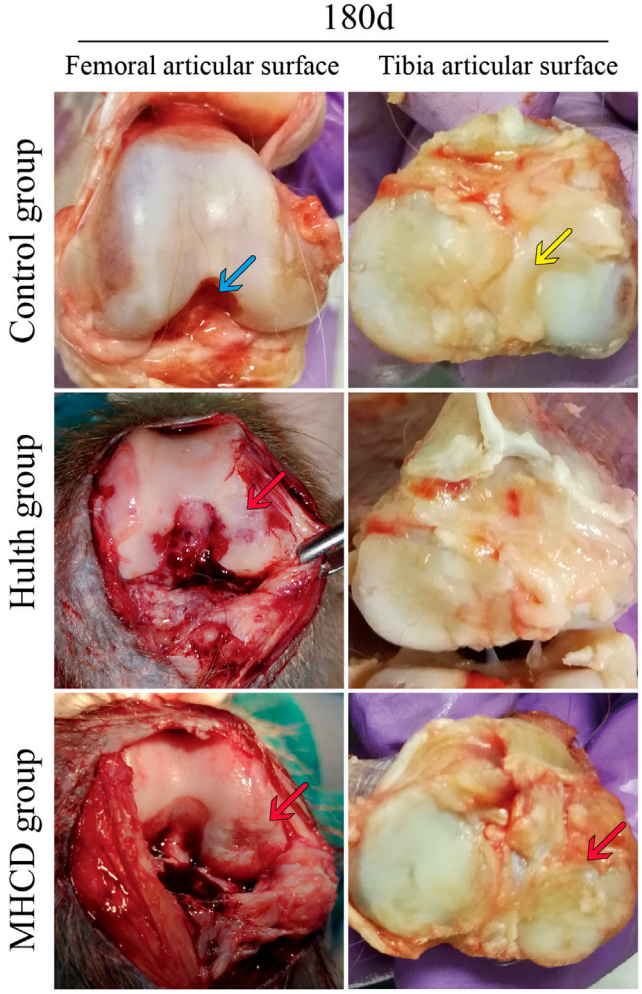

FIGURE 6 | Gross observations on Day 180, showing abrasion of the weight-bearing surface of the medial femoral condyle and femoral posterior condylar cartilage in the Hulth group, but more serious abrasion in the MHCD group (blue arrows, ACL; yellow arrows, medial meniscus; red arrows, cartilage defects).

addition, the size of the cartilage defect was significantly larger in the MHCD than in the Hulth group on Days 60 ($p < 0.01$) and 120 ($p < 0.05$) (**Figure 4B**). On Day 180, the articular cartilage was thicker in the Control group than in the MHCD group (**Figure 4C**).

Morphological Observation of the Knee Joint

Arthroscopic views of the knee joints and the gross appearance of the femoral condyles and tibial plateaus in each group are shown in **Figure 5**. Arthroscopy showed that the articular cartilage in the Control group was smooth, and that the ACL and medial meniscus were present. By contrast, arthroscopy of the knees in the Hulth and MHCD groups showed absence of the ACL and medial meniscus, and wear of the medial femoral condyle cartilage. Gross examination revealed abrasion of the weight-bearing surface of the medial femoral condyle and of the femoral posterior condylar cartilage in the Hulth group, but more serious abrasion in the MHCD group. In addition, significant cartilage degeneration and cartilage thinning of the tibial plateau were evident in the MHCD group, but not in the Control and Hulth groups (**Figure 6**).

Histopathologic Evaluation of Knee Joint

H&E staining of samples from the Hulth and MHCD groups on Day 180 showed damaged cartilage, disorganized chondrocyte clusters, and rough cartilage surfaces (**Figure 7A**). In the Hulth group, the boundary of each layer was obscure, the tidal line was continuous, and the articular hyaline cartilage was replaced gradually by fibrous tissue. In the MHCD group, however, the articular cartilage surface was damaged to different degrees, the structure was disordered, cartilage destruction involved the radiation layer, the tidal line was interrupted and blurred, and the articular cartilage was almost entirely replaced by fibrous tissue. Consistent with the radiographic and gross observations, the Mankin score showed that the severity of cartilage damage was markedly higher in the Hulth group than in the Control group ($p < 0.01$), but lower than in the MHCD group ($p < 0.05$). The Mankin score was also markedly higher in the MHCD than in the Control group ($p < 0.001$) (**Figure 7B**).

Tissue samples obtained after sacrifice on Day 180 were also stained with Safranin O, which detects proteoglycans, a major extracellular matrix component in cartilage. Safranin O staining of samples from the Control group showed a deep red color; the cartilage had a smooth surface; and the chondrocytes displayed normal morphology and were arranged in an orderly manner. By contrast, the intensity of Safranin O staining was reduced markedly in the Hulth group, as was the number of chondrocytes, which also showed disordered layers. Samples from the MHCD group showed almost complete absence of Safranin O staining, the number of chondrocytes was significantly reduced, and subchondral bone remodeling was complete (**Figure 8A**).

Consistent with the results of Safranin O staining, toluidine blue staining of Day 180 samples from the Control group showed a deep blue color, with chondrocytes appearing in distinct layers and arranged in an orderly manner. Samples from the Hulth group showed light blue staining of the articular cartilage, with the number of cells being significantly decreased. Samples from the MHCD group showed lower intensity of toluidine blue staining, with some of the layers showing no staining and the regions in the weight-bearing area being negative for chondrocytes (**Figure 8B**).

Expression of IL-1β, TGF-β1, and MMP-13 in Synovial Fluid

Measurement of IL-1β, TGF-β1, and MMP-13 concentrations in synovial fluid on Day 120 showed that the levels of all three were significantly higher in the Hulth group than in the Control group ($p < 0.01$ each). The levels of IL-1β ($p < 0.001$), TGF-β1 ($p < 0.001$), and MMP-13 ($p < 0.01$) in the MHCD group were much higher than those in the Control group. Moreover, the levels of IL-1β ($p < 0.01$) and TGF-β1 ($p < 0.01$) were

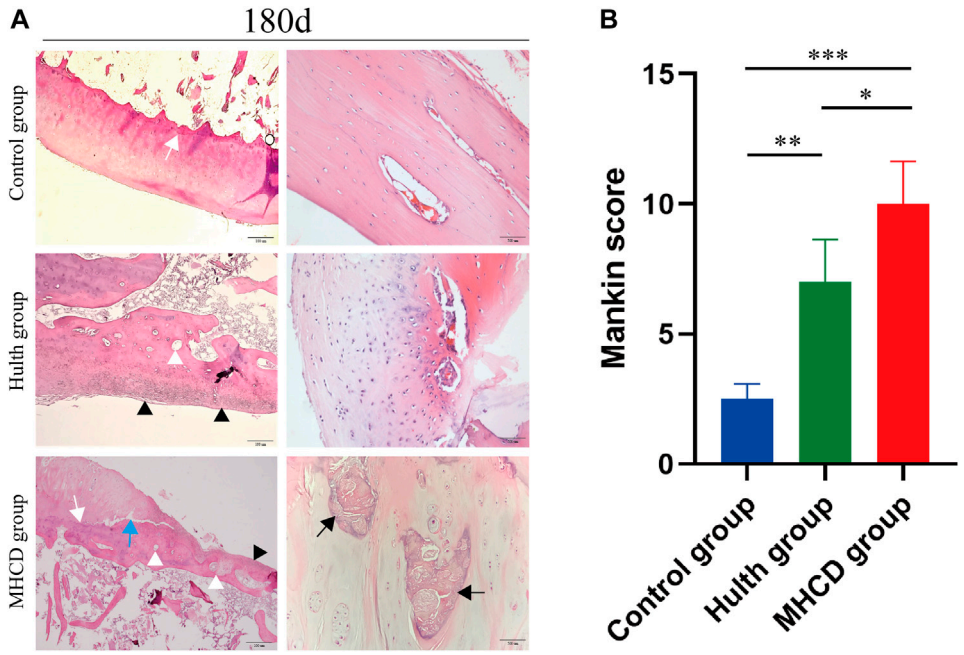

FIGURE 7 | Pathological morphology of articular cartilage 180 days after surgery. **(A)** Representative images showing H&E staining of the weight-bearing surface of the medial femoral condyle and femoral posterior condylar cartilage from the Control, Hulth, and MHCD groups. (White arrow: tidemark, White arrowhead: subchondral cyst, Black arrow: sclerosis, Black arrowhead: fibrocartilage mineralization, Blue arrow: degradation of cartilage matrix) **(B)** Histologic scores of the cartilage lesions in the three groups. $^{*}p < 0.05$, $^{**}p < 0.01$, $^{***}p < 0.001$. Data are presented as the mean ± SD.

significantly higher in the MHCD group than in the Hulth group (**Figures 9A–C**).

DISCUSSION

OA is a common chronic disease characterized by articular cartilage degeneration and bone destruction, which are the main causes of joint pain and disability in patients with advanced disease (Weimer et al., 2012). Development of OA is a complex process, involving several pathological pathways and mechanisms.

Choosing an appropriate animal model of KOA is very important for assessing the mechanisms involved in the development of the disease in humans (Aigner et al., 2010). Spontaneous models are, to some extent, the closest to the natural degeneration of joints in patients with OA, but they take a long time to develop (Teeple et al., 2013). Furthermore, experimental results can be affected by many factors, thereby reducing the reliability of these models (Stone et al., 2015). Transgenic models cannot simulate the pathogenesis of human OA completely because it is driven by a combination of multiple genes and factors (Little and Hunter, 2013). Surgical methods of modeling KOA are used widely because they are rapid, simple, and highly repeatable (Gregory et al., 2012). The Hulth method induces knee joint instability and pathological changes, similar to spontaneous models of OA (Pashuck et al., 2016; Patel et al., 2016). To date, however, effective and reliable models of KOA in animals have not been quick to develop. Compared with the Hulth method, animal models of KOA induced by cartilage injury alone show significantly less damage to the biomechanical stability of the knee joint. The time needed to produce OA-related pathological changes is longer, as weight-bearing interventions are required for the injured limb (Marijnissen et al., 2002). The present study used a modified version of the Hulth method, combining it with cartilage injury to yield a KOA model that closely resembles the pathophysiological process of spontaneous KOA in humans. Furthermore, this modification led to development of KOA in a shorter time than the Hulth method.

Developing an appropriate animal model is important for exploring the pathogenesis and treatment of KOA. Various animal models have been utilized to gain insight into KOA onset and progression, and to aid development and evaluation of advanced diagnostic tools and treatments (Mccoy, 2015). For example, medial meniscectomy in male Lewis rats stimulates the pathological changes of KOA; this rat model was used to explore the effect of antiresorptive and anabolic bone therapy on post-traumatic osteoarthritis (Bagi et al., 2015). A canine spontaneous KOA model may serve as an appropriate animal model that closely mimics pathological changes in humans (Pertovaara, 2012). Moreover, this model may be used in translational pain research to test the safety and efficacy of novel analgesics. KOA was simulated in a rabbit model by transecting the PCL, providing a valuable marker of OA disease severity and progression (Gao et al., 2013). However, differences in knee morphology, biomechanics, and behavior in these animal models can make it difficult to extrapolate the findings to humans (Bailey et al., 2014). In this study, we selected rhesus macaques, a nonhuman primate, as model animals because morphologic progression of cartilage degeneration and KOA are more similar to humans than other animal models.

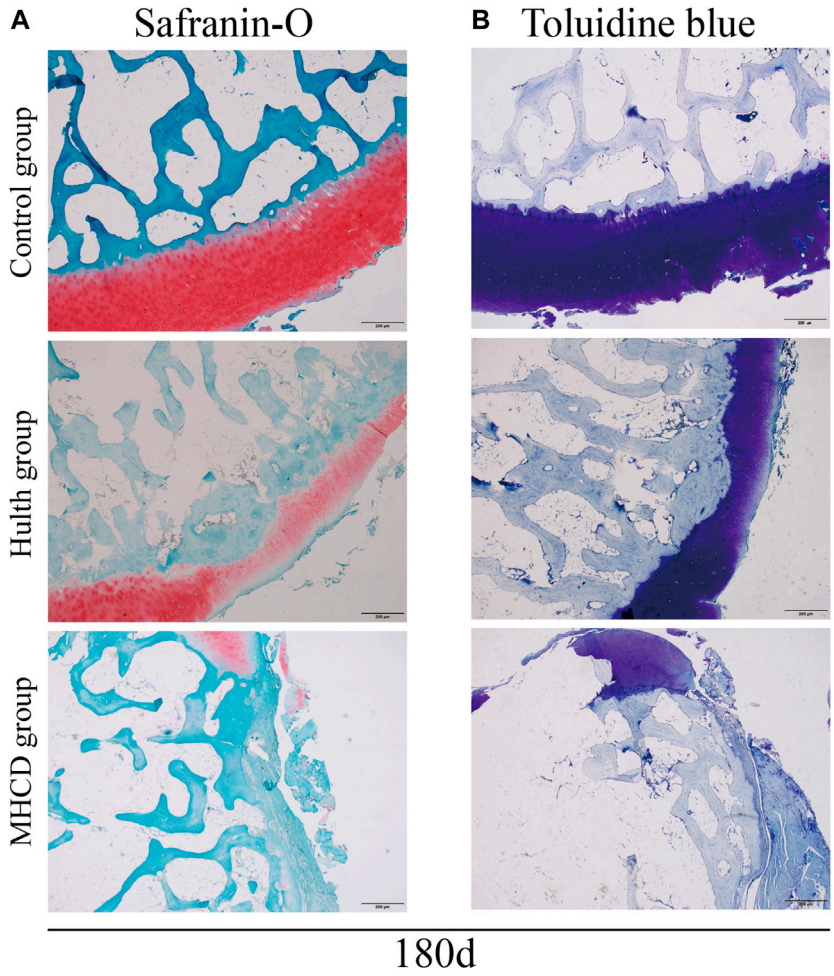

FIGURE 8 | Staining of glycosaminoglycans in articular cartilage 180 days after surgery. Representative images of **(A)** Safranin O and **(B)** toluidine blue staining.

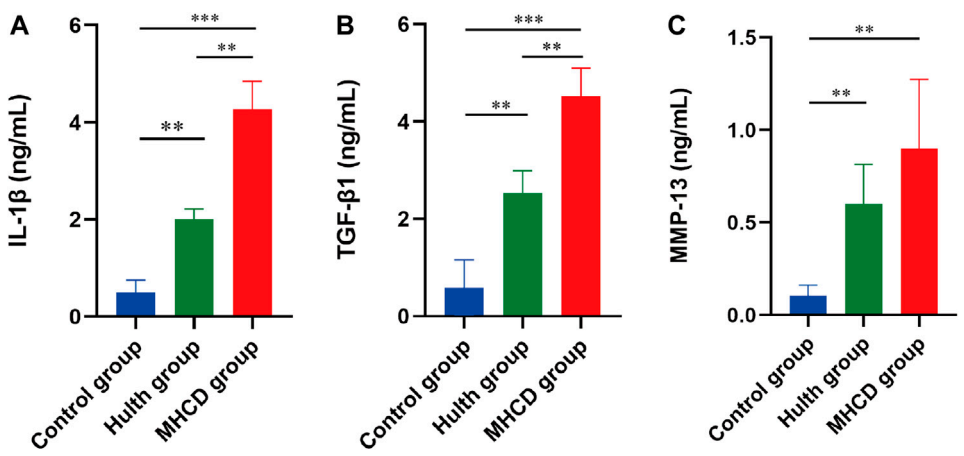

FIGURE 9 | Concentrations of three representative proteins in the synovial fluid of rhesus macaques on Day 120. Concentrations of **(A)** IL-1β, **(B)** TGF-β1, and **(C)** MMP-13 were measured by ELISA. IL-1β, interleukin-1β; TGF-β1, transforming growth factor-β1; MMP-13, matrix metalloproteinase-13. $^{*}p < 0.05$, $^{**}p < 0.01$, $^{***}p < 0.001$. Data are presented as the mean ± SD.

Although the MHCD method increased operation time compared with the Hulth method, it did not increase intraoperative blood loss. The decrease in activity during the first 30 days after surgery in both groups may be associated with postoperative pain. Interestingly, after the plaster cast was removed on Day 14, activity increased significantly in the Hulth group whereas activity in the MHCD group remained low. Damage to the knee cartilage in the MHCD group may have restricted early-stage motor activity. Although late stage (Day 180) motor activity was significantly higher in the Hulth group than in the MHCD group, activity in the Hulth and Control group was similar. The difference between the Hulth and MHCD groups may have been caused by the more significant damage to the articular cartilage in the weight-bearing area of the knee joint in the MHCD group. This result may provide indirect evidence for more rapid development of KOA after the MHCD than the Hulth method.

X-rays and MRI scans are simple and useful methods of preliminarily diagnosing KOA, with a moderate relationship reported between OA imaging features and KOA symptoms (Wu et al., 2012). Radiographic evaluation revealed pathology typical of OA in both the Hulth and MHCD groups, accompanied by severe cartilage degradation and bony changes. OA progression, however, was faster in the MHCD group than in the Hulth group. Radiological results showed that the MHCD method increased the severity of articular cartilage injury, knee joint deformity, and subchondral bone damage, suggesting that the combined method promotes pathological damage to articular cartilage and accelerates OA progression. These changes are similar to those observed for human OA and are consistent with those in previous reports of surgically-induced OA in nonhuman primates (Liu et al., 2018; Zhou et al., 2018). Furthermore, arthroscopic examination and gross morphological and cross-sectional analyses of articular surface wear suggested that pathologic degradation of the cartilage corresponded with radiographic results. Cartilage destruction in the MHCD group was more severe than in the Control and Hulth groups, as determined by the Mankin score. Joint destruction at Day 120 in the MHCD group was similar to that on Day 180 in the Hulth group, with imaging changes and morphological appearance in the MHCD group being closer to the natural degeneration observed in human KOA.

We also found that cartilage pathology was associated with increased secretion of cytokines and MMPs. Previous studies show that serum concentrations of IL-1β and TGF-β1 are higher in OA patients than in control groups, and that these concentrations are closely associated with pain (Hussein et al., 2008; Lee et al., 2011). Inflammation is involved in the pathophysiological mechanism of KOA, as evidenced by the presence of cytokines in both osteoarthritic joints and synovial fluid (Rutgers et al., 2010; Yu and Kim, 2013). These cytokines may be involved in the pathophysiology of OA by regulating expression of MMPs, which induce degradation of the extracellular matrix (Inoue et al., 2005; Haseeb and Haqqi, 2013; Lim et al., 2014). Cytokines and MMPs are involved in the development of cartilage damage (Bondeson et al., 2006; Klatt et al., 2006; Pujol et al., 2008). The present study found that the levels of IL-1β, TGF-β1, and MMP13 in synovial fluid were significantly higher in the MHCD than in the Hulth and Control groups, and were significantly higher in the Hulth than in the Control group. On Day 120, expression of cytokines and MMP-13 in synovial fluid of rhesus macaques with MHCD-induced KOA was similar to that in patients with spontaneous KOA. The inflammatory and biomechanical changes in synovial fluid were less serious animals subjected to the Hulth method.

This study had several limitations. First, due to the lack of suitable experimental animals and funds, groups of animals with spontaneous KOA and those subjected to sham operations were not included. Second, the study included a small number of animals, suggesting caution in interpreting the results. Additional studies are required to compare MHCD-induced and spontaneous models of KOA, as well as KOA in primates of different genders and ages.

In conclusion, the present study describes the development of a primate model of KOA using a modified Hulth method combined with focal cartilage defects. This model is similar to spontaneous models with respect to osteoarthritic and histopathologic grading, as well as changes in expression of inflammatory cytokines and MMPs. Furthermore, compared with the Hulth method, the MHCD method resulted in more rapid development of KOA, suggesting that the MHCD method may be a suitable model for studying the pathogenesis and treatment of OA.

DATA AVAILABILITY STATEMENT

The original contributions presented in the study are included in the article/supplementary material, further inquiries can be directed to the corresponding authors.

ETHICS STATEMENT

The animal study was reviewed and approved by Institutional Animal Care and Use Committee of The Second People's Hospital of Yunnan Province and the Kunming Institute of Zoology. CAS (SCXK(滇)K2017-0008).

AUTHOR CONTRIBUTIONS

XB, TL, and ZC conceived and designed the study. ML, ZW, and JL acquired and 14 analyzed the data. XB, SX, and ZC interpreted the data and drafted the paper. TL, ZW, BL, and JL revised the manuscript. All authors gave final approval of the version to be published and agreed to be accountable for all aspects of the research in ensuring that the accuracy or integrity of any part of the work is appropriately investigated and resolved.

FUNDING

The study was funded by the General Project (2019FE001-264) and Key Project (2019FE001-170) of the Applied Basic Research Project of Science and Technology Department of Yunnan Province & Kunming Medical University.

REFERENCES

Aigner, T., Cook, J. L., Gerwin, N., Glasson, S. S., Laverty, S., Little, C. B., et al. (2010). Histopathology Atlas of Animal Model Systems - Overview of Guiding Principles. *Osteoarthritis and cartilage* 18, S2–S6. doi:10.1016/j.joca.2010.07.013

Alkan, B. M., Fidan, F., Tosun, A., and Ardıçoğlu, Ö. (2014). Quality of Life and Self-Reported Disability in Patients with Knee Osteoarthritis. *Mod. Rheumatol.* 24, 166–171. doi:10.3109/14397595.2013.854046

Bagi, C. M., Berryman, E., Zakur, D. E., Wilkie, D., and Andresen, C. J. (2015). Effect of Antiresorptive and Anabolic Bone Therapy on Development of Osteoarthritis in a Posttraumatic Rat Model of OA. *Arthritis Res. Ther.* 17, 315. doi:10.1186/s13075-015-0829-5

Bailey, J. F., Fields, A. J., Liebenberg, E., Mattison, J. A., Lotz, J. C., and Kramer, P. A. (2014). Comparison of Vertebral and Intervertebral Disc Lesions in Aging Humans and Rhesus Monkeys. *Osteoarthritis and Cartilage* 22, 980–985. doi:10.1016/j.joca.2014.04.027

Blagojevic, M., Jinks, C., Jeffery, A., and Jordan, K. P. (2010). Risk Factors for Onset of Osteoarthritis of the Knee in Older Adults: a Systematic Review and Meta-Analysis. *Osteoarthritis and Cartilage* 18, 24–33. doi:10.1016/j.joca.2009.08.010

Bondeson, J., Wainwright, S. D., Lauder, S., Amos, N., and Hughes, C. E. (2006). The Role of Synovial Macrophages and Macrophage-Produced Cytokines in Driving Aggrecanases, Matrix Metalloproteinases, and Other Destructive and Inflammatory Responses in Osteoarthritis. *Arthritis Res. Ther.* 8, R187. doi:10.1186/ar2099

Cope, P. J., Ourradi, K., Li, Y., and Sharif, M. (2019). Models of Osteoarthritis: the Good, the Bad and the Promising. *Osteoarthritis and Cartilage* 27, 230–239. doi:10.1016/j.joca.2018.09.016

Cross, M., Smith, E., Hoy, D., Nolte, S., Ackerman, I., Fransen, M., et al. (2014). The Global burden of Hip and Knee Osteoarthritis: Estimates from the Global burden of Disease 2010 Study. *Ann. Rheum. Dis.* 73, 1323–1330. doi:10.1136/annrheumdis-2013-204763

Fang, H., and Beier, F. (2014). Mouse Models of Osteoarthritis: Modelling Risk Factors and Assessing Outcomes. *Nat. Rev. Rheumatol.* 10, 413–421. doi:10.1038/nrrheum.2014.46

Gao, S. G., Cheng, L., Zeng, C., Wei, L. C., Zhang, F. J., Tian, J., et al. (2013). Usefulness of Specific OA Biomarkers, Thrombin-Cleaved Osteopontin, in the Posterior Cruciate Ligament OA Rabbit Model. *Osteoarthritis and Cartilage* 21, 144–150. doi:10.1016/j.joca.2012.09.006

Glyn-Jones, S., Palmer, A. J. R., Agricola, R., Price, A. J., Vincent, T. L., Weinans, H., et al. (2015). Osteoarthritis. *The Lancet* 386, 376–387. doi:10.1016/s0140-6736(14)60802-3

Goldring, M. B., and Goldring, S. R. (2010). Articular Cartilage and Subchondral Bone in the Pathogenesis of Osteoarthritis. *Ann. N. Y Acad. Sci.* 1192, 230–237. doi:10.1111/j.1749-6632.2009.05240.x

Gregory, M. H., Capito, N., Kuroki, K., Stoker, A. M., Cook, J. L., and Sherman, S. L. (20122012). A Review of Translational Animal Models for Knee Osteoarthritis. *Arthritis* 2012, 1–14. doi:10.1155/2012/764621

Guilak, F. (2011). Biomechanical Factors in Osteoarthritis. *Best Pract. Res. Clin. Rheumatol.* 25, 815–823. doi:10.1016/j.berh.2011.11.013

Haseeb, A., and Haqqi, T. M. (2013). Immunopathogenesis of Osteoarthritis. *Clin. Immunol.* 146, 185–196. doi:10.1016/j.clim.2012.12.011

Hawker, G. A., Croxford, R., Bierman, A. S., Harvey, P. J., Ravi, B., Stanaitis, I., et al. (2014). All-cause Mortality and Serious Cardiovascular Events in People with Hip and Knee Osteoarthritis: a Population Based Cohort Study. *PLoS One* 9, e91286. doi:10.1371/journal.pone.0091286

Hussein, M. R., Fathi, N. A., El-Din, A. M. E., Hassan, H. I., Abdullah, F., AL-Hakeem, E., et al. (2008). Alterations of the CD4+, CD8+ T Cell Subsets, Interleukins-1β, IL-10, IL-17, Tumor Necrosis Factor-α and Soluble Intercellular Adhesion Molecule-1 in Rheumatoid Arthritis and Osteoarthritis: Preliminary Observations. *Pathol. Oncol. Res.* 14, 321–328. doi:10.1007/s12253-008-9016-1

Inoue, K., Masuko-Hongo, K., Okamoto, M., and Nishioka, K. (2005). Induction of Vascular Endothelial Growth Factor and Matrix Metalloproteinase-3 (Stromelysin) by Interleukin-1 in Human Articular Chondrocytes and Synoviocytes. *Rheumatol. Int.* 26, 93–98. doi:10.1007/s00296-004-0513-6

Johnson, V. L., and Hunter, D. J. (2014). The Epidemiology of Osteoarthritis. *Best Pract. Res. Clin. Rheumatol.* 28, 5–15. doi:10.1016/j.berh.2014.01.004

Klatt, A. R., Klinger, G., Neumüller, O., Eidenmüller, B., Wagner, I., Achenbach, T., et al. (2006). TAK1 Downregulation Reduces IL-1β Induced Expression of MMP13, MMP1 and TNF-Alpha. *Biomed. Pharmacother.* 60, 55–61. doi:10.1016/j.biopha.2005.08.007

Kuyinu, E. L., Narayanan, G., Nair, L. S., and Laurencin, C. T. (2016). Animal Models of Osteoarthritis: Classification, Update, and Measurement of Outcomes. *J. Orthop. Surg. Res.* 11, 19. doi:10.1186/s13018-016-0346-5

Lampropoulou-Adamidou, K., Lelovas, P., Karadimas, E. V., Liakou, C., Triantafillopoulos, I. K., Dontas, I., et al. (2014). Useful Animal Models for the Research of Osteoarthritis. *Eur. J. Orthop. Surg. Traumatol.* 24, 263–271. doi:10.1007/s00590-013-1205-2

Lee, Y. C., Lu, B., Bathon, J. M., Haythornthwaite, J. A., Smith, M. T., Page, G. G., et al. (2010). Pain Sensitivity and Pain Reactivity in Osteoarthritis. *Arthritis Care Res.* 63, a–n. doi:10.1002/acr.20373

Lim, N. H., Meinjohanns, E., Meldal, M., Bou-Gharios, G., and Nagase, H. (2014). *In Vivo* imaging of MMP-13 Activity in the Murine Destabilised Medial Meniscus Surgical Model of Osteoarthritis. *Osteoarthritis and Cartilage* 22, 862–868. doi:10.1016/j.joca.2014.04.006

Little, C. B., and Hunter, D. J. (2013). Post-traumatic Osteoarthritis: from Mouse Models to Clinical Trials. *Nat. Rev. Rheumatol.* 9, 485–497. doi:10.1038/nrrheum.2013.72

Liu, G., Zhang, L., Zhou, X., Zhang, B. L., Guo, G. X., Xu, P., et al. (2018). Selection and Investigation of a Primate Model of Spontaneous Degenerative Knee Osteoarthritis, the Cynomolgus Monkey (Macaca Fascicularis). *Med. Sci. Monit.* 24, 4516–4527. doi:10.12659/MSM.908913

Marijnissen, A. C. A., Van Roermund, P. M., Tekoppele, J. M., Bijlsma, J. W. J., and Lafeber, F. P. J. G. (2002). The Canine 'groove' Model, Compared with the ACLT Model of Osteoarthritis. *Osteoarthritis and cartilage* 10, 145–155. doi:10.1053/joca.2001.0491

Mccoy, A. M. (2015). Animal Models of Osteoarthritis. *Vet. Pathol.* 52, 803–818. doi:10.1177/0300985815588611

Michael, J. W. P., Schlüter-Brust, K. U., and Eysel, P. (2010). The Epidemiology, Etiology, Diagnosis, and Treatment of Osteoarthritis of the Knee. *Deutsches Arzteblatt Int.* 107, 152. doi:10.3238/arztebl.2010.0152

Pashuck, T. D., Kuroki, K., Cook, C. R., Stoker, A. M., and Cook, J. L. (2016). Hyaluronic Acid versus saline Intra-articular Injections for Amelioration of Chronic Knee Osteoarthritis: A Canine Model. *J. Orthop. Res.* 34, 1772–1779. doi:10.1002/jor.23191

Patel, J. M., Merriam, A. R., Culp, B. M., Gatt, C. J., Jr., and Dunn, M. G. (2016). One-Year Outcomes of Total Meniscus Reconstruction Using a Novel Fiber-Reinforced Scaffold in an Ovine Model. *Am. J. Sports Med.* 44, 898–907. doi:10.1177/0363546515624913

Pertovaara, A. (2012). Effective Treatment of Osteoarthritic Pain, Tackling the challenge with Pets. *Scand. J. Pain* 3, 82–83. doi:10.1016/j.sjpain.2012.01.001

Pujol, J.-P., Chadjichristos, C., Legendre, F., Baugé, C., Beauchef, G., Andriamanalijaona, R., et al. (2008). Interleukin-1 and Transforming Growth Factor-SS 1 as Crucial Factors in Osteoarthritic Cartilage Metabolism. *Connect. Tissue Res.* 49, 293–297. doi:10.1080/03008200802148355

Rutgers, M., Saris, D. B., Dhert, W. J., and Creemers, L. B. (2010). Cytokine Profile of Autologous Conditioned Serum for Treatment of Osteoarthritis, *In Vitro* Effects on Cartilage Metabolism and Intra-articular Levels after Injection. *Arthritis Res. Ther.* 12, R114. doi:10.1186/ar3050

Sokolove, J., and Lepus, C. M. (2013). Role of Inflammation in the Pathogenesis of Osteoarthritis: Latest Findings and Interpretations. *Ther. Adv. Musculoskelet.* 5, 77–94. doi:10.1177/1759720X12467868

Stone, A. V., Vanderman, K. S., Willey, J. S., Long, D. L., Register, T. C., Shively, C. A., et al. (2015). Osteoarthritic Changes in Vervet Monkey Knees Correlate with Meniscus Degradation and Increased Matrix Metalloproteinase and Cytokine Secretion. *Osteoarthritis and Cartilage* 23, 1780–1789. doi:10.1016/j.joca.2015.05.020

Teeple, E., Jay, G. D., Elsaid, K. A., and Fleming, B. C. (2013). Animal Models of Osteoarthritis: Challenges of Model Selection and Analysis. *AAPS J.* 15, 438–446. doi:10.1208/s12248-013-9454-x

Thysen, S., Luyten, F. P., and Lories, R. J. U. (2015). Targets, Models and Challenges in Osteoarthritis Research. *Dis. Model. Mech.* 8, 17–30. doi:10.1242/dmm.016881

Van Der Sluijs, J. A., Geesink, R. G. T., Van Der Linden, A. J., Bulstra, S. K., Kuyer, R., and Drukker, J. (1992). The Reliability of the Mankin Score for Osteoarthritis. *J. Orthop. Res.* 10, 58–61. doi:10.1002/jor.1100100107

Weimer, A., Madry, H., Venkatesan, J. K., Schmitt, G., Frisch, J., Wezel, A., et al. (2012). Benefits of Recombinant Adeno-Associated Virus (rAAV)-Mediated Insulinlike Growth Factor I (IGF-I) Overexpression for the Long-Term Reconstruction of Human Osteoarthritic Cartilage by Modulation of the IGF-I axis. *Mol. Med.* 18, 346–358. doi:10.2119/molmed.2011.00371

Wu, P. T., Shao, C. J., Wu, K. C., Wu, T. T., Chern, T. C., Kuo, L. C., et al. (2012). Pain in Patients with Equal Radiographic Grades of Osteoarthritis in Both

Knees: the Value of gray Scale Ultrasound. *Osteoarthritis and Cartilage* 20, 1507–1513. doi:10.1016/j.joca.2012.08.021

Yu, S. M., and Kim, S. J. (2013). Production of Reactive Oxygen Species by Withaferin A Causes Loss of Type Collagen Expression and COX-2 Expression through the PI3K/Akt, P38, and JNK Pathways in Rabbit Articular Chondrocytes. *Exp. Cel Res.* 319, 2822–2834. doi:10.1016/j.yexcr.2013.08.026

Zhou, X., Zhang, L., Guo, X., Liu, G., Wang, G., and Fu, S. (2018). A Macaca Fascicularis Knee Osteoarthritis Model Developed by Modified Hulth Combined with Joint Scratches. *Med. Sci. Monit.* 24, 3393–3404. doi:10.12659/MSM.906626

Conflict of Interest: The authors declare that the research was conducted in the absence of any commercial or financial relationships that could be construed as a potential conflict of interest.

Publisher's Note: All claims expressed in this article are solely those of the authors and do not necessarily represent those of their affiliated organizations, or those of the publisher, the editors and the reviewers. Any product that may be evaluated in this article, or claim that may be made by its manufacturer, is not guaranteed or endorsed by the publisher.

frontiers in Bioengineering and Biotechnology

REVIEW
published: 17 December 2021
doi: 10.3389/fbioe.2021.770655

Strategies for Articular Cartilage Repair and Regeneration

Yanxi Liu[1], *Karan M. Shah*[2]* *and Jian Luo*[1,3]*

[1]*Shanghai Key Laboratory of Regulatory Biology, Institute of Biomedical Sciences and School of Life Sciences, East China Normal University, Shanghai, China,* [2]*Department of Oncology and Metabolism, The Medical School, The University of Sheffield, Sheffield, United Kingdom,* [3]*Shanghai Yangzhi Rehabilitation Hospital (Shanghai Sunshine Rehabilitation Centre), Tongji University School of Medicine, Shanghai, China*

Articular cartilage is an avascular tissue, with limited ability to repair and self-renew. Defects in articular cartilage can induce debilitating degenerative joint diseases such as osteoarthritis. Currently, clinical treatments have limited ability to repair, for they often result in the formation of mechanically inferior cartilage. In this review, we discuss the factors that affect cartilage homeostasis and function, and describe the emerging regenerative approaches that are informing the future treatment options.

Keywords: articular cartilage, chondrocyte, microenvironment, regenerative medicine, articular cartilage repair, osteoarthritis

OPEN ACCESS

Edited by:
Xiaoling Zhang,
Shanghai Jiaotong University, China

Reviewed by:
Yong-Can Huang,
Peking University Shenzhen Hospital, China
Kaili Lin,
Shanghai Jiao Tong University, China

***Correspondence:**
Karan M. Shah
k.shah@sheffield.ac.uk
Jian Luo
jluo@tongji.edu.cn

Specialty section:
This article was submitted to Tissue Engineering and Regenerative Medicine, a section of the journal Frontiers in Bioengineering and Biotechnology

Received: *04 September 2021*
Accepted: *01 December 2021*
Published: *17 December 2021*

Citation:
Liu Y, Shah KM and Luo J (2021) Strategies for Articular Cartilage Repair and Regeneration. Front. Bioeng. Biotechnol. 9:770655. doi: 10.3389/fbioe.2021.770655

INTRODUCTION

Articular cartilage (AC) is a highly specialized connective tissue that covers the surfaces of bones in a synovial joint. Its main function is to allow for an almost friction-less movement of the joints, and facilitate the transmission of loads whilst protecting the subchondral bone. However, the constant mechanical stresses that are experienced by the AC makes it vulnerable to wear, tears, and sports injuries. Moreover, mature AC has a limited ability to self-renew and repair as it is avascular, lacks innervation and has a low cell-density (Chiang and Jiang, 2009). Therefore, without sufficient and potent treatment, cartilage damage can easily lead to progressive tissue deterioration, debilitating joint pain, dysfunction, and eventually the degenerative disease, osteoarthritis (OA) (Borrelli et al., 2019).

Osteoarthritis refers to exposure of subchondral bone to the joint space, which causes inflammation that may be accompanied by osteophyte development, severe pain, and progressive loss of joint function. In fact, retrospective studies with arthroscopic examinations reveal the presence of chondral lesions in nearly 60% of the patients (Chubinskaya et al., 2015). Acute knee injury has also been shown to be a risk factor for OA, with individuals with cartilage damage 7.4 times more likely to develop the disease (Wilder et al., 2002). This is consistent with a more recent study in young adults which identified a risk difference of 8.1 for knee OA, between individuals with and without knee injury at 19 years of follow-up (Snoeker et al., 2020). With the improvement of human life expectancy and the development of social aging process, the incidence of OA will greatly increase during the following decades. In fact, epidemiological study in the Chinese population suggested that the prevalence of knee OA had reached 18% in the country (Wang et al., 2018).

Whilst current treatment options may improve joint function and reduce pain, they fail to elicit regeneration of the articular tissue with its distinct functional characteristics, and therefore are only partially effective. In this review, we begin by discussing the structure and biology of the AC, and then describe the current strategies for its repair, followed by highlighting the recent advances in regenerative technologies that are informing the future treatment options.

ANATOMY OF THE ARTICULAR CARTILAGE

In utero and at birth, AC is a compact, highly cellular tissue with isotropic distribution of chondrocytes, but poor in the extracellular matrix (ECM) (Weiss et al., 1968). As the AC matures and shapes before early adulthood, chondrocytes located in different areas receive AC variant degrees of mechanical, electrical, and physicochemical signals, leading to increased cellular size, accumulation of ECM, and eventually attaining a zonal anisotropic organization (Correa and Lietman, 2017).

The ECM comprises of a fibrillary network of collagen, non-collagenous proteins, proteoglycans, and water; and the orientation of the collagen fibrils along with chondrocyte morphology characterize the three zones of AC (**Figure 1**). In the thin superficial zone, that makes up approximately 10–20% of the AC thickness, the collagen fibrils and chondrocytes are aligned parallel to the articular surface. Chondrocytes are flattened and elongated, and the integrity of this layer is vital for the protection of the deeper layers. This zone confers the tensile properties to the AC, and helps resist the sheer forces experienced by the joint. The middle layer or the transitional zone which makes up 40–60% of the AC thickness is characterized by obliquely organized thicker collagen fibrils, and slightly larger chondrocytes at a relatively lower density. The transitional zone is the first line of resistance to the compressive forces imposed by the articulation. In the deep zone, the collagen fibrils are the thickest and are arranged perpendicular to the articulating surfaces. The very large chondrocytes are typically arranged in columns, parallel to the collagen fibrils. This deep zone which make up nearly 30% of the AC volume, provides the greatest resistance to the compressive forces (Ulrich-Vinther et al., 2003). Calcified cartilage, which lies beneath the deep zone separated by the tide mark, secures the AC by anchoring the collagen fibrils to the subchondral bone (Sophia Fox et al., 2009).

There are three main types of cartilages found in the human body, with differing structures and functions.

Hyaline Cartilage

Hyaline cartilage is the most common type of cartilage and can be seen at the connection sites between the ribs and sternum, trachea, and on the surfaces of the synovial joints. It has a glassy appearance and type II collagen is the most abundant type of collagen in hyaline cartilage, accounting for 90–95% of the collagen in ECM. Additionally, collagen IX links covalently to the type II collagen backbone, with type XI collagen forming the filamentous template of the fibril (Eyre et al., 2006). The matrix of hyaline cartilage is also rich in glycosaminoglycans (GAGs), including negatively charged hyaluronic acid and chondroitin sulfate. Aggrecan (ACAN), is a major proteoglycan in the AC, which interacts with the GAGs to form large aggregates and their high anionic charge allow for increased retention of water molecules thus facilitating shock absorption. In adults, chondrocytes show low anabolic and proliferative activity, and the collagen fibers last life-long, with minimal replacement activity.

Fibrocartilage

Fibrocartilage is mainly found between the vertebral bodies, symphysis pubis, meniscus, and tendon-bone interface. Its matrix is rich in densely braided collagen fibers, making it highly resistant to compressive loads. The chondrocytes are aligned with the thick collagen fibers, and are very few in number. Compared to hyaline cartilage, fibrocartilage contains a large amount of type I collagen in addition to type II collagen (Armiento et al., 2019).

Elastic Cartilage

Elastic cartilage is a type of elastic and flexible tissue that can withstand repeated bending and is found in epiglottis, auricle and eustachian tube. In elastic cartilage, the cell morphology is basically similar to that of hyaline cartilage. Type II collagen and elastic fibers branch densely in multiple directions, and contains relatively low amounts of type III, XII, V collagen (Wachsmuth et al., 2006).

THE ROLE OF MICROENVIRONMENT ON CARTILAGE FUNCTION

Considering the avascular characteristic of AC, chondrocyte metabolism, and thus cartilage homeostasis largely depends on the diffusion of nutrients, oxygen, and other regulatory factors from subchondral bone and synovial fluid through the matrix. In this section, we discuss the current known factors in the chondrocyte microenvironment that regulate cartilage homeostasis and function, with specific focus on mechanical stimulation, oxygen tension, and cytokines and growth factors.

Mechanical Stimulation

The chondrocytes reside in a microenvironment that experiences complex combination of compressive loads, shear, and tensile stress regularly. Sensitivity to such mechanical stimuli and consequent adaptive responses are essential to maintain the joint function. Optimal mechanical stress has been shown to induce chondrogenesis during fetal development and maintains cartilage homeostasis in adults (Zhao et al., 2020). However, impact forces caused by falls, sports injuries and road accidents can lead to substantial damage. Indeed, studies have shown that above a certain threshold, impact forces can cause permanent changes to the mechanical properties and damage the structure of AC (Jeffrey and Aspden, 2006; Verteramo and Seedhom, 2007). Additionally, repetitive heavy loading has been shown to cause chondrocyte mitochondrial dysfunction, decreasing adenosine triphosphate (ATP) levels, exacerbating proton leakage and ROS formation (Coleman et al., 2016). Transforming growth factor-β (TGF- β) signaling is a well-established mediator of mechanical stress based regulation of cartilage. In a recent study, Zhen et al. show that TGF-β activity is concentrated in areas of cartilage that experience high mechanical stress, and it impairs the metabolic activity of chondrocytes, thus disrupting cartilage homeostasis (Zhen et al., 2021). Other pathways including MAPK-ERK, Wnt and Indian hedgehog signaling have been shown to play a role in regulating mechanotransduction in chondrocytes, and have been reviewed elsewhere (Zhao et al., 2020) (**Figure 2A**).

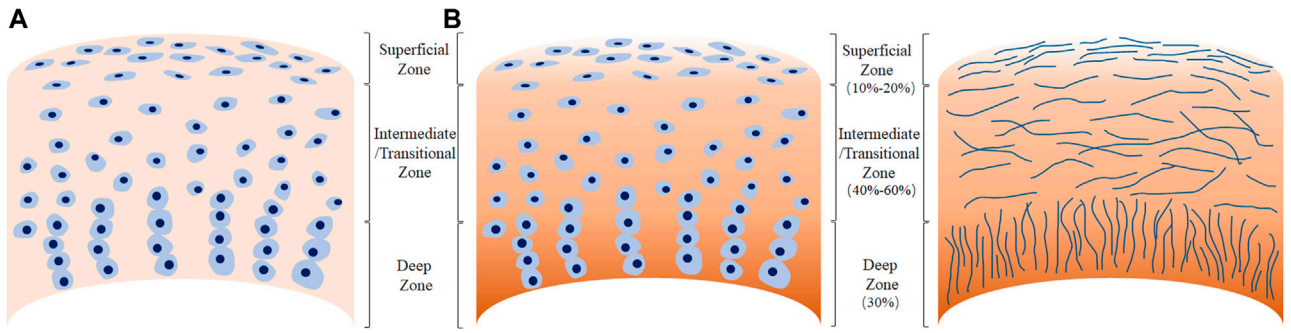

FIGURE 1 | Morphology of human adult articular cartilage. **(A)**, chondrocytes organization in the different tissue zones. **(B)**, arrangement of collagen fibers.

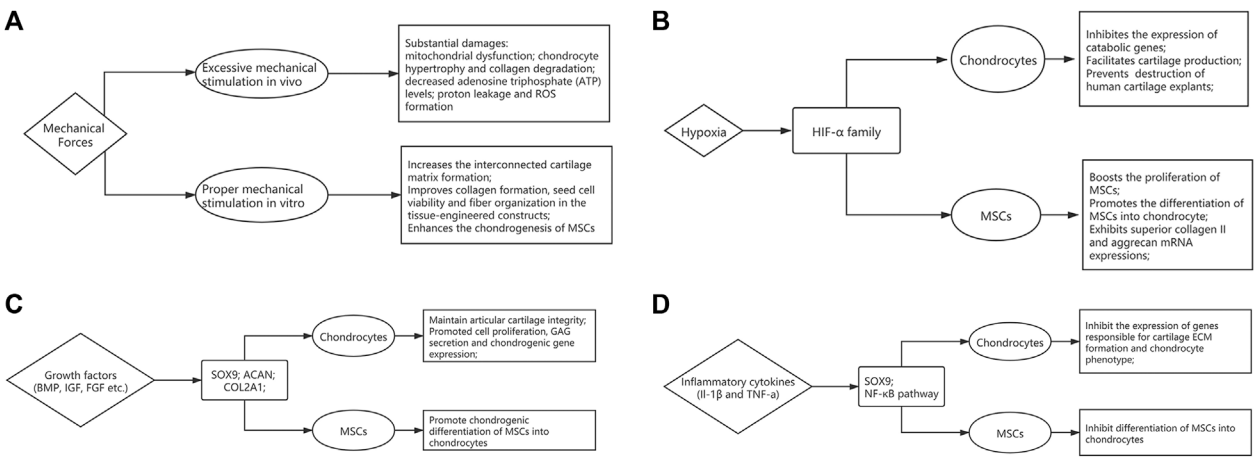

FIGURE 2 | The influence of microenvironmental factors on articular cartilage homeostasis and function. The flow-chart describes the effects of **(A)** mechanical forces, **(B)** Oxygen tension, **(C)** growth factors and **(D)** inflammatory cytokines.

The insights of mechanobiology can provide new strategies in regenerative medicine. In order to mimic the natural environment of AC, mechanical stimulation can be added during expansion cultures of cell-based therapies (see **section 4.2**). At the cellular level, using biomechanics to enhance the chondrogenesis of mesenchymal stem cells has been well documented, which could be attributable to increased TGF-β meditated chondrogenic signaling (Li et al., 2010; Fahy et al., 2018). Low level of shear stress has shown to stimulate hMSC migration through JNK and p38 MAPK pathways mediated by SDF-1/CXCR4 axis (Yuan et al., 2013). In addition, mechanical loading enhances the angiogenic capacity, which could be attributed to FGFR and VEGFR signaling cascades (Kasper et al., 2007). Furthermore, optimal mechanical stimulation also has the potential to improve collagen formation, cell viability and fiber organization in the tissue-engineered constructs (Li et al., 2017; Salinas et al., 2018).

Oxygen Tension

AC microenvironment is generally hypoxic due to the lack of capillary network, and several studies have highlighted the relationship between hypoxia and AC development and homeostasis. The oxygen tension in the AC may be as low as 1–3% compared to 21% under normoxic conditions. Hypoxic environment has long been acknowledged as a positive influence that drives cartilage matrix accumulation, supporting a healthy chondrocyte phenotype (Murphy et al., 2009). Hypoxia-inducible factors (HIFs) are essential regulators that respond to hypoxia. They consist of an oxygen-regulatory α subunit, and a constitutively expressed β subunit. Under normal oxygen tension, the α subunit is degraded following hydroxylation by prolyl hydroxylases. However, it is stabilized under hypoxic conditions, dimerizes with the β subunit, and translocates to the nucleus to regulate gene expression. HIF-1α has been shown to be essential for chondrocyte survival and development of murine growth plates (Schipani et al., 2001). Furthermore, hypoxia has been associated with upregulation in expression of matrix components, and downregulation of degrading enzymes and hypertrophic markers in both healthy and OA chondrocytes (Murphy and Polak, 2004; Markway et al., 2013). A recently published study demonstrated that HIF-1α has anti-catabolic effects on AC by inhibiting the expression of Mmp13, via

suppression of NF-κB signaling (Okada et al., 2020). Furthermore, using RNA interference, HIF-2α and not HIF-1α, was identified as a critical anabolic regulator of matrix synthesis (Lafont et al., 2007). It was also demonstrated that matrix genes such as aggrecan and type IX collagen were not HIF targets but regulated by hypoxia via SOX9, a cartilage-specific transcription factor (Thoms et al., 2013) (**Figure 2B**).

Several studies have highlighted the role of hypoxia in chondrogenic differentiation of mesenchymal stem cells (MSCs) (Robins et al., 2005; Elabd et al., 2018; Contentin et al., 2020). Proliferation of bone marrow MSCs was enhanced under hypoxia, together with increased chondrogenic ability, and higher type II collagen and aggrecan mRNA expressions (Bornes et al., 2015). Furthermore, hypoxia mediated HIF-1α stabilization led to activation of SOX9 and subsequent differentiation of MSCs to chondrocytes (Robins et al., 2005). Thus, targeting the hypoxic pathways, possibly by inhibiting prolyl hydroxylases (Joharapurkar et al., 2018), could be therapeutic strategy for cartilage repair.

Cytokines and Growth Factors

During development, the synthesis of matrix components by chondrocytes is stimulated by a range of anabolic cytokines including TGF-β (Wang et al., 2014), bone morphogenetic proteins (BMPs) (Kobayashi et al., 2005) and insulin-like growth factor-1 (IGF-1) (Lui et al., 2019). The maintenance of cartilage health requires the bioactive levels of TGF-β to be within a narrow range. Concentrations above or below this optimal range and subsequent alterations in the TGF-β/SMAD2/3 pathway result in abnormal cartilage function (Finnson et al., 2012; Zhai et al., 2015). High concentrations of TGF-β induced by mechanical stress and platelet-derived growth factor-BB (PDGF-BB) secreted by mononuclear preosteoclasts respectively, cause bone resorption and angiogenesis in subchondral bone. Since subchondral bone is crucial for maintaining AC integrity, pathological changes in subchondral bone exacerbate the progression of OA (Zhen et al., 2013; Su et al., 2020). BMPs have been shown to regulate several chondrocyte specific genes and are involved all phases of chondrogenesis. *In vitro* studies have highlighted the role of BMP-7 in chondrocyte proliferation, GAG secretion and chondrogenic gene expression including ACAN, SOX9 and Col2a1 (Shen et al., 2010). BMP-2 mediated induction of chondrocyte differentiation from MSCs has been shown to occur via TGF-β3 pathway (Shen et al., 2009). BMP-6 has also been shown to promote chondrogenesis and hypertrophic differentiation from MSCs (Sekiya et al., 2001), and stimulate matrix synthesis (Bobacz et al., 2003). IGF-1 also modulates chondrogenesis from MSCs by stimulating cell proliferation, regulating apoptosis, and inducing chondrogenic gene expression (Longobardi et al., 2006; Ikeda et al., 2017). Moreover, mechanical stimulation has a synergistic effect on IGF-1 mediated increase in collagen and proteoglycan synthesis (Bonassar et al., 2001). Furthermore, chronic deficiency in IGF-1 levels has shown to associate with increased severity of AC lesions in OA in a rat model (Ekenstedt et al., 2006) (**Figure 2C**).

In response to trauma or inflammatory disease such as OA, a process of cartilage remodeling initiates. A catabolic response is mediated by inflammatory cytokines interleukin-1 (IL-1) and tumor necrosis factor-a (TNF-α) which suppress Sox9 mRNA and protein levels via the NF-κB pathway. This leads to a marked inhibition in expression of cartilage specific genes responsible for ECM formation and chondrogenesis (Murakami et al., 2000). This was confirmed in a separate study which showed IL-1β and TNF-α mediated inhibition of chondrogenesis by human MSCs through NF-κB dependent mechanisms (Wehling et al., 2009). IL-1β has also been shown to upregulate the expression of matrix metalloproteinase-3 (MMP3) and tumor-necrosis-factor-stimulated gene 6 (TSG6), and downregulate ACAN, further exacerbating the catabolic phenotype (Stöve et al., 2000). TNF-α also induces the expression of cartilage degradation molecules including MMP-9 and MMP-13, and decreases collagen type II and type XI synthesis (Lefebvre et al., 1990; Reginato et al., 1993; Liacini et al., 2003) (**Figure 2D**).

CURRENT AND EMERGING TREATMENT MODALITIES

Articular cartilage lesions, when left untreated, leads to the onset of degenerative OA, and thus demands an effective treatment option for repair and regeneration. Here we discuss the current treatment modalities used for the repair for cartilage lesions, and the emerging technologies.

Surgical Approaches

Surgical approaches for articular cartilage can be divided into three categories: bone marrow stimulation, autografts and allografts, and cell-based therapies. Bone marrow stimulation procedures are widely applied in treatment of osteochondral lesions treatment, which include microfracture, subchondral drilling or abrasion of the subchondral bone. Microfracture generally targets small, contained defects and requires making several perforations in the subchondral plate by using an arthroscopic awl and may result in good clinical outcome for smaller lesions (Sommerfeldt et al., 2016). Nevertheless, microfracture might ultimately induce the formation of fibrocartilage since bone marrow released into the defect forms a blood clot (Goyal et al., 2013; Kwon et al., 2019). Subchondral drilling and subchondral abrasion are alternatives to microfracture, but are less popular due to the risks of thermal necrosis, hypertrophy, or cysts (Chen et al., 2009).

Osteochondral autograft directly delivers mature and viable hyaline cartilage into the defects and therefore realizes a faster rehabilitation compared to most other cartilage repair strategies (Redondo et al., 2018). However, the application of osteochondral autograft transfer is restricted to small chondral defects (<2 cm^2) because of the limitations in graft availability (Hangody et al., 2004). Osteochondral allograft transplantation is a feasible solution for AC repair due to the avascular nature of cartilage which alleviates any immunological concerns (Arzi et al., 2015). Although osteochondral allograft transplantation overcomes the graft availability concerns of osteochondral autograft transfer, the

difficulties in matching allografts to native architecture and improving the viability and longevity of the fresh tissue still exists (Koh et al., 2006; Cook et al., 2016).

Autologous chondrocyte implantation (ACI) is the most widely used surgical approach to treat large chondral defects (>3–4 cm^2), and is the first application of cell engineering strategy in orthopedic surgery. It relies on repopulating the cartilage lesion with mature autologous chondrocytes, and thus requires two surgeries–one to harvest chondrocytes from healthy cartilage, and another to reimplant them into defects after expansion in cultures *in vitro* (Welch et al., 2016). Approximately 22% of patients suffer from hypertrophy of the periosteum after ACI procedures (Gikas et al., 2009). Matrix-induced ACI (MACI) is the second generation of this technique which involves incorporation of chondrocytes onto a collagen scaffold prior to implantation (Nawaz et al., 2014). Although both ACI and MACI show better hyaline or hyaline-like cartilage formation and graft survival, patients have to endure two surgeries, a longer recovery phase and high financial costs (Chimutengwende-Gordon et al., 2020). Furthermore, the chondrocyte can de-differentiate during culture expansion, with downregulation of chondrogenic markers resulting in a limited life-span following implantation (Brittberg et al., 2003).

Cell Based Therapy

Chondrocytes often lose their capacity to produce ECM and proliferate after passaging in culture, a phenomenon referred to as de-differentiation (Goldring et al., 1986; Schnabel et al., 2002). A recent study identified an important role of perlecan, a heparen sulphate proteoglycan, in the repair of defects in human cartilage. The authors also demonstrate that treating the chondrocytes with heperanase increased their proliferative potential and chondrogenic gene expression, with implications for *in vitro* expansion of cells (Garcia et al., 2021). A new population of cells termed as cartilage-derived stem/progenitor cells (CPSCs) have been identified in the cartilage, which unlike the chondrocytes, may have the ability to self-renew (Jiang and Tuan, 2015). The application potential of CPSCs is still unclear, but research is ongoing to better understand this cell phenotype and its therapeutic prospects for AC repair (Jiang et al., 2016; Bauza et al., 2020).

MSCs offer a promising cell source for regeneration and repair of cartilage lesions, as they have the ability to differentiate into chondrocytes, and are easy to harvest, with minimal donor site morbidity (Park et al., 2018). MSCs used for repairing the cartilage lesions are obtained from a variety of autologous tissues including bone marrow (BM-MSCs), adipose tissue (AT-MSCs) and peripheral blood (PB-MSCs) (Reissis et al., 2016). Depending on the specific cartilage pathology, the MSCs can either be implanted into the defect following surgical incision, or administered via intra-articular injection. A post-surgical prognosis study assessing the efficacy of AT-MSCs implantation for cartilage lesions observed 76% of the patients had the repair rated as abnormal or severely abnormal as per the International Cartilage Repair Society standards (Koh et al., 2014). Furthermore, compared to MSCs implantation, intra-articular injections have a higher risk of the cells migrating to non-target tissues (Reissis et al., 2016). Whilst, there have been several studies which have reported improved outcomes following MSC based therapies (Wakitani et al., 2002; Lee et al., 2019) there are some challenges that need to be overcome.

Indeed, multiple novel strategies are being explored to improve the use MSC in cartilage regeneration. For instance, a magnetically actuated microrobot has recently been proposed to improve the targeting efficiency of MSC in tissue regeneration for cartilage lesions (Go et al., 2020). Other studies are exploiting the ability of MSCs to exert their regenerative functions by secreting paracrine molecules that modulate the local immune response or improves chondrocytes cell survival and proliferation (Toh et al., 2017; Zhang et al., 2019; Kim et al., 2020). By using MSCs derived extracellular vesicles, studies have shown improved cartilage regeneration and repair (Vonk et al., 2018; Alcaraz et al., 2019).

Small Molecules

A variety of synthetic or natural small molecule compounds have proven effective in maintaining a stable chondrocyte phenotype, supporting an ideal microenvironment to promote chondrocyte proliferation and chondrogenic differentiation of stem cells (Li et al., 2020). Kartogenin (KGN) can facilitate chondrocyte differentiation by regulating the CBFβ-RUNX1 signaling pathway in BM-MSCs (Johnson et al., 2012). Moreover, KGN can enhance the therapeutic effect of conventional treatment modalities. Intra-articular injection of KGN after microfracture showed increased hyaline-like cartilage formation and better defect filling, indicating an enhanced quality of repair for full-thickness cartilage defects (Xu et al., 2015).

Another small molecule compound TD-198946, a derivative of thienoindazole, can strongly induce chondrogenic differentiation via upregulation of Runx1 expression, preventing and repairing degeneration of the articular cartilage (Yano et al., 2013). A novel synthetic small molecule 5{i,2} was discovered to induce a more directed chondrogenic differentiation of BM-MSCs compared to TGF-β3. Molecule 5 {i,2} is thought to exert its effect by enhancing the transcription of chondrogenic markers including SOX9 and aggrecan (Cho et al., 2012). A small molecule called BNTA was described to target superoxide dismutase 3 (SOD3) in the cartilage microenvironment and induce superoxide anion elimination in chondrocyte culture, promoting generation of ECM components (Shi et al., 2019). Salidroside, isolated from the root of *Rhodiola rosea*, improves chondrocyte proliferation, prevents apoptosis, and drives cartilage specific gene expression via TGF-β/Smad3 and PI3K/Akt signaling pathways (Zhang and Zhao, 2018; Wu et al., 2019). Lastly, berberine chloride, derived from *Coptis chinensis* and *Berberis aristata*, has been verified to stimulate chondrocyte proliferation and upregulate aggrecan and Col II expression through activating Wnt/β-catenin pathways (Zhou et al., 2016).

Such small molecule drugs present an attractive therapeutic strategy for MSC based cartilage regeneration and repair. They have a significant cost advantage compared to biologics, more predictable pharmacokinetic and pharmacodynamic profile and

are usually orally bioavailable, thus making them a convenient option (Ngo and Garneau-Tsodikova, 2018).

Tissue Engineering

Tissue engineering is using a combination of cells, biochemical and physio-chemical factors along with engineering and biomaterials to improve or replace biological function (Musumeci et al., 2014). Tissue engineering in cartilage repair can be divided into two categories, scaffold-dependent and independent approaches. Scaffold refers to a variety of synthetic or natural biomaterials which construct a suitable environment for cell distribution, cell–matrix and cell–cell interactions (Kwon et al., 2019). In addition, an ideal biomaterial scaffold for AC regeneration can now be bioactive, biomimetic, biodegradable and bioresponsive, allowing signaling with spatio-temporal control (Musumeci et al., 2014). Scaffolds can be made of a wide array of materials including polyglycolides, polylactides, silk and decellularized cartilage-derived matrix (Kwon et al., 2019). Hydrogel-based scaffolds are becoming one of the most prevalent treatment strategies in cartilage defect repair. Injectable hydrogels can form irregular shapes that better fill the cartilage defects, provide a high-water content scaffold similar to natural ECM and are minimally invasive (Liu et al., 2017). More recently, injectable thermogels formed by the sol-gel phase transition have been employed to repair cartilage defects. A thermogel of triblock copolymer poly (lactide-co-glycolide)-block-poly (ethyleneglycol)-block-poly (lactide-co-glycolide) (PLGA–PEG–PLGA) dissolves in water at low temperatures, but gels spontaneously at body temperatures. In a rabbit model of full-thickness cartilage defect, the BM-MSC incorporated PLGA–PEG–PLGA thermogel regenerated cartilage with high expression of GAGs and type II collagen, and comparable biomechanical properties to normal cartilage (Zhang et al., 2018).

While scaffolds provide an initial mechanical stability, it has several limitations including degradation-associated toxicity, hindrances to remodelling, stress shielding, and altered cell phenotypes (Athanasiou et al., 2013). Therefore, investigations were directed into developing scaffold-free strategies. Three dimensional (3D) bioprinting is the placing of cells in a 3D space to generate a cohesive tissue microarchitecture akin to the *in vivo* characteristics (Moldovan et al., 2019). Hydrogels are fast becoming a common printing media which are then jetted with cells, an approach referred to as bio-ink based hybrid bioprinting (Laternser et al., 2018; Moldovan et al., 2019). Hydrogels can differ in their physical properties including viscosity and rigidity, which has implications for the mechanical environment, and the amount of natural cell binding motifs. This may in turn influence cell spreading and cell–matrix interactions. Therefore, the choice of bioink is crucial considering the chondrocyte phenotype varies in fibrocartilage and hyaline cartilage (Daly et al., 2016). In addition, the scaffold free cell-sheet engineering wherein 3D MSC sheets are developed to create a transplantable hyaline-like cartilage tissue have successfully shown chondrogenic differentiation capability (Thorp et al., 2020).

At present, most of the research on the role of tissue microenvironment on regulating AC and chondrocyte phenotype rely on *in vitro* experiments, and requires further exploration *in vivo*. Better understanding of the influence of the microenvironment on chondrocytes and MSCs can provide vital insights for development of novel therapies. For instance, the use of chondrogenic growth factors in scaffolds can improve cartilage synthesis and improve implantation outcomes (Chen et al., 2020). The application of platelet-rich plasma (PRP) in cartilage repair is an excellent example of combining the understanding of molecular biology with regenerative medicine to treat cartilage injury (Abrams et al., 2013; Kennedy et al., 2018). PRP consists of concentrated platelets, white blood cells, plasma, and various other growth factors. On one hand, PRP can be used as a natural scaffold for tissue engineering (Wu et al., 2009; Vinod et al., 2019). Once activated, PRP acts as a gelatinous scaffold that supports the growth of seeded cells and lubricates the articular cartilage, reducing the coefficient of friction and wear. On the other hand, PRP also contains growth factors that can directly promote cartilage repair. Studies have shown that PRP can regulate synovial inflammation and reduce pain through the inflammatory NF-κB signaling pathway. PRP also improves the expression of TGF-β, aggregan, and type II collagen, thus promoting cell migration, proliferation, and differentiation of progenitor/stem cells (Mascarenhas et al., 2015; Sakata and Reddi, 2016; Moussa et al., 2017). Therefore, PRP has potential applications in improving the efficacy of traditional surgical treatment, cell therapy, and tissue engineering.

CONCLUSION AND FUTURE OUTLOOK

Articular cartilage regeneration and repair is a dynamic multidisciplinary field that is continuously evolving. The current clinical approaches have achieved limited success, however, the rapid advances in cell-based therapies, biomaterials, and developments in mechanobiology have the potential to provide long-term solutions for cartilage repair and regeneration. Comprehensive treatment modalities with lower financial costs, shorter recovery period, and reduced surgical recovery is expected in the future.

The formation of fibrocartilage remains a major obstacle in cartilage repair. Fibrosis is characterized by activation and proliferation of fibroblasts or fibrogenic cells, accompanied by an over deposition of ECM (Novo et al., 2009; Sakai and Tager, 2013). In case of AC, the repair procedures after cartilage injury may lead to excessive secretion and deposition of ECM proteins, which may result in fibrocartilage formation (Pearle et al., 2005; Chan et al., 2018). In addition, the inadequate number of stem cells and progenitor cells recruited to the injured site after cartilage damage or microfracture surgery can exacerbate the formation of fibrocartilage (Im, 2016; Hu et al., 2021). The fundamental objective for treating cartilage injury remains the regeneration of hyaline cartilage, or transplant mature hyaline cartilage tissue. However, the potential reparative role of fibrocartilage has been largely neglected due to its inferior mechanical properties. Preventing hyaline cartilage fibrosis and promoting the hyalinization of fibrocartilage may provide new therapeutic ideas for repairing cartilage damage (Shi and Li, 2021).

There are two strategies that could be employed to prevent hyaline cartilage fibrosis. The first is to reshape the microenvironment of the injury site. By adding appropriate cytokines, the spontaneous inflammatory response after injury can be alleviated and cell proliferation and differentiation can be promoted. The three-dimensional structure and physical properties of the grafts used in ACI and MACI could also be optimized to closely simulate the structure of articular cartilage, display better response to mechanical pressure and other stimuli, and therefore be more suitable for the growth of resident cells. The avascular nature of AC makes it difficult for nutrients to diffuse, and the ECM of AC is relatively dense. These factors contribute to the difficulty for mesenchymal stem cells and progenitor cells to migrate to injury sites. The second strategy could be to promote migration of the endogenous skeletal or mesenchymal stem/progenitor cells to the AC. Application of chemoattractants could facilitate this migration of resident mesenchymal stem/progenitor cells, and thus improve the repair capacity (Dwyer et al., 2007; Park et al., 2015; Wang et al., 2017).

Finally, in order to achieve fibrocartilage hyalinization, it is necessary to identify where the cells within the fibrosis tissue come from. Studies have shown that chondrocytes originated from synovium-derived mesenchymal stem cells and articular chondrocytes have similar gene expression profiles, suggesting that synovial and AC are formed from the same precursors (Zhou et al., 2014; Caldwell and Wang, 2015). This may explain why repair of cartilage damage with synovium-derived mesenchymal stem cells shows less de-differentiation and fibrosis, and thus better outcomes in some cases than with other types of mesenchymal stem cells (Sakaguchi et al., 2005; Pei and He, 2012). However, the origins of fibrocartilage after injury still remain unclear. In addition, changes in cell behavior in fibrotic tissue (such as cytoskeletal activity, cell metabolism, etc.), and alterations in gene expression at transcriptional and translational levels need to be clarified. This is essential to thoroughly explore the mechanism of fibrocartilage formation and screen suitable stimulus factors and small molecule drugs that can modify the microenvironment to minimize the fibrocartilage phenotype and promote hyalinization of the cartilage.

AUTHOR CONTRIBUTIONS

YL and JL conceived of the study. YL made literature review and drafted the manuscript. KM was involved in literature review and the revision of the manuscript. JL supervised and revised the manuscript. All authors read and approved the content of the manuscript.

REFERENCES

Abrams, G. D., Frank, R. M., Fortier, L. A., and Cole, B. J. (2013). Platelet-rich Plasma for Articular Cartilage Repair. *Sports Med. Arthrosc. Rev.* 21, 213–219. doi:10.1097/JSA.0b013e3182999740

Alcaraz, M. J., Compañ, A., and Guillén, M. I. (2019). Extracellular Vesicles from Mesenchymal Stem Cells as Novel Treatments for Musculoskeletal Diseases. *Cells* 9, 98. doi:10.3390/cells9010098

Armiento, A. R., Alini, M., and Stoddart, M. J. (2019). Articular Fibrocartilage - Why Does Hyaline Cartilage Fail to Repair? *Adv. Drug Deliv. Rev.* 146, 289–305. doi:10.1016/j.addr.2018.12.015

Arzi, B., Duraine, G. D., Lee, C. A., Huey, D. J., Borjesson, D. L., Murphy, B. G., et al. (2015). Cartilage Immunoprivilege Depends on Donor Source and Lesion Location. *Acta Biomater.* 23, 72–81. doi:10.1016/j.actbio.2015.05.025

Athanasiou, K. A., Eswaramoorthy, R., Hadidi, P., and Hu, J. C. (2013). Self-organization and the Self-Assembling Process in Tissue Engineering. *Annu. Rev. Biomed. Eng.* 15, 115–136. doi:10.1146/annurev-bioeng-071812-152423

Bauza, G., Pasto, A., Mcculloch, P., Lintner, D., Brozovich, A., Niclot, F. B., et al. (2020). Improving the Immunosuppressive Potential of Articular Chondroprogenitors in a Three-Dimensional Culture Setting. *Sci. Rep.* 10, 16610. doi:10.1038/s41598-020-73188-9

Bobacz, K., Gruber, R., Soleiman, A., Erlacher, L., Smolen, J. S., and Graninger, W. B. (2003). Expression of Bone Morphogenetic Protein 6 in Healthy and Osteoarthritic Human Articular Chondrocytes and Stimulation of Matrix Synthesis *In Vitro*. *Arthritis Rheum.* 48, 2501–2508. doi:10.1002/art.11248

Bonassar, L. J., Grodzinsky, A. J., Frank, E. H., Davila, S. G., Bhaktav, N. R., and Trippel, S. B. (2001). The Effect of Dynamic Compression on the Response of Articular Cartilage to Insulin-like Growth Factor-I. *J. Orthop. Res.* 19, 11–17. doi:10.1016/s0736-0266(00)00004-8

Bornes, T. D., Jomha, N. M., Mulet-Sierra, A., and Adesida, A. B. (2015). Hypoxic Culture of Bone Marrow-Derived Mesenchymal Stromal Stem Cells Differentially Enhances *In Vitro* Chondrogenesis within Cell-Seeded Collagen and Hyaluronic Acid Porous Scaffolds. *Stem Cel Res Ther* 6, 84. doi:10.1186/s13287-015-0075-4

Borrelli, J., Jr., Olson, S. A., Godbout, C., Schemitsch, E. H., Stannard, J. P., and Giannoudis, P. V. (2019). Understanding Articular Cartilage Injury and Potential Treatments. *J. Orthop. Trauma* 33 (6), S6–s12. doi:10.1097/bot.0000000000001472

Brittberg, M., Peterson, L., Sjögren-jansson, E., Tallheden, T., and Lindahl, A. (2003). Articular Cartilage Engineering with Autologous Chondrocyte Transplantation. *The J. Bone Jt. Surgery-American.* 85 (3), 109–115. doi:10.2106/00004623-200300003-00017

Caldwell, K. L., and Wang, J. (2015). Cell-based Articular Cartilage Repair: the Link between Development and Regeneration. *Osteoarthritis and Cartilage* 23, 351–362. doi:10.1016/j.joca.2014.11.004

Chan, D. D., Li, J., Luo, W., Predescu, D. N., Cole, B. J., and Plaas, A. (2018). Pirfenidone Reduces Subchondral Bone Loss and Fibrosis after Murine Knee Cartilage Injury. *J. Orthop. Res.* 36, 365–376. doi:10.1002/jor.23635

Chen, H., Sun, J., Hoemann, C. D., Lascau-Coman, V., Ouyang, W., Mckee, M. D., et al. (2009). Drilling and Microfracture lead to Different Bone Structure and Necrosis during Bone-Marrow Stimulation for Cartilage Repair. *J. Orthop. Res.* 27, 1432–1438. doi:10.1002/jor.20905

Chen, L., Liu, J., Guan, M., Zhou, T., Duan, X., and Xiang, Z. (2020). Growth Factor and its Polymer Scaffold-Based Delivery System for Cartilage Tissue Engineering. *Ijn* 15, 6097–6111. doi:10.2147/ijn.S249829

Chiang, H., and Jiang, C.-C. (2009). Repair of Articular Cartilage Defects: Review and Perspectives. *J. Formos. Med. Assoc.* 108, 87–101. doi:10.1016/s0929-6646(09)60039-5

Chimutengwende-Gordon, M., Donaldson, J., and Bentley, G. (2020). Current Solutions for the Treatment of Chronic Articular Cartilage Defects in the Knee. *EFORT Open Rev.* 5, 156–163. doi:10.1302/2058-5241.5.190031

Cho, T.-J., Kim, J., Kwon, S.-K., Oh, K., Lee, J.-A., Lee, D.-S., et al. (2012). A Potent Small-Molecule Inducer of Chondrogenic Differentiation of Human Bone Marrow-Derived Mesenchymal Stem Cells. *Chem. Sci.* 3, 3071–3075. doi:10.1039/C2SC20362F

Chubinskaya, S., Haudenschild, D., Gasser, S., Stannard, J., Krettek, C., and Borrelli, J., Jr. (2015). Articular Cartilage Injury and Potential Remedies. *J. Orthop. Trauma* 29 (12), S47–S52. doi:10.1097/bot.0000000000000462

Coleman, M. C., Ramakrishnan, P. S., Brouillette, M. J., and Martin, J. A. (2016). Injurious Loading of Articular Cartilage Compromises Chondrocyte Respiratory Function. *Arthritis Rheumatol.* 68, 662–671. doi:10.1002/art.39460

Contentin, R., Demoor, M., Concari, M., Desancé, M., Audigié, F., Branly, T., et al. (2020). Comparison of the Chondrogenic Potential of Mesenchymal Stem Cells

Derived from Bone Marrow and Umbilical Cord Blood Intended for Cartilage Tissue Engineering. *Stem Cel Rev Rep* 16, 126–143. doi:10.1007/s12015-019-09914-2

Cook, J. L., Stannard, J. P., Stoker, A. M., Bozynski, C. C., Kuroki, K., Cook, C. R., et al. (2016). Importance of Donor Chondrocyte Viability for Osteochondral Allografts. *Am. J. Sports Med.* 44, 1260–1268. doi:10.1177/0363546516629434

Correa, D., and Lietman, S. A. (2017). Articular Cartilage Repair: Current Needs, Methods and Research Directions. *Semin. Cel Developmental Biol.* 62, 67–77. doi:10.1016/j.semcdb.2016.07.013

Daly, A. C., Critchley, S. E., Rencsok, E. M., and Kelly, D. J. (2016). A Comparison of Different Bioinks for 3D Bioprinting of Fibrocartilage and Hyaline Cartilage. *Biofabrication* 8, 045002. doi:10.1088/1758-5090/8/4/045002

Dwyer, R. M., Potter-Beirne, S. M., Harrington, K. A., Lowery, A. J., Hennessy, E., Murphy, J. M., et al. (2007). Monocyte Chemotactic Protein-1 Secreted by Primary Breast Tumors Stimulates Migration of Mesenchymal Stem Cells. *Clin. Cancer Res.* 13, 5020–5027. doi:10.1158/1078-0432.Ccr-07-0731

Ekenstedt, K. J., Sonntag, W. E., Loeser, R. F., Lindgren, B. R., and Carlson, C. S. (2006). Effects of Chronic Growth Hormone and Insulin-like Growth Factor 1 Deficiency on Osteoarthritis Severity in Rat Knee Joints. *Arthritis Rheum.* 54, 3850–3858. doi:10.1002/art.22254

Elabd, C., Ichim, T. E., Miller, K., Anneling, A., Grinstein, V., Vargas, V., et al. (2018). Comparing Atmospheric and Hypoxic Cultured Mesenchymal Stem Cell Transcriptome: Implication for Stem Cell Therapies Targeting Intervertebral Discs. *J. Transl Med.* 16, 222. doi:10.1186/s12967-018-1601-9

Eyre, D., Weis, M. A., Weis, M., and Wu, J.-J. (2006). Articular Cartilage Collagen: an Irreplaceable Framework? *eCM* 12, 57–63. doi:10.22203/ecm.v012a07

Fahy, N., Alini, M., and Stoddart, M. J. (2018). Mechanical Stimulation of Mesenchymal Stem Cells: Implications for Cartilage Tissue Engineering. *J. Orthop. Res.* 36, 52–63. doi:10.1002/jor.23670

Finnson, K. W., Chi, Y., Bou-Gharios, G., Leask, A., and Philip, A. (2012). TGF-beta Signaling in Cartilage Homeostasis and Osteoarthritis. *Front. Biosci.* S4, 251–268. doi:10.2741/s26610.2741/266

Garcia, J., Mccarthy, H. S., Kuiper, J. H., Melrose, J., and Roberts, S. (2021). Perlecan in the Natural and Cell Therapy Repair of Human Adult Articular Cartilage: Can Modifications in This Proteoglycan Be a Novel Therapeutic Approach? *Biomolecules* 11, 92. doi:10.3390/biom11010092

Gikas, P. D., Bayliss, L., Bentley, G., and Briggs, T. W. R. (2009). An Overview of Autologous Chondrocyte Implantation. *J. Bone Jt. Surg. Br.* 91-B, 997–1006. doi:10.1302/0301-620x.91b8.21824

Go, G., Jeong, S.-G., Yoo, A., Han, J., Kang, B., Kim, S., et al. (2020). Human Adipose–Derived Mesenchymal Stem Cell–Based Medical Microrobot System for Knee Cartilage Regeneration *In Vivo*. *J. Sci. Robotics* 5, eaay6626. doi:10.1126/scirobotics.aay6626

Goldring, M. B., Sandell, L. J., Stephenson, M. L., and Krane, S. M. (1986). Immune Interferon Suppresses Levels of Procollagen mRNA and Type II Collagen Synthesis in Cultured Human Articular and Costal Chondrocytes. *J. Biol. Chem.* 261, 9049–9055. doi:10.1016/s0021-9258(19)84486-1

Goyal, D., Keyhani, S., Lee, E. H., and Hui, J. H. P. (2013). Evidence-based Status of Microfracture Technique: a Systematic Review of Level I and II Studies. *Arthrosc. J. Arthroscopic Relat. Surg.* 29, 1579–1588. doi:10.1016/j.arthro.2013.05.027

Hangody, L., Ráthonyi, G. K., Duska, Z., Vásárhelyi, G., Füles, P., and Módis, L. (2004). Autologous Osteochondral Mosaicplasty. *J. Bone Jt. Surgery-American.* 86, 65–72. doi:10.2106/00004623-200403001-00009

Hu, H., Liu, W., Sun, C., Wang, Q., Yang, W., Zhang, Z., et al. (2021). Endogenous Repair and Regeneration of Injured Articular Cartilage: A Challenging but Promising Therapeutic Strategy. *Aging Dis.* 12, 886–901. doi:10.14336/ad.2020.0902

Ikeda, Y., Sakaue, M., Chijimatsu, R., Hart, D. A., Otsubo, H., Shimomura, K., et al. (2017). IGF-1 Gene Transfer to Human Synovial MSCs Promotes Their Chondrogenic Differentiation Potential without Induction of the Hypertrophic Phenotype. *Stem Cell Int.* 2017, 1–10. doi:10.1155/2017/5804147

Im, G.-I. (2016). Endogenous Cartilage Repair by Recruitment of Stem Cells. *Tissue Eng. B: Rev.* 22, 160–171. doi:10.1089/ten.TEB.2015.0438

Jeffrey, J. E., and Aspden, R. M. (2006). The Biophysical Effects of a Single Impact Load on Human and Bovine Articular Cartilage. *Proc. Inst. Mech. Eng. H* 220, 677–686. doi:10.1243/09544119jeim31

Jiang, Y., Cai, Y., Zhang, W., Yin, Z., Hu, C., Tong, T., et al. (2016). Human Cartilage-Derived Progenitor Cells from Committed Chondrocytes for Efficient Cartilage Repair and Regeneration. *STEM CELLS Translational Med.* 5, 733–744. doi:10.5966/sctm.2015-0192

Jiang, Y., and Tuan, R. S. (2015). Origin and Function of Cartilage Stem/progenitor Cells in Osteoarthritis. *Nat. Rev. Rheumatol.* 11, 206–212. doi:10.1038/nrrheum.2014.200

Joharapurkar, A. A., Pandya, V. B., Patel, V. J., Desai, R. C., and Jain, M. R. (2018). Prolyl Hydroxylase Inhibitors: A Breakthrough in the Therapy of Anemia Associated with Chronic Diseases. *J. Med. Chem.* 61, 6964–6982. doi:10.1021/acs.jmedchem.7b01686

Johnson, K., Zhu, S., Tremblay, M. S., Payette, J. N., Wang, J., Bouchez, L. C., et al. (2012). A Stem Cell-Based Approach to Cartilage Repair. *Science* 336, 717–721. doi:10.1126/science.1215157

Kasper, G., Dankert, N., Tuischer, J., Hoeft, M., Gaber, T., Glaeser, J. D., et al. (2007). Mesenchymal Stem Cells Regulate Angiogenesis According to Their Mechanical Environment. *Stem Cells* 25, 903–910. doi:10.1634/stemcells.2006-0432

Kennedy, M. I., Whitney, K., Evans, T., and Laprade, R. F. (2018). Platelet-Rich Plasma and Cartilage Repair. *Curr. Rev. Musculoskelet. Med.* 11, 573–582. doi:10.1007/s12178-018-9516-x

Kim, Y. G., Choi, J., and Kim, K. (2020). Mesenchymal Stem Cell-Derived Exosomes for Effective Cartilage Tissue Repair and Treatment of Osteoarthritis. *Biotechnol. J.* 15, 2000082. doi:10.1002/biot.202000082

Kobayashi, T., Lyons, K. M., Mcmahon, A. P., and Kronenberg, H. M. (2005). BMP Signaling Stimulates Cellular Differentiation at Multiple Steps during Cartilage Development. *Proc. Natl. Acad. Sci.* 102, 18023–18027. doi:10.1073/pnas.0503617102

Koh, Y. G., Choi, Y. J., Kwon, O. R., and Kim, Y. S. (2014). Second-Look Arthroscopic Evaluation of Cartilage Lesions after Mesenchymal Stem Cell Implantation in Osteoarthritic Knees. *Am. J. Sports Med.* 42, 1628–1637. doi:10.1177/0363546514529641

Kwon, H., Brown, W. E., Lee, C. A., Wang, D., Paschos, N., Hu, J. C., et al. (2019). Surgical and Tissue Engineering Strategies for Articular Cartilage and Meniscus Repair. *Nat. Rev. Rheumatol.* 15, 550–570. doi:10.1038/s41584-019-0255-1

Lafont, J. E., Talma, S., and Murphy, C. L. (2007). Hypoxia-inducible Factor 2α Is Essential for Hypoxic Induction of the Human Articular Chondrocyte Phenotype. *Arthritis Rheum.* 56, 3297–3306. doi:10.1002/art.22878

Laternser, S., Keller, H., Leupin, O., Rausch, M., Graf-Hausner, U., and Rimann, M. (2018). A Novel Microplate 3D Bioprinting Platform for the Engineering of Muscle and Tendon Tissues. *SLAS Technol. Translating Life Sci. Innovation* 23, 599–613. doi:10.1177/2472630318776594

Lee Koh, J., Kowalski, A., and Lautenschlager, E. (2006). The Effect of Angled Osteochondral Grafting on Contact Pressure. *Am. J. Sports Med.* 34, 116–119. doi:10.1177/0363546505281236

Lee, W. S., Kim, H. J., Kim, K. I., Kim, G. B., and Jin, W. (2019). Intra-Articular Injection of Autologous Adipose Tissue-Derived Mesenchymal Stem Cells for the Treatment of Knee Osteoarthritis: A Phase IIb, Randomized, Placebo-Controlled Clinical Trial. *STEM CELLS Translational Med.* 8, 504–511. doi:10.1002/sctm.18-0122

Lefebvre, V., Peeters-Joris, C., and Vaes, G. (1990). Modulation by Interleukin 1 and Tumor Necrosis Factor α of Production of Collagenase, Tissue Inhibitor of Metalloproteinases and Collagen Types in Differentiated and Dedifferentiated Articular Chondrocytes. *Biochim. Biophys. Acta (Bba) - Mol. Cel Res.* 1052, 366–378. doi:10.1016/0167-4889(90)90145-4

Li, K., Zhang, C., Qiu, L., Gao, L., and Zhang, X. (2017). Advances in Application of Mechanical Stimuli in Bioreactors for Cartilage Tissue Engineering. *Tissue Eng. Part B: Rev.* 23, 399–411. doi:10.1089/ten.TEB.2016.0427

Li, T., Liu, B., Chen, K., Lou, Y., Jiang, Y., and Zhang, D. (2020). Small Molecule Compounds Promote the Proliferation of Chondrocytes and Chondrogenic Differentiation of Stem Cells in Cartilage Tissue Engineering. *Biomed. Pharmacother.* 131, 110652. doi:10.1016/j.biopha.2020.110652

Li, Z., Kupcsik, L., Yao, S.-J., Alini, M., and Stoddart, M. J. (2010). Mechanical Load Modulates Chondrogenesis of Human Mesenchymal Stem Cells through the TGF-β Pathway. *J. Cel Mol Med* 14, 1338–1346. doi:10.1111/j.1582-4934.2009.00780.x

Liacini, A., Sylvester, J., Li, W. Q., Huang, W., Dehnade, F., Ahmad, M., et al. (2003). Induction of Matrix Metalloproteinase-13 Gene Expression by TNF-α Is Mediated by MAP Kinases, AP-1, and NF-Kb Transcription Factors in Articular Chondrocytes. *Exp. Cel Res.* 288, 208–217. doi:10.1016/s0014-4827(03)00180-0

Liu, M., Zeng, X., Ma, C., Yi, H., Ali, Z., Mou, X., et al. (2017). Injectable Hydrogels for Cartilage and Bone Tissue Engineering. *Bone Res.* 5, 17014. doi:10.1038/boneres.2017.14

Longobardi, L., O'rear, L., Aakula, S., Johnstone, B., Shimer, K., Chytil, A., et al. (2006). Effect of IGF-I in the Chondrogenesis of Bone Marrow Mesenchymal Stem Cells in

the Presence or Absence of TGF-β Signaling. *J. Bone Miner Res.* 21, 626–636. doi:10.1359/jbmr.051213

Lui, J. C., Colbert, M., Cheung, C. S. F., Ad, M., Lee, A., Zhu, Z., et al. (2019). Cartilage-Targeted IGF-1 Treatment to Promote Longitudinal Bone Growth. *Mol. Ther.* 27, 673–680. doi:10.1016/j.ymthe.2019.01.017

Markway, B. D., Cho, H., and Johnstone, B. (2013). Hypoxia Promotes Redifferentiation and Suppresses Markers of Hypertrophy and Degeneration in Both Healthy and Osteoarthritic Chondrocytes. *Arthritis Res. Ther.* 15, R92. doi:10.1186/ar4272

Mascarenhas, R., Saltzman, B., Fortier, L., and Cole, B. (2015). Role of Platelet-Rich Plasma in Articular Cartilage Injury and Disease. *J. Knee Surg.* 28, 003–010. doi:10.1055/s-0034-1384672

Moldovan, N., Maldovan, L., and Raghunath, M. (2019). Of Balls, Inks and Cages: Hybrid Biofabrication of 3D Tissue Analogs. *Int. J. Bioprint* 5, 167. doi:10.18063/ijb.v5i1.167

Moussa, M., Lajeunesse, D., Hilal, G., El Atat, O., Haykal, G., Serhal, R., et al. (2017). Platelet Rich Plasma (PRP) Induces Chondroprotection via Increasing Autophagy, Anti-inflammatory Markers, and Decreasing Apoptosis in Human Osteoarthritic Cartilage. *Exp. Cel Res.* 352, 146–156. doi:10.1016/j.yexcr.2017.02.012

Murakami, S., Lefebvre, V., and De Crombrugghe, B. (2000). Potent Inhibition of the Master Chondrogenic FactorSox9 Gene by Interleukin-1 and Tumor Necrosis Factor-α. *J. Biol. Chem.* 275, 3687–3692. doi:10.1074/jbc.275.5.3687

Murphy, C. L., and Polak, J. M. (2004). Control of Human Articular Chondrocyte Differentiation by Reduced Oxygen Tension. *J. Cel. Physiol.* 199, 451–459. doi:10.1002/jcp.10481

Murphy, C. L., Thoms, B. L., Vaghjiani, R. J., and Lafont, J. E. (2009). HIF-mediated Articular Chondrocyte Function: Prospects for Cartilage Repair. *Arthritis Res. Ther.* 11, 213. doi:10.1186/ar2574

Musumeci, G., Castrogiovanni, P., Leonardi, R., Trovato, F. M., Szychlinska, M. A., Di Giunta, A., et al. (2014). New Perspectives for Articular Cartilage Repair Treatment through Tissue Engineering: A Contemporary Review. *Wjo* 5, 80–88. doi:10.5312/wjo.v5.i2.80

Nawaz, S. Z., Bentley, G., Briggs, T. W. R., Carrington, R. W. J., Skinner, J. A., Gallagher, K. R., et al. (2014). Autologous Chondrocyte Implantation in the Knee. *J. Bone Jt. Surg Am* 96, 824–830. doi:10.2106/jbjs.L.01695

Ngo, H. X., and Garneau-Tsodikova, S. (2018). What Are the Drugs of the Future? *Med. Chem. Commun.* 9, 757–758. doi:10.1039/c8md90019a

Novo, E., Valfrè di Bonzo, L., Cannito, S., Colombatto, S., and Parola, M. (2009). Hepatic Myofibroblasts: a Heterogeneous Population of Multifunctional Cells in Liver Fibrogenesis. *Int. J. Biochem. Cel Biol.* 41, 2089–2093. doi:10.1016/j.biocel.2009.03.010

Okada, K., Mori, D., Makii, Y., Nakamoto, H., Murahashi, Y., Yano, F., et al. (2020). Hypoxia-inducible Factor-1 Alpha Maintains Mouse Articular Cartilage through Suppression of NF-Kb Signaling. *Sci. Rep.* 10, 5425. doi:10.1038/s41598-020-62463-4

Park, M. S., Kim, Y. H., Jung, Y., Kim, S. H., Park, J. C., Yoon, D. S., et al. (2015). *In Situ* Recruitment of Human Bone Marrow-Derived Mesenchymal Stem Cells Using Chemokines for Articular Cartilage Regeneration. *Cel Transpl.* 24, 1067–1083. doi:10.3727/096368914x681018

Park, Y.-B., Ha, C.-W., Rhim, J. H., and Lee, H.-J. (2018). Stem Cell Therapy for Articular Cartilage Repair: Review of the Entity of Cell Populations Used and the Result of the Clinical Application of Each Entity. *Am. J. Sports Med.* 46, 2540–2552. doi:10.1177/0363546517729152

Pearle, A. D., Warren, R. F., and Rodeo, S. A. (2005). Basic Science of Articular Cartilage and Osteoarthritis. *Clin. Sports Med.* 24, 1–12. doi:10.1016/j.csm.2004.08.007

Pei, M., and He, F. (2012). Extracellular Matrix Deposited by Synovium-Derived Stem Cells Delays Replicative Senescent Chondrocyte Dedifferentiation and Enhances Redifferentiation. *J. Cel. Physiol.* 227, 2163–2174. doi:10.1002/jcp.22950

Redondo, M., Beer, A., and Yanke, A. (2018). Cartilage Restoration: Microfracture and Osteochondral Autograft Transplantation. *J. Knee Surg.* 31, 231–238. doi:10.1055/s-0037-1618592

Reginato, A. M., Sanz-Rodriguez, C., Diaz, A., Dharmavaram, R. M., and Jimenez, S. A. (1993). Transcriptional Modulation of Cartilage-specific Collagen Gene Expression by Interferon γ and Tumour Necrosis Factor α in Cultured Human Chondrocytes. *Biochem. J.* 294 (Pt 3), 761–769. doi:10.1042/bj2940761

Reissis, D., Tang, Q. O., Cooper, N. C., Carasco, C. F., Gamie, Z., Mantalaris, A., et al. (2016). Current Clinical Evidence for the Use of Mesenchymal Stem Cells in Articular Cartilage Repair. *Expert Opin. Biol. Ther.* 16, 535–557. doi:10.1517/14712598.2016.1145651

Robins, J. C., Akeno, N., Mukherjee, A., Dalal, R. R., Aronow, B. J., Koopman, P., et al. (2005). Hypoxia Induces Chondrocyte-specific Gene Expression in Mesenchymal Cells in Association with Transcriptional Activation of Sox9. *Bone* 37, 313–322. doi:10.1016/j.bone.2005.04.040

Sakaguchi, Y., Sekiya, I., Yagishita, K., and Muneta, T. (2005). Comparison of Human Stem Cells Derived from Various Mesenchymal Tissues: Superiority of Synovium as a Cell Source. *Arthritis Rheum.* 52, 2521–2529. doi:10.1002/art.21212

Sakai, N., and Tager, A. M. (2013). Fibrosis of Two: Epithelial Cell-Fibroblast Interactions in Pulmonary Fibrosis. *Biochim. Biophys. Acta (Bba) - Mol. Basis Dis.* 1832, 911–921. doi:10.1016/j.bbadis.2013.03.001

Sakata, R., and Reddi, A. H. (2016). Platelet-Rich Plasma Modulates Actions on Articular Cartilage Lubrication and Regeneration. *Tissue Eng. Part B: Rev.* 22, 408–419. doi:10.1089/ten.TEB.2015.0534

Salinas, E. Y., Hu, J. C., and Athanasiou, K. (2018). A Guide for Using Mechanical Stimulation to Enhance Tissue-Engineered Articular Cartilage Properties. *Tissue Eng. Part B: Rev.* 24, 345–358. doi:10.1089/ten.TEB.2018.0006

Schipani, E., Ryan, H. E., Didrickson, S., Kobayashi, T., Knight, M., and Johnson, R. S. (2001). Hypoxia in Cartilage: HIF-1α Is Essential for Chondrocyte Growth Arrest and Survival. *Genes Dev.* 15, 2865–2876. doi:10.1101/gad.934301

Schnabel, M., Marlovits, S., Eckhoff, G., Fichtel, I., Gotzen, L., Vécsei, V., et al. (2002). Dedifferentiation-associated Changes in Morphology and Gene Expression in Primary Human Articular Chondrocytes in Cell Culture. *Osteoarthritis and Cartilage* 10, 62–70. doi:10.1053/joca.2001.0482

Sekiya, I., Colter, D. C., and Prockop, D. J. (2001). BMP-6 Enhances Chondrogenesis in a Subpopulation of Human Marrow Stromal Cells. *Biochem. Biophysical Res. Commun.* 284, 411–418. doi:10.1006/bbrc.2001.4898

Shen, B., Wei, A., Tao, H., Diwan, A. D., and Ma, D. D. F. (2009). BMP-2 Enhances TGF-B3-Mediated Chondrogenic Differentiation of Human Bone Marrow Multipotent Mesenchymal Stromal Cells in Alginate Bead Culture. *Tissue Eng. A* 15, 1311–1320. doi:10.1089/ten.tea.2008.0132

Shen, B., Wei, A., Whittaker, S., Williams, L. A., Tao, H., Ma, D. D. F., et al. (2009). The Role of BMP-7 in Chondrogenic and Osteogenic Differentiation of Human Bone Marrow Multipotent Mesenchymal Stromal Cells *In Vitro*. *J. Cel. Biochem.* 109, a–n. doi:10.1002/jcb.22412

Shi, D., and Li, J. (2021). Research Progress of Fibrocartilage Hyalinization. *J. Clin. Surg.* 29, 388–391. doi:10.3969/j.issn.1005-6483.2021.04.026

Shi, Y., Hu, X., Cheng, J., Zhang, X., Zhao, F., Shi, W., et al. (2019). A Small Molecule Promotes Cartilage Extracellular Matrix Generation and Inhibits Osteoarthritis Development. *Nat. Commun.* 10, 1914. doi:10.1038/s41467-019-09839-x

Snoeker, B., Turkiewicz, A., Magnusson, K., Frobell, R., Yu, D., Peat, G., et al. (2020). Risk of Knee Osteoarthritis after Different Types of Knee Injuries in Young Adults: a Population-Based Cohort Study. *Br. J. Sports Med.* 54, 725–730. doi:10.1136/bjsports-2019-100959

Sommerfeldt, M. F., Magnussen, R. A., Hewett, T. E., Kaeding, C. C., and Flanigan, D. C. (2016). Microfracture of Articular Cartilage. *JBJS Rev.* 4. doi:10.2106/jbjs.Rvw.15.00005

Sophia Fox, A. J., Bedi, A., and Rodeo, S. A. (2009). The Basic Science of Articular Cartilage: Structure, Composition, and Function. *Sports Health* 1, 461–468. doi:10.1177/1941738109350438

Stöve, J., Huch, K., Günther, K.-P., and Scharf, H.-P. (2000). Interleukin-1β Induces Different Gene Expression of Stromelysin, Aggrecan and Tumor-Necrosis-Factor-Stimulated Gene 6 in Human Osteoarthritic Chondrocytes *In Vitro*. *Pathobiology* 68, 144–149. doi:10.1159/000055915

Su, W., Liu, G., Liu, X., Zhou, Y., Sun, Q., Zhen, G., et al. (2020). Angiogenesis Stimulated by Elevated PDGF-BB in Subchondral Bone Contributes to Osteoarthritis Development. *JCI Insight* 5. doi:10.1172/jci.insight.135446

Thoms, B. L., Dudek, K. A., Lafont, J. E., and Murphy, C. L. (2013). Hypoxia Promotes the Production and Inhibits the Destruction of Human Articular Cartilage. *Arthritis Rheum.* 65, 1302–1312. doi:10.1002/art.37867

Thorp, H., Kim, K., Kondo, M., Grainger, D. W., and Okano, T. (2020). Fabrication of Hyaline-like Cartilage Constructs Using Mesenchymal Stem Cell Sheets. *Sci. Rep.* 10, 20869. doi:10.1038/s41598-020-77842-0

Toh, W. S., Lai, R. C., Hui, J. H. P., and Lim, S. K. (2017). MSC Exosome as a Cell-free MSC Therapy for Cartilage Regeneration: Implications for Osteoarthritis Treatment. *Semin. Cel Developmental Biol.* 67, 56–64. doi:10.1016/j.semcdb.2016.11.008

Ulrich-Vinther, M., Maloney, M. D., Schwarz, E. M., Rosier, R., and O'Keefe, R. J. (2003). Articular Cartilage Biology. *J. Am. Acad. Orthopaedic Surgeons* 11, 421–430. doi:10.5435/00124635-200311000-00006

Verteramo, A., and Seedhom, B. B. (2007). Effect of a Single Impact Loading on the Structure and Mechanical Properties of Articular Cartilage. *J. Biomech.* 40, 3580–3589. doi:10.1016/j.jbiomech.2007.06.002

Vinod, E., Vinod Francis, D., Manickam Amirtham, S., Sathishkumar, S., and Boopalan, P. R. J. V. C. (2019). Allogeneic Platelet Rich Plasma Serves as a Scaffold for Articular Cartilage Derived Chondroprogenitors. *Tissue and Cell* 56, 107–113. doi:10.1016/j.tice.2018.12.006

Vonk, L. A., Van Dooremalen, S. F. J., Liv, N., Klumperman, J., Coffer, P. J., Saris, D. B. F., et al. (2018). Mesenchymal Stromal/stem Cell-Derived Extracellular Vesicles Promote Human Cartilage Regeneration *In Vitro*. *Theranostics* 8, 906–920. doi:10.7150/thno.20746

Wachsmuth, L., Söder, S., Fan, Z., Finger, F., and Aigner, T. (2006). Immunolocalization of Matrix Proteins in Different Human Cartilage Subtypes. *Histol. Histopathol* 21, 477–485. doi:10.14670/hh-21.477

Wakitani, S., Imoto, K., Yamamoto, T., Saito, M., Murata, N., and Yoneda, M. (2002). Human Autologous Culture Expanded Bone Marrow Mesenchymal Cell Transplantation for Repair of Cartilage Defects in Osteoarthritic Knees. *Osteoarthritis and Cartilage* 10, 199–206. doi:10.1053/joca.2001.0504

Wang, B., Xing, D., Dong, S., Tie, R., Zhang, Z., Lin, J., et al. (2018). Prevalence and Disease burden of Knee Osteoarthritis in China: a Systematic Review. *CHINESE JOURNAL EVIDENCE-BASED MEDICINE* 18, 134–142. doi:10.7507/1672-2531.201712031

Wang, W., Rigueur, D., and Lyons, K. M. (2014). TGFβ Signaling in Cartilage Development and Maintenance. *Birth Defect Res. C* 102, 37–51. doi:10.1002/bdrc.21058

Wang, Y., Sun, X., Lv, J., Zeng, L., Wei, X., and Wei, L. (2017). Stromal Cell-Derived Factor-1 Accelerates Cartilage Defect Repairing by Recruiting Bone Marrow Mesenchymal Stem Cells and Promoting Chondrogenic Differentiation. *Tissue Eng. Part A* 23, 1160–1168. doi:10.1089/ten.TEA.2017.0046

Wehling, N., Palmer, G. D., Pilapil, C., Liu, F., Wells, J. W., Müller, P. E., et al. (2009). Interleukin-1β and Tumor Necrosis Factor α Inhibit Chondrogenesis by Human Mesenchymal Stem Cells through NF-κb-dependent Pathways. *Arthritis Rheum.* 60, 801–812. doi:10.1002/art.24352

Weiss, C., Rosenberg, L., and Helfet, A. J. (1968). An Ultrastructural Study of normal Young Adult Human Articular Cartilage. *J. Bone Jt. Surg.* 50, 663–674. doi:10.2106/00004623-196850040-00002

Welch, T., Mandelbaum, B., and Tom, M. (2016). Autologous Chondrocyte Implantation: Past, Present, and Future. *Sports Med. Arthrosc. Rev.* 24, 85–91. doi:10.1097/jsa.0000000000000115

Wilder, F. V., Hall, B. J., Barrett, J. P., Jr., and Lemrow, N. B. (2002). History of Acute Knee Injury and Osteoarthritis of the Knee: a Prospective Epidemiological Assessment. *Osteoarthritis and Cartilage* 10, 611–616. doi:10.1053/joca.2002.0795

Wu, M., Hu, R., Wang, J., An, Y., Lu, L., Long, C., et al. (2019). Salidroside Suppresses IL-1β-Induced Apoptosis in Chondrocytes via Phosphatidylinositol 3-Kinases (PI3K)/Akt Signaling Inhibition. *Med. Sci. Monit.* 25, 5833–5840. doi:10.12659/msm.917851

Wu, W., Zhang, J., Dong, Q., Liu, Y., Mao, T., and Chen, F. (2009). Platelet-rich Plasma - A Promising Cell Carrier for Micro-invasive Articular Cartilage Repair. *Med. Hypotheses* 72, 455–457. doi:10.1016/j.mehy.2008.11.032

Xu, X., Shi, D., Shen, Y., Xu, Z., Dai, J., Chen, D., et al. (2015). Full-thickness Cartilage Defects Are Repaired via a Microfracture Technique and Intraarticular Injection of the Small-Molecule Compound Kartogenin. *Arthritis Res. Ther.* 17, 20. doi:10.1186/s13075-015-0537-1

Yano, F., Hojo, H., Ohba, S., Fukai, A., Hosaka, Y., Ikeda, T., et al. (2013). A Novel Disease-Modifying Osteoarthritis Drug Candidate Targeting Runx1. *Ann. Rheum. Dis.* 72, 748–753. doi:10.1136/annrheumdis-2012-201745

Yuan, L., Sakamoto, N., Song, G., and Sato, M. (2013). Low-level Shear Stress Induces Human Mesenchymal Stem Cell Migration through the SDF-1/CXCR4 axis via MAPK Signaling Pathways. *Stem Cell Development* 22, 2384–2393. doi:10.1089/scd.2012.0717

Zhai, G., Doré, J., and Rahman, P. (2015). TGF-β Signal Transduction Pathways and Osteoarthritis. *Rheumatol. Int.* 35, 1283–1292. doi:10.1007/s00296-015-3251-z

Zhang, R., Ma, J., Han, J., Zhang, W., and Ma, J. (2019). Mesenchymal Stem Cell Related Therapies for Cartilage Lesions and Osteoarthritis. *Am. J. Transl Res.* 11, 6275–6289.

Zhang, Y., Zhang, J., Chang, F., Xu, W., and Ding, J. (2018). Repair of Full-Thickness Articular Cartilage Defect Using Stem Cell-Encapsulated Thermogel. *Mater. Sci. Eng. C* 88, 79–87. doi:10.1016/j.msec.2018.02.028

Zhang, Y., and Zhao, Q. (2018). Salidroside Attenuates Interleukin-1β-induced Inflammation in Human Osteoarthritis Chondrocytes. *J. Cel Biochem* 120, 1203–1209. doi:10.1002/jcb.27076

Zhao, Z., Li, Y., Wang, M., Zhao, S., Zhao, Z., and Fang, J. (2020). Mechanotransduction Pathways in the Regulation of Cartilage Chondrocyte Homoeostasis. *J. Cel Mol Med* 24, 5408–5419. doi:10.1111/jcmm.15204

Zhen, G., Guo, Q., Li, Y., Wu, C., Zhu, S., Wang, R., et al. (2021). Mechanical Stress Determines the Configuration of TGFβ Activation in Articular Cartilage. *Nat. Commun.* 12, 1706. doi:10.1038/s41467-021-21948-0

Zhen, G., Wen, C., Jia, X., Li, Y., Crane, J. L., Mears, S. C., et al. (2013). Inhibition of TGF-β Signaling in Mesenchymal Stem Cells of Subchondral Bone Attenuates Osteoarthritis. *Nat. Med.* 19, 704–712. doi:10.1038/nm.3143

Zhou, C., Zheng, H., Seol, D., Yu, Y., and Martin, J. A. (2014). Gene Expression Profiles Reveal that Chondrogenic Progenitor Cells and Synovial Cells Are Closely Related. *J. Orthop. Res.* 32, 981–988. doi:10.1002/jor.22641

Zhou, Y., Tao, H., Li, Y., Deng, M., He, B., Xia, S., et al. (2016). Berberine Promotes Proliferation of Sodium Nitroprusside-Stimulated Rat Chondrocytes and Osteoarthritic Rat Cartilage via Wnt/β-Catenin Pathway. *Eur. J. Pharmacol.* 789, 109–118. doi:10.1016/j.ejphar.2016.07.027

Conflict of Interest: The authors declare that the research was conducted in the absence of any commercial or financial relationships that could be construed as a potential conflict of interest.

Publisher's Note: All claims expressed in this article are solely those of the authors and do not necessarily represent those of their affiliated organizations, or those of the publisher, the editors and the reviewers. Any product that may be evaluated in this article, or claim that may be made by its manufacturer, is not guaranteed or endorsed by the publisher.

frontiers in Bioengineering and Biotechnology

ORIGINAL RESEARCH
published: 21 December 2021
doi: 10.3389/fbioe.2021.752677

Regeneration of Subcutaneous Cartilage in a Swine Model Using Autologous Auricular Chondrocytes and Electrospun Nanofiber Membranes Under Conditions of Varying Gelatin/PCL Ratios

Rui Zheng[1,2†], Xiaoyun Wang[3†], Jixin Xue[4†], Lin Yao[5,6†], Gaoyang Wu[1], Bingcheng Yi[1], Mengjie Hou[1,5], Hui Xu[2], Ruhong Zhang[1], Jie Chen[1,5], Zhengyu Shen[2], Yu Liu[5,6]* and Guangdong Zhou[1,5,6]**

[1]Department of Plastic and Reconstructive Surgery, Shanghai 9th People's Hospital, Shanghai Jiao Tong University School of Medicine, Shanghai Key Laboratory of Tissue Engineering, Shanghai Stem Cell Institute, Shanghai, China, [2]Department of Dermatology, Shanghai 9th People's Hospital, Shanghai Jiao Tong University School of Medicine, Shanghai, China, [3]Department of Cosmetic Surgery, Tongren Hospital, Shanghai Jiao Tong University School of Medicine, Shanghai, China, [4]Department of Orthopaedics, The Second Affiliated Hospital and Yuying Children's Hospital of Wenzhou Medical University, Wenzhou, China, [5]National Tissue Engineering Center of China, Shanghai, China, [6]Research Institute of Plastic Surgery, Weifang Medical College, Weifang, China

The scarcity of ideal biocompatible scaffolds makes the regeneration of cartilage in the subcutaneous environment of large animals difficult. We have previously reported the successful regeneration of good-quality cartilage in a nude mouse model using the electrospun gelatin/polycaprolactone (GT/PCL) nanofiber membranes. The GT/PCL ratios were varied to generate different sets of membranes to conduct the experiments. However, it is unknown whether these GT/PCL membranes can support the process of cartilage regeneration in an immunocompetent large animal model. We seeded swine auricular chondrocytes onto different GT/PCL nanofiber membranes (GT: PCL = 30:70, 50:50, and 70:30) under the sandwich cell-seeding mode. Prior to subcutaneously implanting the samples into an autologous host, they were cultured *in vitro* over a period of 2 weeks. The results revealed that the nanofiber membranes with different GT/PCL ratios could support the process of subcutaneous cartilage regeneration in an autologous swine model. The maximum extent of homogeneity in the cartilage tissues was achieved when the G5P5 (GT: PC = 50: 50) group was used for the regeneration of cartilage. The formed homogeneous cartilage tissues were characterized by the maximum cartilage formation ratio. The extents of the ingrowth of the fibrous tissues realized and the extents of infiltration of inflammatory cells achieved were found to be the minimum in this case. Quantitative analyses were conducted to determine the wet weight, cartilage-specific extracellular matrix content, and Young's modulus. The results indicated that the optimal extent of cartilage formation was observed in the G5P5 group. These results indicated that the GT/PCL nanofiber membranes could

OPEN ACCESS

Edited by:
Laura Creemers, University Medical Center Utrecht, Netherlands

Reviewed by:
Zigang Ge, Peking University, China
Feng-Huei Lin, National Taiwan University, Taiwan

***Correspondence:**
Guangdong Zhou
guangdongzhou@126.com
Yu Liu
yuliu1211@163.com
Zhengyu Shen
neuronszy@sina.com

[†]These authors have contributed equally to this work

Specialty section:
This article was submitted to Tissue Engineering and Regenerative Medicine, a section of the journal Frontiers in Bioengineering and Biotechnology

Received: *03 August 2021*
Accepted: *12 November 2021*
Published: *21 December 2021*

Citation:
Zheng R, Wang X, Xue J, Yao L, Wu G, Yi B, Hou M, Xu H, Zhang R, Chen J, Shen Z, Liu Y and Zhou G (2021) Regeneration of Subcutaneous Cartilage in a Swine Model Using Autologous Auricular Chondrocytes and Electrospun Nanofiber Membranes Under Conditions of Varying Gelatin/PCL Ratios. Front. Bioeng. Biotechnol. 9:752677. doi: 10.3389/fbioe.2021.752677

serve as a potential scaffold for supporting subcutaneous cartilage regeneration under clinical settings. An optimum GT/PCL ratio can promote cartilage formation.

Keywords: cartilage regeneration, large animal, subcutaneous environment, electrospun nanofiber membrane, inflammatory reaction

1 INTRODUCTION

Cartilage defects in the subcutaneous environment (such as ear, nose, and trachea) due to congenital disease (microtia), cancer removal, or trauma are very common in plastic and reconstructive surgery (Wiggenhauser et al., 2017). The defects can significantly alter the appearance, psychological status, and physiological function of the patients. Traditional methods followed to repair these defects involve the implantation of a pre-shaped prosthetic graft made from silastic or high-density polyethylene (Medpor®) or the transplantation of sculpted autologous cartilage (usually harvested from the rib, nasal septum, or auricle) (Brent, 1999; Bateman and Jones, 2000; Kim, et al., 2011). The poor bioactivity of the prosthetic grafts can potentially result in extrusion and infection, while the use of grafts developed from autologous cartilage can cause severe donor-site morbidity. The process is characterized by a prolonged operative time, and the success of the process is heavily dependent on the skill of the surgeon. An ideal cartilaginous substitute with a pre-designed shape and characterized by the minimum donor-site morbidity can be developed using tissue engineering technology. This can help address the problems faced when the traditional cartilage reconstructive approaches are followed (Sterodimas et al., 2009; Bichara et al., 2012). Recently, good progress has been made in the field of cartilage engineering. Materials and methods that can be used for nasal, auricular, and tracheal reconstruction have been developed. Some of the materials developed have entered the stage of proof-of-feasibility clinical trials (Zang et al., 2013; Fulco et al., 2014; Bichara et al., 2014; Pomerantseva et al., 2016). However, a method to achieve reliable and stable cartilage regeneration in the subcutaneous environment is yet to be developed. This is because the clinical outcomes vary from patient to patient. The fluctuations in the clinical outcomes can be potentially attributed to the inflammatory reactions triggered by the use of the engineered cartilaginous grafts for subcutaneous implantation.

The subcutaneous environment is different from the environment of the immune privileged articular tissue (Huang et al., 2016). The subcutaneous environment is characterized by a high extent of immune activities and the absence of endogenous chondrogenic cues (Nayyer et al., 2012). The implanted engineered cartilaginous grafts face acute immune attack, which may significantly hinder the process of cartilage formation, resulting in the absorption of the implanted grafts. This phenomenon is particularly observed when the grafts engineered from polymeric scaffolds such as polyglycolic acid/polylactic acid (PGA/PLA), whose degradation products promote antigenicity, are used (Asawa et al., 2012). We have previously proposed a long (>8 weeks) *in vitro* pre-culture scheme that can be used to implant the engineered grafts when the scaffolds have been significantly degraded. The extent of postimplantation inflammation realized could be decreased, and stable subcutaneous cartilage could be formed in an autologous preclinical goat model using the PGA/PLA-engineered cartilage (Liu et al., 2016). However, the process of prolonged *in vitro* culture results in an increase in the grafting time. This can potentially increase the risk of contamination. Under these conditions, the cost of executing the method also increases. It is important to identify or develop a scaffold characterized by low immunogenicity to support the formation of stable subcutaneous cartilage and reduce the time taken for the *in vitro* pre-culture process.

Electrospun nanofibers can mimic microscopic aspects of the extracellular matrix (ECM) and help to establish a tissue-specific microenvironment that maintains and regulates cell behavior and function (Kanani and Bahrami, 2010; Qian et al., 2018). Gelatin (GT) and polycaprolactone (PCL) exhibit significantly low immunogenicity. GT is a biosafety scaffold that exhibits good biocompatibility but poor mechanical strength. The scaffold is characterized by a rapid degradation time. PCL is a synthetic polymer characterized by a good mechanical strength and prolonged degradation time. It can be used to complement the disadvantages of using GT. Electrospun nanofibers fabricated by blending GT with PCL exhibit excellent physiochemical, biomechanical, and biocompatible properties. These nanofibers have been widely used as scaffolds to conduct *in vitro* cellular studies with a variety of tissues (Chong et al., 2007; Ji et al., 2013; Jiang et al., 2017). There are a few papers that report the feasibility of engineering a three-dimensional (3D) tissue using the electrospun GT/PCL membranes. The lack of information can be potentially attributed to the limitations posed by the thicknesses of the materials. There is also a dearth of information in the field of 3D tissue regeneration in large animals used in preclinical trials. We have previously reported the ability of the electrospun GT/PCL membranes to support cartilage formation following a sandwich strategy using nude mouse models (Xue et al., 2013; Zheng et al., 2014). The results revealed that a combination of GT and PCL (high GT and low PCL contents; aGT: PCL = 70:30) could be used to achieve cartilage formation in nude mice. Successful regeneration of human ear-shaped cartilage could be achieved (Zheng, et al., 2014).

However, it is unknown if the formation of cartilage can be realized using this scaffold in a large animal model used in preclinical trials. It should also be tested if the optimized GT/PCL ratio used for cartilage regeneration in a nude mouse can be effectively used for cartilage regeneration in a preclinical large animal model. It has been reported that the electrospun nanofibrous membranes function as anti-inflammatory barriers

that help alleviate inflammatory reactions (Wang et al., 2016; Luo et al., 2016). We also studied if the electrospun GT/PCL membranes can be used to alleviate inflammatory reactions to improve the quality of the 3D cartilage regenerated in a large animal model.

We used the electrospun GT/PCL membranes with different GT/PCL ratios to construct cartilage-like tissues (*in vitro*) using the previously established sandwich strategy to predict the potential of using the scaffold in the field of clinical translation. Following this, the regenerated cartilage-like tissue was implanted into an autologous subcutaneous environment in a swine model to evaluate the feasibility of forming subcutaneous cartilage and study the effect of different GT/PCL ratios on the cartilage regeneration process in a large preclinical model. The results presented herein provide direct experimental evidence required to promote the clinical translation of cartilage regeneration using electrospun GT/PCL membranes.

2 MATERIALS AND METHODS

2.1 Isolation and Expansion of Chondrocytes

A total of five adult swine (16 weeks old; Shanghai Jiagan Biological Technology Co., Ltd., Shanghai, China) were used for the studies. All animals received humane care according to the guidelines laid down in 2006 by the National Ministry of Science in the "Guide for Care of Laboratory Animals." The animal care and experiment committee of the Shanghai Jiao Tong University School of Medicine approved the animal studies conducted by us. A biopsy of the auricular cartilage (2.0 × 1.0 cm) obtained from the autologous swine sample was conducted under conditions of endotracheal anesthesia. The surrounding fibrous tissue and perichondrium were removed, and the cartilage biopsy was minced into fragments (dimension: 1.0 mm^3). The samples were pretreated with 0.25% trypsin (HyClone, Logan, UT, USA) at 37°C over a period of 30 min. Following this, the sample was washed with phosphate-buffered solution (PBS). Subsequently, the sample was digested with 0.3% collagenase NB4 (Worthington Biochemical Corp., Freehold, NJ, United States) for 8 h at 37°C. The isolated cells were cultured and expanded using Dulbecco's modified Eagle's medium (DMEM, Gibco BRL, Grand Island, NY, United States) containing 10% fetal bovine serum (FBS, HyClone, Logan, UT, United States), penicillin (100 U/ml), and streptomycin (100 μg/ml), following previously reported protocols (Feng et al., 2012). Chondrocytes in passage two (P2) were harvested for scaffold seeding.

2.2 Preparation of Scaffolds Under Conditions of Varying GT/PCL Ratios

As previously described (Xue et al., 2013; Zheng et al., 2014), GT/PCL membranes with GT:PCL ratios (by weight) of 70:30 (G7P3), 50:50 (G5P5), and 30:70 (G3P7) were fabricated and trimmed to form round-shaped samples (diameter: 9 mm). The samples were irradiated with UV light over a period of 30 min to obtain sterilized samples. Prior to conducting the cell seeding process, the samples were lyophilized using a vacuum free-drier (VirTis BenchTop 6.6; SP Industries, Gardiner, NY, United States).

2.3 Mechanical Analysis of the Scaffolds

The mechanical properties of the electrospun fibrous membranes in their dry state were determined using a tabletop uniaxial material testing machine (H5K-S, Hounsfield, United Kingdom). Rectangular specimens (10 × 50 mm) were stretched at a constant cross-head speed of 10 mm/min (Feng et al., 2012). At least eight samples were tested for each type of membrane. The tensile strength, Young's modulus, and strain at break for all the groups were calculated and analyzed based on the stress–strain curve.

2.4 Scanning Electron Microscopy

For the cell-loaded group, 2.0×10^5 chondrocytes in 1.0 ml of the medium (DMEM with 10% FBS) were evenly dropped onto the GT/PCL membrane and incubated at 37°C under conditions of 95% humidity and 5% CO_2 (incubation time: 24 h). The cell-loaded or non-loaded membranes were rinsed with PBS, fixed in 0.05% glutaraldehyde at 4°C overnight, dehydrated through a graded series of ethanol, critical-point dried, and analyzed using the SEM technique (JEOL-6380LV, Tokyo, Japan). The extent of adhesion achieved and the distribution of the chondrocytes on the membranes were studied following previously reported methods (Xue et al., 2013; Zheng et al., 2014).

2.5 Macrophages and GT/PCL Membranes

2.5.1 Macrophage Seeding

GT/PCL membranes were punched into 14-mm discs to fit 24-well plates. The samples were disinfected with 70% ethanol and washed thoroughly with PBS prior to conducting the cell seeding process. Raw 264.7 macrophages at 80% confluence were detached using trypsin. Subsequently, the cells were centrifuged and resuspended in the medium. The seeding density of the macrophage on the scaffolds was 5×10^5 cells/cm^2. The cell-seeded scaffolds were transferred to an incubator and cultured at 37°C. The medium was changed every 2 days. The samples were harvested at predesignated time points for further analysis.

2.5.2 Confocal Microscopy

The biocompatibility of the macrophages with the GT/PCL membranes was analyzed using the confocal microscope (Leica, TCS SP8 STED 3X, Wetzlar, Germany) technique. On day 2, the cell-seeded scaffolds were harvested and fixed with 4% paraformaldehyde and permeabilized with 0.1% Triton X-100 (time: 5 min). Subsequently, the treated samples were incubated with rhodamine-conjugated phalloidin for 30 min at room temperature in the dark. DAPI was used to stain the nuclei. The samples were imaged using a confocal microscope.

2.5.3 Enzyme-Linked Immunosorbent Assay

The supernatant obtained when the macrophages were cultured was collected after 24 h of incubation. The supernatant was used to conduct ELISA. Mouse IL-6 ELISA Kit, Mouse TNF-α ELISA Kit, and Human/Mouse Arginase 1/ARG1 ELISA Kit (all ELISA

kits: MultiSciences, Hangzhou, China) were used for the studies. The protocols outlined by the manufacturers were followed. The macrophages directly seeded inside the 14-mm dishes were used as the negative controls. The macrophages treated with a solution of lipopolysaccharide (LPS; 2.5 μg/ml) were used as the positive controls. Cell culture experiments were performed in groups of four, and the experiments were repeated three times (Zheng et al., 2021).

2.5.4 Histological Analysis

Paraformaldehyde fixed macrophage-seeded GT/PCL membranes (14 mm diameter) were embedded in paraffin at days 2, 4, and 6. Sections were stained with hematoxylin and eosin (H&E) (Wang et al., 2021).

2.6 Preparation of Chondrocyte-Scaffold Constructs

The chondrocyte-GT/PCL constructs were prepared following the sandwich approach reported in the literature (Gong et al., 2011). Briefly, a chondrocyte suspension (5 μl) with a cell density of 100×10^6 cells/ml was seeded onto one slice of the GT/PCL membrane. The process was followed by stacking another slice of the GT/PCL membrane onto the previous one. Subsequently, it was seeded with the same number of chondrocytes until a 10-layer membrane stack was formed. The constructs were incubated for 2.5 h (37°C, 95% humidity, 5% CO_2) to allow the cells to get attached. Following this, a pre-warmed medium (DMEM with 10% FBS) was applied gently to cover the constructs. The medium was changed twice per week. After 2 weeks, the constructs were either subjected to the conditions of gross, histological, and immunohistochemical analyses or subcutaneously implanted into autologous swine members to conduct *in vivo* tests.

2.7 Subcutaneous Implantation

After 2 weeks of *in vitro* culture, the chondrocyte-GT/PCL constructs were implanted subcutaneously into autologous swine (time: 3 and 6 weeks). Under conditions of endotracheal anesthesia, individual subcutaneous pockets were created in the abdominal area. One construct was implanted into each pocket. The incisions were closed, and the animals were allowed to recover. Penicillin was injected intramuscularly over a period of 3 days, commencing on the first-day post operation.

2.8 Gross Evaluation

The *in vivo* samples were harvested after 3 and 6 weeks had passed post subcutaneous implantation. The surrounding fibrous tissues were carefully removed, and the appearance (color and texture) and wet weight of the samples were studied.

2.9 Histological and Immunohistochemical Analyses

All the constructs targeted for histological analysis were bisected post gross evaluation. One-half of each construct was stored at −80°C for biochemical assays. The other half was fixed with 4% paraformaldehyde (fixing time: 24 h), embedded in paraffin, sectioned into slices (diameter: 5 μm), and mounted on glass slides. Sections were stained with hematoxylin and eosin (H&E) or Safranin O following standard protocols. Type II collagen, CD3, and CD68 were detected following the principles of immunohistochemistry. Mouse anti-human type II collagen monoclonal antibody (1: 200 in PBS, Santa Cruz, CA, United States), mouse anti-human CD3 monoclonal antibody (1:200 in PBS, Santa Cruz, CA, United States), and mouse anti-human CD68 monoclonal antibody (1:200 in PBS, Santa Cruz, CA, United States) were used to study all the samples. Horseradish peroxidase (HRP)-conjugated anti-mouse antibody (1:200 in PBS, Santa Cruz, CA, United States) was then applied as a secondary antibody. Color development was achieved using diaminobenzidine tetrahydrochloride (DAB, Santa Cruz, CA, United States), and cell nuclei were counterstained with hematoxylin according to previously established techniques (Liu et al., 2016).

2.10 Biomechanical and Biochemical Analyses

Young's moduli of thatic compression; biomechanical analyzer, Instron-5542, Canton, MA, United States) (Yan, et e 3- and 6-weeks specimens were detected and analyzed following previously established methods (Yan, et al., 2009). After mechanical testing, the samples were collected and minced for biochemical analysis. The sulfated glycosaminoglycan (GAG) content was determined by conducting the dimethylmethylene blue chloride (DMMB, Sigma-Aldrich, St. Louis, MO, United States) assay, and the results were expressed in mg/g wet weight (Farndale et al., 1982). The content of type II collagen was determined following an enzyme-linked immunosorbent assay approach (Zhou et al., 2018). Five samples were analyzed in each group, and all assays were performed in duplicate as per the manufacturer's instructions.

2.11 Semi-Quantification Analysis

The areas corresponding to cartilage formation, undegraded scaffold, and inflammatory infiltration were quantified using the software used for picture analysis (ImageJ, National Institutes of Health (NIH), Bethesda, MD, United States). The corresponding regions were studied by analyzing the specific histological features. Subsequently, the total area in each structure was summed, and the corresponding areas of each parameter were divided by the total area of the samples.

2.12 Statistical Analysis

The quantitative data were recorded as mean ± standard deviation (SD). The differences among the groups in wet weight, GAG content, type II collagen content, and Young's moduli (for the 3- and 6-week specimens) were analyzed by conducting the one-way ANOVA tests (n = 5). The area proportions corresponding to the cartilage tissue, undegraded scaffold, and inflammatory infiltration recorded for the 3-week specimens were also analyzed by conducting the one-way

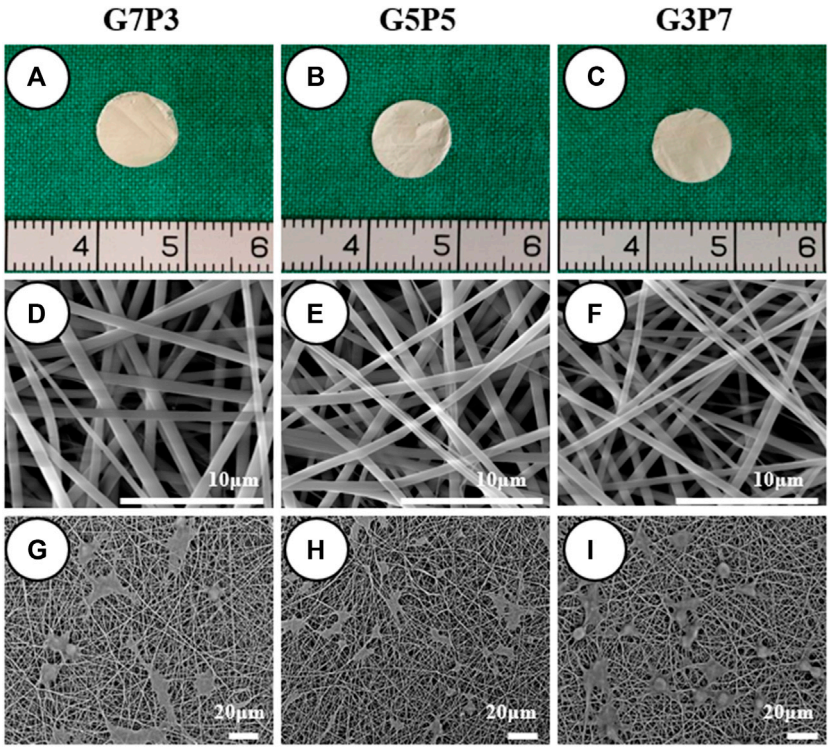

FIGURE 1 | Gross view, microstructure, and cell compatibility of GT/PCL membranes. The membranes are easily trimmed into round shape, and no visible differences are observed among different GT/PCL content groups **(A–C)**. SEM shows a similar fibrous microstructure while the fiber diameter slightly decreased with GT content **(D–F),** and chondrocytes can spread well on the surfaces of all the membranes after 24 h of cell seeding **(G–I)**.

ANOVA tests (n = 5). A p-value less than 0.05 was considered statistically significant.

3 RESULTS

3.1 Influence of the GT/PCL Ratio on the Basic Properties of the Scaffolds and Chondrocyte Compatibility

We first examined the gross appearance, microstructure, and chondrocyte compatibility of the GT/PCL membranes. The results revealed that the GT/PCL membranes characterized by varying GT/PCL ratios appeared ivory-white. The diameters of the membranes were calculated to be 9 mm (gross observation; **Figures 1A–C**). Analysis of the SEM images revealed that the diameter of the fiber decreased slightly with an increase in the GT content (**Figures 1D–F**). Additional mechanical analyses were conducted. Significant differences in the mechanical properties were observed among the three groups of the GT/PCL membranes. The tensile strengths and Young's moduli of the membranes increased significantly while the strain at break decreased with an increase in the PCL content (**Supplementary Figure S1**). The chondrocytes adhered and spread well on the membranes in all groups after 24 h of cell seeding. This indicated that all the GT/PCL membranes exhibited good biocompatibility with the chondrocytes (**Figures 1G–I**).

3.2 Influence of the GT/PCL Ratio on the Biocompatibility, Immunomodulatory Behavior, and Cell Distribution of the Macrophages (*in vitro*)

Analysis of the confocal microscopy images revealed that the macrophages grew well on the membranes with different GT/PCL contents after 24 h of incubation (**Supplementary Figures S2A–C**). No significant differences in TNF-α (M1 marker), IL-6 (M1 marker), and Arg-1 (M2 marker) were observed among the three groups, indicating that the GT/PCL membranes characterized by varying GT/PCL ratios exhibited low immunogenicity. The results also revealed the difficulty in realizing the polarization of the macrophages (**Supplementary Figures S2D–F**). Results from histological analyses revealed that the macrophages grew well on the surface of the GT/PCL membranes. It was also observed that the macrophages could not infiltrate the membranes even after 2 and 4 days (**Supplementary Figures S3A–F**). This indicated that the membranes provided a physical barrier that blocked macrophage infiltration. When G5P5 and G3P7 were studied, it was observed that the effect of the cell barrier could be observed at day 6 (**Supplementary Figures S3H,I**). For the G7P3 group, a small number of the macrophages could be detected inside the membranes at day 6 (**Supplementary Figure S3G**). This indicated that the **barrier effect** started to deteriorate under these conditions. This could be attributed to the rapid degradation of the G7P3 membranes.

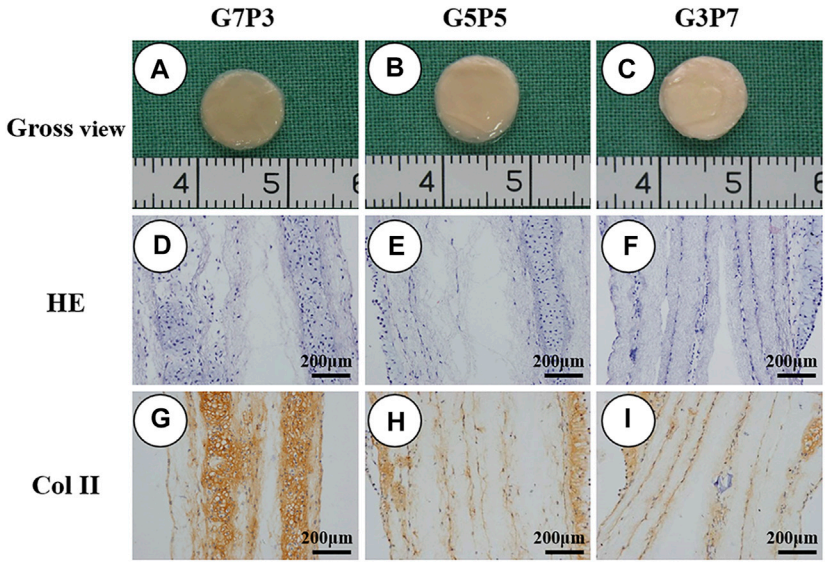

FIGURE 2 | Gross view and histological examination of engineered tissues at 2 weeks *in vitro*. All the samples basically maintain the cylinder shape after cell seeding and retain the original shape after *in vitro* implantation **(A–C)**. The samples in all groups form cartilage-like tissue with typical lacuna structure and positive staining of type II collagen **(D–I)**. In the G7P3 group **(G)**, the samples show obviously positive staining of type II collagen than the other two groups **(H,I)**.

3.3 Influence of the GT/PCL Ratio on the Process of *in vitro* Cartilage Formation

Before conducting the process of subcutaneous implantation, the samples generated *in vitro* were studied for cartilage formation following the processes of gross observation and histological staining. It was observed that the chondrocyte-GT/PCL constructs in all groups retained their original shapes and sizes when they were subjected to conditions of *in vitro* culture over 2 weeks (**Figures 2A–C**). Histologically, all the samples formed cartilage-like tissues with typical lacuna-like structures. The type II collagen could be positively stained (**Figures 2D–I**). The extent of ECM deposition observed in the cartilage present in the G7P3 group was higher than the extent of cartilage ECM depositions observed in the other two groups. This was revealed by analyzing the staining patterns of type II collagen (**Figure 2G**). In addition, the samples belonging to the G7P3 group exhibited better neocartilage integration. These samples did not exhibit the lamellar structure. Relatively loose lamellar structures separated by the GT/PCL membranes were observed in the G3P7 group. The results obtained from the *in vitro* studies indicated that the GT/PCL membranes characterized by low PCL contents could promote the formation of cartilage *in vitro*.

3.4 Influence of the GT/PCL Ratio on the Early Stage of Subcutaneous Cartilage Formation

We studied the early stages of cartilage formation *in vivo* using the GT/PCL membranes under conditions of varying GT/PCL ratios. We used a swine model for our studies. After 3 weeks of subcutaneous implantation (in autologous swine), the samples belonging to the G7P3 group shrank significantly and appeared yellow. The texture of the samples was soft (**Figure 3A**). Under the same conditions, the samples belonging to the G5P5 and G3P7 groups retained the original sizes and formed cartilage-like tissues that were hard and elastic (**Figures 3B,C**). The wet weight, Young's moduli, GAG content, and Collagen II content recorded for the G7P3 group were lower than those recorded for the G5P5 and G3P7 groups (**Figures 3D–G**). No significant difference in the data was observed for the G5P5 and G3P7 groups.

Results obtained by conducting histological evaluations agreed well with the results obtained from gross view and quantitative analyses. Samples belonging to the G7P3 group formed sparse cartilage islands surrounded by abundant inflammatory cells and fibrous tissues (continuous lamellar scaffolds were absent), indicating that low PCL content was not favorable for cartilage regeneration in a large animal model (**Figures 4A–E**). The results did not reflect the results obtained by conducting *in vitro* studies. The results also did not agree well with the results obtained by studying a nude mouse model (**Figure 2**) (Zheng et al., 2014). The cartilage formed in the interior regions of the samples belonging to the G5P5 and G3P7 groups were more homogenous than those formed in the interior regions of the samples belonging to the G7P3 group. These cartilage were characterized by a typical lacuna-like structure. Positive staining of GAG and type II collagen (exception: some undegraded lamellar scaffolds) was observed in the neocartilage (**Figures 4F–O**). The formation of homogenous cartilage with fine interlayer integration was observed at the edge of the samples belonging to the G5P5 group. Significant levels of invasion of the fibrous tissues or

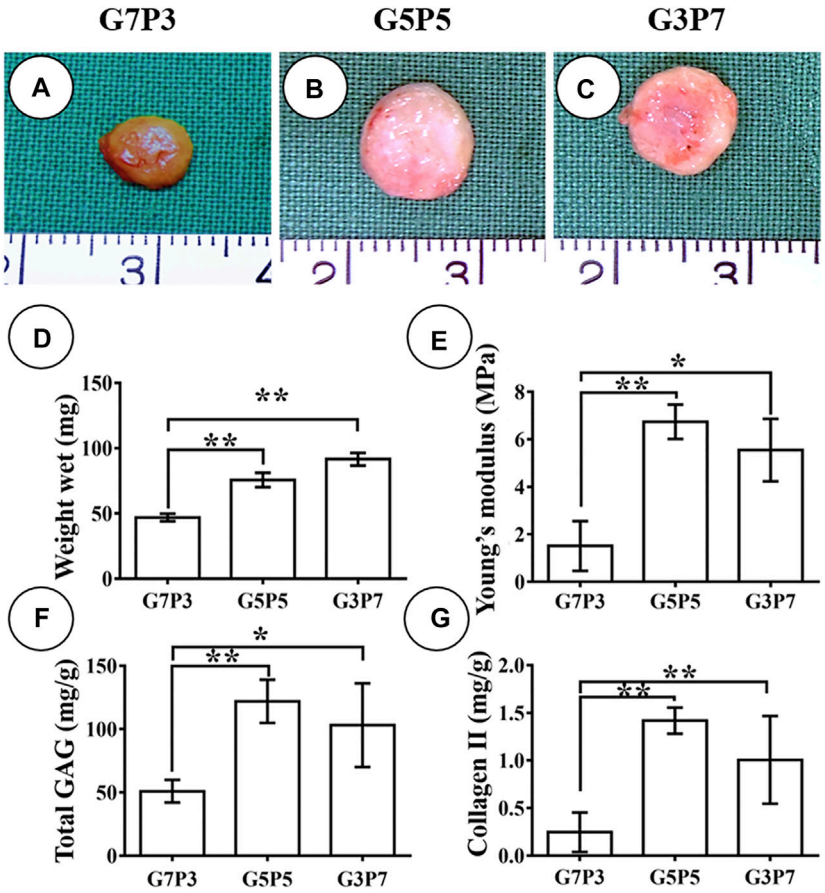

FIGURE 3 | Gross view and quantitative analysis of engineered tissues at 3 weeks *in vivo*. The samples in G7P3 remarkably shrink and show yellowish appearance **(A)** while the samples in G5P5 and G3P7 groups retained the original size and show ivory-white appearance **(B,C)**. Quantitative analysis demonstrates that the samples in the G7P3 group show lower values in wet weight, Young's modulus, total GAG, and Collagen II than those in G5P5 and G3P7 groups **(D–G)**. No obvious differences are observed in terms of wet weight, Young's modulus, total GAG, and Collagen II between the G5P5 group and the G3P7 group **(D–G)**. *Indicating significant differences (*$p < 0.05$; **$p < 0.01$).

inflammatory cells toward the interior of the sample were not observed (**Figure 4G**). The extent of tissue aggregation observed at the edge of the samples belonging to the G3P7 group was relatively lower than the extent of tissue integration observed in the G5P5 group. A significant amount of the fibrous tissues invaded the interior of the sample along with the lamellar scaffolds (**Figure 4L**). These results indicated that a significantly high PCL content was not favorable for cartilage regeneration in a large animal model.

The results obtained from semiquantitative analyses revealed significant differences among the three groups in terms of the area percentages corresponding to the cartilage tissues, fibrous tissues, and undegraded scaffolds (**Figures 4P–R**). According to the statistical results, the samples belonging to the G5P5 group presented the maximum percentage for the cartilage tissue area, the minimum percentage for the fibrous tissue area, and a moderate percentage for the undegraded scaffold area. This indicated that an optimum GT to PCL ratio helped the extent of cartilage regeneration achieved. It also helped reduce the extent of invasion of the fibrous tissue in a large animal model.

3.5 Influence of the GT/PCL Ratio on the Maturation of the Subcutaneous Cartilage

We then evaluated the *in vivo* fate of the engineered cartilage after a long period (6 weeks) following subcutaneous implantation. Analysis of **Figure 5** reveals that the size of the 6-week-old specimen belonging to the G7P3 group is much smaller than the size of the 6-week-old specimen belonging to the G5P5 and G3P7 groups (**Figures 5A–C**). The wet weight, Young's moduli, GAG contents, and collagen II contents recorded for the samples belonging to the G7P3 groups were significantly lower than those recorded for the samples belonging to the G5P5 and G3P7 groups (**Figures 5D–G**). It was also observed that Young's moduli and collagen II contents recorded for the samples belonging to the G5P5 group were higher than those recorded for the samples

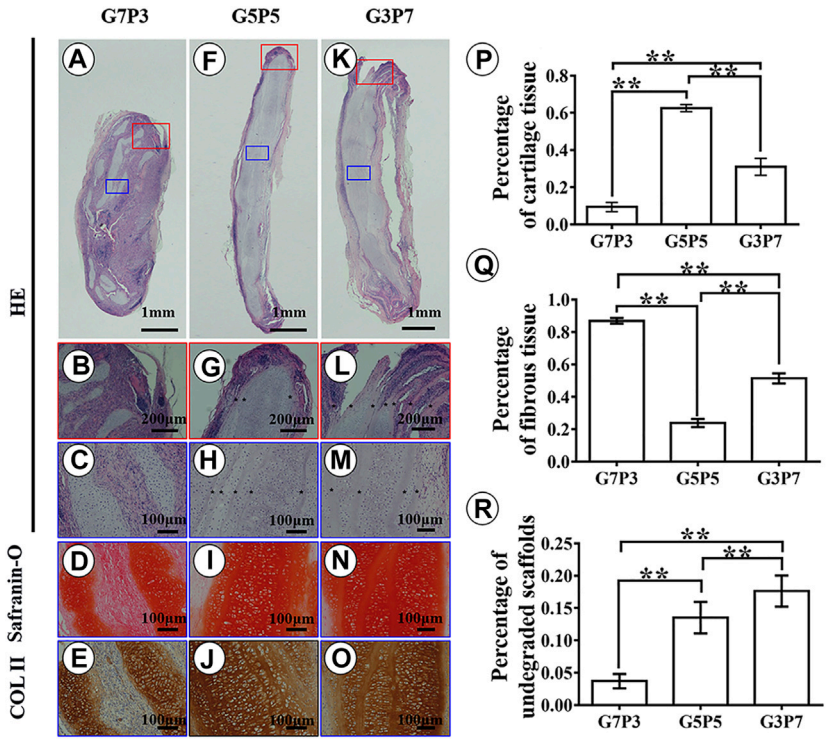

FIGURE 4 | Histological examination and semiquantitative analysis in engineered tissues at 3 weeks *in vivo*. In the G7P3 group, the samples show sparse cartilage islands surrounded by abundant inflammatory cells, fibrous tissue, and discontinuous laminar scaffolds **(A–E)**. In the G5P5 and G3P7 groups, relatively homogenous cartilage is observed in the interior regions (blue box) of the samples with typical lacuna structure and positive staining of GAG and type II collagen **(H–J,M–O)**, and continuous undegraded lamellar scaffolds (marked with *) are still observed among neocartilage **(H,M)**. At the edge of the samples (red box), the G5P5 group shows relatively homogenous cartilage formation with fine interlayer integration and no obvious fibrous tissue invades toward the interior of the sample **(G)**. In the G3P7 group, relatively inferior tissue integration is observed at the edge of the samples and obvious fibrous tissue invades toward the interior of the sample along with the interlayer gap **(L)**. The semiquantitative analysis shows significant differences in area percentage of cartilage tissue, fibrous tissue, and undegraded scaffolds among the three groups **(P–R)**. *Indicating significant differences (*$p < 0.05$; **$p < 0.01$).

belonging to the G3P7 group (**Figures 5E,G**). The results from histological analyses further confirmed the above observation. The samples belonging to the G7P3 group formed cartilage islands isolated by fibrous tissue (**Figures 6A–E**), and the samples belonging to the G5P5 and G3P7 groups formed continuous and homogenous cartilage in the interior of the samples (**Figures 6H–J**). The extent of distribution of the cartilage and fibrous tissues realized in the samples was consistent with the distribution of the tissues realized after 3 weeks. Satisfactory levels of cartilage integration were observed in the edge regions in the samples of the G5P5 group (**Figure 6G**). A small extent of fibrous tissue invasion was observed in this case. Poor tissue integration and significantly high levels of fibrous tissue invasion were observed at the edges of the samples belonging to the G3P7 group (**Figure 6L**).

Results obtained by conducting semiquantitative analyses revealed significant differences in terms of the area percentages corresponding to cartilage tissues, fibrous tissues, and undegraded scaffolds among the three groups. The G5P5 group exhibited the best extent of cartilage formation. The formation of the minimum amount of fibrous tissues and the presence of a moderate scaffold residual were also observed in this case. This indicated that an optimum GT to PCL ratio promoted cartilage regeneration in a large animal model (**Figures 6P–R**). Noticeably, the area percentages corresponding to the cartilage tissues, fibrous tissues, and undegraded scaffolds recorded for the 6-week samples were consistent with the results obtained for the 3-week samples. Significant differences among the groups were not observed, indicating that the results obtained for the 3- and 6-week-old samples could predict long-term results.

3.6 Influence of the GT/PCL Ratio on the Inflammatory Reaction (*in vivo*)

The 3-week specimens were further subjected to conditions of immunohistochemical staining using CD3 [T-cell marker (van Dongen et al., 1988)] and CD68 [monocyte/macrophage markers (Holness and Simmons, 1993)] to determine the status of the subcutaneous postimplantation inflammation. The results revealed that after 3 weeks of subcutaneous implantation (in autologous swine), the CD3- and CD68-positive cells presented highly consistent distribution in all the samples. The samples in different groups presented different distribution trends for CD3- and CD68-positive cells. A large number of CD3- and CD68-positive cells were observed throughout the samples surrounding the sparse cartilage islands and scaffold

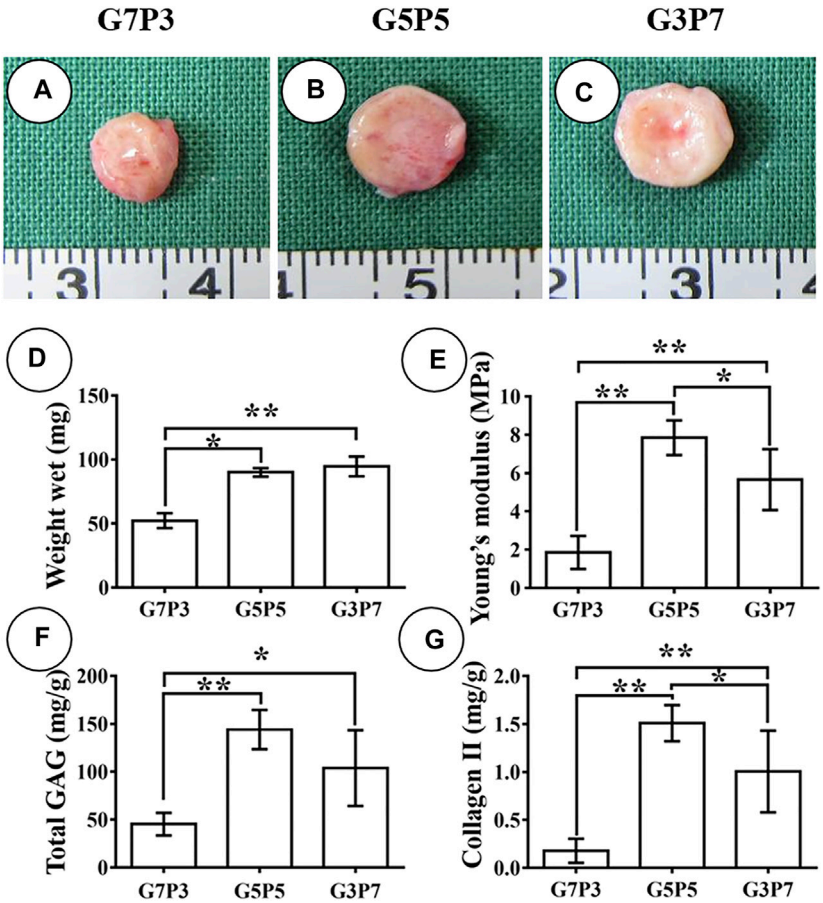

FIGURE 5 | Gross view and quantitative analysis of engineered tissues at 6 weeks *in vivo*. The samples in the G7P3 group remarkably shrink **(A)** while the samples in the G5P5 and G3P7 groups retain the original size **(B,C)**. Quantitative analysis reveals that the samples in the G7P3 group show lower values in wet weight, total GAG, Collagen II, and Young's modulus **(D–G)** than those in the G5P5 and G3P7 groups. The samples in the G5P5 group show higher Young's modulus and collagen II content compared to those in the G3P7 group **(E,G)**. *Indicating significant differences (*$p < 0.05$; **$p < 0.01$).

pieces (**Figures 7A–C**, **Figures 8A–C**) in the specimens belonging to the G7P3 group. This indicated that a low PCL content could potentially facilitate the infiltration of the inflammatory cells. In the G5P5 and G3P7 groups, CD3- and CD68-positive cells were only observed in the outer and edge regions. The presence of continuous, homogenous cartilage blocks characterized by a continuous layer of undegraded scaffolds (**Figures 7D–I**, **Figures 8D–I**) was observed at the central region. This indicated that a high PCL content could potentially help prevent the infiltration of the inflammatory cells. The presence of a large number of CD3- and CD68-positive cells was observed in the layered undegraded scaffolds at the edges of the specimens belonging to the G3P7 group. The tissue integration levels (between the layered undegraded scaffolds) (**Figure 7I**, **Figure 8I**) observed, in this case, were lower than the tissue integration levels observed in the samples belonging to the G5P5 group (with better cartilage-like tissue integration between the layered undegraded scaffolds) (**Figure 7F**, **Figure 8F**). This indicated that a significantly high PCL content might not be favorable for the prevention of inflammatory cell infiltration. This can be attributed to the low extents of cartilage regeneration and tissue integration achieved.

4 DISCUSSION

The subcutaneous environment of large animals is an immune environment that is similar to the environment of the human body. Successful cartilage construction realized in the subcutaneous environment of large animals can have important guiding significance in the field of clinical transformation. We have previously reported that the electrospun GT/PCL nanofiber membrane was a promising scaffold for cartilage regeneration. We had also observed that the GT/PCL membranes characterized by low PCL content promoted cartilage construction in a nude mouse model (Xue et al., 2013; Zheng et al., 2014). The results presented herein reveal that the membranes with different GT/PCL ratios can support the process of subcutaneous cartilage regeneration in an autologous swine model. The cartilage tissues formed in the samples belonging to the G5P5 group were more homogeneous than

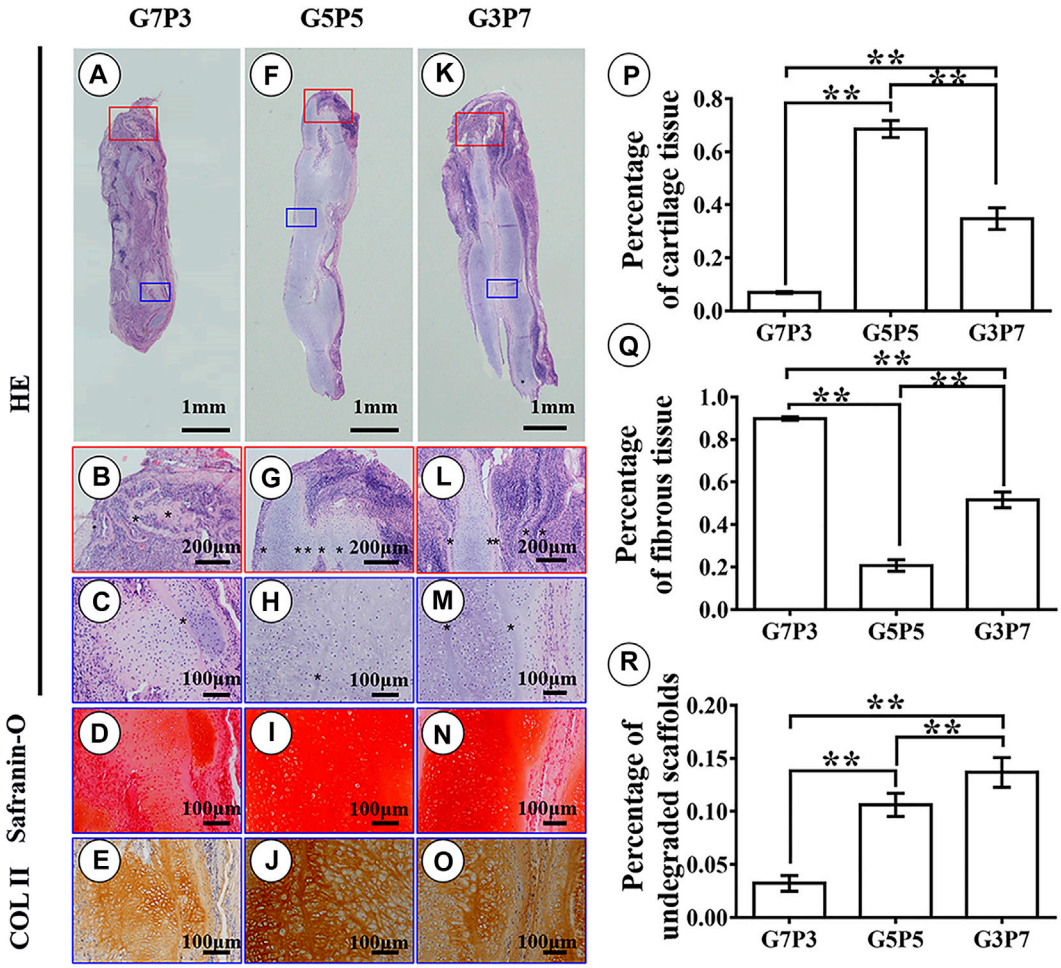

FIGURE 6 | Histological examination and semiquantitative analysis in engineered tissues at 6 weeks *in vivo*. Histological evaluation shows that the samples in the G7P3 group form cartilage islands isolated by fibrous tissue and discontinuous lamellar scaffolds **(A–E)** while the samples in the G5P5 and G3P7 groups form continuous and homogenous cartilage with continuous undegraded lamellar scaffolds in the interior area of the samples **(H–J,M–O)**. The edge regions in the G5P5 group **(G)** show relatively satisfactory cartilage integration with little fibrous tissue invasion while the edge regions in the G3P7 group present relatively inferior tissue integration (separated by undegraded lamellar scaffolds *) with obvious fibrous tissue invasion **(L)**. The semiquantitative analysis shows significant differences in area percentage of cartilage tissue, fibrous tissue, and undegraded scaffolds among the three groups **(P–R)**.

the cartilage tissues formed in the members of the other groups. The maximum cartilage formation area ratio, the minimum extent of fibrous tissue ingrowth, and the minimum extent of infiltration of the inflammatory cells were also observed in this case. These results indicated that the GT/PCL nanofiber membrane could serve as a good scaffold that could be used to support the process of subcutaneous cartilage regeneration in future clinical translation. An optimum GT/PCL ratio helped promote cartilage formation.

The scarcity of ideal scaffolds is one of the bottlenecks that restrict the clinical translation of cartilage regeneration technology. Many scaffolds are not suitable for subcutaneous cartilage regeneration in an immunocompetent large animal model, even though these scaffolds can be used to successfully generate cartilage *in vitro* or in nude mouse models (Asawa et al., 2012; Dumont et al., 2015; Francesca et al., 2018). The unsuitability of these scaffolds can be attributed to aggressive immune activities. We have previously reported that chondrocytes combined with the PGA/PLA scaffold could be used to successfully construct cartilage *in vitro* or in nude mice. However, these could not be used to regenerate good-quality cartilage in the subcutaneous environment of large animals as severe inflammation response results in the rapid degradation of the PGA fiber (Liu et al., 2010; Luo et al., 2013). Prolonged *in vitro* pre-culture methods should be conducted (>8 weeks) to dissipate the degradation products before implantation (Liu et al., 2016; Zhou et al., 2018) to realize satisfactory cartilage regeneration. However, a long-term *in vitro* culture method is time-consuming and expensive. The process also increases the risk of contamination. The GT/PCL electrospun membrane used in the current study is composed of the naturally occurring GT and polymeric PCL. GT is an accepted biosafety scaffold that has been widely used to realize multiple tissue regeneration. However, poor mechanical strength and rapid degradation time severely restrict its application in the field of cartilage regeneration (Huang et al., 2004; Aldana and Abraham,

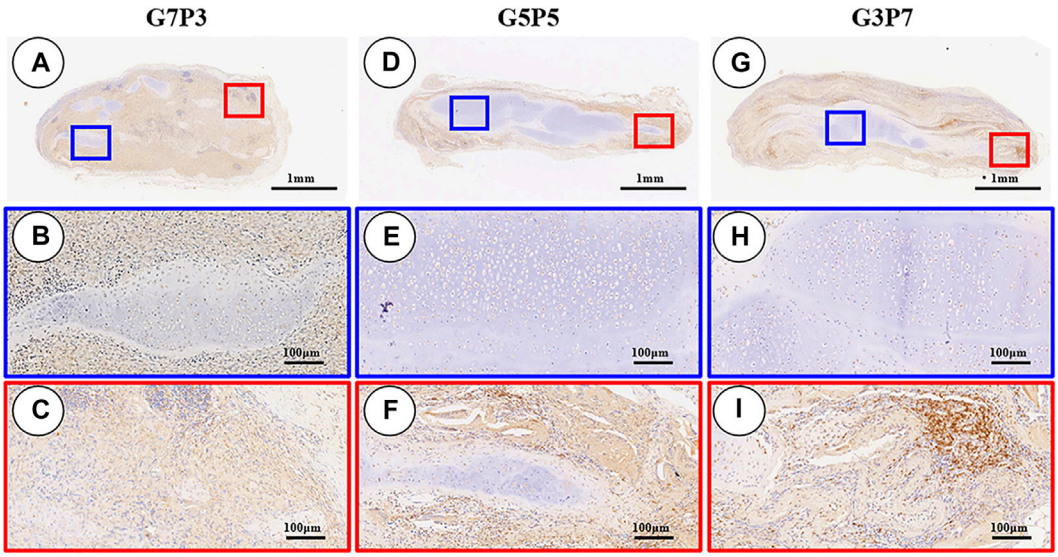

FIGURE 7 | Inflammatory reaction characterized by CD3 staining. The samples in the G7P3 group show small and sparse cartilage islands surrounded by abundant CD3-positive cells **(A–C)**. In the G5P5 and G3P7 groups, CD3-positive cells are observed in the outer and edge regions but not in the central regions **(D–I)**. Compared to the G5P5 group **(F)**, more CD3-positive cells are observed among layered undegraded scaffold in the edge regions of the G3P7 group **(I)**.

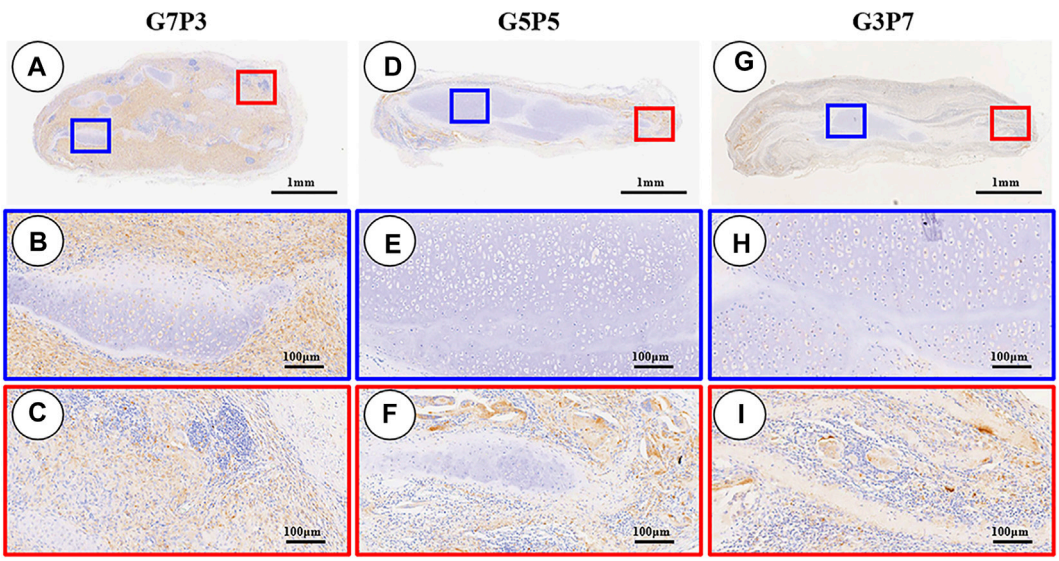

FIGURE 8 | Inflammatory reaction characterized by CD68 staining. The samples in the G7P3 group show small and sparse cartilage islands surrounded by abundant CD68-positive cells **(A–C)**. In the G5P5 and G3P7 groups, CD68-positive cells are observed in the outer and edge regions but not in the central regions **(D–I)**. More CD68-positive cells are observed among layered undegraded scaffolds in the edge regions of the G3P7 group **(I)** compared to the G5P5 group **(F)**.

2017). PCL is characterized by adequate mechanical strength, high elasticity, and long degradation time and can complement the weaknesses of GT (Woodward et al., 1985; Pham et al., 2006). Importantly, PCL and GT are Food and Drug Administration (FDA)-approved non-immunogenic materials that exhibit good biocompatibility. Therefore, theoretically, the use of the GT/PCL membrane should result in the generation of less extent of immune responses in large animal models. As evidenced in the current study, the various GT/PCL membranes (differing in the GT to PCL ratios) could not easily cause the polarization of the macrophages *in vitro*. This directly proved that the materials were characterized by low immunogenicity. Following the process of subcutaneous implantation, inflammatory cell infiltrations were observed in the samples belonging to the G5P5 group, even though an abundance of the layered undegraded scaffolds was observed in the surroundings. This also indicated the low immunogenicity of the GT/PCL

membranes. The chondrocyte-GT/PCL constructs cultured *in vitro* over 2 weeks formed homogenous and mature cartilage-like tissues characterized by typical lacuna-like structures. Positive staining in GAG and collagen II was observed after 3 and 6 weeks of subcutaneous implantation in the autologous swine model. This indicated that the GT/PCL membranes could serve as a promising scaffold to realize subcutaneous cartilage regeneration. The use of these membranes could significantly save the *in vitro* culture time, reduce culture costs, and reduce the risk of contamination.

The quality of the engineered cartilage presented significant differences among the three groups varying in the GT/PCL ratio in the autologous swine model. It was also observed that the influence of the GT/PCL ratio on the efficiency of cartilage regeneration in the swine model did not agree with the influence exerted on the process of cartilage regeneration in a nude mouse model (Zheng et al., 2014). In some cases, opposite trends were observed. We had previously reported that the low-PCL-ratio group could be used to realize the best cartilage regeneration in nude mice. However, the results obtained by studying the autologous swine model indicate that in the presence of the low-PCL-ratio group, the worst cartilage regeneration was realized after 3 and 6 weeks of subcutaneous implantation. A significant extent of infiltration of the inflammatory cells and high levels of ingrowth of fibrous tissues throughout the sample were observed in the samples belonging to the G7P3 group. It was speculated that the nonspecific inflammatory response caused by implantation trauma, changes in the membrane structure, and the rapid degradation of the scaffolds resulted in poor cartilage regeneration in the samples belonging to the G7P3 group. Although the GT/PCL membranes hardly triggered immune responses, the process of implantation could inevitably cause acute trauma and nonspecific inflammatory responses, resulting in the high extent of infiltration of the inflammatory cells and secretion of inflammatory factors. The rapid change in the structure of the membrane with the extent of degradation also contributed to the process. Histological analysis reveals that the membranes with different GT/PCL ratios exhibited a barrier effect that helped block the infiltration of the macrophages (*in vitro*). The rapid degradation of the scaffold, attributable to the high GT content, resulted in the weakening of the barrier effect in the samples belonging to the G7P3 group. The barrier effect observed in this case was weaker than the barrier effect observed in the other two groups. The weakening was initiated on day 6. The GT/PCL membranes subjected to the process of subcutaneous implantation failed to retain their continuous layered structures and thus failed to block the infiltration of the inflammatory cells. It was also observed that the implanted samples cultured *in vitro* over a period of 2 weeks presented loose cartilage structures. This significantly facilitated the infiltration of the inflammatory cells toward the interior of the samples. As a result, the process of cartilage regeneration in the samples of the G7P3 group was significantly disrupted by the presence of inflammatory cells and factors. These results indicated that the GT/PCL membranes characterized by high GT contents could not promote the process of subcutaneous cartilage regeneration in a large animal model.

It was also observed that a high PCL content significantly delayed the process of scaffold degradation in the samples belonging to the G5P5 and G3P7 groups. Thus, the GT/PCL membranes retained the continuous layered structures, and the cell barrier effect was also observed. Nanoscale micropores (the pore size was smaller than the cell size) were present on the continuous layered structures. The presence of these pores can potentially help block the infiltration of the inflammatory cells and macromolecule factors. They can also allow the free transportation of nutrients and metabolized products. These pores potentially impart anti-inflammatory effects to the electrospun nanofibrous membranes (Wang et al., 2016). The results presented herein confirm the feasibility of the concept. In the samples belonging to the G5P5 and G3P7 groups, the CD3- and CD68-positive cells were only observed in the outer regions and edges of the samples. These cells were absent in the inner regions, indicating that the continuous layered structures formed an anti-inflammatory barrier that helped block the invasion of the inflammatory cells. The presence of continuous, homogenous, and stable cartilage was observed in the central region, indicating that the continuous undegraded GT/PCL membranes had no significant influence on the process of transportation of nutrients and metabolized products.

The results indicated that the GT/PCL membranes characterized by high PCL contents could better retain the continuous layered structures. The membranes helped block the infiltration of the inflammatory cells. This, in turn, helped enhance the quality of the engineered cartilage. It was also observed that a significantly high PCL content might not be favorable for the prevention of the process of inflammatory cell infiltration. The number of the CD3- and CD68-positive cells present in the layered undegraded scaffold at the edges of the samples belonging to the G3P7 group was higher than the number of the CD3- and CD68-positive cells present in the samples belonging to the G5P5 group. A relatively low extent of tissue integration (compared to the extent of tissue integration realized in the G5P5 group) between the layered undegraded scaffold was observed at the edges of the samples belonging to the G3P7 group. Better cartilage-like tissue integration was realized at the edge regions of the samples belonging to the G5P5 group. The low extent of tissue integration recorded for the G3P7 group characterized by a significantly high PCL content resulted in an increase in the extent of infiltration of the inflammatory cells. Better tissue integration in the G5P5 group was achieved under conditions of optimum PCL content. The infiltration of the inflammatory cells and factors could be blocked under these conditions. The poor extent of tissue integration observed in the G3P7 group can be potentially attributed to the hydrophilicity and mechanical strength of the high PCL-content material. We have previously reported that a high PCL content in the membranes hindered the process of early cartilage formation (*in vivo*) in 3-week-old nude mice (Zheng et al., 2014). Therefore, only the GT/PCL membranes characterized by an optimum GT/PCL ratio could serve as a

satisfactory scaffold for subcutaneous cartilage formation in a large animal model.

5 CONCLUSION

Homogenous cartilage could be successfully regenerated in the subcutaneous environment of an autologous swine model using electrospun GT/PCL nanofibrous membranes and autologous auricular chondrocytes following 2 weeks of *in vitro* culture. A sandwich construction strategy was followed to regenerate the cartilage. The samples characterized by an optimum GT/PCL ratio (GT: PCL = 50:50) could be used to achieve efficient cartilage regeneration. The anti-inflammatory barrier of the nanofibrous membrane and the extent of tissue integration significantly influenced the process. The samples containing a large amount of GT (GT: PCL = 70:30) could not be used for efficient cartilage formation as under these conditions, the anti-inflammatory barrier attributable to the rapid degradation of the scaffold weakened. A poor extent of tissue integration was realized under conditions of high PCL contents. Thus, the samples characterized by high PCL contents (GT: PCL = 30:70) could not be used for effective cartilage regeneration at the edges. The results presented herein provide important information and a valuable model to realize effective subcutaneous cartilage regeneration in immunocompetent animals. The results can potentially help in the clinical translation of tissue-engineered cartilage.

DATA AVAILABILITY STATEMENT

The original contributions presented in the study are included in the article/**Supplementary Material**; further inquiries can be directed to the corresponding authors.

ETHICS STATEMENT

The animal study was reviewed and approved by the "Guide for Care of Laboratory Animals" formulated by the National Ministry of Science (2006).

AUTHOR CONTRIBUTIONS

RZ: Conceptualization, Methodology, Data curation, Formal analysis, Writing - Original Draft. XW: Methodology, Data Curation. JX: Data Curation, Formal analysis. LY: Data Curation, Formal analysis. GW and BY: Data Curation, HX and RZ: Conceptualization, Resources. MH and JC: Investigation, Resources. ZS: Conceptualization, Writing - Original Draft. YL: Conceptualization, Writing - Review and Editing. GZ: Conceptualization, Methodology, Writing - Review and Editing.

FUNDING

The current research was supported by the National Key Research and Development Program of China (2017YFC1103900), the National Natural Science Foundation of China (81871502, 81974291, 81701843, 31700837, 81671837), the Shanghai Collaborative Innovation Program on Regenerative Medicine and Stem Cell Research (2019CXJQ01), the Program of Shanghai Academic/Technology Research Leader (19XD1431100), the Clinical Research Plan of SHDC (No. SHDC2020CR 2045B), and the Cross-disciplinary Research Fund of Shanghai Ninth People's Hospital, Shanghai JiaoTong University School of Medicine (JYJC201901, JYJC202105).

SUPPLEMENTARY MATERIAL

The Supplementary Material for this article can be found online at: https://www.frontiersin.org/articles/10.3389/fbioe.2021.752677/full#supplementary-material

REFERENCES

Aldana, A. A., and Abraham, G. A. (2017). Current Advances in Electrospun Gelatin-Based Scaffolds for Tissue Engineering Applications. *Int. J. Pharmaceutics* 523, 441–453. doi:10.1016/j.ijpharm.2016.09.044

Asawa, Y., Sakamoto, T., Komura, M., Watanabe, M., Nishizawa, S., Takazawa, Y., et al. (2012). Early Stage Foreign Body Reaction against Biodegradable Polymer Scaffolds Affects Tissue Regeneration during the Autologous Transplantation of Tissue-Engineered Cartilage in the Canine Model. *Cell Transpl.* 21, 1431–1442. doi:10.3727/096368912x640574

Bateman, N., and Jones, N. S. (2000). Retrospective Review of Augmentation Rhinoplasties Using Autologous Cartilage Grafts. *J. Laryngol. Otol.* 114, 514–518. doi:10.1258/0022215001906264

Bichara, D. A., O'Sullivan, N.-A., Pomerantseva, I., Zhao, X., Sundback, C. A., Vacanti, J. P., et al. (2012). The Tissue-Engineered Auricle: Past, Present, and Future. *Tissue Eng. B: Rev.* 18, 51–61. doi:10.1089/ten.teb.2011.0326

Bichara, D. A., Pomerantseva, I., Zhao, X., Zhou, L., Kulig, K. M., Tseng, A., et al. (2014). Successful Creation of Tissue-Engineered Autologous Auricular Cartilage in an Immunocompetent Large Animal Model. *Tissue Eng. A* 20, 303–312. doi:10.1089/ten.tea.2013.0150

Brent, B. (1999). Technical Advances in Ear Reconstruction with Autogenous Rib Cartilage Grafts: Personal Experience with 1200 Cases. *Plast. Reconstr. Surg.* 104, 319335–334338. doi:10.1097/00006534-199908000-00001

Chong, E., Phan, T., Lim, I., Zhang, Y., Bay, B., Ramakrishna, S., et al. (2007). Evaluation of Electrospun PCL/gelatin Nanofibrous Scaffold for Wound Healing and Layered Dermal Reconstitution☆. *Acta Biomater.* 3, 321–330. doi:10.1016/j.actbio.2007.01.002

Dumont, C. M., Park, J., and Shea, L. D. (2015). Controlled Release Strategies for Modulating Immune Responses to Promote Tissue Regeneration. *J. Controlled Release* 219, 155–166. doi:10.1016/j.jconrel.2015.08.014

Farndale, R. W., Sayers, C. A., and Barrett, A. J. (1982). A Direct Spectrophotometric Microassay for Sulfated Glycosaminoglycans in Cartilage Cultures. *Connect. Tissue Res.* 9, 247–248. doi:10.3109/03008208209160269

Feng, B., Tu, H., Yuan, H., Peng, H., and Zhang, Y. (2012). Acetic-acid-mediated Miscibility toward Electrospinning Homogeneous Composite Nanofibers of GT/PCL. *Biomacromolecules* 13, 3917–3925. doi:10.1021/bm3009389

Francesca, T., Manuela, S., Christopher, T., Guillermo, B., Chiara, L., Shi, A., et al. (2018). Biomimetic Tissue Engineering: Tuning the Immune and Inflammatory Response to Implantable Biomaterials. *Adv. Healthc. Mater.* 7, e1800490. doi:10.1002/adhm.201800490

Fulco, I., Miot, S., Haug, M. D., Barbero, A., Wixmerten, A., Feliciano, S., et al. (2014). Engineered Autologous Cartilage Tissue for Nasal Reconstruction after Tumour Resection: an Observational First-In-Human Trial. *The Lancet* 384, 337–346. doi:10.1016/s0140-6736(14)60544-4

Gong, Y. Y., Xue, J. X., Zhang, W. J., Zhou, G. D., Liu, W., and Cao, Y. (2011). A sandwich Model for Engineering Cartilage with Acellular Cartilage Sheets and Chondrocytes. *Biomaterials* 32, 2265–2273. doi:10.1016/j.biomaterials.2010.11.078

Holness, C., and Simmons, D. (1993). Molecular Cloning of CD68, a Human Macrophage Marker Related to Lysosomal Glycoproteins. *Blood* 81, 1607–1613. doi:10.1182/blood.v81.6.1607.bloodjournal8161607

Huang, B. J., Hu, J. C., and Athanasiou, K. A. (2016). Cell-based Tissue Engineering Strategies Used in the Clinical Repair of Articular Cartilage. *Biomaterials* 98, 1–22. doi:10.1016/j.biomaterials.2016.04.018

Huang, Z.-M., Zhang, Y. Z., Ramakrishna, S., and Lim, C. T. (2004). Electrospinning and Mechanical Characterization of Gelatin Nanofibers. *Polymer* 45, 5361–5368. doi:10.1016/j.polymer.2004.04.005

Ji, W., Yang, F., Ma, J., Bouma, M. J., Boerman, O. C., Chen, Z., et al. (2013). Incorporation of Stromal Cell-Derived Factor-1α in PCL/gelatin Electrospun Membranes for Guided Bone Regeneration. *Biomaterials* 34, 735–745. doi:10.1016/j.biomaterials.2012.10.016

Jiang, Y.-C., Jiang, L., Huang, A., Wang, X.-F., Li, Q., and Turng, L.-S. (2017). Electrospun Polycaprolactone/gelatin Composites with Enhanced Cell-Matrix Interactions as Blood Vessel Endothelial Layer Scaffolds. *Mater. Sci. Eng. C* 71, 901–908. doi:10.1016/j.msec.2016.10.083

Kanani, A. G., and Bahrami, S. H. (2010). Review on Electrospun Nanofibers Scaffold and Biomedical Applications. *Trends Biomater. Artif. Organs* 24.

Kim, Y. H., Kim, B. J., and Jang, T. Y. (2011). Use of Porous High-Density Polyethylene (Medpor) for Spreader or Extended Septal Graft in Rhinoplasty. *Ann. Plast. Surg.* 67, 464–468. doi:10.1097/sap.0b013e3182045741

Liu, Y., Li, D., Yin, Z., Luo, X., Liu, W., Zhang, W., et al. (2016). Prolonged *In Vitro* Precultivation Alleviates post-implantation Inflammation and Promotes Stable Subcutaneous Cartilage Formation in a Goat Model. *Biomed. Mater.* 12, 015006. doi:10.1088/1748-605X/12/1/015006

Liu, Y., Zhang, L., Zhou, G., Li, Q., Liu, W., Yu, Z., et al. (2010). *In Vitro* engineering of Human Ear-Shaped Cartilage Assisted with CAD/CAM Technology. *Biomaterials* 31, 2176–2183. doi:10.1016/j.biomaterials.2009.11.080

Luo, L., He, Y., Chang, Q., Xie, G., Zhan, W., Wang, X., et al. (2016). Polycaprolactone Nanofibrous Mesh Reduces Foreign Body Reaction and Induces Adipose Flap Expansion in Tissue Engineering Chamber. *Ijn* 11, 6471–6483. doi:10.2147/ijn.s114295

Luo, X., Liu, Y., Zhang, Z., Tao, R., Liu, Y., He, A., et al. (2013). Long-term Functional Reconstruction of Segmental Tracheal Defect by Pedicled Tissue-Engineered Trachea in Rabbits. *Biomaterials* 34, 3336–3344. doi:10.1016/j.biomaterials.2013.01.060

Nayyer, L., Patel, K. H., Esmaeili, A., Rippel, R. A., Birchall, M., O'Toole, G., et al. (2012). Tissue Engineering. *Plast. Reconstr. Surg.* 129, 1123–1137. doi:10.1097/prs.0b013e31824a2c1c

Pham, Q. P., Sharma, U., and Mikos, A. G. (2006). Electrospun Poly(ε-Caprolactone) Microfiber and Multilayer Nanofiber/Microfiber Scaffolds: Characterization of Scaffolds and Measurement of Cellular Infiltration. *Biomacromolecules* 7, 2796–2805. doi:10.1021/bm060680j

Pomerantseva, I., Bichara, D. A., Tseng, A., Cronce, M. J., Cervantes, T. M., Kimura, A. M., et al. (2016). Ear-Shaped Stable Auricular Cartilage Engineered from Extensively Expanded Chondrocytes in an Immunocompetent Experimental Animal Model. *Tissue Eng. Part A* 22, 197–207. doi:10.1089/ten.tea.2015.0173

Qian, Y., Li, L., Song, Y., Dong, L., Chen, P., Li, X., et al. (2018). Surface Modification of Nanofibrous Matrices via Layer-By-Layer Functionalized Silk Assembly for Mitigating the Foreign Body Reaction. *Biomaterials* 164, 22–37. doi:10.1016/j.biomaterials.2018.02.038

Sterodimas, A., de Faria, J., Correa, W. E., and Pitanguy, I. (2009). Tissue Engineering and Auricular Reconstruction: a Review. *J. Plast. Reconstr. Aesthet. Surg.* 62, 447–452. doi:10.1016/j.bjps.2008.11.046

van Dongen, J., Krissansen, G., Wolvers-Tettero, I., Comans-Bitter, W., Adriaansen, H., Hooijkaas, H., et al. (1988). Cytoplasmic Expression of the CD3 Antigen as a Diagnostic Marker for Immature T-Cell Malignancies. *Blood* 71, 603–612. doi:10.1182/blood.v71.3.603.bloodjournal713603

Wang, K., Hou, W.-D., Wang, X., Han, C., Vuletic, I., Su, N., et al. (2016). Overcoming Foreign-Body Reaction through Nanotopography: Biocompatibility and Immunoisolation Properties of a Nanofibrous Membrane. *Biomaterials* 102, 249–258. doi:10.1016/j.biomaterials.2016.06.028

Wang, X., Zhu, J., Sun, B., Jin, Q., Li, H., Xia, C., et al. (2021). Harnessing Electrospun Nanofibers to Recapitulate Hierarchical Fibrous Structures of Meniscus. *J. Biomed. Mater. Res.* 109, 201–213. doi:10.1002/jbm.b.34692

Wiggenhauser, P. S., Schantz, J. T., and Rotter, N. (2017). Cartilage Engineering in Reconstructive Surgery: Auricular, Nasal and Tracheal Engineering from a Surgical Perspective. *Regenerative Med.* 12, 303–314. doi:10.2217/rme-2016-0160

Woodward, S. C., Brewer, P. S., Moatamed, F., Schindler, A., and Pitt, C. G. (1985). The Intracellular Degradation of Poly(?-Caprolactone). *J. Biomed. Mater. Res.* 19, 437–444. doi:10.1002/jbm.820190408

Xue, J., Feng, B., Zheng, R., Lu, Y., Zhou, G., Liu, W., et al. (2013). Engineering Ear-Shaped Cartilage Using Electrospun Fibrous Membranes of Gelatin/polycaprolactone. *Biomaterials* 34, 2624–2631. doi:10.1016/j.biomaterials.2012.12.011

Yan, D., Zhou, G., Zhou, X., Liu, W., Zhang, W. J., Luo, X., et al. (2009). The Impact of Low Levels of Collagen IX and Pyridinoline on the Mechanical Properties of *In Vitro* Engineered Cartilage. *Biomaterials* 30, 814–821. doi:10.1016/j.biomaterials.2008.10.042

Zang, M., Zhang, Q., Chang, E. I., Mathur, A. B., and Yu, P. (2013). Decellularized Tracheal Matrix Scaffold for Tracheal Tissue Engineering. *Plast. Reconstr. Surg.* 132, 549e–559e. doi:10.1097/prs.0b013e3182a013fc

Zheng, R., Duan, H., Xue, J., Liu, Y., Feng, B., Zhao, S., et al. (2014). The Influence of Gelatin/PCL Ratio and 3-D Construct Shape of Electrospun Membranes on Cartilage Regeneration. *Biomaterials* 35, 152–164. doi:10.1016/j.biomaterials.2013.09.082

Zheng, Z., Chen, Y., Hong, H., Shen, Y., Wang, Y., Sun, J., et al. (2021). The "Yin and Yang" of Immunomodulatory Magnesium-Enriched Graphene Oxide Nanoscrolls Decorated Biomimetic Scaffolds in Promoting Bone Regeneration. *Adv. Healthc. Mater.* 10, 2000631. doi:10.1002/adhm.202000631

Zhou, G., Jiang, H., Yin, Z., Liu, Y., Zhang, Q., Zhang, C., et al. (2018). *In Vitro* Regeneration of Patient-specific Ear-Shaped Cartilage and its First Clinical Application for Auricular Reconstruction. *EBioMedicine* 28, 287–302. doi:10.1016/j.ebiom.2018.01.011

Conflict of Interest: The authors declare that the research was conducted in the absence of any commercial or financial relationships that could be construed as a potential conflict of interest.

Publisher's Note: All claims expressed in this article are solely those of the authors and do not necessarily represent those of their affiliated organizations, or those of the publisher, the editors, and the reviewers. Any product that may be evaluated in this article, or claim that may be made by its manufacturer, is not guaranteed or endorsed by the publisher.

frontiers in Bioengineering and Biotechnology

REVIEW
published: 22 December 2021
doi: 10.3389/fbioe.2021.756930

Tackling the Challenges of Graft Healing After Anterior Cruciate Ligament Reconstruction—Thinking From the Endpoint

*Shiyi Yao, Patrick Shu Hang Yung and Pauline Po Yee Lui**

Department of Orthopaedics and Traumatology, The Chinese University of Hong Kong, Shatin, Hong Kong SAR, China

Anterior cruciate ligament (ACL) tear is common in sports and accidents, and accounts for over 50% of all knee injuries. ACL reconstruction (ACLR) is commonly indicated to restore the knee stability, prevent anterior–posterior translation, and reduce the risk of developing post-traumatic osteoarthritis. However, the outcome of biological graft healing is not satisfactory with graft failure after ACLR. Tendon graft-to-bone tunnel healing and graft mid-substance remodeling are two key challenges of biological graft healing after ACLR. Mounting evidence supports excessive inflammation due to ACL injury and ACLR, and tendon graft-to-bone tunnel motion negatively influences these two key processes. To tackle the problem of biological graft healing, we believe that an inductive approach should be adopted, starting from the endpoint that we expected after ACLR, even though the results may not be achievable at present, followed by developing clinically practical strategies to achieve this ultimate goal. We believe that mineralization of tunnel graft and ligamentization of graft mid-substance to restore the ultrastructure and anatomy of the original ACL are the ultimate targets of ACLR. Hence, strategies that are osteoinductive, angiogenic, or anti-inflammatory should drive graft healing toward the targets. This paper reviews pre-clinical and clinical literature supporting this claim and the role of inflammation in negatively influencing graft healing. The practical considerations when developing a biological therapy to promote ACLR for future clinical translation are also discussed.

Keywords: ACL reconstruction, anterior cruciate ligament, ACL, graft healing, biological therapy, inflammation, osteogenesis, angiogenesis

OPEN ACCESS

Edited by:
Laura Creemers, University Medical Center Utrecht, Netherlands

Reviewed by:
Fei Chen, Shenzhen Institutes of Advanced Technology (CAS), China
Cynthia M. Coleman, National University of Ireland Galway, Ireland

****Correspondence:***
Pauline Po Yee Lui
paulinelui@cuhk.edu.hk
paulinelui00@gmail.com

Specialty section:
This article was submitted to Tissue Engineering and Regenerative Medicine, a section of the journal Frontiers in Bioengineering and Biotechnology

Received: *11 August 2021*
Accepted: *09 November 2021*
Published: *22 December 2021*

Citation:
Yao S, Yung PSH and Lui PPY (2021) Tackling the Challenges of Graft Healing After Anterior Cruciate Ligament Reconstruction—Thinking From the Endpoint. Front. Bioeng. Biotechnol. 9:756930. doi: 10.3389/fbioe.2021.756930

1 INTRODUCTION

1.1 Epidemiology of anterior cruciate ligament tears and current management

The anterior cruciate ligament (ACL) is a band of dense connective tissues that courses from the femur to the tibia, the function of which is to prevent excessive knee anterior–posterior translation and to maintain joint stability (Duthon et al., 2006; Zantop et al., 2006). Tears or ruptures of ACL are very common injuries in sports medicine, representing more than 50% of all knee injuries and affecting more than 200,000 people in the United States each year (Musahl and Karlsson, 2019).

ACL tears can impair knee function and increase the lifetime risk of knee osteoarthritis. Patients without and with meniscal tear had a 0%–13% and 21%–48% higher risk of developing knee osteoarthritis at 10 years after an ACL injury, respectively (Oiestad et al., 2009). The contribution of ACL tears to the burden of degenerative joint disease is substantial, accounting for an increase of 30,000–38,000 patients with symptomatic knee osteoarthritis and an additional 25,000–30,000 total knee arthroplasties each year in the United States. (Mather et al., 2013).

ACL tears are managed by conservative and surgical approaches. Cryotherapy, restrictive bracing, continuous passive motion, electrotherapy, and exercises aimed at reducing inflammation, restricting excessive knee motions, or strengthening muscles to improve knee symptoms and stability as well as to protect the joint are common conservative treatment options. However, conservative approaches for the management of ACL tears are poorly accepted by young active individuals. The continued active lifestyles of these individuals often lead to recurrent knee instability, chondral and meniscal injuries, and early onset of osteoarthritis (Raines et al., 2017).

ACL reconstruction is a surgical procedure that replaces the injured ACL with a tendon graft as the ACL does not heal after injury due to insufficient vascularization. Bone tunnels are artificially created in the distal femur and proximal tibia, and the tendon graft is inserted and fixed to the bone tunnels using staples, sutures, cross-pins, or interference screws. The procedure is usually assisted by arthroscopy to minimize the size of incision and reduce complications. The success rate of ACLR varied from 73% to 95% and the return to pre-injury activity level varied from 37% to 75% (Yunes et al., 2001; Fithian et al., 2005). Graft failure, presented as graft laxity and inferior mechanical properties compared with that of native ACL, is one of the main reasons for poor outcome after ACLR. A graft failure rate ranging from 1.5% to 5.7% has been reported (Yunes et al., 2001). Such graft failure is mainly attributed to surgical errors, traumatic injuries, failure of tendon graft-to-bone tunnel integration, and unsuccessful graft remodeling (George et al., 2006). Graft healing after ACLR is very slow, leading to long periods of carefully monitored rehabilitation and long delays before returning to full activity (Silva et al., 2012).

To tackle the problem of poor graft healing after ACLR, we believe a new research paradigm should be applied. An inductive approach, starting from the ideal endpoint of ACLR, should be adopted. The feasibility of translating the pre-clinical findings into clinical practice should be considered at the pre-clinical stage. This would enhance the future translation of the findings to benefit patients. Using this new paradigm of thinking, we believe that strategies that are osteoinductive, angiogenic, or anti-inflammatory should drive graft healing toward the ultimate goal of restoring ACL function after ACLR. This paper aims to present evidence from the literature to support this claim. The graft healing process is first summarized, with evidence supporting the role of inflammation in negatively influencing the healing response highlighted. Evidence supporting osteoinductive, angiogenic, or anti-inflammatory approaches to promote graft healing will then be systematically reviewed. Important issues requiring consideration when developing biological therapies for ACLR from the perspective of future clinical translation are then discussed.

2 GRAFT HEALING PROCESS AFTER ANTERIOR CRUCIATE LIGAMENT RECONSTRUCTION

Tendon graft-to-bone tunnel healing followed by graft mid-substance remodeling (collectively called "graft healing") are two key healing processes that occur after ACLR (**Figure 1**). After ACLR, an inflammatory response is triggered, and inflammatory cells are recruited to the injury site. They clear cell debris and produce inflammatory cytokines, which attract mesenchymal stromal cells (MSCs) (formerly called mesenchymal stem cells) to the bone tunnel region and the intra-articular graft mid-substance. Next, cell necrosis in the implanted graft occurs. Re-vascularization and repopulation of tendon graft with MSCs then take place. The MSCs terminally differentiate and produce growth factors and extracellular matrix (ECM) to incorporate the tendon graft to the bone tunnel. On the other hand, with the help of the inflammatory cells and MSCs, the graft mid-substance remodels from a tendon to a ligament in a process called ligamentization (Scheffler et al., 2008).

2.1 Tendon graft-to-bone tunnel healing

Tendon graft-to-bone tunnel healing is the weak link in the early stage of ACLR as it requires the attachment of a compliant material-like tendon to a relatively stiff material-like bone. The regeneration of a normal insertion site with formation of a unique transitional tissue called "enthesis" (Petersen and Laprell, 2000), characterized by gradual change in structure, composition, and mechanical behavior, is pivotal for efficient transfer of load and prevention of stress accumulation at the interface. Excessive inflammation (Song et al., 2017) at the graft-to-bone tunnel interface induces the formation of a fibrous scar tissue interface rather than a normal insertion site. The mechanical strength achieved by this scar interface is far from satisfactory.

Depending on how the collagen fibers are attached to bone, there are two types of entheses at the bone–tendon junction—direct and indirect insertions. Direct insertion (also called the fibrocartilaginous enthesis) is composed of four zones (Petersen and Laprell, 2000) in order of gradual transition: tendon, uncalcified fibrocartilage, calcified fibrocartilage, and bone. Indirect insertion has no fibrocartilage interface. The tendon/ligament passes obliquely along the bone surface and inserts at an acute angle into the periosteum and is connected by Sharpey's fibers over a broader area of tendon and bone. Direct and indirect insertions confer different anchorage strength and interface properties at the tendon–bone interface. Although both direct and indirect insertions have been described in the literature as a better healing outcome after ACLR (Liu et al., 1997), it has been more widely accepted that the insertion type after ACLR is an indirect one. Our results have shown that the chondrocytes at the tendon–bone tunnel interface only functioned as an intermediate in endochondral ossification and were replaced by bone with time during healing (Lui et al., 2010). The

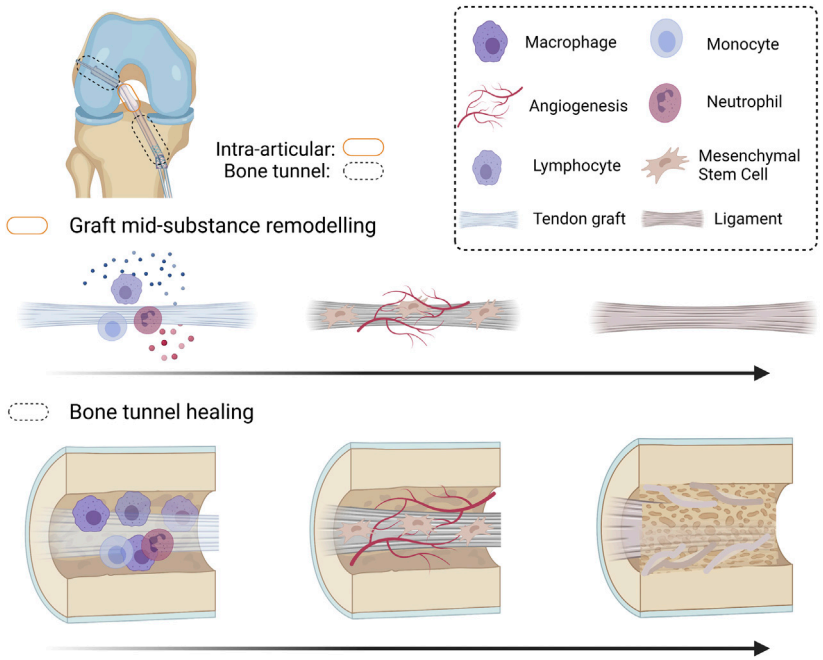

FIGURE 1 | Schematic diagram summarizing the graft healing process after anterior cruciate ligament (ACL) reconstruction. After ACL reconstruction (ACLR), inflammatory occurs, attracting immune cells and mesenchymal stromal cells (MSCs) to the injured site. The original cells in the tendon graft undergo necrosis and are replaced by MSCs infiltrating into the graft. Both MSCs and the inflammatory cells produce angiogenic factors and the MSCs proliferate and differentiate. The differentiated MSCs produce extracellular matrix and remodeling enzymes to incorporate the tendon graft-to-bone tunnel by Sharpey's fibers and is associated with improved biomechanical properties of the healing complex. However, there is regional variation in healing along the bone tunnel. The original ACL insertion site is not re-established. The tendon graft mid-substance theoretically should remodel to a ligament. However, it degenerates due to excessive inflammation and poor angiogenesis after ACLR. Created with BioRender.com.

placement of tendon graft inside an artificially created bone tunnel, while providing a large bone surface area for tendon graft-to-bone tunnel healing, also disrupts the physiological mechanical load, resulting in regional-dependent stress shielding and subsequent bone loss (Lui P. P. Y. et al., 2013; Stolarz et al., 2017). The healing is, therefore, not uniform at different regions of bone tunnel and at different bone tunnels, with some areas exhibiting better healing than the others (Wen et al., 2010; Lui et al., 2015). Tunnel widening and bone resorption negatively influence healing and increase the chance of graft pull-out. Tendon to bone tunnel healing is slow, and the direct insertion site of native ACL is not regenerated. The outcome of graft healing after ACLR, therefore, remains unsatisfactory.

2.2 Graft mid-substance remodeling

As healing progresses, the weak link of graft healing gradually shifts from the tendon graft-to-bone tunnel interface to the graft mid-substance. The tendon graft undergoes "ligamentization," in which the composition and organization of ECM are adapted to the functions of an active ACL.

Ligament fibroblasts have higher DNA content and are more metabolically active compared with tendon fibroblasts. Besides, the ECM of ligament contains more type III collagen and glycosaminoglycans but slightly less total collagen compared with tendons. Due to the direction of mechanical load, the collagen fibers of ligament are less orderly aligned compared with tendon. Moreover, the collagen fibrils in ligament are smaller but have more reducible cross-links compared with the fibrils in tendon (Amiel et al., 1984).

The process of ligamentization, therefore, requires the tendon graft to metabolically, compositionally, and ultrastructurally remodeled to adapt to the function of a ligament. However, the process is not successful as graft degeneration due to poor angiogenesis and ECM degradation were observed both clinically (Marumo et al., 2005) and in animal studies (Lui et al., 2014c; Yung et al., 2020).

3 ROLE OF INFLAMMATION IN INFLUENCING HEALING RESPONSE

Shortly after graft implantation, an inflammatory response, which is important for removing cell debris and activate tissue repair, ensues. Neutrophils and macrophages are recruited to the tendon–bone interface as early as 4 days after surgery (Wall and Board, 2014). They produce inflammatory cytokines and fibrogenic growth factors, which contribute to the formation of a fibrous tissue interface between the graft and host bone at the early healing phase (Ekdahl et al., 2008). While the fibrous tissue fills the gap and provides early mechanical support at the interface, excessive inflammation causes fibrosis, which interferes

TABLE 1 | A summary of the impact of inflammation on the outcomes of anterior cruciate ligament (ACL) graft healing.

Study type	Causes of inflammation[a]/ cells and factors involved	Results	References
Human	(1) IL-6	IL-6 levels were significantly higher in the group with <6 weeks of injury than in the group with >12 weeks since injury. IL-6 was significantly elevated in painful ligamentous injury of knee, showed negative correlation with Lysholm knee scores at 2 months, 6 months, and 1 year of follow-up, and showed negative correlation with Tegner level of sports activity at 1 year of follow-up	Gupta et al. (2021)
Human	(1) IL-6, MMP-3	High concentration of IL-6 and MMP-3 in the synovial fluid early post-ACL injury was associated with aberrant gait biomechanics in the injured limb at 6 months post-ACLR.	Evans-Pickett et al. (2021a)
Human	(1) IL-1α, IL-1ra, MMP-9	At 2 years of follow-up, patients that failed to reach the QOL PASS threshold after surgery (n = 6, 27%) had significantly greater IL-1α, IL-1ra, MMP-9 concentrations on the day of surgery. Patients that failed to reach the IKDC PASS threshold (n = 9, 41%) had significantly greater IL-1α	Lattermann et al. (2018)
Human	(1) (2) MMP-3, IL-6	Individuals with lesser biomechanical loading on the ACLR limb at the 6-month follow-up exam, compared with the contralateral limb, demonstrate greater concentrations of plasma MMP-3 and IL-6 early after ACL injury and during the early postoperative period	Pietrosimone et al. (2017)
Human	(2) IL-8	Patients with Remnant Preserved (RP)-ACLR had better knee stability within 3 months which was associated with higher expression of IL-8 in the synovial fluid compared with the patients with conventional ACLR	Kim et al. (2020)
Human	(2) IL-6, IL-8, TNF-α, M1 Macrophage	Graft loosening was closely related to increased gene and protein expression of inflammatory cytokines (TNF-α, IL-6, and IL-8) within the first year of ACLR. There was a probable role of M1 but not M2 macrophages in the pathological process leading to graft loosening	Song et al. (2017)
Human	(2) IL-10, IL-1β, IL-6, IFN-γ	Increased level of IL-10, IL-1β, IL-6, IFN-γ in the synovial fluid at 3–4 days post-ACLR was associated with a prolonged recovery	Inoue et al. (2016)
Human	(2) IL-1β	There is an association between tibial bone tunnel enlargement and elevated synovial fluid concentrations of IL-1β concentrations postoperatively after ACLR. A lower expression of IL-1β in the synovial fluid after autologous conditioned serum (ACS) treatment was associated with reduced tunnel widening 6 months and 1 year after ACLR.	Darabos et al. (2011a)
Human	(2) TNF-α, IL-6, NO	An elevated synovial fluid concentration of IL-6, TNF-α, and NO at 7 days after ACLR was associated with tibial bone tunnel enlargement at 38 ± 7 weeks after surgery	Zysk et al. (2004)
Rat	(2) MMP1, MMP13, $CD68^+$ cells	The peri-tunnel bone loss correlated with high expression of MMP1, MMP13, and $CD68^+$ cells at the graft–bone tunnel interface at week 6 after ACLR.	Lui et al. (2015)
Rat	(2) MMP1, MMP13, $CD68^+$ cells	Alendronate reduced peri-tunnel bone resorption, increased mineralized tissue inside bone tunnel as well as histologically and biomechanically promoted graft-bone tunnel healing at week 6, probably by reducing the expression of MMP1, MMP13, and CD68-positive cells	Lui et al. (2013a)
Rat	(2) Macrophages	Macrophage depletion following ACLR significantly improved histological and biomechanical properties of the healing tendon–bone interface at 42 days	Hays et al. (2008)
Rat	(3) ED1 macrophages	Short-duration of low-magnitude cyclic axial loading of the ACL graft was associated with more inflammatory ED1 macrophages and less bone formation in the bone tunnel at 5, 14, 28 days post-ACLR.	Brophy et al. (2011)
Rat	(3) ED1macrophages ED2 macrophages	Interface width was smaller and collagen fiber continuity was greater in the immobilized group. Immobilized animals exhibited fewer ED1 + macrophages at the healing interface at 2 and 4 weeks. In contrast, there were more ED2 + macrophages at the interface in the immobilized group at 2 weeks	Dagher et al. (2009)
Mice	(3) MMP -2, -3, -9, -13	A short period of immobilization after ACLR enhanced graft-to-bone tunnel healing by mitigating excessive MMP expression at day 30	Nakagawa et al. (2019)

Note. N.B.

[a]*Causes of inflammation: (1) ACL injury; (2) surgical trauma in ACLR, and (3) tendon graft-to-bone tunnel motion.*

with graft osteo-integration. Excessive inflammation also causes bone tunnel widening, peri-tunnel bone loss, and graft degeneration. Combining histological and molecular analyses, a clear correlation between increased expression of inflammatory cytokines, M1 macrophage infiltration, and graft loosening has been reported in tissue samples of patients who underwent a second-look arthroscopy within the first year after arthroscopic ACLR (Song et al., 2017).

To confirm the association of inflammation with poor outcome of ACL graft healing, a systematic search and analysis of the literature was done (search strategy in **Supplementary Information S1**). The results showed that excessive inflammation due to 1) ACL injury, 2) surgical trauma in ACLR, and 3) tendon graft-to-bone tunnel motion were common reasons for poor tendon graft-to-bone tunnel healing and graft mid-substance degeneration (**Table 1**). These unfavorable biological and mechanical factors induce the release of inflammatory cytokines by macrophages, synoviocytes, or fibroblasts, stimulating the production of matrix metalloproteinases (MMPs), which degrade ECM, and

activating osteoclasts for bone resorption. The role of each of these factors in inducing excessive inflammation and impacting the outcomes of graft healing after ACLR are discussed below.

3.1 Anterior cruciate ligament injury

Synovial fluid is an interstitial fluid produced by synoviocytes in the synovial membrane and functions to absorb shock and reduce friction as well as transport nutrient and waste in the joint. ACL injury has been demonstrated to increase the level of inflammatory cytokines and related substances in the synovial fluid, including TNF-α, IL-1β, IL-6, IL-8, IL-1ra, and IL-10 (Irie et al., 2003). The synovial fluid leaks into the bone tunnel and exposes the tendon graft to the pro-inflammatory cytokines and catabolic enzymes, contributing to bone resorption and poor graft healing. This is evident by Berg et al. (2001), who have reported that tunnel healing was slower and less complete in the articular part of the tunnel than in the tunnel part, which was farther from the synovial environment. Besides, the level of inflammatory cytokines (IL-1) in the synovial fluid taken intra-operatively was associated with higher pain score and anterior knee laxity as well as lower functional outcome and return to sports in patients undergoing ACLR at 1-year follow-up (Gupta et al., 2021). In addition, high concentration of IL-1 and MMP-3 in the synovial fluid early post-ACL injury was also associated with aberrant gait biomechanics in the injured limb at 6 months post-ACLR (Evans-Pickett et al., 2021b). In another clinical study, patients failing to meet the Knee Injury and Osteoarthritis Outcome Score (KOOS QoL) Patient Acceptable Symptom State (PASS) threshold and the International Knee Documentation Committee scores (IKDC) PASS threshold 2 years post-ACLR had significantly higher pre-operative concentrations of inflammatory cytokines and matrix remodeling enzyme in the synovial fluid (Lattermann et al., 2018). These studies support that the inflammatory cytokines in the synovial fluid after ACL tear negatively influences graft healing.

3.2 Surgical trauma in anterior cruciate ligament reconstruction

ACLR constitutes a second trauma to the acutely injured knee, resulting in further elevation of the concentrations of inflammatory cytokines in the synovial fluid (Larsson et al., 2017). In a secondary analysis of data from 14 patients in a clinical trial, ACLR triggered a second inflammatory hit in the knee with an increase in the levels of IL-1β and IL-6 in the synovial fluid (Hunt et al., 2021). In a second-look arthroscopy, there were higher expressions of pro-inflammatory cytokines and signaling mediators in the graft tissues in the graft loosening group compared with the expressions in the normal graft group. The activated M1 macrophages accumulated in the graft tissue, but no M2 macrophages were identified (Song et al., 2017). A significant negative correlation between the expressions of inflammatory cytokines and knee laxity function score was observed in the patient. The level of IL-1β in the synovial fluid at 3–4 days post-surgery predicted poor functional recovery at 3 months after ACLR (Inoue et al., 2016). In another clinical trial, all patients with tibial tunnel enlargement had elevated synovial levels of TNF-α, IL-6, and NO at 7 days post-operation (Zysk et al., 2004). These findings support that inflammation after ACLR negatively impacts graft healing.

The release of inflammatory cytokines attracts inflammatory cells to the injury sites. The inflammatory cells release inflammatory cytokines and stimulate further inflammation in a viscous cycle. Among the limited numbers of studies investigating the temporal changes of inflammatory cells after ACLR, neutrophils and macrophages accumulated sequentially at the healing graft-to-bone interface and repopulated the tendon graft. T-lymphocytes and mast cells were seen occasionally at the graft-to-bone interface (Kawamura et al., 2005). Unlike the allograft group, the ratio of $CCR4^{+}CCR6^{+}$ Th to Treg cells in the synovial fluid post-surgery did not correlate with anterior knee laxity after ACLR in the autograft group in a clinical study (Yang et al., 2012).

Macrophages play an important role in orchestrating graft healing after ACLR. In an animal study of the temporal changes of pro-inflammatory, phagocytic M1 macrophages and anti-inflammatory, regenerative M2 macrophages, the M1 macrophages appeared as early as 4 days after ACLR at the tendon-to-bone interface and led to the formation of a scar-tissue interface rather than the reformation of a normal insertion site. The M2 macrophages did not appear until day 11 after ACLR (Kawamura et al., 2005). Lui et al. (2015) have also reported that higher expressions of M1 macrophages, MMP1 and MMP13 at the peri-tunnel region were associated with greater peri-tunnel bone loss at the tibia after ACLR, and local administration of alendronate can reduce peri tunnel bone resorption, increase mineralized tissue inside bone tunnel probably by reducing the expression of MMP1, MMP13, and CD68-positive cells (Lui P. et al., 2013). Interestingly, the depletion of macrophages following ACLR significantly improved the histological and biomechanical properties of the healing tendon–bone interface (Hays et al., 2008) further supporting that macrophage-induced excessive inflammation caused poor graft healing after ACLR.

3.3 Tendon graft-to-bone tunnel motion

Besides, tendon graft motion inside the bone tunnel also induces an inflammatory response and is one of the mechanisms causing poor graft healing (Rodeo et al., 2006). It induces macrophage infiltration, increases inflammation, increases bone resorption, and impairs graft incorporation. In contrast, inhibition of early graft-to-bone tunnel motion reduces macrophage accumulation, reduces excessive inflammation, and promotes more effective graft incorporation. In this regard, graft healing in the femoral tunnel was inversely proportional to the magnitude of graft-tunnel motion. Daily low-magnitude cyclic axial load of ACL graft in the postoperative period induced greater infiltration of inflammatory macrophages and less bone formation in the bone tunnel compared with the immobilization group in a rat ACLR model (Brophy et al., 2011). On the contrary, there was better graft healing in the immobilization group compared with the graft healing in animals with normal cage activity. Graft failure at the intra-articular portion at a higher maximum load was observed in the immobilization group, whereas graft pullouts

at a lower maximum load were observed in the normal cage activity group (Sakai et al., 2000). In another study, there were fewer M1 macrophages, more M2 macrophages at the tendon–bone interface, smaller interface width, higher collagen fiber continuity, higher failure load, and higher stiffness in the immobilization group compared with the free-cage activity group post-ACLR (Dagher et al., 2009). Therefore, suppressing inflammation by stable graft fixation and early healing with reduced tendon graft-to-bone tunnel motion are both crucial to the success of ACLR.

However, immobilization alone does not provide all the appropriate signals to improve healing. Rather, delayed and controlled mechanical loading after an initial period of immobilization is needed. This is evident by the greater suppression of MMP activities at the graft-to-bone interface and better graft healing in animals immobilized for 5 days or 14 days post-ACLR compared with the MMP activities and graft healing in the animals without immobilization or prolonged immobilization (Nakagawa et al., 2019). In another study, there were significantly fewer inflammatory M1 macrophages and significantly more resident M2 macrophages at the healing graft-to-bone interface in the day-4 and -10 delayed-loading groups compared with the counts in the immediate-loading and prolonged immobilization groups at 2 and 4 weeks after ACLR. There were less scar tissue and more bone formation at the interface as well as higher mechanical strength of the reconstructed ACL complex in the delayed mobilization groups compared with the immediate-loading group and prolonged immobilization group (Packer et al., 2014). Tight control of the mechanical environment at the graft-to-bone tunnel interface is hence, crucial to the maintenance of an anti-inflammatory and regenerative environment favorable for graft healing.

4 AN INDUCTIVE APPROACH FOR DEVELOPING NEW BIOLOGICS FOR IMPROVING GRAFT HEALING

To tackle the problem of biological graft healing, we believe that an inductive approach should be adopted, starting from the optimal endpoint after ACLR, and even the results may not be achievable at present, followed by developing clinically practical strategies to achieve this ultimate target. This would help in refining the scope of the clinical problem and directing us to test for the right strategies.

The motivation for ACLR is to replace the damaged ligament with the tendon graft and transform it into a ligament. Ideally, the tunnel graft should mineralize and completely be replaced by bone with re-establishment of a fibrocartilage transition zone at the original footprints of ACL. Both angiogenesis and inflammation are known to regulate tissue repair. Consequently, we believe that strategies that can enhance osteogenesis at the bone tunnel, promote angiogenesis, and suppress inflammation at the knee and bone tunnels would promote graft healing after ACLR. To support our claim, a systematic review of literature examining the efficacy of biological therapies in the promotion of graft healing was performed (search strategy in **Supplementary Information S2**). The results showed that most (41/49, 83.7%) of the biologics with positive effects on graft healing have either osteogenic, angiogenic, or anti-inflammatory properties (**Table 2**).

4.1 Osteogenesis

As indicated, the tunnel graft should ideally be mineralized, and the fibrocartilage transition zone should be re-established at the original ACL footprints. The importance of bone formation at the early stage of healing is demonstrated by the positive correlation of the mechanical strength of bone-tendon junction with the amount of osseous ingrowth, mineralization, and maturation of healing tissue (Sun et al., 2019; Zhang et al., 2019). Our previous study has shown replacement of tendon graft by bone at some regions at the femoral tunnel and juxta-articular segment of the tibial tunnel in a rabbit ACLR model, and we believe that this may represent the ideal healing inside the bone tunnel (Lui et al., 2010).

In preclinical studies, osteoinductive factors, such as bone morphogenetic protein-2 (BMP-2) (Crispim et al., 2018), α-fibroblast growth factor (α-FGF) (Lu et al., 2018), basic fibroblast growth factor (bFGF) (Kimura et al., 2008), granulocyte colony-stimulating factor (G-CSF) (Sasaki et al., 2008), and transforming growth factor-β1 (TGF-β1) (Yamazaki et al., 2005) enhanced tunnel bone formation and, hence, promoted tendon graft-to-bone tunnel healing after ACLR (**Table 2**). Besides, cells like ACL-derived $CD34^+$ cell (Mifune et al., 2012; Mifune et al., 2013), tendon-derived stem cells (TDSCs) (Lui et al., 2014c), bone marrow-derived MSCs (BMSCs) (Hur et al., 2019), and adipose-derived stem cells (ADSCs) (Matsumoto et al., 2021) had been applied directly or made into cell sheets for the enhancement of bone formation after ACLR. These cells could release osteogenic factors and promote osteogenesis at the graft–bone interface. To enable the stable delivery and controlled release of osteogenic factors, both BMP-2 and TGF-β have been overexpressed in cells (Wang et al., 2010; Dong et al., 2012; Wang et al., 2017) to lengthen the therapeutic window and maximize their effect on bone formation. There was better tendon-to-bone integration and biomechanical properties of the bone–graft–bone complex in these groups compared with those in the control groups after ACLR. In consideration of the potential safety and difficulty in clinical application, weekly intra-articular injection of BMSC-conditioned medium (Sun et al., 2019) containing osteoinductive factors has been developed and is shown to promote tendon graft-to-bone tunnel integration and ligamentization after ACLR.

Clinically, platelet-rich plasma (PRP) containing osteogenic factors is frequently tested for the promotion of graft healing after ACLR with mixed results. It has been reported to prevent tunnel widening (Starantzis et al., 2014) and reduces the rate of revision of ACL surgery (Berdis et al., 2019). However, it has no significant effect on tunnel enlargement (Mirzatolooei et al., 2013; Vadalà et al., 2013) and graft incorporation (Silva and Sampaio, 2009) in

TABLE 2 | A summary of the nature and effects of biologics on graft healing after anterior cruciate ligament reconstruction (ACLR).

	Osteogenesis	Angiogenesis	Suppression of inflammation	Other mechanisms	Outcomes of graft healing (+/-/no effect)	Remarks	References
Animal Studies							
ADSC sheet	V				+	ADSCs stimulate bone-forming activities. ADSC sheets improved biomechanical strength, prevented bone tunnel enlargement, and promoted tendon–bone interface healing and graft remodeling in ACLR	Matsumoto et al. (2021)
BMSCs	V				+	BMSCs stimulate bone formation. It promoted graft osteointegration at the tendon–bone interface after ACLR	Hur et al. (2019)
BMP-2 Binding Peptides	V				+	The incorporation of BMP-2 binding peptides into materials used for ACLR enhanced bone formation and healing inside bone tunnels	Crispim et al. (2018)
BMSCs transfected with TGF-β gene	V				+	BMSCs are stem cells with osteogenic differentiation capacity. TGF-β is an osteogenic growth factor. BMSCs overexpressing TGF-β promoted tendon-to-bone healing after ACLR by upregulating the TGF-β/MAPK signaling pathway	Wang et al. (2017)
PRP + BMSCs	V				+	BMSC has osteogenic differentiation potential and PRP can stimulate this potential. PRP significantly stimulated osteogenic differentiation of BMSCs. The combination of PRP and BMSCs enhanced bone formation, maturation of graft-to-bone tunnel interface, and biomechanical properties of the bone–graft–bone complex	Teng et al. (2016)
SHMSP	V				+	SHMSP is an osteogenic factor. It enhanced tunnel bone formation after ACLR	Al-Bluwi et al. (2016)
AdTGF-β_1	V				+	TGF-β is an osteogenic growth factor. Hamstring tendon transfected with AdTGF-β_1 gene promoted healing of tendon–bone interface after ACLR	Wang et al. (2015b)
hUCB-MSCs	V				+	hUCB-MSCs enhanced tendon-bone healing through broad fibrocartilage formation with higher histological scores and decreased femoral and tibial tunnel widening compared with the control group	Jang et al. (2015)
BMSC infected with BMP-2 gene	V				+	BMSCs have osteogenic differentiation potential. BMP-2 can induce osteogenic and chondrogenic differentiation of pluripotent stem cells and bone progenitor cells. The transplantation of BMSCs genetically modified with BMP-2 enhanced the osseointegration of the tendon graft within the host bone	Dong et al. (2012)

(Continued on following page)

TABLE 2 | (*Continued*) A summary of the nature and effects of biologics on graft healing after anterior cruciate ligament reconstruction (ACLR).

	Osteogenesis	Angiogenesis	Suppression of inflammation	Other mechanisms	Outcomes of graft healing (+/-/no effect)	Remarks	References
Rat kidney cell line transduced with pCMV-BMP-2 gene	V				+	BMP-2 is an osteogenic growth factor. It enhanced osteogenesis at the tendon graft-to-bone tunnel interface after ACLR.	Wang et al. (2010)
PRP/DPB complex	V				+	The mixture of PRP/DPB enhanced chondrogenesis, Sharpey's fiber formation and graft incorporation into the bone tunnel at 60% PRP	Zhao and Zhai, (2010)
TGF-β1	V				+	TGF-β1 is an osteogenic growth factor. It enhanced tunnel bone formation	Yamazaki et al. (2005)
TGF-β+EGF	V				+	TGF-ß increases both collagen and noncollagenous protein synthesis. EGF stimulates fibroblast proliferation *in vitro*. Application of TGF-β and EGF improved the structural properties of the bone–graft–bone complex after ACLR	Yasuda et al. (2004)
Bone-derived extract (Bone Protein, Sulzer Biologics, Wheat Ridge, Colorado)	V				+	Bone-derived extract (Bone Protein, Sulzer Biologics, Wheat Ridge, Colorado) is effective in augmenting bone ingrowth. It improved healing of a tendon graft in a bone tunnel in an intra-articular ligament-reconstruction model	Anderson et al. (2001)
ACL-derived $CD34^+$ cell sheet transduced with VEGF gene or sFLT-1		V			+	ACL-derived $CD34^+$ cells expressing moderate levels of VEGF improved tendon graft maturation and biomechanical strength; however, $CD34^+$ overexpressing VEGF promoting excessive angiogenesis impeded graft healing and mechanical strength. The transplantation ACL-derived $CD34^+$ cell sheet secreting sFLT1, a soluble VEGF inhibitor decreased angiogenesis, delayed graft maturation, and decreased biomechanical strength of the bone–graft–bone complex	Takayama et al. (2015)
VEGF		V			–	VEGF is an angiogenic growth factor. Excessive angiogenesis reduced integrity and stiffness as well as increased laxity of graft	Yoshikawa et al. (2006)
PDGF-BB		V			+	PDGF has a positive effect on revascularization. The local long-term application of PDGF using a biodegradable drug delivery tool biomechanically and histologically improved free tendon graft remodeling after ACLR	Weiler et al. (2004)
Synovium-derived cells pre-treated with TGF-β1 or TGF-β1			V		+	The transplantation of synovium-derived cells cultured in TGF-β1 or TGF-β1 inhibited the deterioration of the intra-articular part of tendon graft after ACLR	Kondo et al. (2011)
PRP	V	V			+	PRP contains PDGF, VEGF, and TGF-β. It increased the bioactivity	Zhang et al. (2019)

(Continued on following page)

TABLE 2 | (*Continued*) A summary of the nature and effects of biologics on graft healing after anterior cruciate ligament reconstruction (ACLR).

	Osteogenesis	Angiogenesis	Suppression of inflammation	Other mechanisms	Outcomes of graft healing (+/-/no effect)	Remarks	References
						of the tendon–bone interface and resulted in histological improvement at the tendon–bone junction	
hBMSC-CM	V	V			+	hBMSC-CM contains a variety of growth factors, including TGF-β, VEGF, and IGF. It accelerated graft osteo-integration and mid-substance ligamentization after ACLR	Sun et al. (2019)
Muscle-Secreted Factors	V	V			+	Muscle-secreted factors influences revascularization and tendon–bone closure. Using a rat model of ACLR showed that conditioned media derived from human muscle tissue accelerated femoral tunnel closure, a key step for autograft integration	Ghebes et al. (2018)
α-FGF	V	V			+	α-FGF is a mitogenic factor of osteoblasts and chondrocytes as well as an angiogenic factor. It induced fibrocartilage formation at the tendon–bone interface after ACLR	Lu et al. (2018)
ACL-derived $CD34^+$ cells transduced with BMP-2	V	V			+	ACL-derived $CD34^+$ cells transduced with BMP-2 can stimulate angiogenesis and osteogenesis at the graft-bone interface. ACL-derived $CD34^+$ cells transduced with BMP-2 accelerated graft–bone integration after ACLR	Kawakami et al. (2017)
BMSCs and VEGF	V	V			+	BMSCs have osteogenic potential and VEGF promotes angiogenesis. All parameters using MRI, collagen type III expression, and biomechanical analysis of pullout strength of the graft showed that application of intra tunnel BM-MSCs and VEGF enhanced tendon-to-bone healing after ACLR	Setiawati et al. (2017)
BMSCs genetically modified with bFGF/BMP-2	V	V			+	bFGF can promote angiogenesis and BMP-2 has osteogenic potential. The addition of BMP-2 or bFGF by gene transfer resulted in better cellularity, new bone formation, and higher mechanical property, which contributed to the healing process after ACLR	Chen et al. (2016)
ADRC	V	V			+	ADRCs secrete significantly larger amounts of growth factors, such as VEGF, hepatocyte growth factor than BMSCs. Local administration of ADRCs promoted the early healing process at the tendon–bone junction, both histologically and mechanically, after ACLR	Kosaka et al. (2016)

(Continued on following page)

TABLE 2 | (*Continued*) A summary of the nature and effects of biologics on graft healing after anterior cruciate ligament reconstruction (ACLR).

	Osteogenesis	Angiogenesis	Suppression of inflammation	Other mechanisms	Outcomes of graft healing (+/-/no effect)	Remarks	References
Fibrin clot	V	V			+	Transplantation of fibrin clot improved graft healing as shown by histology and MRI	Hensler et al. (2015)
TDSC sheet	V	V			+	TDSCs are stem cells with osteogenic differentiation capacity. TDSC sheet expressed bFGF, TGF-β1 and BMP-2 which have angiogenic and osteogenic effects. The transplantation of TDSC sheet promoted bone formation, enhanced graft osteointegration and graft mid-substance integrity, as well as improved biomechanical properties of the bone–graft–bone complex	Lui et al. (2014c)
TGF-β1 plasmid in liposomes	V	V			+	TGF-β1 increases angiogenesis and induces fibroblast, monocyte, and macrophage migration to sites of injury, promoting ligament healing. Injection of TGF-β1 plasmid in liposomes into bone tunnel improved biomechanical characteristics of the bone–graft–bone complex	Qin et al. (2013)
ACL-derived $CD34^+$ cell sheet	V	V			+	$CD34^+$ cells are endothelial cells that secrete angiogenic and osteogenic factors. The transplantation of ACL-derived $CD34^+$ cell sheet enhanced healing of the bone–tendon junction and the grafted tendon by promoting proprioceptive recovery, graft maturation, and biomechanical strength. The outcomes were better after transplantation of the cell sheet compared with cell injection	Mifune et al. (2013)
ACL-derived $CD34^+$ cell	V	V			+	$CD34^+$ cells are endothelial cells which secrete angiogenic and osteogenic factors. Intracapsular injection of $CD34^+$ cells post-ACLR increased biomechanical strength of the bone–graft–bone complex *via* enhancement of angiogenesis and osteogenesis at graft-bone interface at early stage after ACLR	Mifune et al. (2012)
Platelet	V	V			+	Platelet contains PDGF, VEGF, and TGF-β. The addition of blood platelets resulted in significant reduction in anterior-posterior knee laxity after ACLR	Spindler et al. (2009)
G-CSF	V	V			+	G-CSF contributes to angiogenesis and osteogenesis. A local application of G-CSF-incorporated gelatin significantly accelerated bone-tendon interface strength *via* enhanced angiogenesis and osteogenesis	Sasaki et al. (2008)

(Continued on following page)

TABLE 2 | (*Continued*) A summary of the nature and effects of biologics on graft healing after anterior cruciate ligament reconstruction (ACLR).

	Osteogenesis	Angiogenesis	Suppression of inflammation	Other mechanisms	Outcomes of graft healing (+/-/no effect)	Remarks	References
Human Studies							
hUCB-MSCs	V				No effect	The transplantation of allogeneic hUCB-MSCs did not show any clinical advantage such as the prevention of tunnel enlargement, knee laxity, and clinical outcomes	Moon et al. (2021)
PRP	V				+	PRP contained bone growth factors. The administration of PRP decreased the rate of second ACL injury compared with the literature	Berdis et al. (2019)
PRP	V				No effect	The administration of PRP did not prevent tunnel enlargement after ACLR	Sözkesen et al. (2018)
PRP	V				+	PRP contained bone growth factors. The application of PRP prevented femoral tunnel widening in ACLR	Starantzis et al. (2014)
PRP	V				No effect	The application of PRP did not reduce tunnel enlargement after ACLR	Vadalà et al. (2013)
PRP	V				+	PRP contained bone growth factors. It enhanced the formation of focal areas of sclerotic cortical bone with subsequent fusion into a thick tibial tunnel wall after ACLR	Rupreht et al. (2013b)
PRP	V				No effect	The administration of PRP to bone tunnels reduced tunnel widening, but the difference was not statistically significant	Mirzatolooei et al. (2013)
PRP	V				No effect	PRP contained growth factors with osteogenic activities. There was no significant improvement in tendon graft incorporation to the bone tunnel after ACLR	Silva and Sampaio, (2009)
PRPG		V			+	PRPG contains PDGF. It decreased edema and increased vascularity at the tibial tunnel after ACLR	Rupreht et al. (2013a)
PG		V			+	PG contained PDGF. It enhanced vascularization at the tibial tunnel interface and intra-articular part of the graft	Vogrin et al. (2010)
PRF	V	V			No effect	The administration of PRF did not significantly improve graft failure and graft ligamentization up to 12 months post-ACLR	Zeman et al. (2018)
PRP	V	V			No effect	The administration of PRP did not accelerate graft interface healing and graft ligamentization after ACLR	Komzák et al. (2015)
PRFM	V	V			+	PRFM has a substantial amount of growth factors (such as TGF-β1, PDGF, VEGF). PRFM-augmented patients showed a statistically significant higher patient-reported knee function	Del Torto et al. (2015)
PRP	V	V			+	The administration of PRP accelerated graft mid-substance remodeling after ACLR.	Seijas et al. (2013)

(Continued on following page)

TABLE 2 | (*Continued*) A summary of the nature and effects of biologics on graft healing after anterior cruciate ligament reconstruction (ACLR).

	Osteogenesis	Angiogenesis	Suppression of inflammation	Other mechanisms	Outcomes of graft healing (+/-/no effect)	Remarks	References
PRP	V	V			+	PRP contained PDGF, TGF-β1, and VEGF which were osteogenic and angiogenic. The administration of PRP enhanced graft mid-substance remodeling compared with the untreated grafts	Sánchez et al. (2010)
ACS	V		V		+	ACS contains endogenous anti-inflammatory cytokines including IL-1Ra and growth factors (IGF-1, PDGF, and TGF-b1) in the liquid blood phase. Intra-articular administration of ACS decreased bone tunnel widening and reduced the level of IL-1β in the synovial fluid after ACLR	Darabos et al. (2011b)

Note. N.B.

ACS, autologous conditioned serum; ADSC, adipose derived stem cell; ADRC, adipose-derived regenerative cell; AdTGF-β1, adenovirus-mediated transforming growth factor β1; BMP-2, bone morphogenetic protein-2; BMSCs, bone marrow mesenchymal stem cells; hBMSC-CM, hBMSC–conditioned medium; pCMV, plasmid cytomegalo virus; DPB, deproteinized bone; EGF, epidermal growth factor; α-FGF, acidic fibroblast growth factor; bFGF, basic fibroblast growth factor; G-CSF, granulocyte colony-stimulating factor; HGF, hepatocyte growth factor; IGF-1, insulin-like growth factor-1; PDGF-BB, platelet-derived growth factor–BB; PG, platelet gel; PRPG, platelet-rich plasma gel; PRFM, platelet-rich fibrin matrix; PRF, platelet-rich fibrin; PRP, platelet-rich plasma; SHMSP, Sadat–Habdan mesenchymal stimulating peptide; TGF-β, transforming growth factor–β; TDSC, tendon-derived stem cell; hUCB-MSCs, umbilical cord blood-derived mesenchymal stem cells; VEGF, vascular endothelial growth factor.

other studies. This may be due to differences in study design (randomized controlled trials versus case series), PRP preparation, surgical procedures (single-bundle versus double-bundle and graft fixation methods), patient characteristics (adolescents versus adults), and rehabilitation protocols.

In summary, all pre-clinical studies have shown positive effects of osteoinductive factors on the promotion of bone formation and enhancement of tendon graft-to-bone tunnel healing, whereas the graft healing effect of PRP, which contain a complex mixture of bioactive proteins other than osteoinductive factors, remains controversial. More well-controlled studies are needed to confirm the effect of PRP on osteogenesis and graft healing after ACLR.

4.2 Angiogenesis

Adequate revascularization is critical for successful tendon graft-to-bone tunnel healing, by transporting MSCs and growth factors to the injury site. The infiltrated MSCs repopulate the tendon graft, release growth factors, produce collagen, and differentiated into cells of different lineages (bone, interface, or ligament) (Menetrey et al., 2008). Vascular endothelial growth factor (VEGF) has been shown to increase transiently, followed by blood vessel formation in the graft mid-substance at the early phase after ACLR in a rabbit model, suggesting that angiogenesis is involved in the early stage of graft mid-substance remodeling (Yoshikawa et al., 2006). On the other hand, low VEGF expression and vascularization were observed in tendon graft samples harvested in a patient with graft loosening in the second-look arthroscopy within the first year (Song et al., 2017), supporting that angiogenesis is important for successful graft mid-substance remodeling, in addition to tendon graft-to-bone tunnel healing.

The administration of angiogenic factors such as platelet-derived growth factor-BB (PDGF-BB) (Weiler et al., 2004), VEGF (Setiawati et al., 2017), and α-fibroblast growth factor (α-FGF) (Lu et al., 2018) has been reported to promote graft healing in different animal models of ACLR (**Table 2**). Furthermore, the application of cellular biologics in different forms, such as TDSCs (Lui et al., 2014c), ACL-derived $CD34^+$ cell sheet (Mifune et al., 2013), or BMSC-conditioned medium (Sun et al., 2019) containing angiogenic factors, also promoted angiogenesis and accelerated graft healing after ACLR. However, excessive angiogenesis has also been reported to negatively impact the integrity of tendon graft, decrease the biomechanics of the reconstructed ACL, and increase the graft laxity (Yoshikawa et al., 2006). Tight control of the treatment dose and time of angiogenic factors is, hence, required.

There has been a long-term interest in the application of PRP and its related-blood preparations for the promotion of graft healing due to its angiogenic components (Sánchez et al., 2010). The administration of PRP enhanced graft mid-substance remodeling in some clinical studies (Seijas et al., 2013; Zeman et al., 2018), supporting that angiogenesis might be the plausible mechanisms underlying their action. However, there are also studies reporting that PRP was

ineffective in the promotion of graft remodeling after ACLR (Komzák et al., 2015).

4.3 Suppression of inflammation

As discussed, inflammatory cytokines and fibrogenic growth factors contribute to the formation of a fibrous tissue interface between the graft and the bone tunnel at the early healing phase (Ekdahl et al., 2008). While the fibrous interface provides early mechanical support, it interferes with graft incorporation. Moreover, excessive inflammation causes bone tunnel widening, peri-tunnel bone loss, and graft degeneration. A correlation between M1 macrophage infiltration and graft loosening has been reported, while the depletion of inflammatory macrophages (Hays et al., 2008) promoted tendon graft-to-bone tunnel healing. In addition, intra-articular injection of alpha-2 macroglobulin, an MMP inhibitor, was reported to inhibit the enzymatic degradation of ACL after rupture in a rabbit model (Demirag et al., 2004). The collagen network was maintained, and the number of fibroblasts and fibrocytes was reduced in the ruptured ACL in the treatment group compared with that in the control group, supporting that suppression of inflammation can enhance graft integrity, which is crucial for providing mechanical strength of the ACL complex.

In our systematic search for biological interventions, only one preclinical study and one clinical study evaluating the efficacy of anti-inflammatory therapies could be identified. TGF-β1 is an anti-inflammatory growth factor. Kondo et al. transplanted TGF-β1-pretreated synovium-derived cells or TGF-β1 in a fibrin sealant sheet to a sheep ACLR model and found that both the pre-treated cells and TGF-β1 inhibited the deterioration of the intra-articular part of tendon graft with increased maximum load and stiffness of the bone–graft–bone complex at 12 weeks after reconstruction. Similar results were not observed after the transplantation of untreated cells in fibrin sealant sheet, suggesting that TGF-β1-inhibited graft degeneration is crucial for graft healing (Kondo et al., 2011), showing anti-inflammation effect. In a clinical study, intra-articular application of autologous conditioned serum (ACS) containing endogenous anti-inflammatory cytokines, including IL1Ra decreased bone tunnel widening after ACLR (Darabos et al., 2011a). The level of IL-1β in the synovial fluid of patients in the ACS group was significantly lower compared with that in the placebo group at early stage of ACLR, supporting that biological intervention, which inhibits intra-articular inflammation, can improve graft healing.

Despite the existence of clear evidence demonstrating the association of inflammation with poor healing outcomes (*Role of inflammation in influencing healing response* section), there has been relatively few original studies targeting inflammation in graft healing after ACLR compared with the number of studies investigating biological therapies targeting osteogenesis and angiogenesis. Improved understanding of the molecular mechanisms of inflammatory cells and cytokines in graft healing after ACLR would support the identification of new anti-inflammatory therapeutics.

5 PRACTICAL CONSIDERATIONS OF DEVELOPING BIOLOGICS FOR ANTERIOR CRUCIATE LIGAMENT RECONSTRUCTION—BRING IT CLOSER TO CLINICAL APPLICATION

While pre-clinical studies have shown positive effects of various biological therapies on graft healing, additional factors need to be considered for translating them into clinical practices. We suggested considering the following factors when developing new biologics at the early pre-clinical stage for generating clinically viable treatment strategies.

5.1 Compatibility with arthroscopy

Arthroscopy is a minimally invasive surgical procedure on a joint in which an arthroscope is inserted into the joint through a small incision to assist in knee examination and surgery. It is a common orthopedic procedure, and about 60,000 arthroscopic surgeries are performed annually in England only (Jameson et al., 2011). For arthroscopy-assisted ACLR, only two small incisions are made, one for the arthroscope and the other for the surgical instruments to be used in the knee cavity. This reduces recovery time due to trauma of the connective tissue. This is different from animal models of ACLR wherein an open surgery is usually performed. As arthroscopy-assisted ACLR is becoming the standard in clinical practice, and new interventions for improving graft healing must be compatible with arthroscopy. Strategies about how to deliver the biologic through the small incision in the presence of large volume of fluid during arthroscopy need to be developed for the clinical application of the biological therapy.

5.2 Localized and sustained intervention

As tendon graft-to-bone tunnel healing and graft mid-substance remodeling are complex healing processes with different endpoints (Ekdahl et al., 2008), localized and sustained interventions should be considered when developing new interventions. A carrier system that can localize the biologic to a specific site and supports its slow release is desired (Han et al., 2019). Collagen (Lu et al., 2018) and fibrin sealant (Kondo et al., 2011) were the carrier systems commonly used to deliver the biologics. Further studies on innovative carriers that can regulate the release of biologics consistent with the healing processes are needed.

5.3 Quality control

Various sources of cells have been used for ACLR (Wang et al., 2010; Wang et al., 2017; Hur et al., 2019). Issues related to the sources, purity, stability, storage condition, efficacy, safety, and delivery should be considered for clinical translation. MSC-based therapy is generally reported to be safe except in a few early reports wherein ectopic bone and tumor were observed in animal studies (Wang et al., 2015a; Zhong et al., 2017). Our previous study has shown that TDSCs are immune-privileged cells and might be used for allogeneic transplantation. Target TDSCs did not activate the immune system after immunization (Lui et al., 2014b). A low infiltration of T cells, M1 macrophages, M2 macrophages, and mast cells in the

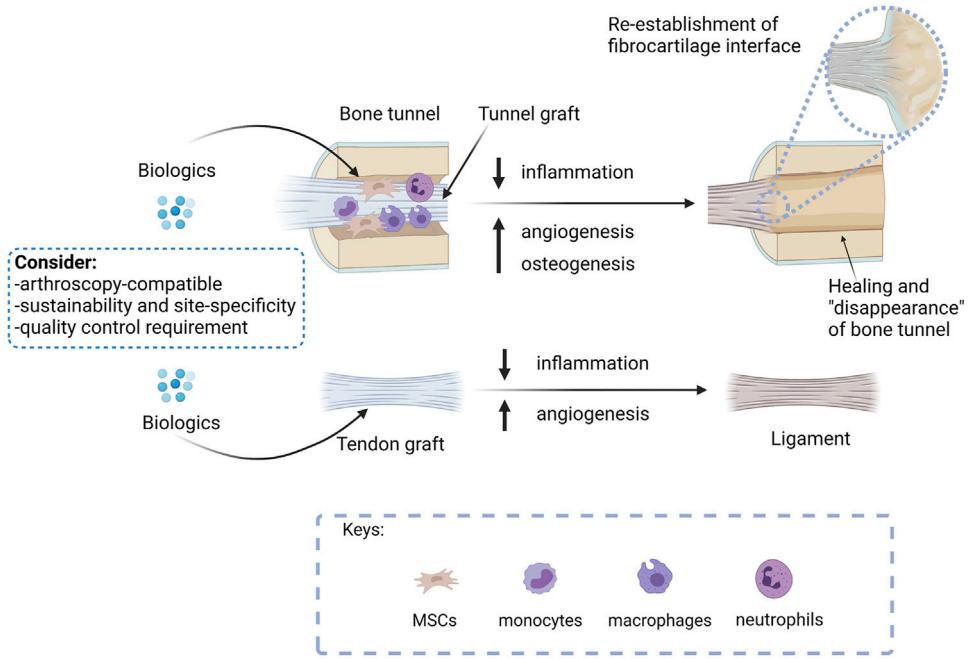

FIGURE 2 | A summary of the treatment approaches and considerations for developing a clinically viable biological therapy for the promotion of graft healing after ACLR. The ultimate goal of ACLR is to replace the tunnel graft by bone with re-establishment of direct insertion at the original ACL footprint and remodel the tendon graft mid-substances to a ligament to meet the functions of an ACL. Biologics that promote bone healing, therefore, should promote tunnel healing, while biologics that enhance angiogenesis are expected to accelerate both tunnel healing and graft remodeling. As inflammation hampers graft healing, biologics that suppress inflammation are anticipated to promote both tunnel healing and graft remodeling. Researches developing osteogenic, angiogenic, or anti-inflammatory biologicals should consider if the proposed intervention is arthroscopy compatible, supports sustainable and site-specific application, and meets quality control requirements for successful future clinical translation. Created with BioRender.com.

window wound was obtained after allogeneic TDSC transplantation to the tendon window wound (Lui et al., 2014a). A clinical-grade Good Manufacturing Practice-compliant (cGMP) stem cell bank and cell preparation protocol should be established for clinical application of stem cells for the augmentation of graft healing after ACLR.

PRP is another complex biological product that has been widely studied for the promotion of graft healing in ACLR both in preclinical and clinical studies with mixed results (Sözkesen et al., 2018; Berdis et al., 2019). There are different PRP preparations with different components including leukocyte-rich PRP, leukocyte-poor PRP, and platelet-rich plasma preparation rich in growth factors (PRGF) (Sánchez et al., 2010; Le et al., 2018). The standardization of PRP preparation with defined growth factor content is needed for its clinical translation.

Except pure proteins, biological therapies are usually complex products. In order to ensure their safety and efficacy in graft healing after ACLR, quality control is required. **Figure 2** summarizes the treatment approaches and considerations for developing a clinically viable biological therapy for the promotion of graft healing after ACLR.

6 CONCLUSION

The adoption of an inductive approach in the research and development of new biologics for improving graft healing after ACLR with the consideration of the feasibility of clinical translation would help in refining the scope of the clinical problem and directing the search for the right strategies.

The bone tunnels in ACLR are artificially created. The ultimate targets after ACLR are to replace the tunnel graft with bone with the re-establishment of a direct insertion at the original ACL footprints and remodeling of graft mid-substance to a functional ACL. However, the remodeling of graft mid-substance always fails due to its avascularity. In addition, there is amble evidence showing that excessive inflammation due to an increase in inflammatory cytokines in the synovial fluid after ACL injury, surgical trauma in ACLR, and graft-to-bone tunnel motion because of unstable fixation and slow healing contribute to tunnel widening, bone resorption, and graft mid-substance degeneration. Therefore, strategies that can promote osteogenesis, angiogenesis, and anti-inflammation have a good chance of enhancing graft healing. This claim is supported by the detrimental effects of excessive inflammation on the healing outcomes, and the osteogenic, angiogenetic, or anti-inflammatory properties of most of the biologics that showed positive effects on graft healing in a systematic literature search. To enhance the translational potential of a new biologic for graft healing, its compatibility with the standard ACL surgical procedures, such as arthroscopy, its localized and sustained release pattern, and its quality

control, are key issues to be considered as early as at the pre-clinical stage.

AUTHOR CONTRIBUTIONS

PL conceived the idea. SY and PL performed the literature search, interpreted the data, and drafted and finalized the manuscript. PY interpreted the data and revised the manuscript. All authors read and approved the final work.

SUPPLEMENTARY MATERIAL

The Supplementary Material for this article can be found online at: https://www.frontiersin.org/articles/10.3389/fbioe.2021.756930/full#supplementary-material

Supplementary Information 1 | Search strategy for articles examining the association of inflammation with poor outcome of ACL graft healing.

Supplementary Information 2 | Search strategy for articles examining the efficacy of biological therapies in the promotion of graft healing.

REFERENCES

Amiel, D., Frank, C., Harwood, F., Fronek, J., and Akeson, W. (1983). Tendons and Ligaments: a Morphological and Biochemical Comparison. *J. Orthop. Res.* 1 (3), 257–265. doi:10.1002/jor.1100010305

Anderson, K., Seneviratne, A. M., Izawa, K., Atkinson, B. L., Potter, H. G., and Rodeo, S. A. (2001). Augmentation of Tendon Healing in an Intraarticular Bone Tunnel with Use of a Bone Growth Factor. *Am. J. Sports Med.* 29 (6), 689–698. doi:10.1177/03635465010290060301

Berdis, A. S., Veale, K., and Fleissner, P. R., Jr. (2019). Outcomes of Anterior Cruciate Ligament Reconstruction Using Biologic Augmentation in Patients 21 Years of Age and Younger. *Arthrosc. J. Arthroscopic Relat. Surg.* 35 (11), 3107–3113. doi:10.1016/j.arthro.2019.05.047

Berg, E. E., Pollard, M. E., and Kang, Q. (2001). Interarticular Bone Tunnel Healing. *Arthrosc. J. Arthroscopic Relat. Surg.* 17 (2), 189–195. doi:10.1053/jars.2001.20958

Brophy, R. H., Kovacevic, D., Imhauser, C. W., Stasiak, M., Bedi, A., Fox, A. J., et al. (2011). Effect of Short-Duration Low-Magnitude Cyclic Loading versus Immobilization on Tendon-Bone Healing after ACL Reconstruction in a Rat Model. *The J. Bone Jt. Surgery-American Volume* 93 (4), 381–393. doi:10.2106/jbjs.I.00933

Chen, B., Li, B., Qi, Y.-J., Ni, Q.-B., Pan, Z.-Q., Wang, H., et al. (2016). Enhancement of Tendon-To-Bone Healing after Anterior Cruciate Ligament Reconstruction Using Bone Marrow-Derived Mesenchymal Stem Cells Genetically Modified with bFGF/BMP2. *Sci. Rep.* 6 (1). doi:10.1038/srep25940

Crispim, J. F., Fu, S. C., Lee, Y. W., Fernandes, H. A. M., Jonkheijm, P., Yung, P. S. H., et al. (2018). Bioactive Tape with BMP-2 Binding Peptides Captures Endogenous Growth Factors and Accelerates Healing after Anterior Cruciate Ligament Reconstruction. *Am. J. Sports Med.* 46 (12), 2905–2914. doi:10.1177/0363546518787507

Dagher, E., Hays, P. L., Kawamura, S., Godin, J., Deng, X.-h., and Rodeo, S. A. (2009). Immobilization Modulates Macrophage Accumulation in Tendon-Bone Healing. *Clin. Orthop. Relat. Res.* 467 (1), 281–287. doi:10.1007/s11999-008-0512-0

Darabos, N., Haspl, M., Moser, C., Darabos, A., Bartolek, D., and Groenemeyer, D. (2011a). Intraarticular Application of Autologous Conditioned Serum (ACS) Reduces Bone Tunnel Widening after ACL Reconstructive Surgery in a Randomized Controlled Trial. *Knee Surg. Sports Traumatol. Arthrosc.* 19 (Suppl. 1), 36–46. doi:10.1007/s00167-011-1458-4

Darabos, N., Haspl, M., Moser, C., Darabos, A., Bartolek, D., and Groenemeyer, D. (2011b). Intraarticular Application of Autologous Conditioned Serum (ACS) Reduces Bone Tunnel Widening after ACL Reconstructive Surgery in a Randomized Controlled Trial. *Knee Surg. Sports Traumatol. Arthrosc.* 19 (Suppl. 1), 36–46. doi:10.1007/s00167-011-1458-4

Del Torto, M., Enea, D., Panfoli, N., Filardo, G., Pace, N., and Chiusaroli, M. (2015). Hamstrings Anterior Cruciate Ligament Reconstruction with and without Platelet Rich Fibrin Matrix. *Knee Surg. Sports Traumatol. Arthrosc.* 23 (12), 3614–3622. doi:10.1007/s00167-014-3260-6

Demirag, B., Sarisozen, B., Durak, K., Blgen, Ö. F., and Ozturk, C. (2004). The Effect of Alpha-2 Macroglobulin on the Healing of Ruptured Anterior Cruciate Ligament in Rabbits. *Connect. Tissue Res.* 45 (1), 23–27. doi:10.1080/03008200490278115

Dong, Y., Zhang, Q., Li, Y., Jiang, J., and Chen, S. (2012). Enhancement of Tendon-Bone Healing for Anterior Cruciate Ligament (ACL) Reconstruction Using Bone Marrow-Derived Mesenchymal Stem Cells Infected with BMP-2. *Ijms* 13 (10), 13605–13620. doi:10.3390/ijms131013605

Duthon, V. B., Barea, C., Abrassart, S., Fasel, J. H., Fritschy, D., and Ménétrey, J. (2006). Anatomy of the Anterior Cruciate Ligament. *Knee Surg. Sports Traumatol. Arthrosc.* 14 (3), 204–213. doi:10.1007/s00167-005-0679-9

Ekdahl, M., Wang, J. H.-C., Ronga, M., and Fu, F. H. (2008). Graft Healing in Anterior Cruciate Ligament Reconstruction. *Knee Surg. Sports Traumatol. Arthr* 16 (10), 935–947. doi:10.1007/s00167-008-0584-0

Evans-Pickett, A., Longobardi, L., Spang, J. T., Creighton, R. A., Kamath, G., Davis–Wilson, H. C., et al. (2021a). Synovial Fluid Concentrations of Matrix Metalloproteinase-3 and Interluekin-6 Following Anterior Cruciate Ligament Injury Associate with Gait Biomechanics 6 Months Following Reconstruction. *Osteoarthritis and Cartilage* 29 (7), 1006–1019. doi:10.1016/j.joca.2021.03.014

Evans-Pickett, A., Longobardi, L., Spang, J. T., Creighton, R. A., Kamath, G., Davis–Wilson, H. C., et al. (2021b). Synovial Fluid Concentrations of Matrix Metalloproteinase-3 and Interluekin-6 Following Anterior Cruciate Ligament Injury Associate with Gait Biomechanics 6 Months Following Reconstruction. *Osteoarthritis and Cartilage* 29, 1006–1019. doi:10.1016/j.joca.2021.03.014

Fithian, D. C., Paxton, E. W., Stone, M. L., Luetzow, W. F., Csintalan, R. P., Phelan, D., et al. (2005). Prospective Trial of a Treatment Algorithm for the Management of the Anterior Cruciate Ligament-Injured Knee. *Am. J. Sports Med.* 33 (3), 335–346. doi:10.1177/0363546504269590

George, M. S., Dunn, W. R., and Spindler, K. P. (2006). Current Concepts Review: Revision Anterior Cruciate Ligament Reconstruction. *Am. J. Sports Med.* 34 (12), 2026–2037. doi:10.1177/0363546506295026

Ghebes, C. A., Groen, N., Cheuk, Y. C., Fu, S. C., Fernandes, H. M., and Saris, D. B. F. (2018). Muscle-Secreted Factors Improve Anterior Cruciate Ligament Graft Healing: An *In Vitro* and *In Vivo* Analysis. *Tissue Eng. A* 24 (3-4), 322–334. doi:10.1089/ten.TEA.2016.0546

Gupta, R., Khatri, S., Malhotra, A., Bachhal, V., Masih, G. D., and Kaur, J. (2021). Pre-operative Joint Inflammation Has No Bearing on Outcome of Arthroscopic Anterior Cruciate Ligament Reconstruction at 1-Year Follow-Up; a Prospective Study. *Joio* 55 (2), 360–367. doi:10.1007/s43465-020-00150-2

Han, L., Hu, Y. G., Jin, B., Xu, S. C., Zheng, X., and Fang, W. L. (2019). Sustained BMP-2 Release and Platelet Rich Fibrin Synergistically Promote Tendon-Bone Healing after Anterior Cruciate Ligament Reconstruction in Rat. *Eur. Rev. Med. Pharmacol. Sci.* 23 (20), 8705–8712. doi:10.26355/eurrev_201910_19264

Hays, P. L., Kawamura, S., Deng, X.-H., Dagher, E., Mithoefer, K., Ying, L., et al. (2008). The Role of Macrophages in Early Healing of a Tendon Graft in a Bone Tunnel. *J. Bone Jt. Surgery-American Volume* 90 (3), 565–579. doi:10.2106/jbjs.F.00531

Hensler, D., Illingworth, K. D., Musahl, V., Working, Z. M., Kobayashi, T., Miyawaki, M., et al. (2015). Does Fibrin Clot Really Enhance Graft Healing after Double-Bundle ACL Reconstruction in a Caprine Model? *Knee Surg. Sports Traumatol. Arthrosc.* 23 (3), 669–679. doi:10.1007/s00167-014-3380-z

Hunt, E. R., Jacobs, C. A., Conley, C. E. W., Ireland, M. L., Johnson, D. L., and Lattermann, C. (2021). Anterior Cruciate Ligament Reconstruction Reinitiates an Inflammatory and Chondrodegenerative Process in the Knee Joint. *J. Orthop. Res.* 39 (6), 1281–1288. doi:10.1002/jor.24783

Hur, C.-I., Ahn, H.-W., Seon, J.-K., Song, E.-K., and Kim, G.-E. (2019). Mesenchymal Stem Cells Decrease Tunnel Widening of Anterior Cruciate Ligament Reconstruction in Rabbit Model. *Ijsc* 12 (1), 162–169. doi:10.15283/ijsc18022

Inoue, M., Muneta, T., Ojima, M., Nakamura, K., Koga, H., Sekiya, I., et al. (2016). Inflammatory Cytokine Levels in Synovial Fluid 3, 4 Days Postoperatively and

its Correlation with Early-phase Functional Recovery after Anterior Cruciate Ligament Reconstruction: a Cohort Study. *J. Exp. Ortop* 3 (1), 30. doi:10.1186/s40634-016-0067-z

Irie, K., Uchiyama, E., and Iwaso, H. (2003). Intraarticular Inflammatory Cytokines in Acute Anterior Cruciate Ligament Injured Knee. *The Knee* 10 (1), 93–96. doi:10.1016/s0968-0160(02)00083-2

Jameson, S. S., Dowen, D., James, P., Serrano-Pedraza, I., Reed, M. R., and Deehan, D. J. (2011). The burden of Arthroscopy of the Knee. *The J. Bone Jt. Surg. Br. volume* 93-B, 1327–1333. doi:10.1302/0301-620x.93b10.27078

Jang, K.-M., Lim, H. C., Jung, W. Y., Moon, S. W., and Wang, J. H. (2015). Efficacy and Safety of Human Umbilical Cord Blood-Derived Mesenchymal Stem Cells in Anterior Cruciate Ligament Reconstruction of a Rabbit Model: New Strategy to Enhance Tendon Graft Healing. *Arthrosc. J. Arthroscopic Relat. Surg.* 31 (8), 1530–1539. doi:10.1016/j.arthro.2015.02.023

Kawakami, Y., Takayama, K., Matsumoto, T., Tang, Y., Wang, B., Mifune, Y., et al. (2017). Anterior Cruciate Ligament-Derived Stem Cells Transduced with BMP2 Accelerate Graft-Bone Integration after ACL Reconstruction. *Am. J. Sports Med.* 45 (3), 584–597. doi:10.1177/0363546516671707

Kawamura, S., Ying, L., Kim, H., Dynybil, C., and Rodeo, S. (2005). Macrophages Accumulate in the Early Phase of Tendon-Bone Healing. *J. Orthopaedic Res.* 23 (6), 1425–1432. doi:10.1016/j.orthres.2005.01.014

Kim, K.-O., Sim, J. A., Choi, J. U., Lee, B. K., and Park, H. G. (2020). The Effect of Interleukin-8 in the Early Stage after Anterior Cruciate Ligament Reconstruction with Remnant Preservation. *Knee Surg. Relat. Res.* 32 (1), 5. doi:10.1186/s43019-019-0024-0

Kimura, Y., Hokugo, A., Takamoto, T., Tabata, Y., and Kurosawa, H. (2008). Regeneration of Anterior Cruciate Ligament by Biodegradable Scaffold Combined with Local Controlled Release of Basic Fibroblast Growth Factor and Collagen Wrapping. *Tissue Eng. C: Methods* 14 (1), 47–57. doi:10.1089/tec.2007.0286

Komzák, M., Hart, R., Šmíd, P., Puskeiler, M., and Jajtner, P. (2015). The Effect of Platelet-Rich Plasma on Graft Healing in Reconstruction of the Anterior Cruciate Ligament of the Knee Joint: Prospective Study. *Acta Chir Orthop. Traumatol. Cech* 82 (2), 135–139.

Kondo, E., Yasuda, K., Katsura, T., Hayashi, R., Azuma, C., and Tohyama, H. (2011). Local Administration of Autologous Synovium-Derived Cells Improve the Structural Properties of Anterior Cruciate Ligament Autograft Reconstruction in Sheep. *Am. J. Sports Med.* 39 (5), 999–1007. doi:10.1177/0363546510390424

Kosaka, M., Nakase, J., Hayashi, K., and Tsuchiya, H. (2016). Adipose-Derived Regenerative Cells Promote Tendon-Bone Healing in a Rabbit Model. *Arthrosc. J. Arthroscopic Relat. Surg.* 32 (5), 851–859. doi:10.1016/j.arthro.2015.10.012

Larsson, S., Struglics, A., Lohmander, L. S., and Frobell, R. (2017). Surgical Reconstruction of Ruptured Anterior Cruciate Ligament Prolongs Trauma-Induced Increase of Inflammatory Cytokines in Synovial Fluid: an Exploratory Analysis in the KANON Trial. *Osteoarthritis and Cartilage* 25 (9), 1443–1451. doi:10.1016/j.joca.2017.05.009

Lattermann, C., Conley, C. E.-W., Johnson, D. L., Reinke, E. K., Huston, L. J., Huebner, J. L., et al. (2018). Select Biomarkers on the Day of Anterior Cruciate Ligament Reconstruction Predict Poor Patient-Reported Outcomes at 2-Year Follow-Up: A Pilot Study. *Biomed. Res. Int.* 2018, 1–9. doi:10.1155/2018/9387809

Le, A. D. K., Enweze, L., DeBaun, M. R., and Dragoo, J. L. (2018). Current Clinical Recommendations for Use of Platelet-Rich Plasma. *Curr. Rev. Musculoskelet. Med.* 11 (4), 624–634. doi:10.1007/s12178-018-9527-7

Liu, S. H., Panossian, V., al-Shaikh, R., Tomin, E., Shepherd, E., Finerman, G. A., et al. (1997). Morphology and Matrix Composition during Early Tendon to Bone Healing. *Clin. Orthopaedics Relat. Res.* 339, 253–260. doi:10.1097/00003086-199706000-00034

Lu, D., Yang, C., Zhang, Z., and Xiao, M. (2018). Enhanced Tendon-Bone Healing with Acidic Fibroblast Growth Factor Delivered in Collagen in a Rabbit Anterior Cruciate Ligament Reconstruction Model. *J. Orthop. Surg. Res.* 13 (1), 301. doi:10.1186/s13018-018-0984-x

Lui, P., Lee, Y. W., Lee, Y., Mok, T., Cheuk, Y., and Chan, K. (2013a). Alendronate Reduced Peri-Tunnel Bone Loss and Enhanced Tendon Graft to Bone Tunnel Healing in Anterior Cruciate Ligament Reconstruction. *eCM* 25, 78–96. doi:10.22203/ecm.v025a06

Lui, P. P. Y., Ho, G., Shum, W. T., Lee, Y. W., Ho, P. Y., Lo, W. N., et al. (2010). Inferior Tendon Graft to Bone Tunnel Healing at the Tibia Compared to that at the Femur after Anterior Cruciate Ligament Reconstruction. *J. Orthopaedic Sci.* 15 (3), 389–401. doi:10.1007/s00776-010-1460-6

Lui, P. P. Y., Kong, S. K., Lau, P. M., Wong, Y. M., Lee, Y. W., Tan, C., et al. (2014a). Allogeneic Tendon-Derived Stem Cells Promote Tendon Healing and Suppress Immunoreactions in Hosts: *In Vivo* Model. *Tissue Eng. Part A* 20 (21-22), 2998–3009. doi:10.1089/ten.TEA.2013.0713

Lui, P. P. Y., Kong, S. K., Lau, P. M., Wong, Y. M., Lee, Y. W., Tan, C., et al. (2014b). Immunogenicity and Escape Mechanisms of Allogeneic Tendon-Derived Stem Cells. *Tissue Eng. Part A* 20 (21-22), 3010–3020. doi:10.1089/ten.TEA.2013.0714

Lui, P. P. Y., Lee, Y. W., Mok, T. Y., and Cheuk, Y. C. (2013b). Local Administration of Alendronate Reduced Peri-Tunnel Bone Loss and Promoted Graft-Bone Tunnel Healing with Minimal Systemic Effect on Bone in Contralateral Knee. *J. Orthop. Res.* 31 (12), 1897–1906. doi:10.1002/jor.22442

Lui, P. P. Y., Lee, Y. W., Mok, T. Y., and Cheuk, Y. C. (2015). Peri-tunnel Bone Loss: Does it Affect Early Tendon Graft to Bone Tunnel Healing after ACL Reconstruction? *Knee Surg. Sports Traumatol. Arthrosc.* 23 (3), 740–751. doi:10.1007/s00167-013-2697-3

Lui, P. P. Y., Wong, O. T., and Lee, Y. W. (2014c). Application of Tendon-Derived Stem Cell Sheet for the Promotion of Graft Healing in Anterior Cruciate Ligament Reconstruction. *Am. J. Sports Med.* 42 (3), 681–689. doi:10.1177/0363546513517539

Marumo, K., Saito, M., Yamagishi, T., and Fujii, K. (2005). The "Ligamentization" Process in Human Anterior Cruciate Ligament Reconstruction with Autogenous Patellar and Hamstring Tendons. *Am. J. Sports Med.* 33 (8), 1166–1173. doi:10.1177/0363546504271973

Mather, R. C., 3rd, Koenig, L., Kocher, M. S., Dall, T. M., Gallo, P., Scott, D. J., et al. (2013). Societal and Economic Impact of Anterior Cruciate Ligament Tears. *J. Bone Jt. Surg Am* 95 (19), 1751–1759. doi:10.2106/JBJS.L.01705

Matsumoto, T., Sato, Y., Kobayashi, T., Suzuki, K., Kimura, A., Soma, T., et al. (2021). Adipose-Derived Stem Cell Sheets Improve Early Biomechanical Graft Strength in Rabbits after Anterior Cruciate Ligament Reconstruction. *Am. J. Sports Med.* 49, 3508–3518. 3635465211041582. doi:10.1177/03635465211041582

Ménétrey, J., Duthon, V. B., Laumonier, T., and Fritschy, D. (2008). "Biological Failure" of the Anterior Cruciate Ligament Graft. *Knee Surg. Sports Traumatol. Arthr* 16 (3), 224–231. doi:10.1007/s00167-007-0474-x

Mifune, Y., Matsumoto, T., Ota, S., Nishimori, M., Usas, A., Kopf, S., et al. (2012). Therapeutic Potential of Anterior Cruciate Ligament-Derived Stem Cells for Anterior Cruciate Ligament Reconstruction. *Cel Transpl.* 21 (8), 1651–1665. doi:10.3727/096368912x647234

Mifune, Y., Matsumoto, T., Takayama, K., Terada, S., Sekiya, N., Kuroda, R., et al. (2013). Tendon Graft Revitalization Using Adult Anterior Cruciate Ligament (ACL)-derived CD34+ Cell Sheets for ACL Reconstruction. *Biomaterials* 34 (22), 5476–5487. doi:10.1016/j.biomaterials.2013.04.013

Mirzatolooei, F., Alamdari, M. T., and Khalkhali, H. R. (2013). The Impact of Platelet-Rich Plasma on the Prevention of Tunnel Widening in Anterior Cruciate Ligament Reconstruction Using Quadrupled Autologous Hamstring Tendon. *Bone Jt. J.* 95-b (1), 65–69. doi:10.1302/0301-620x.95b1.30487

Moon, S. W., Park, S., Oh, M., and Wang, J. H. (2021). Outcomes of Human Umbilical Cord Blood-Derived Mesenchymal Stem Cells in Enhancing Tendon-Graft Healing in Anterior Cruciate Ligament Reconstruction: an Exploratory Study. *Knee Surg. Relat. Res.* 33 (1), 32. doi:10.1186/s43019-021-00104-4

Musahl, V., and Karlsson, J. (2019). Anterior Cruciate Ligament Tear. *N. Engl. J. Med.* 380 (24), 2341–2348. doi:10.1056/NEJMcp1805931

Nakagawa, Y., Lebaschi, A. H., Wada, S., Green, S. J. E., Wang, D., Album, Z. M., et al. (2019). Duration of Postoperative Immobilization Affects MMP Activity at the Healing Graft-Bone Interface: Evaluation in a Mouse ACL Reconstruction Model. *J. Orthop. Res.* 37 (2), 325–334. doi:10.1002/jor.24177

Øiestad, B. E., Engebretsen, L., Storheim, K., and Risberg, M. A. (2009). Winner of the 2008 Systematic Review Competition: Knee Osteoarthritis after Anterior Cruciate Ligament Injury. *Am. J. Sports Med.* 37 (7), 1434–1443. doi:10.1177/0363546509338827

Packer, J. D., Bedi, A., Fox, A. J., Gasinu, S., Imhauser, C. W., Stasiak, M., et al. (2014). Effect of Immediate and Delayed High-Strain Loading on Tendon-To-Bone Healing after Anterior Cruciate Ligament Reconstruction. *J. Bone Jt. Surg Am* 96 (9), 770–777. doi:10.2106/JBJS.L.01354

Petersen, W., and Laprell, H. (2000). Insertion of Autologous Tendon Grafts to the Bone: a Histological and Immunohistochemical Study of Hamstring and Patellar Tendon Grafts. *Knee Surg. Sports Traumatol. Arthrosc.* 8 (1), 26–31. doi:10.1007/s001670050006

Pietrosimone, B., Loeser, R. F., Blackburn, J. T., Padua, D. A., Harkey, M. S., Stanley, L. E., et al. (2017). Biochemical Markers of Cartilage Metabolism Are Associated with Walking Biomechanics 6-months Following Anterior Cruciate Ligament Reconstruction. *J. Orthop. Res.* 35 (10), 2288–2297. doi:10.1002/jor.23534

Qin, J., Hou, Z.-Q., Wang, H., Wang, X.-L., Liu, Y.-Y., Gao, X.-H., et al. (2013). Effects of Gene-Activated Matrix on Autograft Healing of Anterior Cruciate Ligament. *Mol. Med. Rep.* 7 (2), 679–683. doi:10.3892/mmr.2012.1211

Rodeo, S. A., Kawamura, S., Kim, H.-J., Dynybil, C., and Ying, L. (2006). Tendon Healing in a Bone Tunnel Differs at the Tunnel Entrance versus the Tunnel Exit. *Am. J. Sports Med.* 34 (11), 1790–1800. doi:10.1177/0363546506290059

Rupreht, M., Jevtič, V., Serša, I., Vogrin, M., and Jevšek, M. (2013a). Evaluation of the Tibial Tunnel after Intraoperatively Administered Platelet-Rich Plasma Gel during Anterior Cruciate Ligament Reconstruction Using Diffusion Weighted and Dynamic Contrast-Enhanced MRI. *J. Magn. Reson. Imaging* 37 (4), 928–935. doi:10.1002/jmri.23886

Rupreht, M., Vogrin, M., and Hussein, M. (2013b). MRI Evaluation of Tibial Tunnel wall Cortical Bone Formation after Platelet-Rich Plasma Applied during Anterior Cruciate Ligament Reconstruction. *Radiol. Oncol.* 47 (2), 119–124. doi:10.2478/raon-2013-0009

Sadat-Ali, M., Al-Bluwi, M., and Azam, M. Q. (2016). The Effect of Bone Growth Factor in the Tendon to Bone Healing in Anterior Cruciate Ligament Reconstruction: An Experimental Study in Rabbits. *Int. J. App Basic Med. Res.* 6 (1), 23–27. doi:10.4103/2229-516x.174004

Sakai, H., Naoshi, F., Kawakami, A., and Kurosawa, H. (2000). Biological Fixation of the Graft within Bone after Anterior Cruciate Ligament Reconstruction in Rabbits: Effects of the Duration of Postoperative Immobilization. *J. Orthopaedic Sci.* 5 (1), 43–51. doi:10.1007/s007760050007

Sánchez, M., Anitua, E., Azofra, J., Prado, R., Muruzabal, F., and Andia, I. (2010). Ligamentization of Tendon Grafts Treated with an Endogenous Preparation Rich in Growth Factors: Gross Morphology and Histology. *Arthrosc. J. Arthroscopic Relat. Surg.* 26 (4), 470–480. doi:10.1016/j.arthro.2009.08.019

Sasaki, K., Kuroda, R., Ishida, K., Kubo, S., Matsumoto, T., Mifune, Y., et al. (2008). Enhancement of Tendon-Bone Osteointegration of Anterior Cruciate Ligament Graft Using Granulocyte colony-stimulating Factor. *Am. J. Sports Med.* 36 (8), 1519–1527. doi:10.1177/0363546508316282

Scheffler, S. U., Unterhauser, F. N., and Weiler, A. (2008). Graft Remodeling and Ligamentization after Cruciate Ligament Reconstruction. *Knee Surg. Sports Traumatol. Arthr* 16 (9), 834–842. doi:10.1007/s00167-008-0560-8

Seijas, R., Ares, O., Catala, J., Alvarez-Diaz, P., Cusco, X., and Cugat, R. (2013). Magnetic Resonance Imaging Evaluation of Patellar Tendon Graft Remodelling after Anterior Cruciate Ligament Reconstruction with or without Platelet-Rich Plasma. *J. Orthop. Surg. (Hong Kong)* 21 (1), 10–14. doi:10.1177/230949901302100105

Setiawati, R., Utomo, D. N., Rantam, F. A., Ifran, N. N., and Budhiparama, N. C. (2017). Early Graft Tunnel Healing after Anterior Cruciate Ligament Reconstruction with Intratunnel Injection of Bone Marrow Mesenchymal Stem Cells and Vascular Endothelial Growth Factor. *Orthopaedic J. Sports Med.* 5 (6), 232596711770854. doi:10.1177/2325967117708548

Sherman, S., Raines, B., and Naclerio, E. (2017). Management of Anterior Cruciate Ligament Injury? What's in and What's Out? *Indian J. Orthop.* 51 (5), 563–575. doi:10.4103/ortho.IJOrtho_245_17

Silva, A., and Sampaio, R. (2009). Anatomic ACL Reconstruction: Does the Platelet-Rich Plasma Accelerate Tendon Healing? *Knee Surg. Sports Traumatol. Arthrosc.* 17 (6), 676–682. doi:10.1007/s00167-009-0762-8

Silva, F., Ribeiro, F., and Oliveira, J. (2012). Effect of an Accelerated ACL Rehabilitation Protocol on Knee Proprioception and Muscle Strength after Anterior Cruciate Ligament Reconstruction. *Aehd* 3, 139–144. doi:10.5628/aehd.v3i1-2.113

Song, B., Jiang, C., Luo, H., Chen, Z., Hou, J., Zhou, Y., et al. (2017). Macrophage M1 Plays a Positive Role in Aseptic Inflammation-Related Graft Loosening after Anterior Cruciate Ligament Reconstruction Surgery. *Inflammation* 40 (6), 1815–1824. doi:10.1007/s10753-017-0616-3

Sözkesen, S., Karahan, H. G., Kurtulmus, A., Kayali, C., and Altay, T. (2018). PRP on Preventıon of Tunnel Enlargement in ACL Reconstructıon. *Ortop Traumatol. Rehabil.* 20 (4), 285–291. doi:10.5604/01.3001.0012.6462

Spindler, K. P., Murray, M. M., Carey, J. L., Zurakowski, D., and Fleming, B. C. (2009). The Use of Platelets to Affect Functional Healing of an Anterior Cruciate Ligament (ACL) Autograft in a Caprine ACL Reconstruction Model. *J. Orthop. Res.* 27 (5), 631–638. doi:10.1002/jor.20785

Starantzis, K. A., Mastrokalos, D., Koulalis, D., Papakonstantinou, O., Soucacos, P. N., and Papagelopoulos, P. J. (20142014). The Potentially Positive Role of PRPs in Preventing Femoral Tunnel Widening in ACL Reconstruction Surgery Using Hamstrings: A Clinical Study in 51 Patients. *J. Sports Med.* 2014, 1–10. doi:10.1155/2014/789317

Stolarz, M., Ficek, K., Binkowski, M., and Wróbel, Z. (2017). Bone Tunnel Enlargement Following Hamstring Anterior Cruciate Ligament Reconstruction: a Comprehensive Review. *The Physician and Sportsmedicine* 45 (1), 31–40. doi:10.1080/00913847.2017.1253429

Sun, Y., Chen, W., Hao, Y., Gu, X., Liu, X., Cai, J., et al. (2019). Stem Cell-Conditioned Medium Promotes Graft Remodeling of Midsubstance and Intratunnel Incorporation after Anterior Cruciate Ligament Reconstruction in a Rat Model. *Am. J. Sports Med.* 47 (10), 2327–2337. doi:10.1177/0363546519859324

Takayama, K., Kawakami, Y., Mifune, Y., Matsumoto, T., Tang, Y., Cummins, J. H., et al. (2015). The Effect of Blocking Angiogenesis on Anterior Cruciate Ligament Healing Following Stem Cell Transplantation. *Biomaterials* 60, 9–19. doi:10.1016/j.biomaterials.2015.03.036

Teng, C., Zhou, C., Xu, D., and Bi, F. (2016). Combination of Platelet-Rich Plasma and Bone Marrow Mesenchymal Stem Cells Enhances Tendon-Bone Healing in a Rabbit Model of Anterior Cruciate Ligament Reconstruction. *J. Orthop. Surg. Res.* 11 (1), 96. doi:10.1186/s13018-016-0433-7

Vadalà, A., Iorio, R., De Carli, A., Ferretti, M., Paravani, D., Caperna, L., et al. (2013). Platelet-rich Plasma: Does it Help Reduce Tunnel Widening after ACL Reconstruction? *Knee Surg. Sports Traumatol. Arthrosc.* 21 (4), 824–829. doi:10.1007/s00167-012-1980-z

Vogrin, M., Rupreht, M., Crnjac, A., Dinevski, D., Krajnc, Z., and Rečnik, G. (2010). The Effect of Platelet-Derived Growth Factors on Knee Stability after Anterior Cruciate Ligament Reconstruction: A Prospective Randomized Clinical Study. *Wien Klin Wochenschr* 122 (Suppl. 2), 91–95. doi:10.1007/s00508-010-1340-2

Wall, A., and Board, T. (2014). Tendon Healing in a Bone Tunnel: A Biomechanical and Histological Study in the Dog. *Classic Pap. Orthopaedics*, 453–456. doi:10.1007/978-1-4471-5451-8_115

Wang, C.-J., Weng, L.-H., Hsu, S.-L., Sun, Y.-C., Yang, Y.-J., Chan, Y.-S., et al. (2010). pCMV-BMP-2-transfected Cell-Mediated Gene Therapy in Anterior Cruciate Ligament Reconstruction in Rabbits. *Arthrosc. J. Arthroscopic Relat. Surg.* 26 (7), 968–976. doi:10.1016/j.arthro.2009.11.014

Wang, R., Xu, B., and Xu, H.-G. (2017). Up-Regulation of TGF-β Promotes Tendon-To-Bone Healing after Anterior Cruciate Ligament Reconstruction Using Bone Marrow-Derived Mesenchymal Stem Cells through the TGF-β/MAPK Signaling Pathway in a New Zealand White Rabbit Model. *Cell Physiol Biochem* 41 (1), 213–226. doi:10.1159/000456046

Wang, W., Zhong, W., Yuan, J., Yan, C., Hu, S., Tong, Y., et al. (2015a). Involvement of Wnt/β-Catenin Signaling in the Mesenchymal Stem Cells Promote Metastatic Growth and Chemoresistance of Cholangiocarcinoma. *Oncotarget* 6 (39), 42276–42289. doi:10.18632/oncotarget.5514

Wang Xiaoxu, X., Zhai, R., Yang Juntao, J., Zhou, S., Tan, W., and Tan, G. (2015b). Effect of Hamstring Tendon Transfected with Adenovirus- Mediated Transforming Growth Factor B_1 Gene on Histomorphology of Tendon-Bone Interface Healing after Anterior Cruciate Ligament Reconstruction in Rabbits. *Zhongguo Xiu Fu Chong Jian Wai Ke Za Zhi* 29 (12), 1488–1493.

Weiler, A., Förster, C., Hunt, P., Falk, R., Jung, T., Unterhauser, F. N., et al. (2004). The Influence of Locally Applied Platelet-Derived Growth Factor-BB on Free

Tendon Graft Remodeling after Anterior Cruciate Ligament Reconstruction. *Am. J. Sports Med.* 32 (4), 881–891. doi:10.1177/0363546503261711

Wen, C.-Y., Qin, L., Lee, K.-M., Wong, M. W.-N., and Chan, K.-M. (2010). Grafted Tendon Healing in Tibial Tunnel Is Inferior to Healing in Femoral Tunnel after Anterior Cruciate Ligament Reconstruction: a Histomorphometric Study in Rabbits. *Arthrosc. J. Arthroscopic Relat. Surg.* 26 (1), 58–66. doi:10.1016/j.arthro.2009.06.025

Yamazaki, S., Yasuda, K., Tomita, F., Tohyama, H., and Minami, A. (2005). The Effect of Transforming Growth Factor-B1 on Intraosseous Healing of Flexor Tendon Autograft Replacement of Anterior Cruciate Ligament in Dogs. *Arthrosc. J. Arthroscopic Relat. Surg.* 21 (9), 1034–1041. doi:10.1016/j.arthro.2005.05.011

Yang, R., Zhang, Z., Song, B., Wang, P., Wang, L., Li, W., et al. (2012). Ratio of T Helper to Regulatory T Cells in Synovial Fluid and Postoperative Joint Laxity after Allograft Anterior Cruciate Ligament Reconstruction. *Transplantation* 94 (11), 1160–1166. doi:10.1097/TP.0b013e31826dddeb

Yasuda, K., Tomita, F., Yamazaki, S., Minami, A., and Tohyama, H. (2004). The Effect of Growth Factors on Biomechanical Properties of the Bone-Patellar Tendon-Bone Graft after Anterior Cruciate Ligament Reconstruction. *Am. J. Sports Med.* 32 (4), 870–880. doi:10.1177/0363546503261695

Yoshikawa, T., Tohyama, H., Katsura, T., Kondo, E., Kotani, Y., Matsumoto, H., et al. (2006). Effects of Local Administration of Vascular Endothelial Growth Factor on Mechanical Characteristics of the Semitendinosus Tendon Graft after Anterior Cruciate Ligament Reconstruction in Sheep. *Am. J. Sports Med.* 34 (12), 1918–1925. doi:10.1177/0363546506294469

Yunes, M., Richmond, J. C., Engels, E. A., and Pinczewski, L. A. (2001). Patellar versus Hamstring Tendons in Anterior Cruciate Ligament Reconstruction. *Arthrosc. J. Arthroscopic Relat. Surg.* 17 (3), 248–257. doi:10.1053/jars.2001.21242

Yung, P. S.-H., Lee, Y.-W., Fu, S.-C., Chen, C.-H., Rolf, C. G., and Chan, K.-M. (2020). Differential MMP 1 and MMP 13 Expression in Proliferation and Ligamentization Phases of Graft Remodeling in Anterior Cruciate Ligament Reconstruction. *Connect. Tissue Res.*, 1–8. doi:10.1080/03008207.2020.1862806

Zantop, T., Petersen, W., Sekiya, J. K., Musahl, V., and Fu, F. H. (2006). Anterior Cruciate Ligament Anatomy and Function Relating to Anatomical Reconstruction. *Knee Surg. Sports Traumatol. Arthrosc.* 14 (10), 982–992. doi:10.1007/s00167-006-0076-z

Zeman, P., Kasl, J., Tupý, R., Frei, R., Kott, O., and Kautzner, J. (2018). Evaluation of the MRI Findings on a Tendon Graft after the Anatomic Anterior Cruciate Ligament Reconstruction in Patients with versus without the Application of Platelet-Rich Fibrin - Results of the Prospective Randomised Study. *Acta Chir Orthop. Traumatol. Cech* 85 (5), 343–350.

Zhang, M., Zhen, J., Zhang, X., Yang, Z., Zhang, L., Hao, D., et al. (2019). Effect of Autologous Platelet-Rich Plasma and Gelatin Sponge for Tendon-To-Bone Healing after Rabbit Anterior Cruciate Ligament Reconstruction. *Arthrosc. J. Arthroscopic Relat. Surg.* 35 (5), 1486–1497. doi:10.1016/j.arthro.2018.11.014

Zhao, Y., and Zhai, W. (2010). Histological Observation of Tendon-Bone Healing after Anterior Cruciate Ligament Reconstruction by Platelet-Rich Plasma Combined with Deproteinized Bone of Calf. *Zhongguo Xiu Fu Chong Jian Wai Ke Za Zhi* 24 (11), 1323–1329.

Zhong, W., Tong, Y., Li, Y., Yuan, J., Hu, S., Hu, T., et al. (2017). Mesenchymal Stem Cells in Inflammatory Microenvironment Potently Promote Metastatic Growth of Cholangiocarcinoma via Activating Akt/NF-Kb Signaling by Paracrine CCL5. *Oncotarget* 8 (43), 73693–73704. doi:10.18632/oncotarget.17793

Zysk, S. P., Fraunberger, P., Veihelmann, A., Dörger, M., Kalteis, T., Maier, M., et al. (2004). Tunnel Enlargement and Changes in Synovial Fluid Cytokine Profile Following Anterior Cruciate Ligament Reconstruction with Patellar Tendon and Hamstring Tendon Autografts. *Knee Surg. Sports Traumatol. Arthrosc.* 12 (2), 98–103. doi:10.1007/s00167-003-0426-z

Conflict of Interest: The authors declare that the research was conducted in the absence of any commercial or financial relationships that could be construed as a potential conflict of interest.

frontiers in Bioengineering and Biotechnology

REVIEW
published: 05 January 2022
doi: 10.3389/fbioe.2021.777039

Three-Dimensional Printing Strategies for Irregularly Shaped Cartilage Tissue Engineering: Current State and Challenges

Hui Wang[1], Zhonghan Wang[1], He Liu[1], Jiaqi Liu[1], Ronghang Li[1], Xiujie Zhu[1], Ming Ren[1], Mingli Wang[1], Yuzhe Liu[1], Youbin Li[1], Yuxi Jia[1], Chenyu Wang[2]* and Jincheng Wang[1]**

[1]Orthopaedic Medical Center, The Second Hospital of Jilin University, Changchun, China, [2]Department of Plastic and Reconstructive Surgery, The First Hospital of Jilin University, Changchun, China

OPEN ACCESS

Edited by:
Laura Creemers,
University Medical Center Utrecht,
Netherlands

Reviewed by:
Pinar Yilgor Huri,
Ankara University, Turkey
Menekse Ermis Sen,
Terasaki Institute for Biomedical Innovation, United States

***Correspondence:**
Yuxi Jia
jiayuxi@jlu.edu.cn
Chenyu Wang
wangchenyu@jlu.edu.cn
Jincheng Wang
wangjinc@jlu.edu.cn

Specialty section:
This article was submitted to Tissue Engineering and Regenerative Medicine, a section of the journal Frontiers in Bioengineering and Biotechnology

Received: 14 September 2021
Accepted: 07 December 2021
Published: 05 January 2022

Citation:
Wang H, Wang Z, Liu H, Liu J, Li R, Zhu X, Ren M, Wang M, Liu Y, Li Y, Jia Y, Wang C and Wang J (2022) Three-Dimensional Printing Strategies for Irregularly Shaped Cartilage Tissue Engineering: Current State and Challenges. Front. Bioeng. Biotechnol. 9:777039. doi: 10.3389/fbioe.2021.777039

Although there have been remarkable advances in cartilage tissue engineering, construction of irregularly shaped cartilage, including auricular, nasal, tracheal, and meniscus cartilages, remains challenging because of the difficulty in reproducing its precise structure and specific function. Among the advanced fabrication methods, three-dimensional (3D) printing technology offers great potential for achieving shape imitation and bionic performance in cartilage tissue engineering. This review discusses requirements for 3D printing of various irregularly shaped cartilage tissues, as well as selection of appropriate printing materials and seed cells. Current advances in 3D printing of irregularly shaped cartilage are also highlighted. Finally, developments in various types of cartilage tissue are described. This review is intended to provide guidance for future research in tissue engineering of irregularly shaped cartilage.

Keywords: 3D printing, cartilage tissue engineering, irregularly shaped cartilage, shape imitation, bionic performance

1 INTRODUCTION

Cartilage is widely distributed throughout the human body, and is mainly composed of extracellular matrix (ECM) with embedded chondrocytes (Anderson, 1962). The morphologies of the auricle, nose, trachea, and meniscus are irregular. The shape of cartilage varies, often forming irregular arcs or circular patterns depending on its function. These functions include maintaining the specific shape of a tissue or buffering mechanical forces that deform tissues during movement (Honkanen et al., 2016; Zhou et al., 2018). Due to a lack of blood perfusion, cartilage cannot be repaired as easily as other injured structures such as skin and bone that contain blood vessels. Current strategies for restoring damaged cartilage that is irregularly shaped have not met the initially high expectations (Le et al., 2020). For 3D printing of irregularly shaped cartilage, the challenges are specific to each structure.

For repair of auricular and nasal cartilage where aesthetic appearance is the primary consideration, modified autologous costal cartilage is commonly used for transplantation (Foerster, 1966a; Vuyk and Adamson, 1998). However, autologous transplantation may cause damage to the donor site, and patients are often unsatisfied with the appearance of the reconstructed area. In addition, there is a risk of postoperative complications such as infection (Thorne et al., 2001; Yamada, 2018). As an alternative to autologous implantation, commercial auricular prostheses are also a rational choice as they involve pre-assembled scaffolds with C- and Y-shaped frames made of

composite porous polyethylene (Medpor) material (Cenzi et al., 2005). However, surgical implantation is often accompanied by complications like erosion, infection, absorption collapse, inflammation, and displacement (Younis et al., 2010). Furthermore, this treatment is only applicable to total replacement of the auricular scaffold, which is not appropriate for repair of local auricle defects (Yamada, 2018).

Nasal prostheses are not only used in repair of nasal cartilage defects caused by congenital diseases and trauma but also in rhinoplasty. Nasal septal cartilage, auricular cartilage, and alar cartilage are often used as grafts during autogenous cartilage transplantation. Bone grafting can also be used in rhinoplasty, but it is important not to ignore the side effects of rhinoplasty or complications such as open roof, stair-step, and rocker deformities, bony pyramid and nostril asymmetries, and limited donor sites (Vuyk and Adamson, 1998). The trachea and meniscus function in load bearing and supporting, which is difficult to restore following injury due to a lack of blood vessels (Fabre et al., 2013). In this case, the size and shape of the implanted scaffold can be customized with the aid of software according to the patient's needs. In addition, incorporation of acellularized hydrogels into a scaffold can promote biocompatibility after implantation (Mouser et al., 2020).

Taken together, the lack of suitable repair materials of proper morphology, hardness, and biocompatibility is a major problem in cartilage defect repair, and 3D printing has come to the forefront of cartilage tissue engineering to address these problems. In 1986, 3D printing technology was introduced to the public (Hull, 1996). Among 3D printing technologies, fused deposition modeling (FDM) involves melting a polymer so that it flows through a nozzle, allowing the scaffold to be suitably shaped as it is printed layer by layer (Penumakala et al., 2020). In order to construct 3D tissues, 3D bioprinting was developed to build complex structures by incorporating cells and growth factors into a hydrogel and extruding the composite material layer by layer according to a pre-designed 3D model (Gu et al., 2016; Fenton et al., 2019; Mouser et al., 2020) (**Scheme 1**). In addition to precise control of scaffold shape, spatial resolution and mechanical properties can be controlled during 3D printing (Mouser et al., 2017).

This review summarizes studies of 3D printing of irregularly shaped cartilage scaffolds and discusses the current status of that research, including the use of common materials, cells, and related 3D printing technologies (**Scheme 2**). The intend of this review is to provide guidance for future research on irregularly shaped cartilage in tissue engineering.

2 MATERIALS USED FOR 3D BIO-PRINTED IRREGULARLY SHAPED CARTILAGE

3D printing technology has the potential to fundamentally enhance regenerative medicine (Rajabi et al., 2021). Several studies of 3D printing of irregularly shaped cartilage have reported the use of high molecular weight polymers, including poly (lactic-co-glycolic acid) (PLGA) (Wei P. et al., 2020), poly (lactic acid) (PLA) (Rosenzweig et al., 2015), poly (ε-caprolactone) (PCL) (Xu et al., 2019; Li et al., 2021), and polyurethane (PU) (Kim H. Y. et al., 2019), to print cartilage scaffolds that are stable due to their optimal mechanical properties. In addition, depending on the experimental requirements, hydrogels with good biocompatibility such as silk fibroin (SF) (Rosadi et al., 2019), alginate, gelatin (Yang et al., 2019), and chitosan (CS) are often chosen as printing materials or used as part of a cartilage scaffold. Such hydrogels can act as a cell matrix to support cell growth (Unagolla and Jayasuriya, 2020). The following sections describe each material in detail.

2.1 Synthetic Macromolecular Polymer Materials

2.1.1 Poly(Lactic-co-Glycolic Acid)

PLGA possesses ideal bio-compatibility and bio-degradation properties. PLGA is approved by the U.S. Food and Drug Administration for clinical applications, including drug synthesis and prosthesis fabrication (Gentile et al., 2014). PLGA is a type of thermoplastic, and its melting temperature is 190°C, which eliminates the possibility of printing PLGA with living cells (Kim et al., 2016). The characteristics of PLGA are determined by its molecular weight, the type of end caps, and the lactic acid (LA)/glycolic acid (GA) ratio. PLGA with an ester end cap is more stable during printing and degrades more slowly. In contrast, PLGA degradation is accelerated by an acid end cap. PLGA viscosity increases with increasing LA/GA ratio. Hence a PLGA scaffold with a higher LA/GA ratio and ester end cap is more suitable for preparation of cartilage scaffolds (Guo et al., 2017; Gradwohl et al., 2021). In addition, PLGA is also used to make electrospun scaffolds. Due to the bridging and pull-out properties of PLGA, materials mixed with PLGA may exhibit ductile fracture during bioprinting (Zhao G. et al., 2020).

2.1.2 Poly(ε-caprolactone)

PCL is a polymer obtained by ring-opening polymerization of ε-caprolactone monomers (Bhattacharjee et al., 2021). The compressive modulus of pure PCL is approximately 4.5 MPa, which is significantly lower than that of PLA and other materials (Popescu et al., 2018). Nevertheless, the elastic modulus of the PCL is about 30 MPa, which is closer to that of native cartilage and makes it more suitable for 3D printing of cartilage (Zhang et al., 2017). The low melting point of PCL (55°C) renders it easier to extrude in 3D printing (Dong et al., 2017). Owing to a low glass transition temperature and high thermal stability, PCL has great potential for tissue engineering (Chia and Wu., 2015). PCL can be fabricated into a scaffold by selective laser sintering (SLS) (Patel et al., 2015) and direct ink writing (Zhang et al., 2020). Because high temperature can damage cells, PCL with a lower melting point is more appropriate for acting as a protective layer on bioactive scaffolds (Kim et al., 2016).

2.1.3 Poly(Lactic Acid)

PLA is a type of thermoplastic polymer made from natural renewable resources, and is biodegradable (Wang et al., 2015).

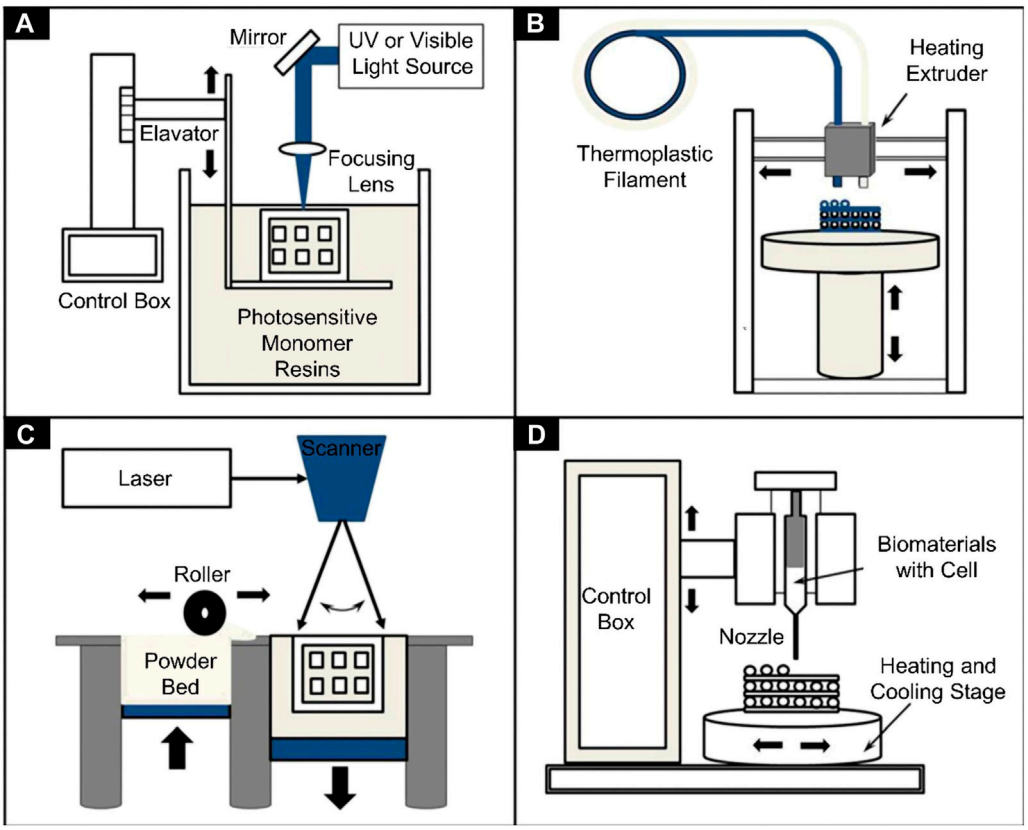

SCHEME 1 | Schematics of different 3D bioprinters used in tissue engineering. **(A)** Vat photopolymerization, **(B)** Fused filament fabrication, **(C)** Selective laser sintering, and **(D)** Inkjet 3D printing (Gu et al., 2016).

PLA can be processed into orthopedic implant materials by FDM, SLS stereolithography (SLA), and other 3D printing technologies (Van den Eynde and Van Puyvelde, 2018; Chen X. et al., 2019). When the temperature rises to 41.5°C, the DNA of cells will be damaged and the cells will die (Akihisa et al., 2004). The high temperature required for printing PLA harms cells seeded onto the surface of the scaffold, but printing PCL between two layers of PLA will make the cell mortality reduce since the melting point of PCL is 60°C. Heated PLA is continuously extruded into three layers by a nozzle, and layers of PCL are extruded between them. Cells encapsulated in sodium alginate are then deposited in the resulting space (Kim et al., 2016). Moreover, printing of scaffolds using layer-by-layer printing technology can improve survival of cells in hydrogel scaffolds (Baena et al., 2019).

When PLA and PCL are used together to prepare 3D-printed scaffolds, not only is cell damage reduced but scaffold mechanical properties are improved. When a PLA mesh covers the surface of a PCL scaffold, its strength significantly increases (Pensa et al., 2019). PLA can be added to a variety of polymers used in 3D-printing. It can also be modified to form poly (L-lactic acid) (PLLA) and poly (D-lactic acid) (PDLA) polymers by incorporating enantiomeric L- and D-lactic acid units, respectively (Masutani and Kimura, 2017). In addition, the toughness of PLLA can be increased by adding PCL to form poly (l-lactide-co-e-caprolactone) (PLCL) (Liu W. et al., 2020).

2.1.4 Polyurethane

PU is usually made from a combination of diisocyanate and polyol (Wang P. et al., 2019), and can be divided into two forms: thermosetting and thermoplastic (Griffin et al., 2020), both of which have good biocompatibility. Compared with other materials, PU has higher elasticity and tensile strength (Griffin et al., 2020). In addition, PU is thermally sensitive and exhibits a sol-gel transition at 37°C (Hsieh and Hsu., 2015). As a result, it has been used to fabricate scaffolds in some soft tissue engineering experiments (Luo K. et al., 2020; Farzan et al., 2020). PU is widely used in various fields of 3D printing by way of fused fiber fabrication (FFF), bio-plotting, SLA (Griffin et al., 2020), and FDM (Xiao and Gao., 2017). The tensile strength and break elongation of thermoplastic polyurethane (TPU) scaffolds printed by FDM can reach 46.7 MPa and 702%, respectively, by arranging the fiber at a 45° angle and forming the scaffold at 215°C (Xiao and Gao., 2017). 3D-printed scaffolds made of PU have excellent shape memory. In addition, they are biodegradable and osteogenic (Wang et al., 2018). Moreover, PU has been used in research on 3D printing of tendons. Scaffolds have been successfully

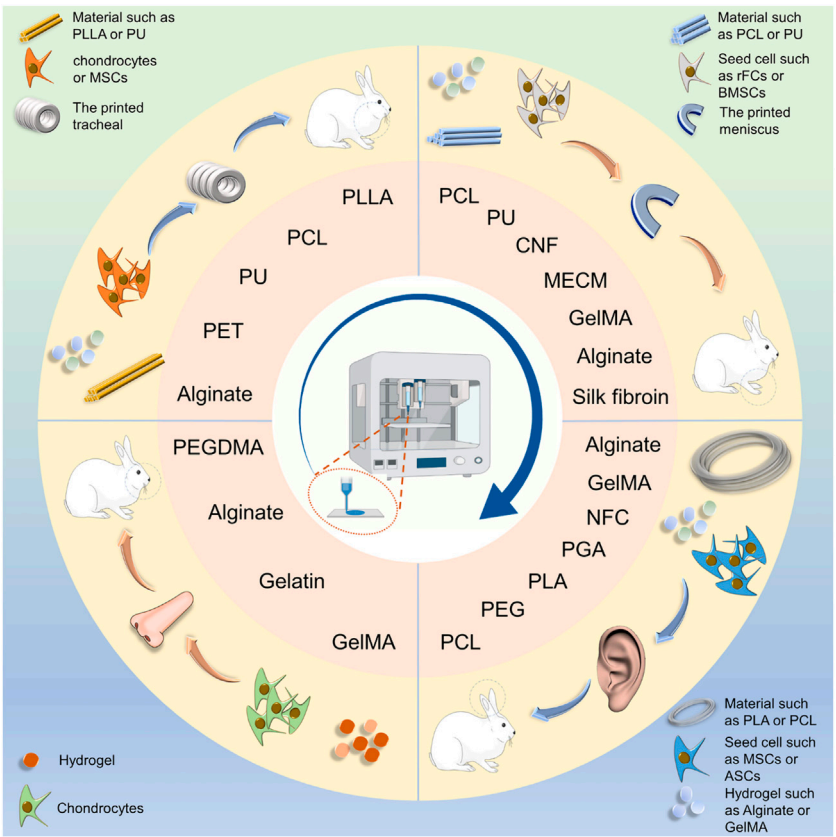

SCHEME 2 | Schematic illustration of scaffold fabrication for cartilage engineering of the auricle, nasal cartilage, trachea, and meniscus. Polymers and hydrogel were made into irregularly shaped cartilage scaffolds using 3D printing technology. PLLA, poly(L-lactic acid); PCL, Poly(ε-caprolactone); PU: Polyurethane; PEG, polyethylene glycol; PEGDMA, polyethylene glycol dimeth-acrylate; PGA, polyglycolic acid; NFC, nanofiber cellulose; MECM, meniscus extracellular matrix.

printed by combining the advantages of PU and PCL (Merceron et al., 2015).

2.2 Natural Materials

2.2.1 Silk Fibroin

SF is a natural material extracted from silkworm cocoons. It is biodegradable and is widely used in medical fields. To date, SF has been used with 3D printing technology to repair defects in skin, bone, cartilage, and vascular tissues (Wang Q. et al., 2019). Pure SF has relatively poor mechanical strength, so it is often mixed with other materials such as hydroxypropyl methylcellulose, gelatin, PEG, and glycerol to improve its properties (Mu et al., 2020). The mixture of SF and hydroxy propyl methyl cellulose of methacrylate (HPMC-MA) has excellent mechanical properties that depend on methacrylate content. The compressive stress of the mixture is 25 KPa (Ni et al., 2020). In addition, the mechanical properties of silk fibroin scaffolds were improved by the technology of biomineralization and pre-mineralization (Neubauer et al., 2021). Biomineralization is the process of metabolizing cells to form minerals (Neubauer and Scheibel, 2020). Graphene oxide, β- Tricalcium phosphate, and nano hydroxyapatite can be added to silk fibroin fibers to pre-mineralize silk fibroin (Liu F. et al., 2020; Wang L. et al., 2020; Zafar et al., 2020). Except for the improvement of mechanical properties, the viscosity of the mixture made of silk fibroin and gelatin will be improved after tyrosinase induced crosslinking (Chameettachal et al., 2016).

In addition to common chemical cross-linking methods, SF can also be cross-linked by physical methods to improve its mechanical properties (Chi et al., 2018). Cartilage acellular matrix (CAM) has properties suitable for cell growth, but its extrusion properties are unsuitable for printing. The addition of SF endows CAM with a fluidity that makes it suitable as a bio-ink for 3D printing (Chi et al., 2018). A solution with useful nanostructural and mechanical properties can be prepared by dissolving SF in a $CaCl_2$ formic acid solution. The maximum elastic modulus and final tensile strength of the stretched SF film in the dry state are 4 GPa and 106 MPa, respectively (Zhang et al., 2015).

2.2.2 Alginate

Alginate can be used in various fields, including wound healing, drug delivery, and tissue engineering (Liu et al., 2019; Wei X. et al., 2020; Oveissi et al., 2020; Khoshnood et al., 2021). Alginate is usually extracted from brown algae and possesses excellent biocompatibility. Ba^{2+} or Ca^{2+} salts can rapidly cross-link sodium

alginate sol into a gel state (Zhang et al., 2019). It has been shown that cell activity in a ring scaffold cross-linked by $BaCl_2$ is stronger than when cross-linked by $CaCl_2$ (Dranseikiene et al., 2020). Cross-linking alginate can also increase its mechanical strength, which provides it with many applications in tissue engineering. Alginate gel is commonly used in 3D printing as it has favorable rheological properties (Kim M. H. et al., 2019). Sodium alginate gels mixed with gelatin to form a hybrid bio-ink possess improved viscosity and elasticity (Cheng et al., 2019; Liu et al., 2019; Soltan et al., 2019). The low degradation rate of alginate gel scaffolds make them poor implants for tissue regeneration. However, using gamma rays to change the molecular weight distribution can accelerate degradation of sodium alginate gels (Kong et al., 2004).

The mechanical strength of an alginate gel is quite low. Mixing PEG and sodium alginate produces a gel with high mechanical strength that is suitable for growth of human bone marrow mesenchymal stem cells (Melo et al., 2019). The rheological properties of alginate gel-based inks influence the shape fidelity and resolution of the printed structure, and they can be improved by mixing alginate gel with carrageenan hydrogels (Kim M. H. et al., 2019). A set of experimental studies has shown that the rheology (viscosity) of the bioprinting ink formed by mixing alginate gel with gelatin is dependent on the printing temperature (Liu et al., 2019). For cells mixed into the hydrogel, adhesion to the gel polymer is essential, and alginate gel modified by dopamine can significantly strengthen cell adhesion (Luo et al., 2019).

2.2.3 Gelatin

Gelatin is a water-soluble and biodegradable polypeptide produced by hydrolysis of collagen. Its enzyme degradation rate is unsatisfactory and it has poor mechanical stability, which limits its applications in biological tissue engineering (Raucci et al., 2019). However, combining gelatin with other materials can improve its viscosity and make it more suitable for 3D printing (Duan et al., 2013; Unagolla and Jayasuriya, 2020). Bio-inks containing gelatin exhibit good fluidity at 35°C, which is conducive to extrusion during 3D printing. After cooling down on the casting platform at 4°C, the scaffold solidifies rapidly (Dutta et al., 2021). In cartilage tissue engineering, MMP2 activity can be induced by gelatin to degrade the synthetic matrix. Then a pericellular zone is formed to accumulate extracellular matrix growth factors and the newly synthesized matrix, so as to the differentiation of chondrocyte is promoted (Chameettachal et al., 2016).

2.2.4 Chitosan

CS is prepared by alkaline deacetylation of chitin. CS has many desirable properties such as natural non-toxicity, histocompatibility, biodegradability, and antibiosis (Long et al., 2019). A fluid suitable for extrusion printers can be prepared by dissolving CS in acid solutions such as GA and LA. A solution made by dissolving CS in 30 wt% GA is suitable for preparation of CS catheters and 3D printing as its tensile strength and Young's modulus are 10.98 ± 0.61 MPa and 12.38 ± 1.19 MPa, respectively (Zhao C. Q. et al., 2020). CS can also be used to improve the performance of other scaffolds. Adhesion of calcium phosphate to PLA can be increased by adding a layer of CS gel to a PLA scaffold, which also improves the mechanical properties of the scaffold (Schneider et al., 2018). Combining CS with mixtures that contain PLA can make the material more hydrophilic (Cheng and Chen, 2017). CS mixed with saline alginate gel can increase its viscosity, making it more suitable for 3D printing (Liu et al., 2018).

3 SEED CELLS USED FOR 3D BIO-PRINTED IRREGULARLY SHAPED CARTILAGE

Depending on the specific requirements, the best biomimetic effect can be achieved by including materials such as seed cells (Kačarević et al., 2018; Zhang and Song, 2018), and selection of an optimal seed cell is of vital importance to achieve cartilage regeneration. Chondrocytes and mesenchymal stem cells (MSCs) are commonly used in cartilage tissue engineering research.

Chondrocytes are often chosen as seed cells, but the tissue sites for obtaining them are limited and vulnerable to injury. Chondrocytes used in cartilage tissue engineering have low immunogenicity, but isolation methods are complex and less well developed than those for MSCs (Francis et al., 2018a)—and considering their multi-directional differentiation potential, MSCs are often preferred (Aggarwal and Pittenger., 2005). In addition, MSCs can inhibit inflammation in scaffolds implanted *in vivo*, and reduce damage resulting from foreign body reactions (Ding et al., 2016).

Some types of MSCs can differentiate toward cartilage cells. Among types of MSCs, bone marrow stem cells (BMSCs) are commonly used in cartilage tissue engineering. As the first identified mesenchymal stem cells, there are many studies on BMSCs (Strioga et al., 2012). BMSCs have the advantage of being plentiful and easy to obtain (Wang Y.-H. et al., 2020), and they have the ability to differentiate toward ecto-, meso-, and endodermal cell lineages, including adipocytes, germ cells, chondrocytes, osteoblasts, pancreatic islet-like cells, hepatocytes, myocytes, annulus fibrosus-like cells, and neuron-like cells (Li et al., 2018). However, BMSCs collected from the elderly are not entirely suitable owing to their limited ability to differentiate and low rate of proliferation (Pittenger et al., 1999; Zaim et al., 2012). There is still a great deal of controversy concerning selection of stem cells. Compared with BMSCs, adipose-derived mesenchymal stem cells (ADSCs) are more plentiful and easier to obtain (Ra et al., 2011; Jo et al., 2014). ADSCs have the potential to differentiate into mesoderm tissue lineages, including bone, cartilage, fat, and muscle (Francis et al., 2018b). Studies have shown that ADSCs are more likely to differentiate into cartilage than are BMSCs (Jang et al., 2015). Umbilical cord blood mesenchymal stem cells (UCB-MSCs) have a greater ability to differentiate into cartilage and express proteins and cytokines than do BMSCs (Lo et al., 2013). However, using BMSCs as seed cells is more conducive to collagen formation and cartilage repair (Contentin et al., 2019). Nevertheless, these conclusions are influenced by the different evaluation criteria

TABLE 1 | Summary of 3D-printed auricular cartilage.

Material	Seed cells	Bioprinting Technology	Key point	References
Nanofibrillated cellulose (NFC)/ Alginate hydrogels	Human nasoseptal chondrocytes (hNC)	Extrusion printing	The hybrid bio-ink, mixed at an 80:20 ratio of NFC to alginate, is printed by an extrusion printer	Markstedt et al. (2015)
PCL/PEG/Alginate hydrogels	Human adipose derived stem cells (ASCs)	Extrusion printing	PEG and PCL were used as the sacrificial and main materials of the framework	Lee et al. (2014)
PCL/methacrylate Gelatin (GelMA)/ Hyaluronic acid (HAMA)/Pluronic F-127 hydrogel	Bone marrow-derived human (BMSCs) Mesenchymal stem cells (MSCs)	Extrusion printing	PCL and GelMA-HAMA were used for hybrid printing, Pluronic F-127 was selected as a sacrificial material	Chung et al. (2020)
Type I collagen gel/PCL	Porcine auricular cartilage	EOS P100 laser sintering system	The cells were embedded in collagen I gel solution and the cell suspension was then pipetted into the PCL scaffolds	Zopf et al. (2015)
PU	Tonsil-derived mesenchymal stem cells	—	3D printing of auricular cartilage scaffold was performed with PU material	Kim et al. (2019a)
PCL	—	Fused deposition system	Creating auricular model and 3D printing with PCL material	Jung et al. (2019)
PCL/PGA/PLA	Picrotia chondrocytes (MCs)	Fused deposition system	The auricular scaffold used PCL as an inner core, which was wrapped with PGA unwoven fibers and coated with PLA.	Zhou et al. (2018)
Gelatin/fibrinogen/hyaluronic acid (HA)/glycerol/PCL/Pluronic F-127 hydrogel	3T3 fibroblasts	An integrated tissue–organ printer (ITOP)	3T3 cells were mixed in the prepared hydrogel, the auricular scaffold structure was printed simultaneously with PCL, and Pluronic F-127 hydrogel was used to print the sacrificial layer to maintain scaffold structure	Kang et al. (2016)

used, and therefore the choice of MSC depends on the purpose of the experiment. It has been shown that a mixture of ADSCs and chondrocytes can be used for seeding cells onto a biodegradable scaffold (Morrison et al., 2018).

4 3D-PRINTED IRREGULARLY SHAPED CARTILAGE SCAFFOLDS

The structural complexity of irregularly shaped cartilage increases the difficulty of manufacturing scaffolds. However, the emergence of 3D printing technology provides a new solution for repair of irregularly shaped cartilage. On this basis, and considering the biocompatibility of materials and selection of seed cells, useful improvements have been made that are adapted to the specific requirements of different structures to facilitate study of 3D printing of irregularly shaped cartilage. This section summarizes progress in 3D printing technology used for reconstruction of four types of irregularly shaped cartilage: auricular, nasal, tracheal and meniscus.

4.1 3D-Printed Auricular Cartilage Tissue

Developments in medical procedures and knowledge have facilitated surgical repair or improvements of features that affect facial beauty. There is a long history of research on auricular repair, including treatment of mild injuries such as earlobe and earring injury, and severe injuries such as when the entire auricle is bitten or cut (Song et al., 2020). Because the auricle is an important facial feature, congenital auricle deformity or injury can damage mental health. 3D-printed auricular cartilage can be used for auricle shape reconstruction. The first step in 3D printing of an auricle is to design its shape, and one of two methods involving CAD software is typically used: either import DICOM files to synthesize auricle shape, or design the required graphics directly (Zhou et al., 2018). The resulting auricle model then needs to be converted into STL (structured template language) form. An iTOP (integrated tissue and organ printer) can also be used to print the ideal ear shape (Kang et al., 2016). Currently there are two main types of 3D-printed auricle scaffold. In the first, the auricle shape is printed directly using hydrogel, and in the second, the support structure of the auricular scaffold is first printed using biomaterials, and then the surface of the scaffold is covered by a cell-containing hydrogel using 3D printing or immersing the scaffold into the hydrogel (Jang et al., 2020).

4.1.1 Preparation of Auricular Scaffolds Using Hydrogel

Because of the pretty biocompatibility of hydrogels, some studies have been devoted to research on 3D printing of auricular scaffolds using hybrid hydrogels. Bio-ink produced by mixing gelatin with SF from two sources (*Philosamia ricini* and *Bombyx mori*) can be used to print auricular cartilage as it gels without cross-linking (Singh et al., 2019), which eliminates potential side effects of the cross-linker. This material shows excellent fidelity, stability, swelling properties, biodegradability, and promotes cell viability (Singh et al., 2019). In addition, a hybrid bio-ink can be photocured during 3D printing by adding methacrylic anhydride and a photoinitiator in a mixture of gelatin and hyaluronic acid. Scaffold degradation becomes prolonged after being freeze-dried, and the compression strength of lyophilized scaffolds is significantly greater than for other scaffolds. This cross-linking method allows sufficient time for preparation of composite materials and development of chondrocytes (Xia et al., 2018).

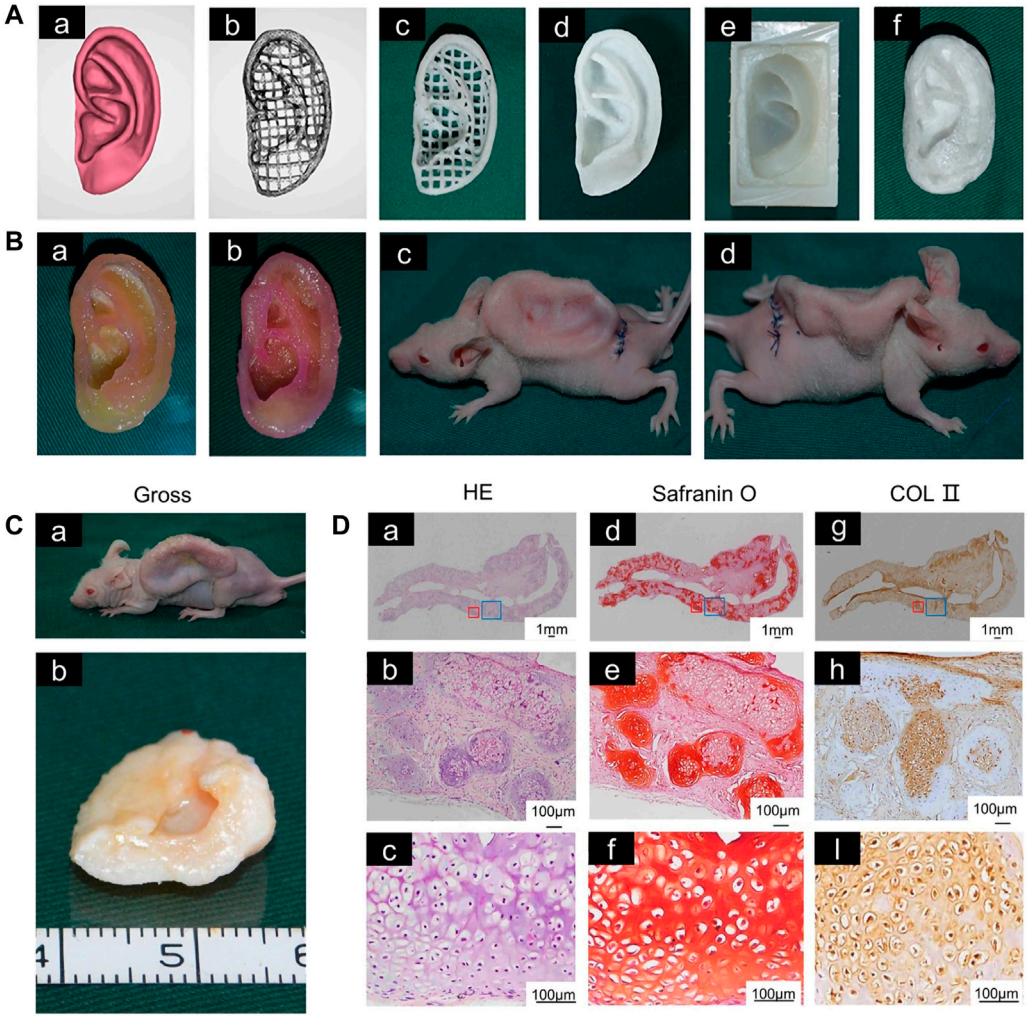

FIGURE 1 | 3D-printed auricular scaffold and *in vivo* experiments. **(A)** Design of a 3D-printed auricle model and the resulting printed scaffold; **(a)** 3D digital model of the human auricle, **(b)** 3D mesh digital model, **(c)** PCL inner core, **(d)** human auricle-shaped PCL positive mold, **(e)** silicone casting mold, and **(f)** ACM/Gelatin-PCL scaffold. **(B)** Auricular scaffold before implantation and after implanting it into a nude mouse for 2 weeks. **(C)** Images of scaffolds cultured *in vivo* for 12 weeks. **(D)** H&E and safranin-O staining showed lacunar structure and cartilage-specific ECM deposition (Jia et al., 2020).

Although freeze-drying results in some improvement in the mechanical properties of hydrogel scaffolds, it remains to be seen whether they remain stable as the gel degrades.

4.1.2 Preparation of Auricular Scaffolds With Polymer Materials and Hydrogel

The other kind of 3D-printed auricular cartilage is that made of composite polymer materials and hydrogel. Polymers such as PLA, PCL, and hydrogels are often combined to fabricate auricular scaffolds (**Table 1**). PCL material is often preferred for auricular cartilage scaffold printing because of its high compression modulus (Olubamiji et al., 2016). The compression modulus of the scaffold is affected by the properties of the material and the diameter of the scaffold, which are related to printing speed. For a given flow rate through the printer nozzle, the higher the printing speed, the smaller the diameter of the extruded stream, which alters the mechanical properties of the printed material. The compression modulus of the PCL scaffold decreases with increasing nozzle diameter, and its flexibility is affected by line spacing and angle. Running the 3D printer nozzle along the 0°/45° direction to print the scaffold will make the scaffold more flexible (Chung et al., 2020). Experimental studies have shown that scaffolds printed with PCL and hydrogel mixed with cells are more conducive to cartilage formation than if the cells are placed on the surface of the composite scaffold (Park et al., 2017).

For the auricular scaffolds printed with PCL, the shape of the pores in the scaffold can affect the cells seeded into it. Spherical pore design not only facilitates chondrocytes adopting a shape characteristic of natural cartilage *in vivo* but also accelerates matrix deposition (Zopf et al., 2018). However, incorporation of hydrogel into scaffold pores cannot guarantee the desired cell content. Scaffolds with a sandwich structure can to some extent reduce the loss of hydrogel and cells. Cell survival has been promising in alginate

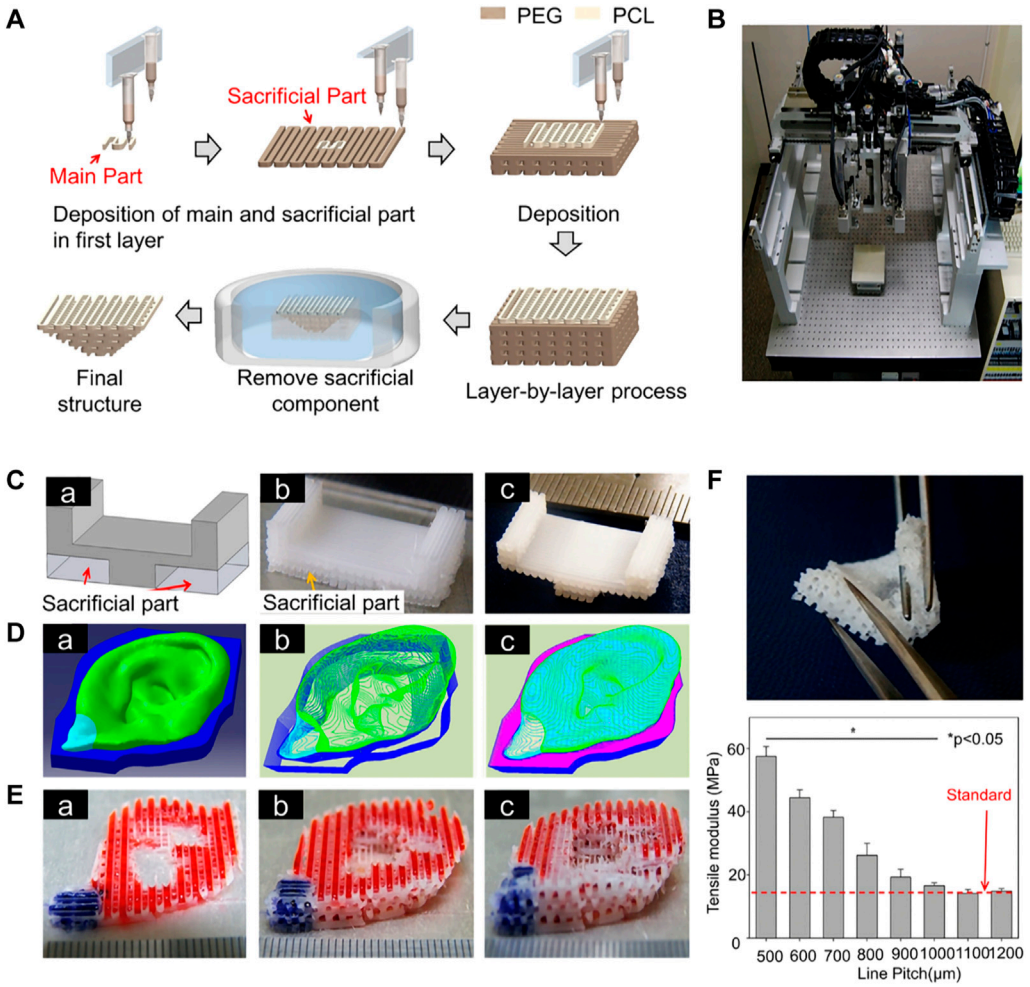

FIGURE 2 | 3D-printed auricular scaffold using sacrificial layer technology. **(A)** Fabrication of inverse porous pyramid structure employing sacrificial layer technology. **(B)** Schematic diagram of the multi-head tissue/organ building system (MtoBS). **(C)** Overhanging structure (20 mm × 10 mm × 6 mm). **(D)** The model designed by CAD software, slicing CAD model, and the Code generation to control XYZ movement of the MtoBS. **(E)** Scaffold after 3D printing. **(F)** The scaffold is flexible, and a line spacing of 1,000–1,200 μm yields a similar tensile modulus to that of the auricle (Lee et al., 2014).

TABLE 2 | Summary of 3D-printed nasal cartilage.

Material	Seed cells	Bioprinting Technology	Key points	References
Gelatin methacryloyl (GelMA)/Polyethylene glycol dimeth-acrylate (PEGDMA)/Gelatin	Chondrocytes	Extrusion printing	The engineered cartilage-like tissue construct was integrated with an electrochemical biosensing system to produce functional olfactory sensations	Jodat et al. (2020)
Gellan/Alginate/BioCartilage	Chondrocytes	Extrusion printing	A novel bio-ink for printing cartilage grafts was developed for use in 3D printing	Kesti et al. (2015)

hydrogels placed between two printed PCL scaffolds to form a sandwich structure for auricle implantation. This new method of constructing auricular cartilage considers both mechanical properties and cell viability (Visscher et al., 2019). When selecting a hydrogel loaded with cells, adding an acellular cartilage matrix (ACM) to the gelatin can produce a hydrogel more similar to that *in vivo*, which is conducive to cell growth (Jia et al., 2020) (**Figure 1**).

Covering a PCL scaffold with PGA has been shown to be beneficial to auricular chondrocytes. The scaffold remained intact and chondrocytes differentiated into cartilage 2.5 years after implantation. This study supported the feasibility of 3D-printed cartilage tissue for clinical applications (Zhou et al., 2018). For 3D printing, in addition to scaffold stability and cell survival in hydrogels, it is also necessary to consider the

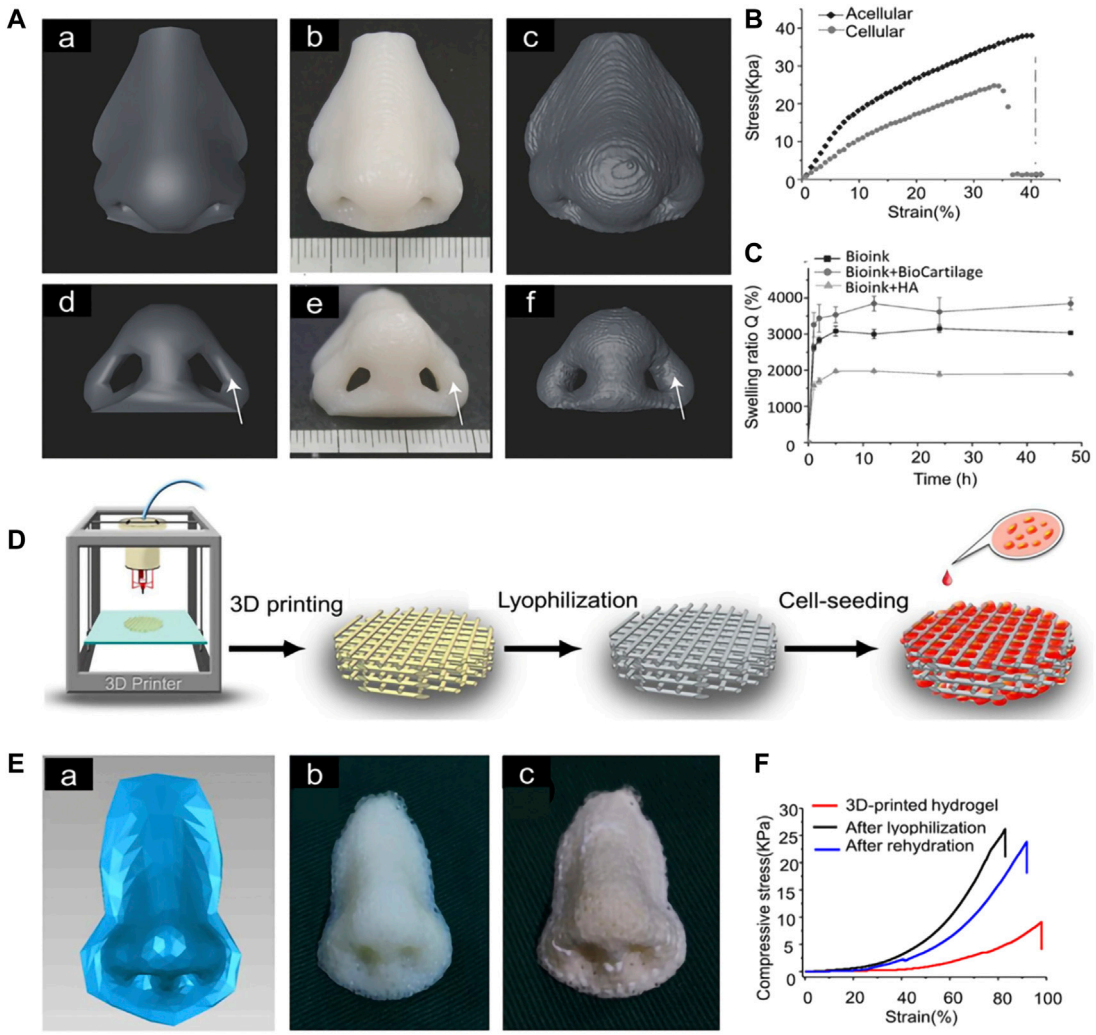

FIGURE 3 | 3D-printed nasal cartilage scaffold. **(A)** The 3D model for printing and comparison of its shape and volume after 2 weeks of swelling **(B)** The Young's modulus of the acellular structure (E = 230 ± 7.0 kPa) was significantly higher than that of the cellular structure (E = 116 ± 6.8 kPa). **(C)** The equilibrium swelling rate of bio-ink + HA was significantly lower than that of bio-ink + biocartilage or bio-ink alone (Kesti et al., 2015). **(D)** Nasal cartilage scaffold was prepared by photocured 3D printing and lyophilization. **(E)** The scaffold printed according to the 3D model was lyophilized. **(F)** compression strength of the scaffold (Xia et al., 2018).

rheological and cross-linking properties of hydrogels. Bio-ink prepared by mixing nanofiber cellulose (NFC) with sodium alginate is promising for bio-printing because of the shear-thinning effect. Moreover, the hybrid material simultaneously offers a dual-cross-linking pattern and greater storage modulus (Markstedt et al., 2015). However, further *in vivo* and clinical trials of hybrid materials are still required to verify their efficacy. On this basis, bacterial nano-cellulose (BNC) was modified by a water-based anti-collision agent, and the Iβ phase of BNC was replaced by the Iα phase, which was more thermodynamically stable. Higher water retention and stronger mechanical properties were obtained in this way (Apelgren et al., 2019). Studies of the feasibility of tissue engineered cartilage have been carried out in animals. As early as 1997, a group of researchers implanted PLGA-PLA structure into mice lacking a thymus, which confirmed the feasibility of auricle construction using chondrocytes and biodegradable polymers (Cao et al., 1997).

4.1.3 3D-Printed Auricular Cartilage With a Sacrificial Layer

To make the 3D-printed scaffold more stable and complex, sacrificial layer technology was used to construct the support, with PEG as the sacrificial layer to stabilize the scaffold structure. At the same time, chondrocytes and adipocytes were implanted into corresponding positions in the scaffolds, including the cartilage and earlobe components for *in vitro* culture (Lee et al., 2014) (**Figure 2**). In recent years, in addition to commonly used materials such as PCL and PEG, the feasibility of using PU materials to print auricular cartilage has also been confirmed. Compared with the Medpor scaffold, PU has better histocompatibility and improved prospects for clinical applications.

TABLE 3 | Summary of 3D-printed tracheal cartilage.

Material	Seed cells	Bioprinting Technology	Key points	References
PCL	Human bronchial epithelial cells (hBECs)/iPSC-derived mesenchymal stem cells (iPSC-MSCs)/iPSC-derived chondrocytes (iPSC-Chds)	Fused deposition system	Combined electrospinning technology and 3D printing technology to print tracheal cartilage	Kim et al. (2020)
PCL	Rabbit chondrocytes	Fused deposition system	The 3D-printed scaffold printed with PCL was loaded with cultured chondrocytes	Gao et al. (2017)
PCL	Goat auricular chondrocytes	Fused deposition system	PCL was used to print the cell scaffold, and the scaffold was cellularized	Xia et al. (2019)
PLLA	Rabbit chondrocytes	Fused deposition system	The 3D-printed scaffolds were seeded with chondrocytes obtained from autologous auricles	Gao et al. (2019)
PU	Mesenchymal stem cells (MSCs)	Liquid-frozen deposition manufacturing (LFDM)	A tracheal scaffold printed by Pu was tested *in vivo*	Hsieh et al. (2018)
PCL/ Alginate	Rabbit bone marrow-derived mesenchymal stem cells (bMSC)/Epithelial Cells		Artificial trachea containing two cell types were fabricated by three-dimensional bioprinting	Bae et al. (2018)

4.2 3D-Printed Nasal Cartilage

Clinically, nasal cartilage defects have a significant impact on a person's facial appearance and olfactory function. In nasal cartilage repair, autologous cartilage or bone is often implanted into the site that needs to be repaired. The materials commonly used for nasal scaffold transplantation include bone or cartilage obtained from the nasal septum, ribs, skull, and ear (Parkhouse and Evans, 1985). However, there is a risk of graft fracture and displacement when using a graft to repair the loss of nasal cartilage (Elik and Aktan, 2019; Cao et al., 2021). Therefore, the application of 3D printing in cartilage tissue engineering can provide a rational alternative for fabrication of nasal cartilage prostheses suitable for a given individual. Many researchers are committed to combining synthetic chemical materials and natural hydrogels into scaffolds using 3D printing. The use of PCL and various kinds of cellular hydrogels for scaffold fabrication has attracted much research interest in recent years (**Table 2**).

4.2.1 Preparation of Nasal Scaffolds With Hydrogel

For 3D printing of nasal cartilage, researchers early on attempted to use pure hydrogel as the 3D printing material for nasal cartilage. However, performance of the printed nasal cartilage scaffolds can be increased by modification of the hydrogels. For example, swelling of the scaffolds can be increased significantly by adding extracellular matrix to the gel. When bio-ink for 3D printing is made of bio-cartilage, gellan gum, and alginate, the swelling rate of the scaffold is significantly greater than when it lacks bio-cartilage (Kesti et al., 2015). For scaffolds printed with hydrogel, the mechanical properties of the scaffolds can be improved by lyophilization (Xia et al., 2018) (**Figure 3**).

4.2.2 Preparation of Nasal Scaffolds With Polymer Materials and Hydrogel

In order to make the mechanical properties of 3D-printed scaffolds approximate those of natural nasal cartilage, polymer and hydrogel were selected for 3D-printed nasal cartilage scaffolds. PCL is the most frequently used polymer. A multi-head disposition system can be applied to print PCL and alginate with both encapsulated cells and TGF-β. The cells in the printed scaffold maintained a high proliferation rate (Kundu et al., 2015). GELMA is also used to load cells and make nasal cartilage scaffolds with PCL. Moreover, 20% w/v gel is considered to be ideal for preparation of cartilage scaffold materials because of its rheology and improved biocompatibility (Ruiz-Cantu et al., 2020). To improve proliferation of chondrocytes on PCL scaffolds, dehydrated porcine nasal cartilage extracellular matrix was incorporated into the scaffold, which showed improved chondrogenic differentiation potential (Wiggenhauser et al., 2019). However, further research is urgently needed.

To improve nasal cartilage scaffolds, in addition to exploration of hydrogels, some have studied PCL as it mainly plays a role in maintaining shape. Filaments of carefully chosen mixtures of PCL and graphene are suitable for preparation of scaffolds by injection molding, which is conducive to growth of cartilage and can improve the mechanical properties of scaffolds (Rajzer et al., 2020). In printing cartilage scaffolds, the flexibility of the scaffold should also be considered in order to make the mechanical properties of the scaffold similar to those of nasal cartilage. Using an octahedral pore structure instead of a cube or lattice structure for 3D-printed nasal scaffolds can increase the flexibility of the scaffold and reduce the risk of prosthesis deformation and infection (Jung et al., 2014). A novel use of laser sintering to process PCL improved cell survival by controlling pore structure and promoting perfusion of the hydrogel (Zopf et al., 2015).

4.2.3 Olfactory Restoration *via* a Novel Nasal Cartilage Scaffold

In addition to focusing on aesthetics in nose reconstruction, the sense of smell should also be considered. A recent study of nasal cartilage 3D printing reported the addition of an olfactory sensing device, which may represent a future direction in nose reconstruction research in which function is considered along with appearance (Jodat et al., 2020). Electrospinning of gelatin fibers on the surface of 3D printing scaffolds can be transformed into gelatin after heating, which helps to capture cells and increase cell adhesion after inoculation. Thus they can be well distributed in the porous PLLA scaffold (Rajzer et al., 2018).

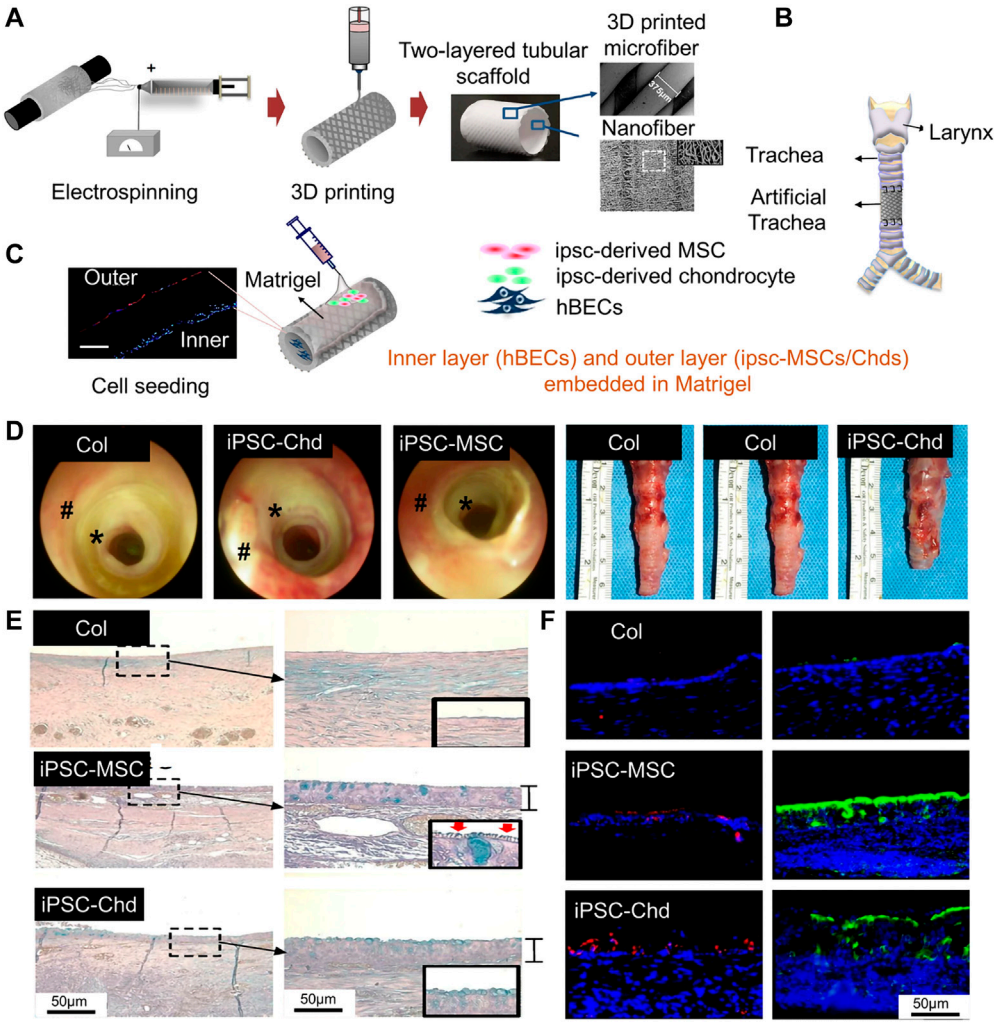

FIGURE 4 | Process diagram for manufacturing a 3D tubular artificial tracheal scaffold. **(A)** A PCL tubular nanofiber layer (inner layer) prepared by electrospinning was wrapped with 3D-printed PCL fiber. **(B)** Tracheal transplantation and endoscopic analysis. **(C)** Induced pluripotent stem cell-derived chondrocytes (IPSC-CHDs) and human bronchial epithelial cells (hBECs) were separately seeded on the outer and inner layers of the scaffold. Each layer was identified by pkh-26 staining (red; IPSC-CHDs) and DAPI (blue; hBECs) staining (scale = 200 μm). **(D)** The endoscopic images at 4 weeks. **(E)** Alcian-blue staining showed mucus (blue) generated by regenerated tracheal epithelium 4 weeks after transplantation. (F) Immunofluorescence staining for β-tubulin and keratin-5 at the implant site (Kim et al., 2020).

4.3 3D-Printed Tracheal Cartilage Tissue

Cricoid hyaline cartilage maintains tracheal shape and guides air flow into and out of the lungs. In addition, the glands in the inner layer of cartilage can release cells and granules into the body by secreting mucus (Brand-Saberi and Schäfer, 2014). There are two kinds of common tracheal diseases: tracheomalacia caused by injuries to the tracheal wall, and tracheal stenosis caused by tumors, congenital defects, and other tracheal diseases (Rich and Gullane, 2012). Severe tracheomalacia leads to tracheal stenosis and can be life threatening. Procedures for assisting breathing include noninvasive ventilation, tracheostomy, and airway stenting (Janssen et al., 2021).

Treatment of tracheal tumors depends on tumor size. If the length of a tracheal resection is greater than 6 cm, it cannot be repaired by end-to-end anastomosis (Fabre et al., 2013); an implantable scaffold offers an alternative approach. When choosing a suitable scaffold, the mechanical strength, cell compatibility, and adhesion of the scaffold should be considered, but at present there is no perfect bionic scaffold (Jagdeep et al., 2017). In addition, for repair of tracheal injury in children, the scaffold must grow with age (Hamilton et al., 2015). Although biological 3D printing may be used to address these issues, hydrogel on its own as a scaffold material is unsuitable as it is too compliant to maintain an open channel for air flow through the trachea.

4.3.1 Preparation of Tracheal Scaffolds Using Polymer Materials Combined With Hydrogel

Macchiarini et al. (2009) were the first to perform trachea replacement using an acellular allogeneic annular trachea. In combination with selecting human tissue to construct trachea, emerging 3D printing technology can provide patients with customized tracheal prostheses. Similar to auricular and nasal cartilage scaffolds, the material used in the initial study of tracheal

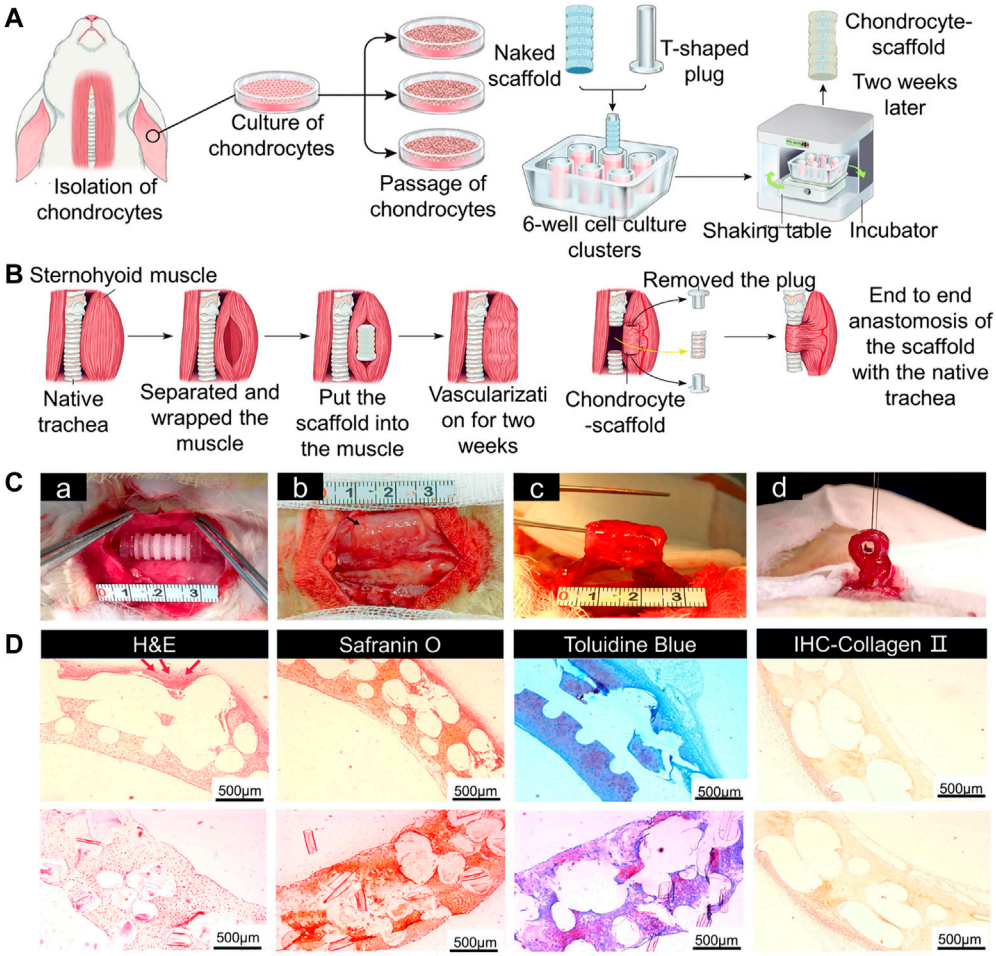

FIGURE 5 | Tracheal cartilage scaffolds were made by 3D printing technology and tested *in vivo*. **(A)** Schematic diagram of 3D-printed PLLA tracheal scaffold. **(B)** Pre-vascularization and tracheal reconstruction of cellular scaffold constructs *in vivo*. **(C)** The scaffold was implanted into sternal muscle for pre-vascularization. A complete segmental tracheal organ unit with pedicle muscle flap was formed. **(D)** The images of H&E, safranin O, and toluidine blue staining, and IHC of type II collagen of chondrocyte-scaffold constructs. (Scale bar: 500 μm; red arrow: small blood vessels around the engineered trachea) (Gao et al., 2019).

printing was mostly PCL (**Table 3**) (She et al., 2021). An optimally structured PCL scaffold can be printed at 90°C with a heating nozzle (Ahn et al., 2019). Given the complexity of tracheal structure, the characteristics of each layer of a tracheal scaffold should be considered in its design. A 3D printing machine with a screw pump system and a pipe manufacturing controller has been used to print tracheal scaffolds composed of alginate combined with PCL and cells (Park et al., 2019). Porous PCL was located both inside and outside the scaffold, and the middle two layers of alginate + cells were separated by pore-free PCL.

The structure of PCL scaffolds can be improved by electrospinning technology, which can improve cell viability (Yu et al., 2021). For example, PCL nanostructured scaffolds were prepared as the inner layer of a tracheal scaffold using an electrostatic spinning technique, into which human bronchial epithelial cells (HBECs) were implanted. In addition, 3D-printed PCL scaffolds have been used as the outer layer of a tracheal scaffold. Induced pluripotent stem cell-derived mesenchymal stem cells (IPSC-MSCs) and induced pluripotent stem cell-derived chondrocytes (iPSC-Chds) were implanted into the outer layer of the scaffold. The outer layer of the scaffold maintained and supported the shape of the trachea. The nanostructure of the internal electrospun scaffold better simulates the extracellular matrix, which is more conducive to the growth of HBECs, enables rapid reconstruction of the mucosal layer, and can also reduce tracheal stenosis caused by incomplete reconstruction (Kim et al., 2020) (**Figure 4**). Comprehensive animal studies will be required before this method can be used for segmental bronchial transplantation.

The composite material obtained by adding chitosan to PCL has been used for electrospinning, which can reduce the diameter of electrospun fibers and improve the mechanical properties of the scaffold (Kim et al., 2021). To provide 3D-printed trachea with improved structure, the sacrificial layer technique has also been used in printing of tracheal cartilage. A sacrificial mold

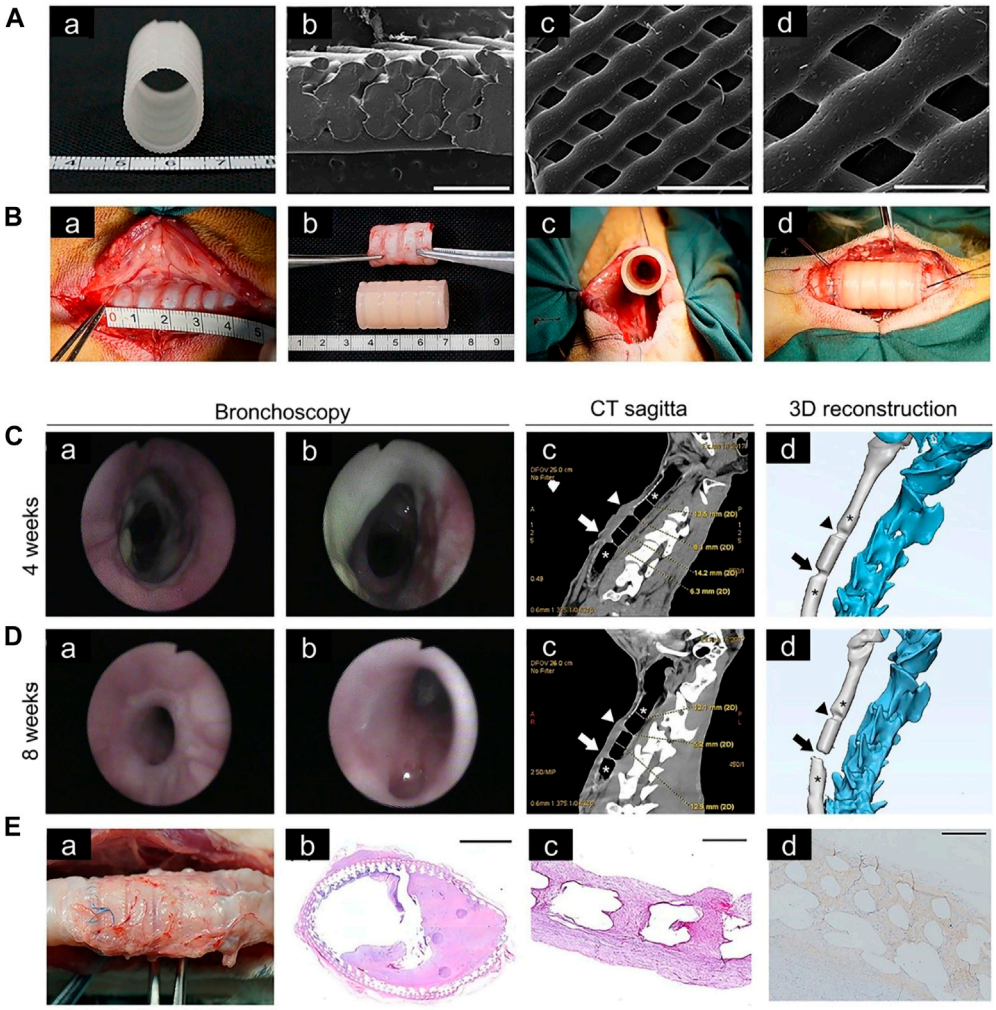

FIGURE 6 | Tracheal cartilage scaffolds were made by 3D printing technology and tested *in vivo*. **(A)** Macroscopic **(a)** and SEM **(b–d)** images of 3D-printed PCL scaffold. **(B)** Implantation of a tracheal cartilage scaffold. **(C)** Four weeks after implantation, tracheal images were acquired at the upper, middle and lower anastomosis sites, respectively **(a,b)**. Computed tomography (CT) sagittal images and representative sections of 3D-printing reconstruction after 4 weeks, in which the narrow area represents the upper and lower anastomoses (arrow) **(c,d)**. **(D)** Bronchoscopy images and CT sagittal images after 8 weeks. **(E)** The scaffold of the experimental group was removed at the time of death **(a)**. Hematoxylin and eosin staining of scaffolds at low magnification **(b)**. Representative safranin O staining **(c)**. Representative collagen II staining **(d)** (Xia et al., 2019).

containing hollow trachea was constructed by 3D printing, and then PLCL was injected into the mold to generate an annular tracheal structure. Gelatin sponges loaded with transforming growth factor-β1 (TGF-β1) and chondrocytes were placed between the annular structures to promote formation of cartilage tissue (Park et al., 2015).

In addition to commonly used PCL materials, two kinds of PU materials with different compositions were used for 3D printing of the hard and soft segments of tracheal wall cartilage, and the printed 3D scaffolds were then implanted into nude mice for 6 weeks. The results showed that the maximum tensile stress, Young's modulus, and elongation of the 3D tracheal scaffold were 4.6 MPa, 21.1 MPa, and 106.2%, respectively, and the MSCs on the scaffold could be induced to differentiate into chondrocytes (Hsieh et al., 2018). TPU has elastic properties appropriate for use as a tracheal support material. Researchers printed TPU scaffolds with wave and straight pattern micro-morphology. Electrospinning was used to cover the inner and outer surfaces of the TPU scaffold to improve its biocompatibility. Electrospinning on 3D-printed tracheal scaffolds can improve cell adhesion to the scaffolds and their elastic properties (Ahn et al., 2019).

4.3.2 Blood Supply Improvement in 3D-Printed Tracheal Scaffolds

Blood vessels can promote growth of airway epithelium on the surface of 3D-printed scaffolds, therefore blood supply should be considered when designing tracheal cartilage scaffolds. As one approach to this problem, PLLA tracheal scaffolds were pre-cultured with chondrocytes *in vitro* and pre-vascularized *in vivo*,

TABLE 4 | Summary of 3D-printed meniscus cartilage.

Material	Seed cells	Bioprinting Technology	Key points	References
PCL	BMSCs	Fused deposition modeling (FDM)	PCL was printed into meniscal scaffolds with different pore sizes using the melt deposition technique	Zhang et al. (2016)
PCL/GelMA	Fibrochondrocytes	Bioscaffolder system (SYS + ENG, SalzgitterBad, Germany)	Agarose and gelatin methcrylate (GelMA) hydrogels were printed on the inside and outside of PCL scaffold, respectively	Bahcecioglu et al. (2019)
Gelatin/Alginate/CNF	Rabbit fibrochondrocytes (rFCs)	Extrusion printing	The gelatin-alginate bio-ink modified with cellulose nanofibers (CNF) has been verified for its feasibility to print meniscus	Luo et al. (2020a)
Silk fibroin/gelatin	Porcine fibrochondrocytes	Extrusion printing	The scaffold made of silk fibroin and gelatin has good performance after freeze-drying	Bandyopadhyay and Mandal (2019)
Meniscus extracellular matrix (MECM)/sodium alginate	Meniscal fibrochondrocytes (MFCs)	Fused deposition modeling (FDM)	The scaffold was made of MECM-alginate bio-ink and 3D-printed PCL.	Chen et al. (2019a)
Decellularized meniscal extracellular matrix (dECM)/ PU/PCL	BMSCs	FDM/Extrusion	Hydrogel made from decellularized extracellular matrix and a mixture of PCL and PU was used to make meniscal scaffolds	Chae et al. (2021)

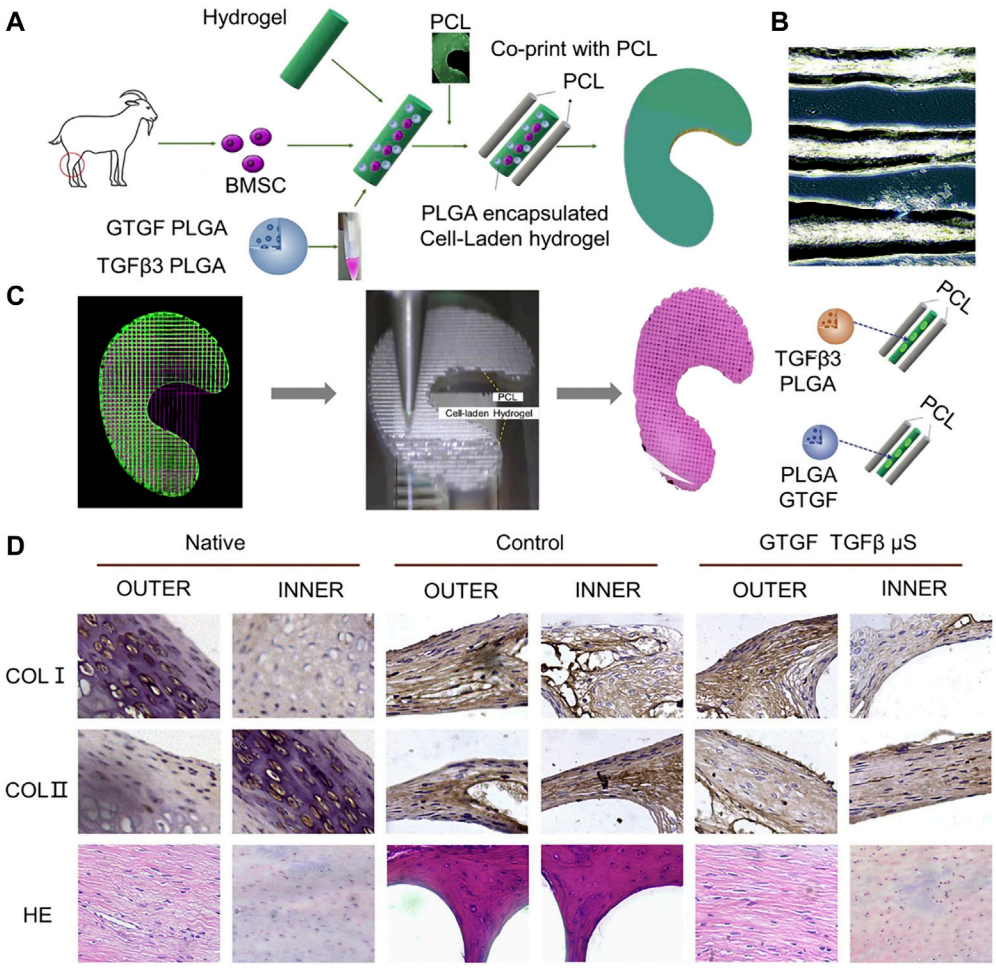

FIGURE 7 | PCL and PLGA encapsulated cell-laden hydrogel was used to make a meniscus scaffold by 3D printing technology. **(A)** Schematic diagram of the design of a bioprinted composite material study for regeneration of a goat meniscus. **(B)** PLGA-encapsulated hydrogels containing MSCs cells exhibited good printability. **(C)** CAD model of the meniscus for 3D printing. The cell hydrogel and PCL were printed into 3D meniscus by 3D printing technology. **(D)** Zone-specific matrix phenotype analysis in engineered versus native tissue (Sun et al., 2020).

and then implanted with a muscle flap into tracheal defects in Manch rabbits (Gao et al., 2019) (**Figure 5**). The same group also transplanted 3D-printed trachea into sheep, which provided a basis for use of 3D-printed trachea in the clinic (Xia et al., 2019) (**Figure 6**).

Studies of segmental bronchial implants must also consider the problem of tracheal stenosis following transplantation. To solve this problem, some researchers use omentum to cover both ends of the prostheses to reduce complications, including luminal stenosis and mesh exposure (Teramachi et al., 1997). This method has also been used to facilitate tracheal scaffold blood flow (Masatsugu et al., 2014). In addition, by implanting a 3D-printed PCL scaffold into an animal's omentum, it was shown that using the omentum as a 3D-printed scaffold bioreactor can not only improve blood flow and reduce the incidence of tracheal stenosis but also promote proliferation of tracheal epithelial cells (Park et al., 2018).

4.4 3D-Printed Meniscus Cartilage Tissue

The knee menisci are two fibrous cartilage discs in the joint that provide for shock absorption and load transmission. The lateral and medial menisci are semicircular and C-shaped, respectively (Chae et al., 2021). A meniscus can be divided into a white-white area, red-red area, and red-white area based on blood supply (Markes et al., 2020). Approximately ninety percent of meniscus injuries require meniscus removal because chondrocytes are not renewable. However, the incidence of osteoarthritis (OA) following meniscectomy is 7.4-fold higher than normal. Therefore, scaffolds with morphology and mechanical properties similar to menisci have attracted much research interest in recent years (Kwon et al., 2019; De Caro et al., 2020). For 3D printing of a tissue engineered meniscus, not only should morphological similarity be considered but also mechanical load-bearing and lubrication. A meniscus scaffold can be printed with PCL using FDM technology (Zheng-Zheng et al., 2016) (**Table 4**).

4.4.1 Preparation of Meniscus Scaffolds With Hydrogel

Among the hydrogels used in meniscus scaffolds, GelMA has superior properties for printing and can maintain higher fidelity (Daly et al., 2016). In addition, gelatin-alginate bio-ink containing cellulose nanofibers (CNF) has been shown to be useful for printing menisci (Luo W. et al., 2020). The mechanical properties of scaffolds made of silk fibroin and gelatin were greatly improved and made more similar to menisci by freeze-drying and cross-linking with EDC (1-ethyl-3-(3-dimethylamino propyl) carbodiimide hydrochloride) and NHS (N-hydroxysuccinimide) (Bandyopadhyay and Mandal, 2019). ECM extracted from menisci mixed with cells and growth factors is promising for use in meniscus tissue engineering (Romanazzo et al., 2017). Hydrogel produced by decellularized ECM and sodium alginate can be combined with PCL to prepare meniscal scaffolds (Chen M. et al., 2019). There are differences in the properties of ECM extracted from the inner and outer menisci: inner meniscus ECM can promote chondrogenesis of fat pad-derived stem cells, while outer meniscus ECM can promote development of cells with thinner and more fibroblast-like phenotypes (Romanazzo et al., 2017).

4.4.1 Preparation of Meniscus Scaffolds With Polymer Materials and Hydrogel

For meniscus scaffolds made of PCL, scaffold pore size influences ECM production, cell behavior, biomechanics, and hence successful repair. A scaffold with an average pore size of 215 μm not only has good tensile and compressive properties but can also promote proliferation and differentiation of MSCs (Zhang et al., 2016). A meniscus scaffold has been constructed of agarose and gelatin methacrylic acid (GelMA) hydrogels printed on both sides of a PCL scaffold. Production of glycosaminoglycans and type II collagen was promoted by agarose, while GelMA promoted production of type I collagen (Bahcecioglu et al., 2019). In addition, a scaffold made by placing silk fibroin on both sides of a 3D-printed PCL mesh also has good biocompatibility and is more suitable for tissue infiltration and blood vessel formation (Cengiz et al., 2019).

PLGA, in addition to being combined with hydrogel and ECM as a carrier of cells, can itself be loaded with cells and growth factors. For instance, PLGA microparticles loaded with MSC cells and TGFβ3 or CTGF can be deposited on a PCL scaffold to make a meniscus scaffold. Activity and proliferation of BMSCs were similar when loaded into seven types of hydrogel (Sun et al., 2020) (**Figure 7**). In addition to growth factors that promote cell proliferation, BMSC-specific-affinity peptide can enhance recruitment and retention of endogenous BMSCs when placed on the surface of composite scaffolds made of SF and PCL, thus reducing cell loss and enhancing scaffold chondrogenicity (Li et al., 2020). In addition to the materials discussed above, silicone can be made into a meniscus scaffold with excellent biocompatibility by using the method of heat-cured extrusion (Luis et al., 2019).

5 FUTURE PROSPECTS

To date there have been several technological advances in 3D printing of tissue-engineered cartilage, and 3D printing of irregularly shaped cartilage has evolved from simple morphological imitation to sophisticated biological tissue engineering. However there is still a need for in-depth research and continuous innovation to improve the effectiveness of complex tissue-engineered cartilage scaffolds.

5.1 Optimization of Technology and Materials Required for 3D Printing

For 3D printing of irregularly shaped cartilage scaffolds, further optimization of 3D printers is needed to increase the range of applications. For example, achieving more precise dynamic control of printing temperature for materials that require high or low temperature would allow for combining polymers and cell-loaded hydrogels into a single scaffold.

In terms of the choice of synthetic macromolecular polymers, the main problem to be solved is whether the hardness of the resulting material is close to that of natural cartilage. PU has been shown to have superior elastic properties, which may make it the first choice among cartilage materials in the future. For selection of cell carriers such as hydrogels, we need to identify biomaterials that can better promote cell viability. At the same time, it is hoped that some drugs, such as antibiotics or growth factors, can be mixed with hydrogels or evenly coated on 3D-printed scaffolds to reduce inflammation or promote cartilage regeneration, respectively. In addition, the material properties of synthetic macromolecular polymers and hydrogels can be modified to increase cell adhesion.

5.2 Optimization of 3D-Printed Cartilage Scaffolds

Research on printing of irregularly shaped 3D cartilage scaffolds has mainly focused on simulation of morphology, while only a few studies, such as those concerned with tracheal scaffolds, have considered optimization of function. For example, improving blood circulation in and around cartilage may increase biocompatibility of the overall scaffold, which may be achieved by implanting 3D-printed cartilage with embedded blood vessels into cartilage repairs. In the future, it may be possible to print auricular and nasal cartilage scaffolds and skin at the same time using 3D printing technology. For printed tracheal cartilage, materials that can adapt to airflow should be further studied. As for the meniscus, because its surface is smooth in the physiological state, this should also be true of the 3D-printed scaffold.

5.3 4D Printing

Based on 3D printing research, 4D printing is gradually being applied in the field of cartilage tissue engineering. The fourth dimension in 4D printing results from changes in conditions, e.g., light, electromagnetic fields, water, or temperature. Some materials with shape memory can restore their original shape under certain conditions (Wu et al., 2018). On this basis, the shape of the hydrogel loaded with a drug could be made to change after being implanted. This technique can not only alter the shape of the scaffold but also slow drug release. Hopefully, complex structural shapes can be optimized by 4D printing. In the future, it may also be possible to inject cells into the closed spaces when the 4D-printed scaffold is deformed in order to prevent loss of cells.

5.4 Applications *In Vivo* and in Clinical Trials

At present, although many kinds of research are devoted to 3D-printed cartilage scaffolds, most lack sufficient clinical trials and are not mature enough to be used in the clinic. A perfect cartilage scaffold needs *in vitro* and *in vivo* experiments to verify its feasibility. If it is to be used in the clinic, follow-up clinical trials are also essential. Therefore, there is still a great need for further research on 3D printing of tissue-engineered cartilage. Nevertheless, some 3D-printed scaffolds are expected to replace implant materials currently on the market.

6 CONCLUSION

3D-printed cartilage has been successfully utilized in various medical fields. This review discusses in detail selection and preparation of various irregularly shaped cartilage scaffolds, including auricle, nasal, tracheal, and meniscus. Using 3D printing technology, scaffolds printed with biocompatible high molecular-weight polymer materials can be combined with hydrogel and chondrocyte matrix to produce ideal irregularly shaped cartilage scaffolds. In addition, we look forward to optimization of 3D printing technology and the materials required for 3D printing. 3D printed cartilage scaffolds can be optimized by increasing blood supply, adding the concept of 4D printing, and increasing research *in vivo* which moves on to clinical trials. We are hopeful that these considerations will be integrated into future research.

AUTHOR CONTRIBUTIONS

HW: Writing-original draft, Funding acquisition. ZHW: Supervision. HL: Supervision. JQL: Conceptualization. RHL: Funding acquisition. XJZ: Conceptualization. MR: Conceptualization. MLW: Conceptualization. YZL: Supervision. YBL: Funding acquisition. YXJ: Funding acquisition. CYW: Investigation. JCW: Investigation and Methodology.

FUNDING

This study was supported by the National Natural Science Foundation of China (82001971, 82102358), the National Key R&D Program of China (2018YFB1105100), the Scientific Development Program of Jilin Province (20200403088SF, 20200802008GH, 20200404202YY, 20200404140YY, 20190304123YY, 20200404190YY, and 20190103087JH), the Program of Jilin Provincial Health Department (2020Q018, 2020SCZT064, 2020SCZT065, 2019SCZT001, 2019SCZT014, 2019SRCJ001, and 2017F007), the Youth Talents Promotion Project of Jilin Province (192004); and the Graduate Innovation Fund of Jilin University (101832020CX297).

REFERENCES

Aggarwal, S., and Pittenger, M. F. (2005). Human Mesenchymal Stem Cells Modulate Allogeneic Immune Cell Responses. *Blood* 105 (4), 1815–1822. doi:10.1182/blood-2004-04-1559

Ahn, C. B., Son, K. H., Yu, Y. S., Kim, T. H., Lee, J. I., and Lee, J. W. (2019). Development of a Flexible 3D Printed Scaffold with a Cell-Adhesive Surface for Artificial Trachea. *Biomed. Mater.* 14 (5), 055001. doi:10.1088/1748-605X/ab2a6c

Anderson, C. E. (1962). The Structure and Function of Cartilage. *J. Bone Jt. Surg.* 44, 777–786. doi:10.2106/00004623-196244040-00020

Apelgren, P., Karabulut, E., Amoroso, M., Mantas, A., Martínez Ávila, H., Kölby, L., et al. (2019). *In Vivo* Human Cartilage Formation in Three-Dimensional Bioprinted Constructs with a Novel Bacterial Nanocellulose Bioink. *ACS Biomater. Sci. Eng.* 5 (5), 2482–2490. doi:10.1021/acsbiomaterials.9b00157

Bae, S. W., Lee, K. W., Park, J. H., Lee, J., Jung, C. R., Yu, J., et al. (2018). 3D Bioprinted Artificial Trachea with Epithelial Cells and Chondrogenic-Differentiated Bone Marrow-Derived Mesenchymal Stem Cells. *Int. J. Mol. Sci.* 19 (6), 1624. doi:10.3390/ijms19061624

Baena, J., Jiménez, G., López-Ruiz, E., Antich, C., Griñán-Lisón, C., Perán, M., et al. (2019). Volume-by-volume Bioprinting of Chondrocytes-Alginate Bioinks in High Temperature Thermoplastic Scaffolds for Cartilage Regeneration. *Exp. Biol. Med. (Maywood)* 244 (1), 13–21. doi:10.1177/1535370218821128

Bahcecioglu, G., Hasirci, N., Bilgen, B., and Hasirci, V. (2019). A 3D Printed PCL/hydrogel Construct with Zone-specific Biochemical Composition Mimicking that of the Meniscus. *Biofabrication* 11 (2), 025002. doi:10.1088/1758-5090/aaf707

Bandyopadhyay, A., and Mandal, B. B. (2019). A Three-Dimensional Printed Silk-Based Biomimetic Tri-layered Meniscus for Potential Patient-specific Implantation. *Biofabrication* 12 (1), 015003. doi:10.1088/1758-5090/ab40fa

Bhattacharjee, J., Sarkar, A., and Panda, T. K. (2021). Alkali and Alkaline Earth Metal Complexes as Versatile Catalysts for Ring-Opening Polymerization of Cyclic Esters. *Chem. Rec.* 21 (11), 1898–1911. doi:10.1002/tcr.202100148

Brand-Saberi, B. E. M., and Schäfer, T. (2014). Trachea. *Thorac. Surg. Clin.* 24 (1), 1–5. doi:10.1016/j.thorsurg.2013.09.004

Cao, Y., Sang, S., An, Y., Xiang, C., Li, Y., and Zhen, Y. (2021). Progress of 3D Printing Techniques for Nasal Cartilage Regeneration. *Aesth Plast. Surg.* doi:10.1007/s00266-021-02472-4

Cao, Y., Vacanti, J. P., Paige, K. T., Upton, J., and Vacanti, C. A. (1997). Transplantation of Chondrocytes Utilizing a Polymer-Cell Construct to Produce Tissue-Engineered Cartilage in the Shape of a Human Ear. *Plast. Reconstr. Surg.* 100 (2), 297–302. discussion 303-294. doi:10.1097/00006534-199708000-00001

Çelik, M., and Aktan, E. (2019). Construction of Bony-Cartilaginous Defects of the Nose. *J. Craniofac. Surg.* 30 (3), E234–E235. doi:10.1097/SCS.0000000000005189

Cengiz, I. F., Pereira, H., Espregueira-Mendes, J., Kwon, I. K., Reis, R. L., and Oliveira, J. M. (2019). Suturable Regenerated Silk Fibroin Scaffold Reinforced with 3D-Printed Polycaprolactone Mesh: Biomechanical Performance and Subcutaneous Implantation. *J. Mater. Sci. Mater. Med.* 30 (6), 63. doi:10.1007/s10856-019-6265-3

Cenzi, R., Farina, A., Zuccarino, L., and Carinci, F. (2005). Clinical Outcome of 285 Medpor Grafts Used for Craniofacial Reconstruction. *J. Craniofac. Surg.* 16, 526–530. doi:10.1097/01.scs.0000168761.46700.dc

Chae, S., Lee, S.-S., Choi, Y.-J., Hong, D. H., Gao, G., Wang, J. H., et al. (2021). 3D Cell-Printing of Biocompatible and Functional Meniscus Constructs Using Meniscus-derived Bioink. *Biomaterials* 267, 120466. doi:10.1016/j.biomaterials.2020.120466

Chameettachal, S., Midha, S., and Ghosh, S. (2016). Regulation of Chondrogenesis and Hypertrophy in Silk Fibroin-Gelatin-Based 3D Bioprinted Constructs. *ACS Biomater. Sci. Eng.* 2 (9), 1450–1463. doi:10.1021/acsbiomaterials.6b00152

Chen, M., Feng, Z., Guo, W., Yang, D., Gao, S., Li, Y., et al. (2019). PCL-MECM-Based Hydrogel Hybrid Scaffolds and Meniscal Fibrochondrocytes Promote Whole Meniscus Regeneration in a Rabbit Meniscectomy Model. *ACS Appl. Mater. Inter.* 11 (44), 41626–41639. doi:10.1021/acsami.9b13611

Chen, X., Chen, G., Wang, G., Zhu, P., and Gao, C. (2019). Recent Progress on 3D-Printed Polylactic Acid and its Applications in Bone Repair. *Adv. Eng. Mater.* 22 (4), 1901065. doi:10.1002/adem.201901065

Cheng, L., Yao, B., Hu, T., Cui, X., Shu, X., Tang, S., et al. (2019). Properties of an Alginate-Gelatin-Based Bioink and its Potential Impact on Cell Migration, Proliferation, and Differentiation. *Int. J. Biol. Macromolecules* 135, 1107–1113. doi:10.1016/j.ijbiomac.2019.06.017

Cheng, Y.-L., and Chen, F. (2017). Preparation and Characterization of Photocured Poly (ε-Caprolactone) Diacrylate/poly (Ethylene Glycol) Diacrylate/chitosan for Photopolymerization-type 3D Printing Tissue Engineering Scaffold Application. *Mater. Sci. Eng. C* 81, 66–73. doi:10.1016/j.msec.2017.07.025

Chia, H. N., and Wu, B. M. (2015). Recent Advances in 3D Printing of Biomaterials. *J. Biol. Eng.* 9, 4. doi:10.1186/s13036-015-0001-4

Chung, J. H. Y., Kade, J. C., Jeiranikhameneh, A., Ruberu, K., Mukherjee, P., Yue, Z., et al. (2020). 3D Hybrid Printing Platform for Auricular Cartilage Reconstruction. *Biomed. Phys. Eng. Express* 6 (3), 035003. doi:10.1088/2057-1976/ab54a7

Contentin, R., Demoor, M., Concari, M., Desancé, M., Audigié, F., Branly, T., et al. (2019). Comparison of the Chondrogenic Potential of Mesenchymal Stem Cells Derived from Bone Marrow and Umbilical Cord Blood Intended for Cartilage Tissue Engineering. *Stem Cel Rev Rep* 16 (1), 126–143. doi:10.1007/s12015-019-09914-2

Daly, A. C., Critchley, S. E., Rencsok, E. M., and Kelly, D. J. (2016). A Comparison of Different Bioinks for 3D Bioprinting of Fibrocartilage and Hyaline Cartilage. *Biofabrication* 8 (4), 045002. doi:10.1088/1758-5090/8/4/045002

De Caro, F., Perdisa, F., Dhollander, A., Verdonk, R., and Verdonk, P. (2020). Meniscus Scaffolds for Partial Meniscus Defects. *Clin. Sports Med.* 39 (1), 83–92. doi:10.1016/j.csm.2019.08.011

Ding, J., Chen, B., Lv, T., Liu, X., Fu, X., Wang, Q., et al. (2016). Bone Marrow Mesenchymal Stem Cell-Based Engineered Cartilage Ameliorates Polyglycolic Acid/Polylactic Acid Scaffold-Induced Inflammation through M2 Polarization of Macrophages in a Pig Model. *STEM CELLS Translational Med.* 5 (8), 1079–1089. doi:10.5966/sctm.2015-0263

Dong, L., Wang, S.-J., Zhao, X.-R., Zhu, Y.-F., and Yu, J.-K. (2017). 3D- Printed Poly(ε-Caprolactone) Scaffold Integrated with Cell-Laden Chitosan Hydrogels for Bone Tissue Engineering. *Sci. Rep.* 7 (1), 13412. doi:10.1038/s41598-017-13838-7

Dranseikiene, D., Schrüfer, S., Schubert, D. W., Reakasame, S., and Boccaccini, A. R. (2020). Cell-laden Alginate Dialdehyde-Gelatin Hydrogels Formed in 3D Printed Sacrificial Gel. *J. Mater. Sci. Mater. Med.* 31 (3), 31. doi:10.1007/s10856-020-06369-7

Duan, B., Hockaday, L. A., Kang, K. H., and Butcher, J. T. (2013). 3D Bioprinting of Heterogeneous Aortic Valve Conduits with Alginate/gelatin Hydrogels. *J. Biomed. Mater. Res.* 101A (5), 1255–1264. doi:10.1002/jbm.a.34420

Dutta, S. D., Hexiu, J., Patel, D. K., Ganguly, K., and Lim, K.-T. (2021). 3D-printed Bioactive and Biodegradable Hydrogel Scaffolds of Alginate/gelatin/cellulose Nanocrystals for Tissue Engineering. *Int. J. Biol. Macromolecules* 167, 644–658. doi:10.1016/j.ijbiomac.2020.12.011

Fabre, D., Kolb, F., Fadel, E., Mercier, O., Mussot, S., Le Chevalier, T., et al. (2013). Successful Tracheal Replacement in Humans Using Autologous Tissues: An 8-Year Experience. *Ann. Thorac. Surg.* 96 (4), 1146–1155. doi:10.1016/j.athoracsur.2013.05.073

Farzan, A., Borandeh, S., Zanjanizadeh Ezazi, N., Lipponen, S., Santos, H. A., and Seppälä, J. (2020). 3D Scaffolding of Fast Photocurable Polyurethane for Soft Tissue Engineering by Stereolithography: Influence of Materials and Geometry on Growth of Fibroblast Cells. *Eur. Polym. J.* 139, 109988. doi:10.1016/j.eurpolymj.2020.109988

Fenton, O. S., Paolini, M., Andresen, J. L., Müller, F. J., and Langer, R. (2020). Outlooks on Three-Dimensional Printing for Ocular Biomaterials Research. *J. Ocul. Pharmacol. Ther.* 36 (1), 7–17. doi:10.1089/jop.2018.0142

Foerster, D. W. (1966a). Total Reconstruction of the External Ear. *J. Okla. State. Med. Assoc.* 59 (11), 606–608.

Francis, S. L., Di Bella, C., Wallace, G. G., and Choong, P. F. M. (2018a). Cartilage Tissue Engineering Using Stem Cells and Bioprinting Technology-Barriers to Clinical Translation. *Front. Surg.* 5, 70. doi:10.3389/fsurg.2018.00070

Francis, S. L., Duchi, S., Onofrillo, C., Di Bella, C., and Choong, P. F. M. (2018b). Adipose-Derived Mesenchymal Stem Cells in the Use of Cartilage Tissue Engineering: The Need for a Rapid Isolation Procedure. *Stem Cell Int.* 2018, 1–9. doi:10.1155/2018/8947548

Gao, B., Jing, H., Gao, M., Wang, S., Fu, W., Zhang, X., et al. (2019). Long-segmental Tracheal Reconstruction in Rabbits with Pedicled Tissue-Engineered Trachea Based on a 3D-Printed Scaffold. *Acta Biomater.* 97, 177–186. doi:10.1016/j.actbio.2019.07.043

Gentile, P., Chiono, V., Carmagnola, I., and Hatton, P. (2014). An Overview of Poly(lactic-Co-Glycolic) Acid (PLGA)-Based Biomaterials for Bone Tissue Engineering. *Ijms* 15 (3), 3640–3659. doi:10.3390/ijms15033640

Gradwohl, M., Chai, F., Payen, J., Guerreschi, P., Marchetti, P., and Blanchemain, N. (2021). Effects of Two Melt Extrusion Based Additive Manufacturing Technologies and Common Sterilization Methods on the Properties of a Medical Grade PLGA Copolymer. *Polymers* 13 (4), 572. doi:10.3390/polym13040572

Griffin, M., Castro, N., Bas, O., Saifzadeh, S., Butler, P., and Hutmacher, D. W. (2020). The Current Versatility of Polyurethane Three-Dimensional Printing for Biomedical Applications. *Tissue Eng. B: Rev.* 26 (3), 272–283. doi:10.1089/ten.TEB.2019.0224

Gu, B. K., Choi, D. J., Park, S. J., Kim, M. S., Kang, C. M., and Kim, C.-H. (2016). 3-dimensional Bioprinting for Tissue Engineering Applications. *Biomater. Res.* 20 (1), 12. doi:10.1186/s40824-016-0058-2

Guo, T., Holzberg, T. R., Lim, C. G., Gao, F., Gargava, A., Trachtenberg, J. E., et al. (2017). 3D Printing PLGA: a Quantitative Examination of the Effects of Polymer Composition and Printing Parameters on Print Resolution. *Biofabrication* 9 (2), 024101. doi:10.1088/1758-5090/aa6370

Hamaji, M., Kojima, F., Koyasu, S., Tsuruyama, T., Komatsu, T., Ikuno, T., et al. (2014). Development of a Composite and Vascularized Tracheal Scaffold in the Omentum for *In Situ* Tissue Engineering: a Canine Model. *Interactive CardioVascular Thorac. Surg.* 19 (3), 357–362. doi:10.1093/icvts/ivu177

Hamilton, N. J., Kanani, M., Roebuck, D. J., Hewitt, R. J., Cetto, R., Culme-Seymour, E. J., et al. (2015). Tissue-Engineered Tracheal Replacement in a Child: A 4-Year Follow-Up Study. *Am. J. Transplant.* 15 (10), 2750–2757. doi:10.1111/ajt.13318

Honkanen, J. T. J., Turunen, M. J., Tiitu, V., Jurvelin, J. S., and Töyräs, J. (2016). Transport of Iodine Is Different in Cartilage and Meniscus. *Ann. Biomed. Eng.* 44 (7), 2114–2122. doi:10.1007/s10439-015-1513-2

Hsieh, C.-T., Liao, C.-Y., Dai, N.-T., Tseng, C.-S., Yen, B. L., and Hsu, S.-h. (2018). 3D Printing of Tubular Scaffolds with Elasticity and Complex Structure from Multiple Waterborne Polyurethanes for Tracheal Tissue Engineering. *Appl. Mater. Today* 12, 330–341. doi:10.1016/j.apmt.2018.06.004

Hsieh, F.-Y., and Hsu, S.-h. (2015). 3D Bioprinting: A New Insight into the Therapeutic Strategy of Neural Tissue Regeneration. *Organogenesis* 11 (4), 153–158. doi:10.1080/15476278.2015.1123360

Hull, C. W. (1996). *Apparatus for Production of Three-Dimensional Objects by Stereolithography*. US5556590 A.

Jang, C. H., Koo, Y., and Kim, G. (2020). ASC/chondrocyte-laden Alginate Hydrogel/PCL Hybrid Scaffold Fabricated Using 3D Printing for Auricle Regeneration. *Carbohydr. Polym.* 248, 116776. doi:10.1016/j.carbpol.2020.116776

Jang, Y., Koh, Y. G., Choi, Y.-J., Kim, S.-H., Yoon, D. S., Lee, M., et al. (2015). Characterization of Adipose Tissue-Derived Stromal Vascular Fraction for Clinical Application to Cartilage Regeneration. In Vitro *Cell.Dev.Biol.-Animal* 51 (2), 142–150. doi:10.1007/s11626-014-9814-6

Janssen, A., Mastouri, M., Boboli, H., Demarche, M., Brandt, H., Moonen, V., et al. (2021). Treatment of Tracheo(broncho)malacia in Children. *Rev. Med. Liege* 76 (3), 145–151.

Jia, L., Zhang, Y., Yao, L., Zhang, P., Ci, Z., Zhang, W., et al. (2020). Regeneration of Human-Ear-Shaped Cartilage with Acellular Cartilage Matrix-Based Biomimetic Scaffolds. *Appl. Mater. Today* 20, 100639. doi:10.1016/j.apmt.2020.100639

Jo, C. H., Lee, Y. G., Shin, W. H., Kim, H., Chai, J. W., Jeong, E. C., et al. (2014). Intra-Articular Injection of Mesenchymal Stem Cells for the Treatment of Osteoarthritis of the Knee: A Proof-of-Concept Clinical Trial. *Stem Cells* 32 (5), 1254–1266. doi:10.1002/stem.1634

Jodat, Y. A., Kiaee, K., Vela Jarquin, D., De la Garza Hernández, R. L., Wang, T., Joshi, S., et al. (2020). A 3D-Printed Hybrid Nasal Cartilage with Functional Electronic Olfaction. *Adv. Sci.* 7 (5), 1901878. doi:10.1002/advs.201901878

Jung, C. S., Kim, B. K., Lee, J., Min, B.-H., and Park, S.-H. (2018). Development of Printable Natural Cartilage Matrix Bioink for 3D Printing of Irregular Tissue Shape. *Tissue Eng. Regen. Med.* 15 (2), 155–162. doi:10.1007/s13770-017-0104-8

Jung, J. W., Park, J. H., Hong, J. M., Kang, H.-W., and Cho, D.-W. (2014). Octahedron Pore Architecture to Enhance Flexibility of Nasal Implant-Shaped Scaffold for Rhinoplasty. *Int. J. Precis. Eng. Manuf.* 15 (12), 2611–2616. doi:10.1007/s12541-014-0634-0

Jung, B. K., Kim, J. Y., Kim, Y. S., Roh, T. S., Seo, A., Park, K. H., et al. (2019). Ideal Scaffold Design for Total Ear Reconstruction Using a Three-Dimensional Printing Technique. *J. Biomed. Mater. Res. Part B Appl. Biomater.* 107 (4), 1295–1303. doi:10.1002/jbm.b.34222

Kačarević, Ž., Rider, P., Alkildani, S., Retnasingh, S., Smeets, R., Jung, O., et al. (2018). An Introduction to 3D Bioprinting: Possibilities, Challenges and Future Aspects. *Materials* 11 (11), 2199. doi:10.3390/ma11112199

Kang, H.-W., Lee, S. J., Ko, I. K., Kengla, C., Yoo, J. J., and Atala, A. (2016). A 3D Bioprinting System to Produce Human-Scale Tissue Constructs with Structural Integrity. *Nat. Biotechnol.* 34 (3), 312–319. doi:10.1038/nbt.3413

Kesti, M., Eberhardt, C., Pagliccia, G., Kenkel, D., Grande, D., Boss, A., et al. (2015). Bioprinting Complex Cartilaginous Structures with Clinically Compliant Biomaterials. *Adv. Funct. Mater.* 25 (48), 7406–7417. doi:10.1002/adfm.201503423

Khoshnood, N., Zamanian, A., and Abbasi, M. (2021). The Potential Impact of Polyethylenimine on Biological Behavior of 3D-Printed Alginate Scaffolds. *Int. J. Biol. Macromolecules* 178 (4), 19–28. doi:10.1016/j.ijbiomac.2021.02.152

Kim, B. S., Jang, J., Chae, S., Gao, G., Kong, J.-S., Ahn, M., et al. (2016). Three-dimensional Bioprinting of Cell-Laden Constructs with Polycaprolactone Protective Layers for Using Various Thermoplastic Polymers. *Biofabrication* 8 (3), 035013. doi:10.1088/1758-5090/8/3/035013

Kim, H., Lee, J. Y., Han, H., Cho, W.-W., Han, H., Choi, A., et al. (2021). Improved Chondrogenic Performance with Protective Tracheal Design of Chitosan Membrane Surrounding 3D-Printed Trachea. *Sci. Rep.* 11 (1), 9258. doi:10.1038/s41598-021-88830-3

Kim, I. G., Park, S. A., Lee, S.-H., Choi, J. S., Cho, H., Lee, S. J., et al. (2020). Transplantation of a 3D-Printed Tracheal Graft Combined with iPS Cell-Derived MSCs and Chondrocytes. *Sci. Rep.* 10 (1), 4326. doi:10.1038/s41598-020-61405-4

Kim, H. Y., Jung, S. Y., Lee, S. J., Lee, H. J., Truong, M.-D., and Kim, H. S. (2019). Fabrication and Characterization of 3D-Printed Elastic Auricular Scaffolds: A Pilot Study. *The Laryngoscope* 129 (2), 351–357. doi:10.1002/lary.27344

Kim, M. H., Lee, Y. W., Jung, W.-K., Oh, J., and Nam, S. Y. (2019). Enhanced Rheological Behaviors of Alginate Hydrogels with Carrageenan for Extrusion-Based Bioprinting. *J. Mech. Behav. Biomed. Mater.* 98, 187–194. doi:10.1016/j.jmbbm.2019.06.014

Kong, H. J., Kaigler, D., Kim, K., and Mooney, D. J. (2004). Controlling Rigidity and Degradation of Alginate Hydrogels via Molecular Weight Distribution. *Biomacromolecules* 5 (5), 1720–1727. doi:10.1021/bm049879r

Kundu, J., Shim, J.-H., Jang, J., Kim, S.-W., and Cho, D.-W. (2015). An Additive Manufacturing-Based PCL-Alginate-Chondrocyte Bioprinted Scaffold for Cartilage Tissue Engineering. *J. Tissue Eng. Regen. Med.* 9 (11), 1286–1297. doi:10.1002/term.1682

Kwon, H., Brown, W. E., Lee, C. A., Wang, D., Paschos, N., Hu, J. C., et al. (2019). Surgical and Tissue Engineering Strategies for Articular Cartilage and Meniscus Repair. *Nat. Rev. Rheumatol.* 15 (9), 550–570. doi:10.1038/s41584-019-0255-1

Le, H., Xu, W., Zhuang, X., Chang, F., Wang, Y., and Ding, J. (2020). Mesenchymal Stem Cells for Cartilage Regeneration. *J. Tissue Eng.* 11, 204173142094383. doi:10.1177/2041731420943839

Lee, J.-S., Hong, J. M., Jung, J. W., Shim, J.-H., Oh, J.-H., and Cho, D.-W. (2014). 3D Printing of Composite Tissue with Complex Shape Applied to Ear Regeneration. *Biofabrication* 6 (2), 024103. doi:10.1088/1758-5082/6/2/024103

Li, H., Liao, Z., Yang, Z., Gao, C., Fu, L., Li, P., et al. (2021). 3D Printed Poly(ε-Caprolactone)/Meniscus Extracellular Matrix Composite Scaffold Functionalized with Kartogenin-Releasing PLGA Microspheres for Meniscus Tissue Engineering. *Front. Bioeng. Biotechnol.* 9, 662381. doi:10.3389/fbioe.2021.662381

Li, X., Wang, M., Jing, X., Guo, W., Hao, C., Zhang, Y., et al. (2018). Bone Marrow- and Adipose Tissue-Derived Mesenchymal Stem Cells: Characterization, Differentiation, and Applications in Cartilage Tissue Engineering. *Crit. Rev. Eukaryot. Gene Expr.* 28 (4), 285–310. doi:10.1615/CritRevEukaryotGeneExpr.2018023572

Li, Z., Wu, N., Cheng, J., Sun, M., Yang, P., Zhao, F., et al. (2020). Biomechanically, Structurally and Functionally Meticulously Tailored Polycaprolactone/silk Fibroin Scaffold for Meniscus Regeneration. *Theranostics* 10 (11), 5090–5106. doi:10.7150/thno.44270

Liu, P., Shen, H., Zhi, Y., Si, J., Shi, J., Guo, L., et al. (2019). 3D Bioprinting and *In Vitro* Study of Bilayered Membranous Construct with Human Cells-Laden Alginate/gelatin Composite Hydrogels. *Colloids Surf. B: Biointerfaces* 181, 1026–1034. doi:10.1016/j.colsurfb.2019.06.069

Liu, Q., Li, Q., Xu, S., Zheng, Q., and Cao, X. (2018). Preparation and Properties of 3D Printed Alginate-Chitosan Polyion Complex Hydrogels for Tissue Engineering. *Polymers* 10 (6), 664. doi:10.3390/polym10060664

Liu, F., Liu, C., Zheng, B., He, J., Liu, J., Chen, C., et al. (2020). Synergistic Effects on Incorporation of β-Tricalcium Phosphate and Graphene Oxide Nanoparticles to Silk Fibroin/Soy Protein Isolate Scaffolds for Bone Tissue Engineering. *Polymers* 12 (1), 69. doi:10.3390/polym12010069

Liu, W., Feng, Z., Ou-Yang, W., Pan, X., Wang, X., Huang, P., et al. (2020). 3D Printing of Implantable Elastic PLCL Copolymer Scaffolds. *Soft Matter* 16 (8), 2141–2148. doi:10.1039/c9sm02396h

Lo, W.-C., Chen, W.-H., Lin, T.-C., Hwang, S.-M., Zeng, R., Hsu, W.-C., et al. (2013). Preferential Therapy for Osteoarthritis by Cord Blood MSCs through Regulation of Chondrogenic Cytokines. *Biomaterials* 34 (20), 4739–4748. doi:10.1016/j.biomaterials.2013.03.016

Long, J., Etxeberria, A. E., Nand, A. V., Bunt, C. R., Ray, S., and Seyfoddin, A. (2019). A 3D Printed Chitosan-Pectin Hydrogel Wound Dressing for Lidocaine Hydrochloride Delivery. *Mater. Sci. Eng. C* 104, 109873. doi:10.1016/j.msec.2019.109873

Luis, E., Pan, H. M., Sing, S. L., Bastola, A. K., Goh, G. D., Goh, G. L., et al. (2019). Silicone 3D Printing: Process Optimization, Product Biocompatibility, and Reliability of Silicone Meniscus Implants. *3D Printing and Additive Manufacturing* 6 (6), 319–332. doi:10.1089/3dp.2018.0226

Luo, K., Wang, L., Chen, X., Zeng, X., Zhou, S., Zhang, P., et al. (2020a). Biomimetic Polyurethane 3D Scaffolds Based on Polytetrahydrofuran Glycol and Polyethylene Glycol for Soft Tissue Engineering. *Polymers* 12 (11), 2631. doi:10.3390/polym12112631

Luo, W., Song, Z., Wang, Z., Wang, Z., Li, Z., Wang, C., et al. (2020b). Printability Optimization of Gelatin-Alginate Bioinks by Cellulose Nanofiber Modification for Potential Meniscus Bioprinting. *J. Nanomater.* 2020, 1–13. doi:10.1155/2020/3863428

Luo, Y., Wei, X., Wan, Y., Lin, X., Wang, Z., and Huang, P. (2019). 3D Printing of Hydrogel Scaffolds for Future Application in Photothermal Therapy of Breast Cancer and Tissue Repair. *Acta Biomater.* 92, 37–47. doi:10.1016/j.actbio.2019.05.039

Macchiarini, P., Jungebluth, P., Go, T., Asnaghi, M. A., Rees, L. E., Cogan, T. A., et al. (2009). Clinical Transplantation of a Tissue-Engineered Airway. *Lancet* 372 (9655), 2023–2030. doi:10.1016/S0140-6736(08)61598-6

Markes, A. R., Hodax, J. D., and Ma, C. B. (2020). Meniscus Form and Function. *Clin. Sports Med.* 39 (1), 1–12. doi:10.1016/j.csm.2019.08.007

Markstedt, K., Mantas, A., Tournier, I., Martínez Ávila, H., Hägg, D., and Gatenholm, P. (2015). 3D Bioprinting Human Chondrocytes with Nanocellulose-Alginate Bioink for Cartilage Tissue Engineering Applications. *Biomacromolecules* 16 (5), 1489–1496. doi:10.1021/acs.biomac.5b00188

Masutani, K., and Kimura, Y. (2017). "Present Situation and Future Perspectives of Poly(lactic Acid)," in *Synthesis, Structure and Properties of Poly(lactic Acid)*, 279, 1–25. doi:10.1007/12_2016_16

Melo, B. A. G., Jodat, Y. A., Mehrotra, S., Calabrese, M. A., Kamperman, T., Mandal, B. B., et al. (2019). 3D Printed Cartilage-Like Tissue Constructs with Spatially Controlled Mechanical Properties. *Adv. Funct. Mater.* 29 (51), 1906330. doi:10.1002/adfm.201906330

Merceron, T. K., Burt, M., Seol, Y.-J., Kang, H.-W., Lee, S. J., Yoo, J. J., et al. (2015). A 3D Bioprinted Complex Structure for Engineering the Muscle-Tendon Unit. *Biofabrication* 7 (3), 035003. doi:10.1088/1758-5090/7/3/035003

Morrison, R. J., Nasser, H. B., Kashlan, K. N., Zopf, D. A., Milner, D. J., Flanangan, C. L., et al. (2018). Co-culture of Adipose-Derived Stem Cells and Chondrocytes on Three-Dimensionally Printed Bioscaffolds for Craniofacial Cartilage Engineering. *The Laryngoscope* 128 (7), E251–E257. doi:10.1002/lary.27200

Mouser, V. H. M., Levato, R., Bonassar, L. J., D'Lima, D. D., Grande, D. A., Klein, T. J., et al. (2017). Three-Dimensional Bioprinting and its Potential in the Field of Articular Cartilage Regeneration. *Cartilage* 8 (4), 327–340. doi:10.1177/1947603516665445

Mouser, V. H. M., Levato, R., Mensinga, A., Dhert, W. J. A., Gawlitta, D., and Malda, J. (2020). Bio-ink Development for Three-Dimensional Bioprinting of Hetero-Cellular Cartilage Constructs. *Connect. Tissue Res.* 61 (2), 137–151. doi:10.1080/03008207.2018.1553960

Mu, X., Fitzpatrick, V., and Kaplan, D. L. (2020). From Silk Spinning to 3D Printing: Polymer Manufacturing Using Directed Hierarchical Molecular Assembly. *Adv. Healthc. Mater.* 9 (15), 1901552. doi:10.1002/adhm.201901552

Neubauer, V. J., Döbl, A., and Scheibel, T. (2021). Silk-Based Materials for Hard Tissue Engineering. *Materials* 14 (3), 674. doi:10.3390/ma14030674

Neubauer, V. J., and Scheibel, T. (2020). Spider Silk Fusion Proteins for Controlled Collagen Binding and Biomineralization. *ACS Biomater. Sci. Eng.* 6 (10), 5599–5608. doi:10.1021/acsbiomaterials.0c00818

Ni, T., Liu, M., Zhang, Y., Cao, Y., and Pei, R. (2020). 3D Bioprinting of Bone Marrow Mesenchymal Stem Cell-Laden Silk Fibroin Double Network Scaffolds for Cartilage Tissue Repair. *Bioconjug. Chem.* 31 (8), 1938–1947. doi:10.1021/acs.bioconjchem.0c00298

Olubamiji, A. D., Izadifar, Z., Si, J. L., Cooper, D. M. L., Eames, B. F., and Chen, D. X. (2016). Modulating Mechanical Behaviour of 3D-Printed Cartilage-Mimetic PCL Scaffolds: Influence of Molecular Weight and Pore Geometry. *Biofabrication* 8 (2), 025020. doi:10.1088/1758-5090/8/2/025020

Oveissi, F., Tavakoli, N., Minaiyan, M., Mofid, M. R., and Taheri, A. (2020). Alginate Hydrogel Enriched with *Ambystoma mexicanum* Epidermal Lipoxygenase-Loaded Pectin Nanoparticles for Enhanced Wound Healing. *J. Biomater. Appl.* 34 (8), 1171–1187. doi:10.1177/0885328219896704

Park, H. S., Lee, J. S., Jung, H., Kim, D. Y., Kim, S. W., Sultan, M. T., et al. (2018). An Omentum-Cultured 3D-Printed Artificial Trachea: *In Vivo* Bioreactor. *Artif. Cell Nanomedicine, Biotechnol.* 46 (Suppl. 3), S1131–S1140. doi:10.1080/21691401.2018.1533844

Park, J.-H., Yoon, J.-K., Lee, J. B., Shin, Y. M., Lee, K.-W., Bae, S.-W., et al. (2019). Experimental Tracheal Replacement Using 3-dimensional Bioprinted Artificial Trachea with Autologous Epithelial Cells and Chondrocytes. *Sci. Rep.* 9, 2103. doi:10.1038/s41598-019-38565-z

Park, J. H., Hong, J. M., Ju, Y. M., Jung, J. W., Kang, H.-W., Lee, S. J., et al. (2015). A Novel Tissue-Engineered Trachea with a Mechanical Behavior Similar to Native Trachea. *Biomaterials* 62, 106–115. doi:10.1016/j.biomaterials.2015.05.008

Park, J. Y., Choi, Y.-J., Shim, J.-H., Park, J. H., and Cho, D.-W. (2017). Development of a 3D Cell Printed Structure as an Alternative to Autologs Cartilage for Auricular Reconstruction. *J. Biomed. Mater. Res.* 105 (5), 1016–1028. doi:10.1002/jbm.b.33639

Parkhouse, N., and Evans, D. (1985). Reconstruction of the Ala of the Nose Using a Composite Free Flap from the Pinna. *Br. J. Plast. Surg.* 38 (3), 306–313. doi:10.1016/0007-1226(85)90233-4

Patel, J. J., Modes, J. E., Flanagan, C. L., Krebsbach, P. H., Edwards, S. P., and Hollister, S. J. (2015). Dual Delivery of EPO and BMP2 from a Novel Modular Poly-ε-Caprolactone Construct to Increase the Bone Formation in Prefabricated Bone Flaps. *Tissue Eng. C: Methods* 21 (9), 889–897. doi:10.1089/ten.tec.2014.0643

Pensa, N. W., Curry, A. S., Bonvallet, P. P., Bellis, N. F., Rettig, K. M., Reddy, M. S., et al. (2019). 3D Printed Mesh Reinforcements Enhance the Mechanical Properties of Electrospun Scaffolds. *Biomater. Res.* 23 (1), 22. doi:10.1186/s40824-019-0171-0

Penumakala, P. K., Santo, J., and Thomas, A. (2020). A Critical Review on the Fused Deposition Modeling of Thermoplastic Polymer Composites. *Composites B: Eng.* 201, 108336. doi:10.1016/j.compositesb.2020.108336

Pittenger, M. F., Mackay, A. M., Beck, S. C., Jaiswal, R. K., Douglas, R., Mosca, J. D., et al. (1999). Multilineage Potential of Adult Human Mesenchymal Stem Cells. *Science* 284 (5411), 143–147. doi:10.1126/science.284.5411.143

Popescu, D., Zapciu, A., Amza, C., Baciu, F., and Marinescu, R. (2018). FDM Process Parameters Influence over the Mechanical Properties of Polymer Specimens: A Review. *Polym. Test.* 69, 157–166. doi:10.1016/j.polymertesting.2018.05.020

Ra, J. C., Shin, I. S., Kim, S. H., Kang, S. K., Kang, B. C., Lee, H. Y., et al. (2011). Safety of Intravenous Infusion of Human Adipose Tissue-Derived Mesenchymal Stem Cells in Animals and Humans. *Stem Cell Develop.* 20 (8), 1297–1308. doi:10.1089/scd.2010.0466

Rajabi, M., McConnell, M., Cabral, J., and Ali, M. A. (2021). Chitosan Hydrogels in 3D Printing for Biomedical Applications. *Carbohydr. Polym.* 260, 117768. doi:10.1016/j.carbpol.2021.117768

Rajzer, I., Kurowska, A., Jabłoński, A., Jatteau, S., Śliwka, M., Ziąbka, M., et al. (2018). Layered Gelatin/PLLA Scaffolds Fabricated by Electrospinning and 3D

Printing- for Nasal Cartilages and Subchondral Bone Reconstruction. *Mater. Des.* 155 (OCT), 297–306. doi:10.1016/j.matdes.2018.06.012

Rajzer, I., Kurowska, A., Jabłoński, A., Kwiatkowski, R., Piekarczyk, W., Hajduga, M. B., et al. (2020). Scaffolds Modified with Graphene as Future Implants for Nasal Cartilage. *J. Mater. Sci.* 55, 4030–4042. doi:10.1007/s10853-019-04298-7

Raucci, M. G., D'Amora, U., Ronca, A., Demitri, C., and Ambrosio, L. (2019). Bioactivation Routes of Gelatin-Based Scaffolds to Enhance at Nanoscale Level Bone Tissue Regeneration. *Front. Bioeng. Biotechnol.* 7, 27. doi:10.3389/fbioe.2019.00027

Romanazzo, S., Vedicherla, S., Moran, C., and Kelly, D. J. (2017). Meniscus ECM-functionalised Hydrogels Containing Infrapatellar Fat Pad-derived Stem Cells for Bioprinting of Regionally Defined Meniscal Tissue. *J. Tissue Eng. Regen. Med.* 12 (3), e1826–e1835. doi:10.1002/term.2602

Rich, J. T., and Gullane, P. J. (2012). Current Concepts in Tracheal Reconstruction. *Curr. Opin. Otolaryngol. Head Neck Surg.* 20 (4), 246–253. doi:10.1097/MOO.0b013e328355580e

Rosadi, I., Karina, K., Rosliana, I., Sobariah, S., Afini, I., Widyastuti, T., et al. (2019). *In Vitro* study of Cartilage Tissue Engineering Using Human Adipose-Derived Stem Cells Induced by Platelet-Rich Plasma and Cultured on Silk Fibroin Scaffold. *Stem Cel Res Ther* 10 (1), 369. doi:10.1186/s13287-019-1443-2

Rosenzweig, D., Carelli, E., Steffen, T., Jarzem, P., and Haglund, L. (2015). 3D-Printed ABS and PLA Scaffolds for Cartilage and Nucleus Pulposus Tissue Regeneration. *Ijms* 16 (7), 15118–15135. doi:10.3390/ijms160715118

Ruiz-Cantu, L., Gleadall, A., Faris, C., Segal, J., Shakesheff, K., and Yang, J. (2020). Multi-material 3D Bioprinting of Porous Constructs for Cartilage Regeneration. *Mater. Sci. Eng. C* 109, 110578. doi:10.1016/j.msec.2019.110578

Schneider, M., Günter, C., and Taubert, A. (2018). Co-Deposition of a Hydrogel/Calcium Phosphate Hybrid Layer on 3D Printed Poly(Lactic Acid) Scaffolds via Dip Coating: Towards Automated Biomaterials Fabrication. *Polymers* 10 (3), 275. doi:10.3390/polym10030275

She, Y., Fan, Z., Wang, L., Li, Y., Sun, W., Tang, H., et al. (2021). 3D Printed Biomimetic PCL Scaffold as Framework Interspersed with Collagen for Long Segment Tracheal Replacement. *Front. Cel Dev. Biol.* 9, 629796. doi:10.3389/fcell.2021.629796

Singh, Y. P., Bandyopadhyay, A., and Mandal, B. B. (2019). 3D Bioprinting Using Cross-linker-free Silk-Gelatin Bioink for Cartilage Tissue Engineering. *ACS Appl. Mater. Inter.* 11 (37), 33684–33696. doi:10.1021/acsami.9b11644

Soltan, N., Ning, L., Mohabatpour, F., Papagerakis, P., and Chen, X. (2019). Printability and Cell Viability in Bioprinting Alginate Dialdehyde-Gelatin Scaffolds. *ACS Biomater. Sci. Eng.* 5 (6), 2976–2987. doi:10.1021/acsbiomaterials.9b00167

Song, Y., Yang, Q., Jiang, H., and Dong, W. (2020). Clinical Application of Carving Template with 3D Reconstruction Technique for Personalized and Precise Treatment of Traumatic Ear Defects. *J. Craniofac. Surg. publish ahead print* 32 (4), 1423–1426. doi:10.1097/SCS.0000000000007166

Strioga, M., Viswanathan, S., Darinskas, A., Slaby, O., and Michalek, J. (2012). Same or Not the Same? Comparison of Adipose Tissue-Derived versus Bone Marrow-Derived Mesenchymal Stem and Stromal Cells. *Stem Cell Develop.* 21 (14), 2724–2752. doi:10.1089/scd.2011.0722

Sun, Y., You, Y., Jiang, W., Wu, Q., Wang, B., and Dai, K. (2020). Generating Ready-To-Implant Anisotropic Menisci by 3D-Bioprinting Protein-Releasing Cell-Laden Hydrogel-Polymer Composite Scaffold. *Appl. Mater. Today* 18, 100469. doi:10.1016/j.apmt.2019.100469

Takahashi, A., Matsumoto, H., Nagayama, K., Kitano, M., Hirose, S., Tanaka, H., et al. (2004). Evidence for the Involvement of Double-Strand Breaks in Heat-Induced Cell Killing. *Cancer Res.* 64 (24), 8839–8845. doi:10.1158/0008-5472.CAN-04-1876

Teramachi, M., Okumura, N., Nakamura, T., Yamamoto, Y., Kiyotani, T., Takimoto, Y., et al. (1997). Intrathoracic Tracheal Reconstruction with a Collagen-Conjugated Prosthesis: Evaluation of the Efficacy of Omental Wrapping. *J. Thorac. Cardiovasc. Surg.* 113 (4), 701–711. doi:10.1016/S0022-5223(97)70227-7

Thorne, C. H., Bradley, L. E., Levine, J. P., Hammerschlag, P., and Longaker, M. T. (2001). Auricular Reconstruction: Indications for Autogenous and Prosthetic Techniques. *Plast. Reconstr. Surg.* 107 (5), 1241–1251. doi:10.1097/00006534-200104150-00024

Unagolla, J. M., and Jayasuriya, A. C. (2020). Hydrogel-based 3D Bioprinting: A Comprehensive Review on Cell-Laden Hydrogels, Bioink Formulations, and Future Perspectives. *Appl. Mater. Today* 18, 100479. doi:10.1016/j.apmt.2019.100479

Van den Eynde, M., and Van Puyvelde, P. (2017). "3D Printing of Poly(lactic Acid)," in *Industrial Applications of Poly(lactic Acid)*, 282, 139–158. doi:10.1007/12_2017_28

Virk, J. S., Zhang, H., Nouraei, R., and Sandhu, G. (2017). Prosthetic Reconstruction of the Trachea: A Historical Perspective. *Wjcc* 5 (4), 128–133. doi:10.12998/wjcc.v5.i4.128

Visscher, D. O., Gleadall, A., Buskermolen, J. K., Burla, F., Segal, J., Koenderink, G. H., et al. (2019). Design and Fabrication of a Hybrid Alginate Hydrogel/poly(ε-caprolactone) Mold for Auricular Cartilage Reconstruction. *J. Biomed. Mater. Res.* 107 (5), 1711–1721. doi:10.1002/jbm.b.34264

Vuyk, H. D., and Adamson, P. A. (1998). Biomaterials in Rhinoplasty. *Clin. Otolaryngol.* 23 (3), 209–217. doi:10.1046/j.1365-2273.1998.00133.x

Wang, P., Auhl, D., Uhlmann, E., Gerlitzky, G., and Wagner, M. H. (2019). Rheological and Mechanical Gradient Properties of Polyurethane Elastomers for 3D-Printing with Reactive Additives. *Appl. Rheology* 29 (1), 162–172. doi:10.1515/arh-2019-0014

Wang, Q., Han, G., Yan, S., and Zhang, Q. (2019). 3D Printing of Silk Fibroin for Biomedical Applications. *Materials* 12 (3), 504. doi:10.3390/ma12030504

Wang, R., Yang, R., and Yang, F. (2015). Production of Bamboo Fiber Reinforced Fibrillated Poly(lactic Acid) (PLA) Material Obtained by a Papermaking Process. *J. Wuhan Univ. Technol.-Mat. Sci. Edit.* 30 (2), 429–432. doi:10.1007/s11595-015-1165-y

Wang, L., Fang, M., Xia, Y., Hou, J., Nan, X., Zhao, B., et al. (2020). Preparation and Biological Properties of Silk Fibroin/nano-Hydroxyapatite/graphene Oxide Scaffolds with an Oriented Channel-like Structure. *RSC Adv.* 10 (17), 10118–10128. doi:10.1039/c9ra09710d

Wang, Y.-H., Wang, D.-R., Guo, Y.-C., Liu, J.-Y., and Pan, J. (2020). The Application of Bone Marrow Mesenchymal Stem Cells and Biomaterials in Skeletal Muscle Regeneration. *Regenerative Ther.* 15, 285–294. doi:10.1016/j.reth.2020.11.002

Wang, Y.-J., Jeng, U.-S., and Hsu, S.-h. (2018). Biodegradable Water-Based Polyurethane Shape Memory Elastomers for Bone Tissue Engineering. *ACS Biomater. Sci. Eng.* 4 (4), 1397–1406. doi:10.1021/acsbiomaterials.8b00091

Wei, P., Xu, Y., Gu, Y., Yao, Q., Li, J., and Wang, L. (2020). IGF-1-releasing PLGA Nanoparticles Modified 3D Printed PCL Scaffolds for Cartilage Tissue Engineering. *Drug Deliv.* 27 (1), 1106–1114. doi:10.1080/10717544.2020.1797239

Wei, X., Liu, C., Wang, Z., and Luo, Y. (2020). 3D Printed Core-Shell Hydrogel Fiber Scaffolds with NIR-Triggered Drug Release for Localized Therapy of Breast Cancer. *Int. J. Pharmaceutics* 580, 119219. doi:10.1016/j.ijpharm.2020.119219

Wiggenhauser, P. S., Schwarz, S., Koerber, L., Hoffmann, T. K., and Rotter, N. (2019). Addition of Decellularized Extracellular Matrix of Porcine Nasal Cartilage Improves Cartilage Regenerative Capacities of PCL-Based Scaffolds *In Vitro*. *J. Mater. Sci. Mater. Med.* 30 (11), 121. doi:10.1007/s10856-019-6323-x

Wu, J.-J., Huang, L.-M., Zhao, Q., and Xie, T. (2018). 4D Printing: History and Recent Progress. *Chin. J. Polym. Sci.* 36 (5), 563–575. doi:10.1007/s10118-018-2089-8

Xia, D., Jin, D., Wang, Q., Gao, M., Zhang, J., Zhang, H., et al. (2019). Tissue-engineered Trachea from a 3D-printed Scaffold Enhances Whole-segment Tracheal Repair in a Goat Model. *J. Tissue Eng. Regen. Med.* 13 (4), 694–703. doi:10.1002/term.2828

Xia, H., Zhao, D., Zhu, H., Hua, Y., Xiao, K., Xu, Y., et al. (2018). Lyophilized Scaffolds Fabricated from 3D-Printed Photocurable Natural Hydrogel for Cartilage Regeneration. *ACS Appl. Mater. Inter.* 10 (37), 31704–31715. doi:10.1021/acsami.8b10926

Xiao, J., and Gao, Y. (2017). The Manufacture of 3D Printing of Medical Grade TPU. *Prog. Addit Manuf* 2 (3), 117–123. doi:10.1007/s40964-017-0023-1

Xu, Y., Peng, J., Richards, G., Lu, S., and Eglin, D. (2019). Optimization of Electrospray Fabrication of Stem Cell-Embedded Alginate-Gelatin Microspheres and Their Assembly in 3D-Printed Poly(ε-Caprolactone) Scaffold for Cartilage Tissue Engineering. *J. Orthopaedic Translation* 18, 128–141. doi:10.1016/j.jot.2019.05.003

Yamada, A. (2018). Autologous Rib Microtia Construction. *Facial Plast. Surg. Clin. North America* 26 (1), 41–55. doi:10.1016/j.fsc.2017.09.006

Yang, Y., Yang, G., Song, Y., Xu, Y., Zhao, S., and Zhang, W. (2019). 3D Bioprinted Integrated Osteochondral Scaffold-Mediated Repair of Articular Cartilage Defects in the Rabbit Knee. *J. Med. Biol. Eng.* 40 (1), 71–81. doi:10.1007/s40846-019-00481-y

Younis, I., Gault, D., Sabbagh, W., and Kang, N. V. (2010). Patient Satisfaction and Aesthetic Outcomes after Ear Reconstruction with a Branemark-type, Bone-Anchored, Ear Prosthesis: a 16 Year Review. *J. Plast. Reconstr. Aesthet. Surg.* 63 (10), 1650–1655. doi:10.1016/j.bjps.2009.10.004

Yu, Y. S., Ahn, C. B., Son, K. H., and Lee, J. W. (2021). Motility Improvement of Biomimetic Trachea Scaffold via Hybrid 3D-Bioprinting Technology. *Polymers (Basel)* 13 (6). doi:10.3390/polym1306010.3390/polym13060971

Zafar, B., Mottaghitalab, F., Shahosseini, Z., Negahdari, B., and Farokhi, M. (2020). Silk Fibroin/alumina Nanoparticle Scaffold Using for Osteogenic Differentiation of Rabbit Adipose-Derived Stem Cells. *Materialia* 9, 100518. doi:10.1016/j.mtla.2019.100518

Zaim, M., Karaman, S., Cetin, G., and Isik, S. (2012). Donor Age and Long-Term Culture Affect Differentiation and Proliferation of Human Bone Marrow Mesenchymal Stem Cells. *Ann. Hematol.* 91 (8), 1175–1186. doi:10.1007/s00277-012-1438-x

Zhang, B., Guo, L., Chen, H., Ventikos, Y., Narayan, R. J., and Huang, J. (2020). Finite Element Evaluations of the Mechanical Properties of Polycaprolactone/hydroxyapatite Scaffolds by Direct Ink Writing: Effects of Pore Geometry. *J. Mech. Behav. Biomed. Mater.* 104, 103665. doi:10.1016/j.jmbbm.2020.103665

Zhang, B., and Song, J. (2018). 3D-Printed Biomaterials for Guided Tissue Regeneration. *Small Methods* 2 (9), 1700306. doi:10.1002/smtd.201700306

Zhang, F., You, X., Dou, H., Liu, Z., Zuo, B., and Zhang, X. (2015). Facile Fabrication of Robust Silk Nanofibril Films via Direct Dissolution of Silk in CaCl2-Formic Acid Solution. *ACS Appl. Mater. Inter.* 7 (5), 3352–3361. doi:10.1021/am508319h

Zhang, J., Wehrle, E., Vetsch, J. R., Paul, G. R., Rubert, M., and Müller, R. (2019). Alginate Dependent Changes of Physical Properties in 3D Bioprinted Cell-Laden Porous Scaffolds Affect Cell Viability and Cell Morphology. *Biomed. Mater.* 14 (6), 065009. doi:10.1088/1748-605X/ab3c74

Zhang, Z.-Z., Jiang, D., Ding, J.-X., Wang, S.-J., Zhang, L., Zhang, J.-Y., et al. (2016). Role of Scaffold Mean Pore Size in Meniscus Regeneration. *Acta Biomater.* 43, 314–326. doi:10.1016/j.actbio.2016.07.050

Zhang, Z.-Z., Jiang, D., Ding, J.-X., Wang, S.-J., Zhang, L., Zhang, J.-Y., et al. (2016). Role of Scaffold Mean Pore Size in Meniscus Regeneration. *Acta Biomater.* 43, 314–326. doi:10.1016/j.actbio.2016.07.050

Zhang, Z.-Z., Wang, S.-J., Zhang, J.-Y., Jiang, W.-B., Huang, A.-B., Qi, Y.-S., et al. (2017). 3D-Printed Poly(ε-Caprolactone) Scaffold Augmented with Mesenchymal Stem Cells for Total Meniscal Substitution: A 12- and 24-Week Animal Study in a Rabbit Model. *Am. J. Sports Med.* 45 (7), 1497–1511. doi:10.1177/0363546517691513

Zhao, C. Q., Liu, W. G., Xu, Z. Y., Li, J. G., Huang, T. T., Lu, Y. J., et al. (2020). Chitosan Ducts Fabricated by Extrusion-Based 3D Printing for Soft-Tissue Engineering. *Carbohydr. Polym.* 236, 116058. doi:10.1016/j.carbpol.2020.116058

Zhao, G., Cui, R., Chen, Y., Zhou, S., Wang, C., Hu, Z., et al. (2020). 3D Printing of Well Dispersed Electrospun PLGA Fiber Toughened Calcium Phosphate Scaffolds for Osteoanagenesis. *J. Bionic Eng.* 17 (4), 652–668. doi:10.1007/s42235-020-0051-2

Zhou, G., Jiang, H., Yin, Z., Liu, Y., Zhang, Q., Zhang, C., et al. (2018). *In Vitro* Regeneration of Patient-specific Ear-Shaped Cartilage and its First Clinical Application for Auricular Reconstruction. *EBioMedicine* 28, 287–302. doi:10.1016/j.ebiom.2018.01.011

Zopf, D. A., Flanagan, C. L., Mitsak, A. G., Brennan, J. R., and Hollister, S. J. (2018). Pore Architecture Effects on Chondrogenic Potential of Patient-specific 3-dimensionally Printed Porous Tissue Bioscaffolds for Auricular Tissue Engineering. *Int. J. Pediatr. Otorhinolaryngol.* 114, 170–174. doi:10.1016/j.ijporl.2018.07.033

Zopf, D. A., Mitsak, A. G., Flanagan, C. L., Wheeler, M., Green, G. E., and Hollister, S. J. (2015). Computer Aided-Designed, 3-dimensionally Printed Porous Tissue Bioscaffolds for Craniofacial Soft Tissue Reconstruction. *Otolaryngol. Head Neck Surg.* 152 (1), 57–62. doi:10.1177/0194599814552065

Conflict of Interest: The authors declare that the research was conducted in the absence of any commercial or financial relationships that could be construed as a potential conflict of interest.

Publisher's Note: All claims expressed in this article are solely those of the authors and do not necessarily represent those of their affiliated organizations, or those of the publisher, the editors and the reviewers. Any product that may be evaluated in this article, or claim that may be made by its manufacturer, is not guaranteed or endorsed by the publisher.

frontiers in Bioengineering and Biotechnology

BRIEF RESEARCH REPORT
published: 28 January 2022
doi: 10.3389/fbioe.2021.789621

Fibronectin Adherent Cell Populations Derived From Avascular and Vascular Regions of the Meniscus Have Enhanced Clonogenicity and Differentiation Potential Under Physioxia

Girish Pattappa[1], Franziska Reischl[1], Judith Jahns[1], Ruth Schewior[1], Siegmund Lang[1], Johannes Zellner[1,2], Brian Johnstone[3], Denitsa Docheva[1,4] and Peter Angele[1,2]*

[1]Laboratory for Experimental Trauma Surgery, Department of Trauma Surgery, University Regensburg Medical Centre, Regensburg, Germany, [2]Sporthopaedicum Regensburg, Regensburg, Germany, [3]Department of Orthopaedics and Rehabilitation, Oregon Health and Science University, Portland, OR, United States, [4]Department of Musculoskeletal Tissue Regeneration, Orthopaedic Hospital König-Ludwig-Haus, University of Wurzburg, Wurzburg, Germany

OPEN ACCESS

Edited by:
Zhen Li,
AO Research Institute, Switzerland

Reviewed by:
Ryan Michael Porter,
University of Arkansas for Medical Sciences, United States
Zoran Ivanovic,
Établissement Français du Sang (EFS), France
Helen Elizabeth McCarthy,
Cardiff University, United Kingdom

***Correspondence:**
Girish Pattappa
girish.pattappa@ukr.de

Specialty section:
This article was submitted to Tissue Engineering and Regenerative Medicine, a section of the journal Frontiers in Bioengineering and Biotechnology

Received: *05 October 2021*
Accepted: *20 December 2021*
Published: *28 January 2022*

Citation:
Pattappa G, Reischl F, Jahns J, Schewior R, Lang S, Zellner J, Johnstone B, Docheva D and Angele P (2022) Fibronectin Adherent Cell Populations Derived From Avascular and Vascular Regions of the Meniscus Have Enhanced Clonogenicity and Differentiation Potential Under Physioxia. Front. Bioeng. Biotechnol. 9:789621. doi: 10.3389/fbioe.2021.789621

The meniscus is composed of an avascular inner region and vascular outer region. The vascular region has been shown to contain a progenitor population with multilineage differentiation capacity. Strategies facilitating the isolation and propagation of these progenitors can be used to develop cell-based meniscal therapies. Differential adhesion to fibronectin has been used to isolate progenitor populations from cartilage, while low oxygen or physioxia (2% oxygen) enhances the meniscal phenotype. This study aimed to isolate progenitor populations from the avascular and vascular meniscus using differential fibronectin adherence and examine their clonogenicity and differentiation potential under hyperoxia (20% oxygen) and physioxia (2% oxygen). Human vascular and avascular meniscus cells were seeded onto fibronectin-coated dishes for a short period and monitored for colony formation under either hyperoxia or physioxia. Non-fibronectin adherent meniscus cells were also expanded under both oxygen tension. Individual fibronectin adherent colonies were isolated and further expanded, until approximately ten population doublings (passage 3), whereby they underwent chondrogenic, osteogenic, and adipogenic differentiation. Physioxia enhances clonogenicity of vascular and avascular meniscus cells on plastic or fibronectin-coated plates. Combined differential fibronectin adhesion and physioxia isolated a progenitor population from both meniscus regions with trilineage differentiation potential compared to equivalent hyperoxia progenitors. Physioxia isolated progenitors had a significantly enhanced meniscus matrix content without the presence of collagen X. These results demonstrate that combined physioxia and fibronectin adherence can isolate and propagate a meniscus progenitor population that can potentially be used to treat meniscal tears or defects.

Keywords: meniscus, hypoxia, tissue engineeering, meniscus progenitor cells, chondrogenesis

INTRODUCTION

The menisci are located on the medial and lateral tibial plateau of the knee joint that aids in load bearing, force transmission (e.g., compression, tension, and shear), and lubrication during joint motion. It also protects the underlying articular cartilage from high impact forces that can induce cartilage lesions and result in early osteoarthritis (Makris et al., 2011; Madry et al., 2016; Verdonk et al., 2016). The meniscus is a fibrocartilaginous tissue that has two distinct regions: an inner avascular region and an outer vascularized region. The avascular region resembles articular cartilage with a high proportion of collagen type II and glycosaminoglycans, while the vascular region of the meniscus contains a higher proportion of collagen type I (Ghadially et al., 1983; McDevitt and Webber, 1990; Verdonk et al., 2005). Meniscal tears or lesions are a common injury with a high annual incidence (66 per 100,000) throughout the world (reviewed by Bansal et al., 2021). Patients with meniscal tears undergo partial or total meniscectomy, but this leads to exposure of the underlying cartilage, resulting in altered joint biomechanics that increases risk of developing early osteoarthritis (Englund et al., 2009; Paradowski et al., 2016). Nowadays, clinicians have begun to preserve the meniscus, although the capacity for repair depends on the localization of the injury. Specifically, tears in the vascular region can be healed by applying sutures, whilst tears in the avascular region have a limited repair capacity, partially due to the low vascularity in this part of the meniscus. Methods to treat meniscus tears are required to prevent further damage to the meniscus and underlying tissues, thus preventing the onset of early osteoarthritis.

Cell-based treatment strategies for meniscus repair have focused on treating the avascular region of the tissue. Studies using mesenchymal stromal cells (MSCs) have shown their superior regenerative properties compared to meniscal cells (Pabbruwe et al., 2010; Nakagawa et al., 2015; Whitehouse et al., 2017; Zellner et al., 2017). The use of these cells in patients has also resulted in improved clinical outcomes (Whitehouse et al., 2017; Olivos-Meza et al., 2019; Sekiya et al., 2019). However, studies using MSCs have demonstrated the induction of cartilage hypertrophy that upon *in vivo* implantation, leads to ectopic bone formation (Pelttari et al., 2006). Furthermore, many countries only permit the use of homologous approaches for treating tissues, which limits the use of MSCs from various tissue sources for clinical treatments.

Previous studies have demonstrated that the meniscus from both animal (e.g., bovine and rabbit) and human sources contains a progenitor population with the ability to differentiate to the adipogenic, osteogenic, and chondrogenic lineage (Mauck et al., 2007; Muhammad et al., 2014; Huang et al., 2016; Gamer et al., 2017; Seol et al., 2017; Chahla et al., 2021; Wei et al., 2021). Specifically, these progenitors were mainly located in the vascular region and horns of the meniscus (Mauck et al., 2007). Muhammad et al. (2014) and Seol et al. (2017) showed that a meniscus progenitor cell population can also be isolated *via* cell migration from meniscus explants derived from bovine or human tissues. The former study showed that these progenitor populations were derived from the superficial layer of the meniscus (Muhammad et al., 2014). A recent investigation has also demonstrated the presence of progenitor population within the avascular meniscus regions (Chahla et al., 2021).

A method to isolate progenitor populations is the use of differential adhesion to fibronectin. Fibronectin is present in both the stem cell niche and meniscus tissues (Salter et al., 1995). It enables selection of progenitor populations due to the presence of alpha-5/beta-1 integrin on their cell surface (Dowthwaite et al., 2004). Previous investigations have isolated multipotent progenitors from skin and bone marrow using this technique (Jones and Watt, 1993; D'Ippolito et al., 2004; Williams et al., 2010). Articular cartilage progenitor cells (ACPs) isolated *via* fibronectin adhesion were found to express stem cell markers (e.g., CD90, CD105, and Notch), increased telomerase activity, and have multilineage differentiation potential. In contrast to MSCs, use of ACPs in an animal model resulted in cartilage regeneration with no evidence of bone formation (Dowthwaite et al., 2004; Williams et al., 2010). Furthermore, a recent study has shown that fibronectin adherent populations exist in osteoarthritic meniscus tissue that are clonogenic, have a high proliferation capacity, express MSC surface markers and maintain differentiation potential at high passages compared to non-fibronectin adherent meniscus cells (Korpershoek et al., 2021). Thus, differential fibronectin adherence has the potential to isolate an appropriate cell type from the tissue that can be used for meniscus treatment or regeneration.

In vivo, the meniscus is under a low oxygen environment or physioxia (2%–5% oxygen) similar to articular cartilage (Lund-Olesen, 1970; Ivanovic, 2009; Lafont, 2010; Ivanovic and Vlaski, 2015). In general, physioxia has shown a donor-dependent enhancement in cartilage-related gene expression and matrix content for chondrocytes and chondrogenic MSCs under physioxia compared to normal oxygen tension (20% oxygen) or hyperoxia (Pattappa et al., 2019b). In the case of meniscus cells, studies have also demonstrated that physioxia has a beneficial effect on their gene expression and matrix content (Adesida et al., 2006; Adesida et al., 2007; Adesida et al., 2012; Berneel et al., 2016; Liang et al., 2017; Szojka et al., 2021). Studies examining stem cells also indicate that low oxygen tension helps maintain their stemness and extends their proliferation capacity compared to normal oxygen tension (D'Ippolito et al., 2006).

The present investigation combined the use of differential fibronectin adhesion and physioxic culture to investigate the presence of progenitor cells from avascular and vascular regions of human meniscus. Isolated progenitor populations expanded under hyperoxia and physioxia, subsequently underwent differentiation to the adipogenic, osteogenic and chondrogenic lineage at passage 2 (≈ 10 population doublings). In-depth analysis of chondrogenic differentiation was investigated to determine the matrix-forming capacity of these progenitors and their potential in treating meniscus tears. In parallel, experiments were replicated for non-fibronectin adherent (NFA) avascular and vascular meniscus cells. Based on previous investigations, it was hypothesized that fibronectin facilitated the isolation of a meniscus progenitor population and that physioxia has a beneficial effect on the clonogenicity and differentiation potential of these cells.

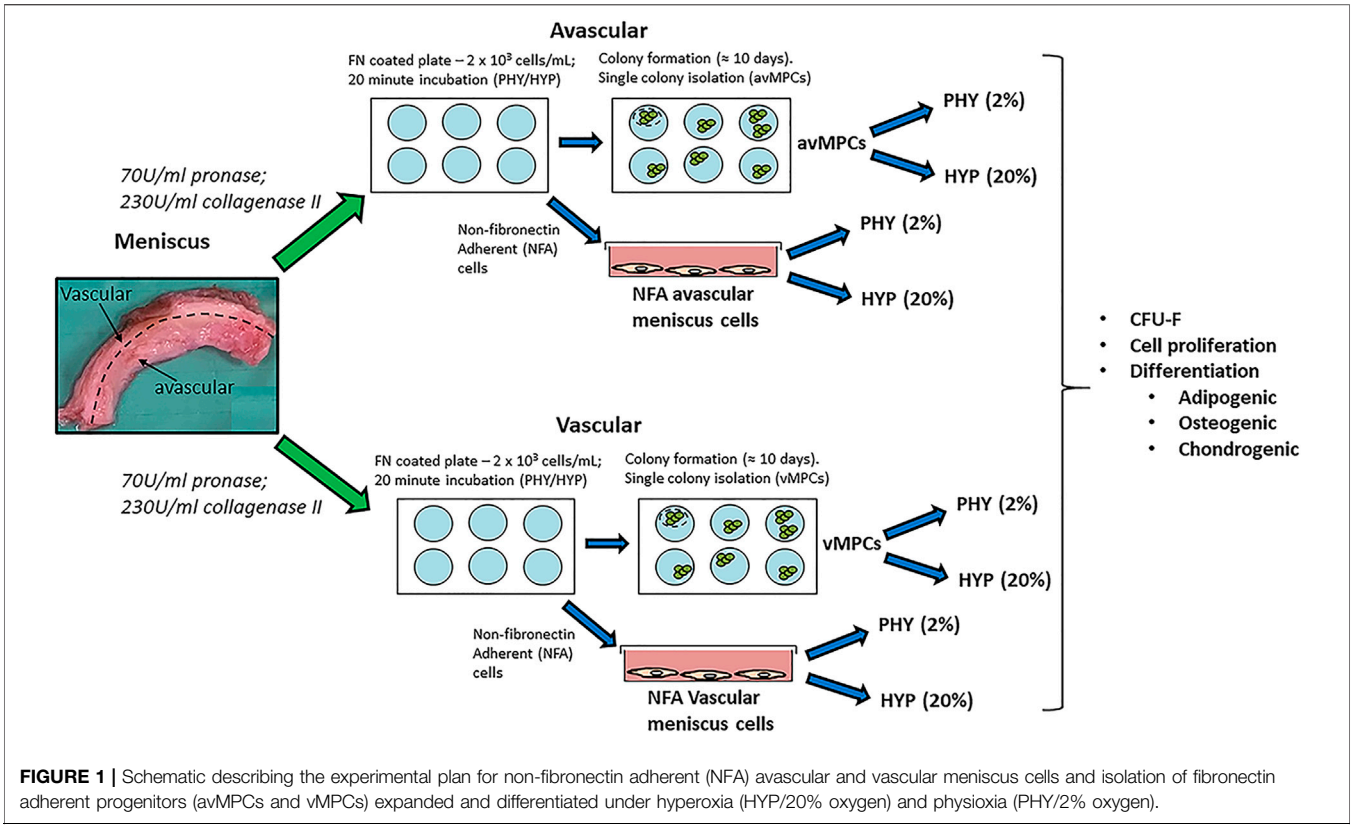

FIGURE 1 | Schematic describing the experimental plan for non-fibronectin adherent (NFA) avascular and vascular meniscus cells and isolation of fibronectin adherent progenitors (avMPCs and vMPCs) expanded and differentiated under hyperoxia (HYP/20% oxygen) and physioxia (PHY/2% oxygen).

MATERIALS AND METHODS

Meniscus Cell and Fibronectin Isolation

Human meniscus tissue was collected from patients (n = 7; mean age: 60 ± 7) with no previous meniscus injury and undergoing total knee arthroplasty, following informed consent from patients and using procedures approved by the local ethics committee (University Hospital Regensburg; Ethic approval no.: Nr. 18-837-101). Meniscus tissue was split into its two regions (inner two-thirds for the avascular region and outer one-third for the vascular region), minced into small pieces and digested in pronase (70 U/ml; Roche Diagnostics, Switzerland) in DMEM-LG (Invitrogen, Karlsruhe, Germany) + 5% FBS (PAN-Biotech, Aidenbach, Germany) + 1% penicillin-streptomycin (Sigma-Aldrich, Steinheim, Germany) for 45 min and then overnight in collagenase type II (230 U/ml; Worthington) in DMEM-LG + 5% FBS + 1% penicillin-streptomycin at 37°C (**Figure 1**).

For the fibronectin adherence, six-well plates were coated with 10 mg/ml bovine fibronectin (Sigma-Aldrich, Steinheim, Germany) in PBS with magnesium and calcium chloride ions (Sigma-Aldrich, Steinheim, Germany) and incubated overnight at 4°C. Following collagenase digestion, the number of avascular and vascular meniscus cells was counted using a hemacytometer, then each cell type was seeded at 2×10^3 cells/ml (200 cells/cm^2) onto fibronectin-coated plates and incubated for 20 min in either a standard cell culture incubator at 20% oxygen and 5% CO_2 or a low oxygen incubator (ThermoFisher Scientific, Regensburg Germany) set at 2% oxygen and 5% CO_2. For this manuscript, hyperoxia refers to 20% oxygen, while 2% oxygen is termed as physioxia. Following a 20-min incubation period, media containing non-fibronectin adherent meniscus cells was removed and replaced with expansion media composed of DMEM + 10% FBS + 5 ng/ml basic fibroblast growth factor (Peprotech, Hamburg, Germany) + 1 ng/ml TGF-beta1 (R&D Systems, Oxford, UK). Non-fibronectin adherent avascular and vascular meniscus cells were seeded at 5×10^3 cells/cm^2 with equal numbers of flasks placed under both oxygen tensions and cultured using the same the expansion media. Media changes were performed twice per week using pre-equilibrated media at the same oxygen tension. Upon observation of colonies, individual meniscus progenitor cell colonies were isolated as previously described (Williams et al., 2010). Three clones were evaluated for each meniscus region under their respective oxygen tension. Henceforth, clones isolated *via* fibronectin are either avascular fibronectin adherent meniscus progenitors (avMPCs) or vascular fibronectin adherent meniscus progenitor (vMPCs) cells. Non-fibronectin adherent (NFA) avascular and vascular meniscus cells, avMPCs, and vMPCs were expanded for 50 days and cell counts were recorded for population growth curve using previously described calculations (Pattappa et al., 2020).

Colony-Forming Unit Assay (CFU-F)

Colony-forming unit (CFU) assay was performed on P1 NFA meniscus cells from both oxygen conditions and on uncoated and fibronectin-coated dishes. In brief, 10-cm Petri dishes were

seeded with NFA avascular or vascular meniscus cells at 20, 5, and 2 cells/cm^2 with a set of dishes also coated with 10 mg/ml fibronectin as described above. After 10 days of cultivation, formed colonies were stained using 0.5% crystal violet/methanol and imaged (Sigma, Steinheim, Germany), and individual colonies were counted as previously described (Kohler et al., 2013; Alberton et al., 2015).

Differentiation

All differentiations were performed on passage 2 (≈10 population doublings) NFA avascular and vascular meniscus cells, avMPCs, and vMPCs under their respective expansion oxygen conditions using previously described protocols (Alberton et al., 2015).

Osteogenic Differentiation and Alizarin Red Staining

Cells were seeded at 2×10^3 cells/cm^2 into 12-well plates and incubated under their respective expansion oxygen conditions. Following 24 h after seeding, media was replaced with osteogenic medium [DMEM-HG (Invitrogen, Karlsruhe, Germany) + 10% FBS + 0.05 mM L-ascorbic acid-2-phosphate + 10 mM β-glycerophosphate + 0.1 mM dexamethasone (all Sigma-Aldrich, Steinheim, Germany)] and cultured for 21 days with media refreshed twice per week. For controls, cells were cultured In DMEM-HG + 10% FBS + 1% penicillin-streptomycin for the duration of culture. At 21 days of culture, calcium deposition was visualized using alizarin red staining using previously described protocols (Alberton et al., 2015). Monolayers were imaged using an inverted microscope (Nikon, Japan).

Adipogenic Differentiation and Oil-Red-O Staining

Cells were seeded at 5×10^3 cells/cm^2 into a 24-well plate and then incubated in expansion media till 80% confluence. Media was then replaced with adipogenic induction media composed of DMEM-HG (Invitrogen) + 10% FBS + 1% penicillin-streptomycin + 0.1 mg/ml insulin (PAN Biotech, Aidenbach, Germany) + 1 µM dexamethasone + 0.2 mM indomethacin + 0.1 mg/ml insulin + 1 mM 3-isobutyl-1-methylxanthine (all Sigma Aldrich, Steinheim, Germany). Control cultures were cultured in adipogenic maintenance media composed of DMEM-HG + 10% FBS + 1% penicillin-streptomycin + 0.1 mg/ml insulin. Cells were stimulated for 21 days with a week cycle for adipogenic cultures consisting of 5 days adipogenic induction media and 2 days of adipogenic maintenance media. Lipid vacuoles were visualized by Oil-Red-O staining by using a standard protocol and imaged using an inverted microscope (Olympus, Japan) (Alberton et al., 2015).

Chondrogenesis: GAG Assay and Histological Staining

Hyperoxia and physioxia expanded crude meniscus cells, avMPCs, and vMPCs were used to form pellet cultures as previously described (Pattappa et al., 2019b). In brief, pellets were formed by centrifuging 2×10^5 cells at 250× *g* for 5 min in 300 µl of chondrogenic medium in polypropylene V-bottom 96-well plates. Chondrogenic media consisted of serum-free high-glucose DMEM containing 10 ng/ml TGF-β1 (R&D Systems), 100 nM dexamethasone, 50 µg/ml ascorbic acid-2-phosphate (all Sigma-Aldrich, Steinheim, Germany), 1 mM sodium pyruvate (Invitrogen, Karlsruhe, Germany), and 1% ITS (PAN Biotech GmbH, Aidenbach, Germany). Media changes were performed three times per week and then collected for analysis after 21 days.

Pellets were collected for wet weight and GAG assay using protocols previously described (Pattappa et al., 2019b). A set of pellets were also fixed in 4% PBS buffered paraformaldehyde, rinsed briefly in PBS, and then incubated in increasing sucrose concentrations (10%–30%). Pellets were photographed with an optical microscope (PL 2000, Optech, Germany) and then embedded in Tissue-Tek (Sakura, Zoeterwnde, Netherlands). Cryosections (10 µm thick) were created using a cryotome (HM500 OM; Microm, Berlin, Germany) and then stained with DMMB for visualization of glycosaminoglycans using previously published protocols (Pattappa et al., 2019b; Pattappa et al., 2020).

Sections were immunohistochemically labeled for human type I collagen (mouse monoclonal antibody, 1:50; C256; Sigma-Aldrich), human type II collagen (mouse monoclonal antibody, 1:200; CP18, Calbiochem, Darmstadt, Germany), and type X collagen (mouse monoclonal antibody, 1:50; X53, ThermoFisher Scientific), then labeled with a corresponding fluorescently labeled secondary antibody [tetramethylrhodamine (TRITC)-conjugated anti-mouse IgG (1:200; Jackson ImmunoResearch, Cambridge, UK)] using previously described protocols (Pattappa et al., 2019b). Sections were imaged on an Olympus XC10 camera on an Olympus BX61 fluorescence microscope (Olympus, Japan).

Gene Expression Analysis

RNA was extracted from a pool of six pellets from crude avascular and vascular meniscus cells and avMPCs and vMPCs from each condition using previously described protocols (Pattappa et al., 2019b). Total RNA was quantified and 250 ng was reverse-transcribed using Transcriptor first strand kit (Roche, Mannheim, Germany). qPCR reactions for chondrogenic genes (see **Supplementary Table S1**) were performed using Brilliant SYBR Green QPCR mix (Stratagene, San Diego, CA, United States) and measured using a Biorad CFX96 system (Biorad Laboratories, Munich, Germany). Results were analyzed using the ΔΔCt method with Proteasome subunit beta type-4 (PSMB4) used as a housekeeping gene and then presented as fold change under physioxia relative to hyperoxia for avMPCs, vMPCs, and crude meniscus cells (Pattappa et al., 2019b; Pattappa et al., 2020).

Statistical Analysis

All statistical analysis was performed using GraphPad Prism v7 (GraphPad, La Jolla, CA, United States). Data were checked for normal distribution using a Shapiro-Wilk test. A comparison of pellet wet weight and GAG content between hyperoxia and physioxia was performed using two-way ANOVA with Tukey

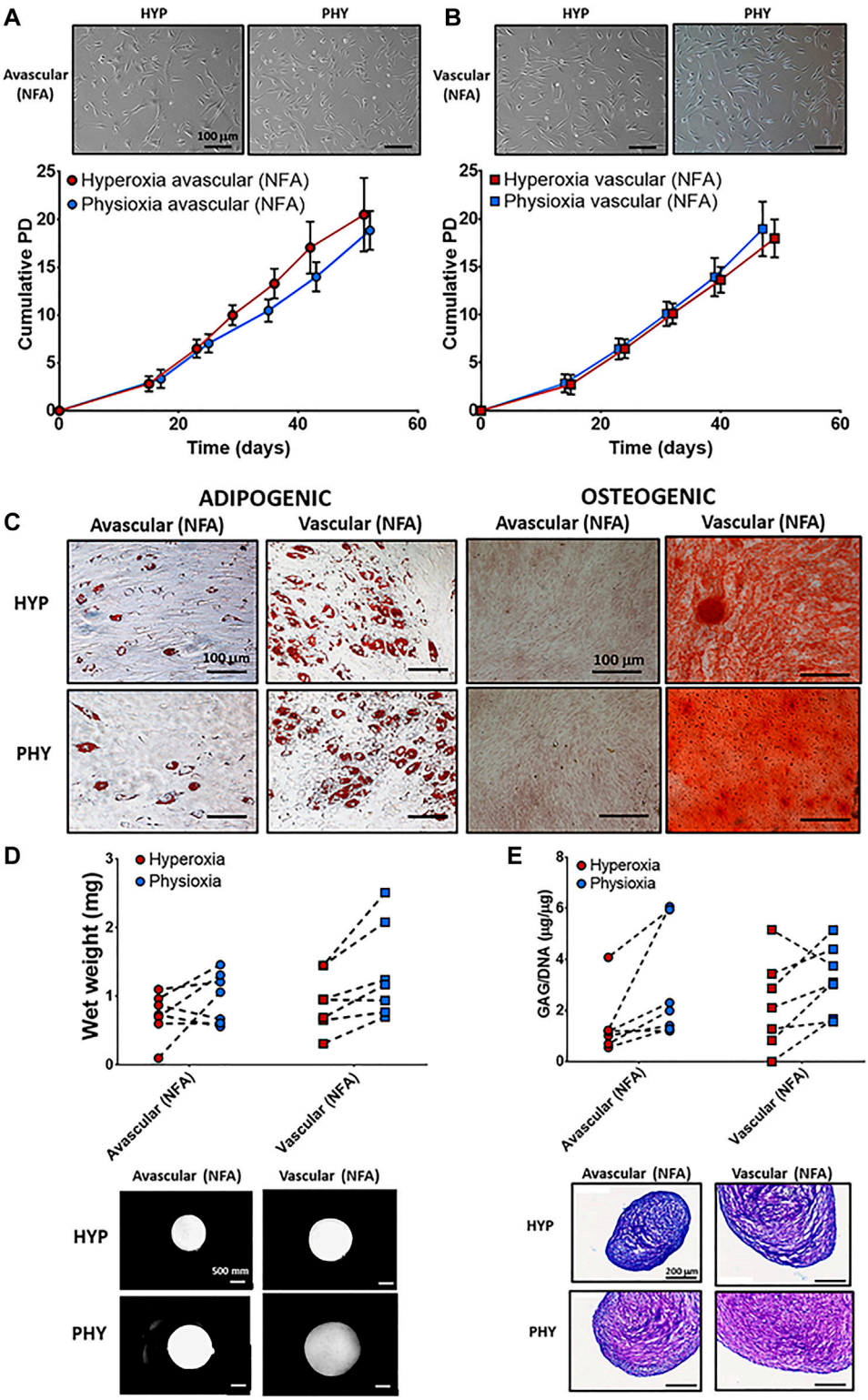

FIGURE 2 | Representative photomicrographs of hyperoxia (HYP) and physioxia (PHY) expanded NFA **(A)** avascular and **(B)** vascular meniscus cells with corresponding population growth curves (n = 7; mean ± S.D.). **(C)** Representative photomicrographs of Oil-red-O staining for lipid droplet and alizarin red staining for calcium deposition for meniscus populations under hyperoxia (HYP) and physioxia (PHY). Pellet **(D)** wet weight **(E)** GAG content for avascular and vascular meniscus cells with representative **(D)** macroscopic and **(E)** DMMB-stained pellets.

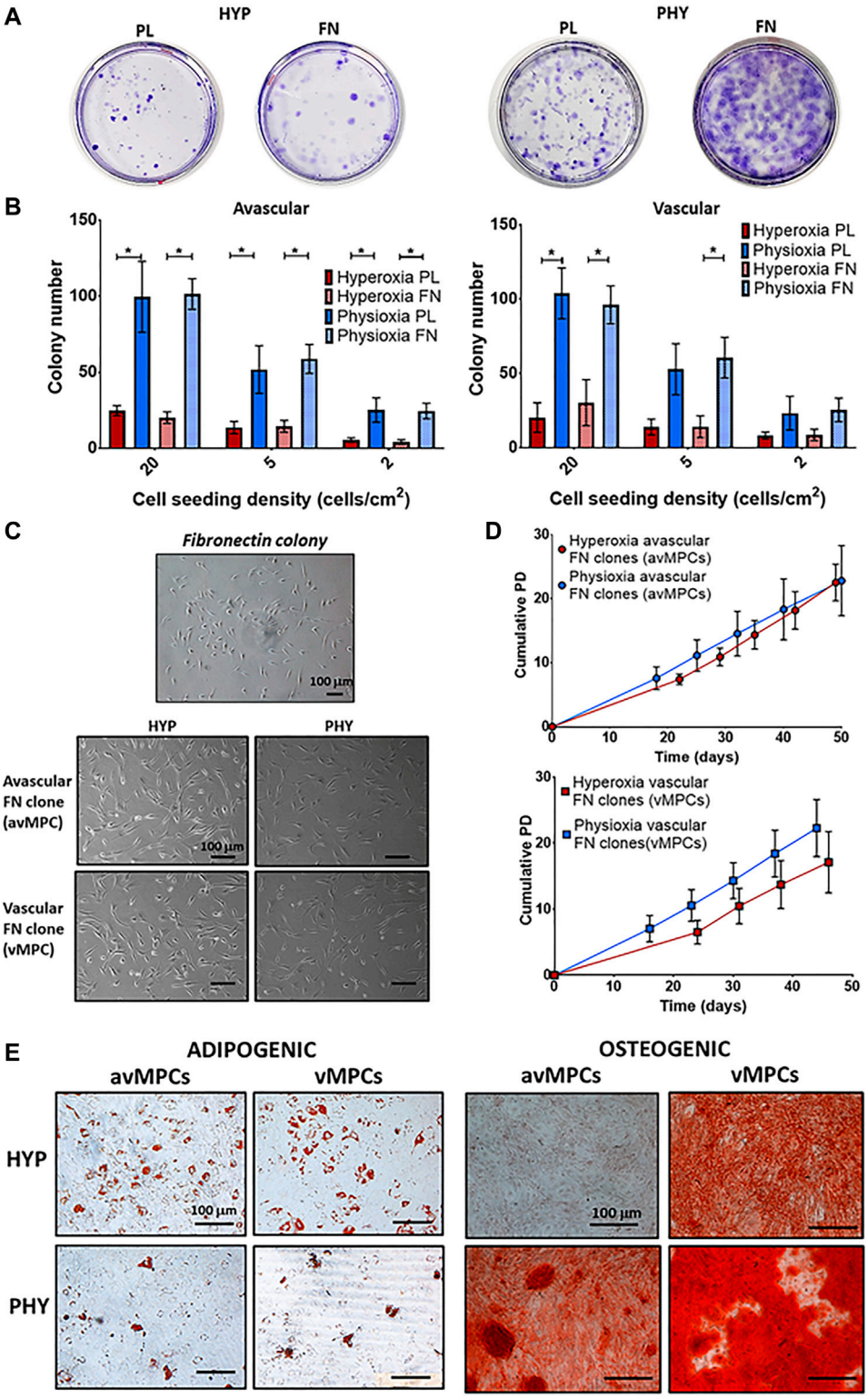

FIGURE 3 | (A) Representative crystal violet-stained colonies cultured under hyperoxia (HYP) and physioxia (HYP) on uncoated (PL) and fibronectin (FN)-coated dishes. **(B)** Number of colonies counted from conditions described in **(A)** from avascular and vascular meniscus cells ($n = 6$; data represent mean ± S.D.; $^*p < 0.05$). **(C)** Representative photomicrographs of a fibronectin colony and avMPCs and vMPCs cultured under hyperoxia and physioxia with **(D)** population growth curves for expanded avMPC and vMPC population under hyperoxia and physioxia [$n = 4$ (3 clones/donor); data represent mean ± S.D.]. **(E)** Representative Oil-red-O staining for lipid droplet formation and alizarin red staining for calcium deposition for avMPCs and vMPCs.

post-hoc test, with significance set at $p < 0.05$. Gene expression data were calculated as a fold change in physioxia relative to hyperoxia and then analyzed using a Mann–Whitney test with significance set at $p < 0.05$.

RESULTS

Non-Fibronectin Adherent Vascular Meniscus Cells Contain a Progenitor Population With Trilineage Differentiation Potential

No differences were observed in cellular morphology between NFA avascular (**Figure 2A**) and vascular (**Figure 2B**) meniscus cells under hyperoxia and physioxia. There was no difference in cumulative cell doublings between NFA avascular and vascular meniscus cells expanded under hyperoxia or physioxia (**Figures 2A,B**). Lipid droplet formation was observed for both meniscus populations (NFA) independent of oxygen tension with avascular meniscus cells (NFA) observed to have fewer lipid vacuoles compared to vascular meniscus cells (**Figure 2C**). In contrast, osteogenic differentiation of meniscus cells showed only positive alizarin red staining for vascular meniscus cells (NFA) under both oxygen conditions, whereas avascular meniscus cells showed no alizarin red staining independent of oxygen tension (**Figure 2C**).

There was no significant difference in pellet wet weight and GAG deposition between meniscus regions under different oxygen tension for chondrogenic differentiation (**Figures 2D,E**). Examination of individual donors demonstrated that 70% of donors had an increase in pellet wet weight and GAG deposition under physioxia compared to hyperoxia for both meniscus cell types (**Figures 2D,E**). Macroscopic images and DMMB staining of a donor that was physioxia responsive showed that avascular and vascular meniscus pellets appeared larger and had greater metachromasia staining compared to corresponding hyperoxia pellets (**Figures 2D,E**). There was an upregulation in SOX9, COL2A1, COL1A1, and ACAN under physioxia for both meniscus regions, while there was a downregulation in COL10A1 under physioxia for vascular meniscus cells (**Supplementary Figure S1A**). Increased type I collagen and type II collagen staining for avascular and vascular meniscus cells was observed under physioxia, while there was no staining for collagen X for both regions independent of oxygen tension (**Supplementary Figure S1B**).

Fibronectin Adherence and Physioxia Isolates a Progenitor Population From the Avascular and Vascular Regions of Meniscus With High Clonogenic and Multilineage Differentiation Capacity

CFU-F evaluation showed that physioxic cultures had increased colony formation compared to hyperoxic cultures, with fibronectin adherent colonies observed to have larger diameter colonies compared to those formed on uncoated plates (**Figure 3A**). Physioxia significantly increased colony number for avascular and vascular meniscus cells on both plastic and fibronectin-coated dishes compared to corresponding dishes cultured under hyperoxia (*$p < 0.05$; **Figure 3B**). Furthermore, a similar pattern was observed for the CFU-F efficiency, whereby a higher efficiency was observed under physioxia with a tendency towards increased CFU-F efficiency upon combining physioxia and fibronectin (*$p < 0.05$; **Supplementary Figure S2**). There was no difference in avMPCs and vMPCs cell morphology between oxygen conditions (**Figure 3C**). Specifically, physioxic vMPCs appeared to have greater cumulative population doublings compared to equivalent hyperoxic vMPCs (**Figure 3D**). However, no significant difference was observed between cumulative population doublings or doubling time at each passage under physioxia compared to hyperoxia for avMPCs or vMPCs (**Figure 3D**). Adipogenesis was exhibited by both hyperoxic and physioxic avMPCs and vMPCs with greater lipid vacuoles formed for hyperoxic avMPCs and vMPCs (**Figure 3E**). In contrast, alizarin red staining for osteogenesis indicated a mineralized matrix by hyperoxic vMPCs, while both physioxic avMPCs and vMPCs also stained for alizarin red (**Figure 3E**).

Physioxia Isolated avMPCs and vMPCs Show Enhanced Matrix Capacity With Minimal Collagen X Expression

Physioxia vMPCs showed a significant increase in both wet weight (*$p < 0.05$; **Figure 4A**) and GAG deposition (*$p < 0.05$; **Figure 4B**) compared to hyperoxic vMPCs. Physioxic avMPCs had both an increase in wet weight and a significant increase in GAG content compared to hyperoxic avMPCs (*$p < 0.05$; **Figure 4B**). Macroscopic images and DMMB staining showed larger pellets and greater DMMB staining formed for physioxia meniscus progenitors (**Figures 4A**,**B**).

A significant upregulation in SOX9, and matrix genes COL2A1, COL1A2, and ACAN was observed for physioxic avMPCs or vMPCs compared to corresponding hyperoxic progenitors (*$p < 0.05$; **Figure 4C**). An increase in type I and II collagen staining was also observed for physioxia avMPCs and vMPCs compared to corresponding hyperoxic progenitors (**Figure 4D**). Furthermore, there was no collagen X staining for progenitors cultured under either oxygen condition (**Figure 4D**).

DISCUSSION

The present study has demonstrated that a progenitor population can be isolated *via* combined differential fibronectin adhesion and physioxia from the avascular and vascular regions of the meniscus with enhanced clonogenicity and differentiation potential of these populations (**Figure 3**). Similar to previous studies using ACPs, physioxic culture of avMPCs or vMPCs demonstrated an increase in matrix content by these cells with minimal presence of collagen X (**Figure 4**) (Anderson et al., 2016). In comparison, examination of non-fibronectin adherent meniscus population only indicated that the vascular region of the meniscus contained a population with trilineage

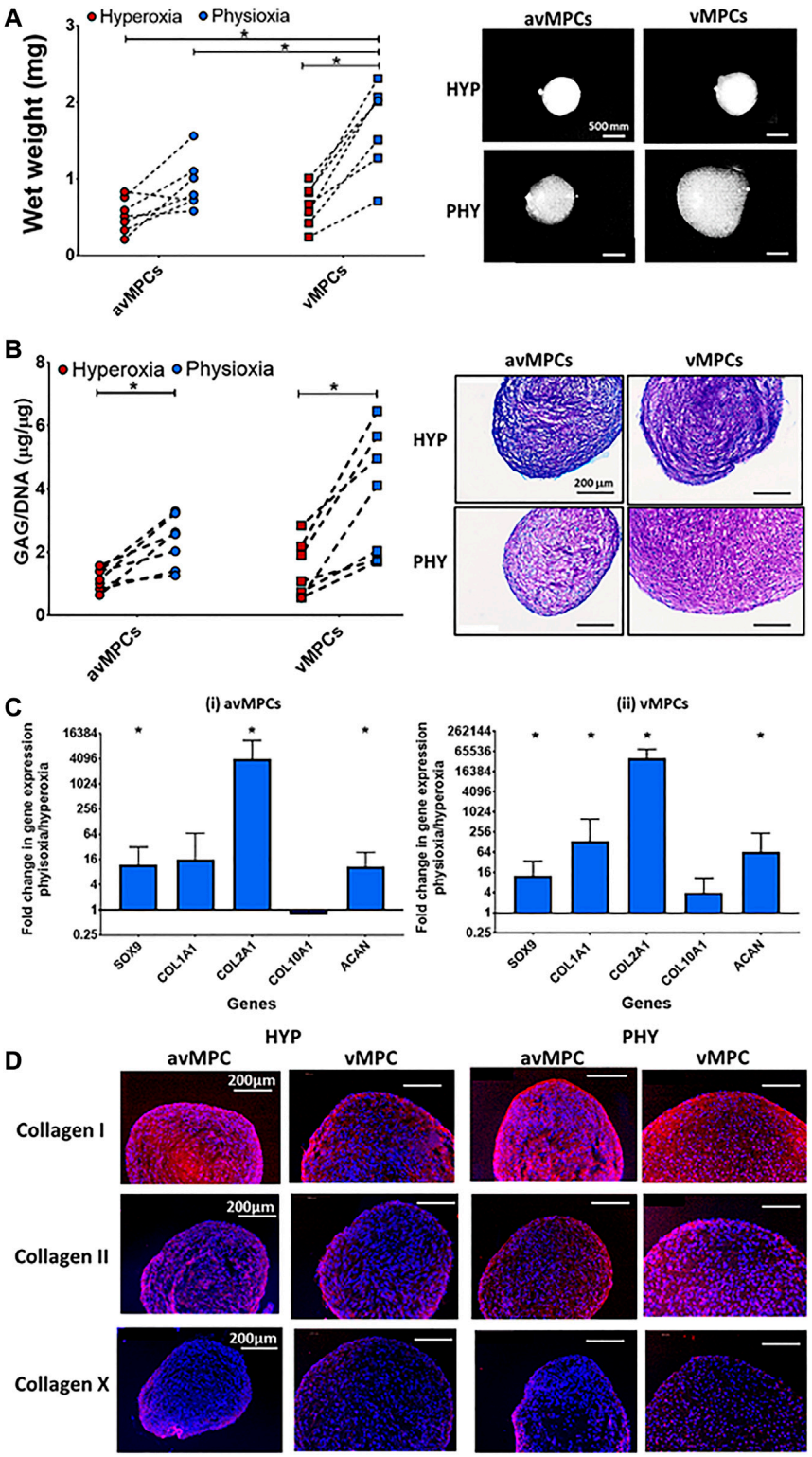

FIGURE 4 | Chondrogenic differentiation of avMPCs and vMPCs under hyperoxia and physioxia. Dot plot for pellet **(A)** wet weight and **(B)** GAG content for isolated clones (each dot represents mean of individual three clones) cultured under hyperoxia and physioxia with representative **(A)** macroscopic and **(B)** DMMB-stained pellets. **(C)** Gene expression data for meniscus matrix genes for (i) avascular and (ii) vascular MPCs. Data represent fold change for (i) avascular and (ii) vascular MPCs cultured under physioxia relative to corresponding clones under hyperoxic conditions (data represent mean ± S.D.; $n = 5$ donors; $^*p < 0.05$). **(D)** Representative images of avMPC and vMPCs pellets stained with collagen I, collagen II, and collagen X cultured under hyperoxia and physioxia. Positive and negative controls are in **Supplementary Figure S1**.

differentiation potential with no difference in cell expansion between oxygen tensions (**Figure 2**).

Previous studies have described the presence of multipotent meniscus cell populations from either animal sources (e.g., bovine), human meniscus tissue, or debris (Mauck et al., 2007; Muhammad et al., 2014; Gamer et al., 2017; Liang et al., 2017; Seol et al., 2017; Sun et al., 2020; Chahla et al., 2021; Wei et al., 2021). Specifically, the horns and vascular regions of the tissue appear to contain progenitor populations (Mauck et al., 2007). However, few studies have investigated their differentiation potential under physioxia. Liang et al. (2017) showed that physioxia enhanced and maintained the adipogenic and chondrogenic potential of meniscus cells for up to 10 population doublings, with no osteogenesis observed under both oxygen tensions. However, there was no separation between regions in the stated study. The results of the non-fibronectin adherent meniscus cells suggest that the vascular region of the meniscus contained a population with trilineage differentiation potential under both oxygen conditions similar to the previously stated investigations (**Figure 2**). The results of the chondrogenic data showed a donor-dependent increase in matrix deposition for meniscus cells under physioxia, similar to recent studies for chondrocytes or chondrogenic MSCs (Anderson et al., 2016; Pattappa et al., 2019a; Pattappa et al., 2019b). An upregulation in COL1A1 and COL2A1 expression and greater collagen I and II staining was observed for avascular and vascular meniscus cells (NFA) under physioxia compared to hyperoxia expanded cells, similar to results from previous studies (**Supplementary Figure S1**) (Adesida et al., 2006; Adesida et al., 2007; Berneel et al., 2016).

The second part of this study combined physioxia with differential fibronectin adherence to understand whether progenitor populations can be directly isolated from both avascular and vascular regions of the meniscus using this method (**Figures 3**, **4**). Isolation using differential fibronectin adherence for articular cartilage yielded a population with increased telomerase activity that enabled it to undergo high population doublings with maintenance of their differentiation capacity in both healthy and osteoarthritic cartilage (Dowthwaite et al., 2004; Williams et al., 2010). A recent investigation demonstrated that from OA meniscus tissue, fibronectin adherence enabled the isolation of a progenitor population that maintained both its clonogenicity and multipotency at high passages with expression of stem cell markers (e.g. CD90 and CD105) compared to non-fibronectin adherent meniscus cells (Korpershoek et al., 2021). In contrast to the stated study and the results from the non-fibronectin adherent meniscus cells, the present study demonstrated that the combined use of differential fibronectin adherence and physioxia yielded a progenitor population from both the avascular and vascular meniscus regions with trilineage differentiation capacity (**Figures 3**, **4**). This result supports the results of recent investigations that have demonstrated the presence of progenitor populations in avascular regions of the meniscus (Muhammad et al., 2014; Chahla et al., 2021). Additionally, the presence of fibronectin has a tendency to increase CFU-F efficiency of avascular and vascular meniscus cells under physioxia, indicating that fibronectin could efficiently isolate meniscus progenitor populations (**Supplementary Figure S2**).

It should be noted that the osteogenic lineage demonstrated variable differentiation among the avMPCs and vMPCs examined, particularly upon physioxic culture. Previous publications have contrasting data regarding whether physioxia either inhibits (D'Ippolito et al., 2006) or enhances (Wagegg et al., 2012; Yu et al., 2019) osteogenic differentiation. Our results show that the majority of clonal progenitors studied differentiated to the osteogenic lineage under physioxia. However, there were also progenitors with no osteogenic induction that may be related to physioxia inhibiting osteogenesis. Furthermore, this could also be related to inherent multipotency of the specific clonal progenitor. Loncaric et al. (2019) demonstrated that even within MSC cultures, only 40% of clonal populations derived from a single cell exhibit multipotency and sustain their clonogenicity at high passages (Loncaric et al., 2019). Thus, further clonal progenitor isolation would need to be performed for fibronectin adherent meniscus cells (avMPCs and vMPCs) with single cells taken from these clones to understand whether these are true multipotent progenitors. Additionally, this would also show whether the inhibited osteogenesis for avMPCs and vMPCs under physioxia was due to the oxygen tension or inherent differentiation capacity.

To demonstrate that the avMPCs and vMPCs are progenitor populations, examination of their cell surface marker expression needs to be performed. Single-cell RNAseq analysis has identified progenitor populations within healthy and osteoarthritic meniscus (Sun et al., 2020). They showed that a CD146-positive population had progenitor characteristics within healthy meniscus, while in osteoarthritic meniscus, this changed to a CD318-positive population *via* attenuation of TGF-β-related pathways (Sun et al., 2020). CD146-positive cells are termed pericytes and found to be present near vasculature (e.g., bone marrow) and have stem cell characteristics (Crisan et al., 2008). Korpershoek et al. (2021) showed a significant increase in CD318 expression in their fibronectin adherent meniscus progenitors compared to non-fibronectin-adherent meniscus cells, indicating that these are dervied from osteoarthritic meniscus. Future investigations would study cell surface markers from the populations described in the present study.

The use of physioxia significantly enhanced the clonogenicity of the meniscus population with fibronectin producing colonies with larger diameter (**Figures 3A**,**B**). This is potentially related to the stem cell property of cellular migration that assists in self-renewal and cellular proliferation and has been known to be enhanced upon culture on fibronectin (Singh and Schwarzbauer, 2012). The subsequent growth under both oxygen conditions demonstrates that the avMPCs and vMPCs under both oxygen conditions have the potential to be expanded to high population doublings with no discernible changes in doubling time or differentiation potential (**Figure 3D**). Further analysis is required to see whether their differentiation potential remains the same with passage for this clonal population compared to non-fibronectin adherent meniscus cells

(Korpershoek et al., 2021). However, in spite of combined fibronectin and physioxia isolating progenitors from both meniscus regions, there remains an open question regarding the additional benefit of fibronectin towards creating a cell-based therapy for meniscus regeneration. Previous studies have shown that physioxia helps maintain the stemness and expression of stem cell genes (D'Ippolito et al., 2006), whilst fibronectin adherent progenitors have demonstrated similar properties with the additional benefit of increased telomerase activity compared to non-fibronectin adherent populations (Dowthwaite et al., 2004; Williams et al., 2010). Due to the similarities in their effect on progenitor populations, future investigations would seek to understand the specific effects of fibronectin on isolation of meniscus progenitors both on its own and in combination with physioxia. Furthermore, this would help justify the use of fibronectin for meniscus progenitor isolation, as this step adds additional costs towards the creation of cell-based therapies for meniscus treatment.

Physioxic culture of avMPCs and vMPCs had a significant increase in cartilage matrix genes, GAG deposition, and collagen I/II staining for both meniscus regions compared to hyperoxic cultures (**Figure 4**). Furthermore, similar to findings for ACPs, no collagen X staining was found in these progenitor populations, independent of oxygen tension (Anderson et al., 2016). A limitation of bone marrow MSCs for chondrogenesis is that it expresses markers for hypertrophy *in vitro* and forms bone upon *in vivo* implantation, inspite of physioxic expansion (Pelttari et al., 2006; Pattappa et al., 2019b). Thus, the present results demonstrate the importance of physioxia for the induction of a meniscus phenotype, specifically for matrix deposition and preventing collagen X expression that could lead to hypertrophy *in vivo*. Future studies would evaluate the feasibility of these meniscus progenitors for clinical translation by isolating progenitors from animal meniscus and then test their healing potential in treating either meniscal tears or pars intermedia defects (Angele et al., 2008; Koch et al., 2019). Additionally, the presence of these progenitor populations provides an additional rationale for the development of biomaterial-based technologies that allow cellular migration *via* suitable chemoattractants, which enables natural healing of meniscus tears without the necessity for extensive cell culture (Qu et al., 2017).

CONCLUSION

Physioxia enhances the clonogenicity of avascular and vascular meniscus cells, with larger diameter colonies formed on fibronectin. Combined physioxia and fibronectin adherence isolated a progenitor population with trilineage differentiation potential from the avascular and vascular meniscus regions. Specifically for meniscus tissue engineering, these progenitor cells were observed to have enhanced matrix content under physioxia with suppression of collagen X that could make them less susceptible to hypertrophy upon *in vivo* implantation. Therefore, combined differential fibronectin adherence and physioxia is a potential method for isolating progenitor populations from the meniscus that can be used for the development of cell-based therapies for the treatment of meniscus tears/defects.

DATA AVAILABILITY STATEMENT

The original contributions presented in the study are included in the article/**Supplementary Material**. Further inquiries can be directed to the corresponding author.

ETHICS STATEMENT

The studies involving human participants were reviewed and approved by Ethikcommission an der Univeristat Regensburg. Ethical approval no: 18-83-101, Isolation and characterization of human meniscus derived cells. The patients/participants provided their written informed consent to participate in this study.

AUTHOR CONTRIBUTIONS

GP, JZ, BJ, DD, and PA conceived the study. GP, DD, and PA designed the experiments for the study. GP, FR, JJ, RS, and SL carried out the experiments. GP, FR, and JJ analyzed the experimental results. GP wrote the manuscript draft. All authors review and edited the final manuscript.

FUNDING

This was supported by European Union Horizon 2020 research and innovation programme (EU No.: 814444 (MEFISTO)).

ACKNOWLEDGMENTS

The authors would like to acknowledge Philip von Roth (Sporthopaedicm Regensburg) for providing the meniscus donors used in the study.

SUPPLEMENTARY MATERIAL

The Supplementary Material for this article can be found online at: https://www.frontiersin.org/articles/10.3389/fbioe.2021.789621/full#supplementary-material

REFERENCES

Adesida, A. B., Grady, L. M., Khan, W. S., Millward-Sadler, S. J., Salter, D. M., and Hardingham, T. E. (2007). Human Meniscus Cells Express Hypoxia Inducible Factor-1α and Increased SOX9 in Response to Low Oxygen Tension in Cell Aggregate Culture. *Arthritis Res. Ther.* 9 (4), R69. doi:10.1186/ar2267

Adesida, A. B., Mulet-Sierra, A., Laouar, L., and Jomha, N. M. (2012). Oxygen Tension Is a Determinant of the Matrix-Forming Phenotype of Cultured Human Meniscal Fibrochondrocytes. *PLoS One* 7 (6), e39339. doi:10.1371/journal.pone.0039339

Adesida, A., Grady, L., Khan, W., and Hardingham, T. (2006). The Matrix-Forming Phenotype of Cultured Human Meniscus Cells Is Enhanced after Culture with Fibroblast Growth Factor 2 and Is Further Stimulated by Hypoxia. *Arthritis Res. Ther.* 8 (3), R61. doi:10.1186/ar1929

Alberton, P., Dex, S., Popov, C., Shukunami, C., Schieker, M., and Docheva, D. (2015). Loss of Tenomodulin Results in Reduced Self-Renewal and Augmented Senescence of Tendon Stem/progenitor Cells. *Stem Cell Dev.* 24 (5), 597–609. doi:10.1089/scd.2014.0314

Anderson, D. E., Markway, B. D., Bond, D., McCarthy, H. E., and Johnstone, B. (2016). Responses to Altered Oxygen Tension Are Distinct between Human Stem Cells of High and Low Chondrogenic Capacity. *Stem Cel Res Ther* 7 (1), 154. doi:10.1186/s13287-016-0419-8

Angele, P., Johnstone, B., Kujat, R., Zellner, J., Nerlich, M., Goldberg, V., et al. (2008). Stem Cell Based Tissue Engineering for Meniscus Repair. *J. Biomed. Mater. Res.* 85A (2), 445–455. doi:10.1002/jbm.a.31480

Bansal, S., Floyd, E. R., Kowalsk, M. A., Kowalski, M., Elrod, P., Burkey, K., et al. (2021). Meniscal Repair: The Current State and Recent Advances in Augmentation. *J. Orthop. Res.* 39 (7), 1368–1382. doi:10.1002/jor.25021

Berneel, E., Philips, C., Declercq, H., and Cornelissen, R. (2016). Redifferentiation of High-Throughput Generated Fibrochondrocyte Micro-aggregates: Impact of Low Oxygen Tension. *Cells Tissues Organs* 202 (5-6), 369–381. doi:10.1159/000447509

Chahla, J., Papalamprou, A., Chan, V., Arabi, Y., Salehi, K., Nelson, T. J., et al. (2021). Assessing the Resident Progenitor Cell Population and the Vascularity of the Adult Human Meniscus. *Arthrosc. J. Arthroscopic Relat. Surg.* 37 (1), 252–265. doi:10.1016/j.arthro.2020.09.021

Crisan, M., Yap, S., Casteilla, L., Chen, C.-W., Corselli, M., Park, T. S., et al. (2008). A Perivascular Origin for Mesenchymal Stem Cells in Multiple Human Organs. *Cell Stem Cell* 3 (3), 301–313. doi:10.1016/j.stem.2008.07.003

D'Ippolito, G., Diabira, S., Howard, G. A., Menei, P., Roos, B. A., and Schiller, P. C. (2004). Marrow-isolated Adult Multilineage Inducible (MIAMI) Cells, a Unique Population of Postnatal Young and Old Human Cells with Extensive Expansion and Differentiation Potential. *J. Cel Sci* 117 (Pt 14), 2971–2981. doi:10.1242/jcs.01103

D'Ippolito, G., Diabira, S., Howard, G. A., Roos, B. A., and Schiller, P. C. (2006). Low Oxygen Tension Inhibits Osteogenic Differentiation and Enhances Stemness of Human MIAMI Cells. *Bone* 39 (3), 513–522. doi:10.1016/j.bone.2006.02.061

Dowthwaite, G. P., Bishop, J. C., Redman, S. N., Khan, I. M., Rooney, P., Evans, D. J. R., et al. (2004). The Surface of Articular Cartilage Contains a Progenitor Cell Population. *J. Cel Sci* 117 (Pt 6), 889–897. doi:10.1242/jcs.00912

Englund, M., Guermazi, A., Roemer, F. W., Aliabadi, P., Yang, M., Lewis, C. E., et al. (2009). Meniscal Tear in Knees without Surgery and the Development of Radiographic Osteoarthritis Among Middle-Aged and Elderly Persons: The Multicenter Osteoarthritis Study. *Arthritis Rheum.* 60 (3), 831–839. doi:10.1002/art.24383

Gamer, L. W., Shi, R. R., Gendelman, A., Mathewson, D., Gamer, J., and Rosen, V. (2017). Identification and Characterization of Adult Mouse Meniscus Stem/progenitor Cells. *Connect. Tissue Res.* 58 (3-4), 238–245. doi:10.1080/03008207.2016.1271797

Ghadially, F. N., Lalonde, J. M., and Wedge, J. H. (1983). Ultrastructure of normal and Torn Menisci of the Human Knee Joint. *J. Anat.* 136 (Pt 4), 773–791.

Huang, H., Wang, S., Gui, J., and Shen, H. (2016). A Study to Identify and Characterize the Stem/progenitor Cell in Rabbit Meniscus. *Cytotechnology* 68 (5), 2083–2103. doi:10.1007/s10616-016-9949-2

Ivanovic, Z. (2009). Hypoxia or *In Situ* Normoxia: The Stem Cell Paradigm. *J. Cel. Physiol.* 219 (2), 271–275. doi:10.1002/jcp.21690

Ivanovic, Z., and Vlaski, M. (2015). *Anaerobiosis and Stemness: An Evolutionary Paradigm for Therapeutic Applications*. Cambridge, Massachusetts: Academic Press.

Jones, P. H., and Watt, F. M. (1993). Separation of Human Epidermal Stem Cells from Transit Amplifying Cells on the Basis of Differences in Integrin Function and Expression. *Cell* 73 (4), 713–724. doi:10.1016/0092-8674(93)90251-k

Koch, M., Hammer, S., Fuellerer, J., Lang, S., Pfeifer, C., Pattappa, G., et al. (2019). Bone Marrow Aspirate Concentrate for the Treatment of Avascular Meniscus Tears in a One-step Procedure-Evaluation of an *In Vivo* Model. *Int. J. Mol. Sci.* 20 (5), 1120. doi:10.3390/ijms20051120

Kohler, J., Popov, C., Klotz, B., Alberton, P., Prall, W. C., Haasters, F., et al. (2013). Uncovering the Cellular and Molecular Changes in Tendon Stem/progenitor Cells Attributed to Tendon Aging and Degeneration. *Aging Cell* 12 (6), 988–999. doi:10.1111/acel.12124

Korpershoek, J. V., Rikkers, M., de Windt, T. S., Tryfonidou, M. A., Saris, D. B. F., and Vonk, L. A. (2021). Selection of Highly Proliferative and Multipotent Meniscus Progenitors through Differential Adhesion to Fibronectin: A Novel Approach in Meniscus Tissue Engineering. *Int. J. Mol. Sci.* 22 (16), 8614. doi:10.3390/ijms22168614

Lafont, J. E. (2010). Lack of Oxygen in Articular Cartilage: Consequences for Chondrocyte Biology. *Int. J. Exp. Pathol.* 91 (2), 99–106. doi:10.1111/j.1365-2613.2010.00707.x

Liang, Y., Idrees, E., Andrews, S. H. J., Labib, K., Szojka, A., Kunze, M., et al. (2017). Plasticity of Human Meniscus Fibrochondrocytes: A Study on Effects of Mitotic Divisions and Oxygen Tension. *Sci. Rep.* 7 (1), 12148. doi:10.1038/s41598-017-12096-x

Loncaric, D., Labat, V., Debeissat, C., Brunet de la Grange, P., Rodriguez, L., Vlaski-Lafarge, M., et al. (2019). The Majority of Cells in So-Called "mesenchymal Stem Cell" Population Are Neither Stem Cells Nor Progenitors. *Transfus. Clinique Biologique* 26 (4), 316–323. doi:10.1016/j.tracli.2018.08.157

Lund-Olesen, K. (1970). Oxygen Tension in Synovial Fluids. *Arthritis Rheum.* 13 (6), 769–776. doi:10.1002/art.1780130606

Madry, H., Kon, E., Condello, V., Peretti, G. M., Steinwachs, M., Seil, R., et al. (2016). Early Osteoarthritis of the Knee. *Knee Surg. Sports Traumatol. Arthrosc.* 24 (6), 1753–1762. doi:10.1007/s00167-016-4068-3

Makris, E. A., Hadidi, P., and Athanasiou, K. A. (2011). The Knee Meniscus: Structure-Function, Pathophysiology, Current Repair Techniques, and Prospects for Regeneration. *Biomaterials* 32 (30), 7411–7431. doi:10.1016/j.biomaterials.2011.06.037

Mauck, R. L., Martinez-Diaz, G. J., Yuan, X., and Tuan, R. S. (2007). Regional Multilineage Differentiation Potential of Meniscal Fibrochondrocytes: Implications for Meniscus Repair. *Anat. Rec.* 290 (1), 48–58. doi:10.1002/ar.20419

McDevitt, C. A., and Webber, R. J. (1990). The Ultrastructure and Biochemistry of Meniscal Cartilage. *Clin. Orthopaedics Relat. Res.* 252, 8–18. doi:10.1097/00003086-199003000-00003

Muhammad, H., Schminke, B., Bode, C., Roth, M., Albert, J., von der Heyde, S., et al. (2014). Human Migratory Meniscus Progenitor Cells Are Controlled via the TGF-β Pathway. *Stem Cel Rep.* 3 (5), 789–803. doi:10.1016/j.stemcr.2014.08.010

Nakagawa, Y., Muneta, T., Kondo, S., Mizuno, M., Takakuda, K., Ichinose, S., et al. (2015). Synovial Mesenchymal Stem Cells Promote Healing after Meniscal Repair in Microminipigs. *Osteoarthritis and Cartilage* 23 (6), 1007–1017. doi:10.1016/j.joca.2015.02.008

Olivos-Meza, A., Pérez Jiménez, F. J., Granados-Montiel, J., Landa-Solís, C., Cortés González, S., Jiménez Aroche, C. A., et al. (2019). First Clinical Application of Polyurethane Meniscal Scaffolds with Mesenchymal Stem Cells and Assessment of Cartilage Quality with T2 Mapping at 12 Months. *Cartilage* 13, 197S–207S. doi:10.1177/1947603519852415

Pabbruwe, M. B., Kafienah, W., Tarlton, J. F., Mistry, S., Fox, D. J., and Hollander, A. P. (2010). Repair of Meniscal Cartilage white Zone Tears Using a Stem Cell/collagen-Scaffold Implant. *Biomaterials* 31 (9), 2583–2591. doi:10.1016/j.biomaterials.2009.12.023

Paradowski, P. T., Lohmander, L. S., and Englund, M. (2016). Osteoarthritis of the Knee after Meniscal Resection: Long Term Radiographic Evaluation of Disease Progression. *Osteoarthritis and Cartilage* 24 (5), 794–800. doi:10.1016/j.joca.2015.12.002

Pattappa, G., Johnstone, B., Zellner, J., Docheva, D., and Angele, P. (2019a). The Importance of Physioxia in Mesenchymal Stem Cell Chondrogenesis and the Mechanisms Controlling its Response. *Int. J. Mol. Sci.* 20 (3), 484. doi:10.3390/ijms20030484

Pattappa, G., Schewior, R., Hofmeister, I., Seja, J., Zellner, J., Johnstone, B., et al. (2019b). Physioxia Has a Beneficial Effect on Cartilage Matrix Production in Interleukin-1 Beta-Inhibited Mesenchymal Stem Cell Chondrogenesis. *Cells* 8 (8), 936. doi:10.3390/cells8080936

Pattappa, G., Krueckel, J., Schewior, R., Franke, D., Mench, A., Koch, M., et al. (2020). Physioxia Expanded Bone Marrow Derived Mesenchymal Stem Cells Have Improved Cartilage Repair in an Early Osteoarthritic Focal Defect Model. *Biology* 9 (8), 230. doi:10.3390/biology9080230

Pelttari, K., Winter, A., Steck, E., Goetzke, K., Hennig, T., Ochs, B. G., et al. (2006). Premature Induction of Hypertrophy during *In Vitro* Chondrogenesis of Human Mesenchymal Stem Cells Correlates with Calcification and Vascular Invasion after Ectopic Transplantation in SCID Mice. *Arthritis Rheum.* 54 (10), 3254–3266. doi:10.1002/art.22136

Qu, F., Holloway, J. L., Esterhai, J. L., Burdick, J. A., and Mauck, R. L. (2017). Programmed Biomolecule Delivery to Enable and Direct Cell Migration for Connective Tissue Repair. *Nat. Commun.* 8 (1), 1780. doi:10.1038/s41467-017-01955-w

Salter, D. M., Godolphin, J. L., and Gourlay, M. S. (1995). Chondrocyte Heterogeneity: Immunohistologically Defined Variation of Integrin Expression at Different Sites in Human Fetal Knees. *J. Histochem. Cytochem.* 43 (4), 447–457. doi:10.1177/43.4.7897185

Sekiya, I., Koga, H., Otabe, K., Nakagawa, Y., Katano, H., Ozeki, N., et al. (2019). Additional Use of Synovial Mesenchymal Stem Cell Transplantation Following Surgical Repair of a Complex Degenerative Tear of the Medial Meniscus of the Knee: A Case Report. *Cel Transpl.* 28 (11), 1445–1454. doi:10.1177/0963689719863793

Seol, D., Zhou, C., Brouillette, M. J., Song, I., Yu, Y., Choe, H. H., et al. (2017). Characteristics of Meniscus Progenitor Cells Migrated from Injured Meniscus. *J. Orthop. Res.* 35 (9), 1966–1972. doi:10.1002/jor.23472

Singh, P., and Schwarzbauer, J. E. (2012). Fibronectin and Stem Cell Differentiation - Lessons from Chondrogenesis. *J. Cel Sci* 125 (Pt 16), 3703–3712. doi:10.1242/jcs.095786

Sun, H., Wen, X., Li, H., Wu, P., Gu, M., Zhao, X., et al. (2020). Single-cell RNA-Seq Analysis Identifies Meniscus Progenitors and Reveals the Progression of Meniscus Degeneration. *Ann. Rheum. Dis.* 79 (3), 408–417. doi:10.1136/annrheumdis-2019-215926

Szojka, A. R. A., Liang, Y., Marqueti, R. d. C., Moore, C. N., Erkut, E. J. N., Kunze, M., et al. (2021). Time Course of 3D Fibrocartilage Formation by Expanded Human Meniscus Fibrochondrocytes in Hypoxia. *J. Orthop. Res*. Online ahead of print. doi:10.1002/jor.25046

Verdonk, P. C. M., Forsyth, R. G., Wang, J., Almqvist, K. F., Verdonk, R., Veys, E. M., et al. (2005). Characterisation of Human Knee Meniscus Cell Phenotype. *Osteoarthritis and Cartilage* 13 (7), 548–560. doi:10.1016/j.joca.2005.01.010

Verdonk, R., Madry, H., Shabshin, N., Dirisamer, F., Peretti, G. M., Pujol, N., et al. (2016). The Role of Meniscal Tissue in Joint protection in Early Osteoarthritis. *Knee Surg. Sports Traumatol. Arthrosc.* 24 (6), 1763–1774. doi:10.1007/s00167-016-4069-2

Wagegg, M., Gaber, T., Lohanatha, F. L., Hahne, M., Strehl, C., Fangradt, M., et al. (2012). Hypoxia Promotes Osteogenesis but Suppresses Adipogenesis of Human Mesenchymal Stromal Cells in a Hypoxia-Inducible Factor-1 Dependent Manner. *PLoS One* 7 (9), e46483. doi:10.1371/journal.pone.0046483

Wei, Y., Sun, H., Gui, T., Yao, L., Zhong, L., Yu, W., et al. (2021). The Critical Role of Hedgehog-Responsive Mesenchymal Progenitors in Meniscus Development and Injury Repair. *Elife* 10, e62917. doi:10.7554/eLife.62917

Whitehouse, M. R., Howells, N. R., Parry, M. C., Austin, E., Kafienah, W., Brady, K., et al. (2017). Repair of Torn Avascular Meniscal Cartilage Using Undifferentiated Autologous Mesenchymal Stem Cells: From *In Vitro* Optimization to a First-In-Human Study. *Stem Cells Transl Med.* 6 (4), 1237–1248. doi:10.1002/sctm.16-0199

Williams, R., Khan, I. M., Richardson, K., Nelson, L., McCarthy, H. E., Analbelsi, T., et al. (2010). Identification and Clonal Characterisation of a Progenitor Cell Sub-population in normal Human Articular Cartilage. *PLoS One* 5 (10), e13246. doi:10.1371/journal.pone.0013246

Yu, X., Wan, Q., Ye, X., Cheng, Y., Pathak, J. L., and Li, Z. (2019). Cellular Hypoxia Promotes Osteogenic Differentiation of Mesenchymal Stem Cells and Bone Defect Healing via STAT3 Signaling. *Cell Mol Biol Lett* 24, 64. doi:10.1186/s11658-019-0191-8

Zellner, J., Pattappa, G., Koch, M., Mueller, M. B., Nerlicht, M., Angele, P., et al. (2017). Autologous Mesenchymal Stem Cells or Meniscal Cells: what Is the Best Cell Source for Regenerative Meniscus Treatment in an Early Osteoarthritis Situation? *Stem Cel Res Ther* 8 (1), 225. doi:10.1186/s13287-017-0678-z

Conflict of Interest: The authors declare that the research was conducted in the absence of any commercial or financial relationships that could be construed as a potential conflict of interest.

Publisher's Note: All claims expressed in this article are solely those of the authors and do not necessarily represent those of their affiliated organizations, or those of the publisher, the editors and the reviewers. Any product that may be evaluated in this article, or claim that may be made by its manufacturer, is not guaranteed or endorsed by the publisher.

Advantages of publishing in Frontiers

OPEN ACCESS
Articles are free to read for greatest visibility and readership

FAST PUBLICATION
Around 90 days from submission to decision

HIGH QUALITY PEER-REVIEW
Rigorous, collaborative, and constructive peer-review

TRANSPARENT PEER-REVIEW
Editors and reviewers acknowledged by name on published articles

Frontiers
Avenue du Tribunal-Fédéral 34
1005 Lausanne | Switzerland

Visit us: www.frontiersin.org
Contact us: frontiersin.org/about/contact

REPRODUCIBILITY OF RESEARCH
Support open data and methods to enhance research reproducibility

DIGITAL PUBLISHING
Articles designed for optimal readership across devices

FOLLOW US
@frontiersin

IMPACT METRICS
Advanced article metrics track visibility across digital media

EXTENSIVE PROMOTION
Marketing and promotion of impactful research

LOOP RESEARCH NETWORK
Our network increases your article's readership